





Smithsonian  
Contributions to Astrophysics

VOLUME 7

PROCEEDINGS OF THE SYMPOSIUM  
ON THE  
ASTRONOMY AND PHYSICS OF METEORS

Held at

SMITHSONIAN ASTROPHYSICAL OBSERVATORY

Cambridge, Massachusetts

August 28–September 1, 1961



Sponsored by  
Smithsonian Astrophysical Observatory, Cambridge, Mass.,  
and

Geophysical Research Directorate,  
Air Force Cambridge Research Laboratories,  
Office of Aerospace Research, U.S. Air Force.

Coordinated by  
Wentworth Institute, Boston, Mass.

SMITHSONIAN INSTITUTION

*Washington, D.C.*

1963

## *Publications of the Astrophysical Observatory*

This series, *Smithsonian Contributions to Astrophysics*, was inaugurated in 1956 to provide a proper communication for the results of research conducted at the Astrophysical Observatory of the Smithsonian Institution. Its purpose is the "increase and diffusion of knowledge" in the field of astrophysics, with particular emphasis on problems of the sun, the earth, and the solar system. Its pages are open to a limited number of papers by other investigators with whom we have common interests.

Another series is *Annals of the Astrophysical Observatory*. It was started in 1900 by the Observatory's first director, Samuel P. Langley, and has been published about every 10 years since that date. These quarto volumes, some of which are still available, record the history of the Observatory's researches and activities.

Many technical papers and volumes emanating from the Astrophysical Observatory have appeared in the *Smithsonian Miscellaneous Collections*. Among these are *Smithsonian Physical Tables*, *Smithsonian Meteorological Tables*, and *World Weather Records*.

Additional information concerning these publications may be secured from the Editorial and Publications Division, Smithsonian Institution, Washington, D.C.

FRED L. WHIPPLE, *Director,*  
*Astrophysical Observatory,*  
*Smithsonian Institution.*

Cambridge, Mass.

# Contents

	<b>Page</b>
<b>Session 1</b>	
<i>Welcoming address:</i> Col. Ernest A. Pinson, USAF . . . . .	3
<i>Limitations of radar techniques for the study of meteors:</i> J. S. Greenhow . . . . .	5
<i>The initial radius of ionized meteor trails:</i> B. L. Kashcheyev and V. N. Lebedinets . . . . .	19
<i>The initial diameter of meteor trails:</i> G. S. Hawkins . . . . .	23
<i>The relation between visual magnitudes of meteors and the durations of radar echoes:</i> B. A. Lindblad . . . . .	27
<i>Radio-echo measurements of meteor mass distributions:</i> A. A. Weiss . . . . .	41
<i>A preliminary report on radar meteor counts:</i> P. M. Millman and B. A. McIntosh . . . . .	45
<i>The Harvard radio meteor project:</i> G. S. Hawkins . . . . .	53
<i>Meteor rates observed by radio-echo techniques during the IGY-IGC period:</i> B. L. Kashcheyev and K. V. Kostilyov . . . . .	63
<i>The orbits of meteor streams determined by radio-echo techniques:</i> B. L. Kashcheyev, V. N. Lebedinets, and M. F. Lagutin . . . . .	67
<b>Session 2</b>	
<i>The distribution of small interplanetary dust particles in the vicinity of Earth:</i> C. W. McCracken and W. M. Alexander . . . . .	71
<i>Micrometeorite measurements from Midas II (Satellite 1960 <math>\zeta</math> 1):</i> R. K. Soberman and L. Della Lucca . . . . .	85
<i>Micrometeorite collection from a recoverable sounding rocket. I:</i> R. K. Soberman, C. L. Hemenway, T. G. Ryan, S. A. Chrest, J. Frissora, and E. F. Fullam . . . . .	89
<i>Micrometeorite collection from a recoverable sounding rocket. II:</i> C. L. Hemenway, R. K. Soberman, E. F. Fullam, J. J. Balsamo, J. Cole, D. Hallgren, P. Yedinak, A. Goodman, and G. Hoff . . . . .	93
<i>Micrometeorite collection from a recoverable sounding rocket. III:</i> R. K. Soberman and C. L. Hemenway . . . . .	99
<i>Rocket and satellite studies of meteoric dust:</i> T. N. Nazarova . . . . .	105
<i>Cosmic dust showers by direct measurements:</i> M. Dubin, W. M. Alexander, and O. E. Berg . . . . .	109
<i>Discussion:</i> . . . . .	115
<b>Session 3</b>	
<i>A general survey of meteor spectra:</i> P. M. Millman . . . . .	119
<i>Meteor spectra with high dispersion:</i> Zd. Ceplecha and J. Rajchl . . . . .	129
<i>A short note on meteor spectra with low dispersion:</i> J. Rajchl . . . . .	155
<i>Spectrographic observations of meteors in U.S.S.R. in 1957-1960:</i> E. N. Kramer, K. A. Liubarsky, and V. I. Ivanikov . . . . .	157

	Page
<i>Diffusion effects observed in the wake spectrum of a Geminid meteor: I. Halliday . . . . .</i>	161
<i>On the frequency of occurrence of the auroral green line (5577A) in Perseid spectra: J. A. Russell . . . . .</i>	171
<b>Session 4</b>	
<i>Negative ions and luminosity in meteor trains: T. R. Kaiser . . . . .</i>	175
<i>Luminosity from large meteoric bodies: H. J. Allen and K. K. Yoshikawa . . . . .</i>	181
<i>Preliminary notes on some results of photographic multiple meteorite fall of Přebram: Zd. Ceplecha . . . . .</i>	195
<i>Results from an artificial iron meteoroid at 10 km/sec: R. E. McCrosky and R. K. Soberman . . . . .</i>	199
<i>Luminous efficiency of iron and stone asteroidal meteors: A. F. Cook, L. G. Jacchia, and R. E. McCrosky . . . . .</i>	209
<i>Meteor ionization and the mass of meteoroids: D. M. Lazarus and G. S. Hawkins . . . . .</i>	221
<i>Statistical verification of the physical theory of meteors: B. J. Levin and S. V. Majeva . . . . .</i>	229
<i>On the color index of meteors: J. Davis . . . . .</i>	233
<i>Image-orthicon photographs of meteors: J. Spalding, G. Colter, C. L. Hemenway, J. A. Cole, and J. F. Dugan . . . . .</i>	237
<i>Meteoritic erosion in space: F. L. Whipple . . . . .</i>	239
<i>The absence of magnetic micropulsations of meteor origin: C. Ellyett and G. B. Gillion . . . . .</i>	249
<b>Session 5</b>	
<i>The density distribution of telescopic meteors around the earth's orbit: L. Kresák and M. Kresáková . . . . .</i>	253
<i>Atmospheric trajectories of telescopic meteors: L. Kohoutek and J. Grygar . . . . .</i>	259
<i>Statistics of meteor streams: R. B. Southworth and G. S. Hawkins . . . . .</i>	261
<i>Orbital elements of photographic meteors: P. Babadjanov . . . . .</i>	287
<i>On the structure of the <math>\delta</math>-Aquadrid meteor stream: A. K. Terentjeva . . . . .</i>	293
<i>Masses of Comet Giacobini-Zinner and the Draconid meteor stream: Y. V. Yevdokimov . . . . .</i>	297
<i>Dynamical evolution of the Perseids and Orionids: R. B. Southworth . . . . .</i>	299
<i>A note on the cometary nature of the Tungus meteorites: V. Fessenkov . . . . .</i>	305
<i>A short note on the origin and age of the Quadrantids: S. E. Hamid and Mary N. Youssef . . . . .</i>	309
<hr/> <i>Abstracts of other papers . . . . .</i>	313

**PROCEEDINGS OF THE SYMPOSIUM  
ON THE  
ASTRONOMY AND PHYSICS OF METEORS**



## Welcoming Address

By Col. Ernest A. Pinson, USAF <sup>1</sup>

It is my great pleasure to extend a welcome to this distinguished assembly on behalf of the Geophysics Research Directorate of the Air Force Cambridge Research Laboratories. We are pleased to be associated with the Smithsonian Astrophysical Observatory in cosponsoring this symposium, and with the Wentworth Institute as coordinating agency. Our long-standing interests in astrophysics are emphasized this week in this symposium and in another international astrophysical symposium on the Solar Corona, which we are sponsoring at Cloudcroft, N. Mex., during this same week. The latter is Symposium No. 16 of the International Astronomical Union.

The U.S. Air Force is interested in studies that can be applied to the solution of specific problems of the space environment. However, we fully recognize that theoretical and experimental studies that appear, on the surface, only to increase knowledge of our universe invariably lead to useful applications and solutions of specific problems.

As most of you know, the last international meteor physics symposium was held at Jodrell Bank in 1954. A brief examination of the proceedings of that symposium reveals the tremendous growth in meteor measurement and observation techniques that has taken place during the past few years. This meeting is the first opportunity for people specializing in meteor physics to gather at an international symposium to discuss measurements made *above* the earth's atmosphere. The advent of rocket and satellite vehicles has opened tremen-

dous potentialities for research in this field. A good example of new opportunities for controlled experimentation is the recent artificial meteor experiment, which will be discussed in detail during the meeting.

Meteor physics experiments have now become global in nature, requiring ever greater cooperation among world scientists. It is encouraging to note that international cooperation in this field is flourishing; information is being exchanged on a personal basis and appears in the open literature as soon as it has been reduced and analyzed. Our fervent hope is that such cooperation will continue and even increase. In this regard, I am happy to offer the use of any space available on our research vehicles to worthy meteor experiments that may be forthcoming.

The extent and degree of international cooperation that may soon be required is illustrated by our consideration of the possibility of using a ground-based network of photographic and radio observations of natural meteoric phenomena for determining high-altitude winds and densities.

Briefly, the 1954 symposium spoke in terms of local, ground-based meteor studies, and of international cooperation. Soon, the meteor physicist will be unrestricted—within our solar system—as to mode and place of observation. International cooperation is therefore even more essential.

May I again extend the greetings of the Air Force Cambridge Research Laboratories and our best wishes for a fruitful and provocative exchange in this important area of research.

<sup>1</sup> Vice commander, Air Force Cambridge Research Laboratories.



# Limitations of Radar Techniques for the Study of Meteors

By J. S. Greenhow<sup>1</sup>

Radar techniques are widely used for the study of the physics and astronomy of meteors, and observations of echoes from the ionized trails have also been used as a tool for the study of the upper atmosphere. Various scattering theories have been developed that give the amplitudes and durations of the radar echoes in terms of the ionization densities in the trails, the ambipolar diffusion coefficient, and the parameters of the equipment.

Although it was realized that departures from the simple theories would occur at very high frequencies (Eshelman, 1956), it has been assumed hitherto that there are no serious limitations at frequencies of a few tens of Mc/sec. In view of recent work on the initial radii of the ionized trails (Greenhow and Hall, 1960a,b) and the loss of electrons by attachment processes (Davis, Greenhow, and Hall, 1959), it is now apparent that even at frequencies as low as 20 Mc/sec serious deviations from theory occur. The deviations are of sufficient magnitude to introduce very considerable uncertainties into much of the previous meteor work concerned with measurements of linear electron density and of mass and velocity distributions, and with investigations of upper atmospheric pressure and scale height.

The probable errors arising in each of the above measurements made with typical radars operating at frequencies of about 5 to 600 Mc/sec are the subject of this paper. Only the case of backscattering will be considered.

<sup>1</sup>Dr. Greenhow died in November 1962. At the time of this symposium he was associated with Royal Radar Establishment, Malvern, England.

## The scattering theories

*Linear electron densities less than  $10^{12}$  cm<sup>-1</sup>.*—When the linear electron density  $\alpha$  is less than approximately  $10^{12}$  cm<sup>-1</sup>, the scattering equation derived by Lovell and Clegg (1948) is appropriate, where the received power  $\epsilon_0$  at time  $t=0$  after the formation of the trail is given by

$$\epsilon_0 = \frac{PG^2\alpha^2\lambda^3}{32\pi^2R^3} \left(\frac{e^2}{mc^2}\right)^2 \text{ watts,} \quad (1)$$

where  $P$  is the peak transmitted power;  $G$  the aerial gain;  $\lambda$  the wavelength;  $R$  the range;  $e$  the electronic charge;  $m$  the electronic mass; and  $c$  the velocity of light.

The echo amplitude decays exponentially in the manner

$$A = A_0 \exp(-16\pi^2Dt/\lambda^2), \quad (2)$$

where  $A_0$  is the initial amplitude, and  $D$  the ambipolar diffusion coefficient (Herlofson, 1947).

*Linear electron densities greater than  $10^{12}$  cm<sup>-1</sup>.*—In the case of the "over-critically dense" trails with  $\alpha > 10^{12}$  cm<sup>-1</sup>, giving rise to long duration echoes, the scattering equations given by Greenhow (1952a) can be applied, where

$$\epsilon_m = \frac{PG^2\alpha^4\lambda^3}{108\pi^3R^3} \left(\frac{e^2}{mc^2}\right)^4, \quad (3)$$

with  $\epsilon_m$  the maximum received power.

The echo duration  $T_D$ , determined by the time for the effects of diffusion to reduce the electron density  $n_e$  on the axis of the trail below the critical density  $n_c$ , is

$$T_D = \frac{\alpha\lambda^2}{4\pi^2D} \left(\frac{e^2}{mc^2}\right). \quad (4)$$

*Departures from the scattering theories.*—A number of simplifications are made in the derivations of equations (1) to (4), and more rigorous solutions, taking account of polarization and plasma resonance effects, have been given by Kaiser and Closs (1952). The modifications to the echo amplitude are only of the order 2 for certain values of  $\alpha$ , and as we will be discussing departures from the simple scattering theories that are of several orders of magnitude, these refinements need not be considered. These very large departures from theory are due to the effects of finite velocity, the initial trail radius, and the loss of electrons by attachment.

First, it is assumed in the derivation of equations (1) and (3) that the meteor trail is formed instantaneously, and that the echo is obtained from a complete Fresnel zone of radius  $(R\lambda/2)^{1/2}$ . A sufficient condition for this in the case of  $\alpha < 10^{12}$  cm<sup>-1</sup> is that the meteor should reach the end of the first Fresnel zone before the ionized column at the beginning of the trail has diffused to a radius of  $\lambda/2\pi$ , or

$$V \frac{\lambda^2}{16\pi^2 D} \gtrsim (R\lambda/2)^{1/2}, \quad (5)$$

where  $V$  is the meteor velocity.

In the case of  $\alpha > 10^{12}$  cm<sup>-1</sup>, the condition is that the meteor should reach the end of the first Fresnel zone before the electron density on the axis of the trail at the beginning of the zone falls below  $n_c$ , or

$$V \frac{\alpha \lambda^2}{4\pi^2 D} \left( \frac{e^2}{mc^2} \right) \gtrsim (R\lambda/2)^{1/2}. \quad (6)$$

The effects of finite meteor velocity on the echo characteristics have been computed by a number of workers (Eshelman, 1956; Loewenthal, 1956; Hawkins, 1956). As the appropriate values for  $V$  and  $D$  for a given meteor are usually known approximately, the magnitude of the effect can be determined. Although the reduction in echo amplitude or duration may be large, there is no particular wavelength or height at which these reductions become catastrophic.

The second important assumption made in the derivation of the scattering equations is that the initial trail radius  $r_i$  is small compared

with  $\lambda/2\pi$ . When  $\alpha < 10^{12}$  cm<sup>-1</sup>, this condition implies that all the electrons in any cross section of the trail scatter in phase. When  $r_i$  is finite, the echo intensity given by equation (1) is reduced by a factor

$$\eta = \exp [2(2\pi r_i/\lambda)^2]. \quad (7)$$

When  $r_i = \lambda/2\pi$ , the reduction in intensity is only 9 db and the corresponding reduction in echo amplitude is a factor of 2.7, giving rise to a similar error in the determination of  $\alpha$ . This is equivalent to approximately one stellar magnitude in the corresponding visual scale, and can be regarded as the maximum acceptable uncertainty in  $\alpha$ . An increase in  $r_i$  or a decrease in  $\lambda$  by a factor of only 3, however, increases the attenuation to almost 80 db, introducing an error of  $10^4$  in  $\alpha$ . Thus, once the initial trail radius reaches the order of  $\lambda/2\pi$ , this effect quickly assumes overwhelming importance, and the echoes from such trails become virtually undetectable.

In the case of an "overdense" trail, equation (3) can be applied if the initial trail radius is sufficiently small so that the electron density is greater than  $n_c$  on the axis of the trail at zero time, or

$$r_i \lesssim \alpha^{1/2} \frac{\lambda}{\pi} \left( \frac{e^2}{mc^2} \right)^{1/2}. \quad (8)$$

The effect of increasing  $r_i$  above this value will ultimately cause the echo to appear as if it were from an underdense trail, with a much reduced amplitude and value of  $\alpha$ .

Third, while the echo decay times from underdense trails given by equation (2) are less than about 1 second for most practical values of  $\lambda$  and  $D$ , equation (4) readily permits echo durations of several hundred seconds for bright meteors. With times greater than a few seconds, the loss of electrons by attachment to neutral oxygen molecules is found to be more important than the effects of diffusion (Davis, Greenhow, and Hall, 1959), and it has been shown that the echo duration given by equation (4) may be in error by several orders of magnitude. Thus values of  $\alpha$  determined from the echo duration will be liable to these large errors. The choice of suitable radar parameters for observing these bright meteors will be considered in this paper.

### The height variation of trail radius, attachment function, and meteor velocity

Previously the tacit assumption had been made that most meteors ionize in a fairly narrow band of heights centered about 95 km, an assumption apparently supported by the radio observations. However, it was overlooked that this concentration in heights may be due primarily to the failure of radars to detect the ionized trails at heights much above 100 km. Recent work (Greenhow and Hall, 1960b) has now shown that even with equipment of moderate sensitivity, the majority of echoes above 100 km should be observable if the effect of initial trail radius is negligible. However, echoes above 100 km are not detected in large numbers because of the effects of the large trail radii.

As radar observations are widely used for studies of the astronomy and physics of meteors, it is of considerable interest to investigate the effects of the finite initial radius on the observations. In order to carry out this investigation, we must construct models for the variation of the height of maximum ionization with meteor velocity and linear electron density, and for the variation of trail radius and attachment time constant with height. This construction involves a considerable degree of extrapolation from the limited experimental evidence available, but the extrapolations must be carried out before the results of previous experiments can be assessed, and further experiments planned.

*The model for the variation of meteor heights with  $V$  and  $\alpha_{\max}$ .*—Measurements of the variation of height of occurrence with meteor velocity and the maximum linear electron density  $\alpha_{\max}$  have been reviewed by Greenhow and Hall (1960a). Between values of  $\alpha_{\max}$  from about  $10^{11}$  to  $10^{16}$   $\text{cm}^{-1}$ , and velocities of 15 to 70 km/sec, the height variation of the point of maximum ionization agrees approximately with that derived from the theoretical relation

$$\rho_{\max} \propto \alpha_{\max}^{1/3} V^{-3}, \quad (9)$$

where  $\rho_{\max}$  is the atmospheric density at the point of  $\alpha_{\max}$ .

The curve for  $\alpha_{\max} = 10^{12}$   $\text{cm}^{-1}$  in figure 1 has been determined from a balance between

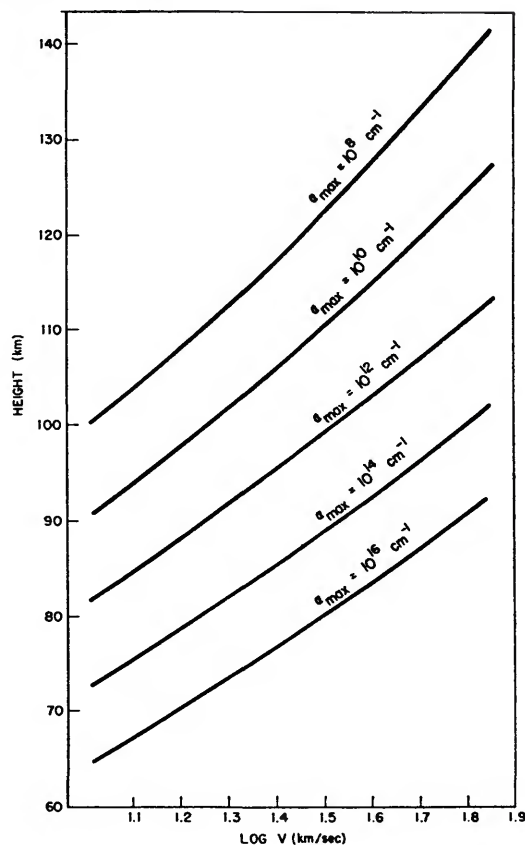


FIGURE 1.—The model adopted for the variation of the mean height of maximum ionization for meteors of various  $\alpha_{\max}$  and  $V$ .

the Super-Schmidt camera observations of faint visual meteors with  $\alpha_{\max} \sim 10^{13}$   $\text{cm}^{-1}$  (Hawkins and Southworth, 1958), and some low frequency radar observations of meteors with  $\alpha_{\max} \sim 5 \times 10^{11}$   $\text{cm}^{-1}$  (Greenhow and Hall, 1960b). This curve has been taken as a standard, and curves for other values of  $\alpha_{\max}$  have been obtained by extrapolation from equation (9). The curves in figure 1 give only the mean height of  $\alpha_{\max}$  for a given velocity, and in any velocity group there is a spread of observed heights about this mean value of about  $\pm H$ , where  $H$  is the atmospheric scale height.

Rocket Panel (1952) density gradients have been used in the extrapolations.

*The height variation of  $r_1$ .*—The only available measurements of the initial trail radius for meteors with  $\alpha_{\max} < 10^{13}$   $\text{cm}^{-1}$ , with which we

are primarily concerned, are due to Greenhow and Hall (1960b). These measurements were made on meteor trails with values of  $\alpha_{\max}$  between  $10^{11}$  and  $10^{12}$   $\text{cm}^{-1}$  at heights between 90 and 115 km; it has therefore been necessary to extrapolate to greater heights over a further 25 km in order to include all values of  $V$  and  $\alpha_{\max}$  given in figure 1. The extrapolation has been carried out with a reference value of  $r_i=140$  cm at a height of 98 km, adopting the experimentally determined relationship

$$r_i \propto \rho^{-0.35}. \quad (10)$$

This value of  $r_i$  at a height of 98 km is several times greater than Manning's (1958) theoretical estimate of 14 ionic mean free paths, although it agrees approximately with Öpik's (1955) value. Both theories, however, predict a more rapid height variation of the form  $r_i \propto \rho^{-1}$ . A variation of this type would have an even more catastrophic effect on the radar observations of meteors than that discussed in the following paragraphs.

*The attachment time constant.*—The parameter of importance for the effects of attachment is the attachment time constant  $T_\beta=1/\beta n_0$ , where  $\beta$  is the two-body attachment coefficient, and  $n_0$  the density of particles capable of forming negative ions. There is a possibility that three-body attachment is the relevant mechanism at meteor heights (Greenhow and Hall, 1961) when  $T_\gamma=1/\gamma n_0 n_a$ ;  $\gamma$  is the three-body attachment coefficient; and  $n_a$  is the density of particles effective in the collision processes.

Values of  $T_\beta$  or  $T_\gamma=50$  sec at a height of 95 km, based on the measurements of Davis et al. (1959) have been assumed, again using Rocket Panel density variations to extrapolate to other heights.

#### The effects of finite trail radius upon the radar observations of faint meteors

*The measurement of linear electron density.*—Equation (1) is generally used to determine the linear electron densities in meteor trails from a measurement of the echo amplitude and from a knowledge of the equipment parameters. However, any observations carried out in the region where  $r_i \gtrsim \lambda/2\pi$  are of doubtful value, as errors of several orders of magnitude in  $\alpha$  may

readily be introduced. Curves of the attenuation in the theoretical echo due to finite  $r_i$ , for meteors of velocity 15, 30, and 60 km/sec occurring at their most probable heights are therefore given in figure 2. The curves are drawn for reductions in intensity up to 80 db, for a selection of frequencies greater than 5 Mc/sec. That such high attenuations may occur we can deduce from some very high frequency observations (see p. 12); beyond this point we would expect that departures from an assumed radial gaussian distribution of electron density would eventually become significant in determinations of echo intensity.

The horizontal broken lines in figure 2 show where  $r_i=\lambda/2\pi$ , and the selection of a suitable operating point should be restricted to the region above this line. For a velocity of 60 km/sec, it can be seen that 20 Mc/sec is the highest frequency that can reasonably be used to observe meteors with  $\alpha_{\max}$  down to  $10^{12}$   $\text{cm}^{-1}$ . At 40 Mc/sec the echo amplitudes for trails with this value of  $\alpha_{\max}$  are already 100 times below the predicted values. The position becomes much worse for very faint meteors with  $\alpha_{\max}$  in the region from  $10^8$  to  $10^{10}$   $\text{cm}^{-1}$ , where even at 20 Mc/sec the echo amplitude is 1000 times below the expected value. In order to observe these meteors, we would need to use a frequency between 5 and 10 Mc/sec.

Decay-type echoes due to fast meteors with linear electron densities apparently of the order of  $10^{11}$  to  $10^{12}$   $\text{cm}^{-1}$  are observed at frequencies at least as high as 70 Mc/sec. However, these echoes are very probably due to overdense trails with  $\alpha$  of the order  $10^{13}$   $\text{cm}^{-1}$ , but with such large initial radii that the electron density on the axis of the trail is already below the critical density (Greenhow and Hall, 1960b, para. 5b).

The situation improves for meteors of smaller velocity that ionize lower in the atmosphere; for  $V=15$  km/sec, a frequency of 50 Mc/sec would be suitable for observing meteors with  $\alpha_{\max} \sim 10^{12}$   $\text{cm}^{-1}$ , and 20 Mc/sec for trails with  $\alpha_{\max} \sim 10^8$   $\text{cm}^{-1}$  (fig. 2a).

*Measurement of velocity distributions: the fraction of meteors observed.*—The effects of finite trail radius on echo amplitude will have a marked influence upon the observed distributions of meteor velocities, which will differ considerably from the true curves. It is difficult

to predict the exact way in which the velocity distributions will be modified, as this will depend upon the shape of the height distributions that are centered about the mean heights given in figure 1, and also upon the mass distributions. The following attempt has therefore been made to deduce the fraction of meteors in each velocity group that will be observed, for two limiting equipment sensitivities.

The number distribution of meteor trails as a function of  $\alpha$  is generally assumed to be of the form

$$N(\alpha)d\alpha \propto \alpha^{-s}d\alpha. \quad (11)$$

Although the value of  $s$  for faint meteors is not known accurately (p. 11), it is likely to be of the order 2, and in this case equations

(11) and (1) predict that the number of echoes of given amplitude observed with any equipment is inversely proportional to the amplitude. Accepting this proportionality, and assuming no spread in heights for meteors in a given velocity group, we find that the fraction of the true numbers of meteors in each velocity group that are actually observed will be of the order  $\eta^{\frac{1}{2}}$ .

The variation of this fraction, expressed as a percentage of the true numbers, is given in figure 3 for various frequencies and values of  $\alpha_{\min}$ . ( $\alpha_{\min}$  is the minimum value of  $\alpha$  that can be detected with a given equipment, assuming equation (1) to be valid.) It can be seen that when  $\alpha_{\min} \sim 10^{11} \text{ cm}^{-1}$ , about 85 percent of the slowest meteors are seen at

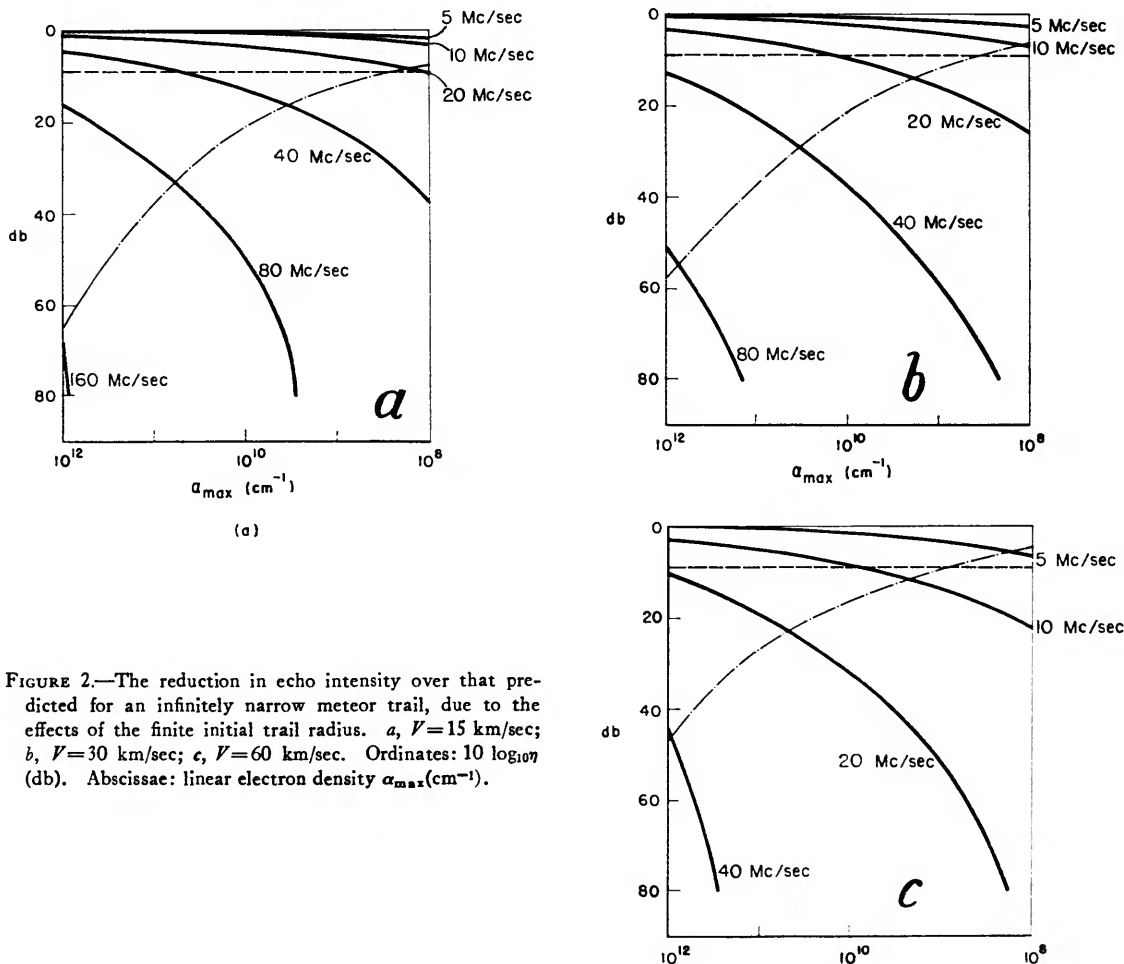


FIGURE 2.—The reduction in echo intensity over that predicted for an infinitely narrow meteor trail, due to the effects of the finite initial trail radius. *a*,  $V=15 \text{ km/sec}$ ; *b*,  $V=30 \text{ km/sec}$ ; *c*,  $V=60 \text{ km/sec}$ . Ordinates:  $10 \log_{10} \eta$  (db). Abscissae: linear electron density  $\alpha_{\max}(\text{cm}^{-1})$ .

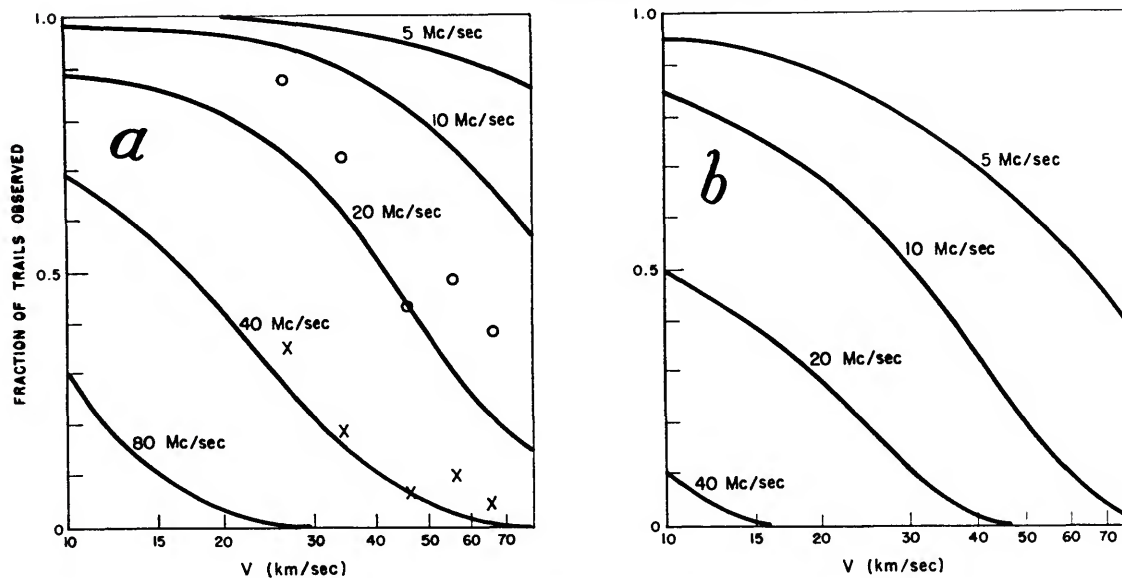


FIGURE 3.—The fraction of the true number of meteor trails with  $\alpha > \alpha_{\min}$  which give detectable echoes, as a function of meteor velocity and frequency. *a*, For a theoretical limiting sensitivity of  $\alpha_{\min} \sim 10^{11} \text{ cm}^{-1}$ . Experimental points:  $\times$ , 36 Mc/sec;  $\circ$ , 17 Mc/sec. *b*, For a theoretical limiting sensitivity of  $\alpha_{\min} \sim 10^8 \text{ cm}^{-1}$ .

$f=20 \text{ Mc/sec}$ , but only 15 percent of those with velocities of 70 km/sec. These percentages improve at lower frequencies, but decrease

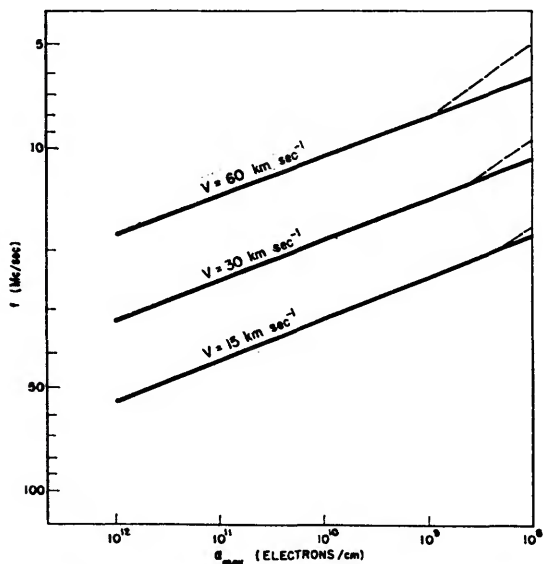


FIGURE 4.—Curves giving the maximum usable frequency  $f$  for the reliable observation of meteors of velocities 15, 30, and 60 km/sec, as a function of  $\alpha_{\max}$ .

very rapidly as the frequency increases. Thus at 80 Mc/sec the echo rate for velocities of 15 km/sec would be 10 percent of the true rate, falling effectively to zero (<1 percent) for velocities greater than 30 km/sec.

The form of these curves has been verified at frequencies of 17 and 36 Mc/sec (Greenhow and Hall, 1960b); the experimental points are shown in figure 3a. There is reasonable agreement with the theoretical curves. Figure 3b is an extrapolation to a lower limiting linear electron density of approximately  $10^8 \text{ cm}^{-1}$ , when it can be seen that a frequency of only 5 Mc/sec would be required to give a reasonably accurate velocity distribution.

These results are summarized in figure 4, where the maximum usable frequency is shown as a function of  $\alpha$  and  $V$ . The criterion  $r_1 \leq \lambda 2\pi$  has been taken as the limiting condition under which acceptable observations can be made.

*Measurement of velocity distributions: The effect of finite meteor velocity.*—An effect not previously taken into account in deriving the echo attenuation curves is that of finite meteor velocity, since this factor, although it may be

large, will generally be negligible in comparison with the effects of trail radius. However, finite velocity limitations will mean that even if large reductions in echo amplitude due to the finite initial radii could be tolerated, the echoes might not show the diffraction effects that enable us to determine meteor velocities.

Curves given by Loewenthal (1956) show that the zone formation is effectively smoothed out when the expression  $c$ , given by

$$c = \frac{8\pi D}{V\lambda^2} (R\lambda/2)^{\frac{1}{2}}, \quad (12)$$

is less than about 0.5, at which point the reduction in echo amplitude is about 2.7 greater than that given by equation (1). With this criterion, the areas under the broken curves in figure 2 define the regions in which meteor velocities would become indeterminate. This condition is also indicated by the broken lines in figure 4.

*Meteor mass distributions.*—Determinations of the  $s$  in equation (11) have been made by measuring the distribution of meteor echo amplitudes, on the assumption that the scattering equation (1) is valid. This exponent is of considerable interest as it can be related to the

meteor mass and magnitude distributions; it would appear that sensitive radars could be used to extend the measurements of the mass distribution from the faintest photographic meteors (about +3 absolute magnitude,  $\alpha_{\max} \sim 6 \times 10^{12} \text{ cm}^{-1}$ ) to about +15 magnitude ( $\alpha_{\max} \sim 10^8 \text{ cm}^{-1}$ ). This method has been used by a number of workers, and values of  $s$  lying within the range  $s=2 \pm 0.2$  are usually found, irrespective of radar wavelength or equipment sensitivity. In view of the effects of finite initial trail radius, we must therefore consider the significance of these measurements.

As an example of the results obtained if this method is used, the differential number-amplitude distributions for two entirely different radars working at the very low frequency of 32 Mc/sec (Greenhow and Watkins, unpublished) and the very high frequency of 500 Mc/sec (Barber, Sutcliffe, and Watkins, 1962) are illustrated in figure 5. The limiting sensitivities of the two equipments, obtained by substituting the equipment parameters in equation 1, were  $\alpha_{\min} \sim 2 \times 10^{10}$  and  $10^8 \text{ cm}^{-1}$  respectively. The slopes of the best straight lines in figures 5a and 5b correspond to values of  $s=1.85$  at 32 Mc/sec, and  $s=2.0$  at 500

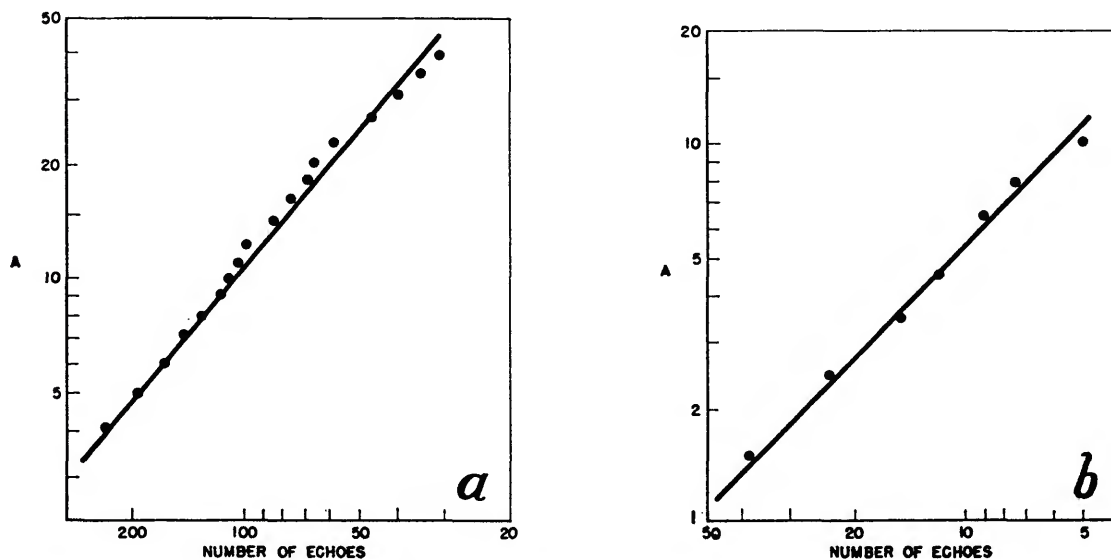


FIGURE 5.—Number/amplitude distributions for echoes observed at frequencies of 32 Mc/sec and 500 Mc/sec. Ordinates: Echo amplitude  $A$  (arbitrary units  $\sim$  receiver noise). Abscissae: Number of echoes with amplitudes  $\geq A$ . *a*,  $f=32$  Mc/sec; limiting theoretical sensitivity  $\alpha_{\min} \sim 2 \times 10^{10} \text{ cm}^{-1}$ . *b*,  $f=500$  Mc/sec; limiting theoretical sensitivity  $\alpha_{\max} \sim 10^8 \text{ cm}^{-1}$ .

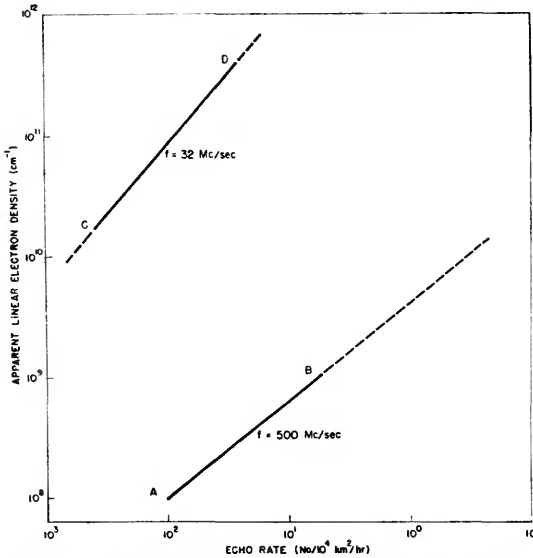


FIGURE 6.—Number/apparent linear electron density distributions. Ordinates: Apparent linear electron density. Abscissae: Echo rate from trails with apparent linear electron densities  $\geq \alpha$ . An approximate absolute scale is given, where "No" is the number of echoes observed per  $10^4 \text{ km}^2$  in the plane 100 km above the earth per hour.

Mc/sec in reasonable agreement with previous measurements for sporadic meteors.

However, when the absolute echo rates on the two equipments are compared, an anomalous situation arises. A value  $s=2$  implies that if similar areas of sky are illuminated by the aerial beams, then the echo rate with an equipment of  $\alpha_{\min} \sim 10^8 \text{ cm}^{-1}$  should be 200 times the rate when  $\alpha_{\min}$  is only  $2 \times 10^{10} \text{ cm}^{-1}$ . In fact, when corrections are made for the different polar diagrams, the observed echo rate on the 500 Mc/sec equipment is found to be only about 0.2 times the 32 Mc/sec rate (fig. 6), a deviation by a factor  $10^3$  from the expected rate at the apparent value of  $s$ . Thus it is clear that the curve AB in figure 6 cannot represent the true distribution of values of  $\alpha$  in the region  $10^8 < \alpha < 10^9$  as the lines AB and CD should be colinear. This is not surprising in view of the expected effects of trail radius. Similarly, the 32 Mc/sec curve CD will not represent the true distribution, as the majority of meteor trails in the appropriate electron density range are not detected. The measured values of  $s$ , using radars at frequencies greater than 5 to 20 Mc/sec, cannot therefore be interpreted as

giving a measurement of the meteor mass or electron density distributions. Instead, equation (11) with  $s \sim 2$  must be regarded only as an empirical relationship that shows that for a given radar, more small echoes will be detected than large ones.

*Echo rate as a function of wavelength.*—For equipments with the same theoretical limiting sensitivity, the echo rate will decrease rapidly because of the differential effects of a finite trail radius. The observed echo rate for meteor trails with  $\alpha$  apparently greater than  $10^{11} \text{ cm}^{-1}$ , where  $\alpha$  is determined from the echo amplitude and equation (1), is shown as a function of radio frequency in figure 7. The points for 17, 36, and 69 Mc/sec are from Greenhow and Hall (1960b), while the points for 300 and 500 Mc/sec are derived from the observations of Barber, Sutcliffe, and Watkins (1962). It can be seen that the observed echo rate falls from 0.4 of the true rate of  $f=17$  Mc/sec, to only 0.01 at 100 Mc/sec, and to 0.00001, at  $f=500$  Mc/sec. This is an extremely rapid variation, giving an approximate  $f^{-3}$  dependence of echo rate between frequencies of 30 and 500 Mc/sec.

At frequencies significantly greater than 100 Mc/sec, it is unlikely that the echoes detected are from underdense meteor trails with  $\alpha < 10^{12} \text{ cm}^{-1}$ . The few echoes that are observed are more likely to be due to overdense trails whose amplitudes have been drastically reduced. In the case of the 500 Mc/sec observations with  $\alpha_{\min} \sim 10^8 \text{ cm}^{-1}$ , for example, the echo rate is only about  $10^{-5}$  of the true value. Thus it is probable that the echoes actually

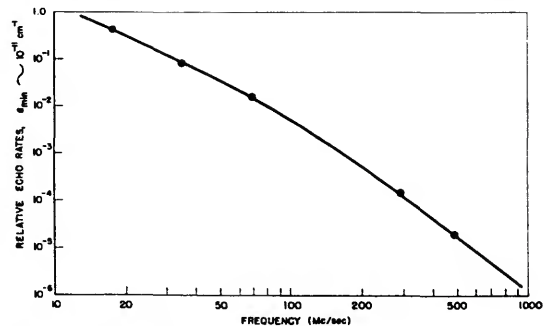


FIGURE 7.—Observed echo rate as a function of frequency, for equipments that have the same theoretical sensitivity based on equation (1). The observed rate for  $\alpha \geq 10^{11} \text{ cm}^{-1}$  is shown as a fraction of the estimated true rate.

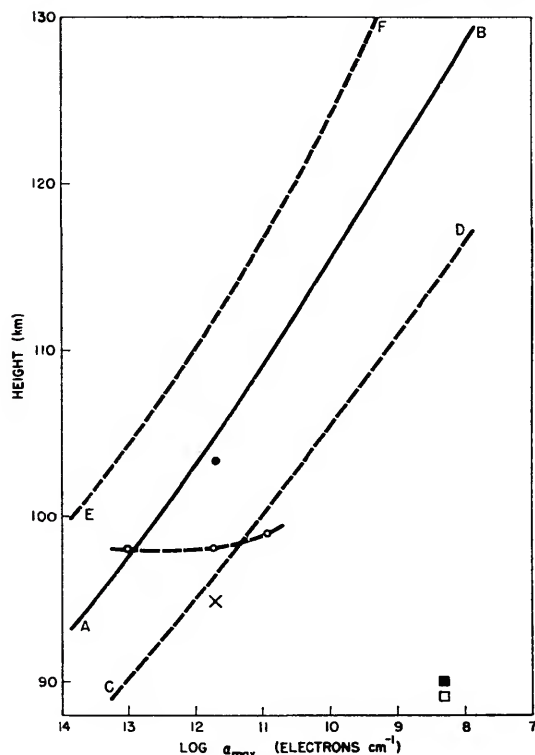


FIGURE 8.—The predicted mean heights (*AB*) and R.M.S. height spreads (*CD, EF*) for meteors with  $V=40$  km/sec as a function of linear electron density. Experimental points:  $\circ$ , 36 Mc/sec;  $\times$ , 69 Mc/sec;  $\bullet$ , 17 Mc/sec (Greenhow and Hall, 1960b, and unpublished observations);  $\square$ , 300 Mc/sec;  $\blacksquare$ , 500 Mc/sec (Barber, Sutcliffe, and Watkins, 1962).

recorded are from trails with  $\alpha \gtrsim 10^{13}$   $\text{cm}^{-1}$ , which are about  $10^5$  times less numerous than those with  $\alpha \sim 10^8$   $\text{cm}^{-1}$ , and whose intensities have been reduced by about 80 db below the predicted values. Further evidence for this supposition is given by the echo heights, discussed in the following section.

*The height distributions of echoes.*—In addition to affecting the number counts and velocity distributions, the trail radius effects will cause the observed height distributions to differ markedly from the true curves for meteors of given  $V$  and  $\alpha_{\max}$ . As an example, the expected variations of mean height and R.M.S. height spread, for meteors of velocity 40 km/sec, are given in figure 8. Some measured values of the mean heights for various apparent values of  $\alpha$ , and at a number of widely spaced frequencies are also shown. Thus at 36 Mc/sec a decrease in  $\alpha$  from  $10^{13}$  to  $10^{11}$   $\text{cm}^{-1}$

produces little change in the mean height of the echoes, although it should have increased by about 12 km. On the other hand, an increase in mean height for a given apparent value of  $\alpha$  is observed as the frequency decreases. Thus the mean height of the observed echoes is seen to rise from 95 to 103 km as the frequency decreases from 69 to 17 Mc/sec. This result supports the view that faint radio meteors ionize at the predicted heights, but that at high frequencies the radar echoes are not detected because of the departures from the simple scattering theory.

The 300 and 500 Mc/sec observations of Barber, Sutcliffe, and Watkins (1962) are extreme examples of the suppression of echoes from faint meteors at their most probable heights of occurrence. The observed mean heights are 89 at 300 Mc/sec and 90 km at 500 Mc/sec, 35 km below the expected heights for meteors with  $\alpha \sim 10^8$   $\text{cm}^{-1}$ . It is therefore apparent that the echoes that do occur at these frequencies must be from trails with  $\alpha \gtrsim 10^{13}$   $\text{cm}^{-1}$ , which ionize near an altitude of 90 km. This would also be consistent with the low echo rates that are observed.

#### The radar observations of bright meteors ( $\alpha_{\max} > 10^{12}$ $\text{cm}^{-1}$ )

*Effect of attachment.*—Three important errors arise in the use of equations (3) and (4) for the study of meteor trails of high linear electron densities: (i) the loss of electrons by attachment processes becomes important, so that diffusion is not the major factor in determining echo duration; (ii) the large initial trail radii may cause the initial volume electron densities to be less than the critical value; and (iii) distortion of an initially linear trail by irregular winds may cause multiple reflections from widely spaced centers. The effects of winds on the trails have been studied in detail elsewhere (for example, Greenhow, 1952 a,b; Greenhow and Neufeld, 1959; Manning, 1959) and will not be considered further in the present paper.

From the method discussed by Davis, Greenhow, and Hall (1959) to allow for the effects of attachment, the echo duration from the point of maximum ionization is shown as a function of frequency and  $\alpha_{\max}$ , for several meteor velocities, in figure 9. Figures 9a-c

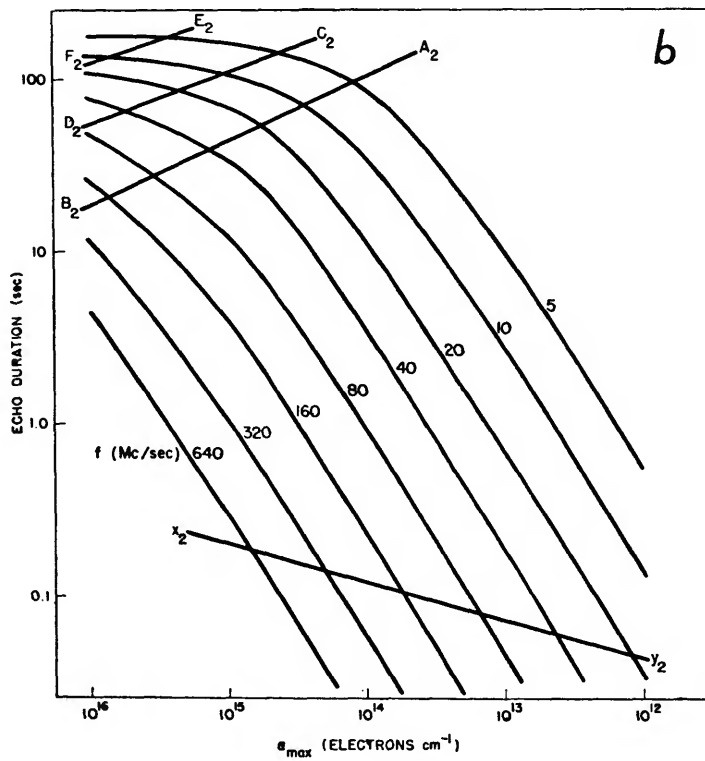
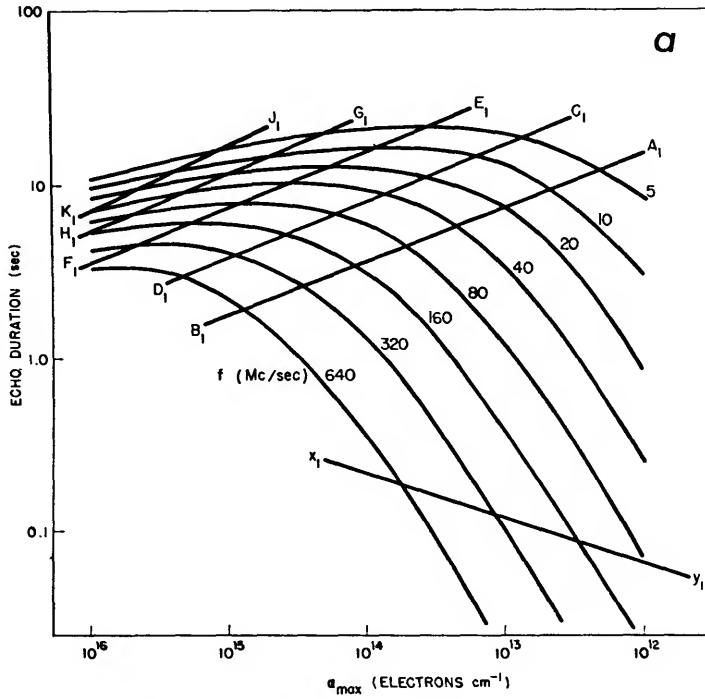
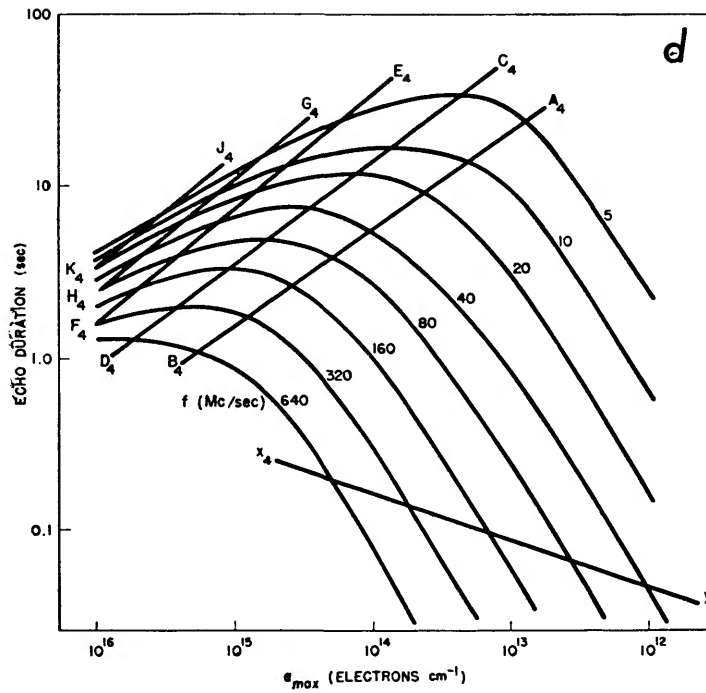
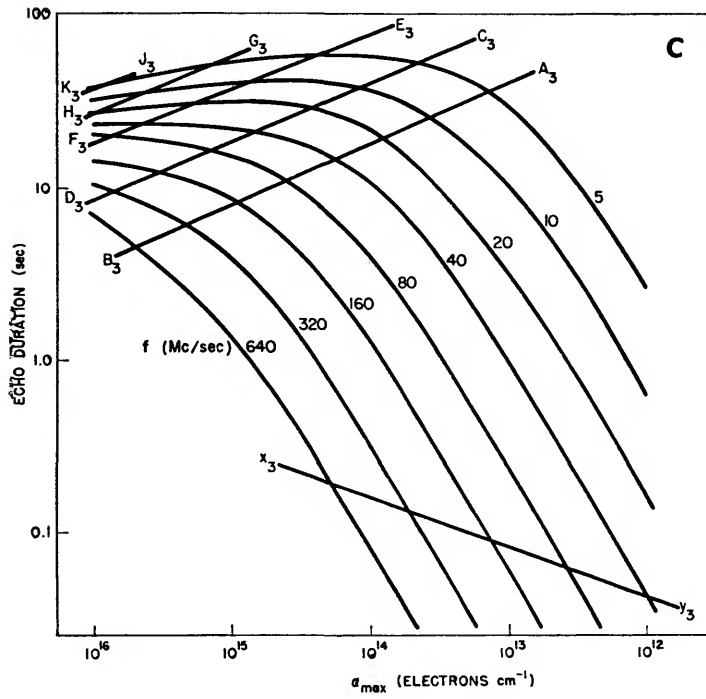


FIGURE 9.—Echo durations from the points of maximum ionization as a function of frequency and  $\alpha_{max}$  allowing for the effects of attachment.  $a-c$  are for a two-body attachment process with  $V=15, 30,$  and  $60$  km/sec respectively;  $d$  is for a three-body attachment process with  $V=30$  km/sec.  $AB, CD, EF, GH, JK$  show where the echo durations are reduced to  $\epsilon^{-1}, 10^{-1}, 10^{-2}, 10^{-3},$  and  $10^{-4}$  of the values expected considering diffusion alone;  $xy$  shows where the effects of the finite initial trail radius become important.



are for a two-body attachment process, and figure 9d is for a three-body reaction.

Let us consider figure 9c for  $V=30$  km/sec as typical of meteors of average velocity. The series of lines  $A_3 B_3, C_3 D_3$ , etc., shows the points where attachment reduces the echo duration to  $e^{-1}, 0.1, 0.01$ , etc., of the value expected considering the effects of diffusion alone. Below  $A_3 B_3$ , equation (4) can therefore be regarded as applicable for all points along a given trail when echo duration is proportional to  $\alpha\lambda^2D^{-1}$ . Above  $A_2 B_3$ , the echo duration increases very slowly with increasing  $\alpha$ , and indeed in some cases the echo duration for a very bright meteor can be less than that from a fainter trail ionizing at a greater height. Thus at a frequency of 20 Mc/sec, for example, a trail with  $\alpha_{\max}\sim 10^{14}$  cm $^{-1}$  gives an echo duration of about 25 seconds from the point of maximum ionization. Increasing  $\alpha_{\max}$  to  $10^{16}$  cm $^{-1}$  increases the echo duration to only 30 seconds, instead of to the  $3\times 10^4$  seconds expected from diffusion theory. For such trails, of course, the longest enduring echoes would normally be obtained from some height above the region of maximum ionization, and curves showing the magnitude of this effect have been given by Davis et al. (1959).

For comparison, the effects of a three-body attachment process for a meteor velocity of 30 km/sec are shown in figure 9d. The echo durations are still further reduced, causing the line  $A_4 B_4$  to move to lower values of duration for a given  $\alpha_{\max}$ .

It is clear that the influence of attachment on echo duration can be so large as to render the duration of little value for the determination of  $\alpha$ . In order to measure the electron densities in the trails of bright meteors, we would need to observe in the region below lines such as  $A B$ , where the normal diffusion equation can be applied. Thus no single wavelength can be used to observe the full range of possible values of  $\alpha$ . Precise measurements of height might be of assistance, but even so the correction factors can be so large, and the precise nature of the attachment effects so uncertain, that it is doubtful if any significant improvement would be gained.

*Effect of finite initial trail radius.*—The value of linear electron density at which the initial

trail radius is such as to cause the initial axial electron density to be less than the critical value for trails with  $\alpha_{\max}>10^{12}$  cm $^{-1}$  are shown by the curves  $x_1 y_1, x_2 y_2$ , etc., in figure 9. Thus, for  $V=30$  km/sec it can be seen that at frequencies above 40 Mc/sec the echoes from overcritically dense trails will begin to assume the characteristics of decay-type echoes. However, as the initial radii of the ionized columns will necessarily be  $>\lambda/2\pi$ , the echo intensities will be very much reduced. At frequencies of 300 to 600 Mc/sec for example, trails with linear electron densities as high as  $10^{14}$  cm $^{-1}$  may be undercritically dense initially. As the trail radii are of the order of 1 meter ( $\sim 10\lambda/2\pi$ ), the reduction in echo intensity given by equation (7) is enormous ( $\sim 800$  db). In this case, it is probable that the echo intensity will be determined by some second-order reflection mechanism, such as partial reflection from the sharp boundary in ionization near the meteor itself. Such echoes would have the same general amplitude-time characteristics as those from low electron density trails under conditions of extremely rapid diffusion (Eshelman, 1956). The two classes of echoes will therefore become indistinguishable.

Thus, in order to make satisfactory observations of overcritically dense meteor trails, we would need to select an observing frequency such that the operating point lies within the region defined by areas similar to  $ABxy$  in figure 9. Simultaneous measurements of two wavelengths would also be of great value in determining whether factors other than diffusion were affecting the observations.

## References

- BARBER, D.; SUTCLIFFE, H. K.; AND WATKINS, C. D.  
1962. Some observations of meteors and aurorae at 300 and 500 Mc/s using a large radio telescope. *Journ. Atmosph. Terr. Phys.*, vol. 24, pp. 585-597.
- DAVIS, J.; GREENHOW, J. S.; AND HALL, J. E.  
1959. The effect of attachment on radio echo observations of meteors. *Proc. Roy. Soc. London, ser. A*, vol. 253, pp. 130-139
- ESHELMAN, V. R.  
1956. Short wave length radio reflections from meteoric ionization. I. Theory for low density trails. Stanford Univ. Contract AF 19(604)-1031, Rep. No. 5.

- GREENHOW, J. S.  
 1952a. Characteristics of radio echoes from meteor trails. III. The behaviour of the electron trails after formation. Proc. Phys. Soc. London, vol. 65B, pp. 169-181.  
 1952b. A radio echo method for the investigation of atmospheric winds at altitudes of 80 to 100 km. Journ. Atmosph. Terr. Phys., vol. 2, pp. 282-291.
- GREENHOW, J. S., AND HALL, J. E.  
 1960a. The variation of meteor heights with velocity and magnitude. Monthly Notices Roy. Astron. Soc., vol. 121, pp. 174-182.  
 1960b. The importance of initial trail radius on the apparent height and number distributions of meteor echoes. Monthly Notices Roy. Astron. Soc., vol. 121, pp. 183-196.  
 1961. Attachment processes in meteor trails. Journ. Atmosph. Terr. Phys., vol. 21, pp. 261-271.
- GREENHOW, J. S., AND NEUFELD, E. L.  
 1959. Turbulence at altitudes of 80-100 km and its effects on long-duration meteor echoes. Journ. Atmosph. Terr. Phys., vol. 16, pp. 384-392.
- HAWKINS, G. S.  
 1956. Radar echoes from meteor trails under conditions of severe diffusion. Proc. Inst. Radio Eng., vol. 44, p. 1192.
- HAWKINS, G. S., AND SOUTHWORTH, R. B.  
 1958. The statistics of meteors in the earth's atmosphere. Smithsonian Contr. Astrophys., vol. 2, no. 11, pp. 349-364.
- HERLOFSON, N.  
 1948. The theory of meteor ionization. Phys. Soc., Rep. Progr. Phys., vol. 11, pp. 444-454.
- KAISER, T. R., AND CLOSS, R. L.  
 1952. Theory of radio reflections from meteor trails. I. Phil. Mag., ser. 7, vol. 43, pp. 1-32.
- LOEWENTHAL, M.  
 1956. Meteor echoes from underdense trails at very high frequencies. TR Technical Report 132, Lincoln Laboratory, Massachusetts Inst. Techn.
- LOVELL, A. C. B., AND CLEGG, J. A.  
 1948. Characteristics of radio echoes from meteor trails. I. The intensity of the radio reflections and electron density in the trails. Proc. Phys. Soc. London, vol. 60, pp. 491-498.
- MANNING, L. A.  
 1958. The initial radius of meteoric ionization trails. Journ. Geophys. Res., vol. 63, pp. 181-196.  
 1959. Air motions and the fading, diversity, and aspect sensitivity of meteoric echoes. Journ. Geophys. Res., vol. 64, pp. 1415-1425.
- ÖPIK, E. J.  
 1955. Meteors and the upper atmosphere. Irish Astron. Journ., vol. 3, pp. 165-181.
- ROCKET PANEL  
 1952. Pressures, densities, and temperatures in the upper atmosphere. Phys. Rev., vol. 88, pp. 1027-1032.

### Abstract

A brief review of the basic theories concerning the scattering of radio waves from the ionized trails produced by meteors is given. Some of the fundamental assumptions used in the derivation of the various scattering equations are discussed, and are shown to be incorrect.

Although it has been realized that the simple picture of an initially narrow trail would break down at very high frequencies, it is now apparent that the initial radius can be an appreciable fraction of a wavelength even at frequencies as low as 20 Mc/sec. This effect has a profound influence on the observation of meteors fainter than about +4 absolute visual magnitude.

The second major cause of the breakdown of the scattering theories is the loss of electrons by attachment processes, in addition to ambipolar diffusion. This effect can be serious in the case of long duration echoes, associated with meteors brighter than about +2 magnitude, and the predicted echo durations may be reduced by several orders of magnitude.

It is shown that much of the previous work on the determination of linear electron densities in meteor trails, and the measurements of meteor mass distributions, velocity distributions, and upper atmospheric pressures and scale heights, is in error. The interpretation of future radar observations of meteors must be treated with considerable caution.



# The Initial Radius of Ionized Meteor Trails

By B. L. Kashcheyev <sup>1</sup> and V. N. Lebedinets <sup>1</sup>

Atoms evaporating from the surface of a meteoroid possess energies as high as hundreds of electron-volts. The resulting meteor trail rapidly diffuses outward until the atoms lose their cosmic energy. From the diffusion equation, the trail radius  $r$  for a time  $t$  after the meteor has traversed a given point is:

$$r = (4Dt)^{1/2} = \left(\frac{4}{3} N\lambda^2\right)^{1/2},$$

where  $D$  is the coefficient of diffusion,  $N$  is number of collisions, and  $\lambda$  is the mean free path. As  $\lambda$  depends upon the velocity of the meteor, in the above formula  $\sum_{k=0}^N \lambda_k^2$  should be substituted for  $N\lambda^2$ , where  $\lambda_k$  is the mean free path after the  $k$ th collision. Then

$$r = \left(\frac{4}{3} \sum_{k=0}^N \lambda_k^2\right)^{1/2}. \quad (1)$$

From their quantum-mechanical computations, Massey and Sida (1955) found four values for the cross section of diffusion  $Q_d$  for collisions of atoms of Ca and Ne possessing various values of energy  $E$ . They proposed an approximation of  $Q_d(E)$ , which is, however, too complex for mathematical computations. A better form of approximation is:

$$Q_d = \frac{C_1}{\sqrt{E + C_2}}, \quad (2)$$

which does not differ greatly from that proposed by Massey and Sida for high values of energies, and gives the right value of  $Q_d$  under normal temperatures.

Experimental evidence (Massey and Burhop, 1952) indicates that for collisions between

ions and atoms of neon and argon, respectively, in the range of meteoric velocities the following relationship holds true:

$$Q_d^i \approx 4.5 Q_d. \quad (3)$$

According to Loeb (1934), for normal temperatures the relationship is about the same. Hence in  $Q_d^i(E)$  diffusion cross section depends upon the value of energy in about the same manner as it does in the case of neutral particles.

From equation (2) the mean free path of ions can be expressed in the form:

$$\lambda_i = F(V + C)\lambda_a, \quad (4)$$

where  $\lambda_a$  is the mean free path of atmospheric molecules, and  $V$  is the velocity of the particles colliding. For the case when the masses of ions and of atmospheric molecules are equal,  $F = 1.4 \times 10^{-6}$  sec/cm, and  $C = 1.8 \times 10^5$  cm/sec. Under the above condition, after one collision an ion retains on the average two-thirds of its initial velocity. The velocity of an ion after  $N$  collisions is given by the formula

$$V_N = V_0 e^{-\alpha N}, \quad (5)$$

where  $\alpha = 0.4$ .

From equations (1), (4), and (5), we obtain

$$r = F \left[ \frac{2V_0^2}{3\alpha} (1 - e^{-2\alpha N}) + \frac{8CV_0}{3\alpha} (1 - e^{-\alpha N}) \right]^{1/2} \lambda_a. \quad (6)$$

The number of collisions before a thermal equilibrium is reached is

$$N_0 = \frac{1}{\alpha} \ln \frac{V_0}{V_a},$$

where  $V_a$  is the mean velocity of atmospheric molecules.

<sup>1</sup> Kharkov Polytechnical Institute, U.S.S.R.

The initial radius of a meteoric ionized trail is

$$r_0 = r(N) = FV_0 \left[ \frac{2}{3\alpha} \left( 1 + \frac{4C}{V_0} \right) \right]^{1/2} \lambda_a. \quad (7)$$

Values of  $r_0/\lambda_a$  for meteors of various velocities are given in table 1. On the average, the initial radius is found to be about 1.5 times greater than the first mean free path of the ions.

The time elapsed between two successive  $N$  and  $N+1$  collisions is given by the expression:

$$\Delta t_N = F \left( 1 + \frac{C}{V_0} e^{\alpha N} \right) \lambda_a.$$

The time taken for  $N$  collisions is

$$t(N) = F \left[ N + \frac{C}{\alpha V_0} (e^{\alpha N} - 1) \right]. \quad (8)$$

The time of initial expansion is given by the equation:

$$t_0 = t(N_0) = F \left( \frac{1}{\alpha} \ln \frac{V_0}{V_a} + \frac{V}{\alpha V_0} \right) \lambda_a \approx 3.3 \times 10^{-5} \lambda_a, \quad (9)$$

where  $\lambda_a$  is in centimeters and  $t_0$  is in seconds. The initial radius is practically reached after fewer than  $N_0$  collisions and  $t_0 \sim 5 \times 10^{-6} \lambda_a$ .

The initial radius of an ionized meteoric trail can be determined by simultaneous radio-echo observations at two different wavelengths. As shown by Dudnik, Kashcheyev, and Lebedinets (1961), the ratio of the maximum amplitudes of echoes reflected from an under-dense meteor trail at wavelengths  $\lambda_1$  and  $\lambda_2$  is:

$$\frac{A_1}{A_2} = \left[ \frac{P_{t_1} G_{t_1} G_{r_1} \lambda_1^3}{P_{t_2} G_{t_2} G_{r_2} \lambda_2^3} \right]^{1/2} \frac{\rho(\Delta_1)}{\rho(\Delta_2)} \exp \left[ 4\pi^2 r_0^2 \left( \frac{1}{\lambda_2^2} - \frac{1}{\lambda_1^2} \right) \right], \quad (10)$$

TABLE 1.—Values of  $r_0/\lambda_a$  for meteors of various velocities

Velocity $V_0$ (km/sec)	10	20	30	40	50	60	70
$r_0/\lambda_a$	2.4	4.2	6.0	7.8	9.7	11.5	13.3

$$\rho(\Delta) = \frac{1 - \exp(-\sqrt{2}\Delta)}{\sqrt{2}\Delta},$$

$$\Delta = \frac{8\pi^2 D \sqrt{R}}{V \lambda^{3/2}}.$$

All other notations are conventional.

From equation (10) we obtain the equation:

$$r_0^2 = \frac{\ln A_1 - \ln A_2 + \frac{1}{2} \ln \frac{P_{t_2}}{P_{t_1}} - \frac{1}{2} \ln \frac{G_{t_1} G_{r_1}}{G_{t_2} G_{r_2}} - \frac{3}{2} \ln \frac{\lambda_1}{\lambda_2} - \ln \frac{\rho(\Delta_1)}{\rho(\Delta_2)}}{4\pi^2 \left( \frac{1}{\lambda_2^2} - \frac{1}{\lambda_1^2} \right)}$$

During the measurements made at the wharkov Polytechnical Institute in 1960, the Kavelengths used were  $\lambda_1 = 8$  meters and  $\lambda_2 = 4$  meters. Identical 5-element director antennas were employed. In order to equalize the effective sensitivities of the equipments, the output power of the transmitter at  $\lambda_2 = 4$  meters was twice as great as its counterpart at  $\lambda_1 = 8$  meters, and the sensitivity of the receiver was also somewhat higher. During the observations the powers and the frequencies of the respective transmitters were continually recorded. Calibration markers enabled the amplitudes to be expressed in terms of microvolts. The identity of the patterns of the two antenna systems was checked experimentally.

Analysis of the errors made in measuring the various quantities in equation (10) showed that the relative errors in the determination of  $r_0$  are as follows:

$$\delta r_0 = \frac{0.06}{r_0^2} \text{ when } r_0 \lesssim 0.6 \text{ m,} \quad (11)$$

$$\delta r_0 = \frac{0.11}{r_0^2} \text{ when } r_0 > 0.6 \text{ m,}$$

where  $r_0$  is in meters.

The errors of measurement increase with greater values of  $r_0$ , since amplitudes of echoes at  $\lambda_2 = 4$  meters are in such cases lower. From equations (11) it should be plain that for the case considered, measurements could be made only where  $0.5 \text{ m} \lesssim r_0 \lesssim 1 \text{ m}$ . The errors for the two extreme values of  $r_0$  are 24 and 11 percent. Hence, when two wavelengths are

used for measurements, only a narrow range of values of  $r_0$  can be measured, and a quantitative relationship between  $r_0$  and heights cannot be obtained.

The most complex consideration in measurements of this type is the determination and selection of meteor trails to which equation (10) is applicable. For over-dense trails equation (10) must give  $r_0=0$ . For intermediate-density trails equation (10) gives values of  $r_0$  that are

less than real if  $r_0 > \frac{\lambda_1}{2\pi}, \frac{\lambda_2}{2\pi}$ ; or greater than real if  $r_0 < \frac{\lambda_1}{2\pi}, \frac{\lambda_2}{2\pi}$ . The appearance of the amplitude-

time curves could not provide a means for determining whether a trail is under-dense or has an intermediate density. A new criterion has been introduced by Dudnik et al. (1961) to determine whether or not equation (10) is applicable in a certain case. The quantity  $\Delta$  was determined for  $\lambda_1=8$  meters in two ways, first, from the ratio of the amplitudes of echoes at the moments of the first and the second maxima, and second, by measuring  $V$ ,  $R$ , and  $D$ . These two values of  $\Delta$  must be equal only for those cases where the following requirements are fully met: (a) linear electron density does not vary considerably within several principal Fresnel zones, and (b) electron density in the trail is so low that only first-order scattering on every electron may be taken into account. As it is on these considerations that equation (10) is based, we can deduce that the agreement of the two values of  $\Delta$  indicates the applicability of equation (10).

The application of this criterion sharply decreased the scatter of values of  $r_0$  with respect to  $D$  and  $V$ , and also narrowed the range of the values of  $D$  and  $V$  where the measurements of  $r_0$  are possible. The values of  $r_0$  were measured for 39 trails. The average values are:  $r_0=80$  cm,  $D=6.4$  m<sup>2</sup>/sec, and  $V=32$  km/sec.

From equation (7), with  $V=32$  km/sec, we obtain

$$r_0 = \lambda_1 \cdot 6.4 \approx 29\lambda_1.$$

From the above theory, for  $r_0=80$  cm and  $D=6.4$  m<sup>2</sup>/sec, we have

$$\lambda_1 = 2.75 \text{ cm.}$$

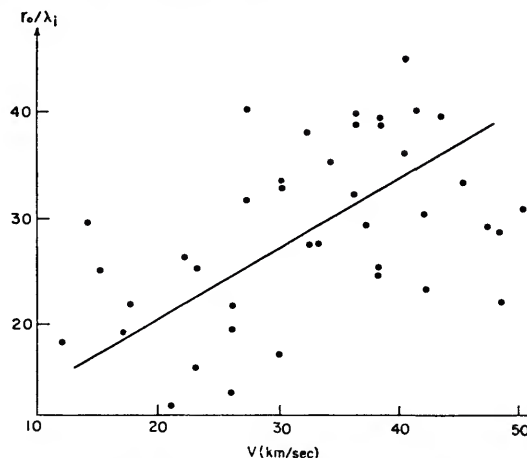


FIGURE 1.—The ratio of the initial radius of a meteoric ionized trail to the mean free path of the ions plotted against the velocity of the colliding particles.

The value of  $\lambda_1$  can be found from the value of the coefficient of ambipolar diffusion  $D$ :

$$D \approx 2D_1 = \frac{2}{3} V \lambda_1. \quad (12)$$

Assuming that  $\mu=29$  and  $\tau=220^\circ$ , we find that

$$\lambda_1 = 2.4 \text{ cm.}$$

Thus, theoretical and measured values are in good agreement.

Figure 1 shows a plot of  $r_0/\lambda_1$  against velocity deduced from the above theory. For simplicity of comparison with the theory, it is assumed that, with  $D=6.4$  m<sup>2</sup>/sec,  $\lambda_1=2.75$  cm. Although the scatter of the points of figure 1 is considerable, the measurements show a high degree of dependence of  $r_0$  upon meteor velocity. A graphic confirmation of the fact that  $V$  greatly influences  $r_0$  is that at  $\lambda_2=4$  meters no meteors were observed whose velocity would be  $V > 50$  km/sec, and whose trail would be under-dense for  $\lambda_1=8$  meters.

Similar measurements of  $r_0$  at  $\lambda_1=17$  meters and  $\lambda_2=8$  meters were made by Greenhow and Hall (1960). As seen from above, their data are most reliable for the cases when  $r_0 \sim 1.5$  meters. They found that, when  $D=13$  m<sup>2</sup>/sec,  $r_0=1.55$  meters. This value is in good agreement with our data and the theory proposed in this paper. Greenhow and Hall found that  $r_0$  depends only slightly upon  $D$  and does not depend at all upon  $V$ . In view of the above

discussion, this may be explained by the fact that their data should be subjected to a stricter analysis. Most of the meteor trails involved in their measurements seem to belong to the intermediate-density type to which equation (10) is not applicable.

#### References

- DUDNIK, B. S.; KASHCHYEV, B. L.; AND LEBEDINETS, V. N.  
1961. Errors in radio-echo measurements of meteor velocities resulting from diffusion. Dokl. Acad. Sci. Ukraine, U.S.S.R., vol. 11, no. 3, pp. 229-302.
- GREENHOW, J. S., AND HALL, J. E.  
1960. The importance of initial trail radius on the apparent height and number distributions of meteor echoes. Monthly Notices Roy. Astron. Soc., vol. 121, pp. 183-196.
- LOEB, L. B.  
1934. Kinetic theory of gases. Ed. 2. McGraw-Hill Book Co., New York.
- MASSEY, H. S. W., AND BURHOP, E. H. S.  
1952. Electronic and ionic impact phenomena. Clarendon Press, Oxford.
- MASSEY, H. S. W., AND SIDA, D. W.  
1955. Collision process in meteor trails. Phil. Mag., ser. 7, vol. 46, pp. 190-198.

# The Initial Diameter of Meteor Trails

By Gerald S. Hawkins <sup>1</sup>

The initial diameter of the column of ionization produced by a meteor is of great importance, since a small increase in its size produces a large increase in the attenuation of a radio echo. Using equation (8-25) of McKinley (1961), we may write the decibel power loss in the echo due to the initial diameter  $d$  as

$$\text{loss} = 85 \left( \frac{d}{\lambda} \right)^2 \text{ decibels,} \quad (1)$$

where  $\lambda$  is the wavelength of the radar. At a wavelength of 8 meters an initial diameter of 4.0 meters produces an attenuation of 21.25 db, whereas the attenuation is only 5.3 db if the diameter is 2.0 meters. Greenhow and Hall (1960), and Greenhow (see this symposium, p. 5) measured the amplitude of echoes at two wavelengths and deduced an average diameter of 4.0 meters for the column at a height of 105 km. It is important to establish whether this value is correct, for if it is, the attenuation at normal radar wavelengths is so severe as to make worthwhile observations virtually impossible.

Öpik (1958) and Manning (1958) have considered theoretically the initial conditions at the meteoroid. Atoms and ions evaporate from the heated surface of the meteoroid and are injected into the atmosphere at the velocity of the meteor. After approximately 14 collisions with air particles, each meteor atom or ion is reduced to thermal velocities, and thereafter normal diffusion takes place. The mean free path of an atom at these velocities is approximately five times greater than that of an ion. Thus two concentric columns will be produced: a narrow column of ionized particles surrounded by a wider shell of neutral atoms. From the known density of the atmosphere,

the initial diameter is given by McKinley's (1961) equation (8-18):

$$\log_{10} d = 0.075H - 7.6 \text{ (meters),} \quad (2)$$

where  $H$  is the height of the meteor column in kilometers. At a height of 105 km the expected diameter of the ion column is 1.9 meters, which is considerably smaller than the value found by Greenhow and Hall (1960). For comparison I have plotted in figure 1 the values of Greenhow and Hall and the values predicted by theory. The experimental values are considerably greater than the theoretical predictions for heights below 105 km. Greenhow and Hall attribute this fact to fragmentation of the meteoroid and attach significance to the discrepancy. On the other hand, their measurements may overestimate the diameter of the column because of an imbalance in the two wavelength channels, a disparity in the antenna patterns, or other causes.

We can obtain an independent estimate of the initial diameter by direct photography. Our understanding of the meteor process is not sufficient at the moment to distinguish clearly between the column of ionization and the coma that is emitting light. We would not, however, expect the region of optical excitation to be any smaller in extent than the region of ionization. In a discussion of meteor spectra, Cook (1955) summarizes the levels of optical excitation that have so far been observed. Meteoric radiation is a mixture of light from both ionized and neutral atoms. We would expect that as a minimum the light would be confined to the ionized column, where excitation and recombination are taking place. At the maximum extent the light could be generated from the core out to the fringes of the neutral atomic column. Although on one occasion Cook and Millman (1955) observed radiation from the heated

<sup>1</sup> Harvard College Observatory, Cambridge, Mass., and Boston University, Boston, Mass.

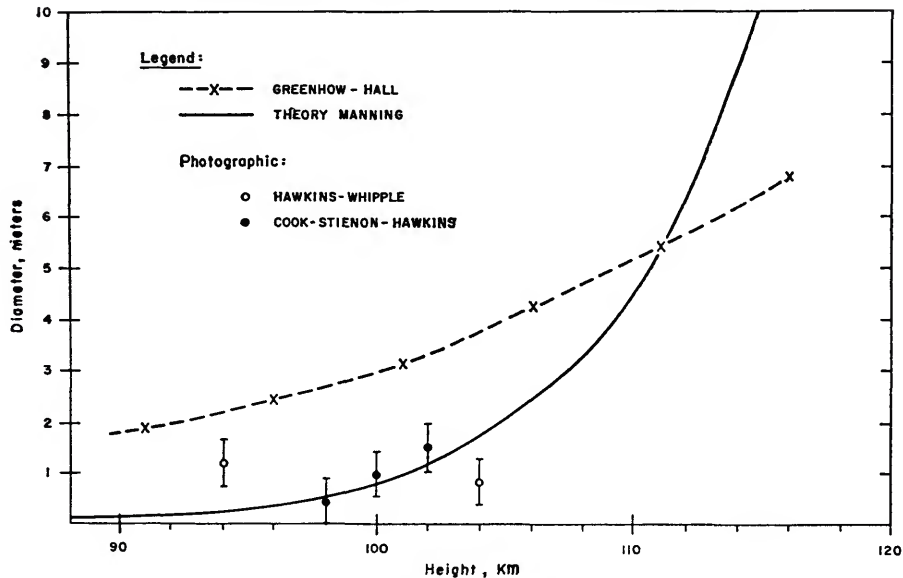


FIGURE 1.—Diameter meteor column as function of height.

surface of the meteoroid, this source of radiation may be neglected for meteors that are fainter than magnitude  $-5$ .

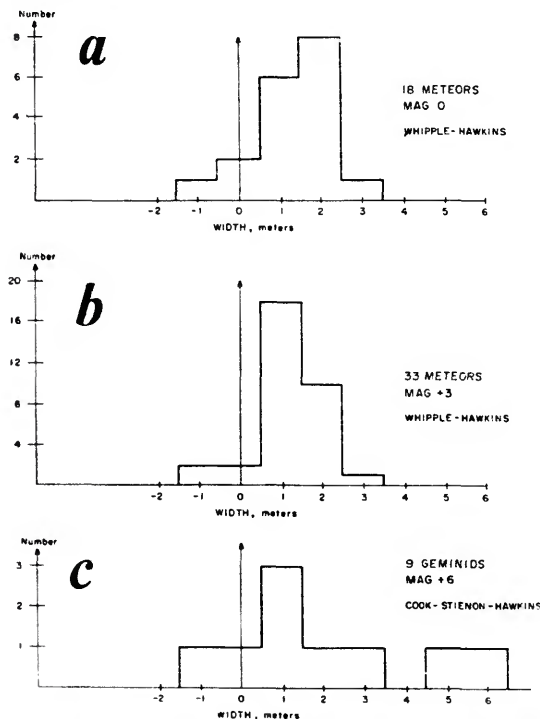


FIGURE 2.—Photographic measures of meteor trail widths.

The photographic data were obtained during two series of observations. The first set of measurements (Hawkins and Whipple, 1958) was taken from the Palomar Sky Atlas, for which meteors had been photographed with the 48-inch Schmidt telescope during the sky survey by the Mount Wilson and Palomar Observatories and the National Geographic Society. Photographic plates were exposed in red and blue light; the average magnitude of the meteors was 0 for red and  $+3$  for blue. The results are summarized in figure 2*a, b*. The mean width of the 18 meteors photographed on the red plates was 1.32 meters; and of the 33 meteors on the blue plates, 1.25 meters. Although these measurements suggest that the brighter meteors produce wider trails, the result is not conclusive since the estimated error of a single measurement was  $\pm 0.5$  meters. We may safely conclude, however, that the width of the optical coma for meteors with magnitude between 0 and  $+3$  is less than the initial diameter found by Greenhow and Hall.

The second set of measurements was obtained by Cook, Stienon, and Hawkins (1960) during the Geminid meteor shower of December 1957. The 48-inch Palomar Schmidt was directed towards the Geminid radiant so that the meteor trails were considerably foreshortened. In this

manner the limiting visual magnitude was extended to +9, and the average magnitude of meteors measured in this program was +6. In their original measurements, Hawkins and Whipple (1958) focused the camera at infinity to record the stellar images, and employed a sidereal drive. These factors introduced some uncertainty in the work since a correction had to be applied to allow for the fact that the meteors, not being at infinity, were slightly out of focus. Also, the width of the meteor trails had to be compared with the diameter of the circular star images. In the measurements of 1957 several photographs were obtained with the plate displaced 50 microns from the focal plane so that the meteor trails were correctly "in focus" and the star images were "out of focus." Since the sidereal drive was not employed, we were able to compare meteor trails directly with star trails. The widths of the nine Geminids that were measured are given in figure 2c. Seven have widths that are distributed symmetrically around a mean value of 0.97 meters. The other two meteors were considerably wider, with values of 5.8 and 5.1 meters. The estimated error for the Geminid meteors was  $\pm 0.4$  meters, slightly less than the value obtained by Hawkins and Whipple (1958).

If we define the 58 meteors in the quasi-symmetrical distributions to be "average meteors," then the width of the optical coma for an average meteor is about 1.2 meters for magnitudes between 0 and +6. If the ionized column is comparable in size to the optical coma, then the attenuation for an 8-meter radar signal for these "average meteors" is less than 2 db. On the other hand, the two Geminids of excessive width would produce an attenuation of more than 40 db, and would be virtually

unobservable by the radio-echo technique. We must regard such meteors as "abnormal." Their excessive width is probably due to explosive fragmentation.

To explore further the disagreement between the radar measurements of Greenhow and Hall (1960) and the optical data, we can consider the dependence of trail width on height. In table 1, I have used the published optical data to group the meteors according to velocity. The mean height of these meteors can be taken from previous photographic data (Hawkins and Southworth, 1958). The Geminid data of Cook, Stienon, and Hawkins (1960) are given, where the mean value for the height of a Geminid of magnitude +6 was taken to be 100 km. The two meteors of excessive width were excluded from this sample. In addition, the trails were reanalyzed to obtain values for the mean diameter of the first half of the trail, and that of the second half of the trail. From table 1 we obtained the five values of diameter that are shown in figure 1. The optical coma corresponds in size to the initial diameter of the ionization column as predicted by Manning (1958). It is difficult to see how the initial ionization column can be any larger in diameter than the measured optical values, i.e., of the order of 1.0 meter over the normal range of meteor heights from 90 to 105 km. Above a height of 110 km, the trails may indeed be extremely wide, but photographic meteors seldom appear in this region of the atmosphere.

The majority of meteors with visual magnitudes between 0 and +6 are narrow enough to avoid the extreme attenuation effects suggested by Greenhow and Hall (1960). There is no optical evidence to support the idea that faint meteors produce an optical coma that is wider than the coma of the brighter photographic meteors.

TABLE 1.—Photographic width as a function of height

	Mean width (meters)	Mean height (kilometers)
(Hawkins, Whipple) Perseids, Orionids	0.79	104
(Hawkins, Whipple) δ Aquarids, Taurids, Quadrantids, Lyrids, Geminids	1.20	94
(Cook, Stienon, Hawkins) Mean value, Geminids	0.97	100
First half	1.53	102
Second half	0.44	98

### References

- COOK, A. F.  
1955. The nature of meteoric radiation. In *Meteors*, ed. T. R. Kaiser, Spec. Suppl. Journ. Atmosph. Terr. Physics, vol. 2, pp. 8-15. Pergamon Press, New York.
- COOK, A. F.; STIENON, F. M.; AND HAWKINS, G. S.  
1960. Meteor trail widths. Interim Report 47, Harvard Radio Meteor Project, Harvard College Observatory, Contract AF 19 (122)-458, Subcontract no. 57.

- COOK, A. F., AND MILLMAN, P. M.  
1955. Photometric analysis of a spectrogram of a Perseid meteor. *Astrophys. Journ.*, vol. 121, pp. 250-270.
- GREENHOW, J. S., AND HALL, J. E.  
1960. The importance of initial trail radius on the apparent height and number distributions of meteor echoes. *Monthly Notices Roy. Astron. Soc.*, vol. 121, pp. 183-196.
- HAWKINS, G. S., AND SOUTHWORTH, R. S.  
1958. The statistics of meteors in the earth's atmosphere. *Smithsonian Contr. Astrophys.*, vol. 2, no. 11, pp. 349-364.
- HAWKINS, G. S., AND WHIPPLE, F. L.  
1958. The width of meteor trails. *Astron. Journ.*, vol. 63, pp. 283-291.
- MANNING, L. A.  
1958. The initial radius of meteoric ionization trails. *Journ. Geophys. Res.*, vol. 63, pp. 181-196.
- McKINLEY, D. W. R.  
1961. *Meteor science and engineering*. McGraw-Hill, New York.
- ÖPIK, E. J.  
1958. *Physics of meteor flight in the atmosphere*. Interscience, New York.

# The Relation Between Visual Magnitudes of Meteors and the Durations of Radar Echoes

By B. A. Lindblad<sup>1</sup>

Observations of the luminous and ionized trails of meteors have shown that meteors in the visual brightness range give rise to radar echoes with durations ranging from a fraction of a second to several minutes. Observational evidence for a relation between the apparent luminosity of a meteor and the duration of the associated radar echo was presented by Millman (1950). This relation has been discussed by various authors (Greenhow and Hawkins, 1952; Kaiser, 1953).

The most extensive observations relating the magnitudes of visual meteors to the lifetimes of the corresponding radar echoes have been made by Millman and McKinley (1956). From a total of 1,405 coincidences obtained during observations of the Perseid shower, these workers found a linear relationship between the logarithm of the echo duration and the absolute magnitude of the meteor. A similar investigation by Lindblad (1956) was based on a rather small sample. The purpose of the present communication is to repeat and extend the previous work, using the larger amount of data which is now available.

The observational data have been collected in the course of Perseid observations carried out at the Onsala Wave Propagation Observatory<sup>2</sup> in Sweden between 1953 and 1960. The experimental technique, which has been described in more detail elsewhere (Lindblad, 1956, 1961), is summarized below.

## Observational techniques

The radar and visual observations of the pro-

gram are designed to cover as completely as possible a limited area of the sky. The radio investigations are conducted with a beamed radar equipment, and the field of the visual observers is restricted to the beamed sky area. During the observations the beam is directed to a point in the sky whose elevation and azimuth differ by 90° and 180°, respectively, from those of the shower radiant.

Visual recording is made by a group of three or four trained meteor observers. The observers estimate meteor magnitude and train duration, and also plot the meteors on star charts. Meteor brightness is estimated to the nearest half magnitude by direct comparison with standard magnitudes within the field of observation.

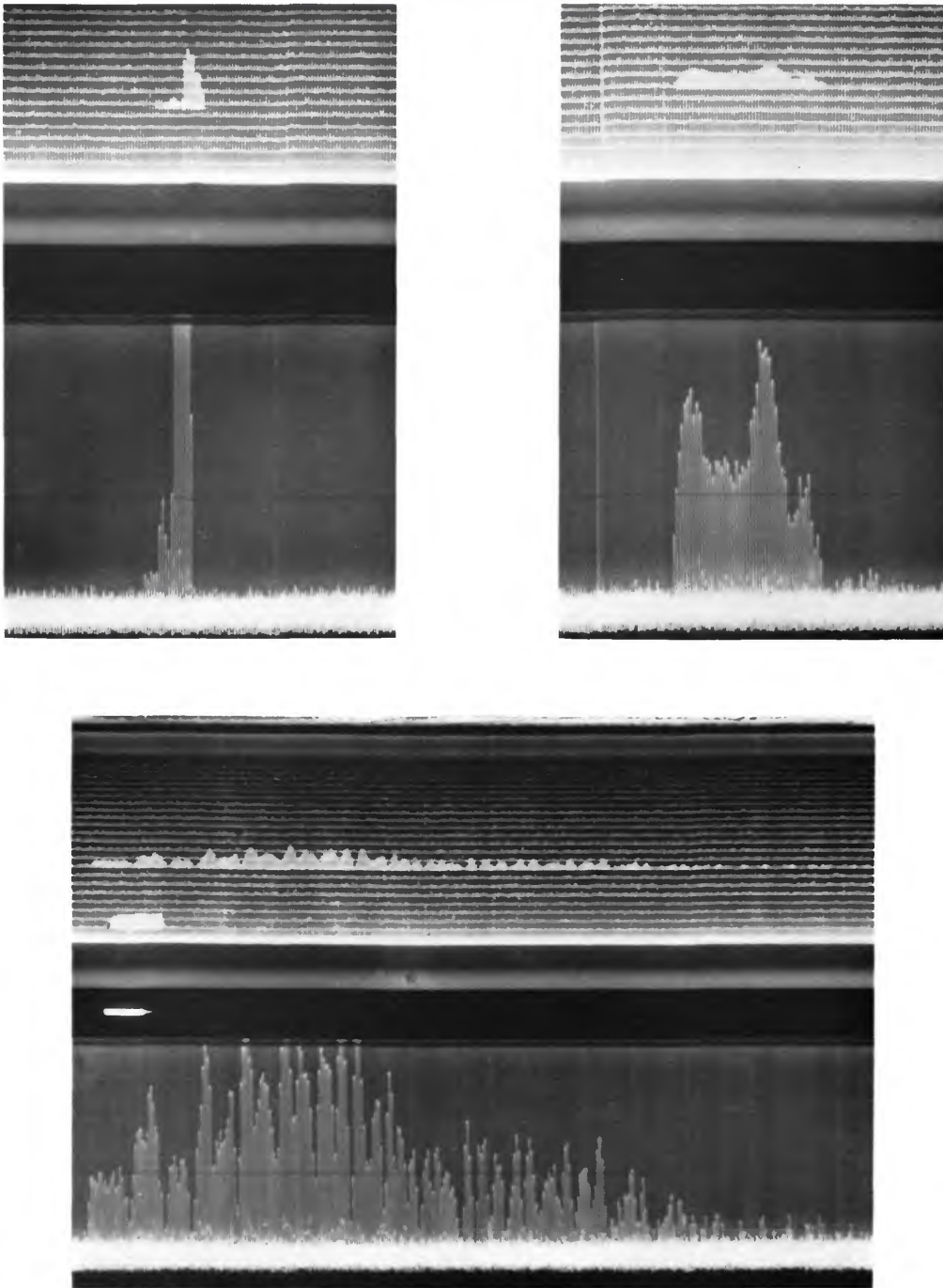
Radar observations are made with a pulsed equipment. The transmitter generates 20–50 kw peak power with a pulse width of 20  $\mu$  sec at a wavelength of 9.2 meters. Repetition frequency is 50 c/s. The receiver has an overall bandwidth of 75 kc/s. The equipment used was essentially the same during the entire program, but the recording technique has been improved from time to time in order to increase the detectability of faint meteors. The present arrangement uses two separate displays, one intensity-modulated range-time display, and one amplitude-time display. Both displays are simultaneously photographed at high film speed (25–50 cm/min). The arrangement permits the individual echo pulses to be recognized and gives good discrimination against the noise background. The shortest echo duration which can be resolved is between 0.04 and 0.02 second. Some typical registration results are shown in plate 1.

<sup>1</sup> Lund Observatory, Sweden.

<sup>2</sup> A division of the Research Laboratory of Electronics of the Chalmers Technical University, Gothenburg.

TABLE 1.—Correlation between (1) zenithal magnitude of meteor and (2) logarithm of duration of associated radar echo. Duration in seconds

log r	Mz												Total			
	-4.0 to -3.6	-3.5 to -3.1	-3.0 to -2.6	-2.5 to -2.1	-2.0 to -1.6	-1.5 to -1.1	-1.0 to -0.6	-0.5 to -0.1	0.0 to +0.4	+0.5 to +0.9	+1.0 to +1.4	+1.5 to +1.9		+2.0 to +2.4	+2.5 to +2.9	+3.0 to +3.4
2.00 to 2.29	1			1		1	7	6		1	1					2
1.70 to 1.99				4	2	5	7			1						28
1.40 to 1.69			2	4	7	13	14	12	7	3						63
1.10 to 1.39				1	7	7	18	17	14	15	4					83
0.80 to 1.09					4	6	12	16	19	13	10		6	3		89
0.50 to 0.79						4	6	20	15	22	22	6				95
0.20 to 0.49						2	5	10	11	16	14	13	2		1	74
-0.10 to +0.19							1	9	12	18	26	17	10	3	1	97
-0.40 to -0.11									5	10	24	19	24	4	2	89
-0.70 to -0.41										6	9	11	12	5	2	47
-1.00 to -0.71											3	5	5	2	1	16
-1.30 to -1.01												2	1	1	1	4
-1.60 to -1.31																
Total	1	2	3	9	21	37	64	92	83	104	113	79	56	17	7	688



Registrations obtained with fast amplitude-time and range-time radar displays. Time difference between consecutive pulses 0.02 second. Lower display, amplitude-time ( $\sim 0-10\mu V$ ); upper display, range-time with superimposed amplitude-time ( $\sim 0-100\mu V$ ). *Top photos*: Short duration echoes with no associated visual meteor. *Bottom photo*: Long duration echo produced by apparent magnitude 2<sup>m</sup>0 Perseid at 22<sup>h</sup>35<sup>m</sup>18<sup>s</sup> M.E.T. on August 12, 1959 (Meteor No. 59-279). Range 180 km. A marker between 40-70 km indicated simultaneous visual recording.



### Reduction of data

The criterion for accepting an association between a visual meteor and a radar echo is mainly one of time coincidence. As a rule, no echo is accepted as a coincidence if the time difference between the signal of the visual observer and the echo is more than 0.5 second. During the period of maximum Perseid activity, the echo rate on the present equipment rarely exceeds 120 echoes per hour. The number of spurious associations in our data is thus less than 2 percent. The possibility of a spurious association is further reduced by stipulating that the accepted radar range should produce a reasonable mean height for the luminous trail of the meteor.

For accepted coincidences the observed meteor magnitudes are corrected to a zenithal or absolute value by adding a correction  $\Delta m = 10 - 5 \cdot \log R$ , where  $R$  is the radio range in kilometers of the associated echo. No correction for absorption was included, since the comparison method of magnitude estimates was used.

The recorded echo lifetimes are durations above a fixed threshold level. Duration is nominally measured to within 0.1 second, with stricter tolerances for echoes lasting less than 0.4 second. Logarithms of echo lifetimes were computed to within 0.01. No corrections were applied to the echo durations.

The magnitude-duration data for each accepted association were collected on a punched card together with other relevant information about the meteor. The data were then grouped in various ways and correlations between magnitude, echo duration, and height were investigated.

### Experimental results I

*Observational data.*—A total of 808 meteors with associated radar echoes was available for analysis. Of these, 688 belonged to the Perseid shower and 120 were either members of various other showers or sporadic objects. Since the Perseid sample was the largest and most homogeneous group, only that group will be discussed.

The first investigation was concerned with

the scatter diagram of log echo duration versus zenithal magnitude. This diagram for 688 Perseid meteors is shown in figure 1. The data of this sample, arbitrarily grouped in intervals of 0.3 in log echo duration and 0<sup>m</sup>5 in zenithal magnitude, are collected in table 1. Inspection of the table shows that in any one array there is a considerable scatter about the mean. Since only a moderate correlation exists between the variates, statistical methods must be used in the presentation and discussion of the data.

Means of rows and columns for the data of table 1 are plotted in figure 2. Inspection of the diagram shows that the points approximate well to two straight lines, although for very bright meteors the means  $\log \tau$  are somewhat low. Within the limited magnitude range covered by this investigation, one may, however, assume that the regression is linear.

Regression lines, computed according to standard procedure, are included in figure 2. The correlation coefficient for the magnitude-duration data is  $-0.725$ , and the slopes,  $b_z$  and  $b_v$ , of the regression lines are  $-0.44$  and  $-0.83$ , respectively. These results are based on computations from ungrouped data.

*Error analysis.*—For a comparison with physical theory it is desirable to express the relation between the variates as a single straight-line relation. The problem is best treated by error analysis. An unknown structural relation is postulated and it is assumed that the scatter about this relation is caused by errors of various kinds. The structural relation is then found if we correct one (or both) of the observed regression lines for the effect of these errors.

Estimates of meteor magnitudes are available from visual observations only, and the observational error in these estimates is not negligible. There is, however, fairly general agreement that the probable error of a magnitude estimate for a trained group of meteor observers is not more than 0<sup>m</sup>3 or 0<sup>m</sup>4. In the present investigation special attention was given to correct magnitude estimates, and all observers had previous experience of astronomical observations. It therefore appears reasonable to adopt as the probable error in our investigation for the combined observa-

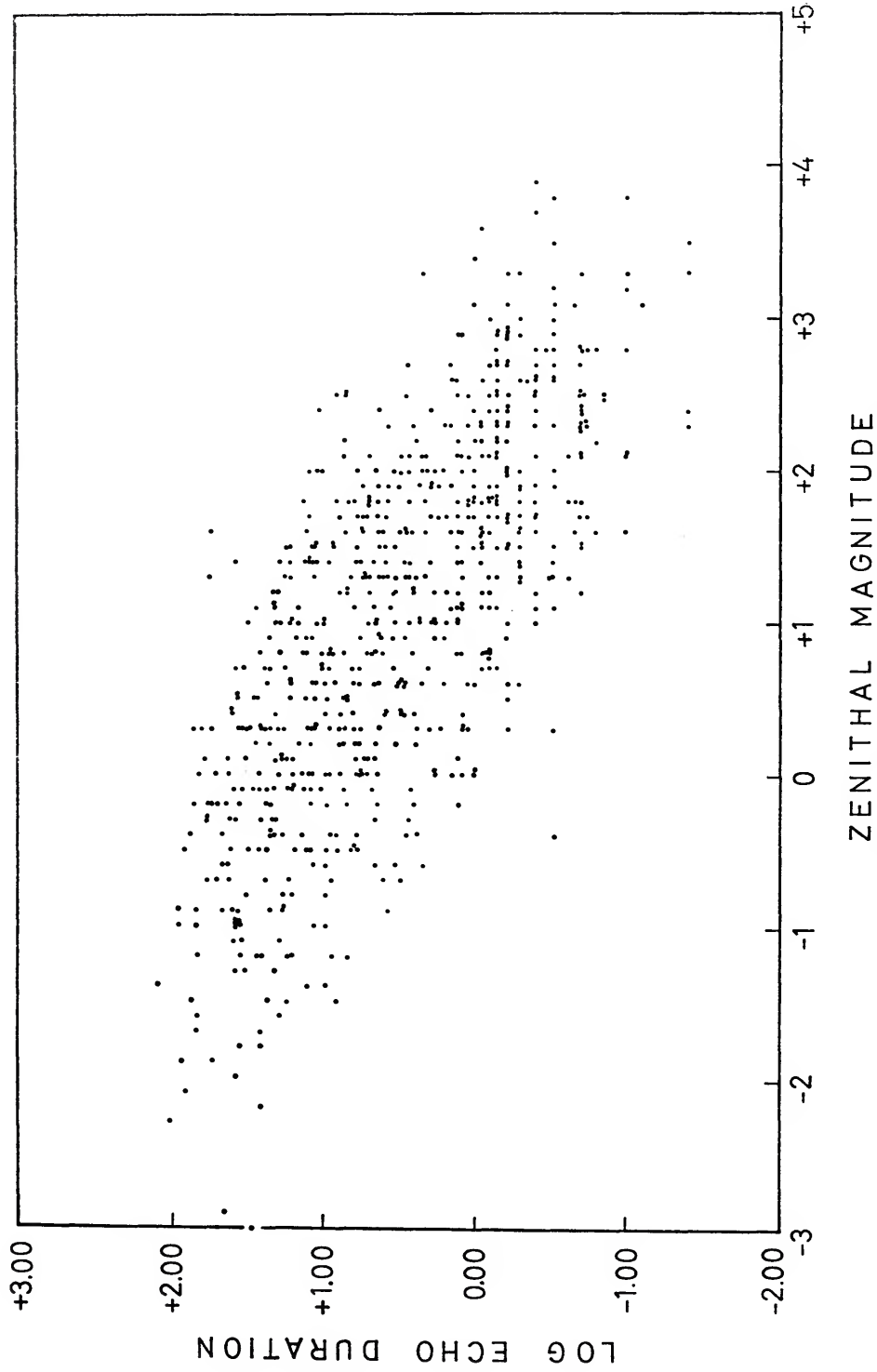


FIGURE 1.—Scatter diagram of log echo duration in seconds versus zenithal magnitude of meteor.

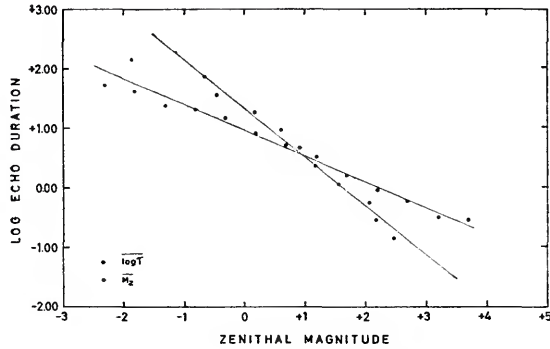


FIGURE 2.—Array means and regression lines for table 1.

tional and reductional error a value of  $0^{m}35$  (standard deviation  $+0^{m}50$ ). On the basis of this assumption it is possible to correct the  $\log \tau$ -line for error in the meteor magnitudes.

Measurements of echo durations are made directly from the radar film. With the display used in our work, sizable errors in these measurements occur only for a few exceptionally long persistent echoes. The duration scatter which is present in meteor data is instead related to the atmospheric and geometrical conditions at the echoing point. It thus appears difficult at this stage to give a numerical estimate of the "errors" in the echo durations, and even more difficult to attempt to correct the  $\bar{M}_z$ -line for these errors.

In view of the above considerations the structural relation behind the experimental data of table 1 is sought by correcting the  $\log \tau$ -line for magnitude error. The correction procedure adopted is summarized in the next section.

*Correction for error.*—Two different correction procedures were investigated. A numerical method for correcting an observed frequency curve, which is described by Eddington (1913), was considered to be the best method. An alternative method given by Seares (1944) was used as a check on the computations.

Eddington's method was applied to the data in the following way: Each separate horizontal array in table 1 was corrected for error dispersion in the magnitudes. A magnitude-error curve based on a slow increase in the magnitude error with meteor brightness was assumed. Eddington's second-order differences were computed from smoothed error curves, deduced from 3-array running means in  $\log \tau$ . Corrected values of the correlation coefficient and the gradient  $b_z$  were then computed. The results of these computations for two models, denoted A and B, are given in table 2. (Both these models were based on a mean probable error of  $0^{m}35$  and differed only in the method of applying the second-order corrections.) In the computations A and B, Sheppard's corrections for grouping have been included.

The correcting of a bivariate distribution by the numerical method and the computing of the corrected regression lines is a rather tedious procedure. The necessity to include corrections for grouping introduces a slight uncertainty in the final result. The error-correction formula given by Seares was therefore also employed. In this method one directly computes the corrected gradient. However, it is necessary to make the assumption that the

TABLE 2.—Correlation data:  $b_z$ , magnitude-duration gradient;  $\bar{x}$ , mean zenithal magnitude;  $\bar{y}$ , mean log echo duration  $\rho$ , correlation coefficient

	$b_z$	$\bar{x}$	$\bar{y}$	$\rho$
Observed values	-0.435	1 <sup>m</sup> 00	0.52	-0.725
Corrected values:				
A	-0.519	1.14	0.52	-0.761
B	-0.480	1.05	0.54	-0.754
C	-0.521	1.00	0.52	
Mean of A and B	-0.500	1 <sup>m</sup> 10	0.53	

magnitude error is independent of magnitude. A constant mean probable error in the magnitudes of 0<sup>m</sup>35 was therefore assumed. The corrected gradient  $b_z$  is listed in table 2 (Model C).

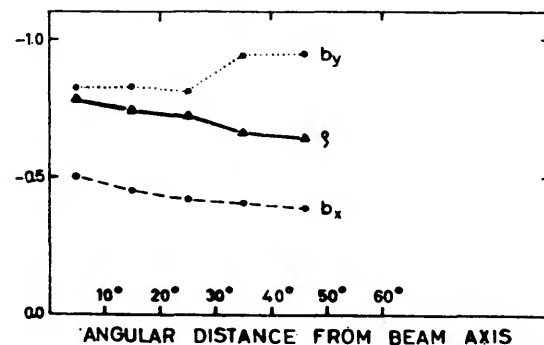
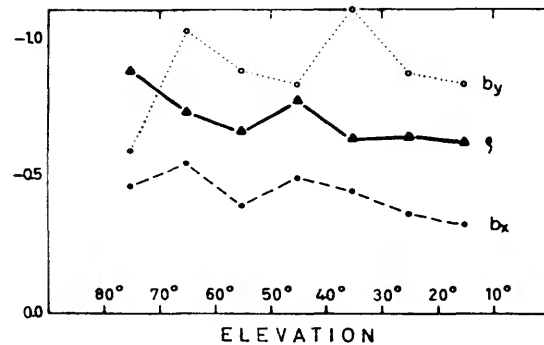
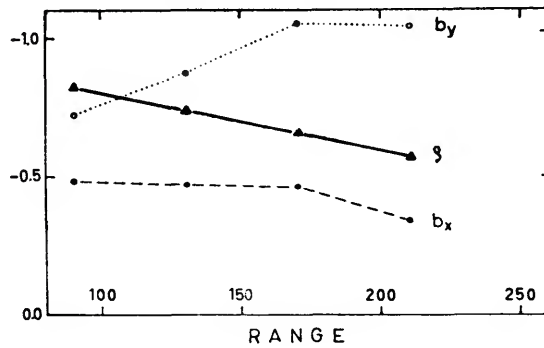


FIGURE 3.—Variations of correlation quantities with range, elevation, and elongation from beam. Symbols:  $\rho$ =correlation coefficient;  $b_z$  and  $b_y$ =gradients of regression lines  $\log \tau$  and  $M_p$ , respectively.

Inspection of table 2 shows that the results of the different methods are in surprisingly good agreement, all indicating similar mass centers and a magnitude-duration gradient after error correction of very nearly  $-0.50$ . The correction for magnitude error has thus only slightly increased the correlation and the slope. It follows that most of the scatter in the diagram of figure 1 must be related to some other factor than magnitude error.

*Observational selection.*—In a following investigation the influence on the computed gradients of different observational selections was studied. *A priori*, one might expect that meteors observed at large distances and low elevations would exhibit peculiar effects and that they might show unduly large scatter when plotted in a magnitude-duration diagram. The Perseid data were therefore grouped according to elevation and range. Correlation coefficients and gradients were then computed for each of these groups. The results of these computations are shown in figure 3. The dependence of the correlation quantities on angular distance from beam is also shown. In view of the paucity of the data, no attempt was made to correct the results of figure 3 for magnitude error.

Although minor irregularities exist, the general trend of the curves of figure 3 is clearly very similar. The trend is such that the correlation coefficient approaches values between  $-0.8$  and  $-0.9$  as the variates approach 90 km, 90°, and 0°, respectively. However, this increase in correlation is associated with a marked decrease in the gradient  $b_y$ , while the gradient  $b_x$  is not affected to the same extent. If Gaussian error functions are assumed, it can be shown that the observed lower value of  $b_y$  indicates a reduced scatter in the echo durations. It thus appears that part of the scatter in the diagram of figure 1 is related to various factors, which influence the recorded echo durations of distant or low-elevation meteors.

Some investigations were made in which other groupings of the meteor data were attempted. One point of interest revealed by these investigations was that the derived

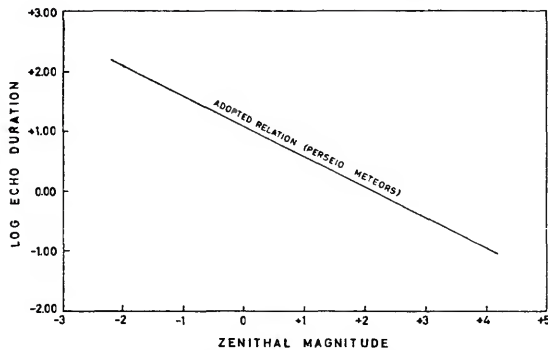


FIGURE 4.—Adopted linear relationship between zenithal magnitude and log echo duration (Perseid meteors).

magnitude-duration relation is independent of trail orientation; i.e., independent of whether the meteors are recorded in a specular reflecting condition or not.

*Adopted magnitude-duration relation.*—The mean elevation of the recorded meteors in our investigation is  $40^\circ$ . If meteors below  $40^\circ$  were rejected, it follows from figure 3 that a slight improvement in the correlation would result. A somewhat higher gradient  $b_z$  would also result. However, the correction for magnitude error is very difficult to apply to a small sample. The overall accuracy of the corrected linear relation between log echo duration and magnitude would therefore not be improved by the rejection procedure.

In view of these considerations, the finally adopted magnitude-duration relation was computed from the total Perseid sample. A mean was taken of the two computations A and B. The resulting coefficients are included in table 2. The adopted linear relationship between magnitude and log echo duration for a radio wavelength of 9 meters is thus

$$\log \tau = -0.50M_z + 1.08.$$

The adopted line is plotted in figure 4. From the diagram it is seen that a Perseid meteor of zenithal magnitude  $0^m0$  produces an echo of duration very nearly 10 seconds and a  $4^m0$  meteor an echo of duration 0.1 second. The relation of these experimental results to the theory of meteor echo durations will be discussed in a following section.

## Experimental results II

*Echo duration and meteor height.*—According to the diffusion theory of meteor echoes, the duration  $\tau$  of a persistent meteor echo is proportional to the electron line density  $\alpha$  and inversely proportional to the diffusion coefficient  $D$ . For an isothermal atmosphere,  $D$  is inversely proportional to density and pressure, and both  $\log D$  and  $\log \tau$  will vary linearly with height for a group of meteors with similar electron line densities.

It thus appears of interest to investigate the relation between  $\log \tau$  and height in a sample of meteors with similar visual magnitudes. In the present investigation approximate meteor heights were obtained from the radar range measurement and from the plot of the trail by the visual observer. Since these latter observations are subject to large errors, the individual height determinations are uncertain, and only mean heights will be used. The magnitude-duration data were arbitrarily grouped in intervals of 0.3 in log echo duration and  $1^m0$  in zenithal magnitude. The mean height computed for each of these cells is listed in table 3. Means computed from less than five observations are given in parentheses.

Inspection of the vertical arrays of table 3 shows that there is a statistical relation between the mean height and the logarithm of the echo duration. It is seen that meteors that lie high in the magnitude-duration diagram are observed at mean heights below 100 km; meteors that lie low in the diagram, are observed at mean heights above 100 km. Inspection of the marginal array indicates, as one would expect, that the relation between mean height and log echo duration is less pronounced when an average is taken over all magnitudes.

*Meteor height versus magnitude.*—Meteor theory predicts that the heights of meteors should decrease with increasing meteor brightness. An experimental verification is provided by the marginal means of table 3. The variation of mean height with magnitude is shown in figure 5 (broken line).

In a subsequent investigation those meteors were selected which showed small scatter about

TABLE 3.—Mean height of Perseid meteor trails as a function of log echo duration and visual magnitude. Meteor heights in kilometers

log $\tau$	$Mz$								Mean height
	-4.0 to -3.1	-3.0 to -2.1	-2.0 to -1.1	-1.0 to -0.1	-0.0 to +0.9	+1.0 to +1.9	+2.0 to +2.9	+3.0 to +3.9	
2.00 to 2.29		(102)	(99)						100.5
1.70 to 1.99		(117)	96	99	95	(98)			98.5
1.40 to 1.69		(91)	97	97	102	(99)			98.4
1.10 to 1.39			93	97	96	98			96.7
0.80 to 1.09			(102)	100	101	100	96		99.8
0.50 to 0.79				99	104	101	91		101.1
0.20 to 0.49				109	97	100	98	(107)	99.6
-0.10 to +0.19				(93)	104	101	98	(105)	101.0
-0.40 to -0.11					108	105	100	99	102.6
-0.70 to -0.41				(94)	(55)	105	100	103	101.0
-1.00 to -0.71						(107)	102	(96)	101.4
-1.30 to -1.01								(100)	
-1.60 to -1.31							(91)		
Mean height		101.7	96.5	98.6	100.4	101.4	98.8	101.2	

the magnitude-duration relation. A maximum variation in log echo duration of  $\pm 0.20$  from the adopted straight-line relation in figure 4 was allowed. This group, consisting of 199 objects, showed a somewhat more pronounced variation of the mean height with magnitude (fig. 5, solid line).

Individual meteors exhibit large scatter about the mean height-magnitude relation of figure 5. It is not possible to explain this scatter as the result of observational errors alone. The question arises whether the height scatter for given visual magnitude is the result of a random breakup of the meteor or if some additional variate is involved (such as the angle of inci-

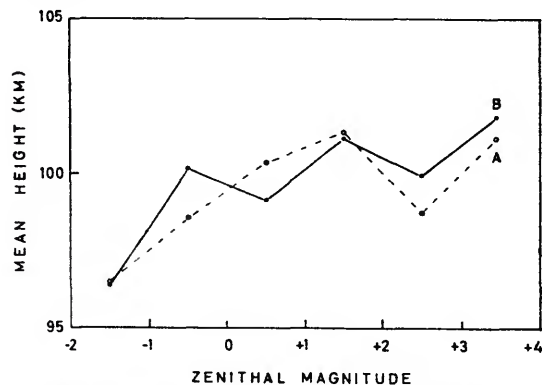


FIGURE 5.—Mean height of Perseid meteor trails as a function of visual magnitude.

dence of the meteor). This point requires further study.

*Duration of persistent visual train.*—Meteors are often accompanied by a persistent train, having a visually observed duration of the order of a second or less. In the present radar-visual program, regular observations of these trains were made, and time durations were estimated by the observers.

The mean train duration in seconds, computed for each of the cells of table 3, is shown in table 4. A meteor with no recorded visual train has been given zero duration in the averaging. Inspection of the marginal mean durations of the table reveals a dependence on visual magnitude and on echo duration. Inspection of the vertical arrays of the table indicates a correlation with echo duration, which is independent of visual magnitude.

From table 4 it may be concluded that meteors that lie high in the magnitude-duration diagram exhibit visual trains of unusual persistence. The durations of meteor trains and meteor ionization are thus intimately connected.

The data of table 4 are published to illustrate qualitatively a general relation. They are representative of observations made at sea level. The measured duration of a persistent train depends critically on the atmospheric transparency—and thus on both locality and meteor

TABLE 4.—Mean duration of persistent train as a function of log echo duration and visual magnitude. Train durations in seconds

log $\tau$	$M_z$								Mean duration
	-4.0 to -3.1	-3.0 to -2.1	-2.0 to -1.1	-1.0 to -0.1	-0.0 to +0.9	+1.0 to +1.9	+2.0 to +2.9	+3.0 to +3.9	
2.00 to 2.29		3.5	7.0						5.3
1.70 to 1.99		3.3	3.6	2.3	1.2				2.4
1.40 to 1.69		1.5	1.0	1.5	0.4	1.3			1.04
1.10 to 1.39			0.6	0.4	0.4	0.2			0.38
0.80 to 1.09			0.3	0.6	0.3	0.4	0.02		0.32
0.50 to 0.79				0.4	0.4	0.14	0.17		0.26
0.20 to 0.49				0.6	0.4	0.30	0.20		0.32
-0.10 to +0.19				3.5	0.3	0.03	0.04		0.12
-0.40 to -0.11					0.2	0.04	0.02		0.04
-0.70 to -0.41					0.2	0.08			0.09
-1.00 to -0.71							0.02		0.02
-1.30 to -1.01									
-1.60 to -1.31									
Mean duration		2.42	1.50	0.98	0.37	0.16	0.05		

elevation angle. Because of the lack of precision of the experimental data, and since the number of trains available for analysis is rather small, no attempt is made in this paper to treat the train data quantitatively.

#### Comparison with other investigations

From radar-visual data obtained on a wavelength of 9.2 meters by Millman and McKinley (1956), linear relations between visual magnitude and log echo duration were reduced for several meteor showers. For Perseid meteors, which represent the largest group, these workers found a magnitude-duration relation (after correction for error) of  $\log \tau = -0.406 M_z + 0.87$ . The gradient value  $-0.406$  is considerably lower than that found in the present investigation. The reason for this discrepancy is not clear at present, but one factor which may be of importance in this connection will be mentioned.

On the basis of the diffusion theory of meteor echoes, one expects a linear relation between log echo duration and visual magnitude. However, Davis, Greenhow, and Hall (1959) have shown that the echo durations of very bright meteors are far less than those to be expected on simple diffusion theory. This has been explained by the removal of electrons from the ionization

trail by attachment to neutral oxygen molecules' to form negative ions. Although this reduction in duration is not of great importance for fast Perseid meteors, which ionize at a mean height of 100 km, a slight indication of some such ceiling effect is evident in the diagrams of figures 1 and 2, where the recorded echo durations for magnitudes  $-1^m$  and  $-2^m$  are slightly less than predicted from diffusion theory.

A comparison of Millman and McKinley's (1956) table III with our table 1 shows that bright meteors are more common in the Canadian observations than in our survey. The discrepancy in magnitude-duration gradient between the two investigations could thus possibly be explained as due to the attachment process, which would systematically lower the durations of the bright meteors in the Canadian investigation and thus also cause a lowering of the computed slope.

A detailed comparison of the two investigations is complicated by the fact that various elevation-dependent corrections are introduced in the reduction of the Ottawa data. It is not known to what extent these corrections influence their observed gradient.

Since a selection according to either elevation or beam elongation is mainly one of distance, the results of figure 3 lend some support to a suggestion of McKinley (1953) that corrections

for attenuation should be applied to echo durations. However, an attempt to apply this type of correction to our data was not very successful, the net result being that the magnitude-duration scatter diagram was shifted upwards, with no pronounced change in the correlation quantities.

### Theoretical relations between magnitude, duration, and height

The ionized trails of meteors can be divided into two main groups, generally referred to as underdense and as overdense trails, in which the linear electron density  $\alpha$  is less or greater than  $2 \times 10^{12}$  electrons/cm.

For low density trails with  $\alpha < 2 \times 10^{12}$  electrons/cm, Herlofson (1948) has shown that the radar echo duration to  $1/e$  of the initial amplitude is independent of  $\alpha$ , and is given by

$$T = \frac{\lambda^2}{16\pi^2 D}, \quad (1)$$

where  $D$  is the diffusion coefficient and  $\lambda$  is the wavelength. The echo duration is thus independent of  $\alpha$ , being determined by the wavelength and the diffusion coefficient.

When  $\alpha > 2 \times 10^{12}$  electrons/cm, the volume electron density in a trail exceeds the critical density  $N_c$ . Under these conditions the duration of a meteor echo is proportional to  $\alpha$ , and with the assumption that the ionization is dissipated mainly by diffusion, Greenhow (1952) and Kaiser and Closs (1952) have shown that the echo duration is given by

$$T = \frac{\alpha}{4\pi D N_c}. \quad (2)$$

*Magnitude-duration relation.*—Meteors in the magnitude range  $-2^m$  to  $+4^m$  will mainly produce overdense ionization trails, and we will assume that equation (2) applies to the majority of the meteors in our survey. We will further assume that the diffusion coefficient is inversely proportional to the atmospheric density  $\rho$ . The radar duration of visual meteors is then given by the relation

$$\log T = \log \alpha + \log \rho + \text{const.} \quad (3)$$

Meteor theory predicts that the electron line density at the point of maximum rate of evapo-

ration of the meteor is related to the atmospheric density at the same point by the relation

$$\rho_{\max} \propto \alpha^{1/3}_{\max}. \quad (4)$$

Meteor magnitudes are defined by the relation

$$\log \alpha = \text{const} - 0.4 M_z. \quad (5)$$

Let  $T_{\max}$  be the predicted echo duration at the point of maximum evaporation. Combining equations (3), (4), and (5) gives

$$\log T_{\max} = \text{const} - 0.533 M_z \quad (6)$$

for the predicted variation of echo duration with magnitude. It is thus assumed that the final echo signal is returned from a segment of trail near the point of maximum ionization.

*Height-magnitude relation.*—A relation between meteor height and visual magnitude is derived as follows. An isothermal atmosphere is assumed with atmospheric density  $\rho$  given by

$$\log \rho = \text{const} - \frac{H}{\mathcal{H}} \log e, \quad (7)$$

where  $H$  and  $\mathcal{H}$  are height and scale height, respectively. Introducing  $H_{\max}$ , the predicted height at maximum evaporation and substituting equations (5) and (7) in equation (4), we find that

$$\frac{H_{\max}}{\mathcal{H}} \log e = \frac{0.4}{3} M_z, \quad (8)$$

or

$$\frac{H_{\max}}{\mathcal{H}} = 0.306 M_z + \text{const}, \quad (9)$$

for the relation between meteor height and zenithal magnitude.

*Echo duration versus meteor heights.*—It is of interest to deduce the predicted variation of echo duration with meteor height for a constant magnitude group. Substituting equations (5) and (7) in equation (3), we find that

$$\log T = \text{const} - 0.4 M_z - \frac{H}{\mathcal{H}} \log e, \quad (10)$$

where  $T$ ,  $M_z$ , and  $H$  are echo duration, meteor luminosity, and meteor height at the echoing point.

### Discussion of results

*Comparison of experimental and predicted gradients.*—The theoretical relationships derived in the preceding section will now be compared with the available experimental observations. Physical interest is focused mainly on the gradients in the magnitude-duration and height-magnitude relationships.

Comparison of the predicted and observed slopes of the magnitude-duration relation shows that the experimental data (table 2) are in very good agreement with the predicted relation (6).

The experimental height-magnitude relationship for Perseid meteors is given in figure 5, which shows that bright meteors penetrate lower into the atmosphere than do faint meteors, as predicted by theory. The observed value of the slope is, however, not consistent with the value inferred from equation (9). For a scale height of 6.5 km the theoretical relation (9) predicts a slope of approximately 1.9 km/magnitude. From the experimental curve (B) a gradient of about 1.2 km/magnitude is deduced. However, taking means of the meteor heights artificially lowers the experimental gradient somewhat, owing to the large scatter which is present in the data. An approximate correction for magnitude error raises the experimental slope to about 1.4 km/magnitude.

It should be observed that the experimental heights refer to the midpoint of the visual track, while the height in equation (9) is the predicted height at maximum light. A correction to the observed heights may be derived from photographic meteor data (Millman, 1958). This correction, which is  $-0.5$  km for a  $3^{m5}$  Perseid and  $-4.0$  km for a  $-2^{m5}$  Perseid, is sufficient to remove the remaining discrepancy between the experimental and predicted slopes.

For the variation of log echo duration with height in a constant magnitude group, the previous theory predicts a slope of approximately  $-0.07 \log \tau/\text{km}$ . An experimental verification of this prediction is, however, not possible since the scatter diagram of log  $\tau$  against  $H$  indicates very large scatter in the data even when a narrow magnitude interval is considered.

*Transitional duration and line density.*—In the present investigation it is assumed that

equation (2) is valid for all visual meteors. The validity of this assumption will now be discussed. For this purpose it is necessary to estimate the approximate echo duration and visual magnitude at which the transition from underdense to overdense ionization trails occurs.

For an underdense trail, the echo duration to  $1/e$  of the initial amplitude may be computed from equation (1), provided the diffusion coefficient is known. For conversion of this duration to threshold duration, an empirical graph of signal-to-noise ratio against zenithal magnitude was constructed and used together with the magnitude-duration relation (fig. 4). Assuming an exponential decay of echo amplitude, appropriate values of threshold duration, relative duration, and visual magnitude may be computed for a number of different values of the diffusion coefficient.

With  $D=4.0 \text{ m}^2/\text{sec}$  we find from equation (1) a relative duration of 0.14 second. This duration corresponds to a meteor of approximate magnitude  $3^{m5}$ , a mean signal-to-noise ratio of 4, and a threshold duration of 0.20 second. The transition between underdense and overdense trails thus occurs near zenithal magnitude  $3^{m5}$ .

For the faint visual meteors in the transition region it may, however, be more appropriate to use a higher value of the diffusion coefficient, since these meteors may be assumed to ionize rather high in the atmosphere. If  $D=13 \text{ m}^2/\text{sec}$ , as determined by Greenhow and Neufeld (1955) for a mean height of 100 km, the computations give relative and threshold durations of 0.04 and 0.05 second, respectively, and a visual magnitude between  $4^{m5}$  and  $5^{m0}$ . In this case, all meteors in a radar-visual survey are of the long persistent type. It thus appears correct to apply equation (2) to all meteors in the present investigation.

The electron-line density in the trail may be computed from the magnitude-duration relation and equation (2), provided the visual magnitude exceeds the transitional value. For  $D=13 \text{ m}^2/\text{sec}$  and  $N_e=1.33 \times 10^7$ , the relation between echo duration and line density is given by

$$T=4.5 \times 10^{-14} \alpha,$$

where  $\alpha$  is the line density per centimeter path. For a fourth-magnitude meteor with an echo duration of 0.1 second, the corresponding density is about  $2.2 \times 10^{12}$  electrons per centimeter. The main uncertainty in these computations rests on the assumed value of the diffusion coefficient.

*Limiting meteor magnitude.*—An experimental curve of the signal-to-noise ratio against meteor magnitude indicated a slow decrease with magnitude. Extrapolation of this curve to faint meteors of zenithal magnitude  $6^m0$  indicated that these meteors should still be detectable. A mean signal-to-noise ratio of two was assumed as the detection limit.

However, the shortest duration which is recorded cannot be appreciably less than the time interval between two consecutive transmitter pulses. For a pulse repetition frequency of 50 c/s, this limiting echo duration is 0.02 second. The corresponding visual magnitude, deduced from figure 4, is very nearly  $5^m5$ . It thus appears that the limiting meteor magnitude of the present equipment is determined by the pulse repetition frequency and that fifth-magnitude meteors represent the limit of detectability.

*Summary of results.*—An analysis has been given of the magnitudes, echo durations, and heights of Perseid meteors. A relation between visual magnitude and log echo duration has been deduced, and some observational factors influencing the determination of this relation have been discussed. The experimental relation is found to be linear over the range of zenithal visual magnitudes from  $-2^m0$  to  $+4^m0$ . The observed slope is very nearly  $-0.50$ , in agreement with theoretical predictions based on equation (6). A variation of meteor height with magnitude has been found in accordance with equation (9). Meteors that brighten up, at heights above the mean height predicted from their magnitude, have shorter echo durations than those given by the magnitude-duration relation; meteors which penetrate lower into the atmosphere have echoes of unusual duration. These meteors also exhibit persistent visual trains. The experimental results as to echo durations are in general accord with the results one might expect on the basis of diffusion theory.

### Acknowledgments

This investigation was carried out at the Onsala Wave Propagation Observatory and at the Lund Observatory. The author is indebted to the directors of these stations, Professors O. Rydbeck and C. Schalén, respectively, for their constant interest in the work. The investigation has been financially supported by the Swedish Natural Science Research Council.

### References

- DAVIS, J.; GREENHOW, J. S.; AND HALL, J. E.  
1959. The effect of attachment on radio echo observations of meteors. *Proc. Roy. Soc. London, ser. A*, vol. 253, pp. 130-139.
- EDDINGTON, A. S.  
1913. On a formula for correcting statistics for the effects of a known probable error of observation. *Monthly Notices Roy. Astron. Soc.*, vol. 73, pp. 359-360.
- GREENHOW, J. S.  
1952. Characteristics of radio echoes from meteor trails: III. The behaviour of the electron trails after formation. *Proc. Phys. Soc. London*, vol. 65B, pp. 169-181.
- GREENHOW, J. S., AND HAWKINS, G. S.  
1952. Ionizing and luminous efficiencies of meteors. *Nature*, vol. 170, pp. 355-357.
- GREENHOW, J. S., AND NEUFELD, E. L.  
1955. The diffusion of ionized meteor trails in the upper atmosphere. *Journ. Atmosph. Terr. Phys.*, vol. 6, pp. 133-140.
- HERLOFSON, N.  
1948. The theory of meteor ionization. *Phys. Soc., Rep. Progr. Phys.*, vol. 11, pp. 444-454.
- KAISER, T. R.  
1953. Radio echo studies of meteor ionization. *Advances in Physics (Phil. Mag. Suppl.)*, vol. 2, pp. 495-544.
- KAISER, T. R., AND CLOSS, R. L.  
1952. Theory of radio reflections from meteor trails: I. *Phil. Mag.*, ser. 7, vol. 43, pp. 1-32.
- LINDBLAD, B. A.  
1956. Combined visual and radar observations of Perseid meteors. I. Observations in 1953. *Medd. Lund Astron. Obs.*, ser. 1, no. 189.  
1961. Combined visual and radar observations of Perseid meteors. II. Observations in 1955. *Medd. Lund Astron. Obs.*, ser. 1, no. 198.
- McKINLEY, D. W. R.  
1953. Effect of radar sensitivity on meteor echo durations. *Canadian Journ. Phys.*, vol. 31, pp. 758-767.

- MILLMAN, P. M.  
1950. Meteoric ionization. Journ. Roy. Astron. Soc. Canada, vol. 44, pp. 209-220.  
1958. The heights of meteors. Journ. Roy. Astron. Soc. Canada, vol. 52, pp. 230-232.
- MILLMAN, P. M., AND MCKINLEY, D. W. R.  
1956. Meteor echo durations and visual magnitudes. Canadian Journ. Phys., vol. 34, pp. 50-61.
- SEARES, F. H.  
1944. Regression lines and the functional relation. Astrophys. Journ., vol. 100, pp. 255-263.

### *Abstract*

This investigation is concerned with the statistical relation between visual magnitudes of meteors and radar echo durations. For 688 Perseid meteors observed at a radio wavelength of 9.2 meters, a linear relation is deduced between the logarithm of the duration of the echo and the absolute magnitude of the meteor. The adopted magnitude-duration relation indicates that a Perseid meteor of zenithal magnitude 0<sup>m</sup>0 produces an echo duration of 10 secs, and a meteor of zenithal magnitude +4<sup>m</sup>0 a duration of 0.1 sec. The scatter of points in the magnitude-duration diagram is discussed. It is shown that this scatter, for constant visual magnitude, is related to the mean atmospheric height of the meteor. It is further shown that meteors which lie high in the magnitude-duration diagram are associated with persistent visual trains.



# Radio-Echo Measurements of Meteor Mass Distributions

By A. A. Weiss <sup>1</sup>

## Method of measurement

Mass distributions have been determined for sporadic meteors and for meteors belonging to the major showers visible in the southern hemisphere, over the years 1957 to 1960. Measurements made with a narrow beam 67 Mc/sec radar equipment were used.

A differential mass distribution of the form  $v_m \propto m^{-s} dm$  has been assumed. Electron line densities  $\alpha$  have been converted to radio magnitudes  $M_r$ , with the relation  $M_r = 35 - 2.5 \log_{10} \alpha$ . The value of  $s$  has been determined in the range  $6.0 < M_r < 7.5$  from the dependence of total echo counts on equipment sensitivity, and in the range  $0 < M_r < 2.5$  from the distributions of echo durations. In the former case (total echo counts) allowance has been made for the aerial polar diagram; and fragmentation of the meteoroid, if present, introduces negligible error into the value of  $s$ . In determining the value of  $s$  for the brighter meteors, it has been supposed that the decay of the echo is due to a progressive reduction of the free electron density within the trail by ambipolar diffusion and the attachment of electrons to neutral molecules. It has not been possible to correct for the influence of irregular atmospheric motions on the echo durations, but in view of the small aerial beamwidth and high operating frequency this effect is not expected to be serious.

A full account of the experimental method will be found in Weiss (1961a).

## Sporadic meteors

Uncertainties in the aerial polar diagram and in the threshold sensitivity of the equipment limit the precision with which the value of  $s$

appropriate to the fainter group of sporadic meteors can be determined. Our observations show, however, that for  $6.0 < M_r < 7.5$  the value of  $s$  is close to the  $s=2.0$  found repeatedly from telescopic observations.

From the echo durations,  $s=2.5$  for  $-3 < M_r < 2.5$ . This may be compared with the careful photographic determination by Hawkins and Upton (1958) of  $s=2.34$  for  $-1 < M_r < 4.5$ .

Even if the absolute accuracy of the present radio determinations is open to some doubt, these methods can still be used to obtain useful comparisons of the mass distributions for shower and sporadic meteors. Such comparisons are valid because (a) the variation of the total echo rate with equipment parameters is insensitive to the degree of fragmentation, and (b) the incidence of trail distortion is identical for all the major showers and for sporadics, at least in the southern hemisphere (Weiss 1961b). There do not seem to be any northern hemisphere observations of the incidence of trail distortion which are directly comparable with those of the southern hemisphere mentioned here, but there is no reason to expect a different result in the northern hemisphere.

## Showery meteors

*Geminids.*—Values of  $s$  for the time of maximum activity of this shower are given in table 1, and are compared with northern hemisphere measurements (Browne, Bullough, Evans, and Kaiser, 1956) in figure 1. The echo amplitude and durations methods used in the Jodrell Bank measurements can be regarded as absolute; the height distribution measurement was obtained by comparison with an assumed value  $s=2.0$  for sporadics.

<sup>1</sup> Commonwealth Scientific and Industrial Research Organization, Radiophysics Laboratory, Sydney, Australia.

TABLE 1.—Values of mass distribution exponents  $s$ 

Shower	$s$		
	$7.5 > M_r > 6.0$	$2.5 > M_r > 1.0$	$1.0 > M_r > 0$
Geminids	1.5	1.7	2.7
$\delta$ Aquarids	1.5	1.9	2.7
$\eta$ Aquarids	1.6	1.4	2.0
Sporadics	2.0	2.5	2.5

Two values of  $s$  are given for the present durations measurements, since it was found that even after allowance for attachment the results could not be fitted by a single value of  $s$  over the whole range of echo durations. Kashcheyev and Lebedinets (1959) have also observed an abrupt increase in the value of  $s$  at about the second radio magnitude, which is most pronounced over the time of maximum activity of the shower and is then too large to be attributed solely to the effects of attachment, which they neglected. A similar trend is also apparent in the Jodrell Bank results, but only the weighted mean for the whole shower has been given in the diagram. The new results suggest that, at least near the time of maximum activity, the maximum concentration of mass per unit magnitude range occurs around  $M_r = +1$ , which is rather brighter than suggested by the Jodrell Bank authors.

*The  $\delta$  Aquarids.*—The mass distribution appears to be identical with that for the Geminids (see table 1). Like the Geminids (Browne et al., 1956), the  $\delta$  Aquarids exhibit

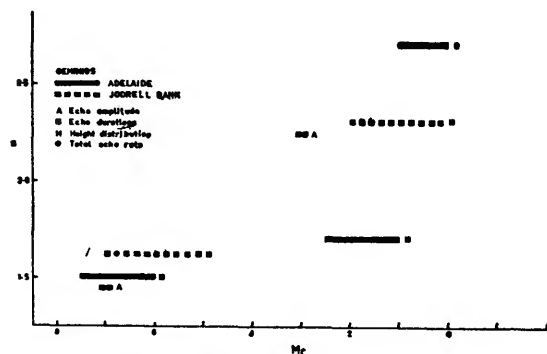


FIGURE 1.—Comparison of mass distribution exponents  $s$  for the Geminid stream, measured at Jodrell Bank and at Adelaide.

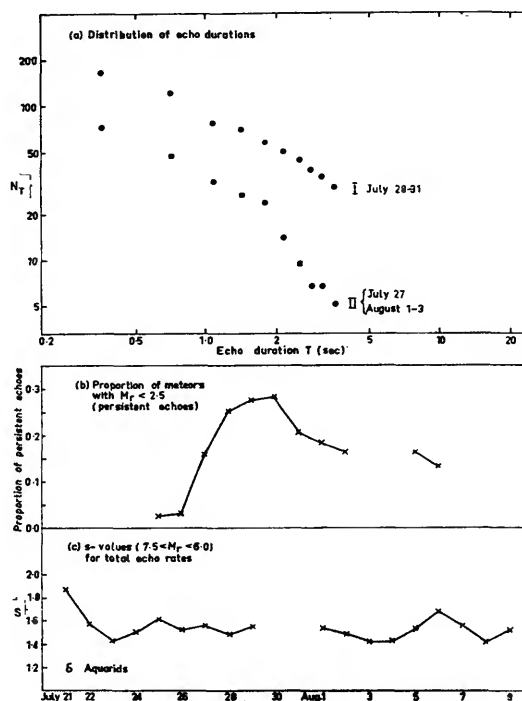


FIGURE 2.—Increases in the proportion of bright and very bright meteors near the time of maximum activity of the  $\delta$ -Aquarid shower, indicating a central condensation of massive meteors within the stream.

a strong concentration of bright meteors to the center of the stream. The evidence for such a central condensation is presented in figure 2. The proportion of persistent echoes increases, and the value of  $s$  for the brightest meteors decreases, for the 4 or 5 days centered on the time of peak activity. At the same time, there is no change in the value of  $s$  for meteors fainter than 5th magnitude.

*The  $\eta$  Aquarids.*—This shower, which is prominent visually, gives a comparatively low echo rate on the radar when the limiting magnitude is reduced to  $M_r = 7.5$ . In fact, during the 1957 apparition, some 30 percent of all echoes detected had  $M_r \leq 2.5$ . These results alone suggest that  $s \ll 2.0$ , and this is confirmed by the more accurate determinations given in table 1. With these values of  $s$ , the predicted proportion of persistent echoes ( $M_r \leq 2.5$ ) to all echoes is about 10 percent. This is only a third of the observed number; the discrepancy is almost wholly due to prolongation of echo durations by atmospheric motions.

### Discussion

These southern hemisphere results confirm the general picture which had emerged from the northern hemisphere radio measurements, that for the major showers the value of  $s$  increases from about 1.5 for meteors of 7th magnitude to values  $\geq 2.0$  for meteors of zero magnitude, and that the mass per unit magnitude range reaches a maximum well above the visual threshold. The more detailed analysis of the durations of persistent echoes has shown that in some cases, notably the Geminids and  $\delta$  Aquarids, there is a very steep rise in the value of  $s$  for  $M_r < +1$ , so steep that it amounts effectively to a cut-off in meteors above the critical mass. Sporadic meteors, by way of contrast, do not share this cut-off, and the value of  $s$  remains substantially constant to the upper limit of the cometary meteoroid mass scale. This characteristic of constant  $s$  amongst the brightest meteors is also shared by some showers (for example, Perseids,  $\eta$  Aquarids).

In conjunction with the Jodrell Bank results, the present observations have shown that the Geminids and the  $\delta$  Aquarids, which have similar mass distributions and in particular share the characteristic of a steep rise in the value of  $s$  for  $M_r < +1$ , both exhibit a strong concentration of bright meteors to the center of the stream. It is interesting to speculate whether these two features of the mass distribution are associated, since in at least one other case (Perseids) a constant value of  $s$  amongst the brightest meteors is coupled with an increase in the relative number of *faint* meteors at the

time of maximum shower activity (Browne et al., 1956).

In conclusion, it is well to emphasize that, so long as the evaporation theory is used to interpret radio-echo data, any appreciable fragmentation, especially amongst the fainter meteors, will result in inconsistencies in the mass distributions derived by different methods (for example, from relative echo rates and from the widths of measured height distributions). This provides us with a means for comparing the physical structure of meteoroids belonging to different streams.

### References

- BROWNE, I. C.; BULLOUGH, K.; EVANS, S.; AND KAISER, T. R.  
1956. Characteristics of radio echoes from meteor trails. II. The distribution of meteor magnitudes and masses. Proc. Phys. Soc. London, vol. 69B, pp. 83-97.
- HAWKINS, G. S., AND UPTON, E. K. L.  
1958. The influx rate of meteors in the earth's atmosphere. Astrophys. Journ., vol. 128, pp. 727-735.
- KASHCHEYEV, B. L., AND LEBEDINETS, V. N.  
1959. On the structure of the Geminid meteor stream. Astron. Journ. U.S.S.R., vol. 36, pp. 629-640.
- WEISS, A. A.  
1961a. The durations of persistent meteor echoes and the derivation of meteor mass distributions. Commonwealth Scientific and Industrial Research Organization Australian Div. Radiophys. Rep. RPR 139.  
1961b. The distribution of meteor masses for sporadic meteors and three showers. Australian Journ. Phys., vol. 14, pp. 102-119.

### Abstract

Mass distributions for sporadic and shower meteors are derived from radio-echo observations at 67 Mc/sec. The data used are total echo rates for the brightness range  $6.0 < M_r < 7.5$ , and durations of persistent echoes for  $M_r < 2.5$ . The mass distributions cannot be represented by simple inverse power laws with constant exponents  $s$ . For sporadic meteors,  $s$  increases from  $\sim 2.0$  for the faint meteor group to 2.5 for the brighter meteors. For the  $\eta$ -Auarid,  $\delta$ -Auarid, and Geminid showers,  $s$  also increases as the brightness increases. In common with the major northern hemisphere showers, the mass per unit magnitude range for these showers reaches a maximum well above the visual threshold.

The  $\delta$  Aquarids are shown to exhibit a concentration of massive meteors towards the center of the stream.



# A Preliminary Report on Radar Meteor Counts

By Peter M. Millman<sup>1</sup> and Bruce A. McIntosh<sup>1</sup>

As part of the Canadian program of the International Geophysical Year, a meteor patrol radar was designed and constructed for use at the Springhill Meteor Observatory a few miles south of Ottawa, latitude  $45^{\circ}11'.8$  N, longitude  $75^{\circ}28'.3$  W, elevation 310 feet above sea level. This radar operates at a frequency of 32.7 mc/sec with a peak power approximately 20 kw, pulse recurrence frequency 117 cps, and a pulse length  $12 \mu$  sec. Independent transmitting and receiving aerials consist of crossed horizontal dipoles, fed  $90^{\circ}$  out of phase and mounted  $0.4 \lambda$  above a wire mesh 105 feet in diameter and some 3 to 4 feet above ground level. The antenna pattern given by this system is essentially uniform at all altitudes and azimuths down to an elevation of  $20^{\circ}$ . Neale gives a more complete description of this meteor radar system.<sup>2</sup> An air view of the Springhill Meteor Observatory appears in plate 1.

Continuous recording of meteor echoes, using a range-time presentation, is made on 35-mm film. A sample record is reproduced in plate 2. Range markers appear as horizontal lines at 20-km intervals, the 100-km range markers being bright, the others dark. Individual seconds-markers appear at top and bottom of the record, with a more prominent marker every tenth second. The serial day number, 713, and the hour and minute of Universal Time, 06.18-06.19, are placed on the film above the trace each minute, while various calibration dials to check the performance of the equipment are photographed at the bottom of the trace every hour. The small triangular markers just below minimum range indicate the times when the

visual observers recorded visible meteors. On certain specified nights a team of eight observers manned the visual station and recorded all meteors seen, for correlation with the radar records.

Both the radio circuitry and the photographic recording unit of this equipment were designed to give maximum reliability of performance and uniform operating characteristics over long periods of time. The radar has been in operation on a 24-hour-per-day schedule since the beginning of October 1957, and the total time lost due to breakdowns of all kinds has been less than 3 percent.

The radar film is read by means of a specially designed viewer coupled with a standard IBM-024 alphabetic key punch. The complete unit is illustrated in plate 1. The projection of the film moves horizontally across the viewing screen past a transparent strip which carries the alphabetic range coding. The operator can vary the speed of motion with a knee pedal. The range of each meteor echo is recorded to the nearest 10 km from 70 km to 370 km. The durations of all echoes are also recorded on a 5-step scale— $<1$  sec, 1 to 2 sec, 2 to 4 sec, 4 to 8 sec, and  $\geq 8$  sec. This information is punched on primary data cards, which are then processed in the IBM-650 computer and give a set of 10-minute summary cards, on each of which the totals are recorded for a 10-minute interval. These cards then are put through the IBM-402 accounting machine, which gives a set of cards with hourly totals and a printed record similar to the one shown in plate 2.

A single sheet of this record tabulates the data for one-quarter of a day. Both individual 10-minute totals and hourly totals are repro-

<sup>1</sup> National Research Council, Ottawa, Ontario, Canada.

<sup>2</sup> M. J. Neale, "Radar Equipment for Continuous Meteor Observations," in press.

duced, the column headings being self-explanatory in most cases. The numbers and letters at the top of the range column correspond to the punching code used. The "CLASS LONGS" columns record the numbers of echoes in various duration classes. The nature of the interference evident on the film is coded in the next-to-last column. Since the sample reproduced here is from a period near the peak of the Geminid shower, both the echo rates and the proportion of long-duration echoes are considerably higher than average.

The data for the period from October 1957 through December 1960 have now been processed as described above, and approximately 4,400,000 meteor echoes were recorded during these 39 months. We have begun a detailed statistical study of this material and give here only a brief outline of some of the preliminary results.

The tabulated rates should be corrected for: (a) The personal equation of the film readers; (b) variation in the performance characteristics of the radar equipment; and (c) interference in the radar reception.

Information for finding correction (a) has been collected, but the correction itself has not yet been determined. In any case it will have little effect on the type of results reported here. The whole instrumental system was designed to keep correction (b) as small as possible, and we believe that, in general, this aim was achieved. The major exception is that, for some reason not entirely explained, the meteor radar seems to have operated somewhat more efficiently during the 1959-60 period than in 1957-58. No attempt has yet been made to allow for this.

A preliminary determination of correction (c) has been made by studying discontinuities in the mean diurnal rate curves, the variation in rates for specific local times in the day, and the variation in the ratios of long duration to total echoes. These data were correlated with the index figures for interference as estimated by the film readers, and a mean correction factor was found. It varies from 1.0 for no interference to 2.5 for maximum interference. In plotting diurnal rate curves the observed rates have been corrected by multiplying by this

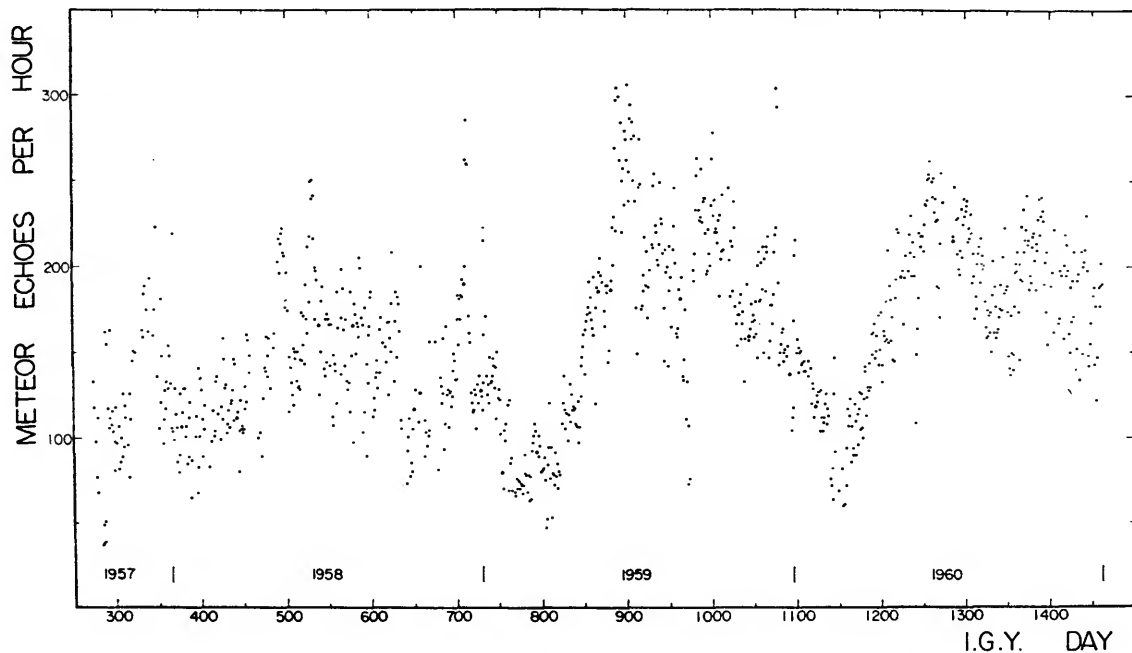


FIGURE 1.—The mean hourly echo rate for each day. The IGY serial day is numbered from 1 on January 1, 1957.

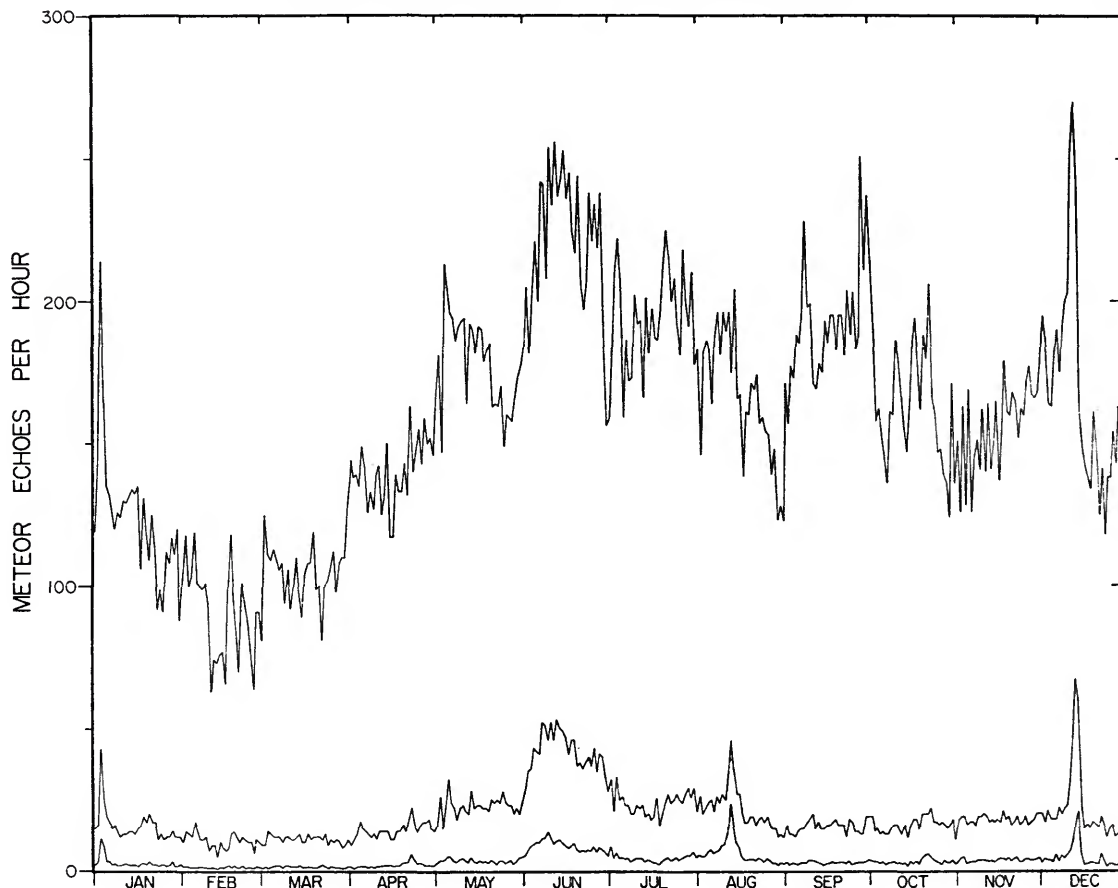


FIGURE 2.—The annual variation of mean hourly echo rate for each day: upper curve, all echoes; middle curve, echoes with durations 1 second or greater; lower curve, echoes with duration 8 seconds or greater.

factor. Periods where the correction factor was 2.0 or more have been omitted from the plotted results. If we consider only the cases where the rates were altered by more than 10 percent, for the first 18 months a correction was made in the case of 40 percent of the observed rates, while for the last 21 months, which were further removed from the sunspot maximum, a correction was made for less than 7 percent of the observed rates.

Uncorrected mean hourly rates of meteor echoes for each day are plotted in figure 1. The IGY serial day number is based on the system used at all the Canadian meteor and auroral stations where January 1, 1957, is taken as Day No. 1 and the days are counted

serially from then on. Note that the mean hourly rates for a day vary from a minimum near 50 during the first few months of each year to peak rates between 250 and 300 in June and December.

To give a general picture of the average variation in meteor rates throughout the year, the values from figure 1 were averaged for each calendar day and are plotted as the upper curve in figure 2. Below this are plotted the mean hourly rates for each day for all echoes with durations of 1 second or greater, and all echoes with durations 8 seconds or greater. Most of the minor fluctuations in these curves are probably accidental and should not be considered as particularly significant. Some of the major

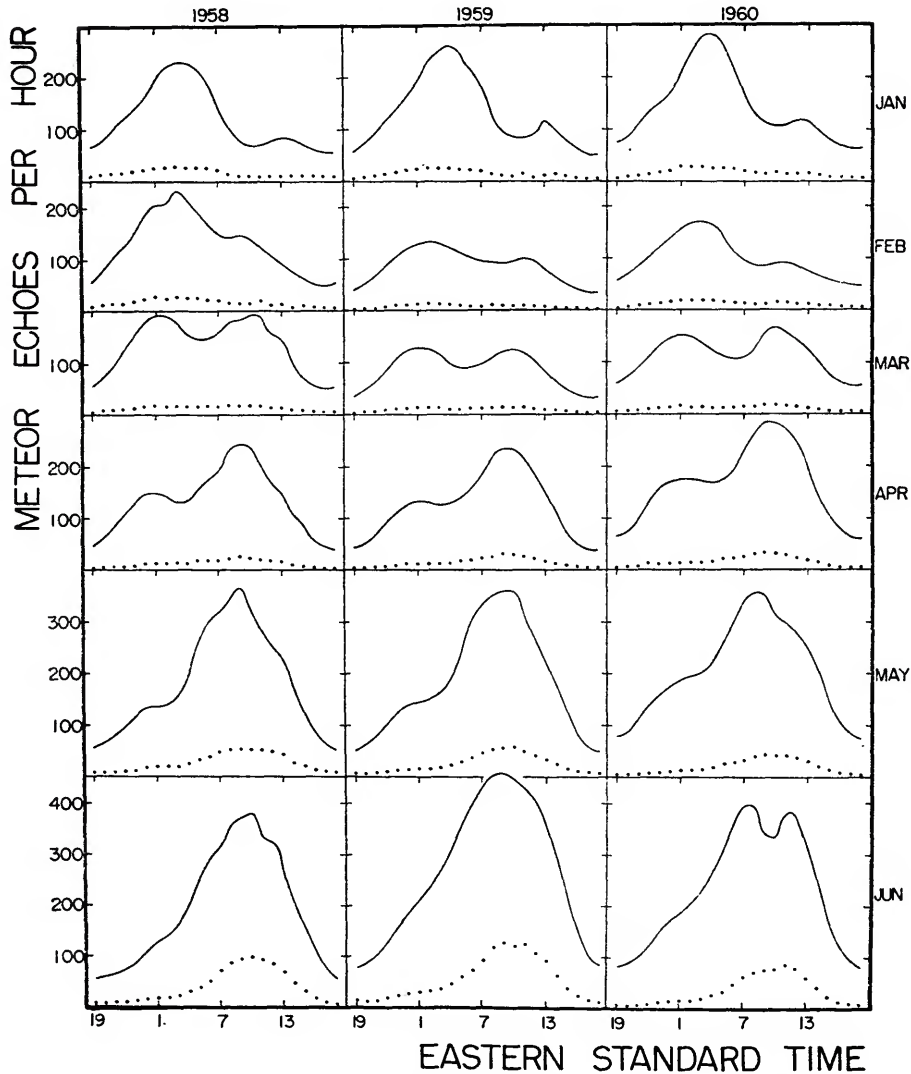


FIGURE 3.—The monthly mean diurnal echo rate curves for January to June: solid line, all echoes; dots, echoes with durations 1 second or greater.

showers, however, stand out clearly, particularly for the lower curves of the long-duration echoes. Good quantitative values for the percentage of meteors in each of these showers must await a much more detailed study of the tabulated records, but qualitative values can be found from figure 2, and are listed in table 1. Eleven well-marked shower peaks were chosen, including the strong daylight shower complex in June, and, in addition, two other peaks near September 8 and September 30. An attempt was made

to estimate the background rate, excluding these major showers, and the values read are given in the first half of the table. The second half of the table shows the peak rates that correspond to the shower meteors only.

It is necessary to remember here that all these rates are based on averages for a complete day. In cases where a shower radiant is below the horizon or at low elevation for part of the day, the peak strength of the shower will appear smaller in the table than it actually is.



Springhill Meteor Observatory near Ottawa, Ontario. The meteor radar antennas appear in foreground and left background. The visual observing station is at upper right.



Meteor radar film reader coupled with IBM-024 alphabetic key punch.



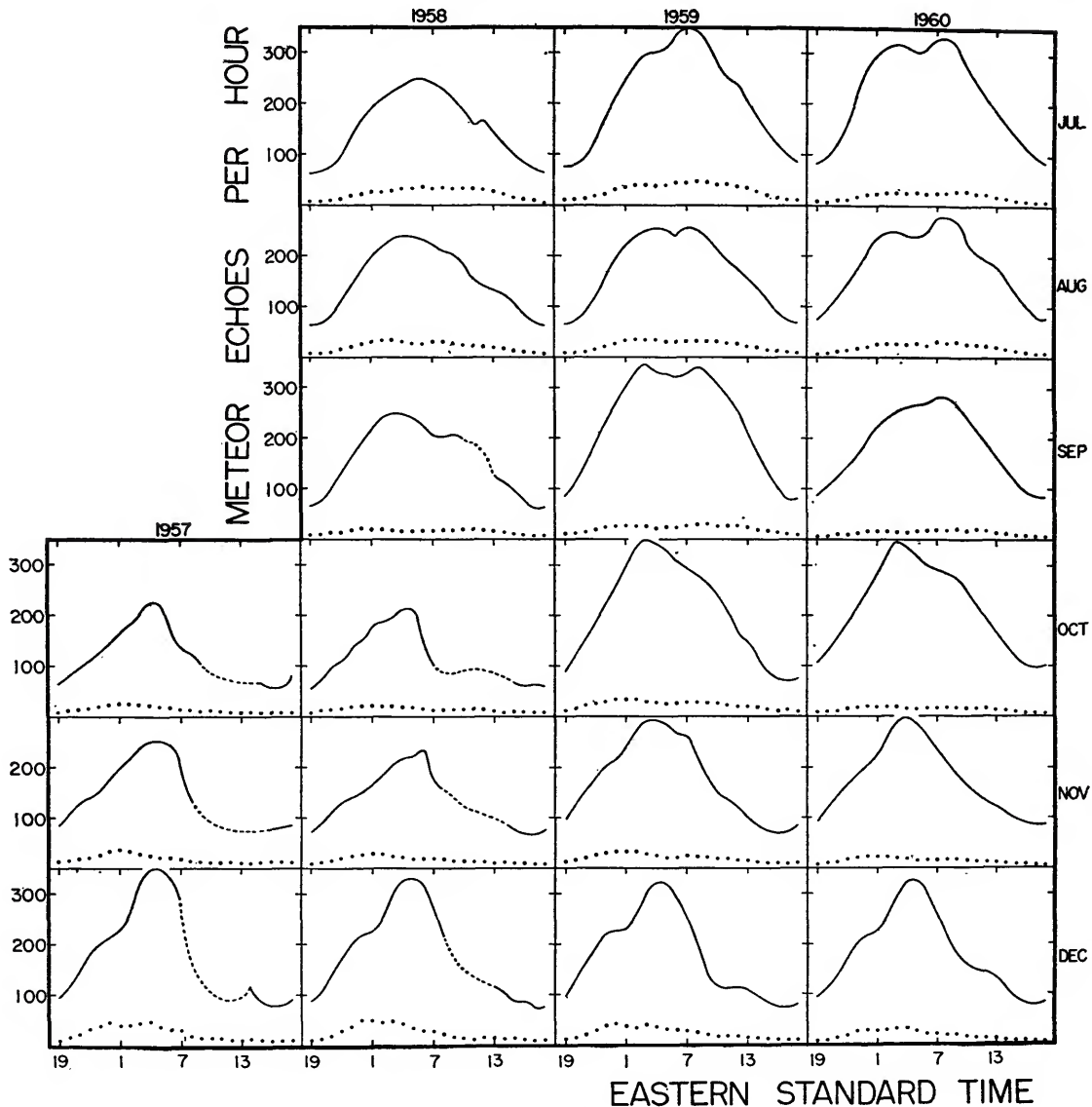


FIGURE 4.—The monthly mean diurnal echo rate curves for July to December: solid line, all echoes; dots, echoes with durations 1 second or greater.

On the basis of the absolute numbers of all echoes, the Geminid shower is by far the strongest, followed by the Quadrantid shower, the June showers, and the peak at September 30. But if we look at the long-duration echoes only, we see that Perseids and Geminids are about equal in strength, while the Quadrantids and June showers are only half as strong, and the rest of the showers much weaker still.

When we study the differences between the meteors of the major showers and those of the general background, the percentage of long-duration echoes is of particular interest. These have been listed in parentheses in table 1. For the background, roughly 10 percent of all echoes have durations 1 second or greater, and 2 percent have durations 8 seconds or greater. We see immediately that most of the showers

TABLE 1.—Mean hourly echo rate for 1 day

Date	Shower	Background echoes			Shower echoes		
		all	≥1 sec	≥8 sec	all	≥1 sec	≥8 sec
Jan. 3	Quadrantid	135	14	2	79	29(37)*	9 (11)
Jan. 20		110	11	1.5	—	—	—
Feb. 20		90	10	1	—	—	—
Mar. 20		105	11	1	—	—	—
Apr. 22	Lyrid	146	16	2	17	6(35)	3.5(20)
May 5	γ Aquarid	160	17	2.5	53	15(28)	2.5 (5)
Jun. 11	Daytime	169	17	3.5	81	35(43)	9.5(12)
Jul. 29	δ Aquarid	170	17	3.5	40	11(28)	2.5 (6)
Aug. 12	Perseid	169	17	3.5	31	29(94)	19.5(63)
Sep. 8	Orionid	165	17	3.5	50	2 (4)	0.5 (1)
Sep. 30		161	16	3	79	3 (4)	0.5 (1)
Oct. 22		156	16	3	49	6(12)	3 (6)
Nov. 20	Geminid	150	16	3	—	—	—
Dec. 13		142	15	2.5	128	52(41)	18.5(14)
Dec. 22		Ursid	137	14	2	13	5(38)
Mean		145	14(10)	2.5(2)			

\*Figures in parentheses are long-duration echo percentages in each category.

have a very much higher percentage of long-duration echoes. The Perseid shower is quite unique in this respect, with over 90 percent of its members having echoes of duration 1 second or greater, and over 60 percent, 8 seconds or greater. Most of the rest of the showers have from 30 to 40 percent of echoes with durations of 1 second or greater, and 10 to 20 percent, 8 seconds or greater. The Orionids and the two September peaks seem to have about the same percentage of long-duration echoes as the background.

A mean diurnal hourly rate curve was now drawn for each month, and corrected for interference using the correction factor described earlier in this paper. These curves, for the entire 39 months, are reproduced in figures 3 and 4. The solid lines represent values for all echoes, and the dots represent echoes with durations of 1 second or longer. Where heavy interference prevented the use of data for more than half the days in a month, the solid line is replaced by a broken line. Examination of the diurnal curve for December 1957 makes it quite obvious that the mean interference correction factor used was not adequate to correct for the actual interference experienced

on this occasion. The problem of correcting for interference became much less acute in 1959 and 1960.

We do not here propose to discuss the monthly diurnal rate curves in detail. Despite various fluctuations from year to year, it is clear that the diurnal curve for any given month shows certain general characteristics throughout. This is true both for all echoes recorded and for the much smaller quantity of data represented by the long-duration echoes. The two diurnal maxima which appear near the equinoxes are particularly prominent in March. The first of these maxima, in the early morning hours, tends to be more prominent before March; the second, during the daylight hours, becomes stronger after March and has a high absolute value as the complex of summer daylight showers becomes evident. The diurnal peak for the long-duration echoes does not always coincide with that for all echoes. This is particularly true in the last quarter of the year, and is no doubt due in part at least to the effect of showers. The general shape of the curves for all echoes reproduced in figures 3 and 4 bears a remarkable similarity to the

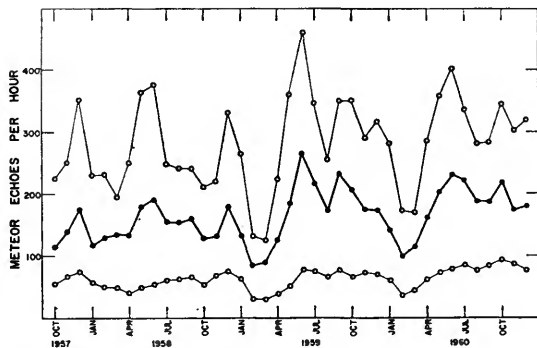


FIGURE 5.—Monthly mean rates for all echoes: top curve, diurnal peak rate; middle curve, overall average rate; lower curve, diurnal minimum rate.

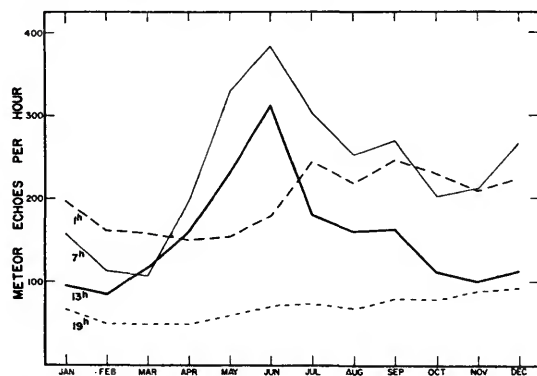


FIGURE 6.—Monthly mean rates for all echoes taken at 4 specific hours of E.S.T.

predicted diurnal curves computed by Hawkins,<sup>3</sup> although the latter were plotted for assumed observational conditions somewhat different from those of the Canadian program reported here.

The mean hourly rates for each month, together with the peak rates and minimum rates taken from the curves of figures 3 and 4, are

<sup>3</sup> G.S. Hawkins, "A Radio Echo Survey of Sporadic Meteor Radiants." *Monthly Notices Roy. Astron. Soc.*, vol. 118, pp. 92-104, 1956.

plotted in figure 5. Here the high peak rates in June are a prominent feature, together with the December peaks and less regular ones in September and October. In the minimum rates the low values during February and March stand out.

To illustrate the changes that occur throughout the year in meteor activity for various hours in the day, the monthly mean rates for four specific hours of E.S.T. are plotted in figure 6. The highest rates definitely tend to occur near 7 hours and the lowest near 19 hours. Here again the high rates for the daylight hours in June are outstanding. The mean rate for 1 hour is definitely higher for the last half of the year, but does not show as much variation as might have been expected.

We have begun a much more detailed study of all these observational data. In particular, the analysis of the range distribution will make it possible to estimate with much greater accuracy both the contributions and the individual characteristics of the various showers. Correlation with the visual observations will aid in calibrating the radar records in relation to the visual data.

#### Acknowledgments

Many individuals have contributed to the success of this Canadian IGY-IGC program. M. J. Neale was chiefly responsible for the design of the meteor radar equipment, and members of the staff of the Upper Atmosphere Research Section at NRC constructed and maintained it. Those assisting with the film reading and the IBM processing include Miss A. M. Baker, Mrs. S. Baron, Mrs. H. Bone, Mrs. E. Bradley, Miss J. Fagen, Miss D. Gibson, Mrs. H. MacLean, Mrs. M. McCall, Mrs. D. M. McKiernan, Miss M. Panet, Miss J. Proudman, and Miss M. Watson.

#### Abstract

A meteor patrol radar equipment was put in operation at Springhill Meteor Observatory near Ottawa at the beginning of October 1957, and a continuous recording of meteor echoes has been carried out since this date. The antennas are omnidirectional, with operating frequency 32.7 mc/sec and peak power 20 kw. Echoes are recorded on 35-mm film in the form of a range-time record. Echo counts for each 10-minute interval, echo ranges and durations, and the intensity of background noise are punched manually on IBM cards from the film record.

All film has been read for the 39 months of operation from October 1, 1957, to December 31, 1960, and over 4,400,000 meteor echoes have been recorded. Mean hourly echo rates range from a diurnal minimum of less than 100 to a diurnal maximum which in June at 8<sup>h</sup> local time may be over 400. The maxima of the major meteor showers show up more distinctly in the rates for the long-duration echoes. There is a tendency for the shape of the monthly mean diurnal rate curve to repeat itself in the same months for successive years.



# The Harvard Radio Meteor Project <sup>1</sup>

By Gerald S. Hawkins <sup>2</sup>

The Radio Meteor Project has been described by Whipple and Hawkins (1956). It is a multistation radar system in which a pulse train is reflected from the ion column of a meteor. The strength of the echo varies with time and the pulses form a Fresnel pattern as described by Davies and Ellyett (1949). The velocity of the meteor can be found from the period of amplitude variations and the measured range, while the angle of approach of the meteor is given by the time delay between the stations. Thus the velocity, radiant, and orbit of individual meteors can be found. Gill and Davies (1956) developed a 3-station system for measuring orbits at Jodrell Bank Experimental Station in England. The Harvard system has been designed to give the same data as the Jodrell Bank equipment and in addition to provide a measurement of height, deceleration, and distribution of ionization along the trail. A high sensitivity was chosen to make possible the detection of meteors at magnitudes +12, some three magnitudes fainter than the limit of Gill and Davies.

## Construction of the system

The work carried out during the construction period has been described (Whipple and Hawkins, 1960). The completed system is shown in figure 1. The various components of the system are described below.

*Antenna.*—A double trough antenna was used at the main site. Two 13-element Yagis were used at the remote sites. Figure 2 shows a sketch of the double trough, and a photograph of this antenna is shown in plate 1.

The antenna pattern for the single trough is shown in figures 3 and 4; the measurements were obtained from a scale model. The main beam, directed at azimuth 113° E of N, has an elevation of 43°, and the side lobes are more than 20 db below the gain of the beam center. The antenna pattern of the double trough in the vertical plane is also represented by figure 3, while the horizontal pattern is shown in figure 5. These patterns were obtained from measurements on the model antenna. The beam width between half-power points is  $\pm 14^\circ$  for the double trough, and  $\pm 25^\circ$  for a single trough. The double trough antenna is used both for transmission and reception and a TR/ATR switch is used to effect the changeover.

*Receivers and radio links.*—Superheterodyne receivers with an intermediate frequency of 3 mc were used. Each receiver was fed from a voltage stabilizer.

The microwave units were standard Raytheon links (MCR-1000) with a transmitter power of 1 watt. The pulses were carried on the links at IF frequency of 3 mc to the Long Branch field site of the Bureau of Standards at Havana, Ill.

*Frequency controls, gate circuits, and display units.*—The master oscillator unit, containing the time base generator, the 150 kc oscillator, and the associated divider units are all housed in the console, shown in plate 1. Plate 2 contains a close-up view of the coaxial lines feeding the double trough antenna, and also a view of the gating, triggering, and bright-up equipment. The Fresnel and range pulses were displayed on single-beam, three-inch tubes.

## Computing program

A detailed computational program had been prepared for the IBM-704 computing machine (Whipple and Hawkins, 1956). The reduction

<sup>1</sup>This research was supported by Lincoln Laboratory, MIT, AF19(122)-458/57; National Bureau of Standards, CST-7282, CST-7067; and National Science Foundation Grant G-14699. It was published in detail as Harvard Radio Meteor Project Final Report of CST-7282, Dec. 13, 1957, to June 30, 1961.

<sup>2</sup>Harvard College Observatory, Cambridge, Mass., and Boston University, Boston, Mass.

HARVARD RADIO METEOR PROJECT STATION , BLOCK DIAGRAM

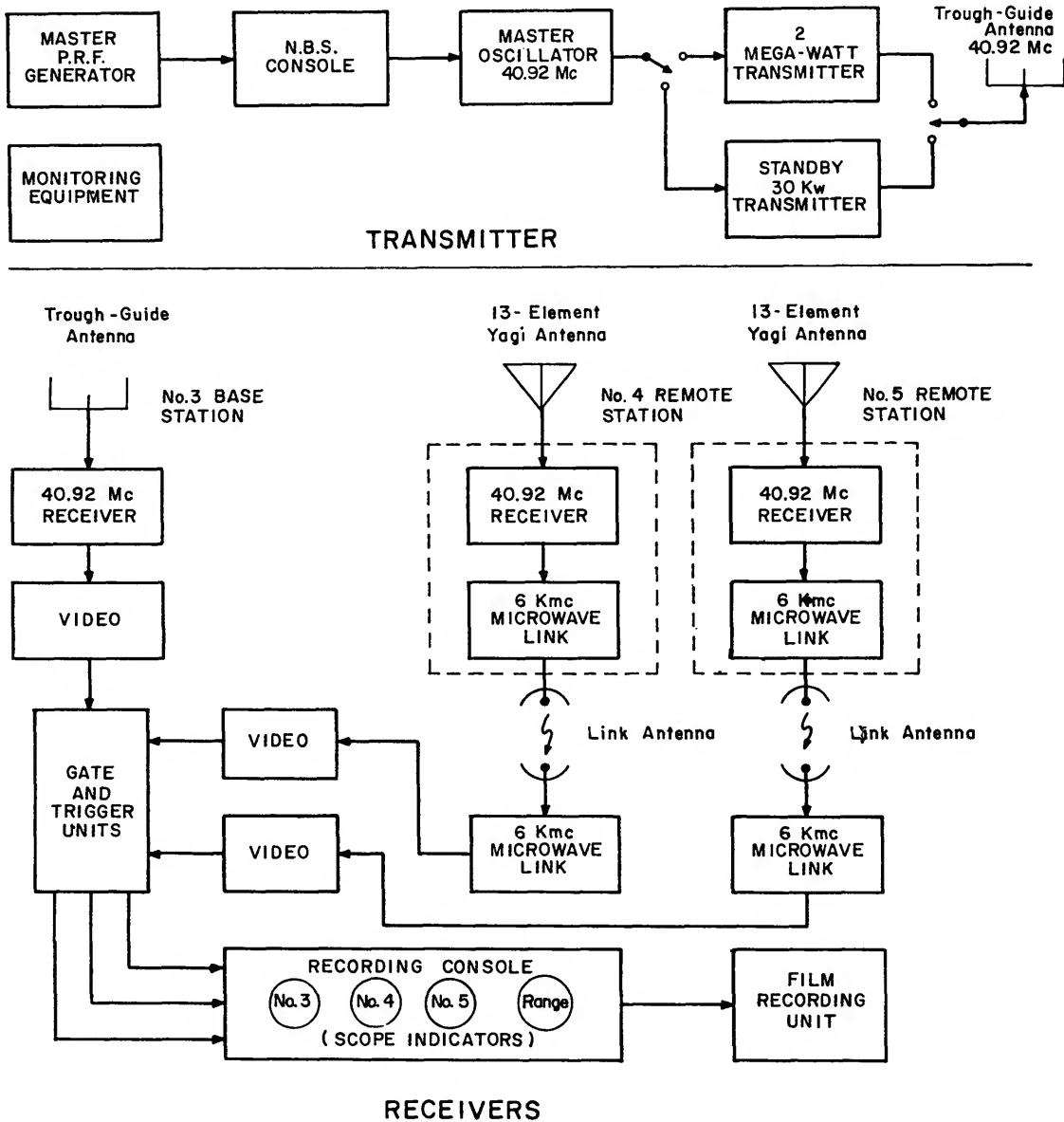


FIGURE 1.—Diagram of Harvard radio meteor project system.

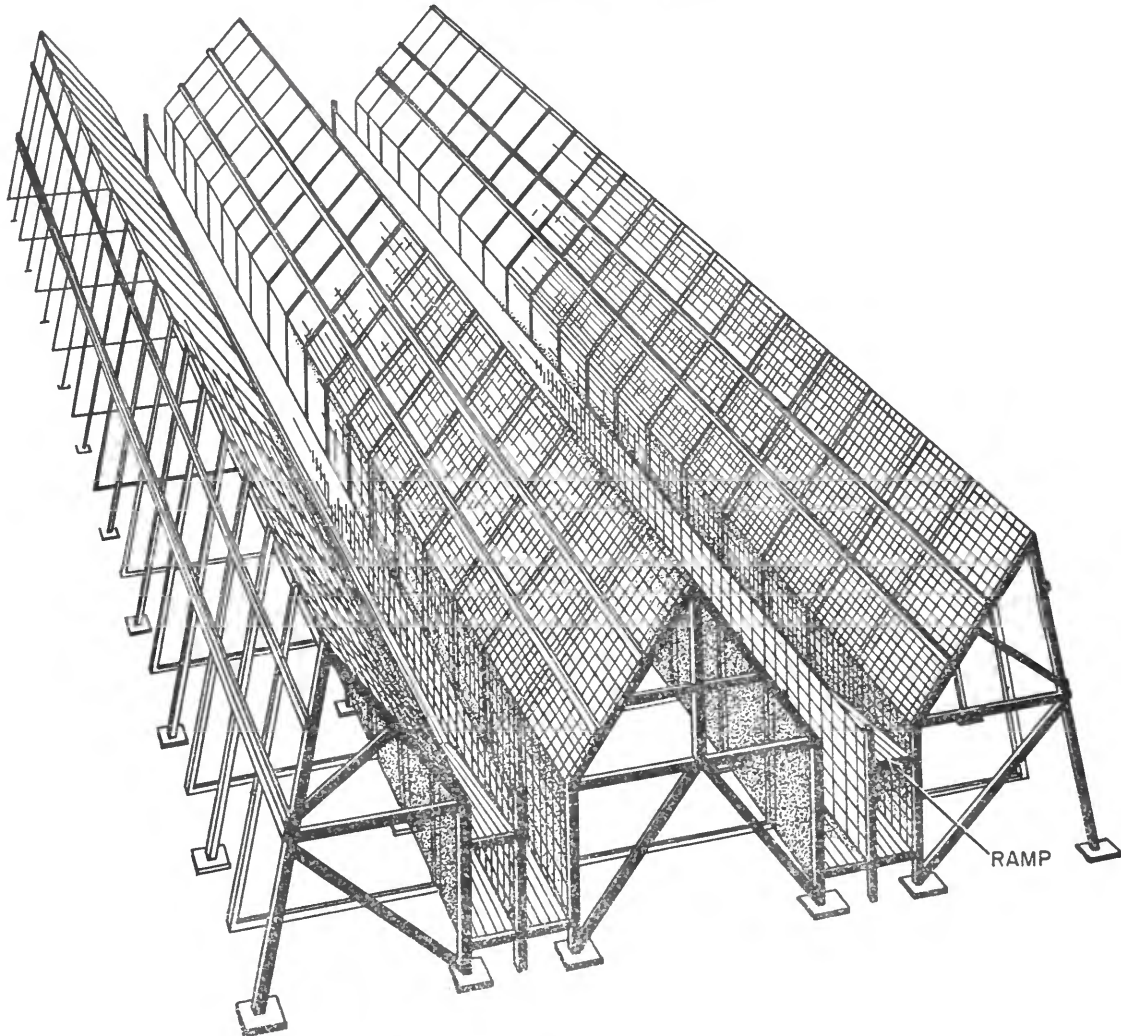


FIGURE 2.—Artist's sketch of double trough antenna.

of the Fresnel patterns is based upon a comparison of the measured pattern with the set of theoretical Fresnel patterns derived by Loewenthal (1956). By comparing the observations with the theoretical pattern, the 90 percent confidence limits are computed for each Fresnel pattern. In this way we can determine whether or not significant deceleration has taken place.

The program was converted from IBM-704 to IBM-7090. A Benson-Lehner film viewer complete with digitizer was used and this was coupled to an IBM card punch.

The majority of the records were obtained with the National Bureau of Standards Collins transmitter with a power output of 25 kilowatts. A small amount of filming was carried out at a power level of 1 megawatt. We estimate the limiting visual magnitude was +6 for the low-power transmitter and +9 for the high-power transmitter.

### Results

A total of 407 meteors has been completely reduced to give radiants, velocities, and orbital parameters, and the results were published in

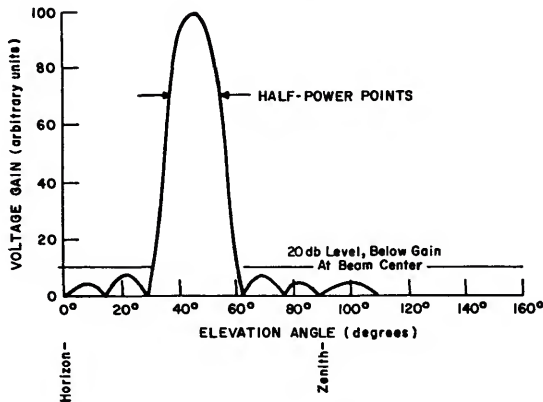


FIGURE 3.—Single trough antenna gain pattern (voltage), vertical plane.

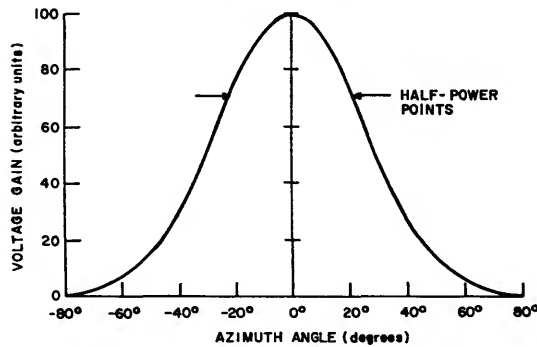


FIGURE 4.—Single trough antenna gain pattern (voltage), azimuthal plane.

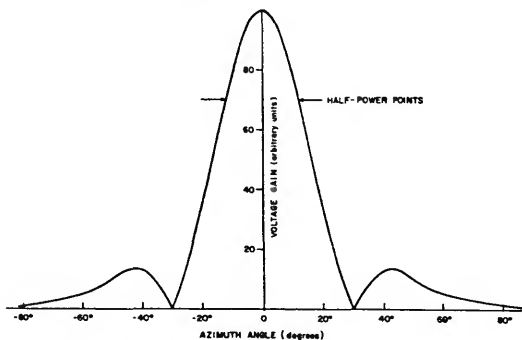


FIGURE 5.—Double trough antenna gain pattern (voltage), azimuthal plane. (Pattern measured from model by Radiation Engineering Laboratory.)

condensed form (tables 1 and 2, Whipple and Hawkins, 1961). Before proceeding with the discussion of the results we give a histogram of observing hours in figure 6, since our observing

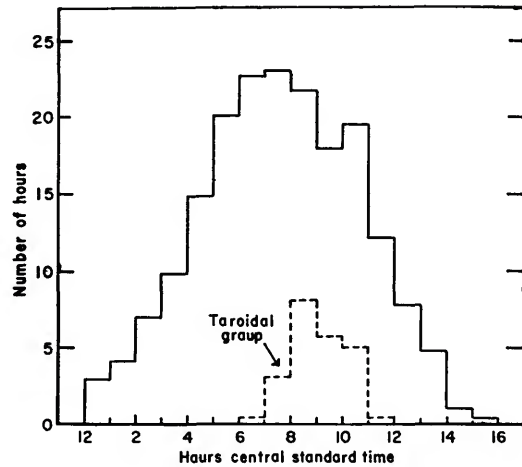


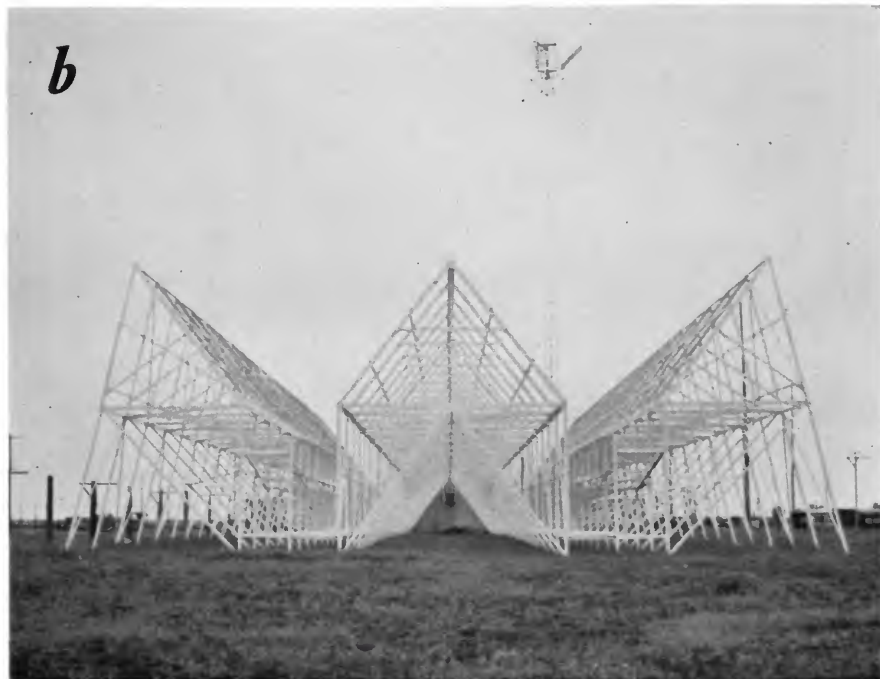
FIGURE 6.—Histogram of hours of observation.

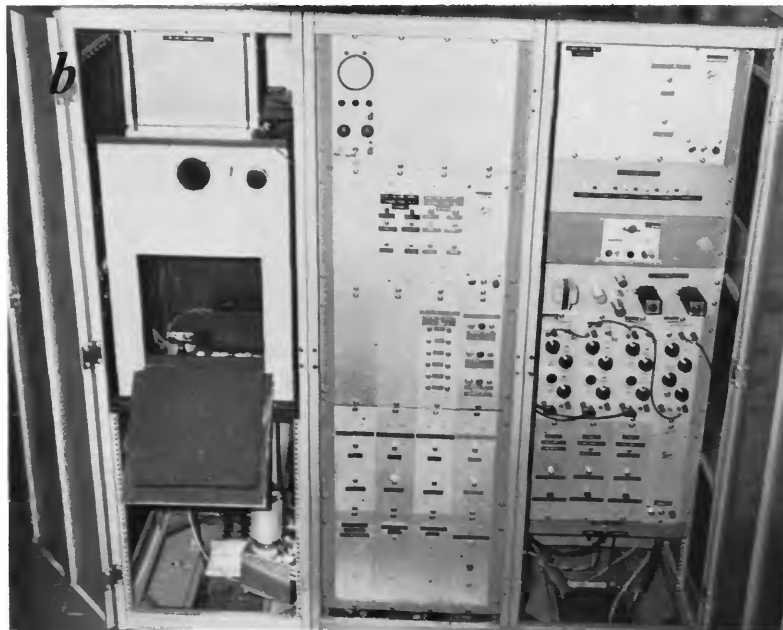
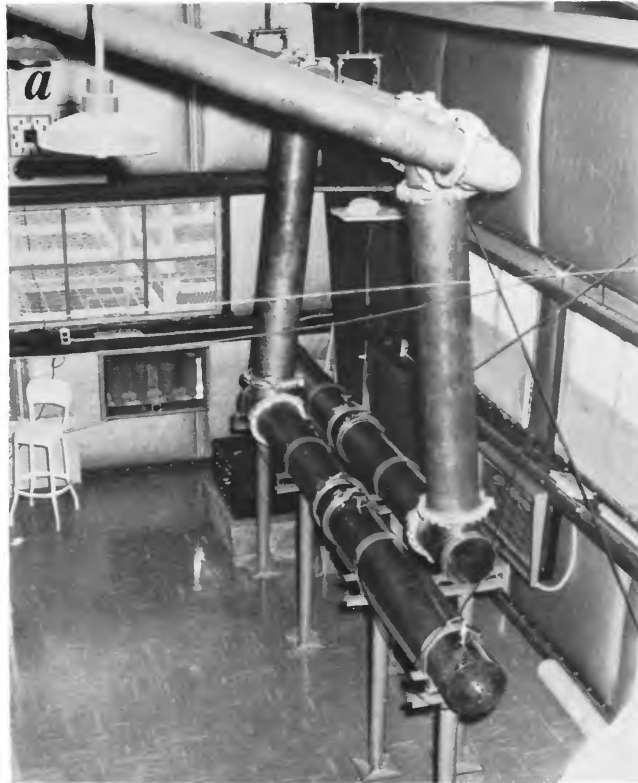
periods will introduce a statistical bias unless we operate on a continuous 24-hour schedule. Not all of the films have been analyzed and the histogram therefore covers only those films selected for analysis. Our observations were made most frequently between 4.00 and 11.00 hours Central Standard Time. This non-uniform coverage was due to many factors, mainly electrical interference. Our observers found that interference was more intense during the daylight hours from 11.00 to midnight, and we therefore chose to operate during the early morning hours when our yield of echoes was higher. We decided that this coverage was satisfactory for preliminary work since we were observing both the antisolar radiants and the apex area of the sky.

The distribution of velocity is given in figure 7. The most frequently observed velocity was between 30 and 35 km/sec, which coincides with the peak found by other radio investigators. The histogram from the Harvard Radio Meteor Project differs markedly from other radio data at the high-velocity end. The Harvard data contain few meteors with velocities greater than 50 km/sec, whereas other observers have found a subsidiary peak between 50 and 70 km/sec. We attribute this difference to a statistical bias in the Harvard data due to the fact that our observations were made during the months of December, January, February, March, and April. At this time of the year the apex of the earth's path is in a low declination region of the



*a*, Console housing the master oscillator unit. *b*, Double trough antenna.





*a*, Close-up view of the coaxial lines feeding the double trough antenna. *b*, View of the gating, triggering, and bright-up equipment.

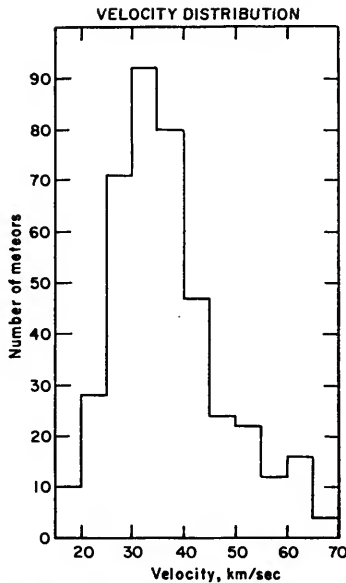


FIGURE 7.—The distribution of velocity.

ecliptic. Our sensitivity decreases as the radiant altitude decreases, and thus our observations of the apex will not be representative until the latter part of the year. The poor observability of low altitude radiants is shown clearly in figure 8, which gives the distribution of observed declinations. At the latitude of the Long Branch Site a radiant with a declination of  $-50^\circ$  never rises above the horizon. A radiant with  $0^\circ$  declination has a maximum altitude of  $50^\circ$ , and one with  $+30^\circ$  declination is in the zenith. Photographic and visual

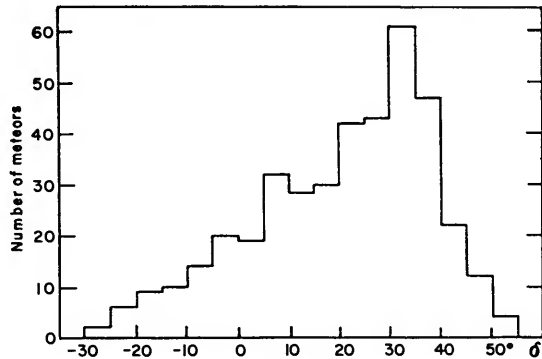


FIGURE 8.—Distribution of observed declinations.

observations have shown that the radiants are fairly uniformly scattered over the sky and that there is a broad concentration of radiants between declinations  $-30^\circ$  and  $+30^\circ$ . We presume that the discrimination of our system against low altitude radiants has caused this asymmetry in the distribution of declination. During the period of observation covered in this report the apex was between declination  $0^\circ$  and  $-23^\circ$ , and the number of meteors observed from this region of the sky was therefore considerably reduced.

Figure 9 shows the distribution of the semi-major axes of the orbits. We have chosen  $1/a$  as our parameter rather than  $a$  since the observational errors in  $1/a$  are almost constant. The most frequent value of  $a$  is 1.0 in our data, whereas the corresponding value obtained at Jodrell Bank was 3.0. In the Harvard data

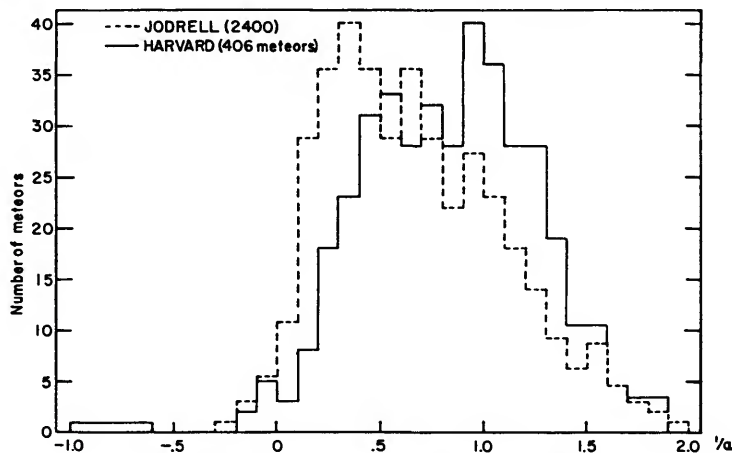


FIGURE 9.—Distribution of the semimajor axes.

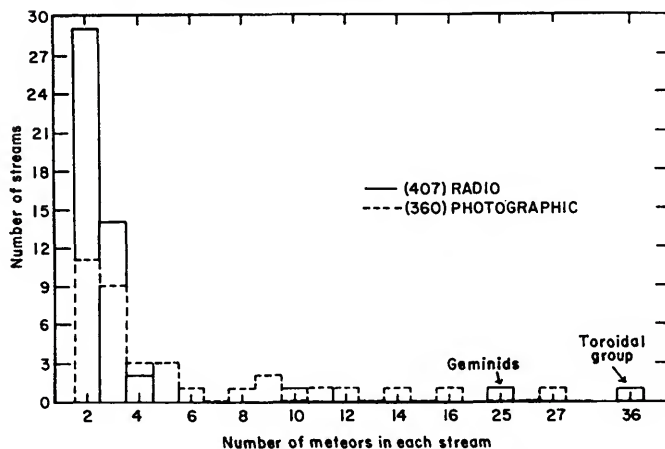


FIGURE 10.—Meteor groups separated by small differences in their orbital elements.

no correction has as yet been made for the deceleration of the meteor in the atmosphere. This deceleration is thought to be insufficient to account for the difference in the two distributions. A small fraction (3 percent) of the orbits in the Harvard survey was hyperbolic. We do not consider this percentage significant; it is the value to be expected from the error in velocity determination.

Southworth (Hawkins and Southworth, 1960) has applied a criterion for identifying minor streams amongst the orbits in this survey. The orbital data were put on punched cards and sorted so as to find meteor groups which were separated by small differences in their orbital elements. The results are shown in figure 10. From the 407 orbits tested, 53 groupings were found. This compares with a total of 35 groups found from a similar search of 360 Super-Schmidt orbits. The percentage of streams in the two sets of data is comparable because allowance must be made for the larger number of radio orbits and the fact that these orbits were concentrated in a 4-month period of the year.

One of the streams found by this automatic selection was, of course, the Geminids of December. This well-known major stream of the nighttime sky serves as a useful check on the radio system. The mean radiant and velocity for twelve Geminids is given in table 1. For comparison we include the mean value of the

Geminids obtained from the Super-Schmidt camera data (Hawkins and Southworth, 1958). The agreement in the radiant distribution is satisfactory, though the difference in declination is a little larger than we would expect. The difference in velocity shows the effects of deceleration; the photographic data have been corrected for deceleration whereas the radio data have not been corrected. Thus we may assume that the average deceleration of the radio meteors in this sample of Geminids is 2.3 km/sec.

TABLE 1.—Geminid data

	Radiant Position		Velocity km/sec
	R.A.	Dec.	
Radio	110°9	+35°0	33.7
Photo	111°4	+32°5	36.0

The stream with the largest membership (36 meteors) represents a very complex system of orbits of high inclination and small eccentricity. These orbits were similar to those found by Davies (1957) in the survey conducted at Jodrell Bank. This grouping of meteors is shown more clearly in figure 11, where we have plotted the distribution in inclination for three values of  $e$ . As the eccentricity of the orbit is

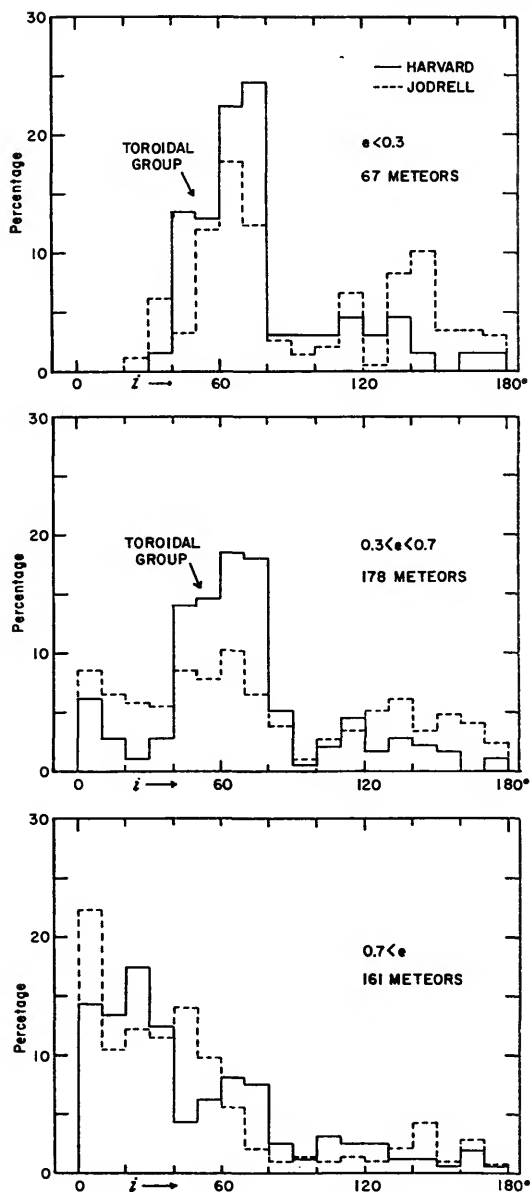


FIGURE 11.—Inclination distribution of meteors.

decreased, there is a tendency for the meteors to occur with inclinations of approximately  $60^\circ$  to the plane of the ecliptic. For comparison we show the Jodrell Bank results, and the agreement is good, though the Harvard data contain a higher percentage of the circular, inclined orbits in the intermediate values of

eccentricity. These orbits are difficult to account for in terms of our present ideas of interplanetary material. Previously the photographic observations had shown a marked concentration of meteor orbits in the plane of the ecliptic, and the high inclination orbits were not detected in any great numbers. For convenience we call this set of orbits the "toroidal group" because the orbits form a cylindrical toroid in space.

The time of appearance of the toroidal group is concentrated at 9.00 hours Central Standard Time, as can be seen from figure 6. Thus the radiant points of this group are approximately at the same longitude as the apex of the earth's path, since the apex passes through the sensitive sector between 9.00 hours and 10.00 hours Central Standard Time.

As far as we can tell there is no reason why the photographic survey should not have located this type of orbit. The radiant occurs at the same longitude as the apex, some  $30^\circ$  north and south of the ecliptic. Figure 12 shows the distribution of radiant points obtained in the photographic survey (Hawkins and Southworth, 1958) plotted in ecliptic coordinates with the sun chosen as a fixed zero point. The photographic data contain a concentration of radiants north of the apex, but the orbits of these meteors were not circular in nature as the ones found by the radio survey.

We do not think that the high inclination orbits found by the radio survey are a result of selection effects due to the orientation of the antenna. To investigate this possibility we have plotted in figure 13 the position of radiants on an altitude-azimuth diagram together with the position of the sensitive sector of the antenna. From the diagram we see that the radiants of meteors are uniformly scattered along the sector (the lack of meteors in the northern half of the sector is caused by our early-model triggering system which could only record meteors coming from the southern quarter of the sky). The radiant points of the high inclination near-circular orbits are scattered fairly uniformly around the sector in a manner similar to that of the other types of orbits. Thus we cannot attribute this grouping of orbits to a side lobe or to an area of high sensitivity in our antenna sector.

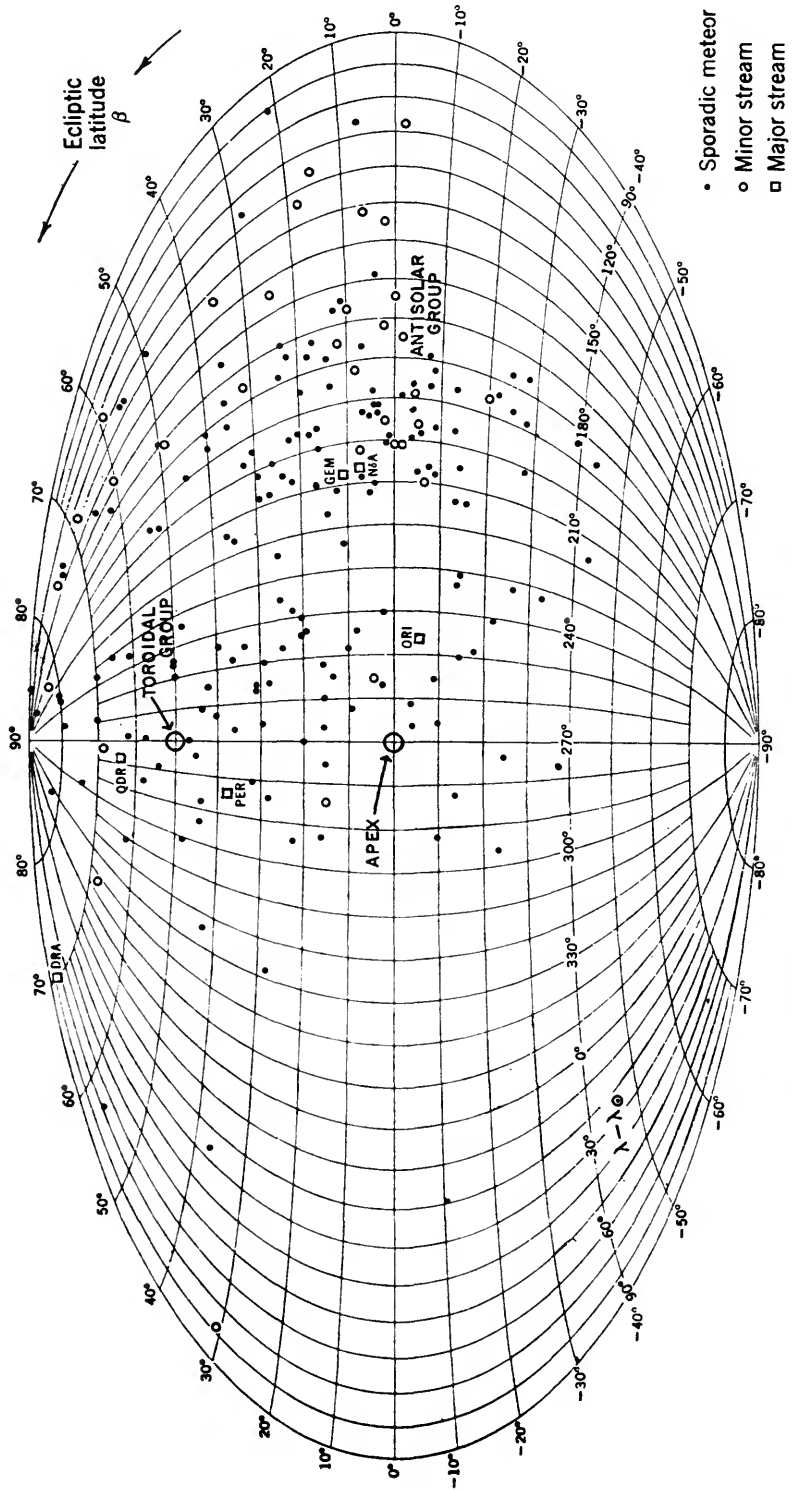


FIGURE 12.—Distribution of radiants of major streams, minor streams, and sporadic streams.

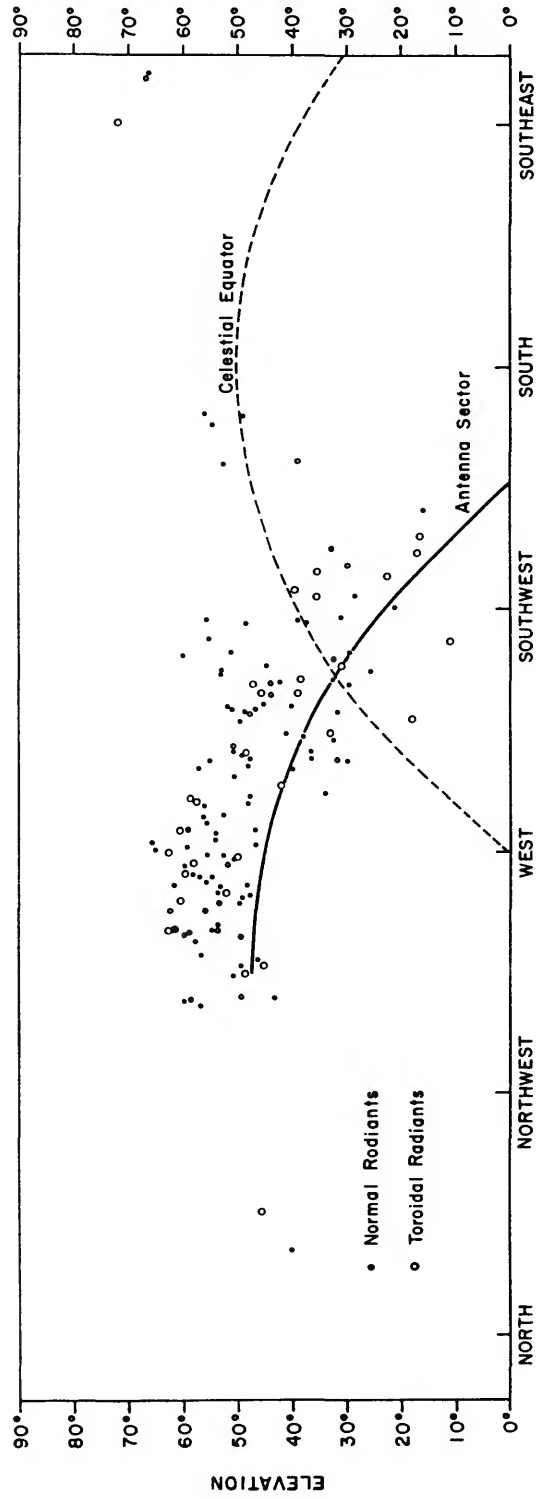


FIGURE 13.—Position of radiants.

## References

- DAVIES, J. G.  
 1957. Radio observations of meteors. *In Advances in Electronics and Electron Physics*, vol. 9, pp. 95-128. Academic Press, New York.
- DAVIES, J. G., AND ELLYETT, C. D.  
 1949. The diffraction of radio waves from meteor trails and the measurement of meteor velocities. *Phil. Mag.*, ser. 7, vol. 40, pp. 614-626.
- GILL, J. C., AND DAVIES, J. G.  
 1956. A radio echo method of meteor orbit determination. *Monthly Notices Roy. Astron. Soc.*, vol. 116, pp. 105-113.
- HAWKINS, G. S., AND SOUTHWORTH, R. B.  
 1958. The statistics of meteors in the earth's atmosphere. *Smithsonian Contr. Astrophys.*, vol. 2, no. 11, pp. 349-364.  
 1960. Statistics of meteor streams. Interim Report No. 44, Harvard Radio Meteor Project, Harvard College Observatory, Contract AF 19(122)-458, Subcontract no. 57.
- LOEWENTHAL, M.  
 1956. Meteor echoes from underdense trails at very high frequencies. Technical Report no. 132, Massachusetts Institute of Technology, Lincoln Laboratory.
- WHIPPLE, F. L., AND HAWKINS, G. S.  
 1956. The Harvard radio meteor program. Final Summary Report, Harvard Radio Meteor Project, Harvard College Observatory, Contract AF 19(122)-458, Subcontract no. 57.  
 1960. Radio meteor project. Final report, Harvard Radio Meteor Project, Harvard College Observatory, Contract CST-7067.  
 1961. Harvard radio meteor project. Final Report, Harvard Radio Meteor Project, Harvard College Observatory. Contract CST-7282.

# Meteor Rates Observed by Radio-Echo Techniques During the IGY-IGC Period

By B. L. Kashcheyev<sup>1</sup> and K. V. Kostilyov<sup>2</sup>

Meteor rates were measured at the Kharkov Polytechnical Institute according to the IGY-IGC program. The measurements were started in December 1957. The wavelength used was 8 meters. Twice since the beginning of the measurements new types of antenna systems have been introduced, and the sensitivity of the receiving equipment has also been increased.

During the first period, from December 1957 to August 1958, a 5-element director antenna and a half-wave dipole were employed; in the second period, from September 1958 to March 1960, an 8-element director antenna and a half-wave dipole were employed for transmission and reception, respectively. During the third period, since April 1960, 5-element director antennas have been used for both transmission and reception. During the observation period the antenna systems were usually oriented eastward.

The sensitivity of the equipment and the analysis of the records show that during the first period mentioned the overwhelming majority of echoes recorded had an absolute visual magnitude brighter than  $+6^m.5$ . For the second period this critical value lay between  $+7^m.5$  and  $+8^m.0$ , while for the third period it was  $+9^m$ . The successive improvements in the equipment resulted in an increase in the diurnal rates of meteors recorded, which were about 1,800, 4,000, and 8,400 for the three periods, respectively.

From December 1957 to December 1960 observations were made during 330 24-hour periods and about 1,300,000 echoes were recorded, some 85,000 of which had a duration of more than 1 second. About 10 to 15 percent of

the echoes can be attributed to major meteor streams—primarily the Arietids, Geminids,  $\delta$  Aquarids,  $\eta$  Aquarids, Perseids, Lyrids, and others. The rest can be attributed to sporadic meteors and the numerous minor meteor streams that cannot be distinguished from the sporadic background unless highly directive antennas are used for the meteor-rate measurements.

It is worth noting that the Perseid stream, although one of the most active for photographic and visual observations, produces a scarcely noticeable increase in the general number of radio echoes. On the other hand, the Perseid stream is clearly discernible because the radio echoes produced by Perseid meteors have a duration of more than 1 second. This can be explained by the fact that high-velocity meteors with a brightness less than  $+5$  magnitude produce weak radio echoes, and that there are few faint meteors in the Perseid stream (Kresáková, 1958). Radio-echo techniques lead to discoveries of new meteor streams that cannot be observed by optical methods. The highest meteor rates are produced by the Arietid stream. Next highest are those of the Geminid, Quadrantid, and other streams that are well known from optical observations.

At the Engelhardt Astronomical Observatory in Kazan, systematic radio-echo measurements of meteor rates were made with fixed and rotating antennas (Kostilyov, 1958). The fixed antenna was directed to the west and the wavelength was 4.2 meters. With the rotating antennas two wavelengths were used:  $\lambda_1=4.2$  meters and  $\lambda_2=8.7$  meters. The antenna system was rotated in steps of  $30^\circ$ , and stayed in each position for 5 minutes. Thus during 1 hour the antenna system turned  $360^\circ$  in a

<sup>1</sup> Kharkov Polytechnical Institute, U.S.S.R.

<sup>2</sup> Kazan State University, U.S.S.R.

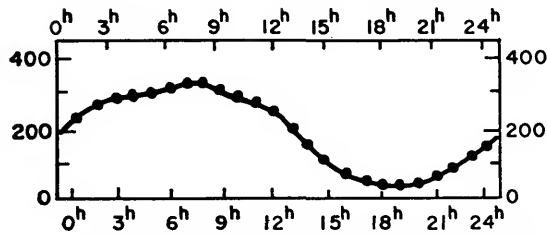


FIGURE 1.—Yearly means of diurnal variations of meteor rates as measured in Kharkov in 1959 ( $\lambda=8$  meters); ordinate, hourly rates; abscissa, hours local time.

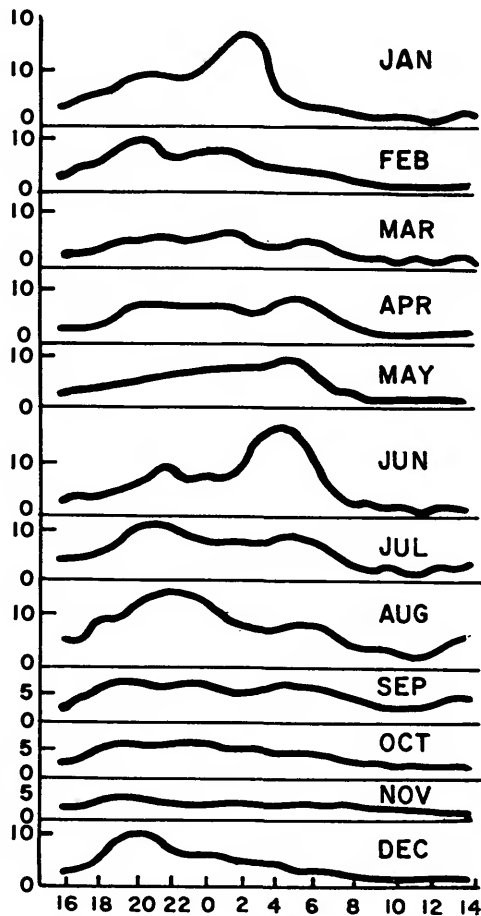


FIGURE 2.—Diurnal variations of meteor rates as measured in Kazan in 1959 ( $\lambda=4$  meters); ordinate, hourly rates; abscissa, hours U.T.

horizontal plane. With  $\lambda_1=4.2$  meters, both the transmitting and the receiving antennas were 7-element directors, raised to the height of  $2\lambda_1$  above the ground. With  $\lambda_2=8.7$  meters,

the antennas were 5-element directors with horizontal jibs, and the height above the ground was  $\lambda_2/2$ .

For the 17 months of observation in the period 1958 to 1960, the equipment with fixed antenna and  $\lambda_1=4.2$  meters was employed during 205 24-hour periods; 35,000 echoes were recorded and the mean daily rate was 160. The equipment with the rotating antenna system ( $\lambda_1=4.2$  meters) was employed during 229 24-hour periods in 1958 to 1960; about 30,000 echoes were recorded and the mean daily rate was 130. The equipment with rotating antenna system and  $\lambda_2=8.7$  meters was employed during 290 24-hour periods in the period 1958 to 1960; about 369,000 echoes were recorded and the mean daily rate was 1,270.

Figures 1 and 2 show the mean diurnal variations of meteor rates, and figures 3 and 4 show the seasonal variations. The diurnal and seasonal rates as obtained in Kazan and in

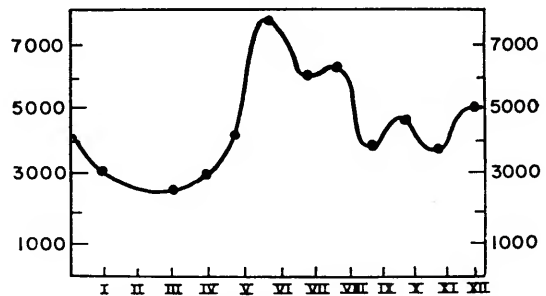


FIGURE 3.—Monthly variations of meteor rates as measured in Kharkov in 1959 ( $\lambda=8$  meters); ordinate, monthly means of daily meteor rates; abscissa, numbers of the months.

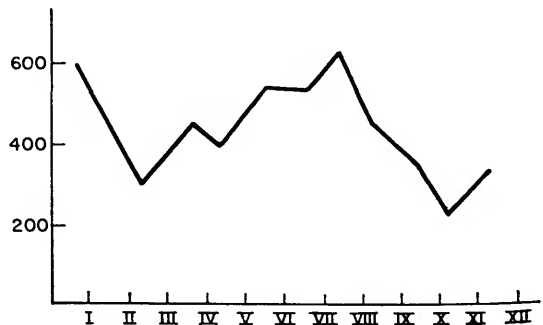


FIGURE 4.—Monthly variations of meteor rates as measured in Kazan in 1959 ( $\lambda=4$  meters); ordinate, monthly means of daily meteor rates; abscissa, numbers of the months.

Kharkov are in good agreement, so that the data can be discussed together. The discussion here, however, will be based mostly upon the data obtained in Kharkov, since most of the echoes were recorded there. The survey of seasonal variations is based upon the measurements made in Kharkov in 1959 because the sensitivity of the equipment was kept constant throughout that year.

The minimum monthly means of diurnal meteor rates in 1959 occurred in February and March and were 2,834 and 2,695, respectively, while the maximum monthly mean, 7,832, occurred in June. Thus there was a threefold change of monthly means within a year. The difference between certain daily rates is still greater: 2,000 echoes for some dates in March and 10,000 echoes in June during the Arietid shower. In December 1959, during the Geminid shower, daily rates reached 8,500.

Hourly meteor rates vary widely from 30 echoes for the period 17<sup>h</sup>00<sup>m</sup> to 19<sup>h</sup>00<sup>m</sup> in January through March, and up to 1,000 for the Arietid, Geminid, and Quadrantid showers. In broad outline, meteor rates show the same daily variations from year to year. During the year, meteor rates reach their maximum in the neighborhood of the moment of the culmination of the apex (6<sup>h</sup> local time). Two more maxima can be observed in the periods about 10<sup>h</sup> to 11<sup>h</sup> and 1<sup>h</sup> to 2<sup>h</sup>. Hawkins (1956) has shown that these maxima are explained by the fact that most meteoroids producing meteors

brighter than +6<sup>m</sup> move directly in orbits whose inclination to the ecliptic is small.

In May and June, the former of the two maxima predominates (10<sup>h</sup> to 11<sup>h</sup>), while in August and September, the latter (1<sup>h</sup> to 2<sup>h</sup>). As has been shown by Kashcheyev, Lebedinets, and Suvorov (1960), twice within the year (in May–June and August–October) the earth crosses in opposite directions a wide belt of meteor orbits which adds to the usual background of sporadic meteors observed in December through April.

### References

- HAWKINS, G. S.  
 1956. A radio echo survey of sporadic meteor radiants. *Monthly Notices Roy. Astron. Soc.*, vol. 116, pp. 92–104.
- KASHCHEYEV, B. L.; LEBEDINETS, V. N.; AND SUVOROV, Y. I.  
 1960. Meteor rates from observations in Kharkov during 1957–1960. *In Meteors, collection of papers, V. V. Tolstov, ed.*, vol. 1, pp. 11–20. Publ. House of Kharkov Univ., Kharkov.
- KOSTYLYOV, K. V.  
 1958. The equipment of the Engelhardt Astronomical Observatory for radio-echo meteor measurements with automatic recording. *Astron. Journ. U.S.S.R.*, vol. 35, pp. 643–651.
- KRESÁKOVÁ, M.  
 1958. On the presence of faint meteors within the Perseid stream. *Bull. Astron. Inst. Czechoslovakia*, vol. 9, pp. 82–88.



# The Orbits of Meteor Streams Determined by Radio-Echo Techniques

By B. L. Kashcheyev,<sup>1</sup> V. N. Lebedinets,<sup>1</sup> and M. F. Lagutin<sup>1</sup>

During the IGY-IGC period, special equipment was developed at the Kharkov Polytechnical Institute for radio-echo determination of orbits of individual meteors.

The observation technique (Kashcheyev, Lebedinets, and Lagutin, 1960) was similar to that used at Jodrell Bank by Gill and Davies (1956). The equipment consisted of a pulse transmitter ( $\lambda=8$  meters) and three receivers. One of the receivers was situated at the transmitter site; the other two receivers were at distances of 4.5 and 7.1 km, and the directions to them from the central station made an approximately right angle. The signals as received by the two receivers were retransmitted to the central station. Three amplitude-time patterns were recorded for every meteor. From these patterns, meteor velocity and time shifts between the corresponding maxima and minima of the diffraction patterns were determined. The orbits were computed according to the scheme proposed by Kleiber (1891).

The electronic computer "Ural" was used for this purpose and it took about 5 minutes to compute each orbit. Meteors brighter than about +8 magnitude were recorded.

Systematic measurements were started in November 1959. In this paper the data given and discussed are those obtained for meteors of the Geminid, Arietid, and  $\delta$ -Aquarid showers as well as for 360 sporadic meteors recorded in November and December 1959.

When observations of the Geminid shower of 1959 were planned, their principal purpose was considered to be the checking of the accuracy obtainable during observations. Dur-

ing the 5 nights of the period from December 9 to December 14, 298 Geminid meteors were recorded. Table 1 shows coordinates of the radiants and orbital elements given as mean values for each night.

The root-mean-square error of velocity measurements for one meteor is  $\pm 1.8$  km/sec. From an analysis it is seen that the following factors contribute to the errors in velocity measurements:

1. Errors made in the evaluation of the atmospheric deceleration involved ( $\pm 0.6$  km/sec).
2. Metering errors ( $\pm 0.75$  km/sec).
3. Errors due to turbulent winds in the atmosphere ( $\pm 0.5$  km/sec).
4. Errors due to diffusion expansion of a meteor trail during the period when principal Fresnel zones are being formed.

The root-mean-square error in the determination of the coordinates of meteor radiants is  $\pm 2^\circ 5'$ . There are two error terms, the first being due to errors in determination of velocity and the second being due to errors in measurements of time delays. The latter, in their turn, are due to turbulent winds in the atmosphere. On the average, the two errors terms are equal.

Throughout the Geminid shower, systematic variations of the elements of the orbit occur as follows:

$$\begin{array}{ll}
 \alpha = 110^\circ 36' + 52' & (\lambda_0 - 260^\circ) \\
 \delta = +32^\circ 18' - 14' & (\lambda_0 - 260^\circ) \\
 V_\infty = 36.15 + 0.30 & (\lambda_0 - 260^\circ) \\
 a = 1.320 + 0.036 & (\lambda_0 - 260^\circ) \\
 e = 0.892 + 0.0045 & (\lambda_0 - 260^\circ)
 \end{array}$$

<sup>1</sup> Kharkov Polytechnical Institute, U.S.S.R.

TABLE 1.—Radiants, orbital elements, and meteor rates for Geminid shower, December 9–14, 1959

Dates	Dec. 9–10	Dec. 10–11	Dec. 11–12	Dec. 12–13	Dec. 13–14
No. meteors	31	40	90	74	62
Orbital elements					
$\alpha$	108°90 ± 0°44	110°28 ± 0°52	111°05 ± 0°28	111°59 ± 0°33	112°50 ± 0°3
$\delta$	+32°57 ± 0°41	+33°30 ± 0°45	+32°43 ± 0°23	+32°00 ± 0°27	+32°07 ± 0°31
$V_{\infty}$	35.48 ± 0.43	35.50 ± 0.31	35.83 ± 0.19	36.06 ± 0.21	36.66 ± 0.20
$a$	1.26 ± 0.04	1.26 ± 0.36	1.29 ± 0.02	1.34 ± 0.03	1.41 ± 0.04
$e$	0.881 ± 0.005	0.881 ± 0.005	0.889 ± 0.003	0.891 ± 0.003	0.898 ± 0.003
$q$	0.138 ± 0.004	0.143 ± 0.005	0.137 ± 0.003	0.139 ± 0.003	0.136 ± 0.003
$i$	22°4 ± 1°1	24°2 ± 0°9	23°3 ± 0°5	22°3 ± 0°6	23°5 ± 0°7
$\Omega$	257°2	258°1	259°2	260°2	261°2
$\omega$	326°0 ± 1°0	325°7 ± 0°8	326°8 ± 0°4	325°6 ± 0°5	325°4 ± 0°5

These variations agree with similar data on 15 orbits determined by Whipple (1954) from photographic observations of Geminid meteors:

$$\begin{aligned} \alpha &= 111^{\circ}35' + 46' & (\lambda_{\odot} - 260^{\circ}) \\ \delta &= +32^{\circ}35' - 9' & (\lambda_{\odot} - 260^{\circ}) \\ V_{\infty} &= 35.95 \pm 0.27 & (\lambda_{\odot} - 260^{\circ}) \\ a &= 1.301 \pm 0.050 & (\lambda_{\odot} - 260^{\circ}) \\ e &= 0.892 \pm 0.0033 & (\lambda_{\odot} - 260^{\circ}) \end{aligned}$$

As was shown by Kashcheyev and Lebedinets (1959), towards the end of the Geminid shower the proportion of large particles increases. An increase in  $a$  and  $e$  as well as a simultaneous increase in the proportion of large particles towards the outer periphery of the stream seems to be due to the evolution of the meteor stream resulting from the Poynting-Robertson effect or from the effect of deceleration by interplanetary matter.

In the period from June 6 to June 18, 1960, 347 meteors of the Arietid stream were recorded. Table 2 shows coordinates of the radiants and orbital elements given as mean values for the period of observations, and compared by statistical methods with those obtained at Jodrell Bank from radio-echo observations in the period 1950 to 1952 (Lovell, 1954). The daily motion of the radiant is  $\Delta\alpha = +48'.4$ ;  $\Delta\delta = +11'.1$ . The data obtained from the two stations show good agreement.

From July 14 to August 14, 1960, orbits of 153 meteors of the  $\delta$ -Aquadrid stream were determined. Table 3 shows coordinates of the radiants and orbital elements, given as mean values for the 153 meteors, and compared with those obtained from five photographic meteors (Wright, Jacchia, and Whipple, 1954). The daily motion of the radiant is  $\Delta\alpha = +51'.0$ ;  $\Delta\delta = +22'.5$ . The coordinates of the radiant are given with respect to the longitude of the sun,  $\lambda_{\odot} = 126^{\circ}.9$ . A satisfactory agreement of the data obtained by the two methods is seen, but the scatter of the individual data in both cases is rather high.

In November and December 1959 measurements were made to obtain orbits of 360 sporadic meteors; of these, 19 orbits were found to be hyperbolic, but this may have been due to measurement errors.

Comparison of our data with those for photographic meteors (Whipple, 1954) shows a rather good agreement in the distribution of orbits according to their eccentricities. For most of the orbits  $0.7 < e < 1.0$ . For 25 percent of the orbits  $e < 0.7$ ; with photographic meteors the percentage is lower, namely 10 percent. The difference is greater when the distribution of the orbits according to their inclinations is analyzed; that is, there is a large group of orbits where  $40^{\circ} < i < 150^{\circ}$ . Figure 1

TABLE 2.—Radiants and orbital elements of Arietid meteors observed from two stations

Station	Orbital elements								
	$\alpha$	$\delta$	$V_{\infty}$	$a$	$e$	$q$	$i$	$\Omega$	$\omega$
Kharkov	44°2	23°3	38.9	1.98	0.941	0.098	18°5	77°5	29°8
Jodrell Bank	44°5	22°7	38.3	1.57	0.943	0.093	17°3	77°5	29°0

TABLE 3.—Orbital data of  $\delta$ -Aquarid meteors, July 14–August 14, 1960

Source	Orbital elements								
	$\alpha$	$\delta$	$V_{\infty}$	$a$	$e$	$q$	$i$	$\Omega$	$\omega$
Kharkov	341°4	−16°4	41.1	2.22	0.96	0.08	28°2	306°9	151°3
Wright, et. al. (1954)	339°2	−16°7	43.0	2.60	0.976	0.061	29°3	302°9	154°7

shows the distribution of the meteor orbits according to their inclination and eccentricity.

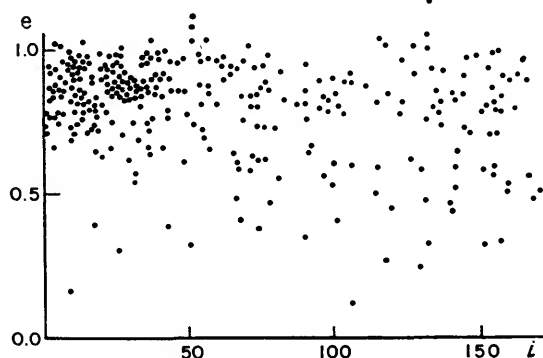


FIGURE 1.—Distribution of meteor orbits according to their inclinations to the plane of the ecliptic and to their eccentricities.

A particular group of orbits (about 13 percent of the total) appears that are not found from photographic observations. These orbits are characterized both by  $40^\circ < i < 150^\circ$  and by  $e < 0.7$ . Orbits of that type were first obtained from radio-echo observations at Jodrell Bank. The importance of orbits of this type for cosmogony is discussed by Davies and Gill (1960).

References

DAVIES, J. G., AND GILL, J. C.  
1960. Radio echo measurements of the orbits of faint sporadic meteors. *Monthly Notices Roy. Astron. Soc.*, vol. 121, pp. 437–462.

GILL, J. C., AND DAVIES, J. G.  
1956. A radio echo method of meteor orbit determination. *Monthly Notices Roy. Astron. Soc.*, vol. 116, pp. 105–113.

KASHCHEYEV, B. L., AND LEBEDINETS, V. N.  
1959. On the structure of the Geminid meteor stream. *Astron. Journ., U.S.S.R.*, vol. 36, pp. 629–640.

KASHCHEYEV, B. L.; LEBEDINETS, V. N.; AND LAGUTIN, M. F.  
1960. The orbit of the Geminids of 1959. In V. V. Tolstov, ed., *Meteors, Collection of papers*, vol. 1, pp. 25–37. Publ. House of Kharkov Univ., Kharkov.

KLEIBER, I. A.  
1891. Determination of orbits of meteor streams. St. Petersburg.

LOVELL, A. C. B.  
1954. *Meteor astronomy*. Clarendon Press, Oxford.

WHIPPLE, F. L.  
1954. Photographic meteor orbits and their distribution in space. *Astron. Journ.*, vol. 59, pp. 201–217.

WRIGHT, F. W.; JACCHIA, L. G.; AND WHIPPLE, F. L.  
1954. Photographic  $\delta$ -Aquarid meteors. *Astron. Journ.*, vol. 59, pp. 400–406.



# The Distribution of Small Interplanetary Dust Particles in the Vicinity of Earth

By C. W. McCracken<sup>1</sup> and W. M. Alexander<sup>1</sup>

One of the components of the solar system is a cloud of dust particles surrounding the sun. The importance of the cloud arises not only from cosmogonical aspects such as the sources and composition of the dust particles, but also from cosmological aspects such as the rapidity with which changes occur in their dynamical characteristics. Properties of the dust particles and the general shape and extent of the dust cloud have been inferred from observations of meteors and from photometric studies of the zodiacal light and the solar corona. Uncertainties in conclusions reached on the basis of such inferences arise because of the differences that possibly exist between the classes of dust particles responsible for the two vastly different phenomena. New and independent methods of determining selected parameters of the dust particles are needed in order to remove the uncertainties that presently exist in the knowledge of their physical characteristics and distributions.

A new technique that holds great promise for supplying some of the most-needed parameters has been developing very rapidly during the past few years. This technique is that of measuring (in space) various parameters of statistical samples of dust particles. The direct measurements that are presently available have been obtained as dust particles impacted onto special sensors mounted on rockets, earth satellites, and other spacecraft.

The sensors that have been flown have necessarily been of very simple design and have provided only limited information about the dust particles. The experiments have been designed primarily to give preliminary infor-

mation about the influx rate or spatial density of dust particles over a limited but astronomically important range of particle mass. More sophisticated experiments capable of defining selected parameters of individual dust particles are possible and technically feasible in the very near future.

Radar, visual, and photographic techniques are used in observing meteoric phenomena produced by meteoroidal dust particles. The dust particles studied by direct measurement techniques are too small to produce meteoric phenomena and cannot be observed by the ground-based techniques common to studies of meteors. The magnetic spherules found in deep-sea deposits and in high-altitude collections of atmospheric aerosols may include extraterrestrial material, but positive identification of this component is extremely difficult. Volatile cometary debris does not appear in either of the collections, and there has been little or no success in the identification of siliceous particles as being of extraterrestrial origin.

One is left with the conclusion that there are basically two effective techniques of experimentally acquiring reliable information about the distributions and physical characteristics of small interplanetary dust particles. The first technique is photometry of the zodiacal light and the solar corona (from outside the atmosphere of Earth as well as from the surface of Earth). The second technique is that of making statistical samples within the dust cloud by the direct-measurements technique. The direct-measurements technique can include the returning to Earth of collections of dust particles from outside the atmosphere of Earth as well as the direct measurements of selected parameters

<sup>1</sup> Goddard Space Flight Center, National Aeronautics and Space Administration, Greenbelt, Md.

of dust particles in space. The two techniques must remain complementary. Each should supply information unique to the method as well as provide information to be used in advancing the other technique.

Spacecraft carrying instruments for obtaining direct measurements can be used for probing comets and meteor streams simultaneously with studies of the dust cloud. Probes sent through comets and meteor streams would provide valuable information about the physical conditions and processes within such collections of dust particles. The direct-measurements technique represents an interesting, useful, and almost unique means of studying small particulate aggregates of matter in selected regions of the solar system as well as in the vicinity of Earth.

#### **Interpretations of direct measurements**

The available direct measurements must be periodically reviewed in order to determine how consistently they fit into one or another pattern that has physical meaning. The direct measurements have, until just recently, been of such a nature that they could be given either of two interpretations. The choice of interpretation depended critically upon the assumptions that one was willing to accept during an analysis of the data.

The two interpretations of direct measurements that could be given prior to obtaining the new direct measurements from Explorer VIII (Satellite 1960 Xi) were: (1) The mass distribution and spatial density of small interplanetary dust particles indicated by the direct measurements differ significantly from those predicted on the basis of linear extrapolations (over about six orders of magnitude) of results from observations of meteors; or (2) the direct measurements indicate the existence of an appreciable geocentric concentration of interplanetary dust particles. The conjectural geocentric concentration mentioned here is of the type proposed by Beard (1959), and should not be confused with concentrations arising from the temporary suspension of dust particles above the temperature inversion layers in the atmosphere of Earth.

The direct measurements obtained with Explorer VIII strongly indicate that the first

of the two interpretations of the presently available direct measurements is the correct one. The second interpretation is not compatible with an analysis in which the direct measurements from Explorer VIII are used as a basis for analyzing other direct measurements. The first interpretation should, therefore, be regarded as correct until direct measurements of the vectorial velocities of impacting dust particles have been obtained. The direct measurements from Explorer VIII serve as the first firm basis for analyzing existing direct measurements of interplanetary dust particles. A review of the available direct measurements (including those from Explorer VIII) obtained with microphone systems is sufficient to demonstrate the validity of the foregoing statements about the interpretation of the direct measurements.

#### **Direct measurements from Explorer VIII**

A definitive set of direct measurements recently was obtained with the satellite Explorer VIII. Two independent systems for studying interplanetary dust particles were mounted on the satellite. The systems provided data from launch on 3 November 1960 until the power supplies were exhausted on 13 December 1960. One of the systems included a photomultiplier tube as the sensor for measuring the luminous energy generated in hypervelocity impacts of dust particles. A microphone was used as the sensor in the other system for the purposes of counting impacts and determining the magnitudes of the impulses delivered by impacting dust particles.

Two sounding boards of the microphone system were mounted on the lower cone of the spin-stabilized satellite. The spin vector of the satellite lay within approximately  $40^\circ$  of the apex of Earth's motion during the active lifetime of the satellite. The "sounding boards" were arranged to detect dust particles for which the radiants generally lay on the hemisphere centered on the antapex of Earth's motion. An average particle velocity of 25 km/sec has been assigned for Explorer VIII until the velocity distribution of interplanetary dust particles can be determined.

The best calibrations that are at present possible for the microphone system show that it

is sensitive to a quantity which is closely related to the momentum of an impacting dust particle. Calibrations have been accomplished with low-velocity particles impacting elastically onto sounding boards to which the microphones were attached. Hypervelocity particle accelerators are now being used in order to obtain more realistic calibrations. The mass sensitivity of a microphone system can be computed from the momentum sensitivity if an average particle velocity is assumed.

The microphone system of Explorer VIII was designed to count impacting dust particles, and to determine in which of three ranges the momentum of each particle lay. A preliminary readout of the data has established approximately the number of dust particles encountered for each of the three ranges of sensitivity. In addition to determining the average influx rate within each range, the data have defined the shape of a section of an average mass-distribution curve. This section extends over a limited but significant range of particle mass, and provides a basis for analyzing all the other available direct measurements of interplanetary dust particles.

A tabulation of the preliminary data from Explorer VIII has not been included in this

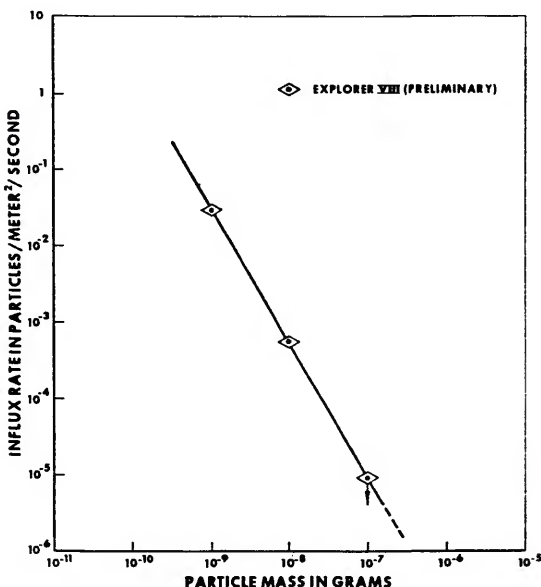


FIGURE 1.—The average distribution curve established by preliminary results from Explorer VIII.

paper, to avoid the unnecessary propagation of preliminary numerical results that may change slightly. The three datum points obtained with the microphone system on Explorer VIII are corrected for the effect of shielding by Earth, and are plotted as a cumulative mass-distribution curve in figure 1. The three datum points represent the impacts of more than 3,100 dust particles registered during an interval of 40 days. The large number of impacts provides statistical weight for the datum points from the two ranges of highest sensitivity. The spacing of the threshold sensitivities allows one to establish definitively the shape of a segment of an average distribution curve that extends over approximately three orders of magnitude in particle mass.

#### Direct measurements from other satellites and spacecraft

Direct measurements have been obtained with rockets, earth satellites, and space probes flown by both the United States and the Soviet Union. Dust-particle sensors carried by these payloads have included microphones, photomultiplier tubes, thin films, erosion grids, wire grids, and pressurized chambers. The microphone system is probably the best calibrated of all the sensors, and certainly has been flown more times and on more payloads than any other sensor.

It is sufficient, for the analysis summarized in this paper, to consider only those direct measurements obtained with microphone systems. The data obtained with microphone systems are entirely adequate to establish an average distribution curve for interplanetary dust particles in the vicinity of Earth. It may be qualitatively stated that the direct measurements obtained with other systems do not indicate that a distribution curve different from the one established by the direct measurements obtained with microphone systems should be considered.

The U.S. satellites and spacecraft for which direct measurements with microphone systems have been obtained are listed, together with the relevant data, in table 1. The data for Explorer I (Satellite 1958 Alpha) and Pioneer I are those given by Dubin (1960). The total number of impacts (145) for Explorer I was used in computing an average influx rate even though approximately one-half the impacts probably

represented a "shower" component (Dubin, 1961). The high influx rate during the "shower" is approximately counteracted by an interval with a low influx rate. An influx rate computed from the total number of impacts serves very well as the average influx rate from Explorer I to be used in establishing an average distribution curve. A factor of 2 was used in correcting the influx rate from Explorer I for the shielding effect of Earth.

The microphone system on Pioneer I registered 25 impacts, of which 17 probably represented dust particles. The average influx rate was computed on the basis of 17 impacts. No correction was made for the shielding effect of Earth because Pioneer I spent most of its time at large geocentric distances (2 to 19 Earth's radii).

Preliminary results for the microphone system on Vanguard III (Satellite 1959 Eta) were reported by LaGow and Alexander (1960). Reading of the telemetered data is still in progress, so the preliminary results shown in table 1 may change slightly. Approximately 6,000 impacts were recorded during 80 days of operation. Approximately 2,800 of the impacts occurred during a 70-hour interval on 16-18 November (Alexander, McCracken, and LaGow, 1961). An average influx rate was computed for Vanguard III on the basis of  $\sim 3,500$  impacts. This number allows for the sporadic background during the 70-hour interval. A factor of 1.5 was used to correct for the shielding effect of Earth. An average particle velocity of 30 km/sec was used in computing the threshold mass sensitivities for the microphone systems on all the spacecraft listed in table 1.

Direct measurements reported by Nazarova (1960) from the microphone systems mounted on Soviet satellites and spacecraft are included in table 2. Portions of the information shown have been computed from information given by Nazarova in order that data from United States and Soviet spacecraft may be included in the same analysis.

The sensitivities for the microphone systems on the Soviet spacecraft were expressed by Nazarova in terms of particle mass. Nazarova computed the mass sensitivities by assuming that the microphone systems were energy-sensitive and that the average particle velocity

was 40 km/sec. McCracken (1959) used 40 km/sec in an early analysis of direct measurements, but this value is almost certainly too high.

Whipple (1957) assigned different values of average velocity to different sizes of dust particles. The velocities varied from 28 km/sec for meteoroids to 15 km/sec for small dust particles of the direct-measurements range of particle size. In order to avoid prematurely constraining the model distribution of interplanetary dust particles, we have assigned a value of 30 km/sec as the average particle velocity when the spacecraft is not oriented or when the dust particle sensors are open to an omnidirectional flux. Average particle velocities for oriented sensors are chosen according to the orientation of the solid viewing angle of the sensor.

The mass sensitivities for the systems on the Soviet spacecraft are reduced by the square of the ratio of 40 to 30 in order to compensate for the difference in the assigned average particle velocities. The spacecraft—Lunik I (Mechta, 2 January 1959), Lunik II (Lunar Probe, 12 September 1959), and Lunik III (Satellite 1959 Theta)—operated at large geocentric distances, so corrections for the shielding effect of Earth are not necessary.

The influx rates measured by Sputnik III (Satellite 1958  $\delta 2$ ) underwent tremendous changes during the first 3 days of operation of the equipment. The influx rates, as reported by Nazarova (1960), were 4 to 11 particles  $m^{-2} sec^{-1}$  on 15 May (launch day),  $5 \times 10^{-4}$  particles  $m^{-2} sec^{-1}$  on 16-17 May, and less than  $10^{-4}$  particles  $m^{-2} sec^{-1}$  during the interval 18-26 May. Nazarova attributes the high influx rates during the first few days to a meteor shower, but the manner in which the influx rate changed could also be suggestive of payload interference. Only the influx rate for the last 9 days of operation of Sputnik III is of any value in establishing an average distribution curve. It is not clear whether Nazarova corrected the influx rate from Sputnik III for the shielding effect of Earth, so the influx rate is left as it was given.

The method of encoding information into the telemetered signal for Lunik I was such that only very crude upper limits for the

TABLE 1.—Direct measurements obtained with microphone systems on the U.S. satellites and space probes

Spacecraft	Momentum sensitivity (dyne seconds)	Mass sensitivity (grams)	Effective area (meter <sup>2</sup> )	Exposure time (seconds)	Exposure (m <sup>2</sup> sec)	Number of particles	Cumulative influx rate (particles/m <sup>2</sup> /sec)	
							Observed	Corrected for earth shielding
Explorer I	$> 2.5 \times 10^{-4}$	$8.3 \times 10^{-10}$	$2.3 \times 10^{-1}$	$7.9 \times 10^4$	$1.8 \times 10^4$	145	$8.4 \times 10^{-3}$	$1.7 \times 10^{-3}$
Pioneer I	$> 1.5 \times 10^{-4}$	$5.0 \times 10^{-11}$	$3.9 \times 10^{-2}$	$1.1 \times 10^5$	$4.2 \times 10^3$	25 (17)	$4.0 \times 10^{-3}$	$4.0 \times 10^{-3}$
Vanguard III	$> 1.0 \times 10^{-4}$	$3.3 \times 10^{-9}$	$4.0 \times 10^{-1}$	$6.9 \times 10^6$	$2.8 \times 10^6$	$\sim 3500$	$1.3 \times 10^{-3}$	$2.0 \times 10^{-3}$

TABLE 2.—Direct measurements obtained with microphone systems on the Soviet satellites and space probes

Spacecraft	Mass sensitivity (grams)		Effective area (meter <sup>2</sup> )	Exposure time (seconds)	Exposure (m <sup>2</sup> sec)	Number of particles	Influx rate (particles/m <sup>2</sup> /sec)	
	$\bar{v}_0 = 40$ km/sec	$\bar{v}_0 = 30$ km/sec					(Nazarova)	Cumulative
Sputnik III	$8.0 \times 10^{-2}$ — $2.7 \times 10^{-3}$	$1.4 \times 10^{-2}$ — $4.8 \times 10^{-3}$	0.34	$\sim 8 \times 10^6$	$\sim 3 \times 10^6$	?	(see text)	$< 1 \times 10^{-4}$
Lunik I	$2.7 \times 10^{-2}$ — $1.5 \times 10^{-7}$	$4.8 \times 10^{-3}$ — $2.7 \times 10^{-7}$	0.2	$3.6 \times 10^4$	$7.2 \times 10^5$	$< 16$	$< 2 \times 10^{-3}$	$< 2.9 \times 10^{-3}$
Lunik II	$1.5 \times 10^{-2}$ — $5.6 \times 10^{-6}$	$2.7 \times 10^{-7}$ — $1.0 \times 10^{-3}$	0.2	$1.1 \times 10^6$	$2.2 \times 10^4$	$< 4$	$< 5 \times 10^{-4}$	$< 7.0 \times 10^{-4}$
Lunik III	$> 5.6 \times 10^{-6}$	$> 1.0 \times 10^{-5}$	0.1	$2.3 \times 10^4$	$2.3 \times 10^5$	$< 1$	$< 1 \times 10^{-4}$	$< 1.4 \times 10^{-4}$
	$2.5 \times 10^{-2}$ — $1.5 \times 10^{-8}$	$4.4 \times 10^{-6}$ — $2.7 \times 10^{-8}$				0	$< 5 \times 10^{-5}$	$9.1 \times 10^{-5}$
	$1.5 \times 10^{-2}$ — $2.0 \times 10^{-7}$	$2.7 \times 10^{-8}$ — $3.6 \times 10^{-7}$				2	$9 \times 10^{-5}$	$3.0 \times 10^{-5}$
	$2.0 \times 10^{-2}$ — $6.0 \times 10^{-9}$	$3.6 \times 10^{-8}$ — $1.1 \times 10^{-8}$				1	$4 \times 10^{-4}$	$2.6 \times 10^{-3}$
	$6.0 \times 10^{-2}$ — $1.5 \times 10^{-8}$	$1.1 \times 10^{-8}$ — $2.7 \times 10^{-8}$				5	$2 \times 10^{-3}$	$2.6 \times 10^{-3}$
	$> 1.5 \times 10^{-3}$	$> 2.7 \times 10^{-8}$				1	$4 \times 10^{-4}$	$4.3 \times 10^{-4}$
	$1.0 \times 10^{-2}$ — $3.0 \times 10^{-9}$	$1.8 \times 10^{-9}$ — $5.3 \times 10^{-9}$						
	$3.0 \times 10^{-2}$ — $8.0 \times 10^{-9}$	$5.3 \times 10^{-9}$ — $1.4 \times 10^{-8}$						
	$> 8.0 \times 10^{-9}$	$> 1.4 \times 10^{-8}$						

TABLE 3.—List of rockets with microphone-type dust-particle sensors

Rocket	Launch time and date	Zenith altitude (kilometers)	Type of data
V-2 Blossom IV-D	8 Dec. 1949	~135	First direct measurement
V-2 Blossom IV-G	31 Aug. 1950	~135	Qualitatively fair data
Aerobee No. 58	14 Sept. 1955	100	Qualitatively fair data
Aerobee No. 77	0819 MST 9 Apr. 1957	27	No data, vehicle failure
Aerobee No. 80	0630 MST 16 July 1957	122	Quantitatively good data
Aerobee No. 81	0730 MST 18 July 1957	----	No data, vehicle failure
Aerobee No. 87	0808 MST 14 Oct. 1957	146	No data, telemetry difficulty
Aerobee No. 88	2212 MST 16 Oct. 1957	114	Quantitatively good data
Nike-Cajun AF-1	0944 MST 24 Apr. 1958	167	No data, thermal interference
Nike-Cajun AF-2	0533 MST 1 May 1958	137	Quantitatively fair data
Nike-Cajun AA6.203	2200 CST 15 Oct. 1958	151	Quantitatively good data
Nike-Cajun AA6.204	0600 CST 14 Oct. 1958	137	Quantitatively good data
Nike-Cajun AA6.205	2125 CST 17 Oct. 1958	143	No data, mechanical failure
Nike-Cajun AA6.206	2145 CST 21 Oct. 1958	157	Quantitatively fair data
Spaerobee 10.01	1047 CST 22 Oct. 1958	177	Quantitatively fair data
Spaerobee 10.02	1327 CST 25 Oct. 1958	420	No data, telemetry failure

influx rates could be set. Only that influx rate measured by the scale of highest sensitivity is of any value in the present analysis.

#### Direct measurements from rockets

Signals that could be ascribed to no other source than the impacts of dust particles onto the skins of rockets were first found on the telemetry records for two V-2 rockets. The rockets were V-2 Blossom IV-D flown on 8 December 1949, and V-2 Blossom IV-G flown on 31 August 1950. Microphones and the associated electronics had been designed and installed by personnel of Temple University under the direction of Prof. J. L. Bohn. The equipment was flown for the purpose of measuring acoustical intensities in the warheads and on the skins of the rockets. Descriptions of the instrumentation and the data have been given in detail by Bohn and Nadig (1950).

Bohn and Nadig tentatively suggested that the unexplained pulses observed on the telemetry records were caused by the impacts of meteoric particles on the skins of the rockets. This explanation may now be regarded as the correct one. The data from these flights were the first direct measurements of interplanetary dust particles ever obtained. Both sets of data should be regarded as being qualitatively fair

but of no use in quantitative discussions of interplanetary dust particles.

The spare equipment from the V-2 flights was mounted on Aerobee No. 58 and flown on 14 September 1955, as has been reported by Dubin (1956). The rocket did not reach a sufficiently high altitude for observation of dust particles that had not been appreciably decelerated by atmospheric drag forces. Signals that probably were caused by the impacts of dust particles were recorded, but the data must be classified as qualitatively fair.

Bohn and Nadig (1950) also proposed that rockets carrying special acoustical systems for counting the impacts of dust particles be flown. Preferably, the rockets were to have nose tips that could be ejected in order to expose a circular diaphragm. Shielding the diaphragm during the passage of the rocket through the lower atmosphere served to eliminate the possibility that spurious counts were being introduced by the aerodynamic heating of the sensor. The type of rocket program that was suggested was carried further under the direction of Mr. M. Dubin, then of the Air Force Cambridge Research Center.

A list of the rockets that have carried microphone systems is given in table 3. Aerobee No. 77 was the fourth rocket to carry a micro-

TABLE 4.—Basic corrected data for the successful OSU rockets

Rocket	Range of momentum sensitivity (dyne seconds)	Effective area (meter <sup>2</sup> )	Time $h \geq 110$ km. (seconds)	Exposure $h \geq 110$ km. (m <sup>2</sup> sec)	Number of impacts
Aerobee No. 80	$6.0 \times 10^{-4} - 3.0 \times 10^{-3}$	0.05	100	5.0	39
	$3.0 \times 10^{-3} - 8.0 \times 10^{-3}$	0.05		5.0	10
	$1.0 \times 10^{-3} - 3.0 \times 10^{-3}$	0.5		50	2
	$3.0 \times 10^{-3} - 1.8 \times 10^{-2}$	0.5		50	1
Aerobee No. 88	$1.3 \times 10^{-4} - 2.0 \times 10^{-3}$	0.05	60	3.0	5
	$2.0 \times 10^{-3} - 2.6 \times 10^{-2}$	0.05		3.0	1
	$4.7 \times 10^{-4} - 1.0 \times 10^{-3}$	0.5		30	10
	$1.0 \times 10^{-3} - 2.8 \times 10^{-3}$	0.5		30	7
Nike-Cajun AF-2	$6.0 \times 10^{-4} - 1.2 \times 10^{-3}$	0.2	154	31	30
	$1.2 \times 10^{-3} - 4.0 \times 10^{-3}$				12
	$4.0 \times 10^{-3} - 3.0 \times 10^{-2}$				3
Nike-Cajun AA6.203	$3.0 \times 10^{-4} - 3.0 \times 10^{-3}$	0.2	186	37	52
	$3.0 \times 10^{-3} - 1.8 \times 10^{-2}$				3
Nike-Cajun AA6.204	$7.0 \times 10^{-4} - 3.0 \times 10^{-3}$	0.2	167	33	31
	$3.0 \times 10^{-3} - 3.0 \times 10^{-2}$				1
Nike-Cajun AA6.206	$1.5 \times 10^{-4} - 1.0 \times 10^{-3}$	0.2	118	24	11
	$1.0 \times 10^{-3} - 6.0 \times 10^{-3}$				1
	$7.0 \times 10^{-4} - 5.0 \times 10^{-3}$				6
Spaerobee 10.01	$5.0 \times 10^{-4} - 7.5 \times 10^{-3}$	0.04	202	8.1	20

phone system and was the first of a series of 13 rockets instrumented with microphone systems and flown by Oklahoma State University under contract with the Air Force. The series of rockets was flown especially for the purpose of directly measuring influx rates and momenta of interplanetary dust particles. Aerobee No. 77, like the other Aerobees in the series, had two crystal microphones mounted on the skin of the instrument compartment, and two microphones mounted on a circular diaphragm that could be exposed by ejecting the nose tip of the rocket at an altitude of about 60 km. The diaphragm had been highly polished by Bohn in the hope of observing hypervelocity craters on the recovered diaphragm. The rocket reached zenith at an altitude of 27 km, which was too low for proper operation of the microphone system. The recovered diaphragm was examined photochemically by Yagoda (Dubin, 1957), who found several tiny craters resembling those formed by hypervelocity impacts of small dust particles.

Seven of the thirteen rockets provided data that are of use in quantitative discussions of interplanetary dust particles. A preliminary readout of the data from six of these rockets was included in an early analysis of direct

measurements by McCracken (1959). A final readout of the uncorrected data from the seven rockets was made available as a final report on the contract, being dated 14 April 1960 (Buck, 1960).

The data for the seven rockets are given in table 4. Corrections have been applied for the counts that possibly could have causes other than the impacts of dust particles. The data from Nike-Cajun AF-2 are slightly rearranged in order to compensate for a change in sensitivity that occurred as a result of a low battery potential during the flight. A corrected tabulation of the data from the OSU rockets has not previously been made available in the open literature because of the series of corrections that were in progress and have only recently been completed.

Only those impacts that occurred when the rockets were at altitudes greater than 110 km are counted. The deceleration of dust particles by atmospheric-drag forces becomes quite appreciable at altitudes below approximately 100 km. The velocities of the dust particles become functions of altitude and zenith angle, making the determination of the velocities of the particles relative to a rocket an almost impossible task. Setting the lower limit on

TABLE 5.—Direct measurements obtained with the OSU rockets

Rocket	Momentum sensitivity (dyne seconds)	Particle velocity (km/sec)	Mass sensitivity (grams)	Number of impacts	Exposure $h \geq 110$ km. (m <sup>2</sup> sec)	Cumulative influx rate (particles/m <sup>2</sup> /sec)
Aerobee No. 80	$6.0 \times 10^{-4}$	70	$8.6 \times 10^{-11}$	49	5.0	9.8
	$3.0 \times 10^{-3}$	70	$4.3 \times 10^{-10}$	10	5.0	2.0
	$1.0 \times 10^{-2}$	40	$2.5 \times 10^{-10}$	3	50	$6.0 \times 10^{-2}$
Aerobee No. 88	$3.0 \times 10^{-3}$	40	$7.5 \times 10^{-10}$	1	50	$2.0 \times 10^{-2}$
	$1.3 \times 10^{-4}$	20	$6.5 \times 10^{-11}$	6	3.0	2.0
	$2.0 \times 10^{-3}$	20	$1.0 \times 10^{-9}$	1	3.0	$3.3 \times 10^{-1}$
Nike-Cajun AF-2	$4.7 \times 10^{-4}$	35	$1.3 \times 10^{-10}$	17	30	$5.7 \times 10^{-1}$
	$1.0 \times 10^{-3}$	35	$2.9 \times 10^{-10}$	7	30	$2.3 \times 10^{-1}$
	$6.0 \times 10^{-4}$	40	$1.5 \times 10^{-10}$	45	31	1.5
Nike-Cajun AA6.203	$1.2 \times 10^{-3}$		$3.0 \times 10^{-10}$	15		$4.8 \times 10^{-1}$
	$4.0 \times 10^{-3}$		$1.0 \times 10^{-9}$	3		$9.7 \times 10^{-2}$
	$3.0 \times 10^{-4}$	35	$8.6 \times 10^{-11}$	55	37	1.5
Nike-Cajun AA6.204	$3.0 \times 10^{-3}$		$8.6 \times 10^{-10}$	3		$8.1 \times 10^{-2}$
	$7.0 \times 10^{-4}$	40	$1.8 \times 10^{-10}$	32	33	$9.7 \times 10^{-1}$
	$3.0 \times 10^{-3}$		$7.5 \times 10^{-10}$	1		$3.0 \times 10^{-2}$
Nike-Cajun AA6.206	$1.5 \times 10^{-4}$	35	$4.3 \times 10^{-11}$	12	24	$5.0 \times 10^{-1}$
	$1.0 \times 10^{-3}$		$2.9 \times 10^{-10}$	1		$4.2 \times 10^{-2}$
	$7.0 \times 10^{-4}$		$2.0 \times 10^{-10}$	6		$2.5 \times 10^{-1}$
Spaerobee 10.01	$5.0 \times 10^{-4}$	60	$8.3 \times 10^{-11}$	20	8.1	2.5

altitude at 110 km allows one to assume that the majority of the dust particles impacting onto the sensors had not been appreciably decelerated by atmospheric-drag forces. Geocentric velocities of dust particles above the atmosphere of Earth lie between 11 and 72 km/sec, so velocities of the dust particles (relative to the rocket) lie approximately between the same limits.

It seems reasonable to assign average particle velocities for each sensor of each rocket until the velocity distribution becomes known. The average particle velocities have been assigned on the basis of the region on the celestial sphere (relative to the apex of Earth's motion) to which each sensor was exposed. The limiting mass sensitivity of each sensor is computed from the momentum sensitivity and the assigned average particle velocity. Table 5 contains the limiting momentum sensitivities, the assigned average particle velocities, the limiting mass sensitivities, and the numbers of impacts from which datum points for a cumulative mass distribution curve were computed.

The direct measurements made with the rockets served as an early and preliminary determination of the influx rate and mass distribution of small interplanetary dust par-

ticles. The data were of considerable importance in the design of the dust-particle experiments for the early satellites and space probes. The degree of importance may be partially illustrated by the fact that the rocket data showed influx rates higher by a factor of  $10^4$  than was expected on the basis of an extrapolation of the tabulation by Watson (1941) of the results from observations of meteors, and higher by a factor of  $10^2$  than was expected on the basis of a similar extrapolation by Whipple (1957). The weight and power allotments on the early satellites did not permit one to build in enough dynamic range to allow for such uncertainties in the influx rate. It is interesting and perhaps of moderate quantitative value if the rocket data agree with and support the more definitive direct measurements now available from satellites. The rocket data probably should not, however, be used as the decisive element in a critical test of the validity of a particular model of the distribution of dust particles in the vicinity of Earth.

#### Analysis of the direct measurements

The available direct measurements that have been obtained with microphone systems on

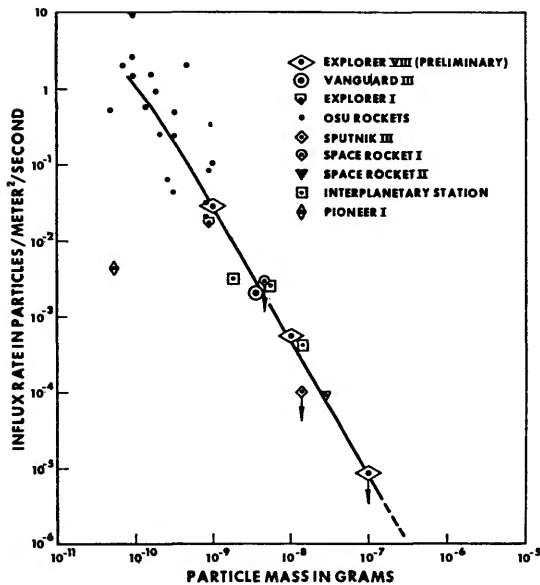


FIGURE 2.—The average distribution curve established by direct measurements from microphone systems for interplanetary dust particles in the vicinity of Earth. (Space Rocket I, Space Rocket II, and Interplanetary Station are referred to in the text as Luniks I, II, and III, respectively.)

the OSU rockets, U.S. spacecraft, and Soviet spacecraft are shown plotted as a cumulative mass-distribution curve in figure 2. The various direct measurements, with the exception of the one from Pioneer I, fit remarkably well onto the distribution curve, regardless of the geocentric distance or sensitivity at which the measurement was made. The departure of the direct measurement for Pioneer I from the average distribution curve can easily be explained on the basis of the actual fluctuations in the influx rates measured with Explorer I, Vanguard III, and Explorer VIII. Pioneer I was active for about 1½ days and easily could have flown during an interval of low dust-particle activity.

The direct measurements listed in tables 1, 2, and 5 encompass a variety of altitudes, sensitivities, lengths of sampling interval, and times of the year. The fact that all except the direct measurement from Pioneer I fit the distribution curve established by Explorer VIII lends substantial support to the validity of the curve shown in figure 2 as an average distribu-

tion curve that can be used until more sophisticated experiments have established the curve over a considerably larger range of particle mass.

It is quite advantageous to the present analysis to point out the uncertainties that are encountered in displaying the direct measurements as a mass distribution. Qualitative discussions of the uncertainties are followed by attempts to assign them numerical values.

The values of average particle velocity assigned in converting from momentum sensitivity to mass sensitivity for the systems may be slightly too high. The correct values depend on the velocity distribution that exists for dust particles in the direct-measurements range of particle size. Lower average velocities would apply if most of the dust particles were in geocentric orbits or direct circular heliocentric orbits. The use of lower particle velocities would tend to shift the direct measurements toward slightly higher values of particle mass without markedly changing the shape of the distribution curve. Even a radical reduction from about 30 km/sec to the value 15 km/sec used by Whipple would lower the threshold mass sensitivities by only a factor of 2.

The impulse delivered to a sensor as a dust particle impacts at hypervelocity is almost certainly greater than the impact-momentum of the dust particle, but the value remains unknown. A value greater than unity (which is used in tables 1, 2, 4, and 5) for the ratio of the impulse to the impact-momentum increases the momentum sensitivities for microphone systems. The proper correction factors probably lie between 2 and 3, and are now being established by hypervelocity accelerators.

Allowing for the impacts of dust particles at angles of incidence appreciably different from 0° effectively decreases the momentum sensitivity, but the decrease is probably less than a factor of 2. This uncertainty can be largely removed through the use of more directional sensors.

The magnitude of the correction for the shielding effect of Earth depends on the velocity distribution of the dust particles. The corrections that have been applied involve the assumption that the dust particles are pre-

dominantly in heliocentric orbits and are not necessarily confined to direct circular orbits. If this assumption is not valid, then slightly smaller corrections would be applied. The factors applied to correct for Earth's shielding of the spacecraft were all less than or equal to 2. Smaller correction factors would shift the direct measurements toward slightly lower values of influx rate without changing the shape of the distribution curve.

Knowing which of the minor corrections to apply requires a better knowledge than exists at present of the mass distribution, velocity distribution, and spatial density of the interplanetary dust particles. All of the direct measurements have been handled in as consistent a manner as possible, so that introducing minor corrections will change only the position of the direct measurements on a plot of mass distribution without changing the shape of the distribution curve. It seems reasonable to assume that likely combinations of the minor uncertainties will leave the distribution curve as it is shown in figure 2. Direct measurements obtained at large distances from Earth and/or a determination of the velocity distribution are needed before much further progress can be made in defining a model distribution of the interplanetary dust particles.

The distribution curve shown in figure 2 can be approximated reasonably well by a straight-line segment. The equation of the straight line is

$$\log I = -17.0 - 1.70 \log m,$$

where  $I$  is the influx rate in particles  $m^{-2} \text{ sec}^{-1}$ , and  $m$  is the particle mass in grams (McCracken, Alexander, and Dubin, 1961). The equation should not be used outside the range  $10^{-10} \text{ gm} \leq m \leq 10^{-6} \text{ gm}$ , and applies for an average particle velocity of 30 km/sec.

The distribution curve shown in figure 2 is intended to be an average for dust particles in the vicinity of Earth. Whether the distribution is the same in interplanetary space is a question that cannot yet be answered. If an appreciable concentration exists near Earth, then the influx rates measured at comparable sensitivities but at different geocentric distances should be functions of the geocentric distance. The influx rates measured at large geocentric

distances (Lunik II,  $3.6 \times 10^6$  km; Lunik III,  $4.7 \times 10^6$  km) should fall appreciably below those from the earth satellite Explorer VIII. The low altitude ( $\sim 150$  km) rockets should have shown influx rates considerably higher than those obtained with Explorer VIII. With the exception of the direct measurement from Pioneer I, the departures of direct measurements from the distribution curve established by Explorer VIII are negligible.

The distribution curve of figure 2 is shown, together with the model distributions of meteors from Watson (1941) and Whipple (1957, 1960), in figure 3. None of the linear extrapolations of the results from observations of meteors fits the direct measurements. The curves labeled "Watson (1941)" and "Whipple (1957)" approximately represent limits for the uncertainty encountered in placing average influx rates for meteors on a mass-distribution curve. The uncertainty of approximately 200 arises because the mass-to-magnitude relationships are not well known for meteors, and exceeds by one to two orders of magnitude the uncertainties that exist for the direct measurements. The curve labeled "Whipple (1960)" represents a revision by Whipple of the curve

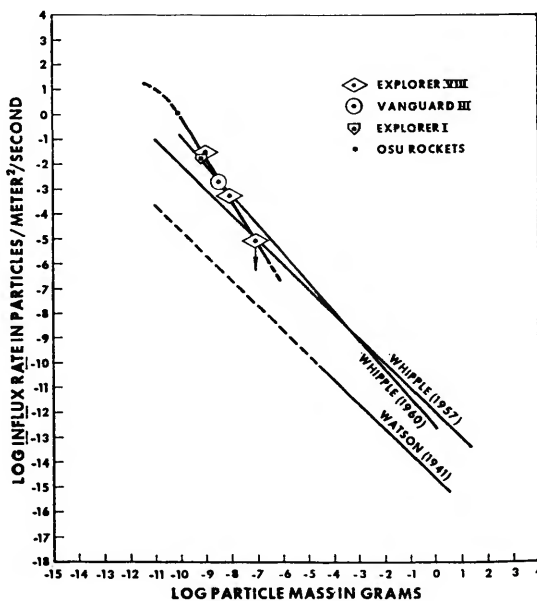


FIGURE 3.—Comparison of model distribution curves obtained from extrapolations of results from observations of meteors.

labeled "Whipple (1957)" made in an attempt to remove the discrepancy between the linearly extrapolated meteor curves and the direct measurements.

Whipple (1960, 1961a, 1961b) performed an analysis of the direct measurements and concluded that "Acoustical impacts of meteoritic dust on counting devices that are carried by satellites and space probes show clearly that a high concentration of interplanetary dust occurs near the earth" (Whipple, 1961b, p. 21). In his analysis, Whipple used the departures of direct measurements from the curve that is labeled "Whipple (1960)" in figure 3 in order to show that the geocentric concentration varied inversely as the 1.4 power of distance from the surface of Earth. Such an interpretation represents the second of the two interpretations that were possible before the direct measurements were obtained with Explorer VIII. Whipple's approach is incompatible with the new direct measurements from Explorer VIII and is not particularly supported by any of the other available direct measurements.

The following paragraphs present arguments against statements that the direct measurements confirm the existence of a geocentric concentration of dust particles.

The datum points representing the largest numbers of impacts (Explorer VIII, Vanguard III, Explorer I, OSU rockets) fit the same straight-line segment (see fig. 2), regardless of the altitude at which a particular direct measurement was obtained.

One must allow for the differences in sensitivity of the various microphone systems before comparing the influx rates to see if an altitude dependence exists. This requires normalizing all the direct measurements to a given value of particle mass. The distribution curve used as the normalization standard is extremely critical to the interpretation of the direct measurements. Using the conjectural curve labeled "Whipple (1960)" as the normalization standard leads one to the conclusion that the direct measurements indicate a geocentric concentration. Using the empirical distribution curve established by Explorer VIII leaves one with no discernible evidence from the direct measurements that a geocentric concentration of dust particles exists.

The slopes of straight-line segments of the distribution curve shown in figure 2, separately indicated by each of the three groups of direct measurements (U.S. spacecraft, Soviet spacecraft, OSU rockets), are between  $-1.5$  and  $-2.0$ . These values differ significantly from the value of approximately  $-1.2$  that was used by Whipple (1960) in order to normalize the direct measurements in such a manner that a geocentric concentration would be evident.

The most critical datum points in Whipple's analysis were the direct measurements from the OSU rockets and those from Explorer VI. It should be pointed out that in adjusting the sensitivities of the systems on the rockets, Whipple has introduced an error of about 15 in the influx rate. The data from Explorer VI have not been placed in the open literature by the experimenters, so it should not be used as a critical point.

### Conclusions

Several interesting conclusions can be reached on the basis of the new distribution curve that has been established by the direct measurements of interplanetary dust particles. Some of the more important are discussed in the following paragraphs.

The average distribution curve established by the direct measurements can be approximately represented over the range of mass  $10^{-10}$  gm  $\leq m \leq 10^{-6}$  gm, by a straight-line segment. The equation of the line segment is

$$\log I = -17.0 - 1.70 \log m,$$

where  $I$  is the omnidirectional influx rate in particles  $m^{-2} \text{ sec}^{-1}$ .

Particulate aggregates of matter accreted by Earth consist primarily of dust particles smaller than the faintest radar meteors, with an accretion rate of approximately  $10^4$  tons per day on Earth. This rate is in good agreement with the earlier estimate (Dubin, 1959) based on the direct measurement from Explorer I.

The convenient constant-mass-per-magnitude relationship, common to discussions of results from observations of meteors, does not hold for dust particles in the direct measurements range of particle mass. The distribution curve

established by the direct measurements departs markedly from the distribution curves obtained by extrapolating linearly the results from observations of meteors.

The available direct measurements extend almost into the range of particle mass where radiation-pressure control becomes important. A rather marked change in the shape of the distribution curve should occur as a result of radiation pressure at values of particle mass slightly lower than those presently covered by the direct measurements.

The distribution curve established by the direct measurements can be joined to a model constant-mass-per-magnitude curve for meteors within the range of particle size typical of the faint radar meteors. Such a junction probably has little physical meaning until the mass-to-magnitude relationship can be established for meteors, or until statistically significant direct measurements can be obtained in the range of particle mass  $10^{-7} \text{ gm} \leq m \leq 10^{-5} \text{ gm}$ .

The direct measurements now available show (within themselves) no discernible evidence for the existence of an appreciable geocentric concentration of interplanetary dust particles. If a geocentric concentration does exist, then its existence can be reliably inferred from the type of direct measurements that is presently available only if future direct measurements obtained at large geocentric distances deviate appreciably from the average distribution curve shown in figure 2.

This curve can be used only to describe average conditions. It is already known from the direct measurements that fluctuations in the influx rate of at least  $\pm 10$  occur within intervals of a few hours for particles with masses of approximately  $10^{-10} \text{ gm}$  (Dubin, Alexander, and Berg, in this symposium, p. 109). The magnitude of the fluctuations presumably becomes quite large for particles near the radiation pressure limit on particle size. The distribution curve is slightly biased toward the autumn of the year because of the distribution in time of year of the direct measurements. If the annual variation in influx rate of dust particles resembles that of meteors, then the curve shown in figure 2 represents influx rates that are slightly higher than the true average values.

Large inconsistencies have been attributed to the direct measurements several times in the literature (Whipple, 1959; Kaiser, 1961). The various direct measurements seem to be remarkably self-consistent when analyzed on the basis of the new measurements from Explorer VIII, in which the authors place much confidence.

### Discussion

*Unidentified speaker.*—I wonder about the assumption of the average velocity of 25 to 40 km/sec for micrometeorites. It appears that the average velocity of meteorites is below 20 km/sec, and I would expect these particles to be in even more circular orbits and therefore at even lower velocities.

*C. W. McCracken.*—I assumed a value of 30 km/sec. That, at most, introduces an uncertainty of a factor of 2 in the placement of the curve on the mass distribution plot.

### References

- ALEXANDER, W. M.; MCCracken, C. W.; AND LA GOW, H. E.  
1961. Interplanetary dust particles of micron-size probably associated with the Leonid meteor stream. *Journ. Geophys. Res.*, vol. 66, pp. 3970-3973.
- BEARD, D. B.  
1959. Interplanetary dust distribution. *Astrophys. Journ.*, vol. 129, pp. 496-506.
- BOHN, J. L., AND NADIG, F. H.  
1950. Researches in the physical properties of the upper atmosphere with special emphasis on acoustical studies with V-2 rockets. Research Institute of Temple University, Report No. 8, pp. 1-26.
- BUCK, R. F.  
1960. Acoustic detection of meteoric particles. Research Foundation, Oklahoma State Univ., Final Report, Contract No. AF 19(604)-1908.
- DUBIN, M.  
1956. Meteoric bombardment. In *Scientific uses of earth satellites*, J. A. Van Allen, ed., pp. 292-300. University of Michigan Press, Ann Arbor.  
1957. Discussion following paper by Thomas C. Poulter. In *Proceedings of the Second Hypervelocity and Impact Effects Symposium*, May 22-24, Washington, D.C., pp. 11-12.

## DUBIN—Continued

1959. Cosmic debris of interplanetary space. *In* *Vistas in astronautics*, M. Alperin and H. F. Gregory, eds., vol. 2, pp. 39–45. Pergamon Press, New York.
1960. IGY micrometeorite measurements. *In* *Space research*, H. K. Bijl, ed., pp. 1042–1058. North-Holland Publishing Co., Amsterdam.
1961. Remarks on the article by A. R. Hibbs, "The distribution of micrometeorites near the earth." *Journ. Geophys. Res.*, vol. 66, pp. 2592–2594.
- KAISER, T. R.  
1961. The incidence of interplanetary dust. *Ann. Géophys.*, vol. 17, pp. 50–59.
- LAGOW, H. E., AND ALEXANDER, W. M.  
1960. Recent direct measurements of cosmic dust in the vicinity of the earth using satellites. *In* *Space research*, H. K. Bijl, ed., pp. 1033–1041. North-Holland Publishing Co., Amsterdam.
- McCRACKEN, C. W.  
1959. An analysis of rocket and Earth satellite measurements of micrometeoritic influx. Thesis, Oklahoma State University. (See also Appendix B, Oklahoma State Univ., Final Report, Contract No. AF 19(604)–1908.)
- McCRACKEN, C. W.; ALEXANDER, W. M.; AND DUBIN, M.  
1961. Direct measurement of interplanetary dust particles in the vicinity of Earth. *Nature*, vol. 192, pp. 441–442.
- NAZAROVA, T. N.  
1960. The results of studies of meteoric dust by means of Sputnik III and space rockets. *In* *Space research*, H. K. Bijl, ed., pp. 1059–1062. North-Holland Publishing Co., Amsterdam.
- WATSON, F. G.  
1941. *Between the planets*. The Blakiston Co., Philadelphia.
- WHIPPLE, F. L.  
1957. The meteoritic risk to space vehicles. Presented at VIIIth Int. Astronautical Congress, Barcelona, 1957. Published in *Proceedings*, pp. 418–428; Springer-Verlag, Vienna, 1958.
1959. Solid particles in the solar system. *Journ. Geophys. Res.*, vol. 64, pp. 1653–1664.
1960. The particulate contents of space. Presented at Third Symposium on the Medical and Biological Aspects of the Energies of Space, Texas, 1960. Published in *Medical and biological aspects of the energies of space*, P. Campbell, ed., pp. 49–70. Columbia University Press, New York, 1961.
- 1961a. The dust cloud about the earth. *Nature*, vol. 189, pp. 127–128.
- 1961b. Dust halo. *Space World*, vol. 1, No. 8, p. 20 ff.

**Abstract**

Existing direct measurements of small interplanetary dust particles in the vicinity of Earth are analyzed on the basis of a new set of data obtained with the satellite Explorer VIII. All but one of the direct measurements made with microphone systems fit remarkably well onto the distribution curve derived from the Explorer VIII data. This good fit allows one to establish an average distribution curve for small interplanetary dust particles in the vicinity of Earth.

The equation of a straight-line segment that approximately fits the new distribution curve for particle masses in the range  $10^{-10}$  gm  $\leq m \leq 10^{-8}$  gm is

$$\log I = -17.0 - 1.70 \log m,$$

where  $I$  is the influx rate in particles  $m^{-2} \text{ sec}^{-1}$ . One of the more important consequences of the new distribution curve is the fact that the particulate matter accreted by Earth is dominated by particles with characteristic dimensions of a few microns.



# Micrometeorite Measurements from Midas II (Satellite 1960 ζ 1)

By R. K. Soberman <sup>1</sup> and L. Della Lucca <sup>2</sup>

To detect micrometeorites in the vicinity of the earth, instruments similar to those used on earlier satellites (Cohen, 1960) were carried on the Midas II (1960 ζ1) earth satellite. Midas II was launched, on May 24, 1960, into an approximately 500-kilometer circular orbit which was inclined 33° with respect to the equatorial plane of the earth.

Five detectors were mounted on the vehicle as shown in figure 1. Three of the detectors were acoustic or microphone type and two were wire-grid type. The dotted lines in the sketch indicate a detector facing outward on the other side of the vehicle.

The vehicle was designed to maintain a stabilized attitude, with the end shown on the right in figure 1 pointing radially outward from the earth. Attitude stabilization was not achieved. Data obtained from other experiments on the vehicle indicate that it was tumbling, but the data are inadequate to determine the attitude history of the vehicle.

Data from the acoustic detectors were acquired only for impacts that occurred while the vehicle was being interrogated by a receiving station. Provision had been made to acquire data over other portions of the orbit, but the vehicle recorders did not operate. The wire grids are inherently data-storage devices. Breaks in the wires that occur during any part of the orbit can be detected by periodically monitoring the continuity of the wires, and the number of breaks is accumulated.

Data (from stations located in Hawaii, California, and Florida) were obtained from parts of four orbits before the telemetry system

failed. Approximately 4,000 seconds of data were acquired from the acoustic detectors, while the grids provided data for 25,000 seconds of exposure.

Although the amount of data is small compared to that accumulated from other satellite vehicles, these are the first reported measurements at this altitude. In the light of recent hypotheses (Whipple, 1961; Hibbs, 1961) regarding the altitude variation of micrometeorite flux, it is felt that these results, although scanty, are worth mentioning.

Sixty-seven impacts were recorded on the three acoustic units, and were distributed over the four partial orbits for which data were acquired, as shown in figure 2. The solid lines indicate the portions of the flight path where a "clean" or noise-free signal was received. Since the total exposed area of the three acoustic plates was 686 square centimeters, the data represent a mean flux of 0.25 particles per square meter per second. The mean momentum sensitivity of the three acoustic units as determined by dropping spherical glass beads on the plates was  $3 \pm 1 \times 10^{-4}$  gm cm/sec. No shielding corrections have been applied. On the assumption of a mean velocity of 15 km/sec, the sensitivity represents a flux measurement of particles of mass greater than  $2 \times 10^{-10}$  gm. Further, if spherical particles of mean density 3 gm/cm<sup>3</sup> are assumed, the impacting particles would be larger than 5 microns in diameter.

No wire grids were broken. An area of 790 square centimeters of grids was exposed. The wire diameter was approximately 20 microns. Previous work (Cohen, Corman, and Dubin, 1959) has indicated that hypervelocity particles 10 microns in diameter or larger should break

<sup>1</sup> Geophysics Research Directorate, Air Force Cambridge Research Laboratories, Bedford, Mass., and Northeastern University, Boston, Mass.

<sup>2</sup> Geophysics Research Directorate, Air Force Cambridge Research Laboratories, Bedford, Mass.

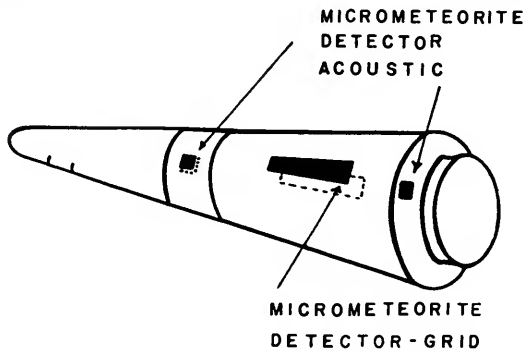


FIGURE 1.—Earth Satellite 1960 ζ1

this size wire. Therefore, the flux of particles larger than 10 microns in diameter is less than  $5 \times 10^{-4}$  particles per square meter per second.

If one assumes the type of distribution function that is commonly arrived at from various data considerations such as Whipple's meteoric risk curve (Whipple, 1958), then the data from the two types of detectors appear to be inconsistent. That is, the ratio of fluxes from the two types of measurements is greater than 500 where the particle sizes differ by a factor of 2 or so, depending upon the assumptions made regarding velocity and density.

One might thus disregard the acoustic measurements with the assumption that the units were not working properly, or that either vehicle noise was being introduced or thermal noise was occurring within the units themselves. This is the usual manner of accounting for high flux rates observed from the first day's data of practically all satellite vehicles.

For several reasons it is felt that the acoustic data should not be discarded. First, the microphones and plates were acoustically isolated from the vehicle. There was only one instance where all three acoustic units were triggered during the one-second interval between readouts. This triple coincidence, shown in figure 2, was not included in the total count or in the flux calculations. Second, although the microphone and grid measurements appear to be inconsistent with each other, more recent information is now available that shows that the values obtained are reproducible. A preliminary reduction of the data from the Satellite 1961 α1 has been completed. These results are not yet in final form and may vary slightly.

They are presented here for comparison purposes only. Satellite 1961 α1 was in a circular polar orbit at approximately the same altitude (about 500 kilometers) as Satellite 1960 ζ1. Similar experiments of approximately the same sensitivities were carried out. Data were obtained from parts of 23 orbits, again only over readout stations. The data from the acoustic units yield a mean influx of 0.34 particles per square meter per second. It should also be pointed out that while the measured acoustic flux shows statistical variations over the 23 orbits, it does not appear to decrease with time. Also on Satellite 1961 α1 eight breaks occurred in the wire grids. These all occurred after the first interrogation somewhat as follows: No break during the first orbit; three breaks in the next 7 orbits; 1 break in the second 7 orbits; and finally 4 breaks in the last 8 orbits. This leads to a flux of particles detectable by the wire grids (i.e., larger than 10 microns in size) of  $8 \times 10^{-4} \text{ m}^{-2} \text{ sec}^{-1}$ . The ratio for the Satellite 1961 α1 acoustic-grid measurements is about 400 as compared with greater than 500 for Midas II. A complete report on the Satellite 1961 α1 measurements will be published shortly.

It is felt that the similarity of the measurements from Satellites 1960 ζ1 and 1961 α1 cannot be ignored. Despite the apparent inconsistency the values appear to be reliable. Varying the assumed values for velocity and density within reasonable limits does not change the particle diameters appreciably since the cube root of these values is involved in the calculation. It may be necessary to re-examine the calibration of these devices by means of hypervelocity techniques now available to resolve the apparent discrepancy. The possibility of a large variation in the distribution function can be eliminated. The acoustic units on board Satellite 1961 α1 had two momentum sensitivities. The lower sensitivity range (with the previously assumed values for velocity and density) should have a threshold of 10 microns. The recorded fluxes are not consistent with the wire-grid data.

The remaining possibility that can be suggested is that fluffy particles of very low density, that might not be able to break the wire grids, are the major constituent of the acoustic flux.

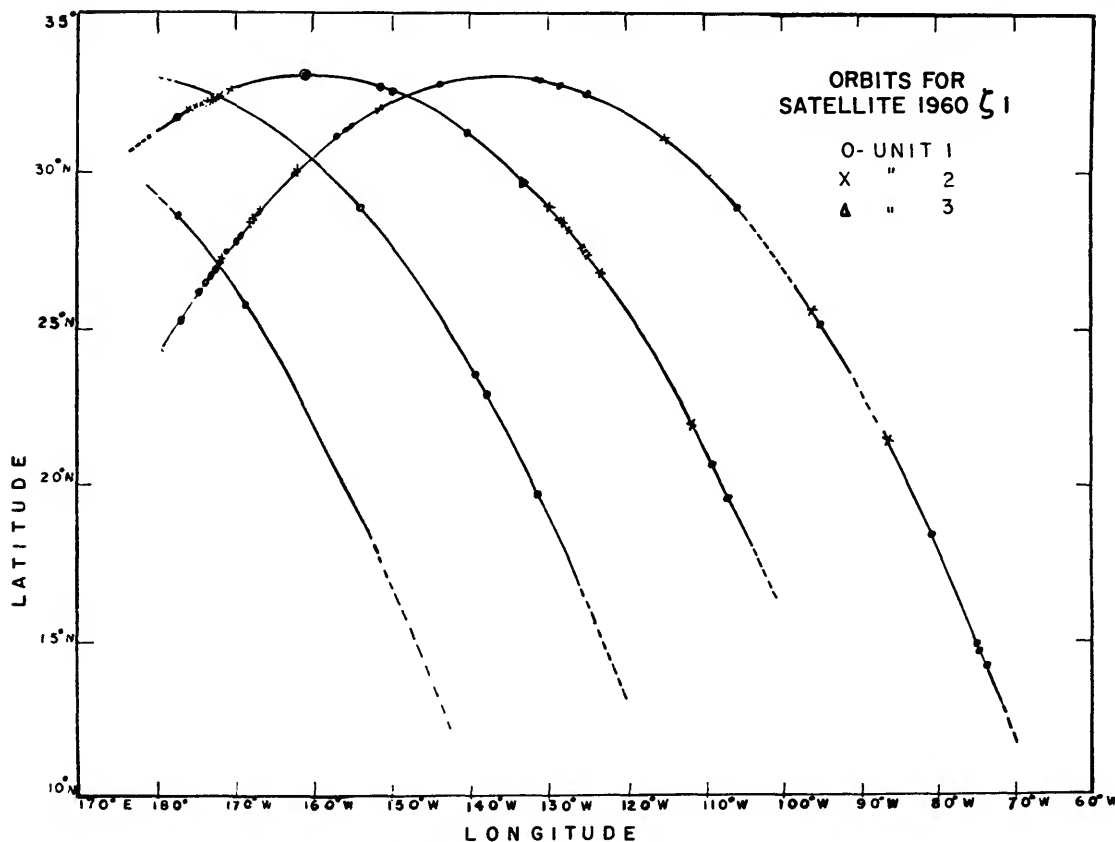


FIGURE 2.—Occurrence of micrometeorite impacts.

This possibility does not agree with empirical formulas of hypervelocity penetration, but cannot be entirely discounted. It is not presently possible to check this hypothesis in the laboratory since techniques for accelerating fluffy particles do not yet exist.

Finally, the relationship between the acoustic data reported here and the altitude variation of micrometeorite flux should be pointed out. Figure 3 shows a curve similar to that given by Whipple (1961). The acoustic flux as measured from Satellite 1960 ζ1 (corrected to a value of  $10^{-9}$  gm by assuming a mass distribution function which is proportional to  $m^{-1.2}$  and a velocity of 15 km/sec) has been added. The corrections are the same as those applied to the other satellite points in Whipple's paper. The early acoustic rocket data, about which there is some dispute, have been deleted and a new curve with a slope of  $-1.1$  has been fitted to the

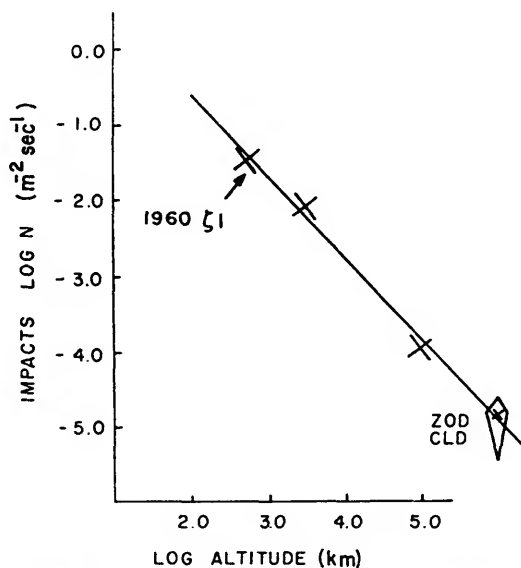


FIGURE 3.—Meteoritic impact (mass= $10^{-9}$  gm) versus altitude from the earth. (Revised from Whipple, 1961.)

points. It should be pointed out that with the exception of the zodiacal cloud, all the points were obtained with satellite acoustic detectors.

In conclusion, the data reported here establish that a discrepancy exists between the acoustic and the wire-grid measurements which must be resolved before the dust content of the interplanetary medium is understood. However, if one considers the acoustic measurements in a purely relative manner, it appears that there is a geocentric variation in the micrometeorite flux.

#### Acknowledgment

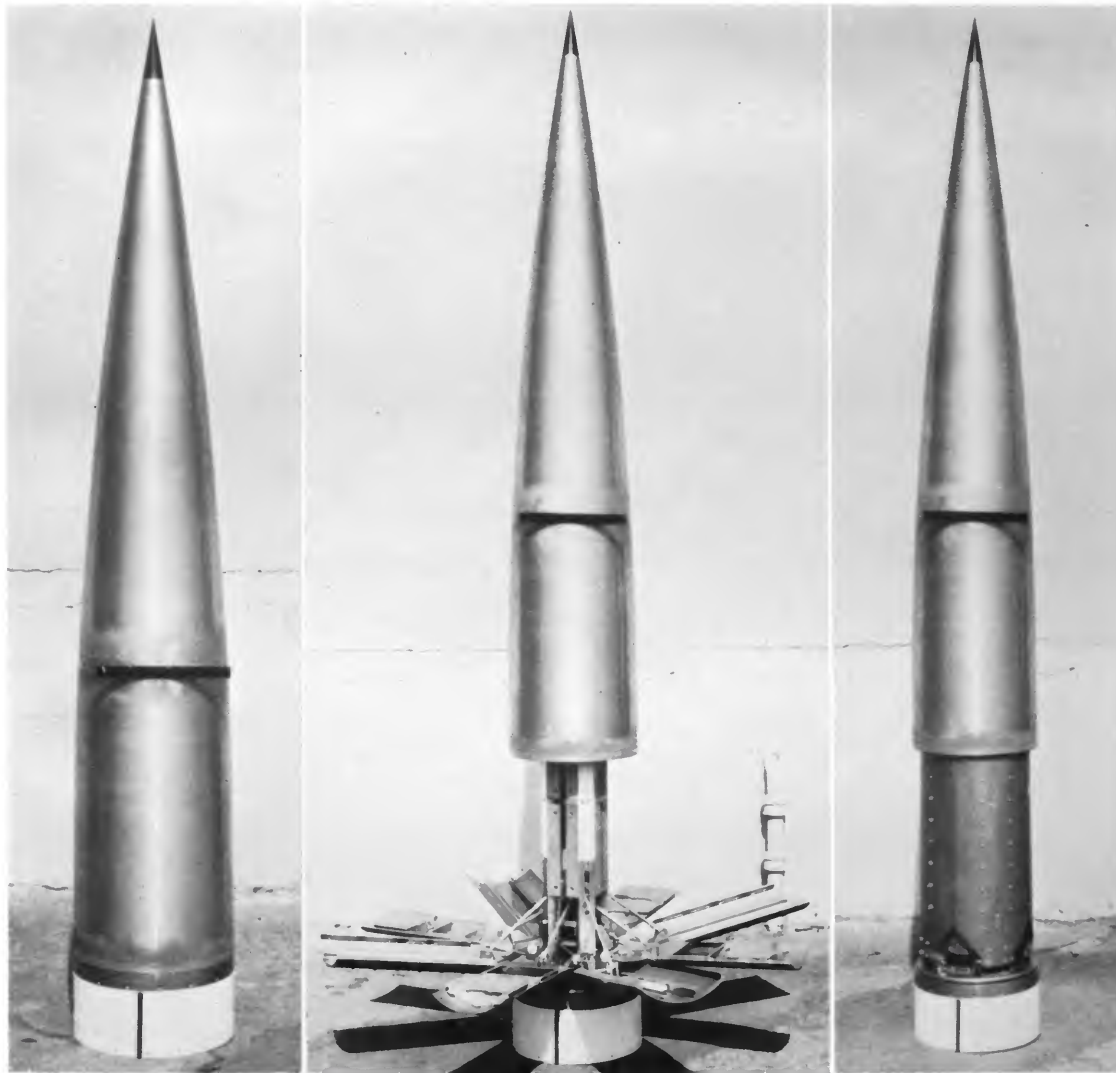
The authors are indebted to Dr. L. Bohn of Temple University for his cooperation and assistance in the preparation of this experiment, and to Mr. H. A. Cohen, who began this experiment.

#### References

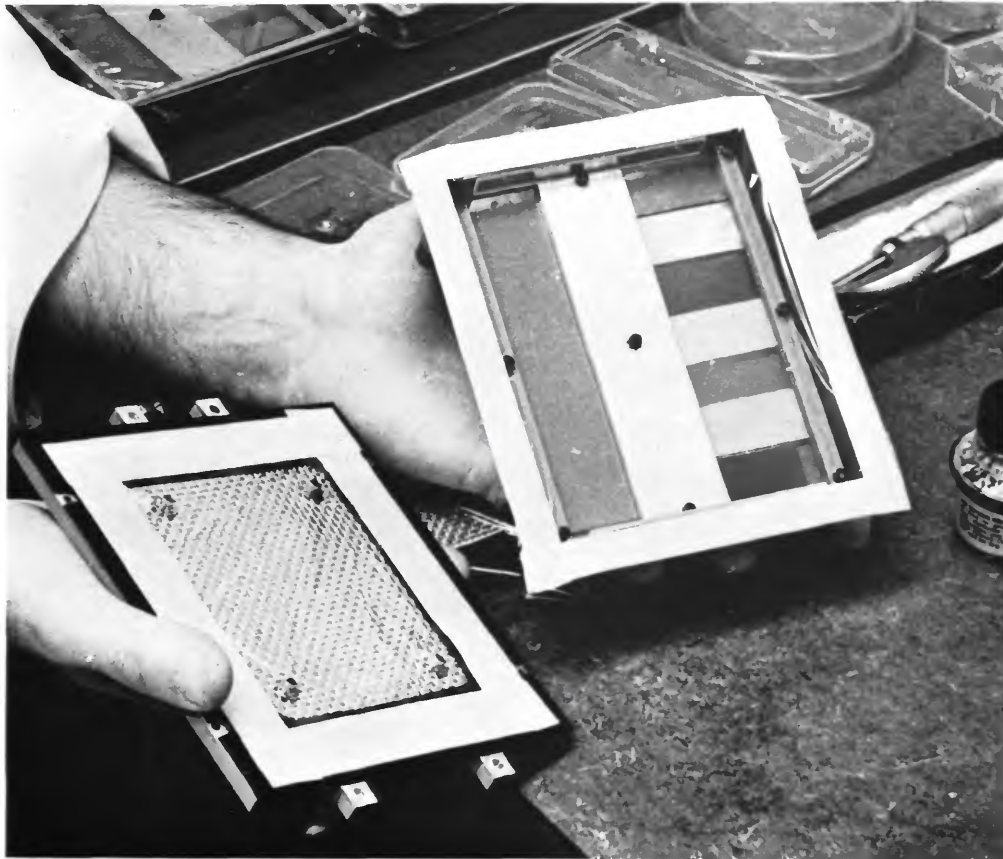
- COHEN, H. A.  
1960. Measurements of flux of small extraterrestrial particles. *Geophys. Res. Dir., Research Notes*, no. 28.
- COHEN, H. A.; CORMAN, A.; AND DUBIN, M.  
1959. Calibration of micrometeoritic detectors used in satellites and rockets. *In Proceedings 3d Symposium on Hypervelocity Impact*, vol. 1, pp. 405-421. Armour Research Foundation, Chicago.
- HIBBS, A. R.  
1961. The distribution of micrometeorites near the earth. *Journ. Geophys. Res.*, vol. 66, pp. 371-377.
- WHIPPLE, F. L.  
1958. The meteoritic risk to space vehicles. *In Proceedings 8th International Astronautical Congress, Barcelona, 1957*, pp. 418-428. Springer-Verlag, Vienna.  
1961. The dust cloud about the earth. *Nature*, vol. 189, pp. 127-128.

#### Abstract

Five micrometeorite sensing devices were carried on board the Midas II (Satellite 1960 f1) which was launched into an approximately 500-kilometer circular equatorial orbit on May 24, 1960. The five devices consisted of three acoustic detectors and two wire-grid detectors. Data were obtained for four partial orbits. These data were recorded in real time. There were no breaks in the wire grids which could record impacts of particles larger than 10 microns. Sixty-seven impacts were recorded on the acoustic detectors which had a momentum threshold of  $3 \times 10^{-4}$  gm cm/sec and a total area of 0.0686 m<sup>2</sup>. These results indicate a flux of 0.25 m<sup>-2</sup> sec<sup>-1</sup> of particles 5 microns in diameter or larger if one assumes a mean velocity of 15 km/sec and a density of 3 gm/cm<sup>3</sup> for the particles. The discrepancy between acoustic and wire-grid data will be discussed. These results will be compared with those obtained from other satellite measurements.



Venus Flytrap nose cone. *Left to right:* fully closed, fully open, and partly open.



Typical micrometeorite collecting box.

# Micrometeorite Collection from a Recoverable Sounding Rocket. I

By R. K. Soberman,<sup>1</sup> C. L. Hemenway,<sup>2</sup> T. G. Ryan,<sup>3</sup> S. A. Chrest,<sup>4</sup> J. Frissora,<sup>4</sup>  
and E. F. Fullam<sup>5</sup>

On June 6, 1961, at 5:31 a.m., M.S.T., an Aerobee 150 rocket, descriptively named the "Venus Flytrap," was successfully fired from the White Sands Proving Ground in New Mexico. Photographs of the nose cone or "payload" section of that rocket are shown in plate 1. The photograph at the left shows the nose cone in the fully closed position in which it was fired and traveled up through the lower atmosphere. An electric motor then raised the outer skin or ogive assembly (photograph at right), and finally another motor, aided by the spin of two revolutions per second, which was applied to the rocket, extended the eight "leaves" outward to complete the opening cycle (middle photograph). The nose cone was designed to fly in this last position through the upper atmosphere, exposing collectors mounted on the tops of the leaves and on the internal structure. Prior to reentry the rocket was "de-spun," thus allowing the nose cone to be resealed, and the booster section was severed explosively from the payload. At an altitude of 6 kilometers a parachute was deployed and the nose cone descended to the ground where recovery was effected.

Four of the leaves carried a penetration experiment (sketched in fig. 1) which covered a total area of 0.24 square meter. The first

two layers were Mylar films 6 microns thick. These films were examined prior to the flight by means of a helium leak detector to insure that there were no holes. In addition to flux, penetration, and cratering data, it was hoped that this experiment might yield some zenith angle information if more than one layer were penetrated by the impinging particles.

A second type of experiment carried on the vehicle were surfaces which were intended to trap particles of lesser momentum (that is, submicron particles if such existed, or somewhat larger particles which had been sufficiently slowed down in the atmosphere). These surfaces were mounted in aluminum boxes for cleanliness. Eight such boxes, each having an open area of 160 square centimeters, were mounted on four of the leaves of the nose cone. The lids of the boxes, on which more collection surfaces were mounted, were fastened to the internal structure of the nose cone. The boxes and their covers were prepared with high-purity materials for this experiment. All boxes were treated and loaded in an identical fashion and were completely interchangeable.

Since the fabrication left the inside of the boxes extremely rough, it was found to be impractical to try to clean the internal surfaces. In order to prevent the collection surfaces from being contaminated with debris from the box, the debris was sealed to the surface with a plastic coating, a high-purity nitrocellulose. All the covers, clamps, screws, and washers were cleaned in benzene to remove grease and other contaminants. The open area inside the gasket on the cover was coated with a nitro-

<sup>1</sup> Geophysics Research Directorate, Air Force Cambridge Research Laboratories, Bedford, Mass., and Northeastern University, Boston, Mass.

<sup>2</sup> Dudley Observatory, Albany, N.Y., and Union College, Schenectady, N.Y.

<sup>3</sup> Geophysics Research Directorate, Air Force Cambridge Research Laboratories, Bedford, Mass.

<sup>4</sup> Northeastern University, Boston, Mass.

<sup>5</sup> Ernest F. Fullam, Inc., Schenectady, N.Y., and Dudley Observatory, Albany, N.Y.

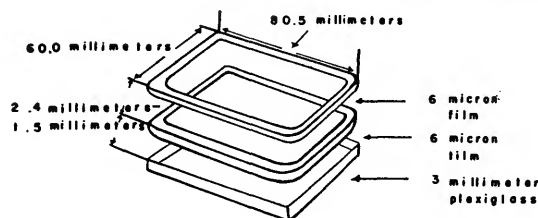


FIGURE 1.—Penetration experiment.

cellulose film 0.003 inch thick. This film was held in place with 10-mesh stainless-steel screening.

Eight different surfaces were loaded in the boxes. There were seven lucite slides, each  $\frac{3}{4}$  by 2 by  $\frac{1}{8}$  inch, covered with various substrates. The eighth surface was a large piece of bare lucite,  $1\frac{1}{2}$  by 5 by  $\frac{1}{8}$  inch. A schematic drawing of the positioning for the various substrates used is shown in figure 2.

All the thin films, each approximately 200 A thick, were supported with 200-mesh copper screening. The coated screening and the self-supporting thick nitrocellulose films (0.003 inch thick) were glued to the lucite slides which were held in place by clamps. Since there was no past experience to go by, a number of substrate materials and handling techniques were tried in an attempt to find the most effective and unambiguous collection system. A photograph of a typical box and cover is shown in plate 2. As can be seen in this photograph, the boxes and their lids were protected by sealed plastic covers.

Extreme care was necessary in handling these boxes to insure that contamination would be kept to a minimum. Therefore the nose cone was thoroughly cleaned prior to the installation of all the experiments. After installation of the experiments, the nose-cone operation was checked by cycling it twice in a precleaned room. During these operations the protective covers were still on the boxes and lids. Finally, a large sealed plastic tent was erected over the nose cone. The air in the tent was allowed to stagnate for some 2 hours, the nose cone was cycled for the final ground test, and during this test the protective covers were removed from the boxes and lids. The boxes and lids were exposed for less than 30 seconds in the tent before being sealed in the nose cone. An identical box was exposed in the handling room to

serve as controls for contamination. In addition, as can be seen from figure 2 and plate 2, there were controls mounted in each box. These controls consisted of an area approximately one-fourth of the surface area which was protected by an aluminum shield placed a half millimeter above the surface so that air could flow freely under the shield. These shielded surfaces were exposed in the same environments and subjected to the same handling procedures, but could not be impinged upon from above.

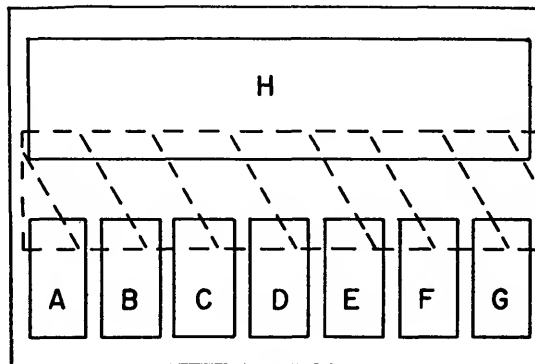


FIGURE 2.—Location of substrates for collection experiment: (A) lucite slide shadow-cast with aluminum, (B) silicon monoxide on thin formvar, (C) thick nitrocellulose film, (D) thin formvar, (E) thick nitrocellulose coated with carbon, (F) thin formvar shadow-cast with aluminum, (G) thin nitrocellulose shadow-cast with aluminum, (H) bare lucite.

The boxes were opened and closed during the flight by the action of the leaves. Upon descent of the nose cone the boxes were sealed by atmospheric pressure. Filtered ports at the base of the nose cone allowed pressure equalization inside the skin of the nose cone. The boxes however, were designed to maintain a vacuum inside.

These extreme precautions were not taken with the penetration experiments, but care was exercised that the film surfaces were protected from any direct contact.

The "Venus Flytrap" system performed as planned. The telemetry record which was used only to monitor the rocket functions indicated that everything operated perfectly and at approximately the preset times. From this telemetry record the angles at which the leaves were exposed were determined. The four leaves containing the penetration experiments

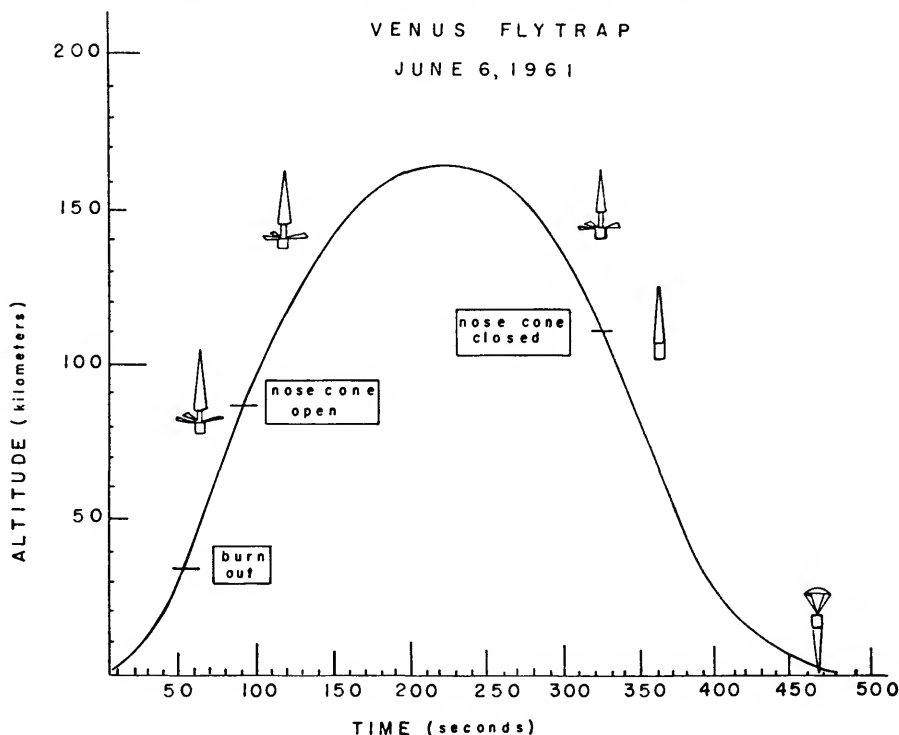


FIGURE 3.—Vehicle altitude plotted against time.

were exposed at an angle of  $73.5^\circ$  with respect to the vertical axis of the rocket. The four leaves on which the boxes were mounted were exposed at an angle of  $66.5^\circ$  with respect to this same axis.

An aspect camera was installed to record the attitude of the rocket. These data have not yet been fully reduced. However, it appears that the rocket axis precessed from about  $10^\circ$  on one side of the vertical to about  $45^\circ$  on the other side of the vertical during the portion of the flight where the nose cone was open. The spin of the rocket was reduced from 2 r.p.s. to 1.4 r.p.s. by the opening of the leaves. A device known as a "yo-yo" threw off two weights and reduced the spin to essentially zero just before the nose cone was closed. This was necessary, since the motor did not have sufficient power to close the leaves while the rocket was spinning.

In figure 3 the altitude of the rocket is plotted against time, and the curve shows that rocket burnout occurred at an altitude of 35 kilometers. It should be pointed out that at burnout the

fuel and oxidizer tanks were valved shut in accordance with standard rocket procedure. The opening of the nose cone was accomplished in about 1 second at an altitude of 88 kilometers. The rocket then ascended for 131 seconds to an apogee of 168 kilometers, and then descended for 105 seconds to an altitude of 116 kilometers where closing was accomplished again in about 1 second. During this entire exposure time the rocket remained in a near vertical attitude (i.e., it precessed, but did not turn over).

In figure 4 the velocity of the rocket is plotted against time and the curve shows that the rocket approximated a free-fall trajectory during the time that the nose cone was open.

The nose cone was found sealed and intact. It lay in the desert for about 1 hour after landing before being placed in a protective plastic bag. Samples of the desert sand were taken for control purposes. On return to the handling room the outer skin was washed down with acetone and the nose cone was wrapped in a clean plastic bag for shipment. One week later in a "dust

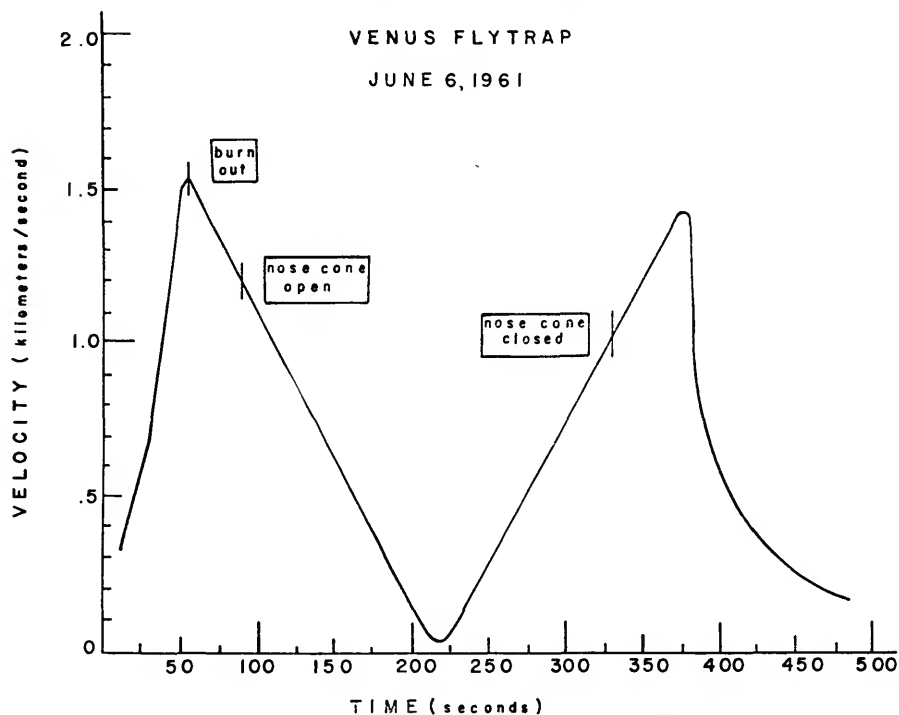


FIGURE 4.—Vehicle velocity plotted against time.

free" environment the nose cone was opened for examination. Five of the eight boxes were found to be still under sufficient vacuum to require opening by injection of clean air with a hypodermic syringe.

This experiment has been described in great detail because we believe that these details have an important bearing upon the validity of the results which are presented in the next paper.

#### Acknowledgments

We acknowledge the debt that this project owes to Mr. H. A. Cohen, who originally began the program. Further, we acknowledge the assistance of Messrs. R. Skrivanek and P.

Gustofson of the Geophysics Research Directorate at the Air Force Cambridge Research Laboratories. We also express our thanks to the staff at Aerojet-General Corp., particularly to Messrs. N. Migdal, J. Smith, and J. McCabe who fabricated the nose cone and assisted in the preparations for the experiment. Finally we thank Capt. T. Smith (USAF), Lt. J. Turpel (USN), and the officers and men of the U.S. Navy Missile Testing Center at White Sands, N. Mex., for their wonderful cooperation and assistance. But for the help of these and many other support groups, the experiment described above would still be "on the drawing boards."

#### Abstract

The "Venus Flytrap" micrometeorite collector rocket was fired from White Sands, N. Mex., on June 6, 1961, at 05:31 a.m., local time. Specially prepared particle impactors were exposed between the altitudes of 88 and 168 kilometers and successfully recovered. The rocket design and performance are discussed. The experimental surfaces consisted of 0.24 square meter of 6-micron-thick Mylar foil for impact and cratering studies, and 0.13 square meter of sealed boxes which were loaded with high-purity materials and surfaces suitable for electron microscopy. In all, eight different materials were used to permit an evaluation of the effectiveness of different materials and techniques for the collection and study of micrometeoritic particles. Some of these materials were shadowed with aluminum before and after the flight to aid in the discrimination of micrometeorite particles from contaminants.

# Micrometeorite Collection from a Recoverable Sounding Rocket. II

By C. L. Hemenway,<sup>1</sup> R. K. Soberman,<sup>2</sup> E. F. Fullam,<sup>3</sup> J. J. Balsamo,<sup>4</sup> J. Cole,<sup>1</sup>  
D. Hallgren,<sup>5</sup> P. Yedinak,<sup>6</sup> A. Goodman,<sup>6</sup> and G. Hoff<sup>1</sup>

As described in the preceding paper, two types of experiments were carried out on the "Venus Flytrap" rocket (i.e., the penetration and the trapping experiments). In this paper the results obtained to date from these experiments are presented.

The mylar films from the penetration experiment were tested by a helium leak detector after return to the laboratory. Three holes, shown in plate 1, were found in top-layer films. There was no evidence of damage on the second-layer films beneath these holes. The holes shown in plate 1*a,b* were found on the same mylar film. The first hole (pl. 1*a*) measures 90 microns across the short axis and 330 microns across the long axis. The second hole (pl. 1*b*) measures 450 microns across the short axis and 1160 microns across the long axis. The third hole (pl. 1*c*) found on another film which was mounted on the same leaf measures 330 microns across the short axis and 550 microns across the long axis. Note the flap structure and curling of the mylar in all three photographs. This flap structure and curling are believed to be indicative of low-velocity impact. From the appearance of the holes it is inferred that they were caused by particles comparable in dimension to the hole size which impacted at relative velocities of less than about 2 kilometers/second. Laboratory

studies are presently being carried out to verify these inferences and to determine the strength of these films under low-velocity impact conditions. Two holes found in an equal number of control films appear to have been caused by handling, and careful examination shows no similarity with the holes that were found on the flight samples.

A careful microscopic examination of the top-layer mylar films was made in the hope of finding imbedded particles or craters. It was immediately noticed that the upper layer of films had more particles on them than the second layer or the controls. But as was mentioned in the preceding paper, extreme cleanliness had not been maintained with these films and therefore this information could not be used. This scanning did not result in any further unambiguous information, since the experiment was designed to look for punctures and no records were kept of film defects.

There have been many attempts in the past to collect micrometeorite particles at ground level, on mountain tops, by balloons, and by high-altitude aircraft. However, all these techniques have been open to criticism because of contamination by terrestrial particles. Since this is a very serious problem, we next discuss the various safeguards which were built into the "Venus Flytrap" experiment to ensure reliable identification of micrometeorites. There were five controls for this portion of the experiment. Some have been described in the preceding paper. All five controls are listed below with brief comments:

1. *Laboratory exposures.*—These were spare boxes prepared at the same time and in the

<sup>1</sup> Dudley Observatory, Albany, N.Y., and Union College, Schenectady, N.Y.

<sup>2</sup> Geophysics Research Directorate, Air Force Cambridge Research Laboratories, Bedford, Mass., and Northeastern University, Boston, Mass.

<sup>3</sup> Ernest F. Fullam, Inc., Schenectady, N.Y., and Dudley Observatory, Albany, N.Y.

<sup>4</sup> Control Equipment Corp., Needham, Mass.

<sup>5</sup> Ernest F. Fullam, Inc., Schenectady, N.Y.

<sup>6</sup> Dudley Observatory, Albany, N.Y.

same way as the flight boxes. One of these spares was exposed in the laboratory for an extended period to study contamination particles from the laboratory. Micrometeorite particles as described below were not found in the laboratory controls.

2. *Rocket preparation exposure.*—A spare box was exposed at White Sands during final rocket testing. As described in the preceding paper, it was necessary to remove the mylar covers from the boxes at the time the nose cone was sealed. The boxes had to be fabricated in such a way that the nose cone could be opened and closed and yet not contaminate the samples while the final checkouts were being made on the nose cone. In the room where the nose cone was being cycled for the final time, a spare box was opened for the full time during which the mylar covers were off prior to the final sealing. This operation was carried out in a plastic tent as described in the preceding paper.

3. *Desert dust examination.*—A sample of desert dust was examined to see what kind of particles could be expected from the air at White Sands. To minimize desert dust contamination, the outside of the nose cone was thoroughly cleaned in the laboratory and kept in a plastic bag until one hour before flight and removed only when the rocket was pressurized. No evidence of desert dust contamination was detected.

4. *Rocket particle examination.*—In a clean environment wipings were made of the inside of the nose cone and were mounted on electron-microscope screens for examination. Some metal chips and some oil were found. None of the types of particles considered to be micrometeorites were found in these wipings.

5. *Shielded flight samples.*—The best controls were the shielded areas inside each box. Approximately one quarter of the area of each box was blocked off in such a way that air flow was allowed beneath the shield, by separating the shield approximately a half millimeter from the control surfaces. Thus, if small particles were drifting around in the air they could wander beneath the shield, yet any particles that would hit at high altitude would be prevented from hitting these control surfaces. Plate 2 of the

preceding paper shows the metal shield in the middle of an open box.

This study utilized three independent teams of electron microscopists using three electron microscopes. It may be relevant here to point out some of the characteristics of electron microscopes. The magnification of an electron microscope is generally very high in comparison with optical techniques and one can scan only a few square millimeters per day. With an electron microscope, the limit of resolution is of the order of 10 to 200 Å, which is a factor of 100 or more better than the resolution possible with optical-microscope techniques. With an electron microscope, one can distinguish surface details and textures of particles, can measure particle sizes accurately, and can see how transparent the particles are to electrons. Finally, while optical microscopes can scan large areas, it is generally extremely difficult to distinguish one small particle from another. When studying micrometeorites one is always working with a "noise" or "background" level, and contaminant particles will always be present. It will be shown that if the textures of the particle surfaces, the shapes and sizes of the particles, and so on, can be studied, contaminants can be recognized and readily ruled out of consideration.

Perhaps the most effective technique utilized in this experiment for micrometeorite identification is the shadowing technique wherein, just before the boxes were loaded, certain of the slides had a coating of aluminum evaporated on the collection surface at an angle of approximately 80° from the normal to the surface. Thus any particles that were on the collection surface before the boxes were loaded would cast a shadow in the direction in which the aluminum was deposited. After the flight, another shadowing at 75° was put on at roughly right angles to the previous shadowing. If a particle was deposited between the two shadowings it should have only the second shadow, and if it was deposited during the scanning process it should have no shadows. Contaminant particles within the films will also be shadowless. This shadowing or flagging technique is a useful way of reducing the ever present contamination level. The flagging techniques had disadvantages. For example, if one attempts electron-diffraction analyses then one may be bothered

by the presence of the aluminum, although it may be convenient for some purposes to have a calibration standard on the same sample.

After a preliminary examination of the various collecting surfaces it was decided, for the initial study of the particles, to concentrate on the surfaces on which the flagging technique was employed. The observer scans first with a magnification of the order of 2000 to 5000 times. He looks for single-flagged particles. However, a single flag is considered to be a necessary but not a sufficient requirement, since it was possible for contaminant particles to be deposited between the two flaggings. The single-flagged particle is examined to determine whether it can be recognized as a contaminant at low magnification. If not, then the magnification is increased to between 15 and 20 thousand times, and the particle examined very carefully. In order to be counted as a micrometeorite the particle has to be of a type not found on *any* of the controls.

There are three types of particles that did not appear on the controls. These were dense spheres with sharp edges ranging in size down to a few tenths of a micron or even less, irregular submicron particles, and extremely irregular particles which were termed "fluffy." In addition, some smashed fluffy particles were found. Also a number of holes were found in some of the thin collecting surfaces. The results described here were obtained with surfaces of nitrocellulose and formvar (approximately 200 A thick).

Plate 1*d* shows an optical micrograph of a portion of a 200-mesh per inch copper screen which has an open area roughly 100 microns along an edge. Plates 2-6 are electron micrographs of a small portion of these open areas in the mesh screen.

Plate 2*a* shows the flagging technique described above. The particle on the left has two shadows and is therefore clearly a contaminant; the particle on the right has one shadow and was identified as an irregular type submicron micrometeorite.

Plate 2*b* shows mica-like contaminants. This type is found on all electron microscope slide materials and apparently is in the air we breathe. There have been no successful tech-

niques to eliminate this type of contaminant from electron microscope specimens. These particles can be readily identified; they are flat, of low density, and have sharp edges.

Plate 3*a* shows a rounded, medium-density, submicron particle of the type initially difficult to identify as a contaminant. Notice the fuzzy edge of this particle. These types of submicron particles were found on both the controls and the flight samples. One reason for using high magnification to aid in the identification of micrometeorites was to discover whether such particles had sharp or fuzzy edges.

Plate 3*b* shows a small spherical micrometeorite with a sharp edge and high density. Notice that it can be readily distinguished from the fuzzy-edged spherical particle in plate 4*a*.

Plate 4*a* shows a large irregular type of particle which looks almost like a museum meteorite. Notice that the surface is characterized by rounded irregularities and is partially transparent to electrons (medium density). This particle was counted as a large irregular micrometeorite; in fact, it is one of the largest single-flagged particles found to date.

Plate 4*b* shows an extremely irregular particle which is termed a "fluffy" particle. All particles not having a compact structure were labelled "fluffy." Like the others obtained in the Venus Flytrap experiment, this type of particle is found in U-2 aircraft collections. Plate 4*c* shows a fluffy particle obtained from a U-2 collection.

Plate 5*a* shows a "sphere" with a hole. Notice that the "sphere" is not quite spherical. It is approximately 2.25 microns in diameter and is the largest of the spheres found thus far. The hole is about 2.4 microns in diameter and apparently the sphere bumped into this 200 A-thick nitrocellulose film, did not get through, and made a flapped hole about the same size and shape as its own body. A number of flapped holes of this type have been found.

Plate 5*b* shows a flapped hole where a smaller spherical particle broke through the thin nitrocellulose completely. Apparently the flapped-hole phenomenon appears over a wide range of dimensions when one deals with low-velocity collisions.

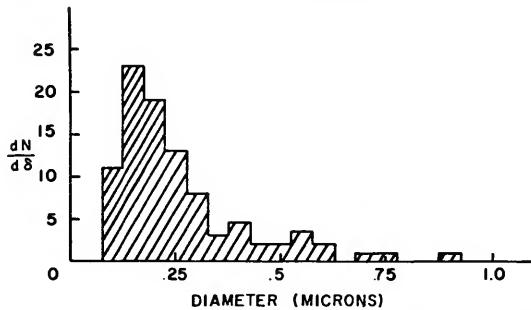


FIGURE 1.—Size distribution of irregular micrometeorites, 0.1 to 1 micron.

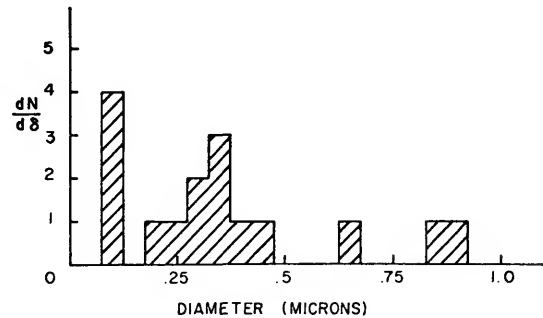


FIGURE 2.—Size distribution of "fluffy" micrometeorites, 0.1 to 1 micron.

Plate 5c shows an elliptical hole where the particle apparently penetrated the thin film at an angle to the surface. Notice the flaps as well as the cracks radiating from the ends of the hole.

Plate 6a shows a portion of a smashed particle, probably a fluffy type. The debris extended over a length of more than 100 microns. Several of these smashed particles have been observed. Such particles are also found in impact-type collections made with U-2 aircraft. An attempt will be made to measure the breaking strength of fluffy particles to determine whether the values obtained correspond to those required to crumble cometary meteoroids.

Plate 6b shows a group of particles. Since it was uncertain whether such particle groups represented debris from the breakup of a larger particle, this type of particle group was not considered in the determination of size distributions.

Figure 1 shows a distribution function for the irregular type of particles. In the figure only particles in the region of 0.1 to 1 micron have been plotted. A few larger and smaller individual particles were found.

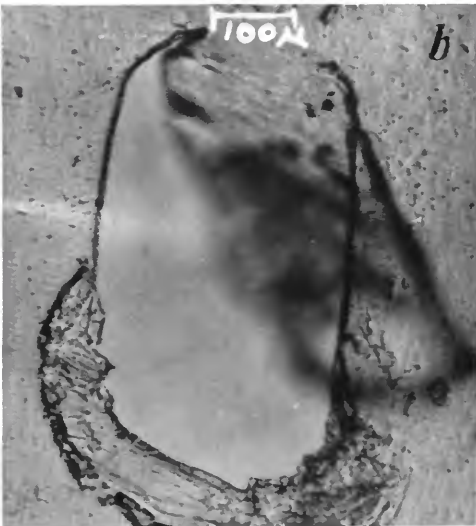
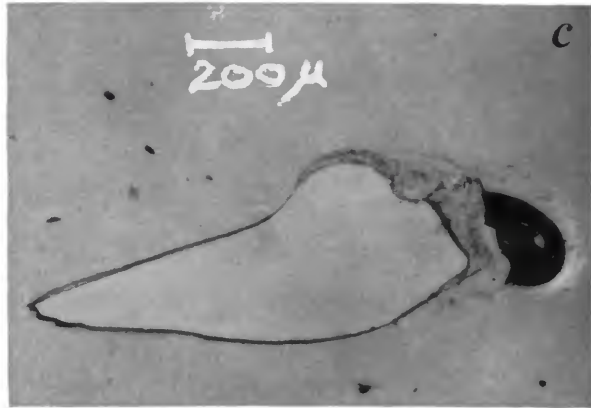
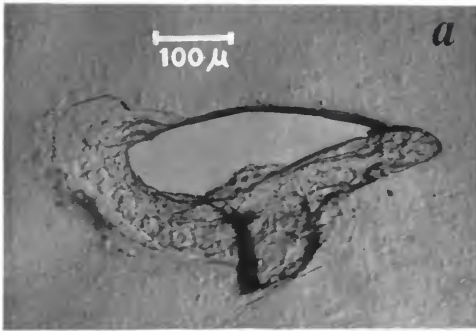
Figure 2 shows a distribution of the "diameters" of the fluffy-type particles. It is rather difficult to determine mean diameters. For this determination the diameters in two perpendicular directions were measured and the particle was assumed to be ellipsoidal.

In figure 3 the size distribution of the spherical-type particles has been plotted. Notice that the size extends down to one-tenth of a micron and apparently the number-per-

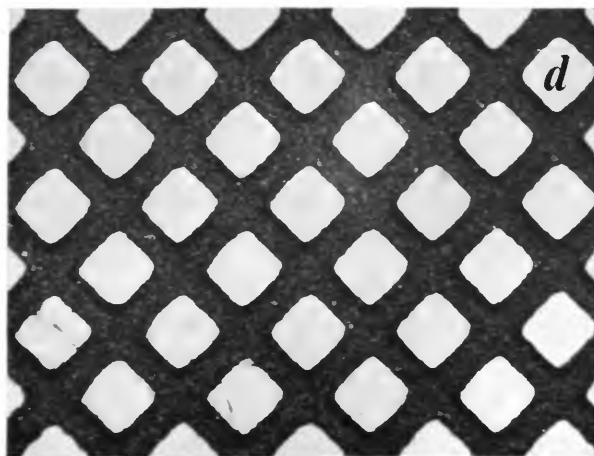
size range is still increasing at that point. There are also some larger spherical particles which are not shown on this distribution.

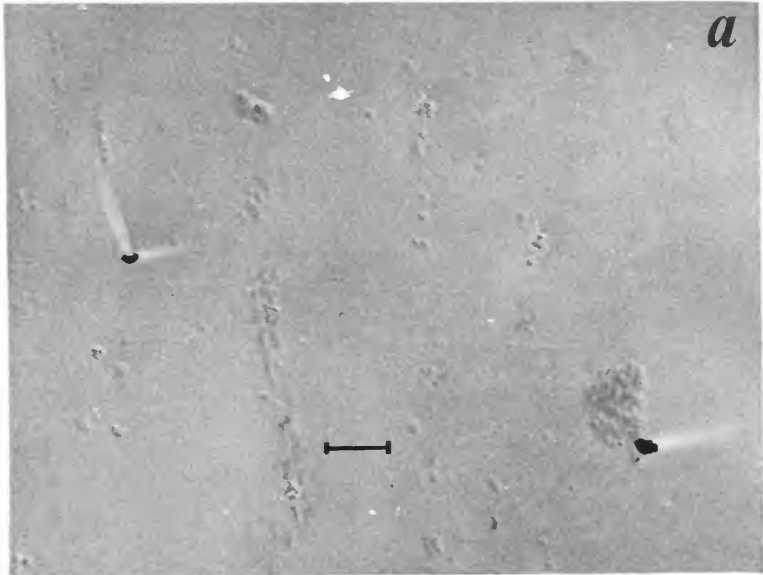
Figure 4 shows the distribution of spherical holes. Notice that there appears to be a cutoff at about 0.3 micron. The fact that the distribution extends down to sizes as small as this, and that spherical particles much larger than the minimum size hole are observed, indicates that there must have been a diversity in the velocities of particles hitting the surfaces.

To date, 133 particles which are believed to be of extraterrestrial origin have been found in the range of 0.1 to 1 micron in diameter. They were found in a total area of 17.84 square millimeters. Eleven particles larger than 1 micron have been found in an area of 18.52 square millimeters. This latter area is a little larger because the less serious laboratory contamination problem associated with larger particles permitted faster scanning. The total number of particles larger than 0.1 micron per unit area was 7.3 per square millimeter. If we separate these particles according to type, 72 percent are irregular with sharp edges and rounded texture, 16 percent are high-density spheres, and 12 percent are of the fluffy type. Of the single-flagged particles examined, two out of every three were judged to be micrometeorites, although this number varied somewhat from sample to sample. In a few cases there was some difficulty in deciding whether or not a particle was a micrometeorite. Each operator was asked how frequently he experienced this difficulty, and the largest number of doubtful cases was found to be 10 percent.



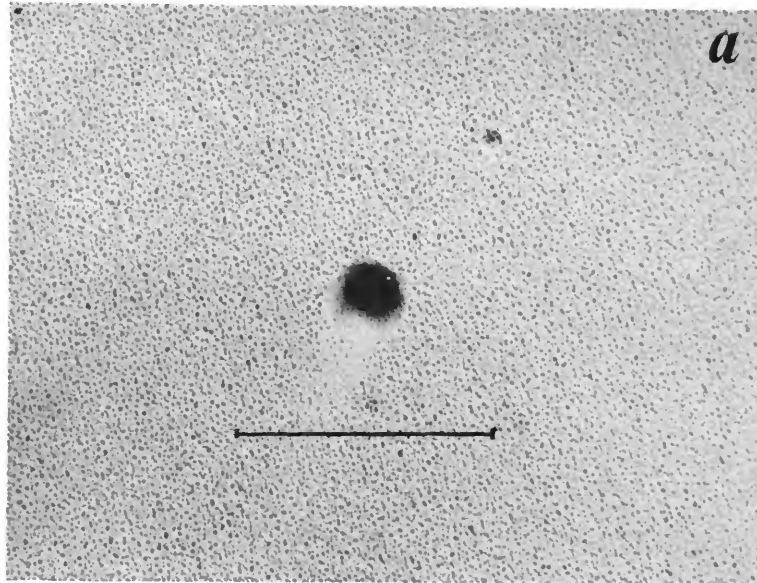
*a-c*, Mylar films showing holes caused by meteorites. *d*, 200-mesh-per-inch copper screen used to support collecting surfaces.



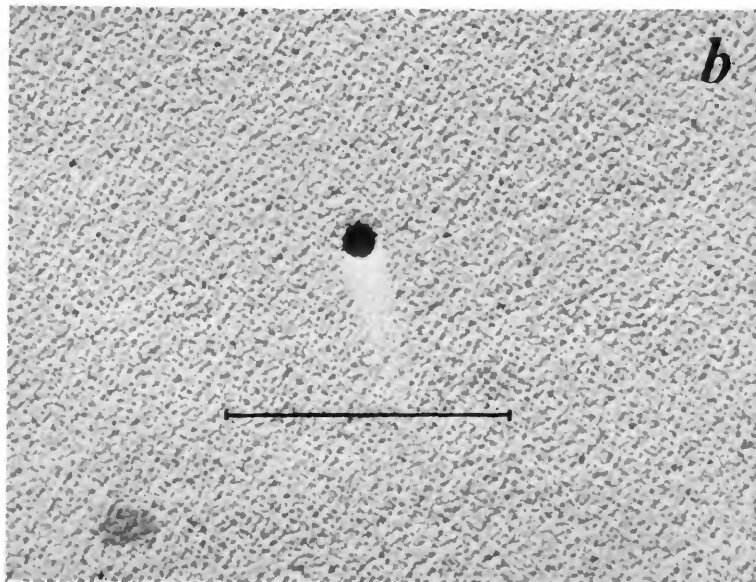


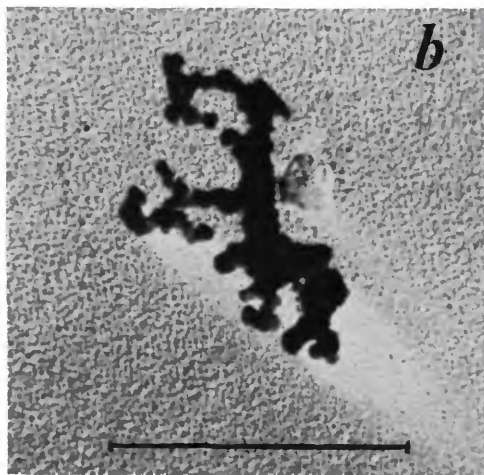
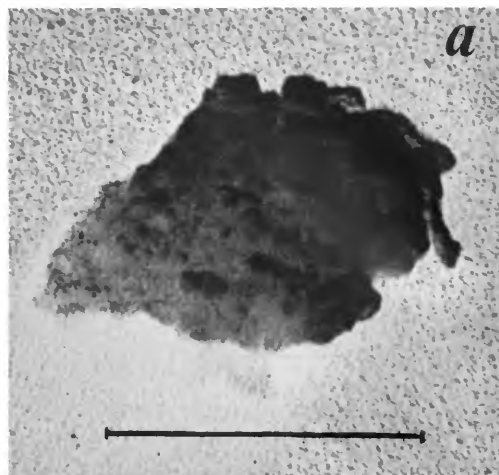
*a*, Illustration of flagging technique used to identify micrometeorites. *b*, Mica-like contaminant particles. Scales, 1 micron.



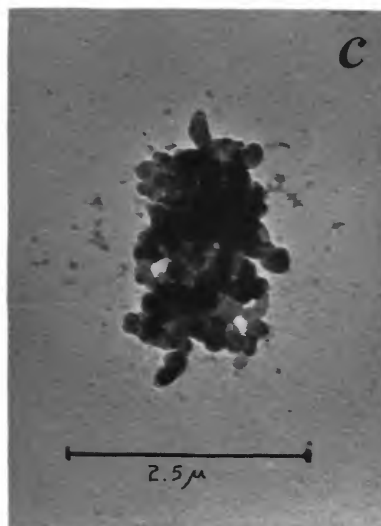


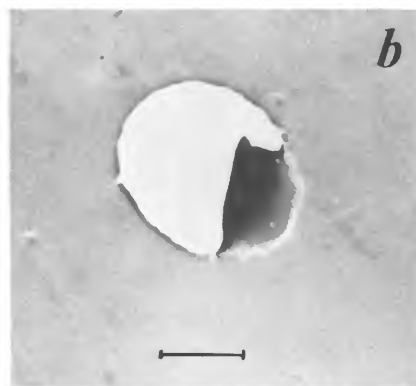
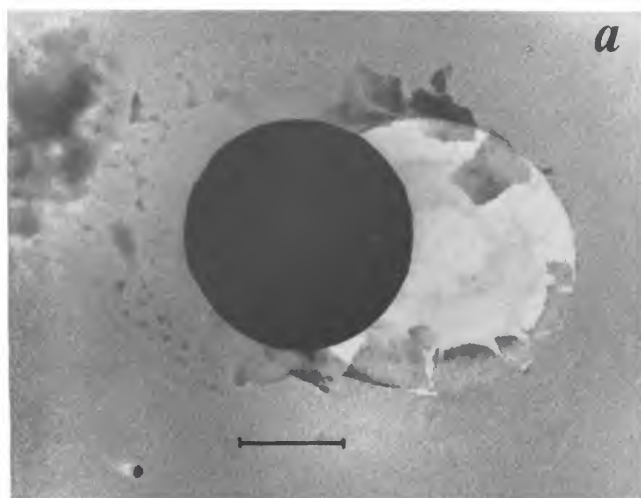
*a*, Submicron contaminant particle. *b*, Submicron spherical micrometeorite.  
Scales, 1 micron.



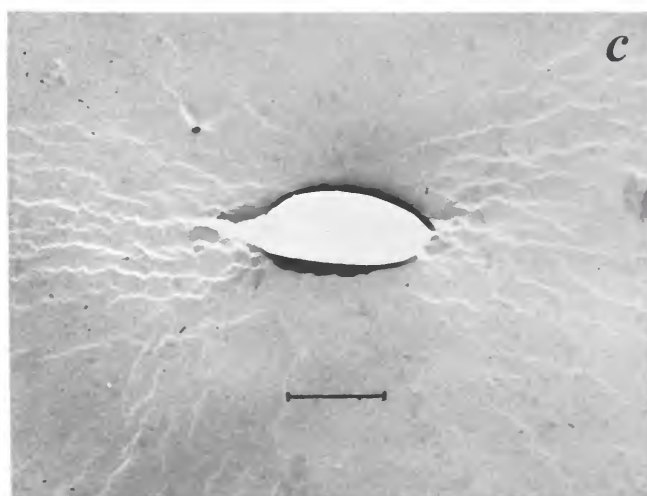


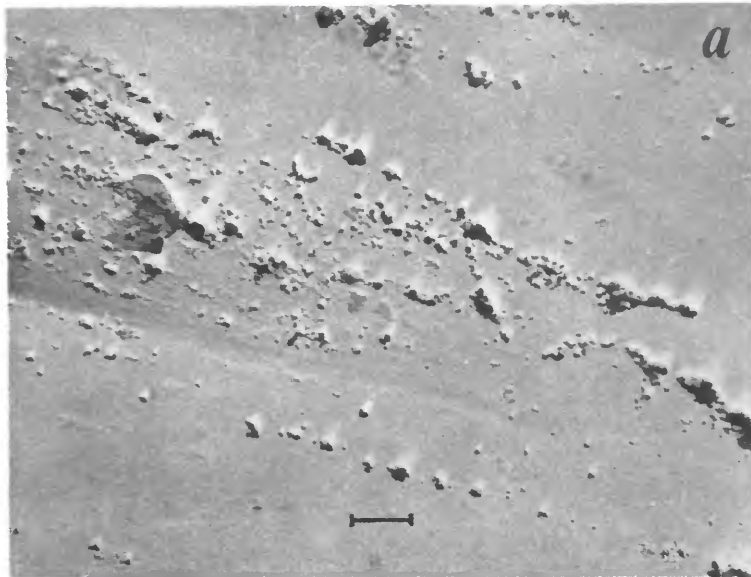
*a*, Irregular micrometeorite. *b*, "Fluffy" micrometeorite. Scales of *a* and *b*, 1 micron. *c*, "Fluffy" particle obtained from U-2 collection.



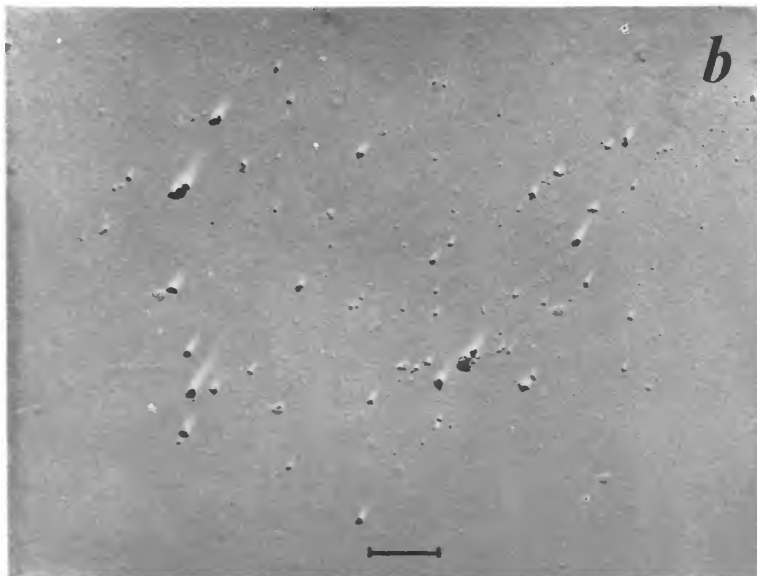


*a*, Spherical micrometeorite and hole. *b*, Circular hole created in 200 Å-thick film by micrometeorite. *c*, Elliptical hole created in 200 Å-thick film by micrometeorite. Scales, 1 micron.





*a*, Remnants of a smashed micrometeorite. *b*, Cluster of irregular micrometeorites.  
Scales, 1 micron.



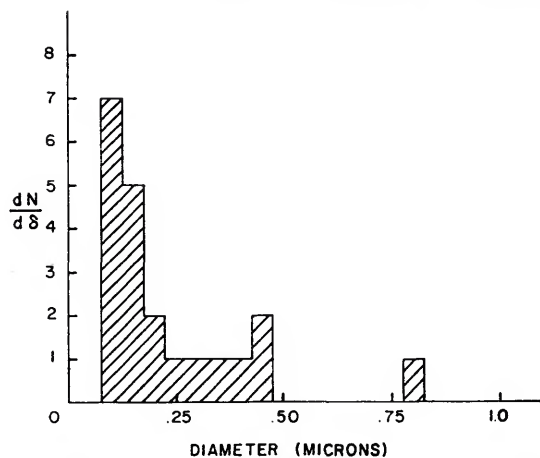


FIGURE 3.—Size distribution of spherical micrometeorites, 0.1 to 1 micron.

All doubtful cases were automatically discarded. Actually, a few particles which really came from beyond the earth's atmosphere were probably discarded because of this conservative policy.

The analysis of these particles has now begun. There are three techniques which offer hope for determining the composition of these particles: electron diffraction, neutron activation, and electron-beam probe techniques.

Thus far no positive results have been obtained with electron diffraction. We are beginning to suspect that micrometeorite particles do not have a crystal structure and that any original crystal structure has been scrambled by cosmic-ray bombardment. We may find that the lack of crystal structure is an appropriate criterion for distinguishing micrometeorites. More work is needed to establish this point.

A second type of analysis involves neutron activation. Gamma-ray spectra studies of activated samples are now in progress. The third technique which will be employed is the electron-beam probe wherein the particles are used as X-ray targets. The wavelengths of the characteristic X-radiation are used to identify the composition of the particle.

In summary, we believe that extraterrestrial particles have been collected. This belief is based on several facts. First, the experiment had a number of controls which were carefully

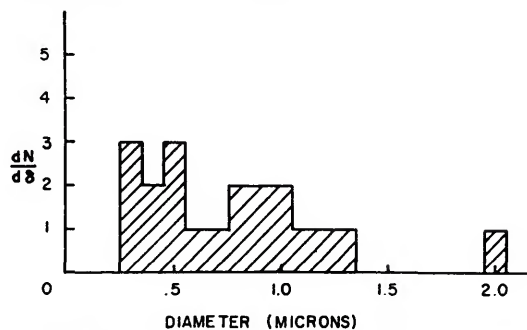


FIGURE 4.—Spherical hole size distribution from 200 A-thick films.

chosen and lend confidence to the results. Second, the particles were collected at altitudes where terrestrial particles are very unlikely to reside for any length of time. The third fact is the distribution of holes found. By dropping particles through a vacuum tube 2 meters long, it was determined that particles of the order of 7 to 10 microns diameter will just break through 200 A-thick nitrocellulose collection film with a velocity of 6 meters/second.

Figure 4 shows holes 0.3 micron in diameter in the flight-collection films. If the strength of the films is energy sensitive, this would suggest relative velocities of the order of 1 or 2 kilometers/second for a particle comparable in size to the smallest hole found. Finally, it should be pointed out that the observers have had a considerable amount of experience looking at the high-altitude particles and at the contaminants which appear in electron microscopy. In fact, four of the observers among them have had a total of 40 years of experience in electron microscopy. This experience increases our confidence that the particles described and pictured in this paper are indeed nonterrestrial in origin.

Although there is much more to be done, particularly on particle analysis, and these results are only preliminary, we feel that further study is not likely to change the present numerical results significantly.

#### Acknowledgments

The authors thank Miss L. Della Lucca, Mr. P. Manning, and Mr. R. Oppenheim for their assistance and cooperation in obtaining some of the results described in this paper.

**Discussion**

*E. L. Fireman.*—Are these particles different from the ones you reported as giving electron diffraction patterns for nickel and nickel oxide?

*C. L. Hemenway.*—Yes. In that paper, we were reporting on extremely small particles found in large profusion on a U-2 flight on November 15, 1960. There was a sufficient concentration of these particles in a cluster to give identifying diffraction patterns. I am now saying that in this experiment and also in the other U-2 flights we have been unable to obtain a diffraction pattern from any of the larger individual particles of suspected extra-terrestrial origin. With terrestrial contaminating

particles, on the other hand, we have always been able to see some diffraction pattern.

*A. F. Cook.*—The low velocities with which you feel most of the particles impacted could be comparable to the rocket velocity at the altitudes where the collector opened.

*R. K. Soberman.*—That would be the right order of magnitude.

*Unidentified speaker.*—The large sphere which you found would have had to strike the film with a very low velocity.

*C. L. Hemenway.*—That would have to be the case. There were a number of similar events.

**Abstract**

Three independent electron microscopes and observer teams have been used to evaluate, count, electron micrograph, and measure the micrometeorite particles. Typical particles and size distributions are shown. Particles have been found in structure and sizes similar to those obtained at lower altitudes with U-2 aircraft and balloon collection techniques. Approximately seven particles per square millimeter were collected during the flight. Most of the particles were submicron in size. The micrometeorite particles collected generally fell into three types: high-density spheres; medium-density irregular particles; and extremely irregular medium-density particles (fluffy particles). Some of the larger particles had sufficient momentum to rupture exposed films. Laboratory and nose-cone control surfaces were carefully studied to permit identification of micrometeorite particles.

# Micrometeorite Collection from a Recoverable Sounding Rocket. III

By R. K. Soberman,<sup>1</sup> and C. L. Hemenway<sup>2</sup>

The preceding papers have presented experimental details and preliminary results of the "Venus Flytrap" experiment, and the reasons for confidence in these results. The present paper introduces interpretations, tentative conclusions, and speculations.

The results indicate first, the apparent existence of submicron particles in the extraterrestrial flux. To account for this, one must suppose a breakup mechanism for larger particles or speculate on the apparent inefficiency of radiation pressure in removing submicron particles from the solar system.

A second surprising result is the low velocity with which the particles impinged on the collectors. Table 1 lists the terminal velocities of particles of various diameters over the altitude range covered by the Venus Flytrap rocket. If one argues that the particles should be arriving at the earth with large radial velocities, then the velocities presented in table 1 (particularly for the larger diameter particles) are much lower than those that

would be observed at the corresponding altitudes. However, if one assumes that the particles had been in orbit about the earth, then tangential deceleration at altitudes of the order of 500 km or less would result in radial velocities equal to, or even less than, the terminal velocities at the altitudes shown. From the lack of high-velocity impacts observed in the experiment, one must accept some form of orbital trapping, or seek a mechanism of radial deceleration or "slow down" which is more effective than atmospheric drag for micrometeoritic particles. Electrostatic deceleration by the ionosphere could conceivably be such a mechanism and should be investigated. Whatever the mechanism, it will be assumed for the present analysis that the particles observed were moving downward with approximately terminal velocities.

The third result is the size distribution and numbers of particles collected per unit area. Figure 1 shows the preliminary results from the collectors which were mounted in the boxes. The number of particles found (larger than a given diameter) are plotted against the diameter. The points were normalized to a total area of 1 square meter, and a line with slope of  $-1.3$  was drawn through these points. It can be seen from the ordinate values that the assumption of low velocities is practically a necessity if these results are to be understood in the light of other meteoric and micrometeoritic work.

With certain assumptions, a value for the extraterrestrial flux can be calculated. If a collector is moving through a column of unit area in which particles are falling (fig. 2), then the number of particles of given size collected can be written as:

TABLE 1.—Particle terminal velocities (km/sec)

Altitude (km)	Diameter (microns)			
	0.1	1.0	10.0	100
168	1.5	4.7	$v_{\infty}$	$v_{\infty}$
148	1.0	3.2	$v_{\infty}$	$v_{\infty}$
128	0.52	1.6	5.2	$v_{\infty}$
108	0.15	0.47	1.5	4.7
88	0.021	0.066	0.21	0.66

<sup>1</sup> Geophysics Research Directorate, Air Force Cambridge Research Laboratories, Bedford, Mass., and Northeastern University, Boston Mass.

<sup>2</sup> Dudley Observatory, Albany, N.Y., and Union College, Schenectady, N.Y.

$$N = \int \phi_c dt = \int \phi_c \frac{dz}{v_c}, \quad (1)$$

where  $\phi_c$  is the flux on the collector, and  $v_c$  is the velocity of the collector. Equation (1) can also be expressed as

$$N = \int n_a [v_p \pm v_c] \frac{dz}{v_c}, \quad (2)$$

where  $v_p$  is the velocity of the particles, and  $n_a$  is the ambient particle density. The minus sign is used when the collector is moving downward. If one assumes a constant ambient flux  $\phi_a$ , then one obtains:

$$N = \phi_a \left[ \int \frac{dz}{v_c} \pm \int \frac{dz}{v_p} \right]. \quad (3)$$

The first integral is the exposure time of the collector. The second term can be evaluated if one assumes that  $v_p$  is the terminal velocity of the particles. That is

$$v_p = \left( \frac{mg}{\rho_a \sigma} \right)^{1/2}, \quad (4)$$

where  $\rho_a$  is the ambient air density, and  $\sigma$  is the cross-sectional area of the particles. Assuming spherical particles, one can write:

$$N = \phi_a \left[ \int dt \pm \int \left( \frac{3\rho_a}{2\delta\rho_p g} \right)^{1/2} dz \right], \quad (5)$$

where  $\delta$  and  $\rho_p$  are the diameter and the density of the particles. For an exponential atmosphere this equation, on integration, yields:

$$N = \phi_a \left[ t \pm 2H \left( \frac{3}{2\delta\rho_p g} \right) (\rho_{a_i}^{1/2} - \rho_{a_f}^{1/2}) \right], \quad (6)$$

where  $H$  is the scale height, and the subscripts  $i$  and  $f$  refer to initial and final values. The quantity in the square brackets (the effective exposure time  $\tau$  of the collectors) is plotted in figure 3.

A mean particle density of 3 gm/cm<sup>3</sup> has been assumed. The calculation was performed by summing equation (6) over regions where the scale height remained reasonably constant. Densities, scale heights, and gravitational accelerations were obtained from the standard atmosphere tables (Minzner, Champion, and Pond, 1959). The summation was cut off

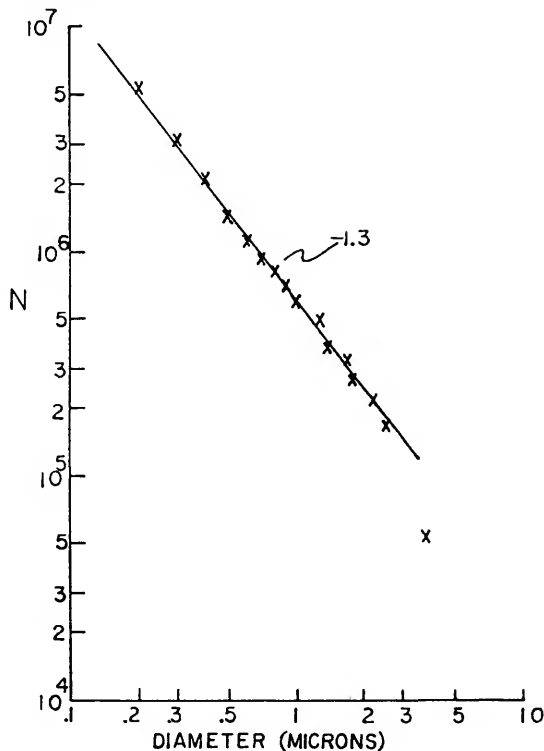


FIGURE 1.—Size distribution of all particles found to date from Venus Flytrap experiment.

where  $v_p = v_c$  when the collector was moving downward. Implicit in these calculations was the assumption of 100 percent collection efficiency. Theoretically this should be true for particles larger than 0.01 micron at the altitudes of interest here. The number of particles of each size collected per square meter divided by the effective collection time for that size is then the flux at all altitudes. The results are plotted in figure 4. The ordinate is the integrated flux (i.e., the flux of particles larger than a given diameter is plotted as a function of the diameter). The correction factors for the exposure angle and any shielding effect of the ogive assembly have been neglected. In the lower right-hand corner of figure 4 the three points from the mylar films (i.e., the particle sizes assumed to have caused the holes) were plotted. These points were normalized in the same manner as the others. Notice that the upper slope has changed to  $-1.2$ . For particle diameters larger than 2 or 3 microns

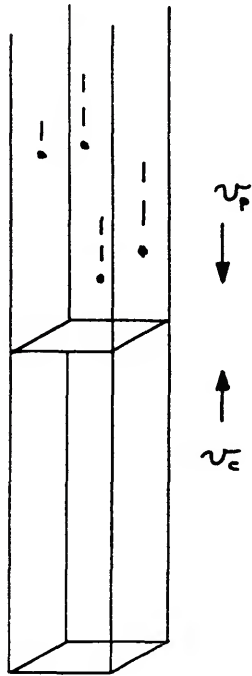


FIGURE 2.—Moving collector in unit area column.

(the solar radiation cutoff) a shaded area with slope  $-3.6$ —which is the best estimate from satellite data for these sizes (Whipple, 1961b)—was somewhat arbitrarily drawn. Thus from the foregoing a flux estimate of approximately 300 particles per square meter per second larger than 3 microns in diameter is obtained. This estimate is based, of course, on preliminary data and may change slightly. It must be remembered, however, that the calculation is based on the assumption of particles moving at terminal velocity. Were the velocities substantially higher, the flux estimate would be raised by the ratio of the assumed effective exposure time to the actual open time of the collector, i.e., the flux estimate for particles 3 microns and larger would be multiplied by a factor of approximately  $4/3$ . On the other hand, if it were shown that the actual particle velocities were lower than terminal velocities in this altitude range, then the estimated flux would be too high. It should also be noted that the present flux estimate does not include the particles which penetrated the 200 A films and were not recovered. If these particles

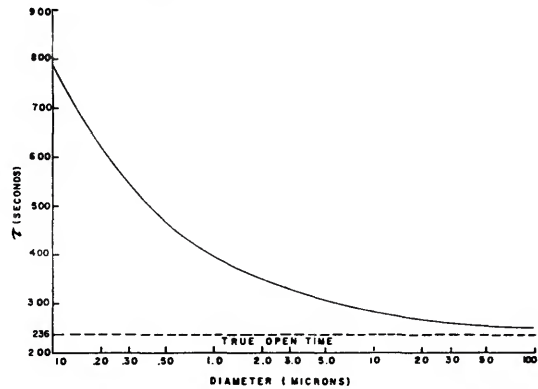


FIGURE 3.—Effective collection time for Venus Flytrap experiment.

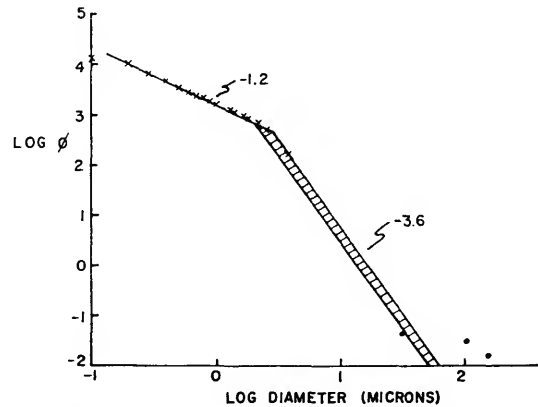


FIGURE 4.—Mircometeorite flux as calculated from Venus Flytrap results.

were included, the flux would increase by approximately 20 percent.

At this point the present estimated fluxes can be compared with measurements made from satellites. At first glance the derived flux value appears to be orders of magnitude higher than any recent measurements or extrapolations. One might, however, compare the present values with a curve for a geocentric distribution of particles. Such a curve is shown in figure 5. This curve, presented by Soberman and Della Lucca (see this symposium, p. 87), is similar to that given by Whipple (1961a). For an assumed spherical particle with uniform density of  $3 \text{ gm/cm}^3$ , this curve represents particles 9 microns in

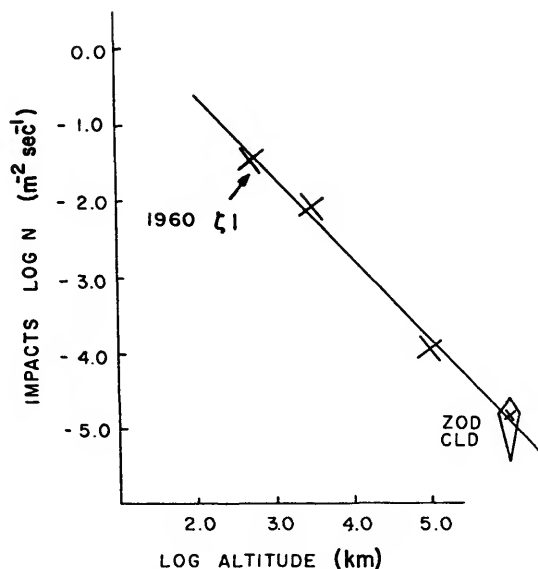


FIGURE 5.—Meteoritic impact plotted against altitude.

diameter and larger. The curve in figure 5 would predict a flux of such particles of  $0.25 \text{ m}^{-2} \text{ sec}^{-1}$  at 100 km. From figure 4, the present estimate would be about 6 particles per square meter per second. If one assumes, however, that the particles measured from satellites were low-density loose agglomerates, and if one uses a density of  $0.1 \text{ gm/cm}^3$ , then a particle with a mass of  $10^{-9} \text{ gm}$  would have a diameter of 27 microns. The present estimate (from fig. 4) of this particle size would be  $0.1 \text{ m}^{-2} \text{ sec}^{-1}$ , which is in much better agreement with the satellite observations.

To speculate briefly on the source of these particles, it is felt that terrestrial origin can be ruled out. A cataclysmic event immediately prior to the firing would be required to raise particles of this size to a 90-km altitude. No such event was observed or reported. A possibility which cannot be ruled out at the moment is that of a sharp increase in flux during the time of the experiment. On June 6th, two daylight radio-meteor showers were in progress, the Arietids which peak on June 8 and the  $\zeta$  Perseids which peak on June 9. No unusually high activity has been reported for this period. If the present experiment was performed during a period of relatively normal activity (future experiments of the same type

will decide this question), then one is forced to look for either a radial "slow-down" or an orbital trapping mechanism. Whatever the choice, one appears to be led to the conclusion that a dust layer (either moving orbitally or settling slowly) exists about the earth. This conclusion follows from the number of particles observed and the low relative velocities. The possible origin or origins of such a dust layer have been discussed by Whipple (1961a) and will not be treated here.

In summary, the three results of this experiment are: (1) A preponderance of submicron particles was observed; (2) the particles were apparently falling at low velocity; and (3) an unexpectedly large number of particles were collected. These results are consistent with one or both of the following assumptions: (1) The breakup of larger low-density "fluffy" particles; and (2) the existence of a dust layer or a geocentric distribution of micrometeoritic particles about the earth.

#### Acknowledgments

The authors thank Miss P. Burnham and Mr. R. Sarkesian for their assistance with the computations.

#### References

- MINZNER, R. A.; CHAMPION, K. S. W.; and POND, H. L.  
1959. The ARDC model atmosphere. AF Surveys in Geophysics No. 115, Geophys. Res. Dir., Air Force Cambridge Res. Lab.
- WHIPPLE, F. L.  
1961a. The dust cloud about the earth. *Nature*, vol. 189, pp. 127-128.  
1961b. The particulate contents of space. In P. Campbell, ed., *Medical and biological aspects of the energies of space*, pp. 49-70. Columbia University Press, New York.

#### Discussion

*C. W. McCracken.*—If we can believe the microphone measurements that you made on the Midas II, any of these results you have submitted give added support to the early rocket-probe data.

*R. K. Soberman.*—We have little, if any, confidence in those early rocket results. Although it might appear, at first glance, that our present measurements lend support, one must recall that we had, in this experiment, 0.25 square meter of puncture area exposed over a trajec-

tory similar to that of the early acoustic rockets. We do not see the large number of high velocity punctures, which one would expect from the interpretation of the acoustic-probe data.

*C. W. McCracken.*—Do you have any hypervelocity measurements showing that particles moving with 6 to 8 km/sec velocities do not form holes with flaps of the type you see in this experiment?

*R. K. Soberman.*—We do not have such measurements, but Richards and Gehring at the Ballistic Research Laboratory measured holes made in mylar by particles down to 5 microns travelling at 12 km/sec and have shown that at this velocity one obtains typical hypervelocity punctures, that is, small circular holes with no flap structure.

*C. W. McCracken.*—We have recent data from tests performed at the Space Technology Laboratories with 1 to 3 micron particles impacting 0.25-mil mylar at 6 to 8 km/sec velocities. It was a shock to us to find small cylindrical cavities instead of the more spherical

craters one might expect. The mylar was aluminum coated and we found small petals of this aluminum around the hole. Therefore, I would question the statement that flapped holes indicate low-velocity impact.

*Unidentified speaker.*—What was the relation between hole size and particle size in those Space Technology Lab tests?

*C. W. McCracken.*—The holes were not more than a factor of two larger than the particles. This was another surprise in that we had expected them to be larger.

*M. Dubin.*—You suggested that many of the particles you observed might have been the result of an earlier breakup. Where might this have occurred and how?

*R. K. Soberman.*—This could have occurred at altitudes below 300 km, where particles undergo deceleration of 1 g and more due to atmospheric drag. Loosely agglomerated particles could break up under such forces. Such a mechanism would explain why solar light pressure does not remove the submicron particles.

### **Abstract**

The interpretation is given of the preliminary results obtained from the "Venus Flytrap" rocket. These results are compared with those from satellite observations. The possible existence of a dust layer is discussed.



# Rocket and Satellite Studies of Meteoric Dust

By T. N. Nazarova<sup>1</sup>

During the last 3 years, investigators in both the Soviet Union and the United States have studied meteoric dust by means of instrumentation carried aloft by rockets and artificial earth satellites. Despite the limited amount of experimental data obtained, and the considerable difficulties associated with both the experiments and the interpretation of the data, the results are of interest to science as a whole and in their application to some engineering problems.

We shall discuss the results of direct investigations of meteoric dust carried out by means of Soviet geophysical rockets, artificial earth satellites (Nazarova, 1961a), and space probes (Nazarova, 1961b). Data provided by non-Soviet publications are also taken into account. In the U.S.S.R., measurements were made by means of ballistic piezoelectric detectors which measure the pulse caused by ejection of detector material when a meteoric particle explodes on the surface of the detector (Isakovich and Roi, 1960; Komissarov *et al*, 1960). From the number of such pulses, the particle impact rate is determined.

In analyzing the experimental results we use the theoretical relationship, derived by Stanyukovich (1961), that the pulse recorded by the detector is a function of the particle energy and can be expressed as  $I = AE$ . This relation ( $I \propto E$ ) is not generally accepted. Lavrentyev (1961) believes the relation should be  $I \propto mv^{1.6}$ , while American investigators usually assume it to be  $I \propto mv$ .

The estimate of the masses of recorded meteoric particles naturally depends on the velocity assumed. We regard Whipple's (1961a) estimate for the impact velocity of meteoric particles with a satellite as reasonable. There-

fore, although earlier publications used the value of 40 km/sec for the particle impact velocity, in this paper we recalculated the recorded masses using a particle impact velocity of 15 km/sec. In some cases, a satellite encounter with meteor streams is possible; actual velocities can then differ considerably from the assumed velocity.

The observational results are listed in table 1. In the experiments which utilized geophysical rockets, the calibration of the instrumentation was redetermined. For these experiments there is an uncertainty of half of an order of magnitude in the recorded meteoric particle impact rate, since the detectors reacted to impacts not only against the operating surface but also against the rocket body. In experiments on Sputnik III and Space Probe I (Lunik I), results were carefully corrected for this effect. The detectors used on Space Probes II and III (Luniks II and III) reacted only to impacts against the operating surface. Table 1 lists, for all experiments, the operating surface area  $S$  (for the geophysical rockets the effective area is given), the time  $t$  of the instrument operation, the impact rate, and the altitude range over which the measurements were made.

To compare data obtained from different experiments, it is necessary to equate them to the same sensitivity. It is known that the integral mass distribution of meteoric particles has the form  $N(m) = km^{-\beta}$ , where  $N(m)$  is the number of particles with masses greater than  $m$ .

Observations of F-corona, gegenschein, and meteors have yielded for  $\beta$  the values 0.5, 0.6, and 1.3, respectively. Comparison of direct measurements from Explorer VI, Vanguard III, and Explorer I has led to the value  $\beta \simeq 1$  (Moroz, 1962).

<sup>1</sup> The U.S.S.R. Academy of Sciences, Moscow, U.S.S.R.

TABLE 1.—*Rocket and satellite meteoric dust data*

Vehicle	Dates	Area $S$ (m <sup>2</sup> )	Time $t$ (sec)	$S. t.$ (m <sup>2</sup> sec)	Alt. range (km)	Mass of recorded particle (with $v=$ 15 km/sec) (gm)	Impact rate (m <sup>-2</sup> sec <sup>-1</sup> )
1. Geophysical rocket	May 24, 1957	4	134	536	100–200	$10^{-3}$	0.06
2. Geophysical rocket	Aug. 8, 1957	4	148	592	100–210	$10^{-3}$	0.05
3. Geophysical rocket	Feb. 22, 1958	4	85	340	126–297	$10^{-3}$	0.75
4. Sputnik III	May 15, 1958 May 16, 17, 1958 May 18–25, 1958	0.34	$1.8 \times 10^4$	$6.0 \times 10^3$	400–1,880 400–700 400–700	$6 \times 10^{-9} - 2 \times 10^{-7}$	4–11 $5 \times 10^{-4}$ $< 10^{-4}$
5. First Cosmic rocket	Jan. 2, 1959	0.2	$3.6 \times 10^4$	$7.2 \times 10^3$	2,000–360,000	$2 \times 10^{-8} - 10^{-7}$ $10^{-7} - 10^{-6}$ $> 10^{-6}$	$< 2 \times 10^{-3}$ $< 5 \times 10^{-4}$ $< 10^{-4}$
6. Second Cosmic rocket	Sept. 12, 1959	0.2	$1.1 \times 10^6$	$2.2 \times 10^5$	2,000–360,000	$10^{-8} - 4 \times 10^{-8}$ $4 \times 10^{-8} - 4 \times 10^{-7}$ $> 10^{-7}$	$< 5 \times 10^{-5}$ $< 5 \times 10^{-5}$ $9 \times 10^{-5}$
7. Third Cosmic rocket	Oct. 4–18, 1959	0.1	$2.3 \times 10^5$	$2.3 \times 10^4$	102,000–470,000	$7 \times 10^{-8} - 2 \times 10^{-8}$ $2 \times 10^{-8} - 6 \times 10^{-8}$ $> 6 \times 10^{-8}$	$4 \times 10^{-4}$ $2 \times 10^{-3}$ $4 \times 10^{-4}$

Figure 1 presents Soviet and American experimental data (LaGow and Alexander, 1960; Dubin, 1960; Whipple, 1961a) equated to the same sensitivity ( $m_{\min} = 10^{-3}$  gm) through the relation  $N(m) \propto m^{-1}$ .

The recorded impact rate is referred to the mean height for each experiment, a procedure which in the case of space probes may lead to additional errors. (The graph was plotted on a logarithmic scale, hence the points are not centered between the altitude limits.) As is evident from figure 1, the observations made by means of geophysical rockets definitely reveal a zone of increased density of dust particles near the earth at an altitude of 100 to 300 km. The existence of this increased concentration is independently confirmed by observations of the twilight sky (Moroz, 1962). At altitudes between 400 and 2,000 km the impact rate is approximately  $10^{-3} \text{ m}^{-2} \text{ sec}^{-1}$ . Measurements made at greater distances from the earth are characterized by a large dispersion in the numerical data obtained. Explorer VI and Pioneer I yielded impact rates of  $5 \times 10^{-6}$  and  $4 \times 10^{-5} \text{ m}^{-2} \text{ sec}^{-1}$ , while the values for Luniks II and III were  $9 \times 10^{-4}$  and  $1 \times 10^{-3} \text{ m}^{-2} \text{ sec}^{-1}$  (all values are corrected to  $m_{\min} = 10^{-8}$  gm).

It should be noted that estimates of the density of matter in the zodiacal cloud, obtained from photoelectric measurements, range between  $\rho = 3 \times 10^{-23}$  and  $3 \times 10^{-21} \text{ gm/cm}^3$ . From

these values the computed impact rates are  $10^{-5}$  and  $10^{-4} \text{ m}^{-2} \text{ sec}^{-1}$ , respectively (Moroz, 1962).

Despite the nonhomogeneity of the experimental data (due in large part to differences in experimental technique, instrument calibration, and assumptions regarding the mass-velocity dependence of the detectors) and the limited amount of such data available, consideration of all the available data allows the supposition that a region of increased concentration of meteoric dust exists at a height of 100 to 300 km above the earth's surface. As already noted, at altitudes between 400 and 2,000 km the impact rate is of the order of  $10^{-3} \text{ m}^{-2} \text{ sec}^{-1}$  (i.e., approximately one order of magnitude larger than the density of the zodiacal cloud would indicate). Because of the great dispersion of points at distances of the order of  $10^4$  to  $10^5$  km from the earth (fig. 1), it is difficult to say at present whether the decreased concentration of meteoric matter (compared with the lower altitudes) is real or whether the dispersion in the experimental data is indicative of fluctuations in the spatial density.

On the basis of direct experiments it may be concluded that the density of meteoric matter in the vicinity of the earth is not constant. At altitudes of 100 to 300 km, variations in the impact rate  $N$  are not greater than one order of magnitude. At the same time, at altitudes of 400 to 2,000 km, sporadic increases in  $N$  are observed.

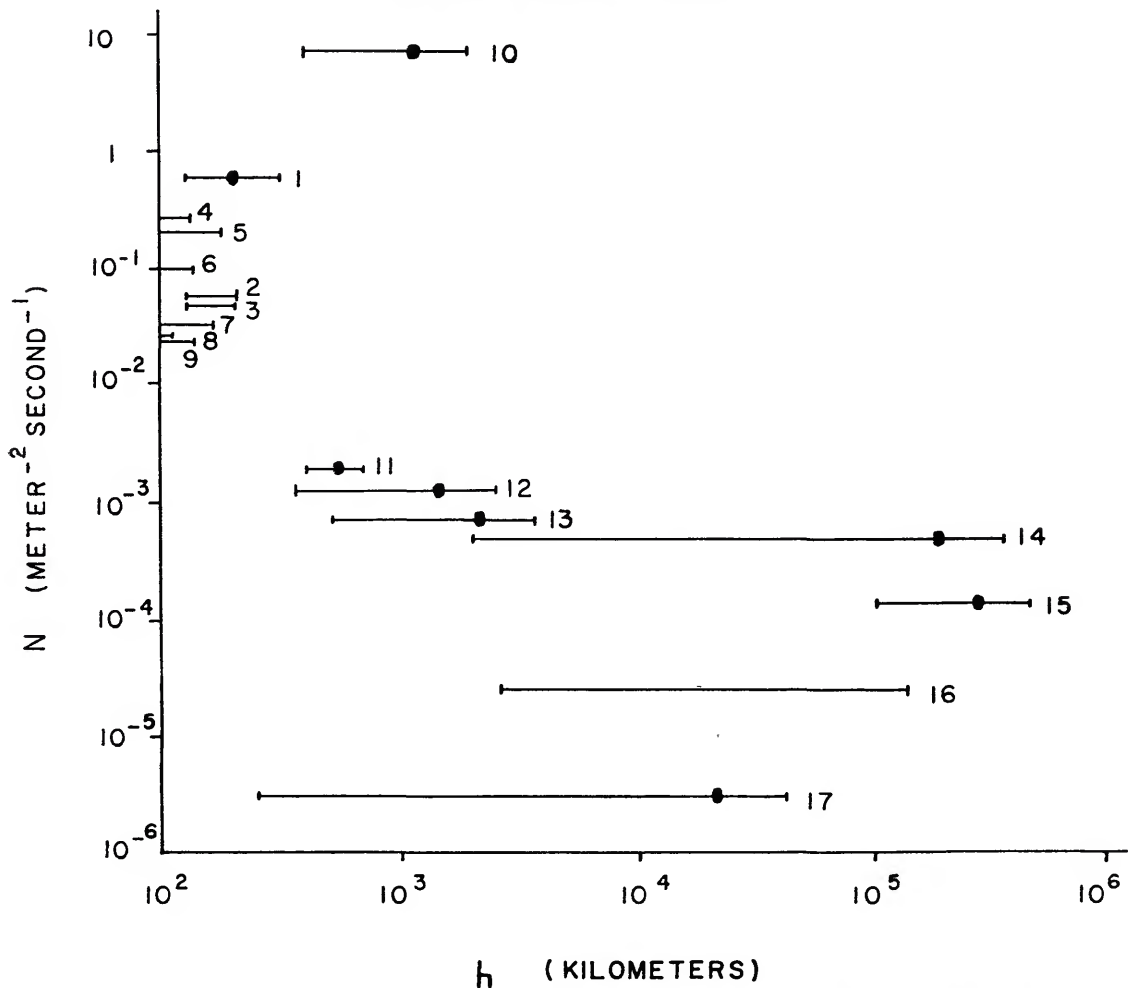


FIGURE 1.—Integral impact rate of meteoric dust  $N$  as a function of altitude  $h$  for masses greater than  $10^{-8}$  gm. Key: 1, 2, 3, Soviet geophysical rockets; 4–9, U.S. Air Force rockets; 10, Sputnik III, May 15, 1958; 11, Sputnik III, May 16, 17, 1958; 12, Explorer I; 13, Vanguard III; 14, Soviet cosmic rocket II; 15, Soviet cosmic rocket III; 16, Pioneer I; 17, Explorer VI.

On May 15, 1958, instruments carried by Sputnik III recorded 4 to 11 impacts per square meter per second.<sup>2</sup> On May 16–17, the impact rate decreased to  $5 \times 10^{-4} \text{m}^{-2} \text{sec}^{-1}$  ( $m_{\text{min}} = 6 \times 10^{-8}$  gm according to present velocity assumptions), which is apparently normal for these altitudes. Since the impact rate changed with a period equal to the precessional rate of the satellite, instrumental origin for this effect

<sup>2</sup> It is likely that the phenomenon observed on May 15 was due to a stream with an unknown radiant. If we assume that the velocity of the stream was 70 km/sec, then the mass of the particles detected in the stream was apparently  $\sim 5 \times 10^{-10}$  gm.

may be almost totally excluded. Explorer I instruments also recorded sporadic increases of the stream in this region. These increases were about an order of magnitude higher than the average impact rate. Of great importance are the diurnal variations in the impact rate which were also observed on Explorer I (Dubin, 1960).

According to Whipple (1961a; 1961b) there is a dust envelope about the earth in which  $N \propto h^{-1.4}$  in a broad region from 100 to 100,000 km. As seen from the above considerations, it is difficult at the present time to encompass

this entire range with a single relationship between  $N$  and  $h$ . In the altitude range from 100 to  $\sim 2,000$  km, we can write  $N \propto h^{-1}$ . From 2,000 km to higher altitudes,  $N$  decreases more slowly. Future experiments will determine the dependence of impact rate on height and latitude.

Several hypotheses have been suggested to explain the existence of the dust cloud about the earth; at the present time, however, no one of these hypotheses can be regarded as final (Moroz, 1962).

### References

- DUBIN, M.  
1960. IGY micrometeorite measurements. *In* Space research, H. K. Bijl, ed., pp. 1042-1058. North-Holland Publishing Co., Amsterdam.
- ISAKOVICH, M. A., AND ROI, N. A.  
1960. An acoustical method for the measurement of the mechanical parameters of meteorites. *In* Artificial earth satellites, L. V. Kurnosova, ed., vol. 2, pp. 105-107 (transl. from Russian). Plenum Press, New York.
- KOMISSAROV, O. D.; NAZAROVA, T. N.; NEUGODOV, L. N.; POLOSKOV, S. M.; AND RUSAKOV, L. Z.  
1960. Micrometeorite studies using rockets and satellites. *In* Artificial earth satellites, L. V. Kurnosova, ed., vol. 2, pp. 68-74 (transl. from Russian). Plenum Press, New York.
- LAWGOW, H. E., AND ALEXANDER, W. M.  
1960. Recent direct measurements of cosmic dust in the vicinity of the earth using satellites. *In* Space research, H. K. Bijl, ed., pp. 1033-1041. North-Holland Publishing Co., Amsterdam.
- LAVRENTYEV, M. A.  
1961. The problem of piercing at cosmic velocities. *In* Artificial earth satellites, L. V. Kurnosova, ed., vol. 3, pp. 85-91 (transl. from Russian). Plenum Press, New York.
- MOROZ, V. I.  
1962. On the dust envelope of the earth. *In* Artificial earth satellites, L. V. Kurnosova, ed., vol. 12 (transl. from Russian). Plenum Press, New York.
- NAZAROVA, T. N.  
1961a. Results of a study of impacting of meteoric matter by means of instruments mounted on space rockets. *In* Artificial earth satellites, L. V. Kurnosova, ed., vol. 5, pp. 524-527 (transl. from Russian). Plenum Press, New York.  
1961b. Study of meteoric particles through instruments on the third Soviet artificial satellite. *In* Artificial earth satellites, L. V. Kurnosova, ed., vol. 4, pp. 402-410 (transl. from Russian). Plenum Press, New York.
- STANYUKOVICH, K. P.  
1961. Elements of the theory of the impact of solid bodies with high (cosmic) velocities. *In* Artificial earth satellites, L. V. Kurnosova, ed., vol. 4, pp. 292-333 (transl. from Russian). Plenum Press, New York.
- WHIPPLE, F. L.  
1961a. The particulate contents of space. *In* Medical and biological aspects of the energies of space, P. Campbell, ed., pp. 49-70. Columbia University Press, New York.  
1961b. The dust cloud about the earth. *Nature*, vol. 189, pp. 127-128.

# Cosmic Dust Showers by Direct Measurements

By M. Dubin,<sup>1</sup> W. M. Alexander,<sup>2</sup> and O. E. Berg<sup>2</sup>

The cometary origin of meteor streams is well established. During the process of disintegration of comets, particles are dispersed along the heliocentric orbit, and it appears reasonable to assume that the age of the meteor stream is related to the uniformity in the counting rate of shower meteors for annually recurring meteor streams. The large number of meteors observed in the Draconid display in 1946 is evidence of the recent formation of the stream from the familiar comet Giacobini-Zinner. Dispersion of dust particles in the meteor stream from interplanetary forces resulting from the Poynting-Robertson effect, corpuscular bombardment, and other radiative forces, is expected to be increasingly pronounced with decreasing dimensions of the dust particles. The extension of the range of measurements of meteoritic material to smaller masses by direct measurements with satellites may, therefore, improve our knowledge of the history and age of meteor streams.

The number distribution of meteors as a function of visual magnitude has been measured by visual and optical methods. Similar distributions as a function of electron line density along the trail have been determined by using radar. Browne, Bullough, Evans, and Kaiser (1956) determined such distributions for the Perseids, Quadrantids, and the Arietids. For the Perseids, for example, they found that compared to the distribution of sporadic meteors there was a depletion of the small meteors for visual magnitudes greater than 7. Weiss (1961) measured distribution functions for the Geminids, the  $\delta$  Aquarids, and the  $\eta$  Aquarids, as well as for the sporadic meteors. Although the distribution function varied for different meteor streams, only the daytime Arietids has

an "s" value (the exponent in the distribution function indicating rate of increase in number with decreasing mass) equal to 2.7 (compared to "s"=2.0 for sporadic meteors). This is the only shower with "s" greater than 2.0.

Direct measurements of micrometeorites or interplanetary dust have been made in the United States on a number of satellites, rockets, and probes. Significant data on four satellites have been obtained: 1958 Alpha, Explorer I, launched February 1, 1958, perigee 355 km, apogee 2550 km (Dubin, 1960a, b, 1961; and Hibbs, 1961a, b); 1959 Eta, Vanguard III, launched September 18, 1959, perigee 509 km, apogee 3751 km (La Gow and Alexander, 1960); 1960 Delta, Explorer VI, launched August 7, 1959, perigee 186 km, apogee 39,000 km; and 1960 Xi, Explorer VIII, launched November 3, 1960, perigee 425 km, apogee 2300 km (McCracken, Alexander, and Dubin, 1961, and McCracken and Alexander, this Symposium, p. 71).

The direct measurements of cosmic dust refer to particle of mass less than  $10^{-8}$  grams or greater than +20 on the visual magnitude scale. Daily variations in the flux of cosmic dust particles greater than an order of magnitude are often observed. We have excellent evidence that two cosmic dust showers or streams have been detected by these direct measurements. One of these dust streams, detected on 1958 Alpha, permitted a determination of an approximate radiant; the other has been detected on more than one occasion and apparently is related to an annually recurring meteor stream.

## Results of Measurements

*Cosmic dust shower, February 1958.*—Evidence of a cosmic dust shower from the data of 1958 Alpha was apparent for a 10-hour period begin-

<sup>1</sup> National Aeronautics and Space Administration, Washington, D. C.  
<sup>2</sup> Goddard Space Flight Center, Greenbelt, Md.

TABLE 1.—*Impacts per station pass for Satellite 1958 Alpha*

February date	Greenwich time	No. hits	Time of pass (secs)	Station	Hits/sec $\times 10^3$
2	1512	2	687	Santiago, Chile	2.9
2	1833	5	159	Woomera, Australia	31.0
2	1930	2	233	Quito, Ecuador	8.5
2	1933	1	69	Fort Stewart, Ga.	14.5
2	2033	4	787	Woomera, Australia	5.1
2	2139	2	221	Fort Stewart, Ga.	9.1
2	2238	2	691	Woomera, Australia	2.9
2	2338	5	192	Ehrlick, Kansas City, Mo.	26.3
2	2339	11	366	Fort Stewart, Ga.	30.0
2	2340	7	174	Havana, Cuba	40.0
3	0043	7	832	Woomera, Australia	8.4
3	0132	2	213	Temple City, Calif.	9.3
3	0138	4	259	Blossom Point, Md.	15.5
3	0139	5	187	Ehrlick, Kansas City, Mo.	26.5
3	0141	12	261	Fort Stewart, Ga.	46.0
3	0142	2	7	Havana, Cuba	286.0
3	0258	3	180	Woomera, Australia	16.7
3	0334	4	213	Temple City, Calif.	18.7
3	0338	1	126	Ehrlick, Kansas City, Mo.	8.1
3	0344	1	71	Fort Stewart, Ga.	14.0
3	0344	2	192	Havana, Cuba	10.4
3	0349	1	—	Antigua, B.W.I.	
3	0539	7	338	JPL, Calif.	20.8
3	0750	2	142	Quito, Ecuador	7.0
3	0958	2	527	Santiago, Chile	3.8
3	1200	0	952	Santiago, Chile	0
3	1405	5	663	Santiago, Chile	7.5
Average impact rate, Feb. 1–Feb. 12, 12 days					1.5
Average impact rate, Feb. 5–Feb. 12, 8 days					0.43

ning on February 2, 1958. The detector was a piezoelectric crystal with an average threshold sensitivity to micrometeoroid impacts of  $2.5 \times 10^{-3}$  dyne-seconds. This is equivalent to detecting particles of mass  $8 \times 10^{-10}$  grams and greater with an average impact velocity of 30 km/sec. The data from Explorer I were in real-time, recorded only while the satellite was over a telemetry receiving station. Table 1 shows the data for each pass over a telemetry station in the interval from February 2, 1512 hours, to February 3, 1405 hours, Greenwich time. Impacts were recorded for every pass but one during the interval of the cosmic dust shower. The table includes the station location, the number of hits during each pass, the time of each pass, and the number of hits per second.

The impact rate from table 1 has been replotted as a polar plot in figure 1 as a function

of time. The inner filled-in circle in the polar plot is the zero level, or zero hits per second. The next ring is the average impact rate of the last 8 days of the 12-day experimental period, i.e.,  $0.43 \times 10^{-3}$  hits/sec. The average impact rate over this period is shown by the next circle, and was  $1.5 \times 10^{-3}$  hits/sec. The plotted points are the real-time readout rates during the shower period. It is quite evident that the impact rates during the shower period were nearly two orders of magnitude greater than the average of the latter two-thirds of the measurement period.

Except for Woomera, Australia, which is represented by the squares, the circular points in figure 1 represent the impact rate for all stations in essentially the same time zone covering about a three-hour period. The local time for these stations in the United States and South America during the maximum of the

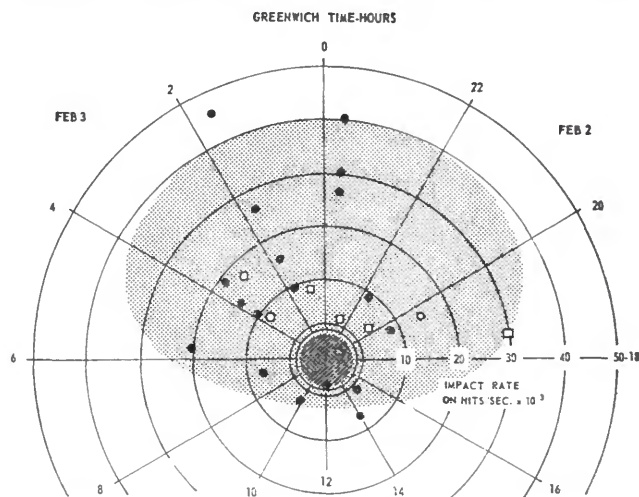


FIGURE 1.—Impact rate for Satellite 1958 Alpha, February 2-3, Greenwich Time.

shower intensity was early evening. This indicates a meteor stream in a direct heliocentric orbit. It is evident that the stream is in the ecliptic since it was detected by receiving stations in both the Northern and Southern Hemispheres. The square-plot points represent the impact rate from five passes over the station at Woomera, Australia. They provide further evidence of a direct heliocentric orbit; the impact rate at Woomera as a function of time is first high, then decreases, and then increases again. This impact rate was near a minimum when at the other stations it was near a maximum. Since the longitude at Woomera differs from other receiving stations by nearly  $180^\circ$ , the earth should have shielded the satellite from this stream. The apogee of 1958 Alpha at 2550 km was located near Woomera on this date. Hence, the earth's shield there would be incomplete. Figure 1 has been shadowed to suggest the extent of the meteor stream, which appeared to have lasted about 10 hours. There is no known meteor stream which may be related to this cosmic dust shower detected on 1958 Alpha.

*Annually Recurring Cosmic Dust Shower in November.*—A cosmic dust shower has been detected with both satellites and sounding rockets in November. It was first recognized from the micrometeoroid data from 1959 Eta, although it was first detected in 1955 from an Aerobee

rocket. Additional data from 1960 Xi are still of a preliminary nature, but support the fact that this shower recurs annually.

A number of rocket flights were carried out by Berg in 1955 (Berg and Meredith, 1956) and in 1960. He used a micrometeorite detector which detected the impact-flash of light resulting from the hypervelocity impact of the particle on an aluminum-coated lucite or quartz surface.

Figure 2 describes the measurements on three separate rocket firings. The first firing of Berg's experiment was carried out on Aerobee NRL-25 on November 17, 1955, at 0215 M.S.T. A 1p21 photomultiplier was used to detect light flashes on impacts of an aluminized lucite cone with a light sensitivity of  $10^{-4}$  lumen seconds/m<sup>2</sup>. On the assumption that 0.002 percent of the impact energy is transformed into visible light, a detector would be able to detect particles of mass greater than  $10^{-13}$  grams. Berg found that 101 impacts were observed on the telemetry record in the 84-second period while the rocket was above an altitude of 85 km. Almost none were observed below this altitude, and the distribution of impacts on the upward and downward trajectory of the rocket was fairly symmetrical. The area of the detector was 75 cm<sup>2</sup>, and the impact rate was  $1.6 \times 10^2$  impacts/m<sup>2</sup>/sec.

This rather high impact rate observed on

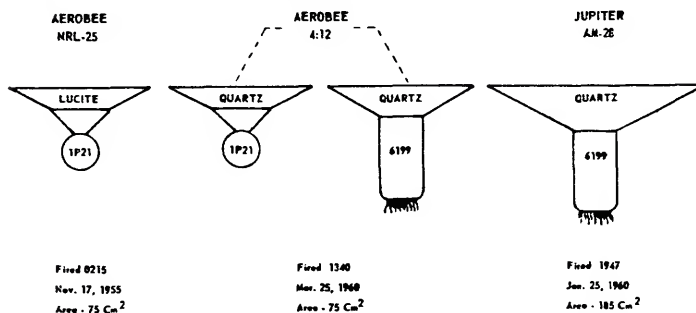


FIGURE 2.—Description of measurements on three separate rocket firings.

NRL-25 remained an anomaly for a number of years. The experiment was repeated by Løvring (1959) in Australia, and no impacts were observed on a single rocket flight. In 1960 Berg repeated the measurement on Aerobee NASA 4.12 and on Jupiter AM-28. He used the 1P21 with lucite and with quartz cones to check for Cerenkov radiation. Aerobee NASA 4.12 was fired on March 25, 1960, at 1340 E.S.T., with a 75 cm<sup>2</sup> detecting surface and with 1P21 and 6199 photomultipliers. One impact was observed on the 1P21 and two events were observed on the 6199. This is equivalent to rate of 1.2 impacts/m<sup>2</sup>/sec and an exposure area-time of 2.4 m<sup>2</sup> sec. On NRL-25 the exposure area-time was 0.64 m<sup>2</sup> sec. Similarly, on Jupiter AM-28, fired on January 25, 1960, a space-oriented detector with 185 cm<sup>2</sup> was exposed at 1947 E.S.T. The 6199 photomultiplier with a quartz cone was used. Included also was a calibrated light source, giving a 50 microsecond light pulse every 26 seconds. The experiment was known to be working correctly, and the area-time of the exposure was 2.4 m<sup>2</sup> sec. Four events were detected, giving an impact rate of 1.6 impacts/m<sup>2</sup>/sec. Thus, of three separate rocket flights similar to the earlier experiment not one could confirm the 1955 results for the impact rate within a factor of 100.

Although it was surmised that a dust shower might explain the rocket data, Alexander, McCracken, and LaGow (1961) provide rather clear confirmation of this hypothesis with their micrometeorite data from 1959 Eta. This experiment consisted of four piezoelectric crystals with a threshold impact sensitivity of

$1 \times 10^{-2}$  dyne-seconds. If we assume an average impact velocity of 30 km/sec, particles of mass greater than  $3.3 \times 10^{-9}$  grams could trigger the counter on the satellite. Except in rare instances, real-time data were not obtained on 1959 Eta, although the sample was much greater than on 1958 Alpha. Data were recorded for 78 days, with the total number of events approximating 5000 impacts.

Figure 3 is a plot of the impact rate (log of the number of impacts per hour) as a function of the date from November 10 through November 20: "C" is the average rate from September 18 through October 9; "B" the average from November 10 to November 20; and "A" the average from November 16 to November 18. It is evident that from November 16 to 18 there are periods when the impact rate was two orders of magnitude greater than the average

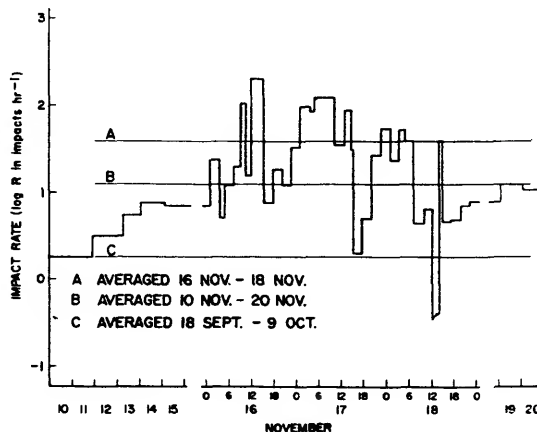


FIGURE 3.—Impact rates during the November 1959 interplanetary dust particle event.

shown in "C", and also than the average of the 78-day period. It is also interesting that there were rapid fluctuations in the rate during the period of the shower, and that several orbits showed no impacts—or very few—even though extremely high rates were observed for small segments of the orbit. These rapid fluctuations are probably real fluctuations in the spatial density of interplanetary dust particles.

The Aerobee NRL-25 was fired on November 17, 1955, at 0215, which was during the same annual period as that of the intense impact rate observed on 1959 Eta. Hence we arrive at the hypothesis that both measurements detected a shower, and that this cosmic dust shower recurs annually and may possibly be related to the Leonid meteor stream. Preliminary analysis of the data from the light-flash micrometeorite experiment using a 6199 photomultiplier with 1000 Å evaporated layer of aluminum on 1960 Xi indicates that an impact rate similar to that observed on NRL-25 was also observed in November 1960 during approximately the same time period. The analysis, however, has not been completed, and it is still not possible to prove or disprove the annual recurrence of this cosmic dust shower. The piezoelectric experiment on Satellite 1960 Xi was so oriented as to be shielded from the Leonid radiant; in fact, the microphone data of this spin-stabilized satellite did not detect a shower at the time.

#### Discussion and conclusions

From the available data on direct measurements of cosmic dust made with satellites and rockets we have presented evidence of large fluctuations in the flux of cosmic dust. In addition to daily variations, which are often greater than an order of magnitude, we have observed sets of conditions which may be attributed to cosmic dust streams. Large fluctuations are also apparent in the streams themselves.

Although the total amount of data available from direct measurements is still fairly small, these two cosmic dust streams represent a large fraction of the total number of impacts recorded on all the satellites. The total number recorded on Satellite 1958 Alpha was 145, of which nearly half may be associated with the cosmic dust shower. Similarly, on 1959 Eta,

of approximately 5000 impacts, about 2800 occurred during the cosmic dust shower between November 16 and November 18. Even if the number of impacts so far recorded on 1960 Xi and all other space vehicles were included, the number of events occurring in these streams represent a considerable fraction of this total. By comparison, the number of meteors in meteor streams observed optically, visually, and by radar is only about 10 percent of the number of sporadic meteors similarly observed. On the other hand, Gallagher and Eshelman (1960) have reported that a large fraction of the meteors observed with their highly sensitive radar equipment, capable of detecting meteors of approximately visual magnitude +14, appear to be in streams. Does this perhaps support the hypothesis of a continuous generation of dust by disintegration of conglomerates of interplanetary material and a short lifetime of the dust in interplanetary space? If so, it would explain the relative unimportance of the space or background density of sporadic dust particles. On the other hand, if the rate of dispersion of dust particles after disintegration from a large conglomerate were rather rapid and if the rate of removal of dust were slow, the large majority of the dust particles would be isotropically dispersed; then the variations in the flux of cosmic dust as detected with satellites would be small, and the number of sporadic dust particles would far outweigh the component of dust in showers. Additional measurements are certainly required to determine the generation and destructive characteristics of interplanetary dust.

#### References

- ALEXANDER, W. M.; McCracken, C. W.; AND LaGOW, H. E.  
1961. Interplanetary dust particles of micron-size probably associated with the Leonid meteor stream. *Journ. Geophys. Res.*, vol. 66, pp. 3970-3973.
- BERG, O. E., AND MEREDITH, L. H.  
1956. Meteorite impacts to altitude of 103 kilometers. *Journ. Geophys. Res.*, vol. 61, pp. 751-754.
- BROWNE, I. C.; BULLOUGH, K.; EVANS, S.; AND KAISER, T. R.  
1956. Characteristics of radio echoes from meteor trails. II. The distribution of meteor magnitudes and masses. *Proc. Phys. Soc. London*, vol. 69B, pp. 83-97.

- DUBIN, M.
- 1960a. Meteoritic dust measured from Explorer I. *Planetary Space Sci.*, vol. 2, pp. 121-129.
- 1960b. IGY micrometeorite measurements. *In* H. K. Bijl, ed., *Space research*, pp. 1042-1058. North-Holland Publishing Co., Amsterdam.
1961. Remarks on the article by A. R. Hibbs, "The distribution of micrometeorites near the earth." *Journ. Geophys. Res.*, vol. 66, pp. 2592-2594.
- GALLAGHER, P. B., AND ESHELMAN, V. R.
1960. "Sporadic shower" properties of very small meteors. *Journ. Geophys. Res.*, vol. 65, pp. 1846-1847.
- HIBBS, A. R.
- 1961a. The distribution of micrometeorites near the earth. *Journ. Geophys. Res.*, vol. 66, pp. 371-377.
- 1961b. Author's reply to the preceding discussion on the article, "The distribution of micrometeorites near the earth." *Journ. Geophys. Res.*, vol. 66, pp. 2595-2596.
- LAGOW, H. E., AND ALEXANDER, W. M.
1960. Recent direct measurements of cosmic dust in the vicinity of the earth using satellites. *In* H. K. Bijl, ed., *Space research*, pp. 1033-1041. North-Holland Publishing Co., Amsterdam.
- LOVERING, J. F.
1959. Micrometeorite impacts to an altitude of 135 km. *Planetary Space Sci.*, vol. 2, pp. 75-77.
- MCCRACKEN, C. W.; ALEXANDER, W. M.; AND DUBIN, M.
1961. Direct measurement of interplanetary dust particles in the vicinity of earth. *Nature*, vol. 192, pp. 441-442.
- WEISS, A. A.
1961. The distribution of meteor masses for sporadic meteors and three showers. *Australian Journ. Phys.*, vol. 14, pp. 102-119.

### *Abstract*

By means of rockets and satellites, direct measurements of cosmic dust over the past several years have yielded two separate sets of data which indicate interplanetary dust showers consisting of particles of mass less than  $10^{-8}$  grams. These cosmic dust showers were observed with micrometeorite detectors using piezoelectric crystals and photomultipliers for detecting the light flash resulting from particle impacts. The Explorer I interplanetary dust stream was detected for about a 10-hour period beginning on February 2, 1958. The peak rate of particles was nearly 50 times the average impact rate over the remainder of the 12-day period of the experiment. From the limited amount of data it may be shown that this stream was nearly in the ecliptic in a direct heliocentric orbit. The shower does not correspond to a known annually recurring meteor shower.

The second stream of interplanetary dust, detected with satellites and from a sounding rocket, appears to recur annually with a peak intensity on November 17. It was detected first in 1955 from an Aerobee rocket and recognized in the November 1959 data from the Vanguard III satellite. Preliminary analysis of the Explorer VIII data indicates that it was probably also detected in 1960. The dust stream corresponds to the Leonids with a heliocentric velocity of 72 km/sec. The data supporting the detection of these two interplanetary dust streams are presented and discussed. The physical significance of these measurements is also reviewed. Although direct measurements from satellites have been made over a period of about four months and during the time of other known meteor streams, so far only these two interplanetary dust streams have been detected by direct measurements.

## Discussion

*F. L. Whipple.*—I think that we should throw the discussion open to all of the papers in this session since they seem to be so intimately related.

I have plotted the number of counts versus the time since launch in a number of these acoustic experiments and have found that this drops off rapidly, so that it is possible that some of these effects are due to noise.

*M. Dubin.*—This is not true for many of the satellites.

I would like to comment on the paper by R. Soberman and C. Hemenway. I believe that there is a fundamental difficulty in relating these results to the rocket and satellite experiments. The rocket in question was opened below 90 km, where the particles have been slowed down by the atmosphere. There is a large uncertainty in the settling rate at these altitudes, and I believe that where the exact altitudes of collection are unknown in this experiment, we should not place too much faith in the flux calculations.

*L. G. Jacchia.*—I have seen some figures quoted for dust at altitudes as high as 90 km for the bright sunsets after the explosion of Krakatoa in 1883; those bright sunsets are said to have persisted for something like 3 or 4 years.

*F. L. Whipple.*—I don't feel that we can accept the validity of those height estimates at that time. Dr. Goody's work has shown that you cannot make a reliable estimate of the amount of material at high altitudes by the sunset method. The fact that something was seen after sunset at that altitude does not prove, I think, that it wasn't secondary scattering. I don't see anything to hold larger particles up there.

*E. L. Fireman.*—One can go the other way and say that these results should lead to a tremendous concentration at the airplane collection altitudes. The relative settling rates

would predict an increase in concentration of something like  $10^7$  at a 15-km altitude. Therefore, I am surprised that people haven't seen many more of these particles in the aircraft collections.

*C. L. Hemenway.*—We do find much higher concentrations of these same types of particles on aircraft collectors.

*F. L. Whipple.*—Some calculations made from the aircraft collections are not completely out of line with these other estimates of the influx rate.

*C. L. Hemenway.*—I might interject that when aircraft collections are made by the filtering technique where the air expands through a hole at subsonic velocities you don't find the fluffy particles breaking up. On the other hand, when you collect by the impactor technique you find a large number of smashed particles that look similar to the ones we have shown today.

*J. Manson.*—We have been working on aircraft collections for some time. We think that possibly the secondary precipitation mechanism of forming sulfate particles at altitudes of about 20 km may hide some of these particles and would certainly speed up their fall rate.

*C. L. Hemenway.*—I would support that. I would say that the extremely small particles that we have seen in aircraft collections and have named nanometeorites for a convenient label were found at U-2 altitudes only in clumps. This would suggest that such a clump had been brought down as a part of a larger particle that partially evaporated under electron-beam bombardment.

*C. Ellyett.*—There is evidently some question as to a possible particle increase at the time of a meteor shower, thus associating the small particles with the larger meteoroids. You propose to fire into a quiet period and a pronounced shower period. I would like to suggest an alternative method, that is, to fire in both the

northern and southern hemispheres at the same time since we have an entirely separate set of showers.

*P. M. Millman.*—I would like to remind the audience of the evidence of the noctilucent clouds and the trains left by large meteors, such as the Tunguska fall, which tend to collect at a preferred height due to the temperature profile. One of the best theories to explain the noctilucent clouds suggests a possible increase in size of these particles due to the formation of ice on a very small solid nucleus. When one is talking about the possibility of particles being held at certain levels I think that this evidence should be carefully considered.

*R. K. Soberman.*—We deliberately opened above the noctilucent cloud altitude, which I believe is consistently in the 80 to 85 km altitude region.

*M. Dubin.*—The estimates of particle concentration in noctilucent clouds (that is, 1 to 5 particles per cubic centimeter) give sufficient numbers at about the altitude of opening to account for your results, and this would explain the low velocity. A higher altitude opening would solve this question. Another point is that Dr. Weiss mentioned in his paper that Dr. Kaiser has measured the distribution of the Arietids in the radio region and found an  $s$  number greater than 2.5, which would give a large number of small particles at the time of that shower.

*C. W. McCracken.*—Earlier Dr. Soberman made the remark that his results from the two satellites did not fit the mass-distribution curve that we presented. I find that if I treat his four datum points as I did the other data, then those four points fall within an order of magnitude of the curve. Also the 300 particles per square meter per second with diameters greater than 3 microns, which he finds from the rocket measurement, is within one order of magnitude of an extrapolation of the mass-distribution curve. Therefore, I don't see any tremendous discrepancies that would lead one to conclude that an appreciable geocentric concentration has been measured.

*F. L. Whipple.*—Referring to the clusters that Dr. Hemenway showed, I have been considering how these particles can be spread out only over a few microns. If they had fallen any distance

through the atmosphere they should have been separated by meters at least. I might suggest that as the rocket goes up there is a lot of degassing going on and the air density in the vicinity of your collectors may be as much as 1000 times greater than ambient. It is quite possible that the particles that survived entering the atmosphere may have broken up when they hit this much denser gas envelope.

*M. Dubin.*—Dr. Soberman said in his papers that he did not trust the earlier rocket acoustic measurements because he did not find any large number of holes in the penetration experiments. Evidence was presented that many of the particles do break up and may not be able to penetrate the mylar films. These particles would still show up as a pulse on the microphone systems. There were cases where we observed clustered pulses that we did not believe. This may be the explanation. Therefore, I do not feel that one can say that these experiments rule out the validity of the earlier acoustic measurements. The velocity of impact, I feel, can still be questioned since the rocket did open close to the so-called noctilucent cloud region.

*R. K. Soberman.*—With regard to noctilucent clouds, there is a half hour per day at these latitudes in which you could see the clouds if they existed in this area. They have not been observed this far south, let alone at 30° N.

*F. L. Whipple.*—But the dust that may form the clouds may exist at all latitudes.

*M. Dubin.*—If these fluffy particles were to strike a wire grid on a satellite, what would be the result?

*C. L. Hemenway.*—I would say that the fluffy particles have no chance of breaking the grid.

*M. Dubin.*—The microphones would still detect them and you could develop a curve of the type that McCracken has shown. But because of the fluffy particles I don't think you can compare the microphone data with the wire-grid breakage rate.

*E. L. Fireman.*—If the statistics are as Dr. Hemenway reported, then fluffy particles are only about 12 percent of the total number.

*R. K. Soberman.*—This is pure speculation, but these irregular particles which we observe and which form the majority of the particles may have been part of larger loose agglomerates.

*C. L. Hemenway.*—Because of our stringent

requirements and the difficulties in classification, I wouldn't trust the percentage breakdown too far. I would trust the size distribution and the over-all numbers of particles per unit area.

*M. Dubin.*—One more point. If you believe the distribution function obtained by microphone systems is as McCracken presented it, plus the fact that there are irregularities in the flux of particles, then you do not have to impose a dust belt to tie in the rocket and the satellite data.

*J. S. Greenhow.*—I would like to show how the measurements of radar rates extrapolate to the micrometeorite measurements. Dr. Weiss showed yesterday that with electron line densities of  $10^{14}$  to  $10^{15}$  per centimeter,  $s$  is about 2.5. These are fairly reliable measurements. I have extended this down to  $10^{11}$  with a value of  $s$  of about 2.4. So over this range of electron line densities  $s$  is of this order. If we look at

the absolute rate for a line density of  $10^{12}$  per centimeter, we find about 30 per  $10^4$  km<sup>2</sup> per hour. We only detect, of course, those at approximately right angles to us; in order to get a true rate we have to multiply by a factor of about 20. This line density corresponds to a mass of about  $10^{-2}$  gram. For micrometeorite, I obtained from the previous graphs a rate of about  $10^{-3}$  per square meter per second for a mass of  $10^{-8}$  gram. If we take this range of  $10^6$  in mass and something like  $5 \times 10^7$  in rate when one puts in the various factors, we find that the  $s$  value required to account for this difference in rates is 2.4. So it seems reasonable that we have an  $s$  value of about 2.4 all the way from these large meteors that are about zero magnitude and  $10^{-2}$  gram down to  $10^{-8}$  gram. It seems to me, therefore, that it would be unreasonable to expect the slope to change in the micrometeorite range and become something else.



# A General Survey of Meteor Spectra

By Peter M. Millman <sup>1</sup>

The study of the spectra of meteors dates from the 1860's when an English astronomer, A. S. Herschel, commenced his visual observations with specially mounted direct-vision binocular prisms. For about 20 years observations were reported by a number of astronomers including Herschel himself, A. Secchi, H. A. Newton, and N. von Konkoly. For a bibliography of the subject during this period see Millman (1932).

Through this early work it was realized that in general meteors had bright-line spectra, though sometimes the intense luminosity of the meteor head caused the lines to blend into each other giving the appearance of a continuous spectrum with a few predominant lines superposed. The orange-yellow lines of neutral sodium and the green lines of neutral magnesium were correctly identified by these nineteenth century observers.

The first meteor spectrum photograph was made on a Harvard patrol plate at Arequipa, Peru, on June 18, 1897 (Pickering, 1897). The first program of meteor spectro-photography was carried out by S. Blajko (1907) at the Moscow Observatory during the spring and summer of 1904. However, at this time there was no general activity in this field of astronomical photography, and by 1930, when I first became interested in the subject, only eight photographic meteor spectra were known. Five of these had been photographed by chance on programs conducted for other purposes. During the last 30 years the number of photographic meteor spectra has grown slowly but steadily and the world total now stands at well over 400.

Even more important than the increase in numbers of spectra has been the advance in quality. This has been due chiefly to the de-

velopment of new photographic emulsions, which are faster and cover a wider range of wave length, and to the use of gratings instead of prisms for the dispersing element. The original spectra were all photographed on blue-sensitive plates. Fast plates sensitive to the yellow-green became available in 1932 (Millman, 1935) and panchromatic plates sensitive to the red in 1933 (Millman, 1934). By 1950 it was possible to use an infrared emulsion to photograph meteor spectra (Millman, 1953). It was also in 1950, on the Ottawa program, that replica transmission gratings were first successfully used. With a grating relatively high dispersors are possible in some of the orders, and lenses of longer focal length can be employed without materially increasing the absorption of the dispersing element. Plates *1a,b* and *2a,b* illustrate spectra photographed with gratings on the Canadian programs.

The photographic observations have confirmed the fact that the luminosity of meteors results primarily from a bright-line atomic spectrum with a small percentage of the light coming from simple molecules, and possibly a continuous background in certain cases. Table 1 lists the multiplets that have been identified with some reliability, the reference numbers being those from the table by Moore (1945). Multiplets found in some recent spectra of high dispersion are included in table 1, while some identified earlier on the basis of poor quality prismatic spectra have not been included. An attempt has been made to select only those multiplets for which it is felt there is independent evidence of their presence. Since meteor spectra as a whole give a consistent picture, an analysis of a weak spectrum of poor definition has been judged in view of what is present in high dispersion spectra of good definition. In other words, the multiplets listed

<sup>1</sup> National Research Council, Ottawa, Canada.

TABLE 1.—*Multiplets identified in meteor spectra* (reference numbers according to Moore, 1945)

(Bold face type indicates the most prominent multiplets; parentheses, those identified with less certainty.)

H I	<b>1</b>									
N I	<b>1</b>									
O I	<b>1</b>	<b>4</b>	<b>5</b>	<b>9</b>	<b>10</b>	(20) <b>11</b>	<b>12</b>	(25) <b>14</b>	<b>23</b>	<b>3F</b>
Na I	<b>1</b>	<b>5</b>	<b>6</b>	(8)	(12)					
Mg I	<b>1</b>	<b>2</b>	<b>3</b>	<b>9</b>	<b>11</b>	<b>14</b>	<b>15</b>			
Al I	<b>1</b>	(5)								
Si I	(2)	(3)	(9)	(10)	(11)	(16)	(17)			
Ca I	<b>1</b>	<b>2</b>	<b>3</b>	<b>4</b>	<b>5</b>	(9)	<b>18</b>	<b>19</b>	(20)	<b>21</b>
	<b>22</b>	(23)	<b>32</b>	(47)						
Cr I	<b>1</b>	<b>7</b>	(9)	<b>22</b>	(31)	(40)				
Mn I	<b>2</b>	<b>5</b>	(6)	<b>16</b>						
Fe I	<b>1</b>	<b>2</b>	<b>3</b>	<b>4</b>	<b>5</b>	<b>6</b>	<b>13</b>	<b>15</b>	<b>16</b>	<b>18</b>
	<b>19</b>	<b>20</b>	<b>21</b>	<b>22</b>	<b>23</b>	<b>24</b>	<b>25</b>	<b>26</b>	<b>36</b>	<b>37</b>
	<b>38</b>	<b>39</b>	<b>41</b>	<b>42</b>	<b>43</b>	<b>45</b>	<b>62</b>	<b>68</b>	<b>71</b>	<b>72</b>
	(74)	152	168	169	207	217	268	278	(280)	318
	<b>350</b>	(352)	<b>354</b>	<b>355</b>	<b>357</b>	<b>383</b>	(385)	<b>409</b>	(476)	<b>482</b>
	<b>522</b>	<b>523</b>	<b>553</b>	<b>558</b>	<b>559</b>	(597)	<b>686</b>	(687)	<b>693</b>	<b>733</b>
	(772)	<b>801</b>	<b>816</b>	<b>965</b>	<b>984</b>	<b>1062</b>	(1066)	<b>1067</b>	<b>1092</b>	<b>1094</b>
	<b>1107</b>	<b>1146</b>	<b>1150</b>	<b>1163</b>	<b>1165</b>	<b>1178</b>				
Co I	(28)	(29)	(31)	(34)	(150)					
Ni I	(1)	(3)	5	(6)	(17)	<b>18</b>	(19)	(20)	(30)	(32)
	<b>33</b>	(35)	(36)	(52)	<b>86</b>					
N II	<b>3</b>	<b>5</b>	<b>8</b>	<b>15</b>	<b>28</b>					
O II	<b>1</b>	<b>2</b>								
Mg II	<b>4</b>	(9)	(10)	(20)						
Si II	<b>1</b>	<b>2</b>	<b>3</b>	<b>4</b>	<b>5</b>	(8)	(9)			
Ca II	<b>1</b>	<b>2</b>								
Fe II	<b>27</b>	<b>28</b>	<b>37</b>	<b>38</b>	<b>42</b>	<b>48</b>	<b>49</b>	<b>74</b>		
Sr II	<b>1</b>									
N <sub>2</sub>	1st positive group, 2d positive group.									

represent my selection on the basis of a study of all the observational data available to date. There is no doubt that it will soon be possible to add to the list a substantial number of additional multiplets.

Table 1 contains multiplets from 13 neutral atoms and 7 singly ionized atoms, and band systems from one molecule. The ionization potentials of the upper levels involved are in general low, particularly for the stronger, more prominent multiplets. Over 80 percent are in the range 2 to 8 eV and most of the remainder are in the range 10 to 14 eV. Only the multiplets from N II and O II have excitation potentials above 20 eV.

Any trailing train luminosity of reasonable strength will be photographed in the breaks of the meteor track, produced by a rotating

shutter. Plate 1*b* illustrates a good example of this effect in a Perseid meteor. The train or wake spectrum exhibits a similar character to the spectrum of the meteor head, but the low excitation multiplets and intercombination lines are much stronger relative to the other multiplets. Except for Ca II the ionized elements are almost entirely lacking. Table 2 lists the multiplets reliably identified in train or wake spectra. Their excitation potentials average 4 eV compared with an average of about 6.5 eV for the multiplets in table 1. The durations of the luminosity photographed in meteor trains or wakes probably range from a few hundredths of a second up to a second or two. Unfortunately, the spectrum of a persistent or long enduring train has not yet been photographed.

Of particular interest in meteor trains is the presence of the forbidden line of oxygen at 5577A (multiplet 3F of O I), often called the auroral green line (see pl. 2b). This was first identified by Halliday (1958) and has since been found in at least 25 spectra including a number photographed by Russell (1959, and this Symposium, p. 171). This feature tends to appear at greater heights than most of the other meteor spectrum lines, and often disappears before the rest of the spectrum has reached maximum intensity. On the average, this oxygen line is brightest between heights of 110 km and 100 km, while the maximum light of the remainder of the meteor spectrum occurs at an average height of 90 km. The green line appears chiefly in the spectra of fast meteors, and this height of 90 km is typical of the maximum light for the spectra of meteors with velocities greater than 50 km/sec. Geminid spectra have the light maximum some 15 km lower on the average, and the spectra of slow sporadic fireballs with velocities near 20 km/sec are brightest at a height of around 60 km. Giacobinid spectra, brightest near a height of 90 km, are abnormally high for their velocity of 23 km/sec.

Of the 318 photographic meteor spectra listed up to the end of 1958 (Millman, 1959), over 70 percent are from the well-known meteor showers. Since meteors of this category do not seem to fall as meteorites, meteor spectra provide the only direct evidence of the composition of these objects. The atomic abundance of the elements in the largest class of stony meteorites, the chondrites, has been

given by Urey and Craig (1953). Of the 15 abundant elements listed by these authors, all except sulphur, potassium, phosphorus, and titanium appear in table 1 above. Neither sulphur nor phosphorus has good low excitation lines in the observed region, and the position of the potassium line in the far red is overlapped by first-order iron lines in the spectra obtained up till now. Titanium, as a minor constituent, is difficult to identify because of the multiplicity of lines and the overlapping with other elements. Three elements not common in meteorites—hydrogen, nitrogen, and strontium—are listed in table 1. The occurrence of hydrogen in meteor spectra may possibly indicate the presence of ices of some form in the cometary meteoroids. Nitrogen must certainly be contributed by the atmosphere, and it is not possible to say whether any of it comes from the meteoroid itself. Strontium, though not common, is found in very small amounts in some meteorites. In summary, it appears that the cometary meteorites do not differ too markedly in general composition from the stony meteorites. The absence of sulphur and potassium from meteor spectra and the presence of hydrogen are probably the most significant indications of possible differences.

Meteor spectra vary greatly in quality, from faint records showing only a single line to high dispersion spectra in which 100 or more separate items have been measured. In any statistical study of spectra it is important to consider this feature, and the following quality scale has been found convenient:

- a - detail of 50 lines or more,
- b - 20 to 49 lines,
- c - 10 to 19 lines,
- d - 9 lines or less.

TABLE 2.—*Multiplets in meteor train and wake spectra*  
(Bold face type indicates the most prominent multiplets; parentheses, those identified with less certainty.)

O I	<b>3F</b>
Na I	<b>1</b>
Mg I	<b>1</b> 2 3 (9)
Ca I	<b>1</b> 2 3 18 (19) (21)
Mn I	<b>2</b>
Fe I	<b>1</b> 2 3 4 5 15 (16) 20 21 (23) 41 42 43 (268)
Ca II	<b>1</b> 2
N <sub>2</sub>	(1st positive group.)

Meteor spectra exhibit a fairly consistent pattern with a few dominant characteristics, and I proposed a simple system of classification some years ago (Millman, 1935). A study of all available data has indicated that this original classification scheme is still useful and it is summarized below, revised slightly to adjust it to the panchromatic emulsions now generally used. Classification of a spectrum is based on its character at light maximum and involves identification of the strongest features

TABLE 3.—Classification of 259 meteor spectra

Meteor	Vel km/sec	Y				X				Z				W d
		a	b	c	d	a	b	c	d	a	b	c	d	
Leonid (L)	72			7	4									
Orionid (O)	66			2	4									3
Perseid (P)	60	9	27	11	45		1	4	4					2
Lyrid (Y)	31-48													
Quadrantid (Q)		1	1	1			1	1					1	
♁ Aquarid (D)														
Taurid (T)														
Geminid (G)	35	1		3	1	1	2	4	12					3
Giacobinid (J)	23						3	9	9		1	2	2	
Miscellaneous (N)	12-70	1	5	9	13	1	6	10	14	2	5	3	4	1
	Totals													
		12	35	35	66	2	13	28	39	2	6	5	10	6
				148				82				23		6

in two wavelength regions, the blue-violet from 3500 to 4500 Å and the orange-green from 5000 to 6000 Å. Four main types are defined below:

Type Y: The H and K lines of Ca II are the strongest features in the blue-violet.

Type X: If not as above, then either the D-lines of Na I, or the lines near 5180Å or 3835Å of Mg I, give the strongest feature in either the orange-green or the blue-violet.

Type Z: If not as above, then the lines of Fe I, or those of Cr I, give the strongest feature in either the orange-green or the blue-violet.

Type W: Not as above.

This classification, though developed on a strictly empirical basis, has some physical significance since Type Y spectra are of higher excitation than Type X. In Type Z spectra most of the elements common in stony meteoroids are weak or absent, and hence a reasonable percentage of Type Z spectra must correspond to iron meteoroids. Type W will include peculiar spectra and those too faint or ill-defined to have other classification features. Since spectrum quality has a direct bearing on what can be identified, it is suggested that a letter for the quality scale be prefixed to the type. For example, a spectrum of 35 lines showing very strong H and K of Ca II would be classified as *bY*, one of 58 lines showing just the iron multiplets would be *aZ*. If it should be found advisable, numbers could be suffixed to the type letters to indicate levels of excitation

within each type. It is suggested that these should be used in the same sense as for stellar spectra, that is, lower numbers referring to higher excitations.

All the meteor spectra secured prior to 1959, for which information is available, have been classified in the above system. Their distribution in type, listed according to velocity, is given in table 3. It will be noted that the fast meteors are predominantly Type Y, meteors of medium speed tend to be Type X though some are of the other types, while slow meteors are confined to Types X and Z. Giacobinid spectra (see pl. 1c) are good examples of what we find in the light of very slow shower meteors.

In the miscellaneous group the Type Y examples probably represent chiefly cometary meteoroids, since asteroidal meteoroids as a class are medium to low velocity objects (Whipple and Hughes, 1955). In table 3 there are probably not more than 30 miscellaneous spectra produced by asteroidal meteoroids, and at least two-thirds of these will be Types Y and X, produced by stony meteoroids. Of the miscellaneous spectra Type Z, it is likely that not more than six represent iron meteoroids. Two examples which are probably in this category are reproduced in plates 1*d* and 2*c*. These spectra exhibit very little other than strong low level iron multiplets and sometimes the ultimate lines of chromium.

A further insight into the relations among meteor spectra may be obtained by an examination

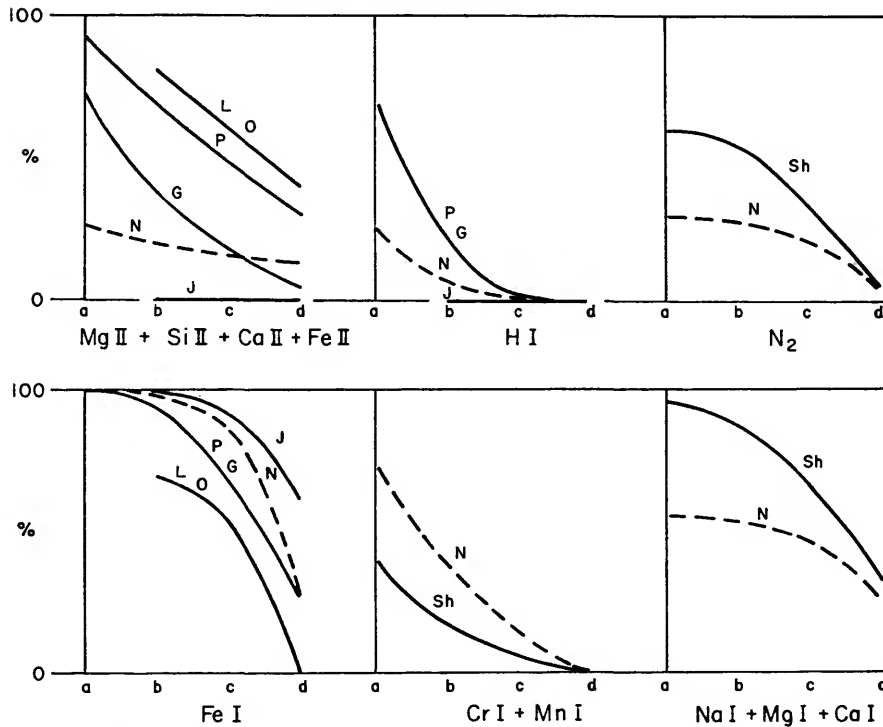


FIGURE 1.—The frequency of identification of various elements in 259 meteor spectra photographed prior to 1959, plotted against the spectrum quality from a to d. The plot has been smoothed to show general trends and should not be used for quantitative values. Abbreviations: L, Leonid; O, Orionid; P, Perseid; G, Geminid; J, Giacobinid; Sh, shower; N, miscellaneous.

of the frequency with which various atoms are identified in any group. Figure 1 illustrates some of these data. The observational material used was the same as that included in table 3. Percentage identification of the atoms is plotted against spectrum quality. These curves are smoothed averages and give qualitative information only and should not be used to give quantitative values. They do, however, clearly demonstrate the danger of drawing general conclusions from spectra of low quality only.

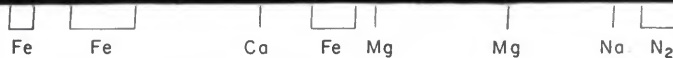
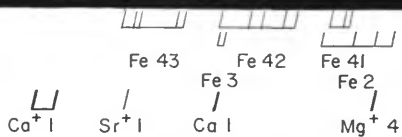
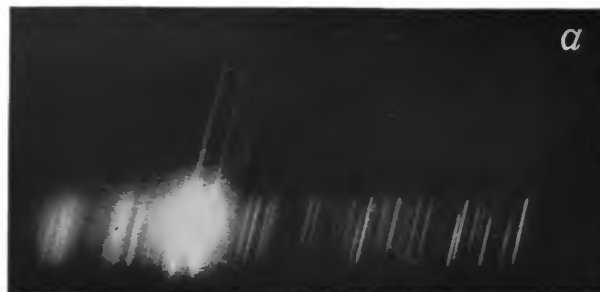
The correlation of the appearance of the ionized elements with the velocity of the meteor, and the universal presence of iron in all spectra of good quality, are quite evident features of the plot. Another interesting point is that the elements Ca, Na, and Mg are more frequently identified in the shower meteors, while Cr and Mn are found more frequently in the miscel-

laneous group which probably contains a significant percentage of nonshower meteors.

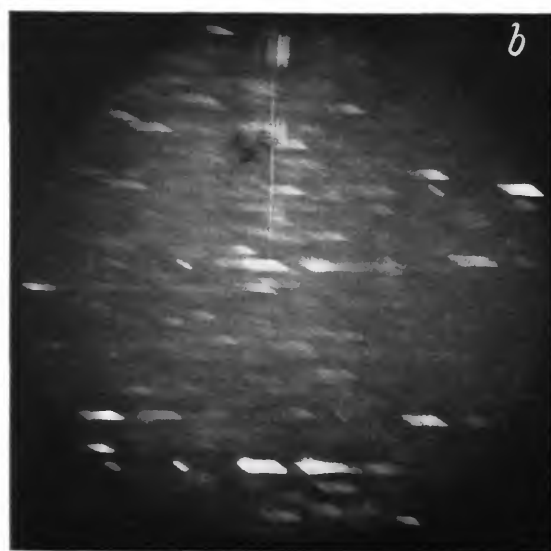
Another way of looking at meteor spectra is to list the features which are strongest in each example. Naturally, this will be greatly modified by the wavelength sensitivity of the grating or prism-lens-emulsion combination. If we consider only the good quality spectra studied here, ionized calcium is the strongest feature in all Perseid spectra. The Geminid spectra are roughly divided into four equal groups with ionized calcium, neutral magnesium, neutral sodium, and neutral iron the strongest in each group respectively. Magnesium is somewhat ahead of the other three elements in frequency, suggesting the possibility that this element is a significant constituent in Geminid meteoroids. Giacobinid spectra are about equally divided between sodium and iron

## EXPLANATION OF PLATE 1

- a: *Meteor Spectrum No. 340, Type aY*, a bright Perseid photographed at the Newbrook Meteor Observatory at 9<sup>h</sup> 27<sup>m</sup> 55<sup>s</sup> UT, August 13, 1959. Lens, focal length 20 cm, aperture 7 cm; grating, 400 lines/mm; emulsion, Kodak Tri-X Aerecon; dispersion in second order 60 Å/mm, no rotating shutter, meteor moving down in figure, observed visually magnitude  $-7$  or  $-8$  with a persistent train of 10-second duration. Halliday (1961) has measured over 100 lines in the spectrum. Note particularly the late appearance in the burst of the low level iron multiplets Fe I 2 and 3 as compared to the higher level multiplets Fe I 41, 42, 43, and the ionized elements. This is a similar effect to that found by Russell (1960) in the spectrum of the terminal burst of another Perseid meteor.
- b: *Meteor Spectrum No. 272, Type aY*, a bright Perseid photographed at the Springhill Meteor Observatory at 6<sup>h</sup> 20<sup>m</sup> 15<sup>s</sup>, August 12, 1958. Lens, focal length 15.0 cm, aperture 3.3 cm; grating, 200 lines/mm; emulsion, Kodak 103 aF spectrographic; dispersion in first order 320 Å/mm, rotating shutter occulting 10/sec, open to closed ratio  $\frac{1}{2}$ , meteor moving up in figure, observed visually magnitude  $-7$  or brighter with persistent train duration 180 sec, photographic trajectory heights from 112 km to 83 km with light maximum at 90 km. Infrared spectrum of this meteor, secured with another camera, studied by Millman and Halliday (1961). Note high relative strength of multiplets Fe I 1, 2, 3, Mg I 1, and Ca I 1 in wake spectrum filling next to last shutter break.
- c: *Meteor Spectrum No. 86, Type bX*, a Giacobinid photographed at North Bay, Ontario, at 3<sup>h</sup> 51<sup>m</sup> 42<sup>s</sup> UT, October 10, 1946. Lens, focal length 15.0 cm, aperture 3.3 cm, prism angle 30°, flint glass; emulsion, Kodak XXX-B plate; mean dispersion H $\delta$ —H $\gamma$  410 Å/mm, rotating shutter occulting 10/sec, open to closed ratio  $\frac{1}{2}$ , meteor moving down in figure, observed visually magnitude  $-2$  with persistent train duration 20 sec, photographic trajectory heights from 109 km to 90 km, light maximum of sodium line 102 km, of magnesium and iron lines 98 km. Note early appearance and disappearance of sodium line.
- d: *Meteor Spectrum No. 24, Type aZ*, nonshower photographed at Flagstaff, Ariz., at 6<sup>h</sup> 35<sup>m</sup> 23<sup>s</sup> UT, February 27, 1933. Lens, focal length 15.0 cm, aperture 3.3 cm, prism angle 30°, flint glass; emulsion, Cramer Iso Presto; mean dispersion H $\delta$ —H $\gamma$  410 Å/mm, no rotating shutter, meteor moving down in figure violet end of spectrum at left, observed visually magnitude  $-9$  with train 2 sec duration. Visually determined heights of major bursts at 75, 73, 71, 69, 66, 65, 63, 59 km respectively. This spectrum has been studied by Millman (1935). Spectrum shows very little besides iron and nickel.



For explanation see facing page.



For explanation see facing page.

## EXPLANATION OF PLATE 2

- a: Meteor Spectrum No. 273, Type bY*, a bright Perseid photographed at the Springhill Meteor Observatory at 6<sup>h</sup> 39<sup>m</sup> 25<sup>s</sup> UT, August 12, 1958. Lens, focal length 20 cm, aperture 7 cm; grating, 200 lines/mm; emulsion, Kodak infrared aerographic; no filter, dispersion in first order 240 Å/mm, rotating shutter occulting 12/sec, open to closed ratio 1/2, meteor moving down in figure, observed visually magnitude -5 with a persistent train duration 30 sec, photographic trajectory heights from 104 km to 79 km with light maximum at 84 km. First order infrared overlaps second order violet. This spectrum has been studied by Millman and Halliday (1961). Note the early appearance of the O I line, and the increase in relative strength of the Ca II lines towards the end of the path.
- b: Meteor Spectrum No. 294, Type dX*, a Perseid photographed at the Newbrook Meteor Observatory at 7<sup>h</sup> 30<sup>m</sup> UT, August 15, 1958. Lens, focal length 6.2 cm, aperture 8.7 cm; grating, 80 lines/mm; emulsion, Kodak I-D spectroscopic; dispersion in first order 1950 Å/mm, rotating shutter occulting 11.6/sec, open to closed ratio 1/2, meteor moving up in figure, approximate heights of photographic trajectory 120 km to 100 km. This spectrum has been studied by Halliday (1960). Note the auroral O I line at 5577 Å which carries across all the shutter breaks, indicating a minimum duration of an appreciable fraction of a second. The sodium D-line appears just to the right of the auroral line, and the magnesium green line just to the left.
- c: Meteor Spectrum No. 26, Type bZ*, nonshower photographed by the Texas Observers at Fort Worth, Tex., at 7<sup>h</sup> 03<sup>m</sup> UT, August 12, 1933. Lens, focal length 30 cm, aperture 7.5 cm; prism angle 20°, flint glass; emulsion, Kodak Hyper Press; mean dispersion Hδ—Hγ 333 Å/mm, no rotating shutter, meteor moving down in figure violet end of spectrum at left, observed visually magnitude -5 with train 1.5 sec duration. Spectrum shows mainly low level multiplets of neutral iron. Note similarity to Spectrum 24 (see pl. 1d).

as the strongest feature. For the miscellaneous group of spectra, sodium comes first, followed by ionized calcium and neutral iron.

Several investigators, including myself, have noted that the character of a meteor spectrum frequently changes along the photographed path. Usually this change is in the sense of progressing to higher excitations, with the associated greater relative strength of the ionized atoms such as Ca II, Mg II, and Si II. Bursts near the end of the path for bright meteors of the faster showers demonstrate particularly well this enhancement of the ionized atoms (Russell, 1949). However, in the case of slow nonshower fireballs it is quite possible for the neutral iron vapor to show a lower excitation at the bursts (Millman, 1935).

Since a meteor generally increases in luminosity over most of the visible path, the change in excitation will be correlated with luminosity. The early part of the path of a fast, bright fireball may show only the nitrogen bands, sodium D-lines, and some iron. This will give an intensity distribution strong in the red and yellow. As the fireball brightens the lines of ionized calcium and ionized magnesium, as well as other features, become relatively stronger and will tend to increase the intensity in the blue and violet. It is found that spectra of the faint meteors of high-velocity showers often appear similar to the early parts of the paths of much brighter meteors of the same shower. This agrees with the observational results of Jacchia (1957), Cepelcha (1959), and Davis (this Symposium p. 233), which indicate a higher color index, and therefore a redder color, for the faint meteors. There are a few very faint Perseid spectra that lack the strong lines of Ca II, a characteristic feature of most spectra of this shower. Cook (1955) has suggested a two-parameter dependence of ionization and excitation in meteor spectra, the major controlling factors being meteor velocity and the ratio of characteristic meteoroid dimension to the mean free path of an evaporated atom. Since the fainter, and hence smaller meteors, disappear higher in the atmosphere, the above suggestion could explain some of the observed correlations, but the situation is probably somewhat more complex in many cases.

In conclusion I express my thanks to I. S. Astapovich, E. N. Kramer, and K. A. Liubarsky, U.S.S.R.; Z. Cepelcha and J. Rajchl, Czechoslovakia; I. Halliday, Canada; H. B. Ridley, England; and J. A. Russell, U.S.A., all of whom have provided me with unpublished details of meteor spectra for this survey.

### References

- BLAJKO, S.  
1907. On the spectra of two meteors. *Astrophys. Journ.*, vol. 26, pp. 341-348.
- CEPLECHA, Z.  
1959. On the colour index of meteors. *Bull. Astron. Inst. Czechoslovakia*, vol. 10, p. 39.
- COOK, A. F.  
1955. The nature of meteoric radiation. *In* T. R. Kaiser, ed., *Meteors, Spec. Suppl. Journ. Atmosph. Terr. Physics*, vol. 2, pp. 8-15. Pergamon Press, New York.
- HALLIDAY, I.  
1958. Forbidden line of O I observed in meteor spectra. *Astrophys. Journ.*, vol. 128, pp. 441-442.  
1960. Auroral green line in meteor wakes. *Astrophys. Journ.*, vol. 131, pp. 25-33.  
1961. A study of spectral line identifications in Perseid meteor spectra. *Publ. Dominion Obs. Ottawa*, vol. 25, pp. 1-16.
- JACCHIA, L. G.  
1957. On the "color index" of meteors. *Astron. Journ.*, vol. 62, pp. 358-362.
- MILLMAN, P. M.  
1932. An analysis of meteor spectra. *Ann. Harvard Coll. Obs.*, vol. 82, pp. 113-146.  
1934. Meteor spectra—list I. *Journ. Roy. Astron. Soc. Canada*, vol. 28, pp. 279-281.  
1935. An analysis of meteor spectra: second paper. *Ann. Harvard Coll. Obs.*, vol. 82, pp. 149-177.  
1953. The typical Perseid meteor spectrum. *Nature*, vol. 172, pp. 853-854.  
1959. Photographic meteor spectra (appendix 7). *Journ. Roy. Astron. Soc. Canada*, vol. 53, pp. 271-276.
- MILLMAN, P. M., AND HALLIDAY, I.  
1961. The near-infra-red spectrum of meteors. *Planetary Space Sci.*, vol. 5, pp. 137-140.
- MOORE, C. E.  
1945. A multiplet table of astrophysical interest. *Contr. Princeton Univ. Obs.*, no. 20, parts 1, 2.
- PICKERING, E. C.  
1897. Spectrum of a meteor. *Astrophys. Journ.*, vol. 6, pp. 461-462.

RUSSELL, J. A.

- 1949a. A composite spectrum of a Perseid meteor of 1948. *Pop. Astron.*, vol. 57, pp. 187-192.
- 1949b. A note on revised wavelenths for a composite spectrum of a Perseid meteor of 1948. *Pop. Astron.*, vol. 57, pp. 344-345.
1959. Some Perseid meteor spectra of the past decade. *Sky and Tel.*, vol. 18, pp. 549-551.
1960. A time-resolved spectrum of the terminal burst of a Perseid meteor. *Astrophys. Journ.*, vol. 131, pp. 34-37.

UREY, H. C., AND CRAIG, H.

1953. The composition of the stone meteorites and the origin of the meteorites. *Geochim. et Cosmochim. Acta*, vol. 4, pp. 36-82.

WHIPPLE, F. L., AND Hughes, R. F.

1955. On the velocities and orbits of meteors, fireballs, and meteorites. *In* T. R. Kaiser, ed., *Meteors, Spec. Suppl. Journ. Atmosph. Terr. Physics*, vol. 2, pp. 149-156. Pergamon Press, New York.

### *Abstract*

Over 400 meteor spectra have now been photographed at various observatories, with most of the data having been obtained in three countries—Canada, the U.S.S.R., and the U.S.A. The range of wavelengths covered extends from 3000A to 9000A. The bright-line emissions for roughly 200 multiplets have now been identified with some certainty. These belong to 13 neutral atoms, 7 singly ionized atoms, and one molecule. The composition of cometary meteoroids does not seem to differ markedly from that of stony meteorites. The excitation in a meteor spectrum depends chiefly upon the velocity of the meteor and its absolute magnitude. A simple system of meteor spectrum classification is suggested, based on an earlier proposal made by the author in 1935.



# Meteor Spectra with High Dispersion

By Zd. Ceplecha<sup>1</sup> and J. Rajchl<sup>1</sup>

This paper is based on the analysis of two photographs of meteor spectra with high dispersion obtained by transmission diffraction gratings in the autumn of 1960 at the Ondřejov Observatory (Rajchl, 1961). The cameras used were provided with Tessar objectives having focal ratios of 1:3.5 and 1:4.5 and focal lengths of 30 cm and 36 cm. The first camera was equipped with a transmission objective grating with 600 grooves per millimeter, and the second one with a grating with 400 grooves per millimeter. The photographic materials used were Agfa Press plates 25° D with dimensions 18×24 cm. A shutter rotating approximately 450 times per minute was used with these cameras.

## The method of wavelength determinations

Since a meteor spectrum photographed with an optical transmission grating is usually off the optical axis of the camera, the ordinary method of wavelength determination is hardly feasible. The diffracted ray falls in the plane determined by the incident ray and the optical axis when the spectrum passes through the optical axis. On the other hand, when the spectrum does not pass through the optical axis, the diffracted rays lie on the surface of a cone, the axis of which is parallel to the grooves. The section of this diffraction cone made by the focal plane is the diffraction hyperbola, along which the spectral record is distributed. Absolute wavelengths can be found from such a spectrum if it includes the zero-order image. A method based on Rowland's (1893) was developed to exploit the full accuracy that could be obtained. Complete details, with equations, have been published (Ceplecha, 1961). We present here a brief description of the principal features of the method.

The spectral plate is measured with the  $y$ -axis placed roughly parallel to the meteor motion, thus leaving the  $x$ -coordinate of any one line only slightly dependent on the position along the track where it is measured. The coordinate system for the whole plate is computed from measurements of zero-order images of stars (Ceplecha, 1951; 1954). The spectrum must be photographed with a rotating shutter. The measurements of one break in three different lines then give the diffraction hyperbola, and thus the connection between the coordinate system of the plate and that of the grating. The coordinate system of the grating directly determines the wavelengths of individual lines if we know the precise number of grooves per millimeter and the direction cosines of the zero-order image of the meteor. Identification of one line will yield this precise number of grooves per millimeter, and comparison with the number of grooves specified by the manufacturer will check the identification. Thus it is possible to say that the wavelengths of all the lines are computed without previous identification, and that they are determined absolutely by the measurements of angles. Of course, because of optical distortions, the coordinate system, defined by zero-order images of three stars and by their apparent spherical coordinates with corrections for atmospheric refraction added, is less accurate than necessary for absolute determinations of wavelengths. It is possible, however, to correct the coordinate system established from three stars at different places of the meteor spectrum by using additional stars. For example, with an undriven camera the intersection points of star images with the meteoric spectral lines may be used for this purpose.

Since the directions of spectral lines in various parts of the spectrum differ slightly, it is necessary to compute the point of intersection of

<sup>1</sup> Astronomical Institute of the Czechoslovak Academy of Sciences, Ondřejov, Czechoslovakia.

diffraction hyperbolae with each line, a somewhat laborious procedure, obviated in the case of hundreds of lines only by the use of an electronic computer. We used NE-803, completing our work on the two spectra in one hour of computer time.

It is very interesting to note incidentally that the dispersion can be chosen along an ellipse, if the grating is inclined to the optical axis of the camera. For our cameras the angle of  $54^\circ$  is sufficient to photograph all meteor spectra with dispersion along an ellipse. Such an experimental arrangement might offer some advantages for photography of meteor spectra.

### Meteor spectrum S 6

This spectrum was photographed September 13, 1960, at  $18^h 59^m$  UT. The spectrum of a single bright flare was well exposed. The flare was shorter than one break (the number of breaks per second was about 15.2). The spectrum is 24 cm long and is near the longer edge of the plate, with the hyperbolic form visible at first sight. Some of the brightest spectral lines also appeared three breaks before the flare. Thus it was possible to determine that the angular velocity was  $6.9^\circ/\text{sec}$ . A direct photograph of this meteor is, however, not available since the meteor flare was only  $28^\circ$  above the horizon at azimuth  $118^\circ$ , where none of our direct cameras was pointed. The spectrum begins with a part of the second order and continues with the third, fourth, fifth, sixth, and seventh orders. The main order contained is the fourth, but the orders overlap, as shown in figure 1. They are on the opposite side from the "blazed" first order. Thus the distribution of the intensity of one line in different orders is relatively smooth. The approximate dispersion, which changes slightly with the place on the plate, is presented in table 1. The dispersion in the fourth order is about 19 Å/mm. With such a high dispersion, it is possible to compute the wavelengths with relatively great precision.

TABLE 1.—Approximate dispersions of meteor spectrum S 6

Order	2	3	4	5	6	7
Dispersion Å/mm	38	25	19	15	13	11

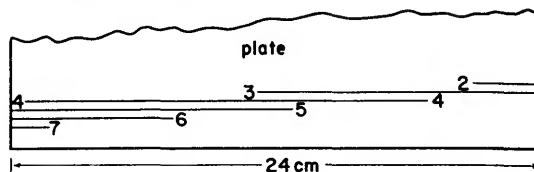


FIGURE 1.—Overlapping of orders in meteor spectrum S 6.

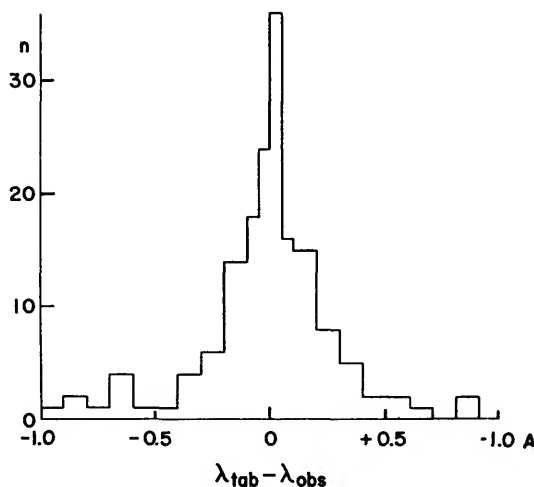


FIGURE 2.—Distribution of the deviations of measured wavelengths from tabular wavelengths of 116 unblended lines.

The disentanglement of the different overlapping orders was very laborious. The wavelengths were computed for every possibility, and identifications of the individual lines were sought in different orders. Some factors, for example the different optical quality of the image depending on the wavelength, simplified the choice of the spectral order, but the most important factor considered was the repetition of one line with corresponding intensities in all spectral orders. The results appear in table 2, which contains 166 lines with their identifications. It is interesting to note that 70 percent (116 lines) are not blended at this high dispersion. The mean deviation of the measured wavelength from the laboratory wavelength for these unblended lines was only  $\pm 0.21$  Å. The distribution of the deviations is given in figure 2.

The basic spectral tables used for the identifications are the Russian tables of Zajdel et al. (1952), from which the intensities  $I_{\text{tab}}$  presented in table 2 are taken for the arc spectra of individual elements. The observed intensities  $I_{\text{obs}}$  of lines of the meteor spectrum were estimated by eye (the scale is given with table 2). The mean wavelengths of table 2 were calculated for each line from wavelengths of different orders by weighting with the number of the order. The mean intensities were computed for the intensity level of the fourth order. The intensities from other orders were reduced to the level of the fourth order by multiplying by the factors derived from comparison of observed intensities of all lines in different spectral orders (the correction factors are given with table 2). Since the spectral sensitivity of the plate was not taken into account, the intensities are only provisional values.<sup>2</sup>

The majority of the lines are iron lines belonging to 76 different multiplets. The multiplet numbers presented in table 2 are from Moore's (1945) tables. The strongest lines are Na doublet 1; Mg triplet 2; ionized Ca doublet 1; Ca line 4226.73; Fe lines 4375.93 of multiplet 2; 4383.55 of multiplet 41; 5328.37 of multiplet 15. Other elements observed are Mn multiplets 2, 4, 5, 6, 22, 23, 24; Ni multiplets 45, 86, 131, 143; Al multiplet 1; Cr multiplets 1, 7, 31, 96; and Co multiplet 34.

The elements usual in meteorites and air, which are not observed in this spectrum, are Cu, P, S, C, Si, K, N, O.

The quality of this meteor spectrum is well demonstrated by the neighborhood of the Ca II line 3933.67 Å. The following lines are separated: Fe line 3927.92; Fe line 3930.30; weak Fe line 3931.12; weak Fe line 3932.63; and Ca II line 3933.67. This is the first instance in which these iron lines were separated from the Ca II line. The closest lines separated in this spectrum are only 0.43 Å apart.

The Ca II doublet in this spectrum is very strong, although the meteor is slow.

As already indicated, direct double-station photographs of this meteor are not available. It is possible, however, to estimate that this

meteor belongs to the Southern Taurid stream. Then the radiant  $\alpha_R=5^\circ$ ,  $\delta_R=0^\circ$ , which lies on the great circle of the meteor, and an assumed velocity of 29 km/sec compared with the observed angular velocity will yield  $11^\circ$  of inclination to the horizontal plane and 76 km for the height of the flare. This is quite acceptable. If the height of the flare is assumed to be in the interval from 90 to 60 km, the velocity lies within a short interval between 34 and 23 km/sec. In any case this meteor can be classified as slow.

### Spectrum of meteor No. 27471

The meteor was observed October 27, 1960, at 0<sup>h</sup>13<sup>m</sup>04<sup>s</sup> UT. Since double-station photographs are available, complete data on the atmospheric trajectory and the orbit can be presented. The detailed study of the velocity changes of this meteor is discussed in a paper by Ceplecha and Davies.<sup>3</sup>

The height of the beginning of this meteor was 86.8 km with the original velocity of  $v_\infty=25.95$  km/sec, which was possible only if the composition of the meteor was iron (Ceplecha, 1958). The observed radiant was  $\alpha_R=39^\circ 09'$ ,  $\delta_R=10^\circ 87'$ , and the elements of the orbit were

$$\begin{aligned} a &= 2.08 \text{ a.u.}, & \omega &= 98^\circ 64', \\ e &= 0.759, & \Omega &= 33^\circ 44', \\ q &= 0.501, & i &= 4^\circ 89'. \end{aligned}$$

This orbit is identical with the association No. 85 observed by Jacchia and Whipple (1961). The brightness of the meteor increased from  $-0^m.5$  at the beginning to the maximum light of  $-5^m.5$  at height 65 km, where the velocity of the meteor was 25.5 km/sec. This part of the trajectory was composed of a series of individual pulsations, the last of which was the maximum itself. After the maximum there were several pulsations; then a relatively long part of the trajectory exhibited almost constant brightness between  $-3^m$  and  $-4^m$ . The end of the trajectory occurred quite suddenly at the height of 41.1 km. The velocity measured at the end was 13.2 km/sec.

<sup>2</sup>The bolometric intensities of lines will be published in Bull. Astron. Inst. Czechoslovakia, vol. 14, no. 2, 1963.

<sup>3</sup>Zd. Ceplecha and J. G. Davies, "On the Change of the Heat-Transfer Coefficient of Bright Meteors," to be published in Bull. Astron. Inst. Czechoslovakia.

TABLE 2.—*Observed wavelengths and identifications of meteor spectrum S 6*

[EXPLANATION: Scale of observed intensities  $I_{obs}$ : 0, not observed; 0.5, weakest lines; 1, very weak; 2, weak; 3, medium intensity; 4, strong; 5, very strong; 6, strongest lines. The correction factors for the level of intensities of the 4th order were derived from comparison of observed intensities in different orders of all observed lines:

Order:            2   3   4   5   6   7  
Correction factor: 0.7 0.8 1.0 1.5 2.0 3.3

The symbol + means that the line was observed but that it was not measured because it was too weak (or not sharp enough) or because it blended with another line. The column headed "Mult." gives the number of multiplet according to Moore (1945). The figures in the last column (ev) represent the energy of the upper excitation level.]

Line observed				Blended with line		Identification				
No.	Order	$I_{obs}$	$\lambda_{obs}$	No.	Order	$\lambda_{tab}$	$I_{tab}$	Mult.	ev	
1.	4	1	3644.27							
	5	1	3643.62							
	6	0.5	3644.87							
	7	1	3644.75							
	<i>Mean:</i>	<i>1.7</i>	<i>3644.44</i>			3644.41	200	Ca I	9 5.30	
2.	4	0		/158 3 \119 4						
	5	2	3681.60				3682.23	400	Fe I	772 6.91
	6	0					3679.92	500	Fe I	5 3.36
	7	0					3683.06	200	Fe I	5 3.41
	<i>Mean:</i>	<i>(0.8)</i>	<i>(3681.60)</i>							
3.	4	1	+	160 3						
	5	1	3696.99							
	6	0								
	7	0					3697.43	100	Fe I	389 6.35
	<i>Mean:</i>	<i>0.6</i>	<i>3696.99</i>				3696.57	100	Mn I	24 6.23
4.	4	1	3700.72							
	5	0.5	+							
	6	0								
	7	0								
	<i>Mean:</i>	<i>0.4</i>	<i>3700.72</i>			3701.09	300	Fe I	385 6.35	
5.	4	1	3705.25							
	5	0.5	+							
	6	0								
	7	0								
	<i>Mean:</i>	<i>0.4</i>	<i>3705.25</i>			3705.57	700	Fe I	5 3.39	
6.	4	2	3719.95							
	5	1	3720.09							
	6	1	3719.94							
	7	0								
	<i>Mean:</i>	<i>1.4</i>	<i>3719.99</i>			3719.94	1000	Fe I	5 3.32	
7.	4	1	3733.93							
	5	1	3733.79							
	6	2	3733.86							
	7	0								
	<i>Mean:</i>	<i>1.6</i>	<i>3733.86</i>			3734.87	1000	Fe I	21 4.18	
						3733.32	400	Fe I	5 3.43	

TABLE 2.—Observed wavelengths and identifications of meteor spectrum S 6—Continued

Line observed				Blended with line		Identification			
No.	Order	$I_{obs}$	$\lambda_{obs}$	No.	Order	$\lambda_{tab}$	$I_{tab}$	Mult.	ev
8.	4	2	3737.27						
	5	2	3737.97						
	6	1	+						
	7	0							
	<i>Mean:</i>	<i>1.8</i>	<i>3737.66</i>			3737.13	1000	Fe I	5 3.35
9.	4	1	3743.00						
	5	0							
	6	1	3743.48						
	7	1	3743.37						
	<i>Mean:</i>	<i>1.6</i>	<i>3743.32</i>			3743.36	200	Fe I	21 4.30
10.	4	2	3745.72						
	5	0.5	+						
	6	1	3745.01						
	7	1	3745.17			3745.56	500	Fe I	5 3.39
	<i>Mean:</i>	<i>2.0</i>	<i>3745.24</i>			3745.90	150	Fe I	5 3.43
11.	4	2	3749.20						
	5	1	+						
	6	1	3749.64						
	7	1	3749.81						
	<i>Mean:</i>	<i>2.2</i>	<i>3749.61</i>			3749.49	1000	Fe I	21 4.22
12.	4	1	3816.06						
	5	0							
	6	0							
	<i>Mean:</i>	<i>0.3</i>	<i>3816.06</i>			3815.84	700	Fe I	45 4.73
13.	4	1	3820.36						
	5	0							
	6	0							
	<i>Mean:</i>	<i>0.3</i>	<i>3820.36</i>			3820.43	800	Fe I	20 4.11
14.	3	1	3822.41						
	4	1	3823.14						
	5	0.5	+						
	6	0				3823.51	75	Mn I	6 5.38
	<i>Mean:</i>	<i>0.6</i>	<i>3822.83</i>			3823.89	50	Mn I	6 5.40
15.	3	2	3824.37	128	3				
	4	2	3824.68						
	5	1	+						
	6	0							
	<i>Mean:</i>	<i>1.3</i>	<i>3824.55</i>			3824.44	150	Fe I	4 3.24
16.	3	0		129	3				
	4	1	3826.27						
	5	0							
	6	0							
	<i>Mean:</i>	<i>0.2</i>	<i>3826.27</i>			3825.88	500	Fe I	20 4.16

TABLE 2.—Observed wavelengths and identifications of meteor spectrum S 6—Continued

Line observed			Blended with line	Identification			
No.	Order	$I_{obs}$ $\lambda_{obs}$	No.    Order	$\lambda_{tab}$	$I_{tab}$	Ident.	Mult. $\epsilon_v$
17.	3	0					
	4	1    3827.78					
	5	1    3828.11					
	6	0					
	<i>Mean:</i>	<i>0.6    3827.96</i>		3827.82	200	Fe I	45    4.79
18.	3	0					
	4	1    3829.36					
	5	1    3829.91					
	6	0					
	<i>Mean:</i>	<i>0.6    3829.67</i>		3829.35	10	Mg I	3    5.94
19.	3	1    3831.69					
	4	1    3832.40					
	5	0					
	6	0					
	<i>Mean:</i>	<i>0.4    3832.10</i>		3832.31	250	Mg I	3    5.94
20.	3	0					
	4	1    3832.93					
	5	0					
	6	0					
	<i>Mean:</i>	<i>0.2    3832.93</i>		3833.31	100	Fe I	221    5.79
21.	3	1    3834.04					
	4	1    3834.10					
	5	1    3834.96		(3834.36	75	Mn I	6    5.39)
	6	0.5    +		(3833.86	75	Mn I	6    5.41)
	<i>Mean:</i>	<i>1.1    3834.44</i>		3834.22	400	Fe I	20    4.19
22.	3	0					
	4	1    3836.49					
	5	1    3837.04					
	6	0					
	<i>Mean:</i>	<i>0.6    3836.80</i>		3836.33	100	Fe I	664    6.53
23.	3	1    3837.86					
	4	1    3838.19					
	5	0.5    +					
	6	0.5    +					
	<i>Mean:</i>	<i>0.9    3838.05</i>		3838.29	300	Mg I	3    5.94
24.	3	0					
	4	1    3839.36					
	5	0					
	6	0					
	<i>Mean:</i>	<i>0.2    3839.36</i>		3839.26	100	Fe I	529    6.27

TABLE 2.—Observed wavelengths and identifications of meteor spectrum S 6—Continued

Line observed				Blended with line		Identification				
No.	Order	$I_{obs}$	$\lambda_{obs}$	No.	Order	$\lambda_{tab}$	$I_{tab}$	Ident.	Mult.	ev
25.	3	0								
	4	1	3839.77							
	5	1	3839.80							
	6	0								
	<i>Mean:</i>	<i>0.6</i>	<i>3839.79</i>			3839.78	100	Mn I	6	5.41
26.	3	0								
	4	1	3840.62							
	5	0								
	6	0								
	<i>Mean:</i>	<i>0.2</i>	<i>3840.62</i>			3840.44	400	Fe I	20	4.22
27.	3	0								
	4	1	3841.21							
	5	0								
	6	0								
	<i>Mean:</i>	<i>0.2</i>	<i>3841.21</i>			3841.05	500	Fe I	45	4.83
28.	3	1	3849.83							
	4	1	3850.32							
	5	1	3850.27							
	6	0				3849.97	500	Fe I	20	4.23
	<i>Mean:</i>	<i>0.8</i>	<i>3850.18</i>			3850.82	200	Fe I	22	4.21
29.	3	0								
	4	1	3852.28							
	5	0								
	6	0								
	<i>Mean:</i>	<i>0.2</i>	<i>3852.28</i>			3852.58	150	Fe I	73	5.99
30.	3	(3)		32	3					
	4	3	3856.52							
	5	2	3856.80							
	6	0								
	<i>Mean:</i>	<i>2.0</i>	<i>3856.68</i>			3856.37	500	Fe I	4	3.25
31.	3	(3)		32	3					
	4	1	3858.38							
	5	1	3858.63							
	6	0								
	<i>Mean:</i>	<i>0.8</i>	<i>3858.52</i>			3958.30	800	Ni I	32	3.63
32.	3	3	3859.79							
	4	3	3859.97							
	5	2	3859.69							
	6	1	+							
	<i>Mean:</i>	<i>2.6</i>	<i>3859.81</i>			3859.91	1000	Fe I	4	3.21

TABLE 2.—Observed wavelengths and identifications of meteor spectrum S 6—Continued

Line observed				Blended with line		Identification			
No.	Order	$I_{obs}$	$\lambda_{obs}$	No.	Order	$\lambda_{tab}$	$I_{tab}$	Mult. ev	
33.	3	2	3872.15						
	4	1	3872.58						
	5	1	3872.55						
	6	1	+						
	<i>Mean:</i>	1.5	3872.46			3872.50	300	Fe I	20 4.19
34.	3	3	3878.21						
	4	(5)		133	3				
	5	2	(3877.47)	165	3				
	6	0				3878.02	400	Fe I	20 4.16
	<i>Mean:</i>	1.8	3878.21			3878.58	300	Fe I	4 3.28
35.	3	4	3886.39						
	4	3	3886.47						
	5	1	3886.66						
	6	0.5	+			(3886.80	125	Cr I	23 4.19)
	<i>Mean:</i>	2.2	3886.53			3886.28	600	Fe I	4 3.24
36.	3	1	+						
	4	1	3892.34						
	5	1	3891.47						
	6	0.5	+						
	<i>Mean:</i>	1.1	3891.86			3891.93	100	Fe I	733 6.60
37.	3	1	(3894.17)	38	3				
	4	1	3893.40	135	3				
	5	0.5	+						
	6	0							
	<i>Mean:</i>	0.6	3893.40			3893.39	100	Fe I	430 6.13
38.	3	1	(3894.17)	37	3				
	4	1	3894.06						
	5	1	3894.12						
	6	0.5	+						
	<i>Mean:</i>	1.1	3894.09			3894.07	1000	Co I	34 4.23
39.	3	2	3895.94						
	4	2	3895.76						
	5	(3)	(3897.01)	166	3				
	6	1	+						
	<i>Mean:</i>	1.9	3895.84			3895.66	400	Fe I	4 3.29
40.	3	1	3898.07						
	4	1	3897.83						
	5	(3)		39	5				
	6	0.5	+	166	3				
	<i>Mean:</i>	0.9	3897.93			3897.90	100	Fe I	280 5.87

TABLE 2.—Observed wavelengths and identifications of meteor spectrum S 6—Continued

Line observed				Blended with line		Identification				
No.	Order	$I_{obs}$	$\lambda_{obs}$	No.	Order	$\lambda_{tab}$	$I_{tab}$	Ident.	Mult.	ev
41.	3	3	3899.82							
	4	2	3899.73							
	5	2	3899.37							
	6	1	+							
	Mean:	2.4	3899.60			3899.71	500	Fe I	4	3.26
42.	3	2	3902.91	137	3					
	4	2	3903.11							
	5	1	3903.63							
	6	0								
	Mean:	1.3	3903.28			3902.95	500	Fe I	45	4.73
43.	3	2	3905.47	139	3					
	4	1	3906.52							
	5	0.5	+							
	6	0.5	+							
	Mean:	1.1	3906.07			3906.48	300	Fe I	4	3.28
44.	3	2	3920.46							
	4	3	3920.26							
	5	0.5	+							
	6	0								
	Mean:	1.3	3920.35			3920.26	500	Fe I	4	3.28
45.	3	3	3922.97							
	4	3	3922.85							
	5	2	3922.97							
	6	1	+							
	Mean:	2.6	3922.93			3922.91	600	Fe I	4	3.21
46.	3	(6)		156	2					
	4	3	3927.90							
	5	1	3927.74							
	6	(6)		156	4					
	Mean:	2.2	3927.81			3927.92	500	Fe I	4	3.26
47.	3	(5)		50	3					
	4	3	3930.34							
	5	1	3930.49							
	6	(6)		157	4					
	Mean:	2.2	3930.42			3930.30	600	Fe I	4	3.24
48.	3	(5)		$\left\langle \begin{array}{l} 50 \\ 47 \end{array} \right.$	3					
	4	0.5	3931.66		3					
	5	0.5	+							
	6	0								
	Mean:	0.4	3941.66			3931.12	35	Fe I	565	6.42

TABLE 2.—Observed wavelengths and identifications of meteor spectrum *S 6*—Continued

Line observed				Blended with line		Identification					
No.	Order	$I_{obs}$	$\lambda_{obs}$	No.	Order	$\lambda_{tab}$	$I_{tab}$	Mult.	ev		
49.	3	(5)		$\left\langle \begin{array}{l} 50 \\ 47 \end{array} \right.$	3						
	4	0.5	3932.63								
	5	0.5	+								
	6	0									
	<i>Mean:</i>	0.4	3932.63					3932.63	80	Fe I	$\left\langle \begin{array}{l} 280 \\ 652 \end{array} \right.$
50.	3	5	3933.64								
	4	4	3933.71								
	5	3	3933.54			(3933.61	200	Fe I	$\left\langle \begin{array}{l} (488 \\ 562 \end{array} \right.$	$\left. \begin{array}{l} 6.22 \\ 6.42 \end{array} \right.$	
	6	3	3933.55			3933.67	600	Ca II	1	3.15	
	<i>Mean:</i>	4.6	3933.60								
51.	3	1	3944.25								
	4	0.5	+								
	5	0.5	+								
	6	0									
	<i>Mean:</i>	0.5	3944.25			3944.01	2000	Al I	1	3.14	
52.	3	0.5	+								
	4	1	3956.33			3957.05	80	Ca I	6	5.02	
	5	0				3957.03	50	Fe I	562	6.40	
	6	0				3956.68	150	Fe I	278	5.80	
	<i>Mean:</i>	0.5	3956.33			3956.46	100	Fe I	604	6.37	
53.	3	1	3961.20								
	4	1	3961.51								
	5	1	3962.29								
	6	0.5	+								
	<i>Mean:</i>	1.1	3961.76			3961.52	3000	Al I	1	3.14	
54.	3	5	3968.45								
	4	4	3968.51								
	5	3	3968.38			3969.26	600	Fe I	43	4.59	
	6	3	3968.08			3968.47	500	Ca II	1	3.12	
	<i>Mean:</i>	4.6	3968.32								
55.	3	1	+								
	4	0.5	+								
	5	0									
	6	1	3984.68			3985.39	125	Fe I	661	6.41	
	<i>Mean:</i>	0.8	3984.68			3983.96	200	Fe I	277	5.83	
56.	3	2	4005.38								
	4	2	4005.18	145	3						
	5	1	+								
	6	0									
	<i>Mean:</i>	1.3	4005.27					4005.25	250	Fe I	43

TABLE 2.—Observed wavelengths and identifications of meteor spectrum S 6—Continued

Line observed				Blended with line		Identification					
No.	Order	$I_{obs}$	$\lambda_{obs}$	No.	Order	$\lambda_{tab}$	$I_{tab}$	Mult.	ev.		
57.	3	3	4030.78	$\left\langle \begin{array}{l} 58 \\ 59 \end{array} \right.$	5	$\left( \begin{array}{l} 4030.50 \\ 4030.76 \end{array} \right.$	$\left( \begin{array}{l} 120 \\ 500 \end{array} \right.$	$\left( \begin{array}{l} \text{Fe I} \\ \text{Mn I} \end{array} \right.$	$\left( \begin{array}{l} 560 \\ 2 \end{array} \right.$	$\left( \begin{array}{l} 6.26 \\ 3.08 \end{array} \right.$	
	4	3	4030.73								
	5	2	+								
	6	0.5	+								
	Mean:		2.1								4030.75
58.	3	2	4032.97	$\left\langle \begin{array}{l} 57 \\ 59 \end{array} \right.$	5	4033.07	400	Mn I	2	3.08	
	4	2	4033.13								
	5	2	+								
	6	0.5	+								
	Mean:		1.5								4033.06
59.	3	2	4034.46	$\left\langle \begin{array}{l} 57 \\ 58 \end{array} \right.$	5	4034.49	250	Mn I	2	3.08	
	4	2	4034.41								
	5	2	+								
	6	0.5	+								
	Mean:		1.5								4034.43
60.	3	(4)	4042.55	61	3	4041.36	100	?	Mn I	5	5.18
	4	1									
	5	0									
	6	0									
	Mean:										
61.	3	4	4045.97			4045.82	400	Fe I	43	4.55	
	4	3	4045.85								
	5	2	+								
	6	1	+								
	Mean:		2.8								4045.90
62.	3	3	4063.69			4063.53	100	Mn I	5	5.21	
	4	2	4063.68								
	5	1	4064.05								
	6	0									
	Mean:		1.5								4063.84
63.	3	1	+			4066.60	40	Fe I	424	6.03	
	4	1	4066.21								
	5	1	4065.33								
	6	0									
	Mean:		0.8								4065.72
64.	3	3	4071.71			4071.74	300	Fe I	43	4.65	
	4	3	4071.86								
	5	0.5	+								
	6	0.5	+								
	Mean:		1.8								4071.80

TABLE 2.—Observed wavelengths and identifications of meteor spectrum S 6—Continued

Line observed				Blended with line		Identification			
No.	Order	$I_{obs}$	$\lambda_{obs}$	No.	Order	$\lambda_{tab}$	$I_{tab}$	Mult.	ev
65.	3	1	4105.13						
	4	1	4104.90						
	5	0.5	+						
	6	0							
	<i>Mean:</i>	<i>0.6</i>	<i>4105.00</i>			4104.13	100	Fe I	$\left\{ \begin{array}{l} 558 \text{ 6.26} \\ 356 \text{ 5.83} \end{array} \right.$
66.	3	1	4127.82						
	4	0.5	+						
	5	0.5	+						
	6	1	4126.33	161	4	4126.19	80	Fe I	695 6.34
	<i>Mean:</i>	<i>1.0</i>	<i>4126.83</i>			4127.61	100	Fe I	357 5.86
67.	3	2	4132.02						
	4	1	4132.11						
	5	(5)		132	4				
	6	0.5	+						
	<i>Mean:</i>	<i>1.2</i>	<i>4132.07</i>			4132.06	300	Fe I	43 4.61
68.	3	(3)		69	3				
	4	1	4143.31						
	5	(2)		69	5				
	6	(1)		69	6				
	<i>Mean:</i>	<i>1.0</i>	<i>4143.31</i>			4143.42	200	Fe I	523 6.03
69.	3	3	4143.80						
	4	3	4143.67						
	5	2	4143.96						
	6	1	4144.07						
	<i>Mean:</i>	<i>2.6</i>	<i>4143.91</i>			4143.87	400	Fe I	43 4.55
70.	3	1	4154.46						
	4	0.5	+						
	5	0				4153.91	120	Fe I	695 6.38
	6	0				4154.81	100	Fe I	694 5.81
	<i>Mean:</i>	<i>0.3</i>	<i>4154.46</i>			4154.50	100	Fe I	355 6.35
71.	3	1	4199.12						
	4	1	4198.99						
	5	0				(4199.97	-	Fe I	3 3.03)
	6	0				4198.31	250	Fe I	152 5.35
	<i>Mean:</i>	<i>0.4</i>	<i>4199.05</i>			4199.10	300	Fe I	522 5.99
72.	3	3	4202.02						
	4	2	4201.82						
	5	1	+						
	6	1	+						
	<i>Mean:</i>	<i>2.0</i>	<i>4201.91</i>			4202.03	400	Fe I	42 4.44

TABLE 2.—Observed wavelengths and identifications of meteor spectrum S 6—Continued

Line observed				Blended with line		Identification			
No.	Order	$I_{obs}$	$\lambda_{obs}$	No.	Order	$\lambda_{tab}$	$I_{tab}$	Mult.	ev
73.	3	1	+						
	4	1	4206.87						
	5	1	+						
	6	0				(4207.13	80	Fe I	352 5.77)
	<i>Mean:</i>	<i>0.8</i>	<i>4206.87</i>			4206.70	125	Fe I	3 3.00
74.	3	1	4210.66						
	4	1	4210.21						
	5	(5)		143	4				
	6	1	4210.42						
	<i>Mean:</i>	<i>1.3</i>	<i>4210.41</i>			4210.35	300	Fe I	152 5.42
75.	3	1	4213.42						
	4	0.5	4213.82						
	5	(5)		143	4				
	6	0.5	4213.73						
	<i>Mean:</i>	<i>0.8</i>	<i>4213.69</i>			4213.65	100	Fe I	355 5.78
76.	3	3	4216.02						
	4	2	4216.24						
	5	(5)		143	4				
	6	1	+						
	<i>Mean:</i>	<i>2.1</i>	<i>4216.15</i>			4216.19	200	Fe I	3 2.94
77.	3	5	4226.74						
	4	4	4226.78						
	5	3	4227.00						
	6	3	4226.98			4227.43	300	Fe I	693 6.25
	<i>Mean:</i>	<i>4.6</i>	<i>4226.90</i>			4226.73	500	Ca I	2 2.93
78.	3	1	+						
	4	1	4242.69						
	5	0.5	+						
	6	1	4242.91						
	<i>Mean:</i>	<i>1.1</i>	<i>4242.82</i>						
79.	3	1	+						
	4	1	4245.09						
	5	0.5	+						
	6	0.5	+			4246.09	80	Fe I	906 6.56
	<i>Mean:</i>	<i>0.9</i>	<i>4245.09</i>			4245.26	80	Fe I	352 5.77
80.	3	1	+						
	4	1	4247.19						
	5	0.5	+						
	6	1	4247.51			4248.23	150	Fe I	482 5.98
	<i>Mean:</i>	<i>1.1</i>	<i>4247.38</i>			4247.43	200	Fe I	693 6.29

TABLE 2.—Observed wavelengths and identifications of meteor spectrum S 6—Continued

Line observed				Blended with line		Identification			
No.	Order	$I_{\text{obs}}$	$\lambda_{\text{obs}}$	No.	Order	$\lambda_{\text{tab}}$	$I_{\text{tab}}$	Mult.	ev
81.	3	(2)	+	82	3				
	4	(2)	+	82	4				
	5	0.5	+						
	6	1	4249.73						
	<i>Mean:</i>	1.4	4249.73			4250.13	250	Fe I	152 5.38
82.	3	(2)	+	81	3				
	4	(2)	+	81	4				
	5	1	4251.13						
	6	1	4250.92						
	<i>Mean:</i>	1.8	4251.02			4250.79	400	Fe I	42 4.47
83.	3	3	4254.48						
	4	2	4254.43						
	5	1	4254.33						
	6	1	4254.42						
	<i>Mean:</i>	2.0	4254.41			4254.35	5000	Cr I	1 2.91
84.	3	1	+						
	4	1	4268.96						
	5	1	4269.07						
	6	1	4268.76			4268.74	30	Fe I	649 6.20
	<i>Mean:</i>	1.3	4268.92			4267.83	125	Fe I	482 6.01
85.	3	4	4271.30						
	4	3	4271.80						
	5	3	4272.20						
	6	2	4271.67			4271.16	400	Fe I	152 5.35
	<i>Mean:</i>	3.7	4271.78			4271.76	1000	Fe I	42 4.39
86.	3	3	4274.33						
	4	2	4274.68						
	5	2	4275.03						
	6	1	4274.70						
	<i>Mean:</i>	2.4	4274.73			4274.80	4000	Cr I	1 2.90
87.	3	1	4282.23						
	4	1	4282.47						
	5	0							
	6	0				(4283.01	40	Ca I	5 4.78)
	<i>Mean:</i>	0.4	4282.37			4282.41	600	Fe I	71 5.07
88.	3	1	+						
	4	1	4285.92						
	5	0							
	6	0							
	<i>Mean:</i>	0.4	4285.92			4285.45	125	Fe I	597 6.12

TABLE 2.—Observed wavelengths and identifications of meteor spectrum S 6—Continued

Line observed				Blended with line		Identification			
No.	Order	$I_{obs}$	$\lambda_{obs}$	No.	Order	$\lambda_{tab}$	$I_{tab}$	Mult.	ev
89.	3	3	4289.64						
	4	2	4289.71						
	5	1	4289.81						
	6	0.5	+						
	<i>Mean:</i>	<i>1.7</i>	<i>4289.73</i>			(4289.36	35	Ca I	5 4.77)
						4289.72	3000	Cr I	1 2.89
90.	3	3	4293.94						
	4	2	4294.20						
	5	1	4294.09						
	6	1	+						
	<i>Mean:</i>	<i>2.0</i>	<i>4294.09</i>			4294.13	700	Fe I	41 4.37
91.	3	1	4299.89						
	4	1	4299.93						
	5	0.5	+						
	6	0							
	<i>Mean:</i>	<i>0.6</i>	<i>4299.91</i>			4299.24	500	Fe I	152 5.29
92.	3	1	+						
	4	1	4302.48						
	5	1	4301.64						
	6	0							
	<i>Mean:</i>	<i>0.8</i>	<i>4302.01</i>			4302.53	50	Ca I	5 4.78
						4302.19	50	Fe I	520 5.92
93.	3	1	+						
	4	1	4305.16						
	5	0							
	6	0							
	<i>Mean:</i>	<i>0.4</i>	<i>4305.16</i>			4305.46	100	Fe I	476 5.89
94.	3	3	4308.25						
	4	3	4307.90						
	5	2	4307.96						
	6	2	4308.03						
	<i>Mean:</i>	<i>3.1</i>	<i>4308.02</i>			(4307.74	45	Ca I	5 4.76)
						4307.91	1000	Fe I	42 4.44
95.	3	0							
	4	0							
	5	1	4312.70						
	6	0							
	<i>Mean:</i>	<i>0.4</i>	<i>4312.70</i>			4312.55	100	Mn I	23 5.81
96.	3	1.5	+	< 97	3				
	4	1	4314.95	98	3				
	5	(4)	+	148	4				
	6	0							
	<i>Mean:</i>	<i>0.5</i>	<i>4314.95</i>			4315.09	500	Fe I	71 5.07

TABLE 2.—*Observed wavelengths and identifications of meteor spectrum S 6—Continued*

Line observed				Blended with line		Identification			
No.	Order	$I_{obs}$	$\lambda_{obs}$	No.	Order	$\lambda_{tab}$	$I_{tab}$	Chemical	Mult. ev
97.	3	1.5	+	96	3	4318.65	60	Ca I	5 4.77
	4	1	4317.98		98				
	5	(4)	+	148	4				
	6	0							
	<i>Mean:</i>	<i>0.5</i>	<i>4317.98</i>						
98.	3	1.5	+	96	3	4320.59	125	Cr I	96 5.76
	4	1	4319.31		97				
	5	(4)	+	148	4	4319.64	100	Cr I	96 5.75
	6	0							
	<i>Mean:</i>	<i>0.5</i>	<i>4319.31</i>						
99.	3	4	4326.07			4325.76	1000	Fe I	42 4.47
	4	3	4325.66						
	5	2	4325.58						
	6	1	4325.96						
	<i>Mean:</i>	<i>2.8</i>	<i>4325.81</i>						
100.	3	0				4374.95	150	Mn I	5.69
	4	0.5	+						
	5	0.5	+						
	6	1	4374.78						
	<i>Mean:</i>	<i>0.8</i>	<i>4374.78</i>						
101.	3	5	4376.56			4375.93	500	Fe I	2 2.83
	4	4	4376.08						
	5	3	4375.96						
	6	3	4376.00						
	<i>Mean:</i>	<i>4.6</i>	<i>4376.10</i>						
102.	3	5	4383.74			4383.55	1000	Fe I	41 4.31
	4	4	4383.51						
	5	3	4383.53						
	6	3	4383.60						
	<i>Mean:</i>	<i>4.6</i>	<i>4383.58</i>						
103.	3	0.5	+	143	5	4393.45	20	Na I	17 4.92
	4	1	4392.79						
	5	1	4393.72						
	6	(4)	+						
	<i>Mean:</i>	<i>1.0</i>	<i>4393.31</i>						
104.	3	1	+			4401.55	1000	Ni I	86 6.00
	4	1	4401.48						
	5	1	+						
	<i>Mean:</i>	<i>1.1</i>	<i>4401.48</i>						

TABLE 2.—Observed wavelengths and identifications of meteor spectrum S 6—Continued

Line observed				Blended with line		Identification			
No.	Order	$I_{obs}$	$\lambda_{obs}$	No.	Order	$\lambda_{tab}$	$I_{tab}$	Mult. ev	
105.	3	3	4404.14						
	4	3	4404.64						
	5	3	4404.72						
	<i>Mean:</i>	<i>3.3</i>	<i>4404.55</i>			4404.75	1000	Fe I	41 4.37
106.	3	2	4406.58						
	4	1	4407.43						
	5	0.5	+						
	<i>Mean:</i>	<i>1.1</i>	<i>4407.07</i>			4407.72	100	Fe I	68 4.99
107.	3	1	4409.10						
	4	0.5	4409.47						
	5	0							
	<i>Mean:</i>	<i>0.4</i>	<i>4409.31</i>			4408.42	125	Fe I	68 5.01
108.	3	2	4414.88						
	4	(6)	+	156	3				
	5	2	4415.29			4414.88	150	Mn I	22 5.69
	<i>Mean:</i>	<i>2.3</i>	<i>4415.14</i>			4415.12	600	Fe I	41 4.42
109.	3	1	4421.81						
	4	(6)	+	157	3				
	5	1	4421.90						
	<i>Mean:</i>	<i>1.2</i>	<i>4421.87</i>			4422.57	300	Fe I	350 5.64
110.	3	3	4427.50						
	4	3	4427.31						
	5	4	4427.37						
	<i>Mean:</i>	<i>3.8</i>	<i>4427.38</i>			4427.31	500	Fe I	2 2.85
111.	3	0.5	+						
	4	0.5	+						
	5	1	4456.11						
	<i>Mean:</i>	<i>0.8</i>	<i>4456.11</i>			4455.89	100	Ca I	4 4.68
112.	3	1	+						
	4	1	4458.31						
	5	0							
	<i>Mean:</i>	<i>0.6</i>	<i>4458.31</i>			4459.12	400	Fe I	68 4.95
113.	3	2	4461.39						
	4	3	4461.72						
	5	3	4461.58						
	<i>Mean:</i>	<i>3.0</i>	<i>4461.58</i>			4461.65	300	Fe I	2 2.86
114.	3	0.5	+						
	4	1	4466.44						
	5	1	4466.23						
	<i>Mean:</i>	<i>1.0</i>	<i>4466.32</i>			4466.55	500	Fe I	350 5.60

TABLE 2.—Observed wavelengths and identifications of meteor spectrum S 6—Continued

Line observed				Blended with line	Identification					
No.	Order	$I_{ob.}$	$\lambda_{ob.}$	No.	Order	$\lambda_{tab}$	$I_{tab}$	Mult.	ev	
115.	3	0.5	+							
	4	1	4471.81							
	5	0								
	<i>Mean:</i>	<i>0.5</i>	<i>4471.81</i>			4472.79	100	Mn I	22 5.72	
116.	3	0.5	+							
	4	1	4475.49							
	5	0								
	<i>Mean:</i>	<i>0.5</i>	<i>4475.49</i>			4476.02	500	Fe I	350 5.61	
117.	3	1	4481.65							
	4	2	4481.71							
	5	2	4482.21			4481.33	100	Mg II	4 11.63	
	<i>Mean:</i>	<i>1.9</i>	<i>4481.90</i>			4482.17	150	Fe I	2 2.82	
118.	3	0								
	4	1	4578.59							
	5	0								
	<i>Mean:</i>	<i>0.3</i>	<i>4578.59</i>			4578.56	80	Ca I	23 5.23	
119.	3	1	+							
	4	2	4601.81	$\left\langle \begin{array}{l} 158 \\ 2 \end{array} \right.$	$\begin{array}{l} 3 \\ 5 \end{array}$					
	5	1	+							
	<i>Mean:</i>	<i>1.4</i>	<i>(4601.81)</i>					4602.94	300	Fe I
120.	3	1	4829.32							
	4	1	4828.87							
	5	0.5	4828.97			4829.38	200	Cr I	31 5.11	
	<i>Mean:</i>	<i>0.8</i>	<i>4829.02</i>			4829.03	300	Ni I	131 6.10	
121.	3	1	+							
	4	1	4891.23							
	5	0				4891.50	70	Fe I	318 5.38	
	<i>Mean:</i>	<i>0.6</i>	<i>4891.23</i>			4890.76	100	Fe I	318 5.41	
122.	3	0								
	4	1	4902.60							
	5	0								
	<i>Mean:</i>	<i>0.3</i>	<i>4902.60</i>			4903.32	500	Fe I	318 5.41	
123.	3	0.5	+							
	4	1	4957.32							
	5	0.5	+			4957.60	300	Fe I	318 5.31	
	<i>Mean:</i>	<i>0.7</i>	<i>4957.32</i>			4957.30	100	Fe I	318 5.35	
124.	3	0.5	+							
	4	0.5	+							
	5	1	4965.99							
	<i>Mean:</i>	<i>0.8</i>	<i>4965.99</i>			4966.10	300	Fe I	687 5.82	

TABLE 2.—Observed wavelengths and identifications of meteor spectrum S 6—Continued

Line observed				Blended with line		Identification			
No.	Order	$I_{obs}$	$\lambda_{obs}$	No.	Order	$\lambda_{lab}$	$I_{lab}$	Mult.	ev
125.	3	1	4984.41						
	4	0.5	+						
	5	1	4984.24			4984.13	500	Ni I	143 6.29
	Mean:		0.9 4984.30			4983.86	200	Fe I	1066 6.59
126.	3	1	5005.96						
	4	1	5005.96						
	5	1	+			5006.13	300	Fe I	318 5.31
	Mean:		1.1 5005.96			5005.72	200	Fe I	984 6.36
127.	3	0.5	+						
	4	2	5012.14						
	5	1	5011.91						
	Mean:		1.3 5012.01			5012.07	300	Fe I	16 3.33
128.	3	2	+	15	4				
	4	1	+						
	5	1	5098.87						
	Mean:		1.4 5098.87			5098.70	200	Fe I	66 4.61
129.	3	1	+	16	4				
	4	1	5101.89						
	5	1	5102.37						
	Mean:		1.1 5102.16			5102.24	80	Fe I	65 4.63
130.	3	1	5109.93						
	4	2	5110.30						
	5	1	5110.39						
	Mean:		1.4 5110.24			5110.41	300	Fe I	1 2.42
131.	3	(3)	+	30	4				
	4	1	5142.21			5142.54	100	Fe I	1092 6.64
	5	0				5141.75	100	Fe I	1090 6.68
	Mean:		0.5 5142.21			5142.93	125	Fe I	114 4.83
									16 3.36
132.	3	5	+	133	3				
	4	5	5167.33			5167.49	700	Fe I	37 3.89
	5	3	5167.38			(5166.29	125	Fe I	1 2.40)
	Mean:		4.5 5167.36			5167.32	100	Mg I	2 5.11
133.	3	5	+	132	3				
	4	5	5172.64						
	5	3	5172.66			(5171.60	300	Fe I	36 3.88)
	Mean:		4.5 5172.65			5172.68	200	Mg I	2 5.11
134.	3	5	+						
	4	5	5183.72						
	5	3	5183.60						
	Mean:		4.5 5183.65			5183.60	500	Mg I	2 5.11

TABLE 2.—Observed wavelengths and identifications of meteor spectrum S 6—Continued

Line observed				Blended with line		Identification				
No.	Order	$I_{\text{obs}}$	$\lambda_{\text{obs}}$	No.	Order	$\lambda_{\text{tab}}$	$I_{\text{tab}}$	Mult.	ev	
135.	3	1	5191.25	37	4					
	4	1	5191.42							
	5	1	+	99	6					
	<i>Mean:</i>	1.1	5191.35			5191.46	400	Fe I	383	5.42
136.	3	1.5	5195.20							
	4	1	5195.25							
	5	2	5195.15			(5195.47	100	Fe I	1092	6.61)
	<i>Mean:</i>	1.7	5195.20			5194.94	200	Fe I	36	3.95
137.	3	2	5204.21	42	4					
	4	2	5205.20							
	5	1	5204.53			5204.58	125	Fe I	1	2.47
	<i>Mean:</i>	1.7	5204.64			5204.52	400	Cr I	7	3.32
138.	3	1	5205.76							
	4	2	5206.34							
	5	1	5205.63							
	<i>Mean:</i>	1.4	5205.90			5206.04	500	Cr I	7	3.32
139.	3	1	5208.71	43	4					
	4	2	5208.44							
	5	1	5208.28			5208.60	200	Fe I	553	5.62
	<i>Mean:</i>	1.4	5208.44			5208.44	500	Cr I	7	3.32
140.	3	1	+							
	4	1	5216.28							
	5	0								
	<i>Mean:</i>	0.6	5216.28			5216.28	300	Fe I	36	3.99
141.	3	3	5227.03							
	4	3	5227.25							
	5	2	5227.13			5226.87	200	Fe I	383	5.41
	<i>Mean:</i>	2.8	5227.14			5227.19	400	Fe I	37	3.93
142.	3	2	5229.48							
	4	1	5228.92							
	5	1	5228.87			5229.86	200	Fe I	1090	6.56
	<i>Mean:</i>	1.4	5229.04						553	5.63
143.	3	5	5269.42							
	4	5	5269.54			(5270.27	20	Ca I	22	4.88)
	5	4	5269.49			5270.36	400	Fe I	37	3.96
	<i>Mean:</i>	5.0	5269.49			5269.54	800	Fe I	15	3.21
144.	3	5	5328.75							
	4	5	5328.08			5328.53	150	Fe I	37	3.87
	<i>Mean:</i>	4.5	5328.37			5328.04	400	Fe I	15	3.23
145.	3	2	5339.98	56	4					
	4	2	5340.04							
	<i>Mean:</i>	1.8	5340.01			5339.94	200	Fe I	553	5.58

TABLE 2.—Observed wavelengths and identifications of meteor spectrum S 6—Continued

Line observed				Blended with line		Identification				
No.	Order	$I_{obs}$	$\lambda_{obs}$	No.	Order	$\lambda_{tab}$	$I_{tab}$	Mult.	ev	
146.	3	1	5341.08	85	5	5341.06	200	Mn I	4	4.44
	4	(3)	+							
	Mean: 0.8		5341.08							
						5341.03	200	Fe I	37	3.91
147.	3	3	5371.26			5371.49	700	Fe I	15	3.26
	4	4	5371.40							
	Mean: 3.2		5371.34							
148.	3	3	5397.07			5397.13	400	Fe I	15	3.21
	4	4	5397.10							
	Mean: 3.2		5397.09							
149.	3	3	5405.59			5405.78	400	Fe I	15	3.28
	4	4	5405.87							
	Mean: 3.2		5405.75							
150.	3	4	5430.11			5429.70	500	Fe I	15	3.24
	4	4	5430.02							
	Mean: 3.6		5430.06							
151.	3	2	5434.42			5434.53	300	Fe I	15	3.29
	4	3	5434.41							
	Mean: 2.3		5434.41							
152.	3	4	5447.19			5446.92	300	Fe I	15	3.25
	4	4	5446.97							
	Mean: 3.6		5447.06							
153.	3	3	5455.83			5455.61	300	Fe I	15	3.28
	4	3	5455.77							
	Mean: 2.7		5455.80							
154.	3	0.5	+			5497.52	150	Fe I	15	3.26
	4	1	5497.71							
	Mean: 0.7		5497.71							
155.	3	0.5	+			5615.65	400	Fe I	686	5.54
	4	1	5615.63							
	Mean: 0.7		5615.63							
156.	2	6	5890.15			5889.95	9000	Na I	1	2.11
	3	6	5889.95							
	4	6	5889.95							
	Mean: 5.0		5889.99							
157.	2	6	5895.66			5895.92	5000	Na I	1	2.10
	3	6	5895.92							
	4	6	5895.97							
	Mean: 5.0		5895.88							

TABLE 2.—Observed wavelengths and identifications of meteor spectrum S 6—Continued

Line observed				Blended with line		Identification					
No.	Order	$I_{obs}$	$\lambda_{obs}$	No.	Order	$\lambda_{tab}$	$I_{tab}$	Mult.	cv		
158.	2	1	6137.79	119	4	6137.70	100	Fe I	207	4.61	
	3	(2)	6136.80		5						
	4	1	6135.77		2						
	Mean: 0.8		6136.56								
159.	2	1	+								
	3	0									
	4	1	6154.11			6154.23	500	Na I	5	4.12	
	Mean: 0.6		6154.11								
160.	2	1	6162.56	3	5	6162.17	40	Ca I	3	3.91	
	3	(2)	6162.34								
	4	1	+								
	Mean: 0.8		6162.43								
161.	2	1	6191.10	66	6	6191.19	500	Ni I	45	3.67	
	3	0.5	+								
	4	1	6190.17								
	Mean: 0.7		6190.48								
162.	2	(3)	+	86	3	6411.66	100	Fe I	816	5.58	
	3	1	6411.96								
	4	1	6411.36								
	Mean: 0.9		6411.62								
163.	2	(3)	+	89	3	6430.85	100	Fe I	62	4.11	
	3	1	6430.24								
	4	0									
	Mean: 0.4		6430.24								
164.	2			89	3	6439.07	150	?	Ca I	18	4.45
	3	1	6437.87								
	4	1	6437.60								
	Mean: 0.9		6437.72								
165.	2	3	6462.22	34	5	6462.57	125	Ca I	18	4.44	
	3	2	6462.39								
	4	1	+								
	Mean: 1.6		6462.32								
166.	2	2	6495.37	39	5	6494.98	400	Fe I	168	4.31	
	3	(3)	6494.98								
	4	1	6495.15								
	Mean: 1.2		6495.14								

The spectrum of this meteor was photographed in the zero order, in the first order with dispersion of 72 Å/mm, and in the blue part of the second order with 36 Å/mm. [The dispersions given by Rajchl (1961) are those of the spectograph and not of the meteor spectra.] The spectral lines of the Na doublet are the most intense lines and are separated one from another in the first order. The beginning of these lines is almost the same as the beginning of the meteor trail photographed by normal cameras. The whole spectrum is photographed in the height interval from 85 km to 56 km. The spectral lines were measured at the maximum brightness at the height of 65 km, and the wavelengths were computed by the method briefly described in this paper. The wavelengths of all 99 measured lines are given in table 3.

The majority of the lines are iron lines belonging to different multiplets. The strongest lines are: Na doublet 1; Mg triplet 2; Fe lines 3720 of multiplet 5; 3856 of multiplet 4; 3860 of multiplet 4; 4045 of multiplet 43; 4383 of multiplet 41; 5269 of multiplets 15 and 37. Other elements observed are Ca I and Ca II, Mg I, Ni I, Cr I, Mn I. The presence of Co I and Si I is questionable. The elements usual in meteorites and air but not observed in this spectrum are: Al, Cu, P, S, C, K, N, O.

The iron line 3930.3 is well separated from the Ca II line 3933.7. This Ca line, in comparison with spectrum S 6, is relatively weak, a fact that may be connected, as previously indicated, with the iron composition of the body. A feature of this Ca II line is quite different from the other lines. It is observable in the maxima of brightness only. In comparison with the others the changes of brightness of this line are very strong. The Ca II doublet is present in this spectrum, although the meteor can be classified as slow.

Artificial spectra of meteoritic material using shock tubes (Nicholls, et al., 1959) also show the Ca II doublet at velocities less than 10 km/sec. Thus it is possible to conclude from all these experimental results that the Ca II doublet is emitted not only by high-velocity meteors but also by slow meteors.

TABLE 3.—*Spectrum of meteor No. 27471*

[The lines with numbers from 1 to 22 are present in the second order only. The lines with numbers from 23 to 33 are present in the first and second order. If one measured wavelength only is presented, it refers to the first order. All other lines from Nos. 34 to 99 are present in the first order only. The dispersion of the meteor spectrum in the first order is approximately 72 Å/mm and in the second order 36 Å/mm. The intensity scale is the same as is used in table 2.]

Line observed No.	Line observed		Identification $\lambda_{tab}$	Mult
	$I_{obs}$	$\lambda_{obs}$		
1	1	3679.6	3679.9 Fe I	5
2	1	3681.1	3682.2 Fe I	772
3	1	3683.5	3683.0 Fe I	5
4	1	3686.8	3687.5 Fe I	21
5	1	3689.6	3689.5 Fe I	369
			3689.5 Fe I	386
6	1	3705.4	3705.6 Fe I	5
7	1	3707.3	3707.8 Fe I	5
8	4	3721.3	3719.9 Fe I	5
9	1	3724.1	3722.6 Fe I	5
10	1	3734.7	3733.3 Fe I	5
11	2	3736.1	3734.9 Fe I	21
12	3	3738.4	3737.1 Fe I	5
13	1	3743.0	3743.4 Fe I	21
14	3	3746.8	3745.6 Fe I	5
			3745.9 Fe I	5
15	2	3749.8	3748.3 Fe I	5
			3749.4 Fe I	21
16	1	3816.6	3815.8 Fe I	45
17	1	3818.8	3816.2 Cr I	40
			3817.8 Cr I	40
			3818.5 Cr I	40
18	2	3821.3	3820.4 Fe I	20
19	2	3825.4	3825.9 Fe I	20
			3824.4 Fe I	4
20	1	3830.1	3829.4 Mg I	3
21	2	3833.1	3832.3 Mg I	3
22	1	3835.0	3834.2 Fe I	20
23	3	3838.9	3838.3 Mg I	3
	3	3839.2		
24	4	3856.5	3856.4 Fe I	4
	2	3857.0		
25	4	3860.8	3859.9 Fe I	4
	4	3860.6	3858.3 Ni I	32
26	1	3866.4	3865.5 Fe I	20
	1	3865.5		
27	1	3868.2	?	
28	2	3878.0	3878.0 Fe I	20
	2	3879.0	3878.6 Fe I	4
29	3	3885.6	3886.3 Fe I	4
	3	3887.2	3886.8 Cr I	23
30	1	3891.5	3891.9 Fe I	733
31	1	3894.4	3895.7 Fe I	4
			3894.1 Co I	34
32	2	3899.2	3899.7 Fe I	4
	1	3900.2		
33	2	3905.2	3906.5 Fe I	4
	1	3905.9	3905.5 Si I	3
34	1	3913.1	3913.6 Fe I	120

TABLE 3.—Spectrum of meteor No. 27471—Continued

Line observed			Identification		Mult
No.	$I_{obs}$	$\lambda_{obs}$	$\lambda_{tab}$		
35	3	3921.3	3922.9	Fe I	4
			3920.3	Fe I	4
36	3	3928.4	3927.9	Fe I	4
			3930.3	Fe I	4
37	3	3932.8	3933.7	Ca II	1
			3933.6	Fe I	488
			3933.6	Fe I	562
38	1	3948.9	3948.8	Fe I	604
39	3	3967.7	3968.5	Ca II	1
			3969.3	Fe I	43
40	1	4004.5	4005.2	Fe I	43
41	2	4032.0	4030.8	Mn I	2
			4033.1	Mn I	2
			4034.5	Mn I	2
			4045.8	Fe I	43
42	4	4045.2		?	
43	1	4052.2			
44	1	4056.6	4055.0	Fe I	218
			4056.5	Fe I	320
45	1	4058.4	4058.0	Mn I	29
			4059.4	Mn I	29
46	3	4063.1	4063.6	Fe I	43
47	3	4070.8	4071.7	Fe I	43
48	1	4078.4	4076.6	Fe I	558
			4078.4	Fe I	217
			4080.2	Fe I	558
49	1	4131.6	4132.1	Fe I	43
50	2	4143.2	4143.9	Fe I	43
			4143.4	Fe I	523
51	1	4200.4	4198.3	Fe I	152
			4199.1	Fe I	522
			4202.0	Fe I	42
52	1	4216.6	4216.2	Fe I	3
53	1	4227.0	4226.7	Ca I	2
			4227.4	Fe I	693
54	1	4250.7	4250.1	Fe I	152
			4250.8	Fe I	42
55	2	4254.5	4254.4	Cr I	1
56	1	4260.8	4260.5	Fe I	152
			4261.4	Cr I	96
57	3	4271.6	4271.2	Fe I	152
			4271.8	Fe I	42
58	1	4290.0	4289.7	Cr I	1
59	1	4294.2	4294.1	Fe I	41
60	3	4308.3	4307.9	Fe I	42
			4307.7	Ca I	5
61	1	4320.4	4319.6	Cr I	96
			4320.6	Cr I	96
62	1	4323.0	4322.7	Fe I	215
63	3	4325.8	4325.8	Fe I	42
64	1	4332.9	4331.6	Ni I	52
65	1	4368.2	4367.9	Fe I	41
66	1	4371.3	4369.8	Fe I	518
			4371.3	Cr I	22
67	3	4376.5	4375.9	Fe I	2
68	4	4383.3	4383.6	Fe I	41
69	1	4395.4		?	
70	2	4404.5	4404.8	Fe I	41
71	2	4414.6	4415.1	Fe I	41
72	2	4427.8	4427.3	Fe I	2

TABLE 3.—Spectrum of meteor No. 27471—Continued

Line observed			Identification		Mult
No.	$I_{obs}$	$\lambda_{obs}$	$\lambda_{tab}$		
73	2	4462.2	4461.6	Fe I	2
74	1	4482.5	4482.2	Fe I	2
			4481.3	Mg II	4
			4481.1	Mg II	4
				?	
75	1	4835.6			
76	1	4878.4	4878.2	Fe I	318
			4878.1	Ca I	35
77	1	4932.6		?	
78	1	4942.0		?	
79	1	4989.6	4989.0	Fe I	1066
			4988.0	Co I	
80	1	5011.9	5012.1	Fe I	16
81	1	5132.5	5133.7	Fe I	1092
82	4	5168.2	5168.8	Fe I	1
			5167.5	Fe I	37
			5167.3	Mg I	2
83	4	5172.4	5172.7	Mg I	2
			5171.6	Fe I	36
84	4	5183.8	5183.6	Mg I	2
85	1	5206.7	5208.4	Cr I	7
			5206.0	Cr I	7
			5204.5	Cr I	7
			5204.6	Fe I	1
86	1	5227.1	5227.2	Fe I	37
87	4	5270.0	5270.4	Fe I	37
			5270.3	Ca I	22
			5269.5	Fe I	15
88	1	5319.6		?	
89	1	5321.4	5322.0	Fe I	112
90	2	5327.9	5328.0	Fe I	15
			5328.5	Fe I	37
91	1	5396.3	5397.1	Fe I	15
92	1	5405.9	5405.8	Fe I	15
93	1	5542.3		?	
94	1	5572.0	5572.8	Fe I	686
			5569.6	Fe I	686
95	1	5622.2	5623.6	Fe I	625
96	1	5681.1	5682.6	Na I	6
97	1	5882.8		?	
98	5	5889.9	5889.9	Na I	1
99	4	5896.2	5895.9	Na I	1

A wave feature in some spectral lines was observed in both spectra. It reaches up to about 1 Å in the spectrum of meteor 27471, and up to about 0.3 Å in the spectrum S 6. We have previously observed the wave-feature of some spectral lines in the low dispersion spectrograms of meteors where it reached up to several Angstrom. A provisional explanation of this phenomenon may lie in the blending of very narrow lines, when one line and another change places as a result of local variations in micro-sensitivity of the photographic emulsion.

The spectrum of meteor No. 27471 is suitable for study of spectral changes during the trajec-

tory. We know accurately the changes of velocity during the trajectory of this meteor. As a result, we have a dynamic determination of the heat-transfer coefficient and of the mass ablation. Thus it will be possible to determine the monochromatic luminosity coefficients.

This is a preliminary report on the subject. Detailed data will be published in Bulletin of the Astronomical Institute of Czechoslovakia.

### References

CEPLECHA, ZD.

1951. The centre of a plate. *Bull. Astron. Inst. Czechoslovakia*, vol. 2, pp. 105-106.
1954. Meteor photographs. III. A reduction method of meteor negatives. *Bull. Astron. Inst. Czechoslovakia*, vol. 5, pp. 9-13.
1958. On the composition of meteors. *Bull. Astron. Inst. Czechoslovakia*, vol. 9, pp. 154-159.
1961. Determination of wavelengths in meteor spectra by using a diffraction grating. *Bull. Astron. Inst. Czechoslovakia*, vol. 12, pp. 246-250.

JACCHIA, L. G., AND WHIPPLE, F. L.

1961. Precision orbits of 413 photographic meteors. *Smithsonian Contr. Astrophys.*, vol. 4, no. 4, pp. 97-129.

MOORE, C. E.

1945. A multiplet table of astrophysical interest. *Contr. Princeton Univ. Obs.*, no. 20, parts 1, 2.

NICHOLLS, R. W.; WATSON, M. D.; and PARKINSON, W. H.

1959. The laboratory excitation of meteoritic spectra in shock tubes. *Journ. Roy. Astron. Soc. Canada*, vol. 53, pp. 223-231.

RAJCHL, J.

1961. Two meteor spectra with high dispersion. *Bull. Astron. Inst. Czechoslovakia*, vol. 12, p. 167.

ROWLAND, H. A.

1893. Gratings in theory and practice. *Astron. and Astrophys.*, vol. 12, pp. 129-149.

ZAJDEL, Z. N.; PROKOFEV, V. K.; and RAJSKIJ, S. M.

1952. Tables of spectrum lines. Moscow. (English translation published by VEB Verlag Technik, Berlin, 1961.)

### Abstract

Analysis of photographs of two meteor spectra with dispersions from 72 Å/mm to 11 Å/mm is presented in this paper. The method of reduction is briefly described. Absolute wavelengths were computed without previous identification of any line, and the zero order of stars for determination of the coordinate system was used. The mean deviation of computed wavelengths from the wavelengths of identified lines is only  $\pm 0.2$  Å in the case of spectrum S 6. The lines of neutral iron predominate in both the meteor spectra.



# A Short Note on Meteor Spectra With Low Dispersion <sup>1</sup>

By J. Rajchl <sup>2</sup>

Up to the present, 16 spectra of meteors with low dispersion (about 200 Å/mm in the blue region, and about 800 Å/mm in the red region of the spectrum) have been photographed at the Ondřejov Observatory. It is evident from these spectra that the emissions of ionized Ca and Mg for some meteors are visible from the beginning of the meteor. For others, these emissions are absent, although as is shown from rocket explorations, ionized Ca and Mg atoms of meteoric origin are present at heights of about 100 km (Istomin, 1961).

From direct photographs it was possible to determine the fundamental dynamical and physical characteristics for three spectra of this collection. Using the mass determined from the photometry and the decelerations, we calculated the diameter of the meteoroid on the assumption that the density of meteoric material is 3.5 gm/cm<sup>3</sup>. Following Baker (1959), we determined the parameter  $B$  (i.e., the ratio of meteor-body diameter to the mean free path of the emitted molecules with respect to the oncoming molecules), and the flow conditions of the interaction between meteoric body and the surrounding atmosphere. The Ca II and Mg II emissions appear when the flow conditions change from transition flow to slip flow. In the case when the slip-flow conditions are already valid from the beginning of meteor light emission, then the ionized emissions occur from the beginning. This is fulfilled for the meteors we investigated in the height interval from 96 to 100 km.

It is interesting to compare this result with my recent finding (Rajchl, 1960) that the slip-flow conditions are also present when a sudden increase in meteor brightness (flare) occurs;

and it is a well-known fact that in flares the emission of ionized Ca and Mg atoms prevails. For example, in our spectral material there are photographs of two meteors that emit light only in the red region of the spectrum. But when a flare occurs, very strong Ca II emission is observable.

Thomas and White (1953) reported that the Ca II emission is absent in the spectra of Giacobinids, and connected this with the low velocity of the shower. Let us suppose, as the highest limit, the same meteoroid diameter for Giacobinids as for our meteors, and let us use the end heights determined for Giacobinids. Then we find that these meteors emit light above the region of slip flow, where transition-flow conditions prevail, and thus according to our results it is impossible to observe Ca II emissions. Similarly, for Super-Schmidt meteors also emitting light above the slip flow, i.e., in transition or free-molecule flow, it is possible to admit from our point of view that the principal blue emissions Ca II and Mg II must be absent and the faint meteors show redder. This fact was recently pointed out by Cepelcha (1959), and was photoelectrically observed by J. Davis (private communication). It is interesting to point out that the height interval at which ionized atoms begin to emit light is the same as that found by Jacchia (1949) for a slight increase of brightness shown by some photographic meteors, and explained by the possible influence of the  $E$ -layer.

We may conclude that Baker's parameter  $B$  is the more important one, governing the processes of light emission and its efficiency  $\tau$ , and perhaps is more important than the meteor velocity itself. But it must be emphasized that our results are only preliminary and more observational material is required for confirmation.

<sup>1</sup> Details of this paper will be published in Bull. Astron. Inst., Czechoslovakia.

<sup>2</sup> Astronomical Institute of the Czechoslovak Academy of Sciences, Ondřejov, Czechoslovakia.

**References**

- BAKER, R. M. L., Jr.**  
1959. The transitional aerodynamic drag of meteorites. *Astrophys. Journ.*, vol. 129, pp. 826-841.
- CEPLECHA, Z.**  
1959. On the colour index of meteors. *Bull. Astron. Inst. Czechoslovakia*, vol. 10, p. 39.
- ISTOMIN, V. G.**  
1961. Nitrogen ions in the earth's upper atmosphere and nighttime ionization in the E layer. *Dokl. Acad. Sci. U.S.S.R.*, vol. 137, p. 1102.
- JACCHIA, L. G.**  
1949. Photographic meteor phenomena and theory. *Harvard Coll. Obs. Reprints*, ser. 2, no. 31.
- RAJCHL, J.**  
1960. A note to the problem of meteor flares. *Bull. Astron. Inst. Czechoslovakia*, vol. 11, pp. 33-34.
- THOMAS, R. N., and WHITE, W. C.**  
1953. The physical theory of meteors. IV. Inquiry into the radiation problem—a laboratory model. *Astrophys. Journ.*, vol. 118, pp. 555-567.

# Spectrographic Observations of Meteors in U.S.S.R. in 1957–1960

By E. N. Kramer,<sup>1</sup> K. A. Liubarsky,<sup>2</sup> and V. I. Ivanikov<sup>3</sup>

The first photographs of meteor spectra were obtained at the Moscow Observatory by S. N. Blajko in 1904. After this only amateurs were engaged in meteor spectrography. However, some good spectra were obtained by K. P. Stanukovich and G. O. Zateishchikov in 1934, G. O. Zateishchikov in 1936, V. M. Chernov in 1939, and K. A. Liubarsky in 1950. During the IGY comparatively powerful spectral patrols came into operation at some observatories.

In the Astrophysical Laboratory of the Physical-Technical Institute, Academy of Sciences of Turkmenian S.S.R., Ashkhabad, U.S.S.R., the patrol consisted of 8 cameras (D:F=1:2.5, F=250 mm) and 2 cameras (D:F=1:5, F=500 mm) with objective prisms made of flintglass, angle 20°, diameter 120 mm. In the Astrophysical Institute, Academy of Sciences of Tadjik S.S.R., Doushanbe, the patrol was designed under the direction of L. A. Katasev and was fully completed in 1960. It consisted of 6 cameras (D:F=1:2.5, F=250 mm) with objective prisms made of flintglass, angle 25°, diameter 250 mm. The calculation of the prisms was published by Ivanikov (1957). The cameras were equatorially mounted and clock driven.

The Odessa Astronomical Observatory ran a patrol of four cameras (D:F=1:4.5, F=125 mm) with objective prisms, angle 17°, and diameter 45 mm.

At the meteor station<sup>4</sup> of the Simferopol section of VAGO, the patrol consisted of six cameras of different types (D:F=1:2, F=125

mm; D:F=1:4.5, F=250 mm; D:F=1:4.5, F=135 mm) with objective prisms, angles 16°, 18°, 30° and diameters 45 and 30 mm. All the stations used panchromatic films.

In the period 1957–1960, 95 spectra were obtained, as follows: 32 in Ashkhabad (Liubarsky), 10 in Odessa (Kramer), 25 in Doushanbe (formerly Stalinabad) (Ivanikov), and 28 in Simferopol (Pushnoy).

The catalog of the spectra with the number of lines  $n \geq 5$  is given in table 1 and is a partial continuation of the list published by Astapovich (1958).

The dispersion on all the spectra is small. In the blue region of the spectrum it is equal to 100–200 Å/mm, and for the Simferopol spectra as high as 1000 Å/mm. Some of the meteors have a small angle between the direction of the dispersion and the meteor trail. As a rule, the stars of spectral type A0–A5 do not appear on the negative near the meteor spectrum, and the irregular distortion of the wide-angle objectives do not permit the use of these stars for purposes of comparison. This is the reason why the stations in Ashkhabad and Odessa, independently of each other, used the method of the construction of the dispersion curve on the base of some line in the meteor spectra, which may be easily identified on the negative. The fact that the identification is correct has been checked by means of the interval coordination of the identification of the other lines (Liubarsky, 1961). For this purpose the list of the most widespread lines in meteor spectra was employed. This method was used partially in Doushanbe.

In Ashkhabad and Doushanbe the method of control based on the multiplets was used; if we identify any line of a multiplet in a

<sup>1</sup> Odessa Astronomical Observatory, U.S.S.R.

<sup>2</sup> Astrophysical Laboratory, Ashkhabad, U.S.S.R.

<sup>3</sup> Astrophysical Institute, Doushanbe (formerly Stalinabad), U.S.S.R.

<sup>4</sup> All Union Astronomical Geodetical Society, U.S.S.R.

TABLE 1.—*Meteor spectra with the number of lines  $n \geq 5$* 

No.	Date	Shower	No. lines	World List* No.	Observatory
1	1957 Aug. 6	Sporadic	10	255	Odessa
2	1958 Aug. 7	?	10	264	Doushanbe
3		12 ?	54	279	Doushanbe
4		13 Perseid	11	281	Odessa
5		13 Sporadic	8	280	Odessa
6	Sept. 7	Sporadic	29	297	Ashkhabad
7		8 ?	12		Doushanbe
8		8 Sporadic	10	298	Odessa
9		9 Sporadic	18	299	Odessa
10	Oct. 21	Orionid	28	307	Ashkhabad
11		22 Orionid	8	308	Ashkhabad
12	1959 Aug. 6	Perseid	7		Ashkhabad
13		11 Perseid	5		Simferopol
14		12 ?	31		Doushanbe
15		12 Perseid	5		Simferopol
16		12 Sporadic	7		Simferopol
17		13 Perseid	9		Simferopol
18		13 Cassiopeid	8		Odessa
19		13 Perseid	7		Simferopol
20		13 Sporadic	7		Simferopol
21	1960 Mar. 28	Sporadic	5		Ashkhabad
22	June 17	Sporadic	6		Ashkhabad
23		18 Sporadic	33		Ashkhabad
24		26 Sporadic	10		Odessa
25	Aug. 3	Perseid	6		Ashkhabad
26		13 Cassiopeid	12		Odessa
27	Oct. 21	?	25		Doushanbe

\* See P. Millman, *Journ. Astron. Soc. Canada*, vol. 53, pp. 271-276, 1959.

spectrum, the other weaker lines of this multiplet must also be in this spectrum. The Ashkhabad station used the method of selection of spectral lines according to the order of their appearance in comparison with the potentials of excitation.

One spectrum in Odessa was reduced by obtaining the mercury spectrum under conditions that are closest to the condition for obtaining the meteor spectrum (Kramer, 1959). The Doushanbe station began the study of the dispersion as a function of the point in the field of view, with the purpose of establishing the standard dispersion curves for every point. In all spectra the lines of neutral and ionized metals were identified: iron, calcium, magnesium, sodium, manganese, cobalt, and chromium. In the spectra of the fast meteors the lines 6340-6350 Å are frequent and strong. They are identified by Cook and Millman (1955) as Si II. This identification, however, is very strange as this line often appears earlier than the D Na I, and the H

and K Ca II lines, but the ionization and excitation potentials of silicon are very large (about 20 eV). Neutral silicon is not identified. Meanwhile any other identifications of this line were not found.

In some spectra the presence of the line near the well-known green line of oxygen (forbidden 5577 Å) was noted. The identification of this line as O I may be erroneous as in this region there is a fairly strong line of neutral calcium Ca I (23).

Most of the spectra show a strong unresolved system N<sub>2</sub> 1 P.G. According to Liubarsky the intensity of the nitrogen bands depends less on the variations of the brightness of the meteor than does the intensity of the metal lines. The Ashkhabad station (1960, June 18) obtained the meteor spectrum in which, except for N<sub>2</sub> 1 P.G., there is a strong system N<sub>2</sub> 2 P.G. Fourteen bands are resolved in this system.

The Doushanbe station (1961, February 9) obtained a spectrum without atomic lines.

This spectrum consists of three unresolved systems of bands; one of these systems may be identified as  $N_2$  1 P.G., but the other two are unidentified.

The Odessa station (1956, October 8) obtained the spectrum of a  $-12^m$  bolide (Kramer, 1958) with cyclical pulsating brightness. The pulsations continued through the bright bursts; the bursts are independent of the pulsations. The cycles of the pulsations begin from sharp double maxima, which are followed by intervals of constant brightness. The brightness increases and falls very rapidly. Toward the end of the trail the intervals between the components of the double maxima as well as between the maxima are shorter. A continuous spectrum appears in the maximum.

Kramer explains these pulsations by arranging a cyclical regime at certain values of the velocity and sizes of a meteor body. Near the boiling point, when the vapor pressure and external pressure are equal, a secondary shock wave arises from the surface of the body and the melting layer instantly evaporates. The bolide flashes up for a second time after the departure of the secondary shock wave.

The Ashkhabad station (1958, September 7) obtained the spectrum of the  $-9^m$  bolide. According to the visual observations of Astapovich, the height of the final point is 20 km and the velocity is about 30 km/sec. The bolide has a metallic spectrum only and the lines of the ionized elements are absent.  $N_2$  1 P.G. is very strong. The bolide showed 14 flares separated by regular intervals. As Liubarsky notes, there are no spectral changes in the flares; the flares may perhaps be due to rotation, but they are not due to the variations in temperature.

For one spectrum (Odessa, 1958, August 12), Komarov tried to find the relative intensities of the lines on the assumption that the density is proportional to the logarithm of the intensity in the density interval 0.4–1.4. He found that in the flares the maximum intensity is displaced toward the blue region of the spectrum and hence the temperature rises. He also found  $\lambda_m$  (the color of the meteor) by using the comparison star  $\alpha$  Lyrae.

Liubarsky noticed the strong asymmetry of the profiles of certain lines (for example, H and K Ca II). The asymmetry may perhaps be caused by the presence of these lines in the meteor train and by drift of the train. It is unlikely that the blending of faint lines may cause such an asymmetry for the H and K lines, but for the weaker lines we must take this possibility into account.

#### References

- ASTAPOVICH, I. S.  
1958. Meteor phenomena in the earth's atmosphere. Publ. House for Physical and Mathematical Literature, Moscow.
- COOK, A. F., AND MILLMAN, P. M.  
1955. Photometric analysis of a spectrogram of a Perseid meteor. *Astrophys. Journ.*, vol. 121, pp. 250–270.
- IVANIKOV, V. I.  
1957. The choice of an objective prism for meteor spectrophotometry. *Bull. Stalinabad Astron. Obs.*, no. 20.
- KRAMER, E. N.  
1958. The spectrum of a bolide from October 8, 1956. *Astron. Circ., Acad. Sci. U.S.S.R.*, no. 195.  
1959. Spectra of three bright meteors. *Proc. Odessa Astron. Obs.*, vol. 5, no. 1.
- LIUBARSKY, K. A.  
1961. Spectral observations of meteors. *Bull. Comiss. Comets and Meteors, Acad. Sci. U.S.S.R.*, no. 5.



# Diffusion Effects Observed in the Wake Spectrum of a Geminid Meteor

By Ian Halliday<sup>1</sup>

The spectrum of a spectacular Geminid meteor was photographed on the night of December 12/13, 1960, at the Meanook Meteor Observatory ( $\varphi = 54^{\circ} 37' N$ ,  $\lambda = 113^{\circ} 21' W$ ). This is one of two meteor observatories operated by the Dominion Observatory in northern Alberta. The spectrum exhibits interesting peculiarities.

The meteor was photographed with a converted K19 aerial camera, focal length 12 inches, focal ratio  $f/2.5$ , using Kodak Spectroscopic I-D emulsion on glass plates 8 by 10 inches. A Bausch & Lomb replica transmission grating with 300 lines per mm was mounted immediately in front of the camera objective. The camera was occulted 12.5 times per second by a rotating shutter with a closed-to-open ratio of 2:1.

The meteor was not observed visually but was recorded on an exposure that began at 3<sup>h</sup>32<sup>m</sup> U.T. and ended at 4<sup>h</sup>05<sup>m</sup> U.T., December 13, 1960. The meteor was initially outside the field of view of the camera, but the zero-order image entered the field before peak luminosity was attained, while the first- and second-order spectra entered the field at progressively lower heights.

The spectrum is reproduced in plate 1. The meteor moved from upper right to lower left. The right-hand edge of the photograph is the edge of the original plate. The first segment of the zero order at the top of the photograph is the sixth segment that appeared on the plate, while the lower end of the zero order (beyond segment 13) has been omitted at the left. The segment numbers are shown opposite each segment of the spectrum along the right-hand edge. Segments 20 and 21 are detectable only

in the first-order image of the Na D lines. A small portion of the first- and second-order spectra of Vega appears in the lower left corner of the photograph.

## Height and velocity measures

Since the meteor was photographed from only one station, no direct measures of height or velocity are possible. Reasonably accurate heights may be obtained, however, by assuming a radiant position and velocity for the Geminid shower and then determining ranges and hence heights from the observed angular velocity.

A standard Geminid radiant at  $\alpha = 113^{\circ}$ ,  $\delta = +32^{\circ}$ , was assumed (Millman, 1954) since the meteor appeared within an hour of the peak of the shower (solar longitude  $261^{\circ}.1$ ). This assumed radiant was displaced to allow for the effect of zenith attraction. It was then found that the observed trail passed through the apparent radiant shortly before the end of the exposure, which gave a computed time for the appearance of the meteor of 4<sup>h</sup>01<sup>m</sup> U.T.

A plot of the observed angular velocities along the trail indicated a marked deceleration in the latter half of the observed trail. The angular velocity at the bottom of segment 4 was assumed to correspond to a meteoric velocity of 36.0 km/sec, and other heights and velocities were based on this assumption. The meteor was  $90^{\circ}$  from the radiant near the end of segment 10, at a minimum range of 106.0 km from the camera. Table 1 lists the computed heights (corrected to sea level) and corresponding velocities at the lower ends of selected segments. Errors in the assumed meteoric velocity, radiant position, and speed of shutter rotation could result in the heights and velocities of table 1

<sup>1</sup> Dominion Observatory, Ottawa, Canada.

being in error by as much as 3 to 5 percent. There is no doubt, however, that the meteor penetrated to unusually low heights in the atmosphere.

TABLE 1.—*Heights and velocities*

Segment	Height of bottom of segment (km)	Velocity (km/sec)
1	72.9	36.1
5	67.2	36.0
9	61.5	35.4
13	55.9	33.7
15	53.3	32.3
17	50.7	30.3
19	48.5	26.7
21	46.6	----

### The meteor spectrum

The dispersions of the first and second orders of the meteor spectrum were found to be 95 and 46 Å/mm, respectively. Atomic emission lines identified in this spectrum are shown in table 2. A total of 95 features are identified. The spectrum appears normal for a meteor of this velocity except that the lines of ionized magnesium, calcium, and silicon are relatively strong compared to those in the spectra of fainter meteors with the same velocity. Almost all the lines in table 2 were also identified in a recent study of Perseid spectra (Halliday, 1961). The only significant addition is the pair of lines of Al I at 3944 and 3961 Å. These are barely detectable by sighting along the lines in a 30× enlargement of the strongest segment of the second order. The much greater relative strength of the H and K lines for fast meteors makes the detection of faint lines in this spectral region very difficult for Perseid spectra.

TABLE 2.—*Measured emission lines in the Geminid spectrum*

$\lambda_{\text{meas}}$	Atom or ion	Mult.	$\lambda_{\text{lab}}$
3683.1	Fe I	5	3679.9
			3683.1
	Fe I	21	3687.5
3705.4	Fe I	5	3705.6
			3707.8
	Fe I	21	3709.2
3719.9	Fe I	5	3719.9
3735.6	Fe I	5	3737.1
	Fe I	21	3734.9
3747.8	Fe I	5	3745.6
			3748.3
	Fe I	21	3749.5

TABLE 2.—*Measured emission lines in the Geminid spectrum—Continued*

$\lambda_{\text{meas}}$	Atom or ion	Mult.	$\lambda_{\text{lab}}$
3797.1	Fe I	21	3795.0
			3798.5
			3799.5
3815.9	Fe I	45	3815.8
3821.0	Fe I	20	3820.4
3825.1	Fe I	20	3825.9
	Fe I	45	3827.8
3832.8	Mg I	3	3829.4
			3832.3
	Fe I	20	3834.2
3839.1	Mg I	3	3838.3
3856.4	Fe I	4	3856.4
	Si II	1	3856.0
3859.7	Fe I	4	3859.9
3878.2	Fe I	4	3878.6
	Fe I	20	3878.0
3886.5	Fe I	4	3886.3
3900.3	Fe I	4	3899.7
3905.5	Fe I	4	3906.5
3921.4	Fe I	4	3920.3
			3922.9
3933.6	Ca II	1	3933.7
3943.6	Al I	1	3944.0
3960.6	Al I	1	3961.5
3968.8	Ca II	1	3968.5
	Fe I	43	3969.3
3997.2	Fe I	276	3998.1
	Fe I	278	3997.4
4005.0	Fe I	43	4005.2
4030.8	Mn I	2	4030.8
4033.5	Mn I	2	4033.1
			4034.8
4046.1	Fe I	43	4045.8
4063.4	Fe I	43	4063.6
4071.7	Fe I	43	4071.7
4132.4	Si II	3	4130.9
	Fe I	43	4132.1
4144.4	Fe I	43	4143.9
	Fe I	523	4143.4
4155.5	Fe I	354	4156.8
	Fe I	355	4154.5
4200.9	Fe I	42	4202.0
	Fe I	152	4198.3
	Fe I	522	4199.1
4217.3	Fe I	3	4216.2
4226.6	Ca I	2	4226.7
	Fe I	693	4227.4
4250.9	Fe I	42	4250.8
	Fe I	152	4250.1
4253.6	Cr I	1	4254.3
4260.6	Fe I	152	4260.5
4272.1	Fe I	42	4271.8
	Fe I	152	4271.2
4274.2	Cr I	1	4274.8
4282.2	Fe I	71	4282.4
	Ca I	5	4283.0

TABLE 2.—*Measured emission lines in the Geminid spectrum—Continued*

$\lambda_{\text{meas}}$	Atom or ion	Mult.	$\lambda_{\text{lab}}$
4290.2	Cr I	1	4289.7
	Ca I	5	4289.4
	Fe I	3, 41	4291.5
4307.6	Fe I	42	4307.9
	Ca I	5	4307.7
4314.2	Fe I	71	4315.1
4325.8	Fe I	42	4325.8
4353.1	Mg I	14	4351.9
	Fe I	71	4352.7
4376.1	Fe I	2	4375.9
4383.6	Fe I	41	4383.5
4404.8	Fe I	41	4404.8
4415.9	Fe I	41	4415.1
4427.1	Fe I	2	4427.3
4461.6	Fe I	2	4461.7
4481.4	Mg II	4	4481.1
			4481.3
			4482.2
4530	Fe I	68	4528.6
4920.4	Fe I	318	4919.0
			4920.5
4955.1	Fe I	318	4957.3
			4957.6
5008.9 <sup>b</sup>	Fe I	16	5012.1
	Fe I	318	5006.1
5041.3	Fe I	16	5041.1
	Fe I	36	5041.8
5108.5	Fe I	1	5110.4
	Fe I	16	5107.5
	Fe I	36	5107.6
5146.1 <sup>b</sup>	Fe I	16	5142.9
			5150.8
	Fe I	383	5139.5
	Na I	8	5148.8
			5153.4
5169.4	Mg I	2	5167.3
			5172.7
	Fe I	1	5166.3
			5168.9
	Fe I	36	5171.6
	Fe I	37	5167.5
5183.6	Mg I	2	5183.6
5207.2	Cr I	7	5204.5
			5206.0
			5208.4
5227.2	Fe I	37	5227.2
	Fe I	383	5226.9
			5232.9
5269.5	Fe I	15	5269.5
	Fe I	37	5270.4
	Fe I	383	5266.6
5328.5	Fe I	15	5328.0
	Fe I	37	5328.5
5341.8	Fe I	37	5341.0
5370.5	Fe I	15	5371.5

<sup>b</sup> Feature noticeably broad.

TABLE 2.—*Measured emission lines in the Geminid spectrum—Continued*

$\lambda_{\text{meas}}$	Atom or ion	Mult.	$\lambda_{\text{lab}}$
5402.8	Fe I	15	5397.1
			5405.8
			5429.7
5429.8	Fe I	15	5429.7
5448.8	Fe I	15	5446.9
5456.9	Fe I	15	5455.6
5499.0	Fe I	15	5497.5
			5501.5
			5506.8
			5528.4
5528.3	Mg I	9	5528.4
5573.2	Fe I	686	5572.9
5587.2	Fe I	686	5586.8
5615.5	Fe I	686	5615.5
5685.8	Na I	6	5682.6
			5688.2
			5709.4
5712	Fe I	686	5709.4
	Mg I	8	5711.1
	Na I	1	5890.0
5892.9			5895.9
			5979.0
5980.2	Si II	4	5979.0
6063	Fe I	207	6065.5
6105	Ca I	3	6102.7
6121.9	Ca I	3	6122.2
6139	Fe I	169	6136.6
	Fe I	207	6137.7
6157.0	Na I	5	6154.2
			6160.7
			6162.2
6162.7	Ca I	3	6162.2
6229	Fe I	207	6230.7
6251	Fe I	169	6252.6
6347.1	Si II	2	6347.1
6369	Si II	2	6371.4
6397.8	Fe I	168	6393.6
	Fe I	816	6400.0
	Ca I	18	6439.1
6438	Ca I	18	6439.1
6461	Fe I	168	6462.7
	Ca I	18	6462.6
6494.4	Fe I	168	6495.0

**Variation in luminosity**

The photograph in plate 1 indicates that this meteor maintained approximately peak luminosity from segments 6 to 16, inclusive, an atmospheric path length of 27 km. Before segment 6, the zero order is considerably weaker, while the spectral lines are fading noticeably by segment 17 and drop abruptly in intensity at segment 19. Peak luminosity appears to occur at about segment 11, near a height of 59 km. The lines in the blue region of the first-order spectrum appear stronger here than in subsequent segments, although the variation between segments 11 and 14 is quite small.

To estimate the peak luminosity the zero-order image of the meteor was compared with zero-order star trails. The meteor trail is definitely weaker than the trail of Vega and appears to match the zero order of  $\alpha$  Cygni. The meteor image trails across the plate at a rate 5,820 times greater than does the image of  $\alpha$  Cygni, corresponding to a difference of 9.4 magnitudes. The apparent magnitude of  $\alpha$  Cygni is +1.3, from which the meteor magnitude is estimated at -8. This is a "panchromatic" magnitude, which may be influenced by such factors as emulsion sensitivity and the blaze of the grating. In other cases (Cook and Millman, 1956; Millman and Cook, 1959), it proved to be only slightly different from photographic magnitudes.

The meteor exhibits a rapid flickering superimposed on the gradual rise and fall in overall intensity. The frequency of the flickering was estimated in each segment by measuring the fraction of a complete segment occupied by the largest number of complete cycles observed within the segment. The results were converted to cycles per second and are shown plotted in figure 1.

Over most of the observed trail the flicker is within the range of 100 to 300 cycles per second. In a sense, it follows the general light curve with a gentle rise to maximum and a steeper decline. The peak of the fre-

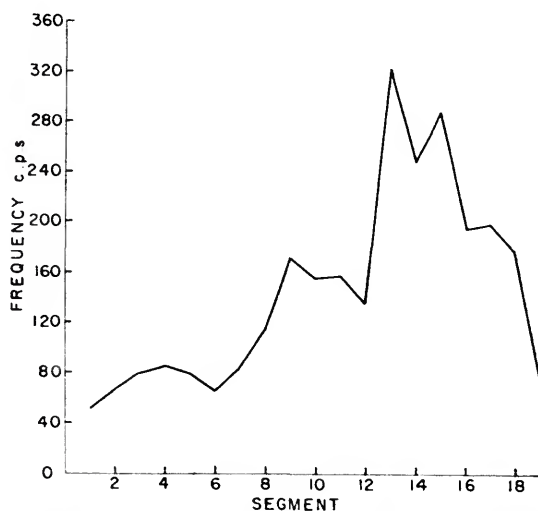


FIGURE 1.—Frequency of the flickering plotted against position along the trail as indicated by segment numbers.

quency curve occurs about two segments after the peak of the light curve. From segments 9 to 12 the frequency is fairly constant near 150 cps, but jumps suddenly at segment 13 to about 320 cps and then declines, only slowly, for another two segments. The amplitude of an individual fluctuation reaches a maximum near segments 10 to 12, resulting in a more pronounced fluting of the spectrum here than at other places.

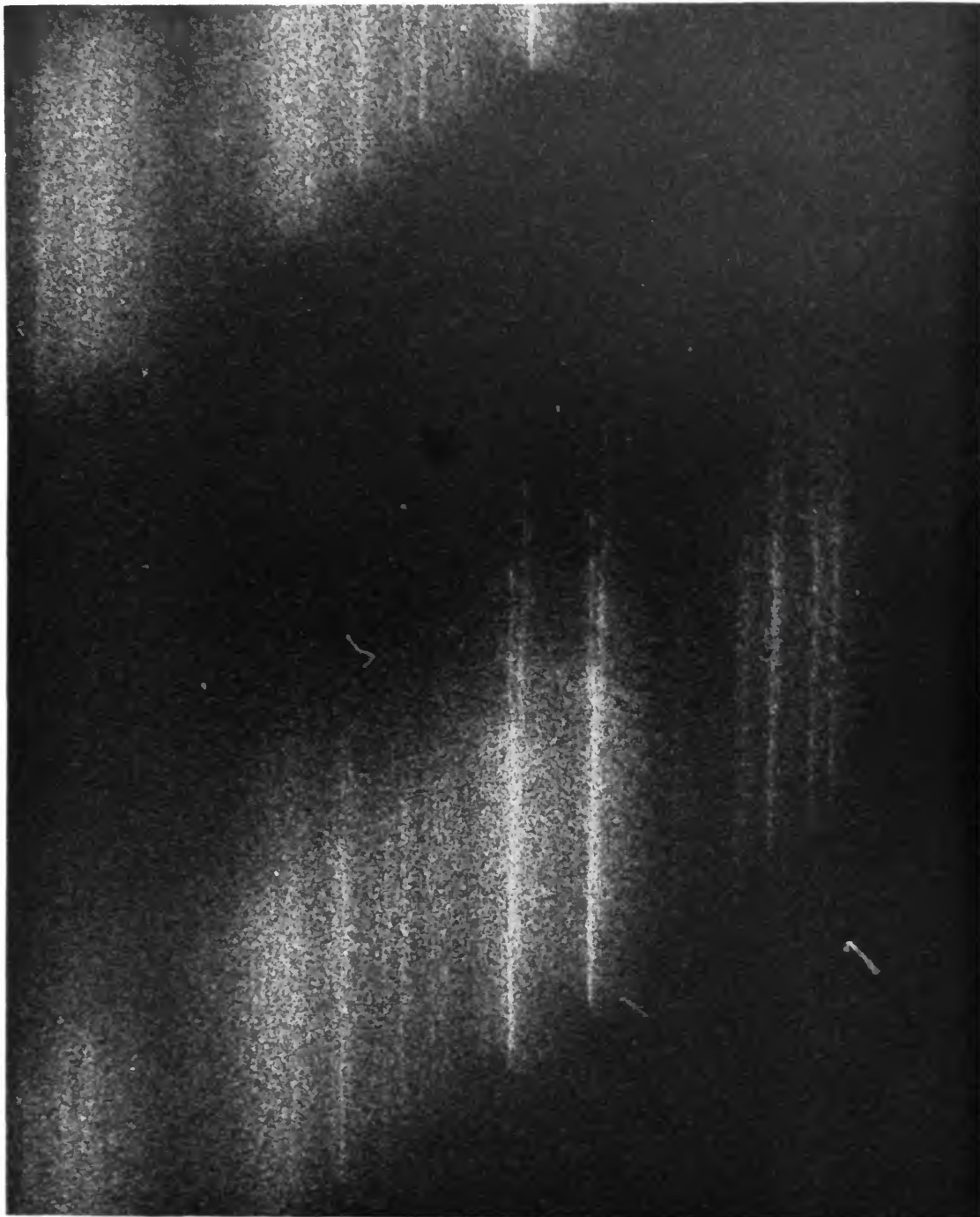
The periodic flaring might be interpreted as indicating the repeated crumbling or fragmentation of minor amounts of material from the main meteoroid in the form of solid fragments. The increased surface area exposed to ablation would then account for the increased luminosity at each minor flare.

Alternatively, the phenomenon might be closely associated with rotation of the meteoroid. If the meteoroid is quite irregular in shape and rotates in such a manner that it alternately presents a large side and a smaller end to the oncoming atmosphere, then the amount of material ablated, in gaseous form, would vary in a periodic manner. The light, of course, is produced by the hot ablated gas and not by the solid surface.

A third possibility, suggested by Dr. L. G. Jacchia, is based on laboratory studies of ultraspeed pellets by Rinehart (Rinehart, Allen, and White, 1952). A flashing phenomenon was observed for the pellets and explained by an oscillation of the pellet during its flight. The luminosity will be low if there is a leading edge of the object, and high when a whole face of the object is exposed to ablation. For a meteor at relatively low heights where continuum flow occurs, as is expected for this Geminid, an oscillation may be set up that would lead to a flickering phenomenon. Sudden jumps in the frequency of the flicker, such as are observed near segment 8 and again just before segment 13, could indicate a tumbling of the meteoroid to oscillate about a new axis. On the rotation hypothesis these changes might be interpreted as a fracturing of the object into two or more pieces with an accompanying increase in rotational velocity for each piece. It is noted, however, that no general increase in luminosity accompanies these changes in the period of the flicker,



A Geminid meteor spectrum showing parts of the zero order (at left), and first- and second-order spectra. Segment numbers are indicated at right.



Greatly enlarged portion of the meteor spectrum showing the split wake-lines of H and K in segment 15 of the second-order spectrum.

which suggests that the effective exposed area is not greatly changed. This would appear to favor the oscillation hypothesis.

### The wake spectrum

The zero-order image shows a slight wake in the gap between the segments, beginning at segment 6. The D lines of Na I show a strong wake where they enter the field of the camera at segment 11, and the wake is observable as far as segment 19. Peak intensity of the wake occurs at segment 15, where the following multiplets can be detected in the wake: Na I, 1; Mg I, 2, 3; Ca I, 2; Ca II, 1; Mn I, 2; Fe I, 1, 2, 4, 5, 15, 20, 21, 41, 42, 43.

Most of these multiplets have been listed in earlier studies of wake spectra (Halliday, 1958), although the manganese lines near 4030 Å have not been listed previously. The wake spectrum shows the usual preference for lines of low excitation potential, but it is less pronounced than in most other cases. The line of Mg I, 2 at 5183.6 Å is moderately intense in the wake, whereas its presence was quite doubtful in most earlier wake spectra. The H and K lines of Ca II are strong in the wake and persist essentially as far back into the gap as the other wake lines, in contrast to some spectra in which the H and K lines decay much faster in the wake than the low-excitation Na I and Fe I lines.

The most significant feature of this spectrum appears to be a clear splitting of the stronger wake lines into two components. It is observable in the second-order spectrum from segments 14 to 18. The H and K lines show the splitting most distinctly because of their strength, but other lines in which it is also observable are:  $\lambda$  4045 of Fe I, 43;  $\lambda$  4226 of Ca I, 2; and  $\lambda$  4383 of Fe I, 41. For the Na D lines, in the first-order spectrum, the situation is complicated by the fact that the splitting is in general comparable to the separation of the two D lines. In segments 18 and 19, however, the separation due to the splitting effect is large enough to show in spite of the duplicity of the spectral feature. For the remainder of the wake lines the intensity in the wake is either too low or the resolution of individual lines is too poor to identify both components of the wake lines.

The two components of one wake line may be considered as "red" and "violet" compo-

nents; i.e., displaced to longer or shorter wavelengths compared to the position of the main spectral line in the adjacent segment of the normal meteor spectrum. The flickering effect can be detected in the wake, although in some cases only one component appears to strengthen. The individual components show distinct curvature in places with little correlation between the two components. In some instances the wake components can be traced down the trail well into the following segment of the meteor spectrum.

Individual descriptions of the components of the H and K lines, in the second order, are given below for segments 14 to 18.

*Segment 14.*—The red component is the stronger, shows some curvature, and appears to fluctuate more due to flickering than does the violet component. The images are within 1 mm of the extreme edge of the plate, which limits the value of this segment.

*Segment 15.*—A large-scale reproduction of this region is shown in plate 2. The red component is strong near the main segment and can be traced back farther than the violet one. The effects of flickering are more evident in the violet component. Both components show some minor kinks, particularly near the main segment.

*Segment 16.*—The red component is very strong in the lower portion of the wake, while the violet component is weak. The violet line strengthens considerably at an earlier flare in this segment of the wake. The red component may be detected higher than the violet one, and also continues about two-thirds of the way through the main part of segment 16. With decreasing height within the segment, the red component approaches the main line but fades out before actually joining the main spectral line.

*Segment 17.*—The violet component is much the stronger in this segment. Just above the main segment the splitting is quite large, while the violet line bends over toward the red component a little farther up in the wake.

*Segment 18.*—The wake is now quite weak, with the violet component stronger than the red component. The splitting of the two components is larger than in earlier segments.

In the first-order Na D lines the two components are not clearly resolved until segment 18. Faint double wake-lines are also detectable in segment 19 for Na D, with an even wider separation than in segment 18.

### Interpretation of the double lines

One obvious explanation to consider for the doubling of the spectral lines in the wake is a physical splitting of the meteoroid into two pieces. This has been observed for some meteors; for example, in spectrum 132 (Millman and Cook, 1959). A splitting of the meteoroid was suggested as one possibility to account for the sudden jump in the frequency of the flicker at segment 13. While this may have occurred it is not the explanation for the double wake-lines, since the wake-lines are generally converging near their lower ends in each segment, while a splitting of the meteoroid would lead to diverging fragments. In segment 16 the red component can be traced for a total distance equivalent to half a complete segment, whereas the exposure time is only one-third of a segment; i.e., the red component is not an exposure on a trailing fragment.

The two components are not due to Doppler effects of an expanding column. The observed splitting would correspond to a relative expansion, transverse to the direction of meteor motion, of about 600 km/sec. This is a most unreasonable value when the initial velocity of the meteor was only 36 km/sec.

The best interpretation is that the wake represents a time exposure of the expanding column of meteoric gas, taken while the luminosity is decaying. Meteor spectrographs are slitless spectrographs, which produce a broad image of a broad source even in monochromatic light. The two wake components apparently represent a side view of a hollow luminous column that shows two well-defined edges because the effective thickness of the luminous portion is small compared to the thickness of the entire column. Note that in comparing the two components at a particular point on the trail, one should compare two points on a line perpendicular to the direction of meteor motion, rather than two points on a line parallel to the spectral dispersion.

Figure 2 shows three computed curves for the intensity profile plotted along a radius of the column from  $x=0$  at the center to  $x=1.0$  at the outer edge. The three curves correspond to an effective thickness  $t$  of the luminous portion of the column of 0.05, 0.15, and 0.40, in units of the column radius. The resolution of the plate is insufficient to rule out very small values of  $t$ , but the components are sharp enough to indicate that the effective value of  $t$  is not much greater than 0.15.

One complete segment corresponds to  $0^{\circ}080$ , made up of an exposure of  $0^{\circ}027$  and an occulted interval of  $0^{\circ}053$ . The wake is observable approximately halfway across an occulted portion, from which it follows that the effective duration of the luminosity is considerably less than one shutter break. For all points within the gap, the total exposure is the same,  $0^{\circ}027$ , but the "age" of the column when the exposure starts is different for each point. A point at the lower end of a normal wake, where the main meteor spectrum segment is starting, receives an exposure from age  $t=0^{\circ}0$  to  $t=0^{\circ}027$ . For a point in the middle of the gap, the exposure runs from  $t=0^{\circ}027$  to  $t=0^{\circ}054$ . This is about the last observable point in most segments; i.e., there is insufficient luminosity emitted after  $t=0^{\circ}03$  to record on the plate.

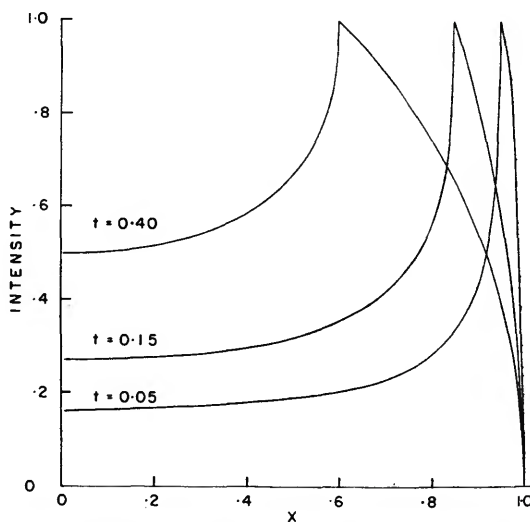


FIGURE 2.—Computed intensity profiles for three values of  $t$ , the effective thickness of the luminous column.

As noted earlier, some of the wake lines, particularly the red components, can be traced down into the following segment. For different points within the segment itself, all exposures start at  $t=0$  but have different durations. The durations decrease linearly with distance down the segment from a maximum exposure of 0<sup>0</sup>27 at the top to 0<sup>0</sup>00 at the bottom (where the shutter occults the camera for the next 0<sup>0</sup>05). In segment 16, it was noted that the red component was observable two-thirds of the way through the segment; i.e., for any exposure duration longer than 0<sup>0</sup>009.

**Magnitude of the splitting**

Once it is known that the split lines correspond to a physical separation of material in the meteor column, it becomes of interest to determine the magnitude of the splitting. The separation of the two components was measured at frequent intervals in each segment of the wake, and the results were plotted. The scales were converted to diameters of the column, in meters, by allowing for the plate scale and the range of the meteor corresponding to each segment.

The results are presented in table 3, where the curves have been read at equal intervals corresponding to 0<sup>0</sup>04 of meteor travel. For example, a time of  $t=0^0012$  indicates a point in the occulted portion from which it took the meteor 0<sup>0</sup>12 to reach the point at which the shutter reopened to begin the next segment of the main spectrum. (The entire gap corresponds to 0<sup>0</sup>53, and although the wake can sometimes be detected at least halfway through the gap, both components are seldom observable for more than one-third of the gap.) The mean splitting within each segment is shown at the bottom of the table.

TABLE 3.—Diameters of the column (meters)

<i>t</i> (sec)	Segment					
	14	15	16	17	18	
0.000	----	31	49	69	78	
0.004		37	34	49	73	82
0.008		42	39	44	61	85
0.012		----	45	49	54	83
0.016			----	53	----	77
0.020				----	----	77
Mean		40	37	49	64	80

In segments 15 and 16, the red components can be traced into the main segment. They begin with separations from the main spectral line (corresponding to a *radius* of the column) of about 24 meters. One-third of the way down through the segment the separation is about 16 meters, and this is maintained for another third of the dash, until the line fades out as noted previously. At the lowest observable points these red components are displaced about 16 meters from the main column, recorded in an exposure which lasted for only 0<sup>0</sup>009.

In all cases where separations for lines of Ca I or Fe I could be measured, the observed points fell quite well on the corresponding curve derived for the H and K lines of Ca II.

The splittings within one segment of the wake are fairly constant; i.e., the red and violet components are nearly parallel. The mean values for the five segments show a curious dependence on height: the splitting increases with decreasing height and may be represented quite well by the linear relation

$$d=550-9.41 h,$$

where  $d$  is the diameter in meters at a height of  $h$  km. The relation is derived from observations between heights of 50 and 55 km.

From the observed rates of expansion, one may compute an equivalent diffusion coefficient. Öpik (1958) has shown that an effective radius  $R$  at time  $t$  may be defined by  $R^2=3Dt$ . For the lowest observed points on the red components,  $t=0^0009$ ,  $R=16$  meters, from which  $D=9.5 \times 10^7$  cm<sup>2</sup>/sec. The effective value of  $t$  should really be smaller, or  $D$  should be somewhat larger. For a typical point in the wake,  $R=30$  meters, and an effective value of  $t$  is about 0<sup>0</sup>03, from which  $D=1.0 \times 10^8$  cm<sup>2</sup>/sec. Öpik tabulates normal diffusion coefficients for these heights of about  $2 \times 10^2$  cm<sup>2</sup>/sec; i.e., the observed expansions exceed those predicted from normal diffusion by a factor of  $5 \times 10^5$ .

**Discussion**

At the low heights of this meteor one should expect a shock front to form around the moving meteoroid. The observed wake luminosity, however, is produced by meteor atoms of calcium, sodium, and iron, not by atmospheric particles. An effective front of expanding me-

teoric material appears to exist inside the heated volume produced by the shock front. Violent collisions at the surface of this meteoric front continue to excite the meteoric atoms for intervals up to about  $0.03$ . As shown earlier, the sharpness of the two components of the strong wake lines indicates that the effective thickness of the luminous portion of the meteor column is not more than about 15 percent of its radius, or else the lines would appear more diffuse.

The wake components indicate a diffusion of meteoric material into the atmosphere, but the effective diffusion coefficients are so large as to suggest the phenomenon is essentially explosive. During the initial stages the diameter of the column is observed to expand at a rate in excess of 3 km/sec. It is not surprising that the expansion should be very rapid compared to normal diffusion since the amount of material deposited by such a bright meteor is so great as to constitute a major change in local density along the meteor trajectory. The rate of diffusion of meteoric material in this case is so great that it seems reasonable to infer that much fainter meteors, perhaps any meteor brighter than 0 magnitude, will also give rise to appreciably more rapid diffusion than is observed by radar for faint meteors. Great care should be taken, then, that normal diffusion coefficients are not considered as a known quantity in calculations involving the gas columns left by bright meteors.

It is of considerable interest to note that the ion column of Ca II ions expands at the same rate as the atom column of Ca I or Fe I. This is not normally considered to be the case, at least for radar observations, which, of course, are for meteors about 10 magnitudes fainter than this Geminid. Manning (1958), for example, quotes Loeb (1934) to support a statement that the ion column will diffuse only one-fifth as fast as the atom column. Loeb's results are based on experiments in which ions were allowed to diffuse through an electric field. He states (p. 548): "the velocity gained from the field between impacts is further supposed small compared with the thermal velocities of agitation." It is not clear that these results are applicable to the meteor case, where the presence of an electric field is unlikely and the systematic velocity of the meteor particles is

very large compared with thermal velocities. Manning mentions that the ion column for a bright meteor may be larger than for a faint one if ionization can still be accomplished during the expansion of the atom column. For calcium, 6.09 eV are required for ionization, which is higher than the excitation of any wake line. This makes it more likely that an ion of Ca II, which emits H or K radiation  $0.03$  after the passage of the meteor, survived nearly all of that interval as an ion, and was then excited with an additional 3.1 eV to radiate, rather than that the ion was formed from a Ca I atom and excited to radiate by any collision occurring later than perhaps  $0.002$  after the atom left the meteoroid.

Rapid rotation or oscillation for this meteoroid is suggested by the regularity of the flickering phenomenon and is supported to some extent by the split wake-lines. The variation in relative intensity between the red and violet components could arise from either mechanism, since varying amounts of material would be ejected from the meteoroid in a manner which is not radially symmetrical. This could also account for some of the curvature observed in the wake lines.

One Perseid spectrum is known which shows a similar but much less pronounced splitting of the wake-lines. It is spectrum 223 in Millman's (1958) list of meteor spectra. The splitting is evident in one segment of the H and K lines, but it is confined to a very short path length near a bright flare. The fact that the phenomenon is so pronounced for the Geminid meteor may be associated with its low height in the atmosphere. The much smaller mean free path may tend to localize the zone where appropriate collisions may occur and effectively shield the inner portion of the wake column, giving rise to the hollow-tube effect.

### References

- COOK, A. F., AND MILLMAN, P. M.  
1956. Photometric analysis of a spectrogram of a Perseid meteor. *Astrophys. Journ.*, vol. 124, pp. 476-477.
- HALLIDAY, I.  
1958. Meteor wakes and their spectra. *Astrophys. Journ.*, vol. 127, pp. 245-252.  
1961. A study of spectral line identifications in Perseid meteor spectra. *Publ. Dominion Obs. Ottawa*, vol. 25, pp. 1-16.

- LOEB, L. B.  
1934. Kinetic theory of gases. Ed. 2. McGraw-Hill Book Co., New York.
- MANNING, L. A.  
1958. The initial radius of meteoric ionization trails. Journ. Geophys. Res., vol. 63, pp. 181-196.
- MILLMAN, P. M.  
1954. A provisional list of the major meteor showers. Journ. Roy. Astron. Soc. Canada, vol. 48, pp. 193-195.  
1958. Photographic meteor spectra (appendix 6). Journ. Roy. Astron. Soc. Canada, vol. 52, pp. 275-276.
- MILLMAN, P. M., AND COOK, A. F.  
1959. Photometric analysis of a spectrogram of a very slow meteor. Astrophys. Journ., vol. 130, pp. 648-662.
- ÖPIK, E. J.  
1958. Physics of meteor flight in the atmosphere. Interscience, New York.
- RINEHART, J. S.; ALLEN, W. A.; AND WHITE, W. C.  
1952. Phenomena associated with the flight of ultra-speed pellets. Part 3. General features of luminosity. Journ. Appl. Phys., vol. 23, pp. 297-299.

### *Abstract*

A study is made of an unusual Geminid meteor spectrum, photographed between heights of 73 and 47 km. Peak luminosity, estimated at magnitude  $-8$ , occurred near 59 km. The meteor exhibited a pronounced flicker, with a frequency varying from 50 to 300 cycles per second. The flicker may be associated with rotation or oscillation of the meteoroid.

A prominent wake spectrum was photographed between 50 and 55 km, consisting of lines of Na I, Mg I, Ca I, Ca II, Mn I, and Fe I. The stronger lines are split into two distinct components attributed to a hollow luminous column rather than splitting of the meteoroid or Doppler effects. The diameter of the column varies from 40 to 80 meters, but shows no variation from one atom or ion to another. Diffusion coefficients computed from the observed rate of expansion exceed the normal values at these heights by a factor of more than  $10^6$ . The expansion in this case might be considered as explosive.



# On the Frequency of Occurrence of the Auroral Green Line (5577 Å) in Perseid Spectra

By John A. Russell<sup>1</sup>

In a note announcing his identification of the forbidden line of O I at 5577 Å in the spectra of three meteors, Halliday (1958) pointed out the difficulty of explaining why the line had not been detected previously. In a subsequent study of old spectra, Millman (1960) located a number of appearances of the auroral line, including one in a spectrum from the 1933 Harvard Leonid campaign and one obtained in 1950 by the author. This latter spectrum, No. 121 on the World List (Millman, 1952), had not been reduced at the time of Millman's identification because of its mediocre quality.

Spectrum No. 121 is one of five Perseid spectra (World Nos. 118-122) obtained in a 31-hour interval with the same instrument: a 30° prism, f/5.6 lens of 130-mm focal length, and Super XX roll film. It is evident that these spectra should provide some information on the consistency with which the green line appears under similar instrumental and atmospheric conditions. Spectrum No. 118 contains only the H and K lines of ionized calcium. In spectrum No. 122 the H and K lines were strong, but the remainder of the spectrum was very weak. In neither of these spectra could the 5577 line be detected. Spectrum No. 120 was reproduced in an earlier paper (Russell, 1953). It was well exposed, but suffered from a poor orientation of the path with respect to the prism edge, from foreshortening as the result of the proximity of the meteor to the radiant, and from the location of the spectrum in the very corner of the photographic film. When the original negative was enlarged and the contrast increased by two successive printings on contrast lantern slide plates, the green line

appeared briefly at the beginning of the trail. Spectrum No. 119 was reproduced in a general paper on Perseid spectra (Russell, 1959) as an example in which the H and K lines, though present, were not dominant. When this spectrum was treated photographically by the process used on No. 120, the auroral green line also became evident.

More recently the presence of the auroral line in two additional spectra, Nos. 103 and 107, obtained in 1948 and 1949 with the same instrument, was detected by careful reexamination of the negatives. This brought the green line identifications to five out of the seven spectra photographed with the same equipment during three consecutive Perseid showers.

We note that the auroral line was not found in the spectrum that showed only the H and K lines, or in the one which showed little besides strong H and K lines. A correlation between the strength of the green line and that of the H and K lines was originally suggested by a Perseid spectrum, No. 198, obtained with different apparatus (Russell, 1959). This was the first Perseid in the author's experience that failed to show H and K lines or that exhibited strongly the O I line, the density of which in this spectrum was second only to that of the sodium D-lines. The extent of this possible correlation was investigated in the following manner. From estimates made visually outside of noticeable bursts, the plates were arranged in order of increasing density of the K line relative to the blend at 3830 Å, and numbered from 1 to 7. The plates were then arranged in order of increasing density of the O I line relative to the D lines and again numbered consecutively. The results are illustrated in figure 1.

<sup>1</sup> Department of Astronomy, University of Southern California, Los Angeles, Calif.

To the extent that so small a sample can be relied upon, the correlation appears to be real. Spectrum No. 198 (photographed 1956) and Halliday's spectrum No. 302 (photographed 1958), which consists solely of the green line, would extend the graph linearly toward the lower right. Why a correlation such as this should exist is not clear. As most of the data plotted in figure 1 are from meteors observed within a period of 31 hours, it may be necessary to explain some of the differences in the spectra as the result of differences in the meteoroids rather than as exclusively the effect of variable atmospheric conditions. Of possible significance is the observation that the strength of the green line is almost entirely unaffected by bursts (Halliday, 1960), whereas the strength of the H and K lines is most strongly influenced by them (Russell, 1950).

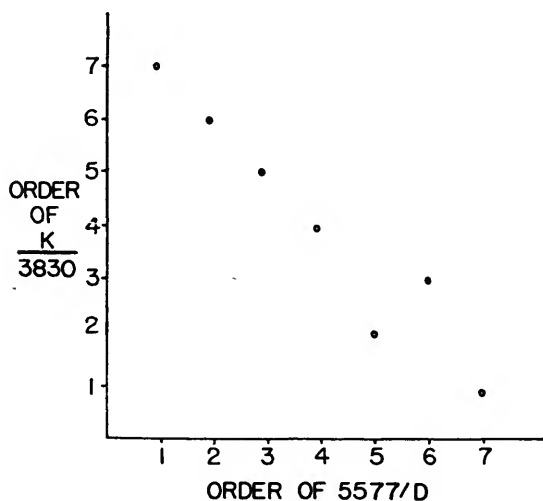


FIGURE 1.—K-line density versus density of 5577 in seven Perseid spectra.

Halliday (1960) finds some evidence for a correlation between the occurrence and depth of penetration of the green line, on the one hand, and geomagnetic and solar activity, on the other. Millman (1960), however, points out that the Leonid spectrum in which he found the green line was photographed at the depth of the sunspot minimum of 1933. The geomagnetic activity and solar activity during the Perseid showers of 1948–1950, 1956, and 1958 are indicated in table 1. The data are

taken from the "Summaries of Mount Wilson Magnetic Observations of Sunspots," which appeared regularly in *Publications of the Astronomical Society of the Pacific* until 1959. No consistent pattern is evident relating the green line to solar activity, although the absence of extreme solar conditions during the period 1948–1950 makes the negative result inconclusive. The atmospheric depth to which the green line penetrates relative to the other lines is remarkably uniform. It generally appears concurrently with the blend of iron lines at 3830 Å and fades about the time that the iron blend at 3740 Å becomes visible. As all of these spectra are of meteors with a common high velocity, they can provide only partial support of Halliday's evidence that the green line is exclusively a high-velocity feature.

TABLE 1.—Relation of auroral line emission to geomagnetic and solar activity

World number of spectrum	Date	Auroral line	Geomagnetic activity	Number sunspot groups that day	Avg. number sunspot groups that month
103	8/12/48	Weak	Great	10	12.4
107	8/13/49	Weak	None	6	8.6
118	8/12/50	Missing	Moderate	6	7.0
119	8/12/50	Weak			
120	8/12/50	Weak			
121	8/13/50	Weak	None	5	
122	8/13/50	Missing			
198	8/11/56	Strong	Great	9	13.5
274	8/12/58	Missing	Not great	14	14.8

When spectra taken with other instruments and emulsions are considered, a broader though less homogeneous base is provided for studying correlations. In 1951, by which time solar activity was below average, a shutter-chopped Perseid, No. 124 (Russell, 1959), which strongly showed H and K lines and the first positive group of nitrogen bands, failed to display the green line. A low-dispersion but fairly well-exposed spectrum of a Geminid, No. 140, obtained in 1953 shows no green line. This absence fits both the low-velocity and the solar-activity correlation. A sporadic meteor of unknown velocity, No. 148, photographed in 1954, showed very strong H and K lines but no green line. Both spectrum No. 198 (1956) and a similar but much fainter spectrum obtained the next night with the same instru-

ment show a relatively strong green line but no H and K lines. Table 1 indicates that a great magnetic storm was in progress at the time and that general solar activity was high.

If general solar activity is a factor in producing the green line, no spectrum obtained by the author should show it better than the Perseid photographed in 1958 with the 18-inch Schmidt at the Mount Palomar Observatory (Russell, 1960). This spectrum, No. 274, shows very strong  $N_2$  bands in the red and 40 measurable features. In the region of the spectrum where the green line would normally appear, there is a broad, amorphous darkening that is a little sharper on one side than on the other. The sharper boundary is close to 5577 Å. This feature was not included in the published discussion as no lines are seen in it under the microscope. It differs from the green line's customary behavior in that it does not appear sooner than the other lines; actually, the  $N_2$  bands appear first, much farther back along the trail. If this feature were produced by the forbidden O I line, blurred by winds during the brief period of radiation, a minimum wind velocity of 5 km/sec would be required to account for the breadth of the line. A. F. Cook (private communication) suggests that this feature is produced by additional, unresolved  $N_2$  bands. The conclusion that the green line is not involved in this spectrum seems strongly justified. Although general solar activity was higher in 1958 than in 1956, no great magnetic storm was in progress at the time of the 1958 shower.

### Conclusions

The seven Perseid spectra obtained with the same instrument over the 3-year period 1948–1950 indicate that (1) there appears to be an

inverse correlation between the strength of the H and K lines and the strength of the auroral green line at 5577 Å; (2) the spectra consistently show the green line except where its absence would be expected in the light of statement (1); (3) the position of the green line relative to the rest of the spectrum was consistently similar. A consideration of several other spectra indicates that (1) any correlation between general solar activity and the occurrence of the green line appears weak, at best; (2) there is no violation of Halliday's findings that the green line is not found in the spectra of low-velocity meteors.

### References

- HALLIDAY, I.  
 1958. Forbidden line of O I observed in meteor spectra. *Astrophys. Journ.*, vol. 128, pp. 441–442.  
 1960. Auroral green line in meteor wakes. *Astrophys. Journ.*, vol. 131, pp. 25–33.
- MILLMAN, P. M.  
 1952. Photographic meteor spectra. *Journ. Roy. Astron. Soc. Canada*, vol. 46, pp. 121–125.  
 1960. The auroral green line in a Leonid spectrum. *Journ. Roy. Astron. Soc. Canada*, vol. 54, pp. 189–192.
- RUSSELL, J. A.  
 1950. Intensity variations in the spectrum of a Perseid meteor. *Contr. Meteorit. Soc.*, vol. 4, pp. 250–254; *Pop. Astron.*, vol. 58, pp. 134–138.  
 1953. Asymmetrical lines in the spectra of meteors. *Meteoritics*, vol. 1, pp. 103–105.  
 1959. Some Perseid meteor spectra of the past decade. *Sky and Tel.*, vol. 18, pp. 549–551.  
 1960. Molecular nitrogen in the spectra of two Perseid meteors. *Publ. Astron. Soc. Pacific*, vol. 72, pp. 291–295.

### Abstract

A reexamination of seven Perseid spectra, obtained with the same instrument, has revealed five instances in which the auroral green line of O I at 5577 Å is visible. All of the seven spectra were photographed during the showers of 1948–50, five of them within a 31-hour period.

An inverse correlation appears to exist in these spectra between the strength of the auroral line and that of the H and K lines of ionized calcium. The points of appearance and disappearance of the auroral line relative to those of other lines were consistently similar.

A consideration of several other meteor spectra indicated little if any correlation between the occurrence of the green line and general solar activity. There is, however, no evidence contrary to Halliday's findings that the green line appears only in the spectra of high-velocity meteors.

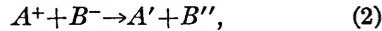
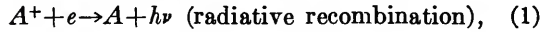


# Negative Ions and Luminosity in Meteor Trails

By T. R. Kaiser <sup>1</sup>

The work reported here forms part of a theoretical study of the processes of dissipation of ionization in meteor trails and, as it is hoped to report this more fully elsewhere, the relevant parts of the theory are given only in outline.

The main causes for decay of volume electron density in a meteor trail are diffusion (molecular and eddy), electron-ion recombination, and negative ion formation. The latter is complicated somewhat through the competing processes of electron detachment and mutual neutralization of positive and negative ions. Both recombination and mutual neutralization can contribute to the meteor train luminescence through the processes



where the primes denote excited states. The positive ions will be the products of collisional ionization and the negative ions will be  $O_2^-$  and  $O^-$ , produced by electron attachment. In the meteor height region molecular oxygen is predominant.

## Formulation of the problem

The expressions for the rate of change of volume density of the various ionic species are:

$$\frac{\partial n_e}{\partial t} = D\nabla^2 n_e - a_1 n_e + a_2 n_- - a_3 n_e n_+, \quad (3)$$

$$\frac{\partial n_-}{\partial t} = D\nabla^2 n_- + a_1 n_e - a_2 n_- - a_4 n_- n_+, \quad (4)$$

$$\frac{\partial n_+}{\partial t} = D\nabla^2 n_+ - a_3 n_e n_+ - a_4 n_- n_+, \quad (5)$$

$$n_+ = n_e + n_-, \quad (6)$$

where  $n_e$ ,  $n_-$  and  $n_+$  are the volume densities

<sup>1</sup> University of Sheffield, England.

of electrons, negative and positive ions respectively. The diffusion coefficient  $D$  is treated as a constant, identical for all species. While this will be essentially true in the absence of heavy negative ions, it is only an approximation in the general case. However, from a generalization of the theory of ambipolar diffusion (Kaiser, 1953), it seems that it is not likely to vary by more than a factor of two. The terms  $a_1$ ,  $a_2$ ,  $a_3$ , and  $a_4$  are the rate coefficients for attachment, detachment, recombination, and mutual neutralization, respectively;  $a_1$  will be proportional either to molecular density  $n \text{ cm}^{-3}$  for radiative attachment, or to  $n^2$  for three-body attachment in which the excited negative ion is stabilized by collision;  $a_2$  will be proportional to  $n$  for collisional detachment or constant for photo-detachment;  $a_3$  will be constant since recombination appears to be radiative (Kaiser and Greenhow, 1953; Kaiser, 1953). The contribution of recombination to train luminosity has been discussed by Kaiser (1955). A reassessment of this process suggests that it may be significant for the brightest meteors but that generally it is likely to be less important than mutual neutralization. In the present analysis, therefore, we will neglect it and put  $a_3 = 0$ .

The most important quantity for radio meteor studies is the electron line density,  $\alpha_e \text{ cm}^{-1}$ . The corresponding quantities for the other species are  $\alpha_+$  and  $\alpha_-$ . Since, if  $a_3 = 0$ , positive ions can disappear only by neutralization with heavy negative ions, the total train intensity is given by the expression,

$$I = -q \frac{d\alpha_{\pm}}{dt}. \quad (7)$$

If we take  $q$  as the mean number of photons produced in reaction (2),  $I$  will be measured in photons per second per cm length of train.

**Solutions to equations 3 to 6 ( $a_3=0$ )**

We will assume the trail is formed with negligible radius at time  $t=0$ .

(i)  $a_2=0$ .

Equation (3) becomes

$$\frac{\partial n_e}{\partial t} = D\nabla^2 n_e - a_1 n_e \tag{8}$$

with the solution (Kaiser, 1953)

$$\alpha_e = \alpha_0 e^{-a_1 t}, \tag{9}$$

where

$$n_e = \frac{\alpha_e}{4\pi Dt} \exp\left(-\frac{r^2}{4Dt}\right) \tag{10}$$

and  $\alpha_0$  is the initial electron and positive ion line density. This solution has been used to derive values of  $a_1$  from long enduring radio echoes (Kaiser, 1953; Davis, Greenhow, and Hall, 1959a, 1959b).

Equations (4) and (5) contain the non-linear neutralization terms and are not amenable to exact analytic solution.

(ii)  $a_4=0$ .

This is not directly helpful for the train problem since it gives  $I=0$ ; however, it is capable of exact solution which may be of value in radio-echo studies and is helpful in obtaining an approximate solution when  $a_4$  is sufficiently small (see below). The solutions are:

$$\alpha_e = \frac{\alpha_+}{1 + a_2/a_1} \left[ a_2/a_1 + \exp(-(a_1 + a_2)t) \right], \tag{11}$$

$$\alpha_- = \frac{\alpha_+}{1 + a_2/a_1} \left[ 1 - \exp(-(a_1 + a_2)t) \right]. \tag{12}$$

$$\alpha_+ = \alpha_0 = \text{constant}$$

For all ionic species

$$n = \frac{\alpha}{4\pi Dt} \exp\left(-\frac{r^2}{4Dt}\right).$$

When  $t$  becomes large compared with  $(a_1 + a_2)^{-1}$ ,

$$\alpha_e \rightarrow \frac{\alpha_0 a_2}{a_1 + a_2},$$

$$\alpha_- \rightarrow \frac{\alpha_0 a_1}{a_1 + a_2}$$

The form of the electron and negative ion decay is illustrated in figure 1.

(iii)  $a_4 \neq 0$ .

Approximate solutions have been found for extreme cases of slow and rapid neutralization.

(a)  $x_4 = \frac{a_4 \alpha_0}{8\pi D} \ll 1$ . Here  $\alpha_e$  and  $\alpha_-$  are given approximately by solutions (11) and (12), with  $\alpha_+$  decreasing with time:

$$\alpha_+ \approx \frac{\alpha_0}{1 + \frac{x_4 a_1}{a_1 + a_2} f(\tau)}, \tag{13}$$

$$-\frac{d\alpha_+}{dt} \approx \frac{x_4 a_1 \alpha_0 (1 - e^{-\tau})}{\tau \left[ 1 + \frac{x_4 a_1}{a_1 + a_2} f(\tau) \right]^2}, \tag{14}$$

where

$$\tau = (a_1 + a_2)t$$

and

$$f(\tau) = \int_0^\tau \frac{1 - e^{-\tau}}{\tau} d\tau.$$

The train luminosity will follow equation (14) and will have decayed significantly when  $\tau \sim 1$ , i.e.,  $t \sim (a_1 + a_2)^{-1}$ .

The initial intensity  $I_0$  is, from equations (7) and (14):

$$I_0 \approx q x_4 a_1 \alpha_0. \tag{15}$$

(b)  $x_4 \gg 1$ . In this case the negative ion volume density rises rapidly (instantaneously for zero initial radius) to  $n_- \approx a_1/a_4$  and maintains this value throughout the region of the column of ionization where  $n_e/n_-$  exceeds  $a_2/a_1$ ; beyond this limit it is proportional to

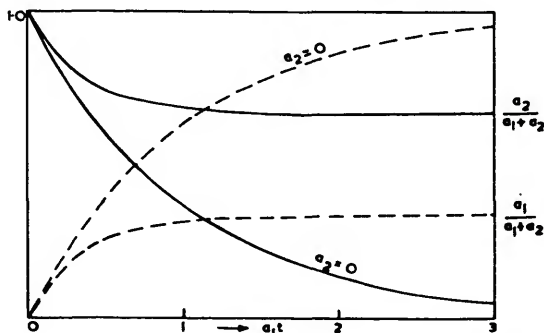


FIGURE 1.—Variation of electron and negative ion line density for  $a_4=0$ . Solid line,  $\alpha_e/\alpha_0$ ; broken line,  $\alpha_-/\alpha_0$ .

$n_e(n_-/n_e \simeq a_1/a_2)$ . If also  $x_4 a_1/(a_1+a_2) \gg 1$ , we get

$$I = -q \frac{d\alpha_+}{dt} \simeq I_0 e^{-a_1 t}, \quad (16)$$

$$I_0 \simeq q a_1 \alpha_0, \quad (17)$$

where equation (16) remains valid to  $t \gg a_1^{-1}$ . If  $x_4 \gg 1$  but  $x_4 a_1/(a_1+a_2) \ll 1$  (which requires  $a_2 \gg a_1$ ) the initial intensity is still approximately as given by equation (17) but the decay is more rapid and it is estimated that the intensity will fall to a fraction of its initial value in a time

$$t \sim \frac{x_4}{a_1+a_2} \ll a_1^{-1}. \quad (18)$$

The significance of the above is that, provided  $x_4 \gg 1$ , negative ions are initially mopped up by neutralization before detachment can operate and, unless  $a_2$  is extremely large compared with  $a_1$ , this will continue to  $t \gg a_1^{-1}$ .

In the limiting case,  $a_2=0$ , it is possible to interpolate graphically to obtain solutions for intermediate values of  $x_4$ ; these are given in figure 2.

#### Interpretation of experimental data

Hawkins and Howard (1959) have analyzed in detail the decay of luminosity in a train photographed with a Baker Super-Schmidt

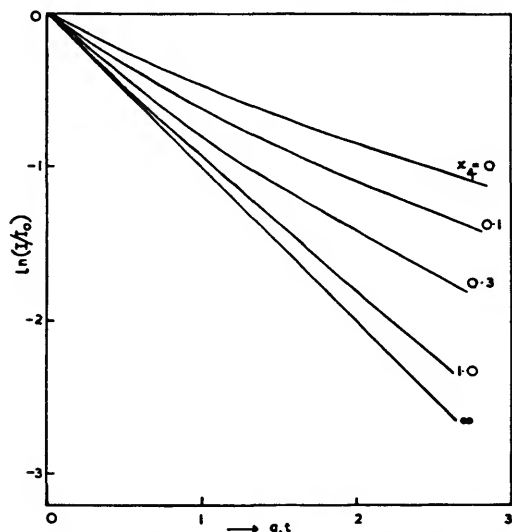


FIGURE 2.—Decay of train intensity for various values of  $x_4$  ( $a_2=0$ ).

camera, over the atmospheric height range 84 to 93 km. They find the decay to be exponential with a duration which increases with height (i.e., with decreasing atmospheric density). They have also estimated the rate of train decay for a long enduring train observed by Liller and Whipple (1954), which suggests that the duration is a maximum at about 92.5 km and decreases above this height. They infer that the decay of light from both normal and long-enduring trains follows an exponential law and that the rate of decay is a well-defined function of height. The decay constants obtained by Howard and Hawkins are plotted in figure 3 as a function of height and atmospheric molecular density  $n \text{ cm}^{-3}$ , the latter as given by Nicolet (1959). The decay constant is defined as  $dM/dt$ , where  $M$  is the train magnitude.

These results strongly suggest that below 92.5 km the decay obeys equation (16) (equation (15) with  $x_4 \ll 1$ , will be shown to lead to too low a value for the initial intensity). Liller and Whipple suggest that the increasing decay constant (decreasing duration) at greater heights is due to diffusion. This would imply that the trails become resolved and hence surface brightness rather than total intensity is recorded.

For an unresolved train, equation (16) gives

$$\frac{dM}{dt} = 1.09 a_1; \quad (19)$$

hence  $a_1$  can be deduced directly from experiment. The theoretical initial decay rate for a finite resolving power has been evaluated on the assumption that the camera records a line source as having a brightness profile  $\exp(-x^2/x_1^2)$ , where  $x$  is measured along the normal from the axis of the image. It is further assumed that  $D \propto n^{-1}$  and the two extremes of radiative and three-body attachment are considered separately.

(a) Radiative attachment,  $a_1 \propto n$ :

$$\frac{dM}{dt} = 1.09 a_{1 \text{ min}} \left( \frac{n}{n_{\text{min}}} + \frac{n_{\text{min}}}{n} \right). \quad (20)$$

(b) Three-body attachment,  $a_1 \propto n^2$ :

$$\frac{dM}{dt} = 1.09 a_{1 \text{ min}} \left[ \left( \frac{n}{n_{\text{min}}} \right)^2 + 2 \frac{n_{\text{min}}}{n} \right], \quad (21)$$

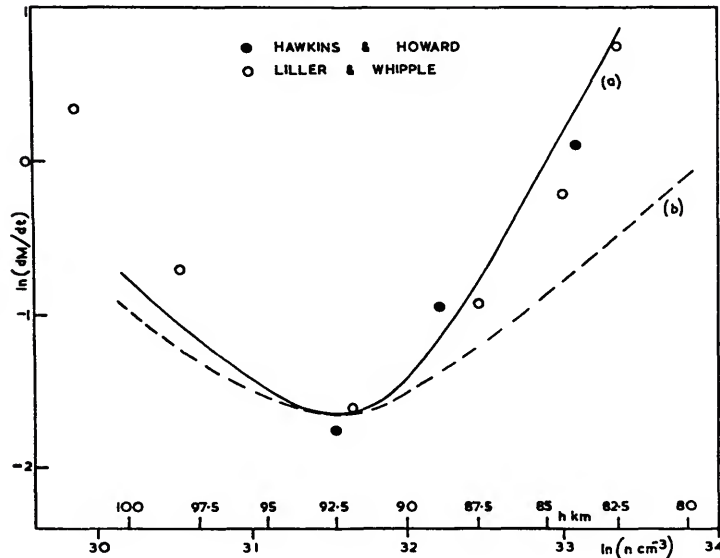


FIGURE 3.—Train decay rate,  $dM/dt$  magnitude  $\text{sec}^{-1}$ , as a function of atmospheric density and height. The theoretical curves, which are discussed in the text, are derived for three-body (a) and two-body (b) attachment.

where the subscript "min" refers to the values corresponding to minimum  $dM/dt$ . The result of fitting the formulas (20) and (21) to the experimental results is illustrated by the curves plotted in figure 3. It is clear that the experimental data strongly support three-body attachment, at least below 92.5 km. In fitting formula (21) we obtain  $a_{1 \text{ min}} = 6 \times 10^{-2}$  and hence

$$a_1 = 2.5 \times 10^{-29} n^2 \text{ sec}^{-1} \quad (22)$$

for the relation between attachment coefficient and total molecular density. The result also implies that  $a_2 \gg a_1$  and  $x_4^2 \gtrsim 1$  up to 92.5 km. If we take  $D = 5 \times 10^4$  at this level (Greenhow and Lovell, 1960) and note that trains have been observed for meteors as faint as magnitude +2.5 (Hughes, 1959) for which  $\alpha_0 \sim 10^{13} \text{ cm}^{-1}$  (Kaiser, 1953) we obtain a limit for the mutual neutralization coefficient, namely,

$$a_4 \gtrsim 10^{-7} \text{ cm}^3 \text{ sec}^{-1}. \quad (23)$$

In deriving expression (21) we obtain a relation for the camera resolution, characterized by  $x_1$ :

$$x_1 = (D_{\text{min}}/a_{1\text{min}})^{1/2}. \quad (24)$$

Substituting the above values we get  $x_1 \sim 9$  meters, which implies a resolvable train diameter of the order of 20 meters. This agrees well with Whipple's estimate of the order of 30 meters for the Baker Super-Schmidt cameras (Liller and Whipple, 1954).

In spite of the above, the explanation of the increasing decay constant above 92.5 km as due to diffusion is not completely convincing, particularly if one considers in more detail the form of the decay in surface brightness with time. However, although one could speculatively suggest additional explanations, this is hardly justified until more experimental data are available.

#### The relation between meteor and initial train magnitude

If the meteor produces  $p$  photons through collisional excitation for each electron and we ignore any difference between meteor and train spectral distribution, then, for  $x_4 \gg 1$ ,

$$\begin{aligned} \delta M &= M_{\text{train}} - M_{\text{meteor}} \\ &\sim 2.5 [\log_{10}(p/q) - \log_{10}(a_1 T)], \quad (25) \end{aligned}$$

provided  $a_1 T < 1$ .  $T$  is the instrumental integrating time and  $M_{\text{train}}$  is the initial train

magnitude. If the ionizing and luminous efficiencies are assumed to be of the same order (Kaiser, 1953), then  $p/q$  will be of order unity and

$$\delta M \sim -2.5 \log_{10} (a_1 T). \quad (26)$$

Thus, for instance, with  $T=0.5$  second for the first train exposure we expect  $\delta M$  to be about zero at 82.5 km, +3 at 90 km, and +7 at 100 km. These values might be optimistic at the lowest height due to the finite delay in operating the camera; generally they appear to be quite reasonable in order of magnitude. They do imply that slow neutralization ( $x_4 \ll 1$ ) would produce much fainter trains than are observed.

It should be noted that for  $p/q \sim 1$ , the integrated train intensity,  $\int_0^\infty I dt$ , will be of the same order as the meteor intensity.

### Discussion

It is suggested that the train decay observed with the Harvard cameras is due to negative ion formation followed by mutual neutralization, leaving the resultant atoms in excited states. The attachment appears to be a three-body reaction and to determine the train decay constant below 92.5 km; at greater heights the increased decay constant may be controlled by diffusion, due to the finite resolving power of the instruments. It would clearly be very useful in future experiments to arrange that the trains remain unresolved at all heights in order to avoid the latter complication. According to Dr. J. Davis (private communication), photoelectric recording of trains is feasible and has some desirable features as compared with the photographic technique, particularly as in principle it can be used to record directly the total light emitted from a small section of a train as a function of time. A comparison between the integrated train intensity  $\int I dt$  and the meteor intensity would lead to an estimate for the ratio  $p/q$ .

Finally, the attachment coefficient arrived at here may be compared with the values estimated from very long-enduring radio echoes. It is interesting to note that the former is associated with the decrease of  $d\alpha_+/dt$  (which is approximately equal to  $d\alpha_e/dt$ ) with time,

whereas the lifetime of the echoes is dependent directly on the decrease of  $\alpha_e$  with time. The importance of attachment in radio echo studies of meteors was pointed out some years ago by the author (Kaiser, 1953) and a value was found for the coefficient which corresponds, in the present terminology, to  $a_1 \sim 0.03 \text{ sec}^{-1}$  at 95 km height. Recently Davis et al. (1959a, 1959b) have derived coefficients for the same height which range between 0.015 and 0.025  $\text{sec}^{-1}$ . In comparison, the relation (22) gives  $a_1 = 0.026 \text{ sec}^{-1}$  at 95 km height.

### Note added October 1962

Further consideration has suggested an alternative (or additional) mechanism to explain the increasing decay constant above 92.5 km in the observations of Liller and Whipple (fig. 3). It arises if the quantity  $x_4 a_1 / (a_1 + a_2)$  is less than unity even though  $x_4 > 1$ , which may occur on the rising portion of the meteor ionization curve if, as suggested,  $a_1 \propto n^2$  while  $a_2 \propto n$ . The minimum decay constant (maximum train duration) will be found near the height at which

$$a_2 \sim a_1 x_4. \quad (27)$$

At greater heights, the train duration, from equation (18), becomes

$$t \sim \frac{a_1 \alpha_0}{8\pi D a_2}. \quad (28)$$

Hence, since  $D \propto n^{-1}$  and  $a_2 \propto n$ , we obtain  $t \propto \alpha_0$ ; i.e., on the rising part of the ionization curve the duration will decrease with increasing height. Since, from intensity considerations, we still require  $x_4 > 1$ , equation (27) enables a lower limit to be set for the detachment coefficient  $a_2$ , namely,  $a_2 > 6 \times 10^{-2} \text{ sec}^{-1}$  at 92.5 km, and generally  $a_2 > 10^{-15} n$ .

### References

- DAVIS, J.; GREENHOW, J. S.; AND HALL, J. E.  
 1959a. Combined photographic and radio echo observations of meteors. Proc. Roy. Soc. London, ser. A, vol. 253, pp. 121-129.  
 1959b. The effect of attachment on radio echo observations of meteors. Proc. Roy. Soc. London, ser. A, vol. 253, pp. 130-139.

- GREENHOW, J. S., AND LOVELL, A. C. B.  
1960. The upper atmosphere and meteors. *In* Physics of the upper atmosphere, J. A. Ratcliffe, ed., pp. 513-549. Academic Press, New York.
- HAWKINS, G. S., AND HOWARD, W. E.  
1959. Decay of light from a meteor train. *Astrophys. Journ.*, vol. 130, pp. 1003-1007.
- HUGHES, R. F.  
1959. Meteor trains. *Smithsonian Contr. Astrophys.*, vol. 3, no. 8, pp. 79-94.
- KAISER, T. R.  
1953. Radio echo studies of meteor ionization. *Advances in Physics (Phil. Mag. Suppl.)*, vol. 2, pp. 495-544.
1955. Meteors. *Spec. Suppl. Journ. Atmosph. Terr. Physics*, vol. 2. Pergamon Press, New York.
- KAISER, T. R., AND GREENHOW, J. S.  
1953. On the decay of radio echoes from meteor trails. *Proc. Phys. Soc. London*, vol. 66B, pp. 150-151.
- LILLER, W., AND WHIPPLE, F. L.  
1954. High-altitude winds by meteor-train photography. *In* Rocket exploration of the upper atmosphere, R. L. F. Boyd and M. J. Seaton, eds., pp. 112-130. Interscience, New York.
- NICOLET, M.  
1959. The constitution and composition of the upper atmosphere. *Proc. Inst. Radio Eng.*, vol. 47, pp. 142-147.

### *Abstract*

The decay of meteoric ionization due to the combined effects of diffusion, electron attachment and detachment, and mutual neutralization of positive and negative ions, has been studied theoretically. It is proposed that the excited neutral atoms resulting from mutual neutralization produce meteor train luminosity. Interpretation of experimental data, in the light of the theory, leads to values for the electron attachment coefficient which agree reasonably with those obtained from radio observations and suggests that attachment occurs through a three-body process.

# Luminosity from Large Meteoric Bodies

By H. Julian Allen<sup>1</sup> and Kenneth K. Yoshikawa<sup>1</sup>

It is usual in meteor theory to ascribe the origin of the luminosity of meteors to collisions of air molecules with the surface molecules of the meteoric body. In this case the rate of removal of mass from the surface is directly proportional to the luminosity, which affords a most convenient means for analysis of meteor flight. It seems not to be generally appreciated that the above procedure must be restricted to meteoric bodies which experience free-molecule flow—that is, to those bodies which are small compared to the mean free path of the air molecules.

For meteoric bodies in continuum flow, wherein the body is large compared to the air mean free path, the air molecules approaching the body enter into a highly compressed layer of gas which precedes the body itself. Lindemann and Dobson (1923) aptly called this layer the “protective gas cap.” The most energetic collisions in the case of such flow occur between the air molecules in the atmosphere and in this gas cap. The resulting luminosity from the gas cap is not a consequence of mass-loss rate of surface molecules, but the radiation from it may be a principal source of aerodynamic heating of the meteoric body and thus cause removal of mass by ablation. Plate 1 gives an illustration of gas-cap radiation from a body as photographed in a shock-tube wind tunnel at Ames Research Center. The airspeed is only 4.3 km/sec with the ideal gas temperature in the shock layer at about 4500° K, yet the luminous gas cap near the bow of the body and near the control surface for this simulated space vehicle is clearly evident. It should be noted that at the instant this photograph was taken, no ablation of the surface of this metal model was occurring.

## Gas-cap radiation

During the development of long-range ballistic missiles and, more recently, of space vehicles intended to enter the atmosphere of earth or other planets, the problem of gas-cap radiation was readily recognized (see, e.g., Allen and Eggers, 1958) by aerodynamicists as one that would require considerable study if satisfactory heat shields were to be designed for such vehicles.

An intensive effort, both theoretical and experimental, has been made to understand the phenomenon (Kivel and Bailey, 1957; Kivel, 1959; Armstrong, 1959; Hochstim, 1957; Ziemer, 1960; Meyerott, Sokoloff, and Nicholls, 1960; Yoshikawa and Wick, 1961; Camm, Kivel, Taylor, and Teare, 1959). The phenomenon is a complex one and far from well understood. The experimental studies, moreover, have not been carried into the speed regimes of most meteors. Thus, in the following paragraphs concerning gas radiation it must be constantly borne in mind that the description of the phenomenon is probably incomplete, and the magnitudes discussed are extrapolations of our present knowledge.

When continuum air is compressed on entering a gas cap of a meteoric body, it is drastically slowed down relative to the body. The high kinetic energy of the stream is then almost entirely converted to heat. The translational, rotational, and vibrational modes of the molecules are first excited. At meteor speed the energy is sufficient, moreover, to dissociate and ionize a large fraction of the air in the cap. These atomic and molecular species become the sources of the radiation. In addition, time is required to establish equilibrium between the gas species during and following the compression transient so that the amount of the radiation is a function of this time of relaxation. The whole process then can be visualized as

<sup>1</sup>National Aeronautics and Space Administration, Ames Research Center, Moffett Field, Calif.

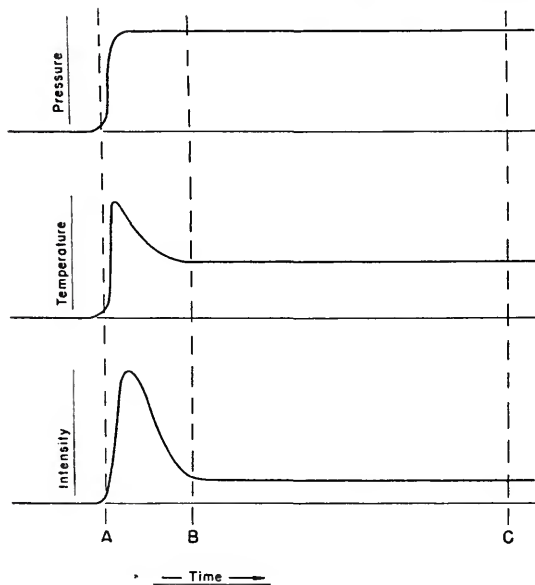


FIGURE 1.—Variation of pressure, temperature, and radiation in air following shock compression.

shown in figure 1. During the initial compression ("A") the temperature attains values approaching that corresponding to an ideal molecular gas; it then decreases as energy is diverted to dissociate and ionize the molecules and to form interim molecules until chemical equilibrium is established. The level of radiation takes somewhat longer to subside to an equilibrium value. The radiation intensity received by the body surface therefore depends upon the position of the surface relative to this time-dependent process. If the air density in

the gas cap is low, the time scale is such that the body surface may be in the position relatively close to the start of the original compression, as at "B" (fig. 1). The radiation will then be principally from "out-of-equilibrium" air. On the contrary, if the gas-cap density is high, the whole of the transient behavior will occur in a much shorter time and hence effectively farther from the body. In this case "C" may represent the position of the body so that the radiation received may be well approximated by the equilibrium value as the integrated mean, provided the density is not so high that reabsorption occurs within the layer. Where reabsorption occurs, the radiation, of course, becomes limited.

Using the results of Yoshikawa and Wick (1961), we have calculated the radiative heat-transfer coefficient in equilibrium flow  $\lambda\sigma_B$ , which the body receives from the gas cap. For this purpose it was assumed that the total volume of the radiating cap is the product of the frontal area of a sphere of radius  $r$  and the thickness of the gas cap. The results are shown in figure 2.

The out-of-equilibrium effects were obtained by extrapolating data from AVCO (Camm, Kivel, Taylor, and Teare, 1959) and Ames Research Center (e.g., Allen, 1961) with the assumption that the total gas-cap radiation is limited to about 15 percent of the total energy as a maximum since body size or reabsorption within the gas would limit further losses. (Note that the "black body" limit was far above this.) The results are shown in figure 3.

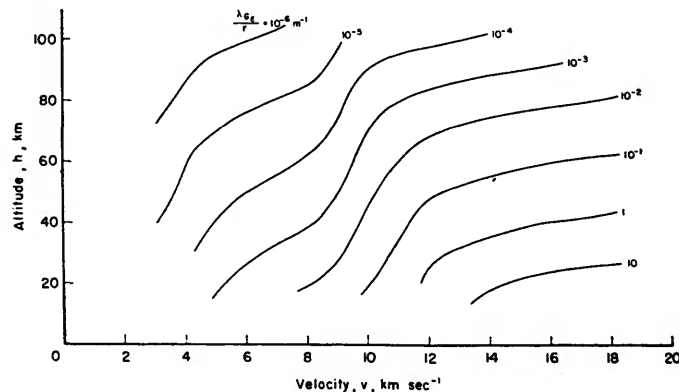


FIGURE 2.—Radiative heat-transfer from the gas cap of a sphere for air in chemical equilibrium

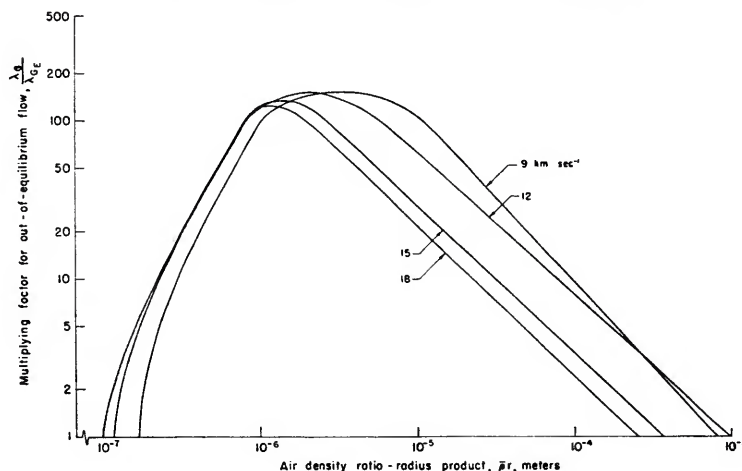


FIGURE 3.—Radiative heat-transfer coefficient for air out of chemical equilibrium.

Thereon  $\lambda_G$  is the radiative heat-transfer coefficient for the air out of chemical equilibrium, and  $\bar{\rho}$  is the ratio of the ambient air density  $\rho$  at altitude  $h$  to that at sea level,  $\rho_0$ . The ratio  $\lambda_G/\lambda_{GE}$  will be less than unity for large values of  $\bar{\rho}r$  when reabsorption becomes important.

**Theory for meteors, including continuum flow**

The equations for acceleration and mass loss rate for all meteor air flow regimes are given in the following. The notation used is that of Jacchia (1948).

The equation of motion, which relates the acceleration of the meteoric body to its mass and to the drag it experiences in flight, is the familiar one

$$\frac{dv}{dt} = -\frac{\gamma \rho v^2 A}{m^{1/3}}, \tag{1}$$

where  $v$  is velocity,  $m$  is mass,  $\rho$  is air density,  $\gamma$  is drag coefficient, and  $Am^{2/3}$  is the effective cross-sectional area.

The time rate of change of mass may, in principle, be obtained in two ways: On the one hand, since for meteoric bodies of all but the smallest in size, (1) the heat radiated from the body is negligible compared to the heat transferred to it, and (2) the rate of heat transfer to the surface is so large that the interior temperature is essentially unchanged during the descent through the atmosphere, heat

input to the body surface must appear as ablation of the surface. Thus

$$\frac{dm}{dt} = -\frac{\lambda \rho v^3 A m^{2/3}}{2\zeta}, \tag{2}$$

where  $\zeta$  is heat of ablation (the heat energy absorbed by a unit mass of the body during ablation), and  $\lambda$  is the heat-transfer coefficient.

On the other hand, it is well known that the ablated mass from meteoric bodies in free-molecule flow emits radiation (see, e.g., Öpik, 1958). For continuum flow it is again to be expected that a fraction of the total radiation resulting from ablation can be related to the time rate of change of mass by the equation

$$\frac{dm}{dt} = -\frac{2(I - I_G)}{\tau_0 v^3}, \tag{3}$$

where  $I$  is the total radiation,  $I_G$  is the gas-cap radiation, and  $\tau_0$  is the luminous efficiency factor.

In the determination of mass loss for meteoric bodies in free-molecule flow (which constitute nearly all of the observed meteors), it has been customary to put all of the reliance on equation (3) rather than equation (2). The reasons for accepting equation (3) are:

(i) The gas-cap radiation ( $I_G$ ) must be zero for free-molecule flow.

(ii) The luminous efficiency can be calculated from rather well-established physical principles.

The reasons for rejecting equation (2) are:

(i) In free-molecule flow, the heat-transfer

coefficient  $\lambda$  is dependent upon the accommodation coefficient which is a relatively unknown quantity at this time. It is true that the drag coefficient  $\gamma$  is also a function of the accommodation coefficient, so it might be thought that in some artful way knowledge of  $\lambda$  could be obtained from its relation with  $\gamma$ . Such a course does not appear profitable because a change in the accommodation coefficient to produce a change in  $\gamma$  from one to about two is sufficient to change  $\lambda$  all the way from one to zero.

(ii) Only the upper limit for  $\zeta$  (i.e., that corresponding to vaporization) can be established. The lower limit is uncertain. If no flaring is observed so that the lower limit can be assumed to be that corresponding to ablation as a liquid, the value of  $\zeta$  may fall as low as one-sixth that for vapor ablation. If flaring occurs (and this is commonly the case), the ablation may have occurred in the solid state (by crumbling due to aerodynamic forces and thermal stress), so  $\zeta$  could conceivably be but a small fraction of the value for vaporization.

For meteors in continuum flow, it is our opinion that the order of preference may well be reversed, particularly in the case of slow meteors, which are commonly meteors of asteroidal origin.

There is less reluctance to accept equation (2) for the following reasons:

(i) The heat-transfer coefficient, which is dependent on both the radiative and the convective heating, is often far better known than it is for free-molecule flow. This is particularly true if the flow in the boundary layer is laminar, and if the gas-cap radiation is close to that for chemical equilibrium. However, as will be discussed later, lack of knowledge of the shape of the meteoric body introduces important uncertainties in the heat-transfer coefficient.

(ii) If care is exercised to exclude as a necessity integration through those trajectory points which, through evidence of flares or observed physical breakup, are suspect as regards the ability to fix  $\zeta$  within the limits of vaporization and fusion, the uncertainty in  $\zeta$  is thereby reduced. However, this uncertainty still remains a serious objection to the use of equation (2).

Perhaps the most important argument for accepting equation (2) is that equation (3) is an even less attractive one for the following reasons:

(i) The value of the gas-cap radiation will generally be a modest-to-large fraction of the total radiation emitted by the meteor, but the gas-cap radiation depends upon the size of the meteor since the gas-cap volume is a direct function of size. Equation (1) can be used to find mass but not size unless the meteor mass density is known, and this is not the usual case. Again, the unknown shape is a complicating factor.

(ii) Values of  $\tau_0$ , while presumably fairly well known for fast meteors in free-molecule flow, are not too well known even for slow meteors in free-molecule flow. In continuum flow it is to be expected that  $\tau_0$  would be much reduced, but by an unknown amount. However, it is clear from laboratory firings in ballistic ranges that  $\tau_0$  is not zero.

Certainly in time the situation will become a less pessimistic one for equation (3). Improvements in ground laboratory measurements should give fair estimates of  $\tau_0$  as well as more precise gas-cap radiation values. For observed meteors for which the meteorites are found, the knowledge of the final mass and shape, and the characteristics of the materials of which they are composed should allow considerably more reliance to be placed on both equations (2) and (3) as means for calculating the instantaneous mass along the trajectory.

#### Application of theory to Meanook Meteor 132

Millman and Cook (1959) analyzed (by equations for free-molecule flow theory) the flight of a bright meteor observed in Canada at the Meanook and Newbrook stations. The data for this meteor are given in table 1, and the observed radiation is indicated by the solid curve in figure 4. These data were of particular interest to us since, as will be demonstrated, this meteor actually experienced continuum flow during the observed portion of its descent through the atmosphere.

To analyze these data it is necessary at the outset to assume a shape for the meteoric body. Allen (1960) indicated that a sphere should approximate a body in most cases for the follow-



Gas-cap radiation from an entry body.



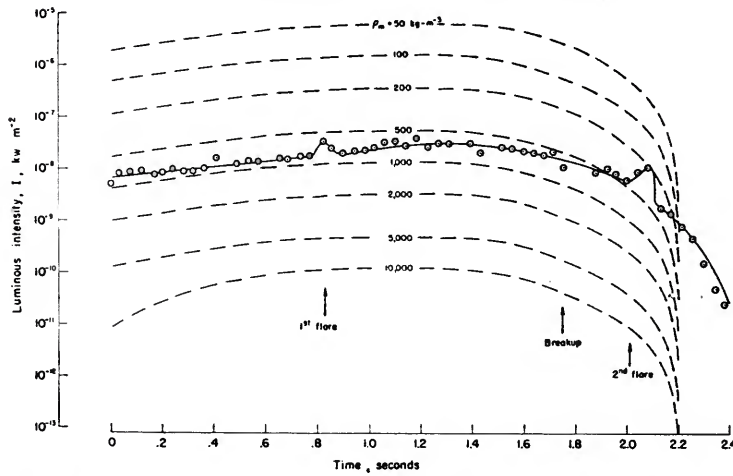


FIGURE 4.—Meanook meteor luminous intensity and comparison with gas-cap radiation for spherical bodies

ing reasons. If the body on entering the atmosphere is tumbling fairly rapidly, the mean drag force experienced will be that of a sphere. When the initial tumbling rate is low, it can be shown that the body will generally stop its rotation and, instead, oscillate about an attitude for which it is aerodynamically stable. Now it should be noted that stable attitudes are not those for which streamline flow would result. Thus rodlike or platelike shapes will assume an attitude for which the largest dimensions are perpendicular to the direction of motion. Such bodies in their high-drag attitude have approximately twice the drag coefficient of a sphere. As an opposite extreme, a right circular cone will fly with its apex forward only if the total cone angle is greater than about 40° of arc. In this case the drag is about one-fourth that for a sphere, but it should be noted that for such a shape the conical point will promptly ablate and hence the drag will be increased. On the average, then, we expect that the assumption of a spherical shape would give an error in the drag coefficient most probably less than a factor of 2. Under the assumption that the meteor is spherical, then

$$\left. \begin{aligned} Am^{2/3} &= \pi r^2 \\ m &= \frac{4}{3} \pi r^3 \rho_m \end{aligned} \right\} \quad (4)$$

where  $\rho_m$  is the meteor density.

For a sphere in continuum flow

$$\gamma = \frac{1}{2}, \quad (5)$$

thus equation (1) can be solved for the radius

$$r = -\frac{3\rho_0}{8\rho_m} \left( \frac{\bar{\rho}v^2}{dv/dt} \right). \quad (6)$$

Of course the meteor density is not known, a priori, and must be determined. Table 1 gives six values of  $v$  (not counting the extrapolated value for  $v_\infty$  given by Millman and Cook) and five of acceleration as a function of  $h$ . These data can be used to obtain a general series expression for  $v$  in the following way: Allen and Eggers (1958) have shown that when no mass is lost

$$v^2 = v_\infty^2 e^{k\bar{\rho}}, \quad (7)$$

where  $k$  is a constant (negative). When mass is lost during descent, as is the case for meteors, then  $k$  must be a function of altitude—or, more conveniently,  $\bar{\rho}$ . Thus we may express the velocity as

$$\ln v^2 = C_0 + C_1\bar{\rho} + C_2\bar{\rho}^2 + C_3\bar{\rho}^3 + \dots \quad (8)$$

so that

$$\frac{dv^2/dh}{v^2} = (C_1 + 2C_2\bar{\rho} + 3C_3\bar{\rho}^2 + \dots) \frac{d\bar{\rho}}{dh} \quad (9)$$

TABLE 1.—Observed data for Meanook Meteor 132 \*

Epoch (t) seconds	Altitude (h) meters	Speed (v) m sec <sup>-1</sup>	Luminous intensity (I) 0 <sub>m.a.g.</sub>	Acceleration (dv/dt) m sec <sup>-2</sup>
0	67.59 × 10 <sup>3</sup>	17.42 × 10 <sup>3</sup>	253.7	-----
.317			363.1	
.538			478.5	
.980			824.0	
1.0	52.71 × 10 <sup>3</sup>	16.58 × 10 <sup>3</sup>	847.5	-1.88 × 10 <sup>3</sup>
1.157			1038.0	
1.4	47.12 × 10 <sup>3</sup>	15.45 × 10 <sup>3</sup>	1087.0	-4.02 × 10 <sup>3</sup>
1.423			1057.0	
1.732			602.5	
1.8	42.11 × 10 <sup>3</sup>	13.10 × 10 <sup>3</sup>	501.5	-8.78 × 10 <sup>3</sup>
1.909			353.2	
2.0	39.98 × 10 <sup>3</sup>	11.28 × 10 <sup>3</sup>	240.0	-9.97 × 10 <sup>3</sup>
2.042			310.4	
2.086			405.5	
2.2	38.21 × 10 <sup>3</sup>	9.16 × 10 <sup>3</sup>	37.35	-11.21 × 10 <sup>3</sup>

\*Additional observations: Two pronounced flares observed at  $t=0.8$  sec and  $t=2.08$  sec (fig. 4); meteoric body observed to break in two pieces at  $t=1.75$  sec ( $h=42.63 \times 10^3$  m); velocity at entrance to atmosphere from extrapolation by Millman and Cook,  $v_{\infty}=17.59 \times 10^3$  m sec<sup>-1</sup>.

Deduced data: entry angle  $Z_R=29.8^\circ$  ( $\cos Z_R=0.868$ ). Radiant power conversion: one zero-magnitude luminous intensity equals  $2.73 \times 10^{-11}$  kilowatts-m<sup>-2</sup>.

But since the density is very nearly an exponential function of  $h$ , that is,

$$\bar{\rho} \cong e^{-\beta h}, \tag{10}$$

where  $\beta$  varies slightly with  $h$ , then

$$\frac{d\bar{\rho}}{dh} = -\bar{\rho} \left( \beta + h \frac{d\beta}{dh} \right), \tag{11}$$

and equation (9) becomes

$$\frac{dv^2}{dh} = -\bar{\rho} v^2 (C_1 + 2C_2 \bar{\rho} + 3C_3 \bar{\rho}^2 + \dots) \left( \beta + h \frac{d\beta}{dh} \right). \tag{12}$$

Now we note that since the flight path is essentially straight so that the vertical velocity is

$$\frac{dh}{dt} = -v \cos Z_R, \tag{13}$$

then

$$\frac{dv}{dt} = \frac{dv}{dh} \frac{dh}{dt} = -\frac{1}{2} \frac{dv^2}{dh} \cos Z_R, \tag{14}$$

so that

$$\frac{dv}{dt} = \frac{\bar{\rho} v^2}{2} \cos^2 Z_R (C_1 + 2C_2 \bar{\rho} + 3C_3 \bar{\rho}^2 + \dots) \left( \beta + h \frac{d\beta}{dh} \right). \tag{15}$$

Thus between equations (8) and (15) one may find the values of as many of the  $C$  coefficients as one has values for  $v$  and  $dv/dt$ , given the variation of density with altitude. In the calculations of this report, the 1959 ARDC atmosphere (AFCRC, 1959) was used for  $\bar{\rho}$  and  $\beta + h(d\beta/dh)$ . Our first attempt to find the  $C$  values using an IBM-704 computer was unsatisfactory because severe oscillations of the functions became evident for low altitudes. It was surmised that this difficulty arose because we had required equations (8) and (15) to have continuity through the altitude 42,630 meters (corresponding to Epoch 1.75 sec) where the body was observed to break into parts. Accordingly, we tried employing two sets of these equations: one above the altitude of the break and one below. These results are reasonably satisfactory, but it was necessary to reduce  $v_{\infty}$  from 17.59 km per second (Millman and Cook extrapolation) to 17.54 km per second to avoid having the radius decrease with increasing altitude at the highest altitudes. The coefficients in equations (8) and (15) in the two altitude regimes are:

for  $h > 42,630$  m

$$\left. \begin{aligned} C_0 &= 0.9772322 \times 10 \\ C_1 &= -0.5223564 \times 10^2 \\ C_2 &= -0.8908289 \times 10^5 \\ C_3 &= 0.6952320 \times 10^8 \\ C_4 &= -0.3252341 \times 10^{11} \\ C_5 &= 0.8007179 \times 10^{13} \\ C_6 &= -0.8640033 \times 10^{15} \end{aligned} \right\}; \quad (16)$$

for  $h < 42,630$  m

$$\left. \begin{aligned} C_0 &= -0.9705839 \times 10 \\ C_1 &= 0.3809221 \times 10^5 \\ C_2 &= -0.3075595 \times 10^8 \\ C_3 &= 0.1302624 \times 10^{11} \\ C_4 &= -0.3065301 \times 10^{13} \\ C_5 &= 0.3800107 \times 10^{15} \\ C_6 &= -0.1940589 \times 10^{17} \end{aligned} \right\}. \quad (17)$$

Oscillations occur also with these functions, and it would probably be best to have allowed similar discontinuities at the altitudes corresponding to the two observed flares (at Epochs  $t=0.8$  sec and  $t=2.08$  sec). However, the results obtained with the above coefficients are certainly adequate for yielding the variation of radius with altitude to evaluate gas-cap radiation  $I_G$  and heat transfer  $\lambda$  to be given later.

The calculated values of  $v$ ,  $dv/dt$ , and the product  $\rho_m r$  are given in table 2 as a function of altitude (along with the values of  $\beta+h(d\beta/dh)$  used), and are shown in figure 5. The observational data of table 1 are also shown as the circled points for comparison. The calculated product  $\rho_m r$  shows a decrease of about 20 per cent at the observed altitude of breakup.

The data of table 2 were used to determine the radius as a function of altitude for values of meteor density from 10,000 to 50  $\text{kg m}^{-3}$ . The gas-cap radiation was then evaluated in accordance with the method indicated earlier. The calculated values of  $I_G$  are plotted on figure 4 along with the total luminous intensity observed for the meteor. If  $\tau_0$  were zero, then  $I_G$  would constitute all the radiation, and the indicated density for the meteor would lie between 1,000 and 500  $\text{kg m}^{-3}$  representing one limit. To evaluate the other limit, it was assumed that Jacchia's (1948) value of  $\log \tau_0 = -18.19$  (in his units) was applicable to the ablated mass-loss rate for this meteor. From the calculated variation of the product  $\rho_m r$ , the time rate of

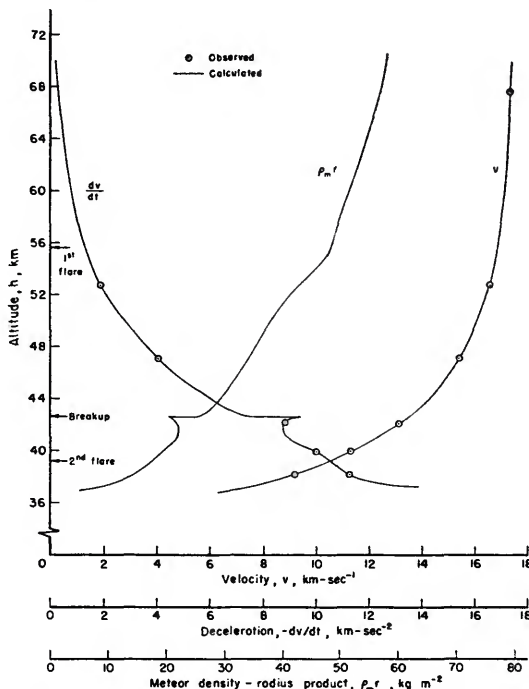


FIGURE 5.—Observed and calculated characteristics for Meanook meteor.

mass loss was calculated for the various assumed densities and the luminous intensity, from the ablated mass evaluated from the equation,

$$I_A = -\frac{1}{2} \tau_0 v^3 \frac{dm}{dt} \quad (18)$$

The sum of  $I_G + I_A$  is plotted along with observed luminous intensity  $I$  in figure 6. This limit indicates the meteor density to lie between 2,000 and 1,000  $\text{kg m}^{-3}$ . Comparing these two limits we chose water density (1,000  $\text{kg m}^{-3}$ ) as the most appropriate value, and evaluated the radius and mass as a function of altitude along with the corresponding Knudsen numbers (ratio of air mean-free-path to body radius) and the Reynolds numbers (the product of the diameter, density, and velocity divided by the absolute viscosity). From the calculated Knudsen numbers (table 2) it is clear that the meteor experienced continuum flow throughout the observed part of the descent. The Reynolds numbers are so low that the flow in the boundary layer must be laminar. With this

TABLE 2.—Calculated data for Meenook Meteor 132

h, m	v, sec <sup>-1</sup>	$\frac{dv}{dt}$ , m sec <sup>-2</sup>	$\rho_{air}$ , kg m <sup>-2</sup>	$\bar{r}$	$\beta + h \frac{d\beta}{dh}$	Kmhdn number	Reynolds number	$\lambda_{CV}$	$\lambda_{CF}$	$\lambda_G$	$(\frac{\lambda}{\sqrt{L}})_V$ sec <sup>-2</sup> m <sup>-2</sup>	$(\frac{\lambda}{\sqrt{L}})_F$ sec <sup>-2</sup> m <sup>-2</sup>	$(\frac{\lambda}{\sqrt{L}})_{exp}$ sec <sup>-2</sup> m <sup>-2</sup>	Epoch, t, sec	$\frac{I_G}{I_0 + I_A}$
70	17.457x10 <sup>3</sup>	0.1962x10 <sup>3</sup>	58.10	0.81696x10 <sup>-4</sup>	1.385x10 <sup>-4</sup>	0.0105	1.06x10 <sup>4</sup>	0.008	0.099	0.121	3.15x10 <sup>-7</sup>	3.15	1.4x10 <sup>10</sup>	-0.168	---
69	17.443	.2259	57.77	.93697	1.357	.0092	1.21	.007	.093	.127	3.42	3.15	---	-1.100	---
68	17.427	.2598	57.38	1.0717x10 <sup>-3</sup>	1.329	.0081	1.32	.007	.087	.132	3.50	3.14	16.34	-.031	---
67	17.409	.2983	56.84	1.2225	1.303	.0072	1.55	.007	.082	.135	3.54	3.11	19.54	.037	0.173
66	17.388	.3432	56.09	1.3910	1.281	.0064	1.75	.006	.078	.138	3.61	3.08	18.12	.104	.190
65	17.363	.3928	55.49	1.5788	1.255	.0057	1.95	.006	.073	.141	3.67	3.06	15.70	.172	.212
64	17.335	.4491	54.78	1.7879	1.231	.0051	2.17	.006	.069	.143	3.72	3.03	15.86	.239	.236
63	17.305	.5129	53.98	.20200	1.209	.0046	2.42	.005	.065	.145	3.76	3.01	15.34	.306	.262
62	17.287	.5847	53.16	.22773	1.188	.0041	2.68	.005	.062	.147	3.80	3.00	13.56	.374	.284
61	17.225	.6646	52.36	.25619	1.167	.0037	2.98	.005	.059	.148	3.82	2.96	11.46	.442	.329
60	17.178	.7527	51.61	.28763	1.146	.0034	3.27	.005	.056	.149	3.84	2.93	10.76	.509	.355
59	17.124	.8522	50.76	.32223	1.129	.0031	3.61	.004	.053	.150	3.86	2.91	9.08	.577	.397
58	17.083	.9590	50.11	.36045	1.109	.0028	3.94	.004	.051	.151	3.88	2.89	7.02	.644	.415
57	16.994	1.0758	49.46	.40239	1.091	.0025	4.33	.004	.049	.152	3.89	2.87	6.08	.712	.443
56	16.917	1.2023	48.86	.44841	1.074	.0023	4.74	.004	.046	.152	3.89	2.83	7.64	.780	.466
55	16.831	1.3550	47.74	.49884	1.071	.0021	5.14	.004	.044	.153	3.92	2.82	12.36	.848	.494
54	16.734	1.5495	45.84	.55401	1.089	.0020	5.44	.004	.043	.153	3.92	2.80	15.80	.916	.258
53	16.619	1.8000	43.46	.61869	1.122	.0019	5.72	.004	.042	.153	3.93	2.79	14.34	.984	.294
52	16.477	2.0918	41.40	.69661	1.151	.0017	6.08	.004	.040	.154	3.94	2.78	11.40	1.053	.339
51	16.316	2.4195	39.53	.78481	1.181	.0016	6.48	.004	.039	.154	3.94	2.76	9.54	1.122	.376
50	16.133	2.7813	37.87	.88396	1.210	.0015	6.91	.003	.037	.154	3.95	2.74	7.80	1.192	.454
49	15.925	3.1733	36.43	.99567	1.236	.0014	7.39	.003	.036	.155	3.95	2.72	6.46	1.261	.511
48	15.690	3.6014	35.11	1.1215x10 <sup>-2</sup>	1.264	.0013	7.91	.003	.034	.155	3.97	2.70	5.60	1.333	.580
47	15.416	4.0799	33.81	.12661	1.292	.0012	8.46	.003	.033	.156	3.98	2.70	5.16	1.407	.624
46	15.083	4.6456	32.40	.14452	1.322	.0011	9.04	.003	.032	.154	3.93	2.65	5.32	1.483	.640
45	14.697	5.3116	30.70	.16495	1.341	.0010	9.52	.003	.030	.151	3.86	2.60	6.12	1.561	.618
44	14.244	6.1351	28.53	.18853	1.341	.0010	9.80	.003	.030	.142	3.64	2.45	7.62	1.641	.558
43	13.705	7.2903	25.53	.21582	1.360	.0009	9.66	.003	.029	.127	3.27	2.23	9.94	1.725	.443
42	13.016	8.9394	22.46	.24742	1.375	.0009	8.85	.004	.030	.102	2.65	1.88	4.04	1.810	.574
41	12.209	8.7518	22.10	.28411	1.392	.0008	9.80	.004	.027	.074	1.94	1.44	2.80	1.900	.489
40	11.303	9.8931	19.32	.32675	1.407	.0008	9.15	.005	.027	.042	1.16	.98	7.68	1.997	.392
39	10.739	10.7939	16.49	.37642	1.423	.0008	8.08	.006	.027	.015	.52	.61	11.08	2.100	.245
38	8.680	13.2018	11.80	.43436	1.441	.0010	5.81	.008	.030	.000	.17	.20	---	2.225	---

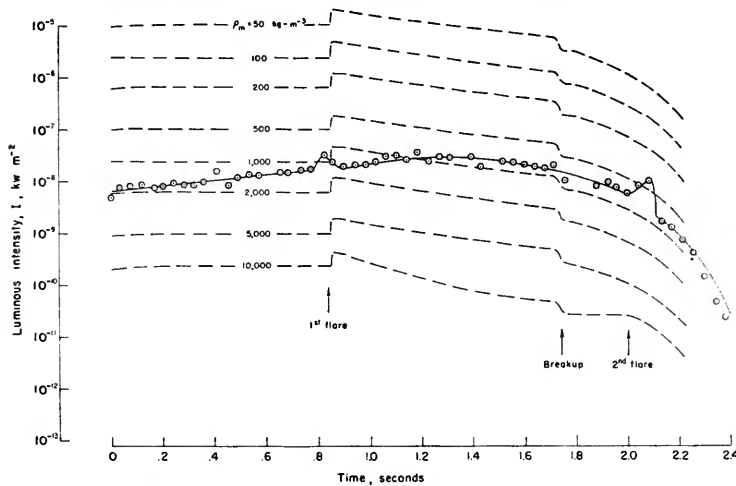


FIGURE 6.—Meanook meteor luminous intensity and comparison with sum of gas-cap and maximum ablative radiation for spherical bodies.

knowledge it is possible to estimate two limiting values for the ratio

$$\frac{\lambda}{\gamma\zeta}$$

corresponding to ablation by vaporization on the one hand, and fusion on the other. The heats of ablation used were  $8 \times 10^6 \text{ m}^2 \text{ sec}^{-2}$  and  $1.4 \times 10^6 \text{ m}^2 \text{ sec}^{-2}$  (usual values for stone), respectively, and again  $\gamma$  of  $\frac{1}{2}$  was employed. The value of the heat-transfer coefficient has two contributions, one due to radiative heating from the gas cap and the other due to the convective heating resulting from the shear in the laminar boundary layer. The radiative component,  $\lambda_{\sigma}$ , was calculated from the total gas-cap radiation as previously discussed assuming an absorptivity of unity for the surface. This value applies if either fusion or vaporization is the process of ablation. This is in contrast to the convective heating, since the convective component for ablation by fusion,  $\lambda_{c_f}$ , differs markedly from that for ablation by vaporization,  $\lambda_{c_v}$ , as discussed by Adams (1959).

For ablation by fusion, the convective heat-transfer coefficient is that which would occur for a solid body. If Lees' (1957) estimate is used (or see Chapman, 1959),

$$\lambda_{c_f} = \frac{0.000216}{\sqrt{\rho r}} \quad (19)$$

When ablation by vaporization occurs, the vapor which is pushed into the boundary layer partially fends off the hot air from the surface, thereby reducing the shear and hence the heat-transfer coefficient. The ratio of convective heat transfer for vapor ablation to that for liquid ablation may be obtained (Adams, 1959) as

$$\frac{\lambda_{c_v}}{\lambda_{c_f}} = \frac{\zeta_v}{\zeta_v + K v^2} \quad (20)$$

where for the constant  $K$  a value of 0.3 is a good average.

In table 2 values for  $\lambda_{c_f}$ ,  $\lambda_{c_v}$ , and  $\lambda_{\sigma}$  are given, and are appropriately combined to give the expected limits for  $\lambda/\gamma\zeta$  for ablation by vapor run-off and liquid run-off. The latter quantities are plotted in figure 7.

Finally, the value of  $\lambda/\gamma\zeta$  can be inferred directly from the experimental data by use of equations (2), (4), (5), and (13):

$$\frac{\lambda}{\gamma\zeta} = \frac{16\rho_m \cos Z_R}{\rho v^2} \left( \frac{dr}{dh} \right) \quad (21)$$

Since  $r$  varies somewhat erratically with  $h$ , the derivative was evaluated at any altitude  $h$  by dividing the value of  $r$  at  $h+1000$  m less  $r$  at  $h-1000$  m by the  $\Delta h=2000$  m. The resulting computed values from equation (21) are given in table 2 and plotted in figure 7. Even with the smoothing the computed values do not pro-

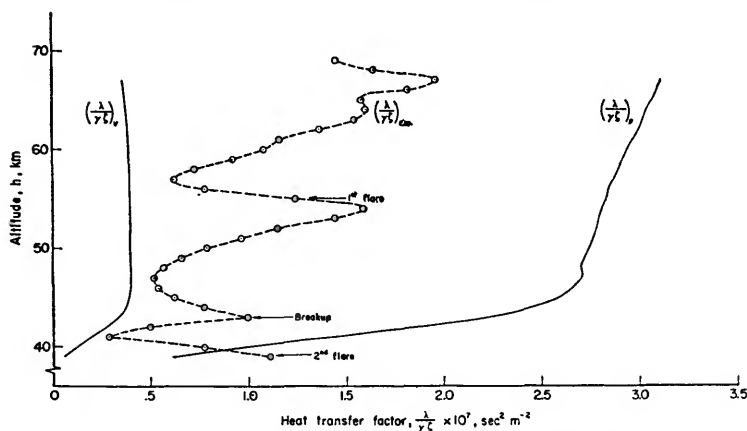


FIGURE 7.—Calculated and experimental values of the heat-transfer factor for Meanook meteor.

duce a smooth variation, but clearly it is evident that the values are reasonably close to the computed limit for vapor ablation. It should be noted, however, that this does not mean that a substantial loss of surface material in the liquid state or even the solid state does not occur, for, as has been shown by Dean R. Chapman in a yet unpublished work on the ablation of tektites, even a small fraction of ablation by vaporization serves to depress the heat transfer by convection.

### Discussion

*Light.*—It is clear, in the present case, that equation (3) for the calculation of mass cannot be used since the appropriate value of  $\tau_0$  and its variation to velocity probably bear no relation to the values and variations suggested by Öpik and Jacchia. In any event,  $\tau_0$  would be expected to be much less than that for the free-molecule regime and, since even using Jacchia's value gives the relative proportion of ablation light to gas-cap light as low as 35 percent as shown in figure 8, the difference between the total radiation and the gas-cap radiation must be so small that no precision from equation (3) could be expected.

There is a disturbing trend of the gas-cap light as compared with the observed luminous intensity shown on figure 6, since, if we match the two at any given point, the calculated gas-cap light exceeds the observed lumination at the higher speeds, but is less than at the lower

speeds. A possible reason for this is that  $\tau_0$  might vary as a negative power of velocity, but the required variation appears far more than can be considered reasonable, particularly since the ablation radiation in the present case must

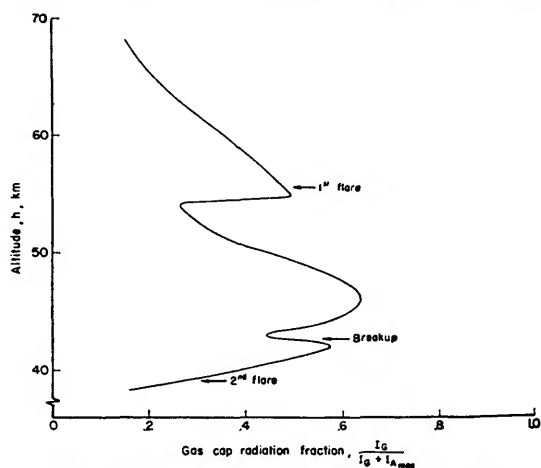


FIGURE 8.—Gas-cap radiation as a function of maximum possible total radiation.

be much smaller than we have assumed. There is no doubt that there can be a considerable error in our estimates of the gas-cap radiation, for, as noted earlier, the actual meteor body may not be near spherical in shape and no doubt changes in shape in the course of descent. Also, the gas cap is well out of chemical equilibrium over most of the range, and the meteor velocities here are beyond those for which we

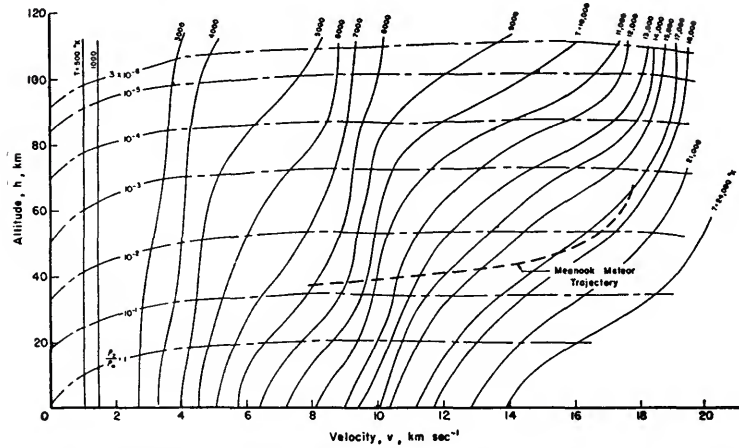


FIGURE 9.—Equilibrium gas temperature as a function of altitude and velocity.

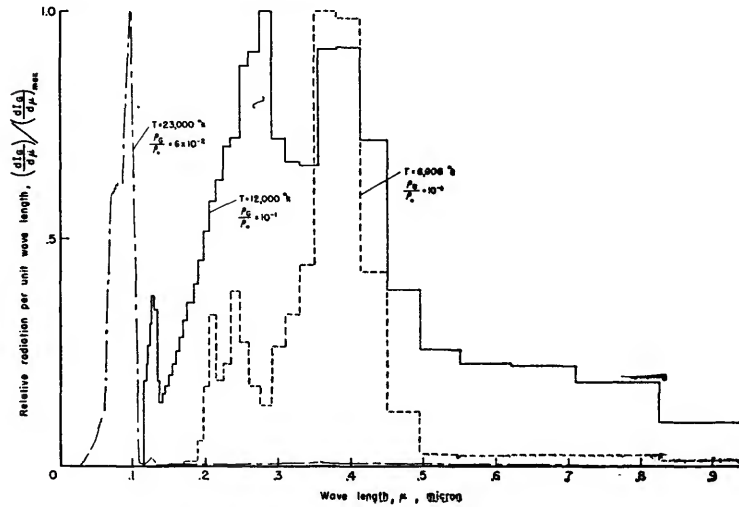


FIGURE 10.—Power spectral density of gas-cap radiation for equilibrium air.

have obtained data for gas radiation, so that the results given had to be extrapolated extensively.

However, it should be noted that errors in assessment of the gas-cap radiation may not be the principal cause for the observed differences, but rather the observed intensity interpreted as the total radiation emitted may be in considerable error itself. This can be seen from the following: In figure 9 are shown the gas-cap temperature and density as a function of velocity and altitude for equilibrium flow. The heavy dashed curve shows the trajectory of the Meanook meteor expressed in these vari-

ables. It is seen that even for equilibrium flow the gas temperature would vary from about 17,000° K early in the entry down to about 8,000° K or less near the end of the flight. For the actual gas flow, which is well out of chemical equilibrium, the maximum temperature would be considerably higher. Figure 10 shows the theoretical estimates of the power spectral density for the gas-cap radiation in equilibrium for 8,000° K and 12,000° K (Meyerott et al., 1960), and for 23,000° K (Armstrong, 1959) for a gas-cap density appropriate for the Meanook meteor. This figure shows that for wavelengths well into the

ultraviolet important contributions exist, particularly when the velocity is high. However, the observed intensity for the meteor was obtained from measurements essentially in the range from 0.3 to above 0.6 micron. Thus the observed luminous intensity approximates the total radiation emitted only near the end of the flight when the speed is low. In the early portion of the flight, when the speeds are high, the total radiation emitted must be much larger than is indicated by the plot in figure 4. In consequence, the disagreement may not be as real as the present evidence indicates. In any event, the density of the meteor is probably less than our analysis has indicated.

*Data reduction.*—It was noted earlier that a better analysis of the series solution for  $v$  and  $dv/dt$  would have been to break the solution (to avoid the necessity for continuity) at the altitudes corresponding to the two observed flares. The data, as presented by Millman and Cook, are insufficient to allow such a procedure. It would clearly be valuable to attempt to reanalyze this meteor using the original unfaired data from as many points as there were shutter breaks on the original films. However, the analysis presented gives results that, in general, agree with the observed behavior of the meteor. In particular, as noted on figure 5, the computed values of the radius-density product show an increase in negative slope at the altitudes corresponding to the flares, as would be expected. Moreover, it was noted by Millman and Cook that when the breakup of a meteor occurred, a small piece was kicked forward ahead of the main body. This could account for the unexpected slope observed for the density-radius product at altitudes just below the altitude for breakup.

*Heat-transfer factor,  $\lambda/\gamma\zeta$ .*—It is of interest to note that the experimental values for  $\lambda/\gamma\zeta$  are consistent with the observations of the flares in that an increase in  $\lambda/\gamma\zeta$  is noted near the altitudes corresponding to the flares. However, there are several other increases noted at altitudes where no flares were observed, but these may result from the fact that in the analysis the velocity function was forced to be continuous at the flare points. The required continuity promotes residual oscillations at

many points if it is called for at the altitudes corresponding to the flares.

The relation of the computed vapor ablation and liquid ablation values to the experimental values of the heat-transfer factor looks reasonable. The actual heat-transfer factor is expected to be more nearly allied with the vapor case even though a sizable fraction of the ablated material is liquid, or even solid, since the vapor blowing in the boundary layer greatly reduces the convective-heat transfer; thus the heat-transfer coefficient is well approximated by the calculated vapor value.

#### Future prospects

It is to be expected that future research in our ground laboratories will prove very useful to the meteor astronomer by providing better values for the total gas-cap radiation and its power spectral density. Moreover, it should be possible to better understand the nature of the radiation from the ablated mass in the future. Future work should also permit much better estimates for the effect of blowing due to vaporization in the boundary layer on the convective-heat transfer. The principal limitations of the ground laboratory work in the past have resulted from the fact that it was not possible to reach even the lowest of meteor speeds in the laboratory. Recently, however, we have managed to enter the meteor speed regime, and have made measurements of gas-cap radiation and ablation radiation up to speeds of 13 kilometers per second. We do not expect ever to be able to reach the highest meteor speeds, but we will probably improve the present situation materially.

Dr. McCrosky recently suggested the construction of a series of optical stations in the Mississippi Valley to track fireballs. The purpose of this system would be primarily to expedite finding the meteorites so that their radioactivity could be analyzed soon after their arrival on earth, thus improving our knowledge of cosmic origin and environment. The system McCrosky proposes could also, in our opinion, provide useful tracking data to obtain a better understanding of the heating of meteors. The analysis of Meanook Meteor 132 is very encouraging in this respect. Clearly, the

present methods are capable of giving the velocities and altitudes and the flight path with about the precision required for such analyses. Examination of the meteorite shape, mass, and material properties would play a very important part in such heat-transfer analyses. However, it is evident that not only should McCrosky's system be designed to give the best coverage for trajectory evaluation, but also the cameras themselves should be designed to give radiation response on the plates for a wide enough range of wavelengths. Also, adequate spectrographic equipment should be provided. In this way very valuable information on gas-cap and ablation radiation would be obtained for speeds far higher than we will probably be able to obtain in the laboratory.

### References

- ADAMS, M. C.  
1959. Recent advances in ablation. *Journ. Amer. Rocket Soc.*, vol. 29, pp. 625-632.
- AIR FORCE CAMBRIDGE RESEARCH CENTER  
1959. Abbreviated English tables of the ARDC model atmosphere. Geophysics Research Directorate, Air Force Cambridge Research Center, ARDC.
- ALLEN, H. J.  
1960. On the motion and ablation of meteoric bodies. In N. J. Hoff and W. G. Vincenti, eds., *Aeronautics and astronautics, Proc Durand Centennial Conference*, pp. 378-416. Pergamon Press, New York.  
1961. Problems in atmospheric entry from parabolic orbits. *Journ. Japanese Soc. Aeron. Space Sci.*, vol. 9, no. 85, pp. 43-50.
- ALLEN, H. J., AND EGGERS, A. J., JR.  
1958. A study of the motion and aerodynamic heating of ballistic missiles entering the earth's atmosphere at high supersonic speeds. Report 1381, NACA.
- ARMSTRONG, B. H.  
1959. Mean absorption coefficients of air, nitrogen, and oxygen from 22,000 to 220,000° K. Report LMSD 49759 (July 15), Lockheed Aircraft Corp.
- CAMM, J. C.; KIVEL, B.; TAYLOR, R. L.; AND TEARE, J. D.  
1959. Absolute intensity of non-equilibrium radiation in air and stagnation heating at high altitudes. Research Report 93, Avco-Everett Research Laboratory.
- CHAPMAN, D. R.  
1959. An approximate analytical method for studying entry into planetary atmospheres. Report 11, National Aeronautics and Space Administration.
- HOCHSTIM, A. R.  
1957. Gas properties behind shocks at hypersonic velocities. I. Normal shocks in air. Convair Zph(GP)-002.
- JACCHIA, L. G.  
1948. Ballistics of the upper atmosphere. Harvard Coll. Obs. and Center of Analysis, Massachusetts Inst. Tech., Tech. Rep. No. 2.
- KIVEL, B.  
1959. Radiation from hot air and stagnation heating. Research Report 79, Avco-Everett Research Laboratory.
- KIVEL, B., AND BAILEY, K.  
1957. Tables of radiation from high temperature air. Research Report 21, Avco-Everett Research Laboratory.
- LEES, L.  
1957. Recent developments in hypersonic flow. *California Inst. Tech. Publ.* 428; also, *Jet Propulsion*, vol. 27, pp. 1162-1178.
- LINDEMANN, F. A., AND DOBSON, G. M. B.  
1923. A theory of meteors and the density and temperature of the outer atmosphere to which it leads. *Proc. Roy. Soc. London*, ser. A, vol. 102, pp. 411-437.
- MEYEROTT, R. E.; SOKOLOFF, J.; AND NICHOLLS, R. W.  
1960. Absorption coefficients of air. Report LMSD 288052, Lockheed Aircraft Corp.
- MILLMAN, P. M., AND COOK, A. F.  
1959. Photometric analysis of a spectrogram of a very slow meteor. *Astrophys. Journ.*, vol. 130, pp. 648-662.
- ÖPIK, E. J.  
1958. *Physics of meteor flight in the atmosphere*. Interscience Publ., New York.
- YOSHIKAWA, K. K., AND WICK, B. H.  
1961. Radiative heat transfer during atmosphere entry at parabolic velocity. Technical Note D-1074, National Aeronautics and Space Administration.
- ZIEMER, R. W.  
1960. Extended hypervelocity gas dynamic charts for equilibrium air. *Space Technology Labs., Inc.*, TR-60-0000-09093.



# Preliminary Notes on Some Results of Photographic Multiple Meteorite Fall of Příbram

By Zd. Ceplecha<sup>1</sup>

This paper is based on the double-station photographs of the meteorite fall of Příbram. The details of this first photographic meteorite fall have been published (Ceplecha, 1961). Ten plates are available of the fall, which was photographed from two stations 40 km apart; the four stony meteorites that were recovered belong to different photographed trajectories of individual fragments.

The photographs allow the determination of the end heights of the individual fragments into which the meteorite was split. The velocity at the end point can also be found by computing the invisible ("dark") part of the trajectory. Thus it seems to be of great importance to derive theoretically the connections among different parameters at the end of the visible ("light") trajectory of a large body. This is simpler than studying the visible trajectory itself, because its end can be taken as the beginning point of the invisible trajectory.

## The end height of the visible trajectory

The thickness of the meteorite crust is usually very small relative to the dimensions of the body itself. Thus we can solve the problem by assuming a semi-infinite space full of meteorite mass, the boundary of which is a plane. Air of density  $\rho$  moves with velocity  $v$  perpendicularly to the surface of this boundary plane. Let the fraction  $\Lambda$  of the total kinetic energy of the moving air be transferred through the boundary plane into the body. Thus  $\Lambda$  is the heat-transfer coefficient. The energy in the body itself can be transferred to the air only by heat conduction. The radiation from the sur-

face is negligible in the range of temperatures under consideration.

We measure the distance  $x$  from the boundary plane into the body, and make  $x=0$  on the boundary plane. Let  $T$  be the temperature of the body in the atmosphere as a function of the time  $t$  and the distance  $x$ . Let  $T_0$  be the temperature of the whole body after a very long time;  $T_0$  is, of course, equal to the temperature of the undisturbed air. We can then define the temperature  $\tau$  according to the equation

$$T = T_0 + \tau. \quad (1)$$

If  $\lambda$  is the heat conductivity,  $\delta$  the density, and  $c$  the specific heat of the body, we can define the coefficient  $\beta$  by the equation

$$\beta^2 = \frac{\lambda}{\delta c}. \quad (2)$$

Then we can formulate our problem by the well-known equation of heat conduction:

$$\frac{\partial \tau}{\partial t} - \beta^2 \frac{\partial^2 \tau}{\partial x^2} = 0. \quad (3)$$

It is useful to choose the zero point of the time at the moment when the light trajectory ends; then

$$t_E = 0. \quad (4)$$

The initial condition for  $\tau$  can then be written in the form

$$\tau(0, 0) = \tau_E, \quad (5)$$

where  $\tau_E$  is the temperature at the surface when the light trajectory ends. The end condition, from equation (1), is then

$$\tau(\infty, x) = 0. \quad (6)$$

<sup>1</sup> Astronomical Institute of the Czechoslovak Academy of Sciences, Ondřejov, Czechoslovakia.

The boundary condition is given by the equation

$$\frac{\partial \tau}{\partial x_{z=0}} = -\frac{\Lambda \rho v^3}{2\lambda} \tag{7}$$

This is the complete mathematical formulation of the problem. The complete solution of equation (3) with the additional conditions in equations (5), (6), and (7) is not possible in analytical form. But it is possible to solve these equations exactly in analytical form if we are satisfied with a solution at one point only. This point will be the point *E*, where the light trajectory ends.

The value  $\rho v^3$  in equation (7) is an unknown transcendental function of time. An analytical function of time can be substituted on the assumption that both these functions are identical in their values and first derivatives. Then the whole problem can be solved by analytical functions.

Let us take

$$\rho v^3 = \rho_E v_E^3 e^{kt}, \tag{8}$$

where the subscript *E* denotes values on the surface of the body at the end of the light trajectory, and *k* is a coefficient which must be determined. If we use the exponential law of the air density

$$\rho = \rho_0 e^{-bz}, \tag{9}$$

then the condition of equal values and derivatives together with the drag equation will yield for *k* the equation

$$k = b v_E \cos z_E - 3\Gamma \frac{s}{m} \rho_E v_E. \tag{10}$$

Here *m* is the constant mass and *s* the constant area of the cross-section;  $\Gamma$  is the drag coefficient, and *z<sub>E</sub>* the zenith distance of the radiant. Now, if we replace the right-hand side of equation (7) by equations (8) and (10), then equations (3), (5), (6), and (7) can be solved. Without going into details of derivation, I write the solution directly

$$\tau_E = \frac{\Lambda \rho_E v_E^3 \beta}{2\lambda (-k)^{1/2}}, \tag{11}$$

where *k* is given by equation (10). This is the exact solution, but it is valid for one point only. However, we are not interested in solutions at other points. Equation (11) contains the nu-

merical factor 2, which originated from equation (7), under the assumption of a plane boundary. The energy in this case goes in only one direction. In reality, the energy is distributed over all directions in space. We shall assume uniform distribution of the energy. This assumption is supported, for the *E*-point, by the fact that there was no difference in the thickness of the crust between the front and the back of the Velka meteorite (one of the Píbram multiple fall). Then the numerical factor 2 in equation (11) will be four times greater and we arrive at the equation

$$\tau_E = \frac{\Lambda \rho_E v_E^3 \beta}{8\lambda (-k)^{1/2}}, \tag{12}$$

which is valid if we can neglect the curvature of the meteorite surface as a factor in the concentration of the heat conducted inwards. This is possible, because the dimensions of the crust of the Píbram meteorites are smaller by three orders of magnitude than the dimensions of the bodies. Numerical computations of the heat-transfer coefficient presented in the following section are based on equation (12).

The solution of the problem contains the term  $(-k)^{1/2}$ , which of course must be real. This is possible only if the equation

$$\rho_E \geq \frac{b \cos z}{3\Gamma \frac{s}{m}} \tag{13}$$

is valid. Equation (13) is a very good criterion for testing whether a meteorite of mass *m* can follow a fireball that ends at a height *h<sub>E</sub>*. The numerical values obtained from equation (13) are presented in table 1.

TABLE 1.—Critical and end heights (km) of a fireball. When *h<sub>E</sub>* of the fireball is less than the presented value, a stony meteorite of mass *m* can follow (for iron meteorites the heights are 3 or 4 km lower)

cos <i>z<sub>E</sub></i>	mass <i>m</i>				
	100 gr	1 kg	10 kg	100 kg	1,000 kg
1	37	32	27	23	17
0.5	42	36	31	27	22
0.1	55	48	42	37	32

**The heat-transfer coefficient**

Equation (12) can be used for the computation of the heat-transfer coefficient  $\Lambda$ , if other values are known. In the case of the Příbram meteorites, we have  $\rho_E$  and  $b$  from the end height  $h_E$  which was directly measured from the double-station plates. The zenith distance of the radiant  $z_E$  was also measured directly. The end velocity  $v_E$  can be computed from the dark-flight distance of meteorites, but the value is only provisional at present, because the wind-tunnel measurements have not yet been completed. The same holds true for the product  $\Gamma \frac{s}{m}$  (Ceplecha, 1961). The surface temperature at the beginning of the light trajectory of a meteor was computed by Levin (1956). It is evident that this value, giving the limiting conditions for the rapid evaporation, is the same for the end of the light trajectory. The density of the meteorites was measured, but the measurements of the heat conductivity are not yet finished. The heat conductivity  $\lambda$  is of course the main factor in equation (12), and strongly determines the numerical results. We have not yet obtained values for the heat conductivity from direct measurements, and therefore use the mean value for stony meteorites as given by Öpik (1958). Thus the numerical values given in tables 2 and 3 must be taken as provisional, and are accurate to an order of magnitude only.

TABLE 2.—Computed end-point velocity  $v_E$  (km/sec). From equation (12), with the following constants:  $\tau_E=2.1 \times 10^8$ ;  $\lambda=2 \times 10^8$ ;  $c=1 \times 10^7$ ;  $\delta=3.6$ ;  $\cos z_E=0.683$

Meteorite	Heat-transfer coefficient $\Lambda$			
	0.01	0.005	0.002	0.001
Luhý	4.0	5.3	7.6	10.1
Velká	5.2	6.9	9.9	13.1
Hojšín	5.8	7.7	11.1	14.6
Dražkov	6.5	8.5	12.3	16.3

TABLE 3.—Computed thickness  $d$  of the meteorite crust ( $m=1.5 \times 10^3$ ,  $\Lambda=0.002$ )

Meteorite	$d$ (cm)
Luhý	0.011
Velká	.009
Hojšín	.006
Dražkov	.015

Equation (12) was used to compute the end velocity  $v_E$ , with different values of  $\Lambda$ , shown in table 2. The end velocities of the same meteorites can be estimated from the computed and the observed dark-flight distances. The end velocity for the Luhý, Velká, and Hojšín meteorites was provisionally estimated to be 7 km/sec, and for the Dražkov meteorite to be 11 km/sec. Thus it is evident from table 2 that the heat-transfer coefficient at the end of the light trajectory was about 0.002 or 0.003.

**The thickness of the meteorite crust**

The solution of equations (3), (5), (6), and (7) can be presented in a more general form if we are not interested in the surface temperature alone. If  $\tau(x)$  is the temperature in the body at the distance  $x$  from the surface, then the equation

$$\tau(x) = \tau_E \exp [ -(-k)^{1/2} x / \beta ] \tag{14}$$

is valid. If we use the temperature of the melting point  $\tau_m$ , the thickness  $d$  of the meteorite crust follows from equation (14):

$$d = \frac{\beta \log \frac{\tau_E}{\tau_m}}{0.434 (-k)^{1/2}} \tag{15}$$

The theoretical thickness of the crust for  $\Lambda=0.002$  is about 0.1 mm for all the meteorites of the Příbram fall. The numerical data are presented in table 3. The measured thickness of the crust for the Velká meteorite is between 0.18 mm and 0.29 mm—about twice or three times the theoretical value. This agreement is quite good, as many provisional values were used in the computations.

**References**

CEPLECHA, ZD.  
 1961. Multiple fall of Příbram meteorites photographed. 1. Double-station photographs of the fireball and their relations to the found meteorites. Bull. Astron. Inst. Czechoslovakia, vol. 12, pp. 21–47.

LEVIN, B. J.  
 1956. The physical theory of meteors and meteoric matter in the solar system. Publ. House Acad. Sci. U.S.S.R., Moscow.

ÖPIK, E. J.  
 1958. Physics of meteor flight in the atmosphere. Interscience, New York.

*Abstract*

The theory presented in this paper can be applied to meteorite falls. The heat-transfer coefficient at the end point of the light trajectory and thickness of the meteorite crust can be computed. The preliminary value of the heat-transfer coefficient at the end points of four Příbram meteorites was estimated to be about 0.002 or 0.003. The definitive numerical values will be published in the Bulletin of the Astronomical Institute of Czechoslovakia in a series of papers entitled "Multiple Fall of Příbram Meteorites Photographed."

# Results from an Artificial Iron Meteoroid at 10 km/sec

By R. E. McCrosky<sup>1</sup> and R. K. Soberman<sup>2</sup>

The results described in this paper are derived from a successful attempt to produce a meteor in the upper atmosphere with a body of known mass and composition. This was accomplished by accelerating a small pellet of stainless steel by an air cavity charge attached to the nose of a high-speed re-entry rocket. The experiment was made possible only through the cooperation of a number of organizations. The test vehicle was a Trailblazer I rocket, developed by the Applied Material and Physics Division of the National Aeronautics and Space Administration at Langley Field, Va., for use in a re-entry research program conducted by the Massachusetts Institute of Technology Lincoln Laboratory. The optical observations described were made by the Harvard Meteor Project with considerable technical assistance from Lincoln Laboratory. The air cavity charge was constructed and tested by the Air Force Cambridge Research Laboratories.

The primary purpose of the experiment was the determination, to within narrower limits than previously available, of the efficiency with which the kinetic energy of a meteoroid is transformed to luminous energy in the photographic region. From a simple inspection of meteor spectra, one can ascertain that a great majority of the meteor luminosity is produced by the excitation of the meteoric atoms, particularly for the luminosity in the photographic (3500 to 5000 Å) region. Whether the ablation is by direct vaporization, melting, or fragmentation, the meteoritic material must be vaporized before appreciable luminosity is produced. The vaporized atoms are then excited by collision. The instantaneous intensity of a meteor must be related to the rate of

mass loss. Presumably the velocity of the meteor will also influence the rate of luminous energy production. As a minimum statement of the problem one can write:

$$I \propto -\frac{dm}{dt} f(v), \quad (1)$$

where  $I$  is the instantaneous intensity,  $m$  the meteoric mass, and  $f(v)$  some function of the velocity. The data obtained from observations of natural meteors are consistent with an expression of the form

$$I = \tau \left[ \frac{1}{2} \left( -\frac{dm}{dt} \right) \right] v^2, \quad (2a)$$

or

$$I = -\frac{\tau_0}{2} \frac{dm}{dt} v^3, \quad (2b)$$

where  $\tau_0$  is the luminosity coefficient and  $\tau = \tau_0 v$  is the ratio of the observable luminous energy to the kinetic energy.

Certainly other factors besides the mass loss and velocity also influence the luminosity, notably the composition of the meteoroid and its aerodynamical properties. But at the present time one must be content, generally, with the simplified theory implicit in equation (2). The considerations of additional factors must await a determination of such basic parameters as the meteor mass and density.

Equation (2b) may be integrated to give

$$m = m_p = \frac{2}{\tau_0} \int_t^\infty \frac{I}{v^3} dt. \quad (3)$$

Since  $I$  and  $v$  are observable quantities, the mass of the meteor can be determined if  $\tau_0$  is known. Masses determined from the observed luminosity are referred to as photometric masses ( $m_p$ ). A number of estimates of this or related quantities are available (Whipple,

<sup>1</sup> Harvard College Observatory, and Smithsonian Astrophysical Observatory, Cambridge, Mass.

<sup>2</sup> Geophysics Research Directorate of the Air Force Cambridge Research Laboratories, Bedford, Mass.

1943; Cook, 1955; Öpik, 1955; McCrosky, 1961; Cook, Jacchia, and McCrosky, in this symposium (p. 209); Lazarus and Hawkins, in this symposium (p. 221). However, the scatter in the values is extreme; a factor of more than  $10^3$  separates the highest from the lowest estimate and this uncertainty, or more, enters essentially into all mass determinations of meteors.

The mass of a meteoroid can also be determined, in principle, from the observed deceleration. The drag equation,

$$\frac{dv}{dt} = -\frac{\Gamma A \delta^{-2/3} \rho v^2}{m^{1/3}}, \quad (4)$$

includes as unknowns the drag coefficient  $\Gamma$ , the mass, and a shaped factor  $A$ . Here  $A \delta^{-2/3} = \mathbf{A} m^{-2/3}$ , where  $\mathbf{A}$  is the presentation area and  $\delta$  the density of the meteoroid. The atmospheric density  $\rho$  is known to sufficient precision at meteor heights. In view of the large uncertainties of  $m$  and  $\delta$ , one is prompted to assume reasonable values for  $\Gamma$  and  $A$  and solve equation (4) for the unknown:

$$m_a \delta^2 = \left( \frac{\Gamma A \rho v^2}{-\dot{v}} \right)^3. \quad (5)$$

If the meteoroid density were known, one could determine a "dynamic mass" ( $m_a$ ) from equation (5). There is considerable evidence (e.g., see Whipple, 1955; McCrosky, 1955; and Jacchia, 1955) that the majority of meteors, those of cometary origin, are extremely fragile. The weak structure may be associated with bodies of low density and one cannot safely assume that the density of these meteoroids is that of meteoritic stone. Until independent measures of meteor densities are made, and this is not immediately likely, equation (5) is of limited value in making estimates of masses.

If the mass can be determined from equation (3), it would appear that the density can be derived from equation (5). However, some caution is required here. The dynamical mass represents the mass of the major meteoroid body, whereas the photometric mass refers to that portion of the entire meteoroid that has not yet produced appreciable luminosity (i.e., that part which is not yet vaporized). If the entire mass consists partly of a parent body and

partly of solid or liquid fragments, these two masses should not agree and are not interchangeable. If fragmentation were the only important factor, the photometric mass would never be smaller than the dynamic mass and equation (5) would yield a lower limit on the density. Unfortunately, however,  $m_p$  may be underestimated. We have assumed in equation (3) that the entire mass has been vaporized by the end of the trajectory. This condition is reasonably well met for high-velocity meteors, but for low-velocity meteors there may be a substantial terminal mass that is not accounted for in  $m_p$ . For this reason,  $m_a$  may exceed  $m_p$  if fragmentation is absent, and the derived value of  $\delta$  would be an upper limit.

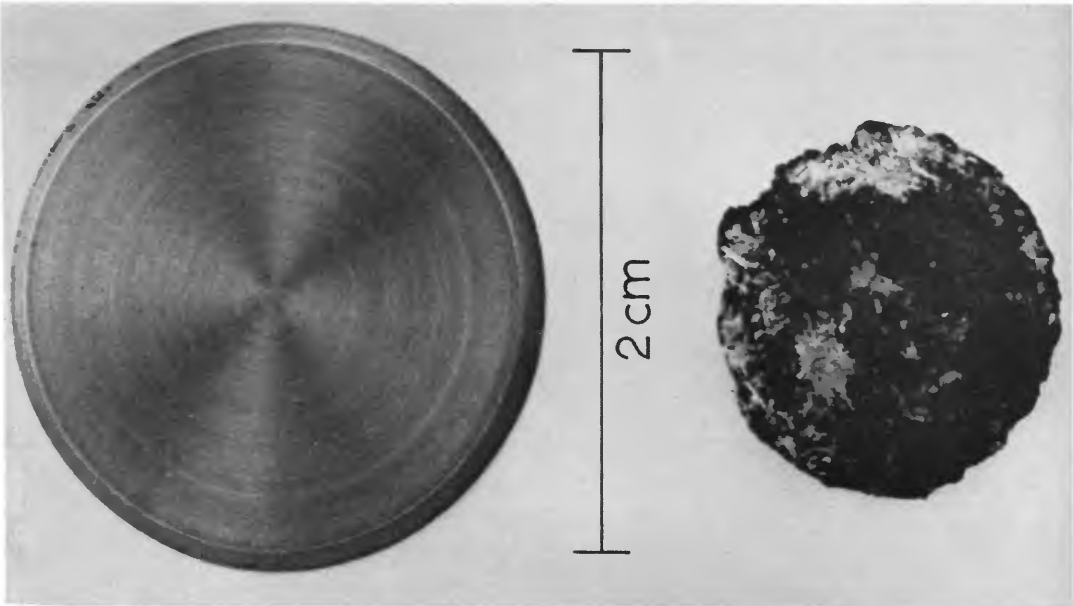
To summarize, observations of natural meteors have not yet yielded reliable data on the luminous efficiency, meteor masses, or meteor densities. The present experiment was intended to supply a reliable value of the luminous efficiency of one meteoric element, iron.

### The experiment

The Trailblazer I rocket (see pl. 1) is normally a 6-stage vehicle; the first three stages lift a velocity package (the final three stages) to an altitude of approximately 300 kilometers and these three stages fire downward in sequence. The last, or sixth stage, is a 5-inch spherical rocket motor which, after burnout, enters the atmosphere at 6 or 7 km/sec and serves as a test object for re-entry studies. In the case of the Trailblazer I used for the meteor experiment, an air cavity charge was mounted on the 5-inch rocket motor as a seventh stage of propulsion (see pl. 1). This explosive projectile accelerator is shown in plate 2. It consists of a chemical delay fuse, a "tetryl" booster and a cylindrical charge of plastic bonded RDX molding explosive. The air cavity in the RDX is sealed by a 5.7-gram pellet of Stainless Steel 304. When ignited, a plane detonation wave—utilizing the air in the cavity as a buffer—propels a portion of the steel pellet forward with a velocity of about 4 km/sec. These projectiles have been recovered intact in the laboratory to determine their mass. Such a recovered projectile is shown, next to an unfired pellet, in plate 2.



*Left, Trailblazer I-G 7th-stage rocket. Right, 6th-stage spherical rocket engine and 7th-stage gun.*



*Top, 7th-stage pellet before and after detonation. Bottom, Disassembled 7th-stage gun showing test pellet.*

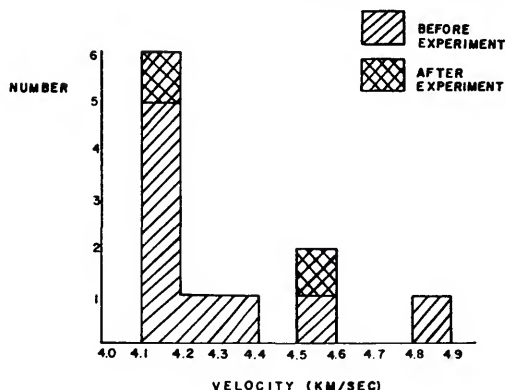


FIGURE 1.—Velocities achieved by air cavity charge during ground tests.

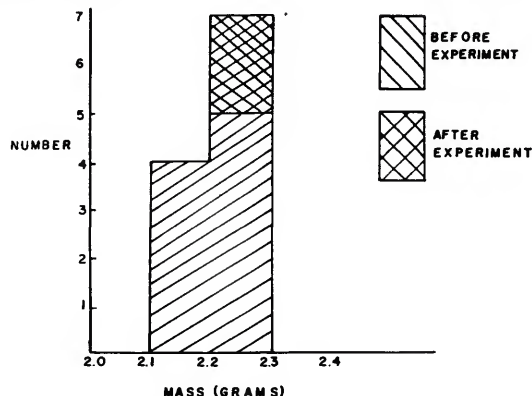


FIGURE 2.—Post-detonation masses of air cavity charge pellet determined from ground tests.

The resultant velocity and mass of these test projectiles are shown in figures 1 and 2. All the charges referred to in these figures, as well as the charge utilized in the experiment, were fabricated in an identical manner from the same batch of materials

In producing the artificial meteoroid, the air cavity charge was to be fired shortly after burnout of the 5-inch rocket motor at an altitude of 195 kilometers.

The seven-stage Trailblazer was fired at 00<sup>h</sup> 56<sup>m</sup> 20<sup>s</sup> E.S.T. on April 21, 1961. The re-entry of the steel pellet was observed visually at 01<sup>h</sup> 02<sup>m</sup> 00<sup>s</sup> by many observers. It was photographed by the Super-Schmidt meteor cameras at the Arbuckle Neck, Va., and the Eastville, Va., stations of the M.I.T. Lincoln Laboratory; and also by smaller cameras operated by the National Aeronautics and Space Administration at Eastville, Va., and at Coquina Beach, N.C. The re-entry of the sixth stage was also observed visually and photographically.

Since it was conceivable that the meteor would be near or below the observable threshold, duplicate observations were made whenever possible. For this reason we relinquished the chance of spectrographic observations with the Super-Schmidt equipped with a prism.

**Observational results**

*Trajectory.*—The probability that the observed meteor was of natural origin and not the result of the experiment is small but must be con-

sidered. The submeteoric velocity (see table 1) of the pellet, although not intentional, is virtual proof of the origin of the body. Furthermore, an upward extrapolation of the trajectories of the sixth and seventh stages indicates a coincidence of these objects in space and in time that agrees, to within the accuracy of the observation, with the position and time at which the seventh stage was intended to fire. The photographs certainly refer to the seventh stage pellet.

The photographs were reduced by the standard precision method described by Whipple and Jacchia (1957). The summary of the results are given in table 1. We followed the usual meteor analysis procedure and, by least squares, fitted the observed distances *D* along the trail by an equation of the form

$$D = a + bt + ce^{kt} \tag{6}$$

The values of the constants, and their probable errors, are included in table 1. *D* and *t* take the value zero at the beginning point.

*Photometry.*—The same photometric techniques described by Whipple and Jacchia have been used to determine the meteor light curve. Each dash (shutter opening) of each Super-Schmidt trail was compared with trailed images of stars in the Harvard Standard region at  $\delta = +15^\circ$ ,  $\alpha = 75^\circ$ . The comparison film had been obtained earlier in an excellent (New Mexico) sky. In addition to the usual corrections for reciprocity failure, the relative trailing rates of star and meteor, and the distance of

TABLE 1.—Trajectory data derived from Super-Schmidt photographs of re-entry pellet

Duration	0.77 sec
Maximum $M_{pe}$	-0.4
Velocity at beginning	9.8 km/sec
Beginning height	69.4 km
End height	62.6 km
Beginning range	254 km
End range	254 km
Zenith distance at midpoint	76°
Radiant (1950)	$\alpha=204^{\circ}.5$ $\delta=37^{\circ}.5$
Zenith distance of radiant, $Z_R$	15°
Constants of equation (6)	
$a=$	$0.012 \pm 0.020$ km
$b=$	$9.787 \pm 0.046$ km/sec
$c=$	$2.8 \times 10^{-6} \pm 0.3 \times 10^{-6}$ km
$k=$	$12.5$ sec <sup>-1</sup>

the meteor, very considerable absorption corrections were also indicated. The sky conditions at the time of the experiment were particularly good for the locale, but the observations were made at a low elevation. Calibration photographs of the re-entry region were made, with each Super-Schmidt camera, within minutes after the event to provide for these absorption corrections. The cameras were kept stationary for these exposures. About 20 star trails on each Super-Schmidt calibration film were compared with star trails on the comparison film. The calibration stars were chosen at about the re-entry azimuth and at zenith distances from 48 to 85 degrees. True apparent photographic magnitudes for these stars were taken from the Henry Draper catalogue, and the apparent absorption values were fitted by least squares to the equation

$$\Delta M_{ab} = a + bZ, \quad (7)$$

where  $Z$  is the air mass above sea-level at the zenith distance of the star. The observed values fit the equation over the entire range of the zenith distance with a mean scatter of 0.3 magnitude. Some of this scatter is certainly due to errors in the Henry Draper magnitudes. We obtained the following values for the two stations:

	$a$	$b$
Arbuckle Neck	0.17	0.30
Eastville	0.77	0.24

The nonzero values of the constant  $a$  can be interpreted as a difference in the film sensitivities

between the comparison and the calibration films. However, the value of the air mass coefficient is surprisingly low for a sky at sea level on the east coast. Perhaps this should be attributed, along with the nonzero value of  $a$ , to a nonuniform sky that was relatively poor near the zenith because of local haze but degrading less rapidly than normal at increasing zenith angle. The cause of this slightly anomalous behavior, whatever it might be, does not concern us. The re-entry film and comparison film were identical emulsions exposed on an identical sky. The photometric measures of both re-entry and calibration films were made against the same comparison film. Thus our "absorption" measures represent corrections that must be applied to the re-entry film whether these departures result from actual absorption or from changes in system sensitivity.

The corrected measures are plotted in figure 3. The agreement between the results from the two stations is generally excellent. The free-hand curve drawn to the points has been taken to be the true light curve for the remainder of this analysis.

#### Luminous efficiency

Equation (3) gives the luminous efficiency as

$$\tau_0 = \frac{2}{m} \int_0^T \frac{I}{v^3} dt, \quad (8)$$

where  $T$  is the duration of the meteor. We will assume at the outset the mass to be 2.2 grams, realizing that the terminal mass may not be negligible for this pellet and that, therefore, the luminous efficiency derived will be a lower limit. The intensity  $I$  is given by the light curve. We have included in the integrated intensity those extrapolated regions at the beginning and the end of the light curve when the meteor was fainter than film limit. The intensity as used here is defined by:

$$M_{pe} = -2.5 \log I. \quad (9)$$

The velocity at the end of the trajectory is rapidly decreasing and not particularly well determined. The formal solution of the trajectory suggests a velocity of 5 km/sec at  $T=0.75$  second. If this velocity is accepted,

the contribution to the integral in the region from 0.7 to 0.9 second becomes inordinately large and unrealistic because of the uncertain extrapolation of the light curve and the poorly determined velocity. If one arbitrarily sets the velocity at 6 km/sec whenever the formal solution yields a lower value, one obtains  $\tau_0=8.6 \times 10^{-19}$  (cgs and  $M_{pe}$ ). If instead of a limiting velocity of 6 km/sec, one chooses 8.5 km/sec (the point on the descending branch of the light curve for which the contribution of  $I/v^3$  first exceeds that of the previous integration step), then  $\tau_0=6.6 \times 10^{-19}$  (cgs and  $M_{pe}$ ). We will take

$$\tau_0=8 \times 10^{-19} \text{ (cgs and } M_{pe}) \quad (10)$$

as the observed value in our discussion.

One must clearly recognize the limitations attached to this value. It is a lower limit to the efficiency of stainless steel at velocities of about 10 km/sec. In attempting to derive other values from this, one must enter areas of speculation. In the following sections we will investigate three corrections that are necessary to convert the value in equation (10) to a luminosity coefficient valid for meteoric material at 10 km/sec. The corrections cannot be derived without assumptions. We offer the following analysis as a "best estimate" for those who may require it. If the mass-luminosity problem of meteor physics is to be solved by the present experimental techniques, observation of a number of materials at several velocities will be necessary.

*Correction for the composition of the pellet.*

—The choice of pellet material was dictated by the physical properties rather than by the chemical composition of the metal, and for this reason the pellet composition does not match either meteoritic iron or the metallic components of meteoritic stone. A comparison of the major constituents of these materials relative to the iron content is given in table 2.

TABLE 2.—Composition of various materials relative to their Fe content

	Stainless 304	Met. stone	Met. iron
Fe	100	100	100
Cr	28	1	trace
Ni	15	5	9
Mn	3	1	

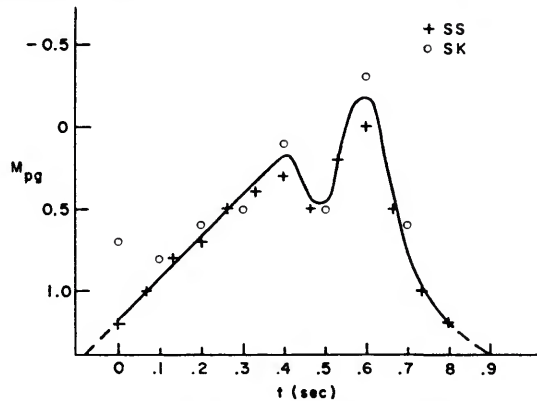


FIGURE 3.—Light curve of the artificial meteor.

The contribution of both Ni and Mn to the luminosity is certainly small and, in any case, is probably comparable to the contribution of a similar mass of iron. However, the gross discrepancy in the relative abundance of Cr is a matter for concern. To derive a value for the luminous efficiency of iron alone, one must first know the ratio of the efficiency of Fe to that of Cr. A few Cr I lines are seen in the best spectrum of a low velocity meteor. They are generally blended with the iron lines which are far more prevalent. If one accepts that the Cr/Fe ratio found in chondritic meteorites or in cosmic material generally ( $\approx 1\%$ ) is also valid for cometary meteoroids, then the available data on meteor spectra and on the absolute oscillator strengths of the important spectral lines of the two elements suggests that the luminous efficiency of Cr does not differ enormously from that of Fe. For the present, we prefer the assumption that  $\tau_0(\text{Cr})=\tau_0(\text{Fe})$ , and that the value given in equation (10) for the steel pellet is representative of pure iron. If, instead, we assume as probable extremes either that  $\tau_0(\text{Cr})=1/10\tau_0(\text{Fe})$  or  $\tau_0(\text{Cr})=10\tau_0(\text{Fe})$ , then the corresponding values for  $\tau_0(\text{Fe})$  become  $1.0 \times 10^{-18}$  and  $2.9 \times 10^{-19}$ , respectively.

*Correction for terminal mass.*—The rate of mass loss from a nonfragmenting meteoroid is proportional to the energy flux and inversely proportional to some energy of ablation  $\xi$  (heat of vaporization or fusion), and is given by

$$\frac{dm}{dt} = -\frac{\Lambda}{2\xi} \rho A v^3, \quad (11)$$

where  $\Lambda$  is the heat-transfer coefficient. Dividing equation (11) by equation (4) and integrating one obtains

$$m_f = m_0 \exp \left[ -\frac{\sigma}{2} (v_0^2 - v_f^2) \right], \quad (12)$$

where  $\sigma = \frac{\Lambda}{2\Gamma_f}$  and the subscripts refer to conditions at two points on the trail. Let  $m_0, v_0$  refer to the beginning of the trail, and  $m_f, v_f$  to the time when all sensible vaporization has ceased. Then the unvaporized terminal mass is given if  $v_f$  and  $\sigma$  are known. The correction to  $\tau_0$  (Fe) can be appreciable if  $\Lambda$  is as low as 0.3, or if  $v_f$  is as high as 7 km/sec. We require estimates of both of these quantities. The estimates will necessarily be rough, and in making the estimates we will lean towards an underestimate of the terminal mass. The corrected luminosity coefficient, therefore, will remain a lower limit.

Vaporization of natural meteors is known to occur at velocities as low as 8 km/sec, and probably continues at still lower velocities. Some estimate of the minimum velocity  $v_f$  can be obtained by requiring a balance between the collisional heating and the radiation loss. We have

$$\frac{1}{2} \Lambda \rho \mathbf{A} v^3 = \sigma \beta \mathbf{A} (T^4 - T_0^4), \quad (13)$$

or, since the equilibrium temperature term  $T_0^4$  is negligible,

$$T^4 = \frac{\Lambda \rho v^3}{8\sigma\beta}, \quad (14)$$

where  $\beta$  is the emissivity and this  $\sigma$  is the Stefan-Boltzmann constant. It appears that the expression is independent of the body size but, in fact,  $\Lambda$  varies with the flow regime and is a function of the body size and of  $\rho$ . Anticipating a later result, we will assume a body radius  $r=1$  mm and compute  $\Lambda$  at the end point altitude of 62.6 km ( $\rho=2.6 \times 10^{-7}$  gm/cm<sup>3</sup>) from the relationship given by Probst and Kemp (1960),

$$\Lambda \approx \left( \frac{1.6L}{r} \right)^{1/2}, \quad (15)$$

where  $L$  is the mean free path in air. From equation (15) we obtained  $\Lambda \approx 0.7$ .

Levin (1956) suggests that intense vaporization will occur at temperatures above 2000°–2800° K. We will assume the higher figure as a conservative value for our purpose. Handbook values for the emissivity of liquid steel are about 0.28. From equation (14),  $v_f=3.5$  km/sec. If instead we take  $T=3500^\circ$  K, the vaporization temperature of iron,  $v_f=4.7$  km/sec. The distinction between these two values is hardly noticeable in equation (12). Let us take  $v_f=4$  km/sec.

The determination of an appropriate value for  $\sigma$  is more critical and not as straightforward as the determination of  $v_f$  for two reasons. First, the heat-transfer coefficient  $\Lambda$  is not well known. Second, since our concern is with the unvaporized remainder, we must investigate the vaporization history of any droplets removed from the pellet—the mass loss of the pellet itself will not necessarily represent the amount of material vaporized. With the aid of several plausible assumptions it is possible to summarize the general mass-loss history of this particular pellet. In addition, some observational verifications of aspects of the presumed history are available and will be summarized at the end of this section.

We suppose the following sequence of events:

(1) The sixth stage of the Trailblazer has a spin about the flight axis of 36 rps. The pellet partakes of this motion plus any perturbation introduced by the detonation wave of the seventh stage. These latter effects have not been adequately observed, but they are thought to be small. We assume that the most likely configuration for the pellet is a spin-stabilized motion about the flight axis (a stable position for supersonic flight even without spin) and therefore about the minor axis of the pellet.

(2) The pellet is heated, to an unknown extent, by the ejection process. In the ground tests, only a minute fraction of the material on the rear surface showed signs of melting; the front surfaces were essentially unaffected. However, the material has been “worked” and some modest temperature rise (100° C?) must occur at this time.

(3) Free molecular flow prevails from ejection to an altitude of about 85 kilometers. In this region the heat-transfer coefficient  $\Lambda$  is near unity and the body is heated further.

It acquires about 10 percent of the energy needed to melt entirely. Conduction prevents any melting of the front surface. Radiative cooling is negligible.

(4) The major heating occurs in the continuum flow regime below 85 kilometers. Some melting must occur before the onset of luminosity. This melt may be spun off, blown off, collect at the edge, or creep to the rear surface. Complete melting is conceivable if sufficient heat is transferred to the rear surface by the flow. It is more likely that melt collecting on the edge begins to be removed by drag and centrifugal forces. The mass-area ratio of these nearly spherical drops will be similar to the major body, and little differential deceleration will occur.

(5) Eventually complete melting must occur. Whether the remaining liquid mass is stable or not depends on the drag load, the angular momentum, and the restoring force of surface tension. The drag load increases through the first half of the trajectory but, in compensation, the angular momentum decreases and the surface tension increases as the body sheds droplets.

(6) If the body is stable, mass loss by melting will cease and the body, after an interval of further heating, will begin to vaporize strongly until the velocity is sufficiently reduced. If the body is unstable, it will break into droplets which will continue to vaporize until the velocity  $v$ , is reached by each droplet.

The beginning of luminosity must be accompanied by either (a) vaporization from the surface of the pellet, (b) vaporization from small droplets thrown off from the pellet, or (c) fragmentation of the pellet into some very small particles. We discard (c) as improbable. If (b) is important, (a) does not occur appreciably; for if the pellet is losing mass efficiently by melting, its temperature cannot approach that necessary for vaporization. To demonstrate that (b) is a possible mechanism, we must show both that the surface can have melted and that there was sufficient force to remove droplets against surface tension. The geometry of the pellet is a determining factor for each of these conditions.

The shapes of pellets recovered on the firing range are roughly that of one-half an oblate spheroid with the plane surface leading. The

major axes are of the order of 12 mm and the semi-minor axes about 3 mm. The body may also be reasonably well characterized as a cylinder 12 mm in diameter and 2.5 mm thick.

Consider a hemispherical drop, of radius  $r$ , on the edge of a cylinder, of radius  $a$ , spinning at a rate  $\omega$ . This drop will be thrown off when the centrifugal force exceeds the surface tension force, or when

$$\frac{2}{3} \pi \delta r^3 a \omega^2 \geq 2\pi S r, \quad (16)$$

where  $S$  is the surface tension. For steel ( $S=1.2 \times 10^3$  dynes/cm and  $\delta=7.9$  gm/cm<sup>3</sup>) the limiting value of  $r$  is about 1 mm. That is, the droplet need have a diameter only comparable to the thickness of the pellet to be unstable against centrifugal force. Spraying will certainly occur whenever molten material reaches the edge. In addition, the drag force on the drops will enhance the spraying process.

The conduction of heat inward from the leading surface will delay melting for a time. The solution for the heat transfer within a cylindrical meteor entering an exponential atmosphere has been given by Levin (1956), and is applicable here. For a thin cylinder of thickness  $D$  and conductivity  $\lambda$ , with the major area presented to the air stream, one finds the temperature to be

$$T(x, t) = \frac{W(t) x_0}{\lambda} e^{-x/x_0} \left[ 1 + \frac{e^{2x/x_0} + 1}{e^{2D/x_0} - 1} \right], \quad (17)$$

where  $W(t) = \frac{\Lambda \rho v^3}{2}$  is the heat flux per unit area

at time  $t$ , and  $x_0$  is a characteristic heating depth given as

$$x_0 = \left( \frac{\lambda \beta}{\delta c v \cos Z_R} \right)^{\frac{1}{2}}. \quad (18)$$

$\beta$  is the scale height of the atmosphere,  $c$  is the specific heat of the material, and  $Z_R$  is the zenith distance of the radiant. For Stainless Steel 304,  $\lambda=2 \times 10^6$  ergs/cm sec degree and  $c=5 \times 10^6$  ergs/gm degree.

Using these values, one finds that if  $\Lambda=0.3$ , sufficient energy to raise the surface to the melting temperature will have been introduced by the time the pellet becomes visible. Since

$\Lambda$  is almost certainly considerably larger than 0.3 (equation (15) gives a value of  $\Lambda \approx 0.5$  at 70 km), some melting must have occurred. We deduce that initial mass loss is due to melting and spraying. The droplets are small enough to be nearly in free-molecular flow and are subject to a heat-transfer coefficient of near unity.

This form of spraying may continue until the pellet is completely melted, or until sufficient angular momentum has been shed with the droplets. Various attempts to describe the mass-loss phenomena in sufficient detail to distinguish between these two events have, not unexpectedly, been unsuccessful. However, the observed light-curve offers a clue, which although indefinite, cannot be ignored. At  $t=0.4$  second (see fig. 3) the intensity subsides temporarily. This is seen on Super-Schmidt films taken from stations separated by 50 kilometers. The decrease is certainly real and not the effect of uneven atmospheric absorption. Compared to the light curves of natural meteors, it is a most unusual event. We suspect that this represents the time when spraying ceased or decreased markedly, and that the delay in the light-curve represents the time required to melt the remaining solids. At this time, at least half of the initial mass remains in the pellet since half of the luminosity is yet to be produced. An approximate analysis suggests that the molten mass might be stable against the flattening brought on by the rotation, but it certainly will not be stable against distortion by drag. Applying the results of an analysis given by Öpik (1958) on the deformation of liquid droplets, one finds that a one gram mass of liquid iron will initially be flattened to an oblate spheroid of semi-minor axis

$$b = 3S/\Gamma\rho v^2 = 0.04 \text{ cm}, \quad (19)$$

and semi-major axis

$$a = (3m/4\pi\delta b)^{1/2} = 0.9 \text{ cm}. \quad (20)$$

In these computations we have used the value of 0.5 for the drag coefficient and the atmospheric density at 65.7 km ( $1.8 \times 10^{-7}$  gm/cm<sup>3</sup>). Öpik suggests also that if  $a/b > 4$ , the droplet will be unstable and a breakup into droplets of dimension  $a/b = 2$  will occur, where  $b$  is given by equation (19). This formulation predicts

that the droplet disintegrates into about  $10^2$  pieces of  $a=1$  mm. Assuming that these particles act independently from the incoming air stream, equation (15) gives  $\Lambda \approx 0.8$ . In all probability the effective body size for each of the particles is larger than its physical dimension since the cluster of droplets will act on the air stream in concert to some extent. But since this value of  $\Lambda$  is an upper limit, it will yield a lower limit in the correction to the luminous efficiency, which is what we seek here.

From the above discussion we arrive at the following best estimate for the terminal mass:

(1) The first half of the mass is introduced as small droplets by spraying at essentially the initial velocity of the meteor and ablates with  $\Lambda \approx 1$  ( $\sigma = 7 \times 10^{-12}$ ) until the velocity of  $v_r$  is reached. For this computation we have used the heat of vaporization of iron,  $6.4 \times 10^{10}$  ergs/gram plus the energy required to raise the melt from 1800° to 3500° K,  $1.1 \times 10^{10}$  ergs/gram. We have presumed free molecular flow and therefore have used  $\Gamma=1$ . Less than 1 percent of the mass remains at 4 km/sec.

(2) For the droplets formed by the disruption of the liquid body we have used  $\Lambda=0.8$  and  $\Gamma=0.5$  as characteristic values for continuum flow. Then  $\sigma = 1 \times 10^{-11}$ . For this portion of the original mass, the terminal mass is again negligible.

No significant correction for the value of luminous efficiency given in the preceding section is necessary. The above analysis is dependent on the assumption of a specific and unusual form of mass loss, but one which can be defended in its broad outline. We give here, without computations, four observations that tend to substantiate the assumptions:

(1) We have already shown that the beginning height of this meteor is consistent with the assumed re-entry geometry. We believe that, without the rapid rotation, the beginning point would have been delayed appreciably. Our estimates of the beginning point of the visible trajectory before the experiment were based on an observation (Halliday, 1960) of a natural iron meteoroid. The rotation was ignored. We used an empirical law (McCrosky, 1955) for the beginning height of meteors  $\rho_{\text{atm}} v^3 = \text{constant}$ , and scaled from Halliday's

example (altitude, 69.4 km.; velocity, 13.4 km/sec) to obtain the estimate of the beginning point. In fact, the natural and simulated meteors appeared first at the same altitude in spite of a difference factor of 2 in the  $v^3$  term.

(2) We have assumed that half of the mass is ablated at  $t=0.4$  second. This assumption is found to be in good agreement with equation (15) if it is supposed that the body loses mass from both the front surface and the edges in such a fashion as to keep constant the shape factor,  $A$ . If, as extreme alternatives, it is assumed that the body loses mass only at the edges, or only from the front surface, equation (15) is reasonably well validated.

(3) The duration of the dip in the light curve, about 0.15 second, is comparable to the time required to liquefy one gram of the material if it is near the melting point and if the heat transfer coefficient is correctly given by equation (15).

(4) The velocity near the end of the trail is in general agreement with that expected from droplets of 1 mm radius introduced into the atmosphere at  $t \approx 0.5$  second.

*Correction for composition of meteoroids.*—Spectra of low velocity meteors show that most of the luminosity observed on a blue-sensitive emulsion arises from iron line emissions, particularly from the  ${}^4\text{D}-{}^4\text{D}^\circ$  and  ${}^4\text{D}-{}^4\text{F}^\circ$  transitions. Thus, a determination of the luminous efficiency of iron leads directly to a determination of the luminous efficiency for meteoritic material if the relative iron content of the meteoroid is known. The abundances in iron and stony meteorites are, of course, known. But no reliable information exists on the composition of the most common body, the cometary meteoroid. It is plausible that the heavier elements and oxygen occur in the same ratio as in stony meteorites and, therefore, approximately in the same relative abundances as in the sun; but these may well be diluted by some lighter elements, particularly H, C, and N. The luminous efficiency of each of these latter elements is certainly very low, and the absence of appreciable luminosity from these in meteor spectra is not necessarily an indication of their rarity. However, unless Fe is excluded in a highly selective fashion in the formation of

comets, it seems unlikely that the iron abundance can be less than 1 percent by weight.

In table 3, we list provisional values for the luminous efficiency based on the iron abundances stated in the table, the luminous efficiency for iron  $\tau_0(\text{Fe})=8 \times 10^{-19}$  as determined from the above results, and the assumption that all the luminosity in the range 3500–5000 Å produced by meteors at 10 km/sec results from iron line emissions. Since other elements will contribute to the luminosity, the values given will be lower limits; the more so for those cases where the iron abundance is low.

TABLE 3.—Provisional values of the luminosity coefficient for meteoric material at 10 km/sec.

Fe abundance	Cometary meteoroids (extreme estimates)			
	Irons 93%	Stones 15%	1%	20%
$\tau_0$	$7.4 \times 10^{-19}$	$1.2 \times 10^{-19}$	$8 \times 10^{-21}$	$1.6 \times 10^{-19}$

In addition to the uncertainties imposed by the composition of the meteoroids, differences in velocity between the simulated meteor and natural photographic meteors (mean velocity  $\approx 25$  km/sec) may introduce appreciable errors if our result is extrapolated to these higher velocities. The velocity function we have employed (see equation 2), although compatible with meteor observations generally, must certainly fail at sufficiently low velocities. There is some evidence (Jacchia, 1949) that the luminous efficiency is decreasing more rapidly than suggested by equation (2) for meteors of  $v < 16$  km/sec. In any case, there is no reason to expect an increase in the efficiency at low velocities and, therefore, extrapolations of our result to higher velocities will give upper limits for the masses of natural meteoroids.

#### Acknowledgment

The research reported here and accomplished at Harvard College Observatory was performed under subcontract to Lincoln Laboratory, a technical center operated by Massachusetts Institute of Technology, with support from the U.S. Advanced Research Projects Agency under Air Force Contract AF19(604)7400 (ARPA Order 13-61).

Many individuals from National Aeronautics and Space Administration, Lincoln Laboratory, A.D. Little, Inc., Harvard College Observatory, and

Air Force Cambridge Research Laboratories contributed to this program. We attribute its success, in large part, to the splendid personal efforts of Mr. Lawrence Prugnarola of Lincoln Laboratory and to Messrs. Stanley Chrest, Thomas Ryan, and Anthony Mandile of Air Force Cambridge Research Laboratories in the preparation of ground observation facilities and the air cavity charge.

### References

- COOK, A. F.  
1955. On the constants of the physical theory of meteors (abstract). *Astron. Journ.*, vol. 60, pp. 156-157.
- HALLIDAY, I.  
1960. The spectrum of an asteroidal meteor fragment. *Astrophys. Journ.*, vol. 132, pp. 482-485.
- JACCHIA, L. G.  
1949. Photographic meteor phenomena and theory. Harvard Meteor Project Technical Report No. 3, Harvard Coll. Obs. Reprints, ser. 2, no. 31.  
1955. The physical theory of meteors. VIII. Fragmentation as a cause of the faint-meteor anomaly. *Astrophys. Journ.*, vol. 121, pp. 521-527.
- LEVIN, B. J.  
1956. The physical theory of meteors and meteoric matter in the solar system. Publ. House Acad. Sci. U.S.S.R., Moscow.
- MCCROSKY, R. E.  
1955. Fragmentation of faint meteors (abstract). *Astron. Journ.*, vol. 60, p. 170.  
1961. Observations of simulated meteors. *Smithsonian Contr. Astrophys.*, vol. 5, no. 4, pp. 29-37.
- ÖPIK, E. J.  
1955. Meteor radiation, ionization and atomic luminous efficiency. *Proc. Roy. Soc. London*, ser. A, vol. 230, pp. 463-501.  
1958. *Physics of meteor flight in the atmosphere*. Interscience, New York.
- PROBSTEIN, R. F., AND KEMP, N. H.  
1960. Viscous aerodynamic characteristics in hypersonic rarefied gas flow. *Journ. Aero. Space Sci.*, vol. 27, pp. 174-192.
- WHIPPLE, F. L.  
1943. Meteors and the earth's upper atmosphere. *Rev. Mod. Phys.*, vol. 15, pp. 246-264.  
1955. On the mass-luminosity relation for meteors (abstract). *Astron. Journ.*, vol. 60, pp. 182-183.
- WHIPPLE, F. L., AND JACCHIA, L. G.  
1957. Reduction methods for photographic meteor trails. *Smithsonian Contr. Astrophys.*, vol. 1, no. 2, pp. 183-206.

# Luminous Efficiency of Iron and Stone Asteroidal Meteors

By A. F. Cook,<sup>1</sup> L. G. Jacchia,<sup>1</sup> and R. E. McCrosky<sup>1</sup>

We shall give a detailed discussion of theory and observation for three meteors, one iron and two stone. The first is known to be a pure iron from its spectrum. The other two yield results consistent with those of the first if they are assumed to be composed of meteoritic stone. Finally, a satisfactory comparison is made with the observed re-entry of an artificial iron meteor. The result is a determination of the luminous efficiency law for iron and solid stone meteors valid in the range of velocity from 9 to 21 km sec<sup>-1</sup>.

## Iron meteors

It is convenient to approach the problem of the luminous efficiency of meteors by starting with objects made of meteoric iron or pure iron. One meteor showing the spectrum of an iron without stone inclusions has been reported by Halliday (1960).

We expect that initially the meteoroid conducted all the heat received at its surface to the interior. The surface temperature must then have been determined by the rate at which heat was received earlier along the trajectory. If the meteoroid were not rotating, the part of the surface normal to the direction of flight would have received a heat flux

$$F = \frac{\Lambda}{2} \rho_a V^3, \quad (1)$$

where  $\Lambda$  is the heat-transfer coefficient,  $\rho_a$  the atmospheric density, and  $V$  the velocity. Since very little change in velocity was observed over the trajectory, we may assume that  $V$  is constant in equation (1).

Two possibilities will be considered. The first is that the meteor may have been near or in free molecular flow; in both cases  $\Lambda$  will be a

constant. For a rough unpolished surface we may expect this constant to approach unity (Öpik, 1958, pp. 52–54). The second possibility is that the meteor may have been in viscous or laminar continuum flow. In that case we expect that (Probstein and Kemp, 1960)

$$\Lambda \simeq (1.6l/r)^{1/2}, \quad (2)$$

where  $l$  is a mean free path in air and  $r$  is the radius of the meteoroid, assumed to be a sphere. Since

$$l = 8.11 \times 10^{-9} \rho_a^{-1}, \quad (3)$$

for  $l$  in cm,  $\rho_a$  in gm cm<sup>-3</sup> (Minzner, Champion, and Pond, 1959), we have

$$\Lambda \simeq 1.14 \times 10^{-4} (r \rho_a)^{-1/2}, \quad (4)$$

and

$$F \simeq 5.7 \times 10^{-8} r^{-1/2} \rho_a^3 V^3. \quad (5)$$

Let us make the further approximation that

$$\rho_a \simeq \rho_a \exp [-(h-h_0)/H], \quad (6)$$

where  $H$  is the scale-height defined by

$$H \equiv \left( \frac{d}{dh} \ln \rho_a \right)^{-1}, \quad (7)$$

and  $h$  denotes height above sea-level. The approximation of equation (6) amounts to the assumption that the scale-height of equation (7) is a constant independent of  $h$ . We now note that

$$h-h_0 = -(s-s_0) \cos Z_R, \quad (8)$$

where  $s$  is the distance along the trajectory from an arbitrary zero point,  $s_0$  is the value of  $s$  corresponding to the height  $h_0$ , and  $Z_R$  is the zenith distance of the radiant. Furthermore,

$$s-s_0 \simeq V(t-t_0), \quad (9)$$

<sup>1</sup> Smithsonian Astrophysical Observatory, and Harvard College Observatory, Cambridge, Mass.

according to the approximate assumption of constant velocity. Substitution of equation (9) into equation (8), substitution of the result into equation (6), and substitution of that result into equation (1) (with  $\Lambda \simeq 1$ ) and into equation (5) yields

$$F \simeq \frac{1}{2} \rho_0 V^3 \exp [(V/H) \cos Z_R(t-t_0)], \quad (10)$$

or

$$F \simeq 5.7 \times 10^{-6} r^{-1/2} \rho_0^{1/2} V^3 \times \exp \left[ \frac{1}{2} (V/H) \cos Z_R(t-t_0) \right], \quad (11)$$

where we adopt the smaller value as correct. Equations (10) and (11) can be written as

$$F = F_0 \exp [(t-t_0)/\tau], \quad (12)$$

where for equation (10) we have

$$F_0 = \frac{1}{2} \rho_0 V^3, \tau = H/(V \cos Z_R), \quad (13)$$

and for equation (11) we have

$$F_0 = 5.7 \times 10^{-6} r^{-1/2} \rho_0^{1/2} V^3, \tau = 2H/(V \cos Z_R). \quad (14)$$

Levin (1956) has shown that for a flux of the form given in equation (12) extending back to  $t = -\infty$ , the following temperature distribution is expected in a semi-infinite medium at negligible initial temperature bounded by a plane surface at  $x=0$ ,

$$T(x, t) = T_0(t) \exp(-x/x_0), \quad (15)$$

$$T_0(t) = F(t) [\tau / (\kappa c_p \rho_m)]^{1/2}, \quad (16)$$

$$x_0 = (k\tau)^{1/2}, \quad (17)$$

where  $x$  is the distance from the surface,  $F(t)$  is given by equation (12),  $\kappa$  is the conductivity,  $c_p$  the specific heat,  $\rho_m$  the density, and  $k$  the thermometric conductivity of meteoric iron. As soon as  $T_0 = 1800^\circ K$  is reached (the melting temperature, Öpik, 1958, pp. 156-158), molten iron will start to flow. To form an idea of the conditions required to remove molten iron from the meteoroid, we must consider the problem of flow of the melt.

### Flow of molten iron

We consider a convex meteoroid with axial symmetry about the direction of flight. Let  $y$  be perpendicular to the surface outward,  $r$  the radius of curvature in the  $xy$ -plane, and  $r_2$  the radius of curvature in the plane normal to the local  $x$ -direction. Let  $\theta$  denote the angle between the  $y$ -direction and the direction of flight. The equation of continuity takes the form

$$\frac{1}{r_2 \sin \theta} \frac{\partial}{\partial x} (r_2 u \sin \theta) + \frac{\partial v}{\partial y} = 0, \quad (18)$$

where  $u, v$  are the  $x$  and  $y$  components of velocity of the iron. The equation for the conduction of heat takes the form

$$u \frac{\partial T}{\partial x} + v \frac{\partial T}{\partial y} = k \frac{\partial^2 T}{\partial y^2}, \quad (19)$$

where a steady state has been assumed and only the dominant term in the Laplacian of the temperature has been kept on the right-hand side. The equation of the transport of the  $u$ -component of momentum is

$$\rho_m u \frac{\partial u}{\partial x} + \rho_m v \frac{\partial u}{\partial y} = \frac{\partial}{\partial y} \left( \mu \frac{\partial u}{\partial y} \right) - \frac{\partial p}{\partial x}. \quad (20)$$

The dynamic viscosity is taken to have the form of a step function of temperature:

$$\begin{aligned} T > 1800^\circ K, \mu &= \infty, \\ T < 1800^\circ K, \mu &= 2 \times 10^{-2} \text{ gm cm}^{-1} \text{ sec}^{-1}, \end{aligned} \quad (21)$$

as given by Öpik (1958, pp. 156-158).

We begin by linearizing equation (20) in  $u, v$ , whence

$$\mu \frac{\partial u}{\partial y} = \mu_0 \left[ \frac{\partial u}{\partial y} \right]_{y=0} + \int_0^y \frac{\partial p}{\partial x} dy',$$

and we denote the rate of flow of shearing momentum across the boundary  $y=0$  by  $\tau_0$ , whence

$$\tau_0 \equiv \mu_0 \left[ \frac{\partial u}{\partial y} \right]_{y=0}, \quad (22)$$

$$\frac{\partial u}{\partial y} = \frac{\tau_0}{\mu} + \frac{1}{\mu} \frac{\partial p}{\partial x} y,$$

$$u(y) = u_0 + \tau_0 \int_0^y \frac{dy'}{\mu} + \frac{\partial p}{\partial x} \int_0^y \frac{y'}{\mu} dy'. \quad (23)$$

We next assume that  $u(\partial T/\partial x) \ll v(\partial T/\partial y)$ , whence the equation for the conduction of heat (19) yields

$$k \frac{\partial^2 T}{\partial y^2} - v \frac{\partial T}{\partial y} = 0. \quad (24)$$

Let  $y_m$  denote the value of  $y$  at which  $T = T_m \equiv 1800^\circ \text{K}$ , the melting point. Then in the range  $0 \geq y \geq y_m$  we have

$$\frac{\partial}{\partial y} \ln \left( \frac{\partial T}{\partial y} \right) = \frac{v}{k}, \quad (25)$$

where we remember that  $y$  is negative below the liquid surface. In the range  $y_m > y > -\infty$  we have  $v = v_w$ , a constant, and

$$\ln (\partial T/\partial y) = \lim_{\substack{y \rightarrow y_m \\ y < y_m}} \ln (\partial T/\partial y) + \frac{v_w}{k} (y - y_m). \quad (26)$$

The conservation of conducted energy requires that

$$k \lim_{\substack{y \rightarrow y_m \\ y > y_m}} (\partial T/\partial y) = k \lim_{\substack{y \rightarrow y_m \\ y < y_m}} (\partial T/\partial y) + \zeta_f \rho_m v_w,$$

where  $\zeta_f$  is the heat of fusion. Then we have

$$\lim_{\substack{y \rightarrow y_m \\ y < y_m}} \frac{\partial T}{\partial y} = \lim_{\substack{y \rightarrow y_m \\ y > y_m}} \frac{\partial T}{\partial y} - \frac{\zeta_f \rho_m}{k} v_w. \quad (27)$$

From equation (25) we have in the range  $0 \geq y > y_m$ ,

$$\ln (\partial T/\partial y) = \ln [(\partial T/\partial y)]_{y=0} + \frac{1}{k} \int_0^y v dy'. \quad (28)$$

The combination of all these results yields

$$0 \geq y > y_m, \quad \frac{\partial T}{\partial y} = \frac{\partial T}{\partial y} \Big|_{y=0} \exp \left( \frac{1}{k} \int_0^y v dy' \right), \quad (29)$$

and

$$y_m > y > -\infty, \quad \frac{\partial T}{\partial y} = \left[ \frac{\partial T}{\partial y} \Big|_{y=0} \exp \left( \frac{1}{k} \int_0^{y_m} v dy' \right) - \frac{\zeta_f \rho_m}{k} v_w \right] \exp \left[ \frac{v_w}{k} (y - y_m) \right]. \quad (30)$$

By substituting equation (21) into equation (23) we obtain

$$0 \geq y \geq y_m, \quad u(y) = \left[ \frac{\tau_0}{\mu_0} + \frac{1}{2\mu_0} \frac{\partial p}{\partial x} (y + y_m) \right] (y - y_m), \quad (31)$$

$$y_m \geq y > -\infty, \quad u(y) = 0, \quad (32)$$

where the condition (eq. 32) corresponding to infinite viscosity of the solid has been imposed at the solid-liquid interface,  $y = y_m$ , and where  $\mu_0$  denotes the dynamic viscosity at the surface of the liquid. Substitution of equations (31) and (32) into the equation of continuity (18) yields

$$v_w \simeq v_0 + \frac{1}{2\mu_0 r_2} \frac{\partial}{\partial x} \left[ r_2 \sin \theta \times y_m^2 \left( \tau_0 - \frac{1}{3} \frac{\partial p}{\partial x} y_m \right) \right]. \quad (33)$$

In free molecular flow the shear transfer to the surface will be

$$\tau_0 = \Lambda' \rho_a V^2 \sin \theta \cos \theta, \quad (34)$$

where  $\Lambda'$  is a constant which we shall call the shear-transfer coefficient. In analogy with the heat-transfer coefficient we shall take it to be unity. In viscous and laminar continuum flow we may make the approximation (Probstein and Kemp, 1960)

$$\Lambda' \simeq (0.84r/l)^{1/2}, \quad (35)$$

whence from equation (3)

$$\Lambda' \simeq 8.3 \times 10^{-5} (r \rho_a)^{1/2} \quad (36)$$

and

$$\tau_0 \simeq 8.3 \times 10^{-5} r^{-1/2} \rho_a^{1/2} V^2 \sin \theta \cos \theta. \quad (37)$$

In free molecular flow the dynamic pressure upon the surface is

$$p_a = \rho_a V^2 \cos^2 \theta. \quad (38)$$

We make the approximation that this relation still holds in viscous and continuum flow. The pressure due to surface tension is

$$p_t = s_t (1/r_1 + 1/r_2), \quad (39)$$

where  $s_t$  is the surface tension which, according to Öpik (1958, pp. 156-158), is 1200 dyne  $\text{cm}^{-1}$ . The sum of the gradients of these two pressures is

$$\frac{\partial p_a}{\partial x} + \frac{\partial p_t}{\partial x} = -2 \frac{\rho_a V^2}{r_1} \sin \theta \cos \theta - s_t \left( \frac{1}{r_1^2} \frac{\partial r_1}{\partial x} + \frac{1}{r_2^2} \frac{\partial r_2}{\partial x} \right). \quad (40)$$

An additional effective component is added to this pressure gradient by the acceleration of the meteor,

$$\frac{\partial p_a}{\partial x} = -\rho_m \frac{dV}{dt} \sin \theta, \quad (41)$$

where we take for the deceleration the standard form

$$\frac{dV}{dt} = -\Gamma A \frac{\rho_a V^2}{\rho_m^{2/3} m^{1/3}}, \quad (42)$$

where  $\Gamma$  is the drag coefficient,  $A$  is a shape factor (1.208 for a sphere), and  $m$  is the mass of the meteoroid. It then follows that the inertial component (41) of the pressure gradient may be written

$$\frac{\partial p_a}{\partial x} = \Gamma A (\rho_m/m)^{1/3} \rho_a V^2 \sin \theta. \quad (43)$$

The sum of equations (40) and (43) is the total pressure gradient to be used in equation (33),

$$\frac{\partial p}{\partial x} = -\rho_a V^2 \sin \theta \left[ \frac{2}{r_1} \cos \theta - \Gamma A (\rho_m/m)^{1/3} \right] - s_t \left( \frac{1}{r_1} \frac{\partial r_1}{\partial x} + \frac{1}{r_2} \frac{\partial r_2}{\partial x} \right). \quad (44)$$

As  $x$  approaches zero,  $\theta$  approaches zero and, by axial symmetry,  $r_2$  approaches  $r_1$ , and the  $x$ -derivatives of  $r_1$ ,  $r_2$ , and  $y_m$  approach zero. In this region equation (33) may be integrated to yield

$$\lim_{x \rightarrow 0} v = v_0 - \frac{\rho_a V^2}{\mu_0 r} \left\{ \Lambda' \left[ (y-y_m)^2 - y_m^2 \right] - \frac{1}{3} \left[ (y-y_m)^3 + 3y_m(y-y_m)^2 - 2y_m^3 \right] \left[ \frac{2}{r} - \Gamma A (\rho_m/m)^{1/3} \right] \right\}, \quad (45)$$

$$r \equiv \lim_{x \rightarrow 0} r_1 \equiv \lim_{x \rightarrow 0} r_2. \quad (46)$$

By substituting  $y=y_m$  we obtain the  $v$ -component of velocity at great depths:

$$\lim_{x \rightarrow 0} v_w = v_0 + \frac{\rho_a V^2}{\mu_0 r} y_m^2 \left[ \Lambda' - \frac{4}{3} \frac{y_m}{r} - \frac{1}{3} y_m \Gamma A (\rho_m/m)^{1/3} \right]. \quad (47)$$

The velocity distribution (eq. 45) enables us to integrate the equations for the temperature gradient (29) and (30) whence, imposing the conditions

$$T(y_m) \equiv T_m, \quad \lim_{y \rightarrow -\infty} T = 0,$$

we find

$$y_m \geq y > -\infty, T(y) = T_m \exp \left[ \frac{v_w}{k} (y-y_m) \right], \quad (48)$$

$$0 \geq y \geq y_m, T(y) = T_0 + \frac{1}{k} (\zeta_r + c_p T_m) \rho_m v_w \\ \times \int_0^y \exp \left\{ \frac{v_0}{2k} (y'-y_m) - \frac{1}{3} \frac{\rho_a V^2}{k \mu_0 r} (y'-y_m) \right\} \\ \times \left[ \Lambda' (y'^2 - 2y_m y' - 2y_m^2) - \frac{1}{6r} \left( 1 - \frac{1}{2} \Gamma A (\rho_m/m)^{1/3} \right) \right. \\ \left. \times (y'^3 - 5y_m y'^2 - 5y_m^2 y' - 5y_m^3) \right] dy'. \quad (49)$$

We assume that all the terms in the exponential are sufficiently small so that equation (49) may be replaced by

$$T(y) \simeq T_0 + \frac{1}{k} (\zeta_r + c_p T_m) \rho_m v_w y,$$

where

$$T_0 \simeq T_m - \frac{1}{k} (\zeta_r + c_p T_m) \rho_m v_w y_m. \quad (50)$$

Thus we have

$$0 \geq y \geq y_m, T \simeq T_m + \frac{1}{k} (\zeta_r + c_p T_m) \rho_m v_w (y-y_m) \quad (51)$$

and

$$y_m \geq y > -\infty, T = T_m \exp \left[ \frac{v_w}{k} (y-y_m) \right]. \quad (52)$$

Equation (47) may be expressed in the form

$$\lim_{\theta \rightarrow 0} (v_w - v_0) = \left( \frac{y_m}{r} \right)^2 \frac{r \rho_a V^2}{\mu_0} \left\{ \Lambda' - 2 \left[ \frac{2}{3} - \frac{1}{3} \Gamma A (\rho_m/m)^{1/3} r \right] \frac{y_m}{r} \right\}. \quad (53)$$

We now assume that vaporization is negligible, i.e.,  $v_0=0$ , and we obtain

$$v_w = \frac{F}{\zeta \rho_m} = \frac{\Lambda}{2} \frac{\rho_a V^3}{\zeta \rho_m} = \frac{r \rho_a V^2}{\mu_0} \left( \frac{y_m}{r} \right)^2 \left\{ \Lambda' - 2 \left[ \frac{2}{3} - \frac{1}{3} \Gamma A (\rho_m/m)^{1/3} r \right] \frac{y_m}{r} \right\}. \quad (54)$$

This is a cubic equation in  $y_m/r$ . The solution of this equation must then be substituted into equation (50) to find  $T_0$ . Next, the assumption that vaporization is always negligible must be verified by computing the rates of loss of mass and heat by vaporization at  $T_0$ . Finally, the assumption that the argument of the exponential in equation (49) is small must also be verified.

Before the computation near  $x=0$  can be undertaken we must return to equation (33) and ask where on the surface the second term on the right-hand side might vanish. At such a point melt would presumably flow past, as it is neither removed nor accumulated by the flow field. At smaller  $x$  the flow field would remove melt, at greater  $x$  it would accumulate melt. On our assumptions the excess accumulation plus the local ablation would be removed by vaporization. If flow of melt without ablation continues past this critical value of  $x$ , it can only do so if  $u(\partial T/\partial x)$  at  $y=0$  dominates over  $v(\partial T/\partial y)$ . We ignore the trivial case of  $T_0 < T_m$ , i.e., when the surface is still solid and  $\mu_0 = \infty$ , and near such a point we expect  $y_m$  to attain a local minimum, whence it follows that

$$\frac{\partial}{\partial x} \left\{ r_1 \sin \theta \left[ \tau_0 - \frac{1}{3} \frac{\partial p}{\partial x} y_m \right] \right\} = 0. \quad (55)$$

The surface tension may be expected to be near a maximum here, and we may thus drop the last term in equation (44).

We now consider the special case of a spherical meteoroid ( $r_1 \equiv r$ ,  $x \equiv r\theta$ ), for which we have

$$\frac{\partial}{\partial \theta} \left\{ \sin \theta \left[ \tau_0 - \frac{1}{3} \frac{\partial p}{\partial x} y_m \right] \right\} = 0. \quad (56)$$

By substituting equations (33) and (44) into equation (56) we obtain

$$\sin \theta \left[ 6 \left( \Lambda' - 4 \frac{y_m}{r} \right) \cos^2 \theta + 9 \Gamma \frac{y_m}{r} \cos \theta - 2 \left( \Lambda' - 4 \frac{y_m}{r} \right) \right] = 0. \quad (57)$$

The root  $\sin \theta = 0$  is extraneous on account of the division by  $\sin \theta$  which occurs in equation (33). We assume that  $y_m/r \ll 1$ , whence we obtain the roots

$$\cos \theta \simeq \pm \frac{\sqrt{3}}{3} - \frac{3 \Gamma}{4 \Lambda'} \frac{y_m}{r}, \quad (58)$$

and by retaining the first root as the only non-extraneous value, we have the result that  $\theta \simeq 54.7^\circ$ . Melt will begin to flow past here as soon as  $T_0$ , by conduction alone according to equation (16), reaches  $T_m$ . If  $r$  is sufficiently large the melt will blow off as droplets, otherwise the surface temperature will rise until vaporization removes the iron. The criterion for the former process is (Öpik, 1958, pp. 83–86)

$$r \gg \frac{7.6 s_1}{\Gamma \rho_a V} \quad (59)$$

In free molecular flow  $\Gamma \simeq 1$ . In continuum flow with negligible shear transfer the dynamic pressure (eq. 38) alone contributes to the drag, and if we integrate over the exposed hemisphere, we find from the local contribution  $p_a \cos^2 \theta$ ,

$$\Gamma \simeq 2 \int_0^{\pi/2} \sin \theta \cos^3 \theta d\theta = \frac{1}{2}$$

We then estimate that in viscous flow

$$\Gamma \simeq \frac{1}{2} (1 + \Lambda'). \quad (60)$$

We also note that the flux is a function of  $\theta$ , and is not given by equation (1) but by

$$F = \frac{\Lambda}{2} \rho_a V^3 \cos \theta. \quad (61)$$

The computation was made for free molecular flow with  $\theta = 54.7^\circ$ ,  $\kappa = 4 \times 10^6$  ergs  $\text{cm}^{-1} \text{sec}^{-1} \text{deg}$ ,  $c_p = 6.91 \times 10^6$  ergs  $\text{gm}^{-1} \text{deg}^{-1}$ , and  $\rho_m = 7.8$  gm  $\text{cm}^{-3}$ . These constants are the same as those adopted by Öpik (1958, pp. 156–158). The ARDC 1959 model atmosphere (Minzner, Champion, and Pond, 1959) was also used. Equation (13) was used for  $\tau$ , equation (61) for  $F$ , and equation (16) for  $T_0 = T_m$ , and we obtain

$$\rho_a = 2\sqrt{3} (k c_p \rho_m / r)^{1/2} (\tau / V)^3, \quad (62)$$

at the onset of ablation. For Halliday's meteor,  $V = 1.32 \times 10^6$  cm  $\text{sec}^{-1}$ , and  $\cos Z_R = 0.48$ . A trial value of  $H$  yields  $\tau$  from equation (13) and  $\rho_a$  from equation (62), whence  $h$  is found and, from the model atmosphere, an

improved value of  $H$ . The process converged rapidly to predict a beginning height somewhat below 74.1 km. This value is too high compared with the observations.

The alternative is to adopt  $h \geq 69.2$  km, whence  $H \leq 6.38 \times 10^5$  cm, and to compute an upper limit on  $\tau$  from eq. (14) and then to solve equation (16) for  $F$ :

$$F = (\kappa c_p \rho_m / \tau)^{1/2} T_0. \quad (63)$$

Then with  $T_0 = T_m$  we find a lower limit for  $F$ . Finally equation (5) may be solved for  $r$ , whence an upper limit is obtained:

$$r = \left( \frac{5.7 \times 10^{-5} \rho_a^{1/2} V^3}{F} \right)^2. \quad (64)$$

This upper limit is a radius of 1.54 cm.

We also consider a second model in rapid rotation about an axis perpendicular to the direction of flight. If the period of rotation is short compared with  $\tau$ , then we may use an average flux. At points where the normal to the surface is parallel to the direction of flight at some orientation during rotation, we have for the average flux

$$\bar{F} = \frac{\Lambda}{2\pi} \rho_a V^3. \quad (65)$$

From the computation for free molecular flow this flux, with  $\Lambda \simeq 1$ , gives an upper limit for the beginning height of 72.2 km, only 3.0 km above the photographed beginning height. This model is valid only for  $r \leq 0.53$  cm (from  $\Lambda = 1$  in eq. (2)). We also require that  $r > x_0$  by equation (17) otherwise the surface temperature will be higher than by equation (16) and ablation will begin at a greater height. We have  $k = 0.004$  cm<sup>2</sup> sec<sup>-1</sup> for meteoric iron from

$$k = \frac{\kappa}{c_p \rho_m}, \quad (66)$$

whence, in viscous or continuum flow,  $x_0 \leq 0.39$  cm, and in free molecular flow with rapid rotation  $x_0 = 0.27$  cm.  $r$  must lie in the range of about 0.3 to 0.5 cm in order that this latter model should be a valid physical picture.

For the nonrotating model,  $r$  must be sufficiently large so that  $\Lambda < 1$  at a height of 74.1 km in order to prevent the onset of ablation

at that height. Thus  $r > 0.23$  cm. In this case the controlling limit becomes  $r > x_0$  for viscous or continuum flow, a condition safely satisfied by  $r > 0.39$  cm. The radius for the model varies from about 0.4 to 1.5 cm. Öpik's criterion (eq. 59) for the shedding of droplets is 0.23 cm at this height for  $r = 1.54$  cm. At  $r = 0.37$  cm it is 0.15 cm, which is smaller due to the increase in  $\Gamma$ . We see that for this meteor this criterion is just satisfied and no more.

Next, for the nonrotating model, we must verify the assumption that vaporization is not important near  $x = 0$ . The highest surface temperature obviously occurs for the largest radius, which exhibits the slowest rate of removal of melt by divergence of the flow field. For a spherical meteoroid we have

$$\Gamma A (\rho_m / m)^{1/3} r = \frac{3}{4} \Gamma. \quad (67)$$

Equation (54) becomes

$$\frac{\Lambda \rho_a V^3}{2 \zeta \rho_m} = \frac{r \rho_a V^2}{\mu_0} \left( \frac{y_m}{r} \right)^2 \left[ \Lambda' - \frac{4}{3} \left( 1 - \frac{3}{8} \Gamma \right) \frac{y_m}{r} \right], \quad (68)$$

where  $\Lambda$  is given by equation (4),  $\Lambda'$  by equation (36),  $\Gamma$  by equation (60), and  $\zeta$  by

$$\zeta = c_{ps} T_m + \zeta_f + c_{pl} (T_0 - T_m), \quad (69)$$

where  $c_{ps}$  is the specific heat of the solid,  $\zeta_f$  the heat of fusion, and  $c_{pl}$  the specific heat of the liquid. Öpik (1958, pp. 156-158) gives  $c_{ps} = 6.91 \times 10^6$  ergs gm<sup>-1</sup> deg<sup>-1</sup>,  $\zeta_f = 2.69 \times 10^9$  ergs gm<sup>-1</sup>,  $c_{pl} = 6.66 \times 10^6$  ergs gm<sup>-1</sup> deg<sup>-1</sup>. We assume that the beginning of ablation occurred at  $h = 69.2$  km. Then the result is  $y_m/r \simeq -3.2 \times 10^{-3}$  for  $T_0 \simeq T_m = 1800^\circ\text{K}$ , and the final results are  $y_m/r = -3.1 \times 10^{-3}$ ,  $T_0 = 1874^\circ\text{K}$ . It may easily be shown from the vaporization law given by Öpik (1958, pp. 156-158) that rates of removal of both heat and mass by vaporization are smaller by three orders of magnitude compared with the rates due to flow of molten iron. Also the characteristic depth of heating is

$$\frac{k}{v_w} = 0.15 \text{ cm},$$

and the depth of the molten layer is  $-y_m = 4.8 \times 10^{-3}$  cm, which is about 1/20th of the depth of

heating. This circumstance makes the exponential in equation (49) nearly unity, and validates the use of equation (50).

**Photometric mass and end point from the light curve**

The light curve has the appearance of a standard light curve (Öpik, 1958, pp. 63–65) collapsed in duration. In the approximation where the scale height is constant, equation (6) may be used. If constant velocity is also assumed, the standard light curve takes the form

$$I(\rho_a) = \frac{27}{4} I_{\max} \frac{\rho_a}{\rho_e} \left(1 - \frac{\rho_a}{\rho_e}\right)^2, \quad (70)$$

where  $\rho_e$  is the ambient atmospheric density at the end point of the trail. Then  $\rho_a$  is given by equation (6),  $h$  by equation (8), and  $s$  by equation (9), which completes the conversion of the independent variable to time. From equation (6) we have

$$\frac{\rho_a}{\rho_e} = \exp[-(h - h_e)/H]. \quad (71)$$

We now propose to alter  $H$  from its true value to one that will fit the observed light curve. We do so for two purposes: to measure the total photographic light emitted by the meteor; and to extrapolate from the observed end point to the true end point of the meteor.

Halliday (1960) gives beginning and end heights determined by the threshold of the emulsion. On such a short trail we assume the threshold to be unchanged from beginning to end. Let us denote the intensity of the meteor at these points by  $I_{B,E}$ . Then the density at maximum intensity  $\rho_{\max}$  is given by

$$\frac{\rho_{\max}}{\rho_e} = \frac{1}{3}, \quad (72)$$

and from equation (71) we have

$$\begin{aligned} \frac{\rho_B}{\rho_{\max}} \left[ \left(1 - \frac{\rho_B}{\rho_e}\right) / \left(1 - \frac{\rho_{\max}}{\rho_e}\right) \right]^2 \\ = \frac{\rho_E}{\rho_{\max}} \left[ \left(1 - \frac{\rho_E}{\rho_e}\right) / \left(1 - \frac{\rho_{\max}}{\rho_e}\right) \right]^2 = \frac{I_{B,E}}{I_{\max}}, \end{aligned}$$

where  $\rho_B, \rho_E$  are the densities at the observed beginning and end points. By substituting

equation (72) into the above expression we find

$$\frac{\rho_B}{\rho_e} \left(1 - \frac{\rho_B}{\rho_e}\right)^2 = \frac{\rho_E}{\rho_e} \left(1 - \frac{\rho_E}{\rho_e}\right)^2 = \frac{4}{27} \frac{I_{B,E}}{I_{\max}} \quad (73)$$

A series of values of  $I_{B,E}/I_{\max}$  may be selected and  $\rho_B/\rho_e$  and  $\rho_E/\rho_e$  found by solving equation (73). For these values we obtain

$$\frac{\rho_{\max}}{\rho_B} = \frac{1}{3} \frac{\rho_e}{\rho_B}, \quad \frac{\rho_E}{\rho_{\max}} = 3 \frac{\rho_E}{\rho_e} \quad (74)$$

From equation (71) these ratios yield

$$h_B - h_{\max} = H \ln(\rho_{\max}/\rho_B), \quad (75)$$

$$h_{\max} - h_E = H \ln(\rho_E/\rho_{\max}), \quad (76)$$

where  $h_B, h_{\max}, h_E$  are the observed height of beginning, maximum intensity, and end, respectively. We now eliminate the scale height  $H$  by obtaining the ratio  $\mathcal{R}$  from equations (75) and (76):

$$\mathcal{R} = \frac{h_B - h_{\max}}{h_{\max} - h_E} = \frac{\ln(\rho_{\max}/\rho_B)}{\ln(\rho_E/\rho_{\max})} \quad (77)$$

The first form is an observed quantity, the second a computed quantity from equations (73) and (74). Thus the computed value must be matched with the observed value to find  $I_{B,E}/I_{\max}$ . Then equation (75) or equation (76) yields the effective scale-height for the light curve,

$$H = \frac{h_B - h_{\max}}{\ln(\rho_{\max}/\rho_B)} = \frac{h_{\max} - h_E}{\ln(\rho_E/\rho_{\max})}, \quad (78)$$

where the ratios have been computed from equation (74). Then from equations (71) and (72) the true end height (complete ablation of the meteoroid) is

$$h_e = h_{\max} - H \ln(\rho_e/\rho_{\max}) = h_{\max} - H \ln 3. \quad (79)$$

The total light emitted up to the disappearance of the meteor at  $t_e$  is

$$\begin{aligned} \int_{-\infty}^{t_e} I dt &= \frac{27}{4} \frac{H}{V} \sec Z_R \cdot I_{\max} \int_0^1 \left(1 - \frac{\rho_a}{\rho_e}\right)^2 d\left(\frac{\rho_a}{\rho_e}\right) \\ &= \frac{9}{4} \frac{H}{V} \sec Z_R \cdot I_{\max}. \quad (80) \end{aligned}$$

The photometric mass introduced by Millman and Cook (1959) is

$$\mathcal{M} = \int_{-\infty}^{t_e} \frac{I}{V^3} dt = \frac{9}{4} \frac{HI_{\max}}{V^4 \cos Z_R}, \quad (81)$$

where the terminal mass is neglected.

From the spectrogram, Halliday (1960) gives  $h_B=68.3$  km,  $h_E=64.9$  km, and from the direct photograph,  $h_B=69.2$  km,  $h_E=64.7$  km. From his figure 1, the ninth of thirteen visible segments of the spectrogram is seen to be the brightest. The corresponding value of  $h_{\max}$  is 66.0 km. Then the two values of  $\mathcal{R}$  are 2 and 2%, respectively, which in turn yield  $H=1.56$  and 1.62 km, and  $h_e=64.3$  km in both cases. Finally, he gives the maximum brightness in panchromatic light as absolute magnitude  $-4.2$ . The spectrum of a slow meteor is overwhelmingly due to iron, except for the D-line of sodium and the first positive group of nitrogen bands (Millman and Cook, 1959); hence, except for these two emissions, the reduction from panchromatic to photographic magnitude should be the same. The contribution of the D-line may safely be neglected, but the first positive group of  $N_2$  is not seen in Halliday's spectrogram, and hence the reduction found by Millman and Cook for a slow cometary meteor of  $+0.2$  magnitude should probably be altered by an unknown negative quantity. It seems best to make no correction at all, hence the intensity at maximum brightness was

$$I_{\max} = 10^{-0.4M_{\max}} = 50,$$

in units of a zero magnitude star. From equation (81) the photometric mass was

$$\mathcal{M} = 1.2 \times 10^{-17} \text{ 0 Mag cm}^{-3} \text{ sec}^4,$$

where  $H=1.59$  km is adopted as the effective scale-height of the light curve. This photometric mass and the end height of 64.3 km are our two fundamental observed quantities.

#### Limits on mass from end height

For the nonrotating model we can set an upper limit on the mass by putting  $\Lambda=1$  in equation (1). Then the total heat input to the end point of the trajectory will be given by

$$\int_{-\infty}^{t_e} F dt = \frac{1}{2} \rho_e V^3 \int_{-\infty}^{t_e} \exp \left[ \frac{V}{H} \cos Z_R (t - t_e) \right] dt = \frac{1}{2} \frac{\rho_e V^2 H}{\cos Z_R},$$

where we have substituted equations (6), (8), and (9), and integrated. For an upper limit on the diameter we neglect conduction of heat in directions other than the direction of flight, and use  $T_0=T_m$  in equation (69) for  $\zeta$ . We then obtain

$$d \leq \frac{\rho_e V^2 H}{2 \zeta \rho_m \cos Z_R}, \quad (82)$$

since all the heat input must ultimately be used for melting. The limit from equation (82) is 2.3 cm, so that the upper limit on the radius is 1.2 cm. A lower limit on the radius can be established by assuming equation (1) to be valid when  $\Lambda=1$  until equation (5) predicts a lower value, and then by using equation (5) with  $r$  fixed therein at its initial value. For a given value of  $r$  the two fluxes are equal when

$$\rho_a = \frac{1.297 \times 10^{-8}}{r}, \quad (83)$$

whence we have

$$\int_{-\infty}^{t_e} F dt = \frac{1}{2} \rho_e V^3 \int_{-\infty}^{t_e} \exp \left[ \frac{V}{H} \cos Z_R (t - t_e) \right] dt + 5.7 \times 10^{-6} r^{-1/2} \rho_e^{1/2} V^3 \int_{t_e}^{t_a} \exp \left[ \frac{1}{2} \frac{V}{H} \cos Z_R (t - t_e) \right] dt,$$

where

$$t_e - t^* = \frac{H}{V \cos Z_R} \ln (r \rho_e / 1.297 \times 10^{-8}).$$

We now find, with  $d=2r$ , that

$$\int_{-\infty}^{t_e} F dt = \frac{1}{2} \frac{\rho_e V^2 H}{\cos Z_R} \frac{1.297 \times 10^{-8}}{r \rho_e} + 1.14 \times 10^{-4} \frac{\rho_e^{1/2} V^2 H}{r^{1/2} \cos Z_R} \left\{ 1 - [1.297 \times 10^{-8} / (r \rho_e)]^{1/2} \right\} = 2 \zeta \rho_m r,$$

then

$$\frac{\rho_e^2 V^2 H}{4 \zeta \rho_m \cos Z_R} \left\{ \frac{1.297 \times 10^{-8}}{r \rho_e} + \frac{2.28 \times 10^{-4}}{(r \rho_e)^{1/2}} \left[ 1 - \frac{1.14 \times 10^{-4}}{(r \rho_e)^{1/2}} \right] \right\} = r \rho_e,$$

and if we put

$$u \equiv \frac{1.14 \times 10^{-4}}{(r \rho_e)^{1/2}} = \left( \frac{1.297 \times 10^{-8}}{r \rho_e} \right)^{1/2}, \quad (84)$$

we obtain

$$u^4 - 2u^3 + 5.19 \times 10^{-8} \frac{\zeta \rho_m \cos Z_R}{\rho_e^2 V^2 H} = 0. \quad (85)$$

The last term in equation (85) has the value 0.0526, and we find  $r \geq 0.61$  cm. This is, however, a closer limit than the upper limit previously found.

For the rotating model, an upper limit can be found as above by putting  $\Lambda=1$ , but using equation (65) instead of equation (1). The limit obtained is a limit on  $r$  rather than on  $d$  and is expressed by

$$r \leq \frac{\rho_e V^2 H}{2\pi \zeta \rho_m \cos Z_R}, \quad (86)$$

which establishes the limit  $r \leq 0.74$  cm.

A lower limit can be established as above but with the left-hand side divided by  $\pi$  for averaging the flux over a rotation and the right-hand side divided by 2, since the radius rather than the diameter sets the limit. The result is

$$\int_{-\infty}^{t^*} F dt' = \frac{1}{2\pi \cos Z_R} \frac{\rho_e V^2 H}{\rho_e} \frac{1.297 \times 10^{-8}}{\rho_e} + \frac{1.14 \times 10^{-4}}{\pi} \frac{\rho_e^{1/2} V^2 H}{r^{1/2} \cos Z_R} \left[ 1 - \left( \frac{1.297 \times 10^{-8}}{r \rho_e} \right)^{1/2} \right] = \zeta \rho_m r,$$

and then

$$u^4 - 2u^3 + 5.19 \times 10^{-8} \frac{\pi \zeta \rho_m \cos Z_R}{2 \rho_e^2 V^2 H} = 0. \quad (87)$$

The last term in equation (87) has the value 0.083, whence we find  $r \geq 0.44$  cm.

From the above analysis we may estimate  $0.5 \leq r \leq 0.9$  cm. The corresponding range for the mass is from 4 to 24 gm. For  $r=0.7$  cm, the mass is 11 gm.

#### Coefficient in formula for luminous efficiency

The coefficient in the law for luminous efficiency, the mass, and the photometric mass are related as follows (Millman and Cook, 1959):

$$m = \frac{2}{\tau_0} \mathcal{M}, \quad \tau_0 = \frac{2\mathcal{M}}{m}, \quad (88)$$

whence we find  $\tau_0 = 6 \times 10^{-18}$  to  $10^{-18}$  0 Mag  $\text{gm}^{-1} \text{cm}^{-3} \text{sec}^4$  as  $r$  varies from 0.5 to 0.9 cm. For  $r=0.7$  cm, we have  $\tau_0 = 2 \times 10^{-18}$  0 Mag  $\text{gm}^{-1} \text{cm}^{-3} \text{sec}^4$ .

On the other hand, McCrosky and Soberman (see this symposium, p. 199) find that, from a re-entering iron pellet of known mass,  $\tau_0 = 8 \times 10^{-18}$  0 Mag  $\text{gm}^{-1} \text{cm}^{-3} \text{sec}^4$ . If we now use the logarithmic mean, we obtain

$$\left. \begin{aligned} \log \tau_0 &= -17.70 \text{ for spectrum no. 210,} \\ \log \tau_0 &= -18.10 \text{ for re-entering pellet,} \\ \log \tau_0 &= -17.90 \text{ adopted pro tempore.} \end{aligned} \right\} \text{Iron}$$

For low velocity meteors the spectrum in the photographic region is almost exclusively dominated by iron lines (Millman and Cook, 1959). Hence we should be able to derive the luminous efficiency of meteoric stone in photographic light from that of iron by multiplying the luminous efficiency of iron by the fraction of the mass of meteoric stone due to iron. According to Öpik (1958, pp. 159-162) this fraction is 0.154, from which we deduce that  $\log \tau_0 = 18.71$  for stone.

#### Coefficient in deceleration equation for stone

The deceleration equation usually appears in the form

$$\frac{dV}{dt} = -\frac{1}{K} \frac{\rho_a V^2}{\mathcal{M}^{1/3}}, \quad (89)$$

where  $K$  is an observable quantity,

$$K = \frac{\rho_a V^2}{\mathcal{M}^{1/3} (-dV/dt)}. \quad (90)$$

In terms of physical parameters, it takes the form

$$K = \frac{2^{1/3} \rho_m^{2/3}}{\tau_0^{1/3} \Gamma A}, \quad (91)$$

where  $A$  is a shape factor. For a sphere we have

$$A = (9\pi/16)^{1/3} = 1.208.$$

If we insert into equation (91) this value of  $A$  and the value of  $\tau_0$  for stone found above, then  $K = 3.4 \times 10^6$  for  $\Gamma=1$ , and  $8.1 \times 10^6$  for  $\Gamma=1/2$ . The corresponding values of the logarithm are  $\log K = 6.61$  and  $6.91$ , respectively. These expected values for stony meteors may be contrasted with  $\log K \simeq 6.29$  observed for cometary

TABLE 1.—Observed data for meteor No. 1242

(Beginning height, 74.9 km on FA 8808; maximum light, 47.1 km on FA 8808 and AI 39336; end height, 38.0 km on FA 8808, 36.6 km on RH 12890;  $\cos Z_R=0.632$ .)

Epoch <i>t</i> (sec)	Height <i>h</i> (km)	Velocity <i>V</i> (km/sec)	Acceleration <i>dV/dt</i> (km/sec <sup>2</sup> )	Air density* $\rho_a$ (gm/cm <sup>3</sup> )	$\mathcal{M}-\mathcal{M}_e$ O Mag cm <sup>-3</sup> sec <sup>4</sup>	I O Mag	I (smoothed) O Mag
1. 0526	62.56	11.93	-0.185	$2.58 \times 10^{-7}$	$7.56 \times 10^{-18}$	3.0	3.0
1. 6842	57.78	11.81	-0.389	$4.49 \times 10^{-7}$	$6.69 \times 10^{-18}$	3.3	3.3
2. 3158	53.10	11.48	-0.660	$7.49 \times 10^{-7}$	$5.64 \times 10^{-18}$	4.8	4.0
2. 9474	48.61	10.94	-1.024	$1.278 \times 10^{-6}$	$4.07 \times 10^{-18}$	4.3	4.0
3. 5790	44.38	10.13	-1.505	$2.195 \times 10^{-6}$	$2.432 \times 10^{-18}$	4.0	3.3
4. 2105	40.57	8.87	-2.23	$3.698 \times 10^{-6}$	$0.885 \times 10^{-19}$	2.1	2.1

\* According to Minzner, Champion, and Pond (1959).

TABLE 2.—Reduced values of parameters on assumption that  $1/K$  and  $\sigma$  are constant for last three epochs

Epoch <i>t</i> sec	Photometric mass $\mathcal{M}$ O Mag cm <sup>-3</sup> sec <sup>4</sup>	$1/K$ O Mag <sup>1/3</sup> gm <sup>-1</sup> cm sec <sup>4/3</sup>	$\sigma/K$ O Mag <sup>1/3</sup> gm <sup>-1</sup> cm <sup>3</sup> sec <sup>-2/3</sup>
1. 0526	$10.09 \times 10^{-18}$	$1.087 \times 10^{-7}$	$8.41 \times 10^{-19}$
1. 6842	$9.22 \times 10^{-18}$	$1.303 \times 10^{-7}$	$6.16 \times 10^{-19}$
2. 3158	$8.17 \times 10^{-18}$	$1.347 \times 10^{-7}$	$5.75 \times 10^{-19}$
2. 9474	$6.60 \times 10^{-18}$	$1.255 \times 10^{-7}$	$5.19 \times 10^{-19}$
3. 5790	$4.96 \times 10^{-18}$	$1.140 \times 10^{-7}$	$4.78 \times 10^{-19}$
4. 2105	$3.42 \times 10^{-18}$	$1.155 \times 10^{-7}$	$5.15 \times 10^{-19}$

TABLE 3.—Deduced values of parameters on assumption that  $1/K$  is constant over trajectory(The values of  $\sigma$  are computed using the mean  $1/K$  deduced for computation of the masses.)

Epoch <i>t</i> sec	Photometric mass $\mathcal{M}$ O Mg cm <sup>-3</sup> sec <sup>4</sup>	$1/K$ O Mag <sup>1/3</sup> gm <sup>-1</sup> cm sec <sup>4/3</sup>	$\sigma/K$ O Mag <sup>1/3</sup> gm <sup>-1</sup> cm <sup>3</sup> sec <sup>-2/3</sup>	$\sigma$ cm <sup>2</sup> sec <sup>-2</sup>
1. 0526	$1.710 \times 10^{-17}$	$1.285 \times 10^{-7}$	$5.92 \times 10^{-19}$	$3.6 \times 10^{-12}$
1. 6842	$1.623 \times 10^{-17}$	$1.573 \times 10^{-7}$	$4.23 \times 10^{-19}$	$2.6 \times 10^{-12}$
2. 3158	$1.518 \times 10^{-17}$	$1.656 \times 10^{-7}$	$3.81 \times 10^{-19}$	$2.3 \times 10^{-12}$
2. 9474	$1.361 \times 10^{-17}$	$1.598 \times 10^{-7}$	$3.20 \times 10^{-19}$	$2.0 \times 10^{-12}$
3. 5790	$1.197 \times 10^{-17}$	$1.529 \times 10^{-7}$	$2.66 \times 10^{-19}$	$1.6 \times 10^{-12}$
4. 2105	$1.042 \times 10^{-17}$	$1.676 \times 10^{-7}$	$2.45 \times 10^{-19}$	$1.5 \times 10^{-12}$

meteors. Two such meteors with anomalously large  $\log K$  have been well photographed in the Harvard Program, and will be discussed in turn.

#### Meteor No. 1242

Meteor No. 1242 was photographed on February 6, 1945, from Harvard College Observatory in Cambridge, Mass., on plate no. AI 39336, and at the Oak Ridge Station (now Agassiz Station) in Harvard, Mass., on plates nos. FA 8808 and RH 12890. The meteor appeared at 5<sup>h</sup> 12<sup>m</sup> 17<sup>s</sup> UT. Table 1 lists the pertinent data from the reductions.

The method of Millman and Cook (1959) is used to determine that  $\mathcal{M}_e=2.5 \times 10^{-18}$  from the last three points. The results are given in table 2. These results are not satisfactory since neither  $1/K$  nor  $\sigma$  is constant.

We next assume that  $1/K$  alone is constant. From the reciprocal of the cube of equation (90) we have

$$\frac{1}{K^3} = \left[ \frac{(-dV/dt)}{\rho_a V^2} \right]^3 \mathcal{M} = \left[ \frac{(-dV/dt)}{\rho_a V^2} \right]^3 \mathcal{M}_e + \left[ \frac{(-dV/dt)}{\rho_a V^2} \right]^3 (\mathcal{M} - \mathcal{M}_e). \quad (92)$$

The coefficient of  $\mathcal{M}_e$  and the entire last term are observed quantities. The equation is to be solved for  $\mathcal{M}_e$  and  $1/K^3$  as unknowns. We do so by grouping the first three epochs and the last three epochs and using average values for each. The results are  $1/K=1.628 \times 10^{-7}$  O Mag gm<sup>-1</sup> cm sec,  $\log K=6.79$ , and  $\mathcal{M}_e=9.54 \times 10^{-18}$  O Mag gm<sup>-3</sup> sec<sup>4</sup> (see table 3). We estimate that  $\Gamma \approx 1/2$  since we are presumably far from free molecular flow, and hence  $\log \tau_0 = -18.36$ .

TABLE 4.—Observed data for Meteor No. 19816

(1/K(obs) = value computed from eq. (90); 1/K(corr) = 1/K(obs) corrected for presence of two equal fragments; beginning height, 91.1 km (SK); maximum light, 60.1 km; end height, 47.1 km (SL);  $\cos Z_R = 0.716$ .)

Camera	<i>t</i> sec	<i>h</i> km	<i>V</i> km/sec	<i>dV/dt</i> km/sec <sup>2</sup>	$\rho_a$ gm/cm <sup>3</sup>	$\mathcal{M} - \mathcal{M}_c$ O Mag cm <sup>-3</sup> sec <sup>4</sup>	<i>I</i> O Mag	1/K(obs) cm sec <sup>4/3</sup>	1/K(corr)	$\sigma$ cm <sup>2</sup> sec <sup>-2</sup>
SK	0.764	80.13	20.67	-0.158	$2.117 \times 10^{-8}$	$6.60 \times 10^{-10}$	1.2	$1.52 \times 10^{-7}$	$1.52 \times 10^{-7}$	$6.0 \times 10^{-12}$
SL	1.135	74.02	20.57	-0.416	$5.739 \times 10^{-8}$	$6.07 \times 10^{-10}$	1.3	$1.45 \times 10^{-7}$	$1.45 \times 10^{-7}$	$2.9 \times 10^{-12}$
SK	1.860	64.16	19.87	-2.02	$2.123 \times 10^{-7}$	$4.43 \times 10^{-10}$	2.5	$1.84 \times 10^{-7}$	$1.84 \times 10^{-7}$	$1.8 \times 10^{-12}$
SL	2.038	61.06	19.27	-2.75	$3.105 \times 10^{-7}$	$3.87 \times 10^{-10}$	2.5	$1.74 \times 10^{-7}$	$1.38 \times 10^{-7}$	$1.7 \times 10^{-12}$
SK	2.425	56.49	17.85	-5.92	$5.178 \times 10^{-7}$	$2.71 \times 10^{-10}$	1.9	$2.32 \times 10^{-7}$	$1.84 \times 10^{-7}$	$1.2 \times 10^{-12}$
SL	2.623	53.75	16.36	-8.45	$6.935 \times 10^{-7}$	$2.05 \times 10^{-10}$	1.9	$2.68 \times 10^{-7}$	$2.13 \times 10^{-7}$	$1.5 \times 10^{-12}$
SK	2.824	51.87	14.63	-9.67	$8.662 \times 10^{-7}$	$1.14 \times 10^{-10}$	1.3	$2.53 \times 10^{-7}$	$2.01 \times 10^{-7}$	$2.6 \times 10^{-12}$
SL	3.124	48.92	10.77	-8.90	$1.231 \times 10^{-6}$	$0.32 \times 10^{-10}$	0.23	$1.98 \times 10^{-7}$	$1.57 \times 10^{-7}$	$6.0 \times 10^{-12}$

Smoothed magnitudes are used at some epochs, primarily because oscillations appear on the FA and AI plates near maximum light. A very short period flicker is found on the RH plate. The following model may be used to represent the observed behavior. The meteoroid is assumed to have been in rapid rotation upon entering the atmosphere. After free molecular flow was left behind, a torque depending upon orientation developed and became stronger. First, the angular velocity of rotation was diminished at all orientations except those for which no torque occurred, and restoring torques were met on either side of these null orientations. The period lengthened until rotation ceased and oscillation began about an equilibrium orientation. This change occurred around maximum light. Thereafter the period of oscillation became progressively shorter. Next, we consider the shape bounded by two right circular cylinders of equal diameter with axes intersecting perpendicularly. We then make the axis of rotation perpendicular to the axes of the cylinders. Finally, we orient the axis of rotation perpendicular to the direction of flight. Such a model does not really deviate much from a sphere, and yet it can be shown that the torques produced upon it are about equal to those required to fit the observed periods. This model can also be made to fit an observed proportionality of the period of oscillation to the inverse square root of the air density along the lower part of the trail.

**Meteor No. 19816**

This sporadic meteor was photographed with the Super-Schmidt meteor cameras (SL 12537

and SK 9821) at the Sacramento Peak and Organ Pass meteor stations in New Mexico. The meteor appeared at 08<sup>h</sup> 50<sup>m</sup> 13<sup>s</sup> UT on December 8, 1958. The entire trajectory of 62 km was photographed on at least one of the cameras, but the initial 12 km and the final 4 km were photographed at only one station.

The light curve is particularly smooth, exhibiting only one brief flare of 0.2 magnitude. During the final portion of the trajectory, two particles are in evidence, and it is likely that the flare represents the time of splitting of the original body. The deceleration history of the separate particles indicates that they have nearly comparable masses. The lifetimes and the total luminosity of each particle are similar. In the following analysis we have made the approximation that the masses and area of the particles are exactly identical although, in fact, some difference between them must exist for differential deceleration to be observed. Apart from this single fracturing, there is no evidence of unusual wake or terminal blending that frequently is visible in meteor trails formed by fragmenting cometary bodies.

The data for this meteor is given in table 4. Four deceleration solutions were made for each trail. The values for  $K^{-1}$  are generally lower for the later solutions, presumably due to the presence of the two fragments. In the penultimate column of table 4, we increased  $K^{-1}$  by  $2^{1/3}$  for those solutions where two fragments existed. The corrected values show no significant trend with time. It appears that the terminal mass is negligible, as would be expected for a meteor with an initial velocity of 21 km/sec. Assuming the same values for  $A$ ,  $\Gamma$ , and  $\rho_m$

TABLE 5.—Orbital elements of asteroidal meteors

Meteor	Corr. rad.		$V_{\infty}$ (km/sec)	$a$	$e$	$q$	$q'$	$\omega$	$\Omega$	$i$	$\pi = \omega + \Omega$
	$\alpha$	$\delta$									
Iron Meteor	332°0	+73°2	13.4	1.05	.117	.928	1.173	247°5	219°1	13°3	106°6
Meteor No. 1242	3°0	+59°2	12.2	1.33	.262	.984	1.68	172°1	317°1	6°9	129°2
Meteor No. 19816	70°5	-0°2	20.7	2.24	.662	.756	3.72	65°4	75°7	12°6	141°1
Přibram Meteorite	191°5	+17°7	20.9	2.42	.674	.790	4.05	241°6	17°1	10°4	258°7

as were used for meteor no. 1242, we find  $\log \tau_0 = -18.24$ . These two values are in excellent agreement.

#### Optimum values of the luminous efficiency factor for iron and stone

Spectrum no. 210 yields, on reduction for the abundance fraction of iron in stone,  $\log \tau_0 = -18.51$  for stone. For the above two meteors  $\log \tau_0 = -18.36$  and  $-18.24$ . The mean of the three values is

$$\log \tau_0 = -18.37 \text{ for stone.}$$

Application of the reduction for the abundance fraction of iron yields  $\log \tau_0 = -17.56$  for iron, while McCrosky and Soberman (see this symposium, p. 199) find  $\log \tau_0 = -18.10$  for a re-entering iron pellet of known mass. This discrepancy corresponds to a deviation in the shape factor (larger than for a sphere) by the antilogarithm of 0.18, or of about 1.51. If we adopt this new corresponding value of the shape factor we have

$$A = 1.83, \log \tau_0 = -18.10 \text{ for iron, and} \\ -18.91 \text{ for stone.} \quad (93)$$

#### Orbits of asteroidal meteors

The meteors discussed in this paper are of unique value because their physical characteristics indicate that the objects are of asteroidal origin. These meteors, together with the Přibram meteorite that was photographed in flight (Ceplecha, 1961), represent a new source of data on the orbits of asteroidal material with small perihelion distance. The information is collected in table 5. Three of the orbits have

been published previously (Halliday, 1960; Whipple, 1954; and Ceplecha, 1961).

It is apparent in the table that these four meteors represent two distinct classes of orbits. However, an inspection of the orbits of the asteroids with small perihelion distance indicates that this is probably a chance grouping.

#### References

- CEPLECHA, ZD.  
1961. Multiple fall of Přibram meteorites photographed. *Bull. Astron. Inst. Czechoslovakia*, vol. 12, pp. 21-47.
- HALLIDAY, I.  
1960. The spectrum of an asteroidal meteor fragment. *Astrophys. Journ.*, vol. 132, pp. 482-485.
- LEVIN, B. J.  
1956. The physical theory of meteors and meteoric matter in the solar system. *Publ. House Acad. Sci. U.S.S.R.*, Moscow. (German translation published by Akademie-Verlag, Berlin, 1961, pp. 47-49.)
- MILLMAN, P. M., AND COOK, A. F.  
1959. Photometric analysis of a spectrogram of a very slow meteor. *Astrophys. Journ.*, vol. 130, pp. 648-662.
- MINZNER, R. A.; CHAMPION, K. S.; AND POND, H. L.  
1959. The ARDC model atmosphere. *Air Force Surveys in Geophysics*, No. 115, Geophysical Research Directorate, Air Force Cambridge Research Laboratories.
- ÓPIK, E. J.  
1958. *Physics of meteor flight in the atmosphere*. Interscience, New York.
- PROBSTEIN, R. F., AND KEMP, N. H.  
1960. Viscous aerodynamic characteristics in hypersonic rarefied gas flow. *Journ. Aerospace Sci.*, vol. 27, pp. 174-192.
- WHIPPLE, F. L.  
1954. Photographic meteor orbits and their distribution in space. *Astron. Journ.*, vol. 59, pp. 201-217.

# Meteor Ionization and the Mass of Meteoroids

By Donald M. Lazarus<sup>1</sup> and Gerald S. Hawkins<sup>2</sup>

The excitation and ionization observed in meteor trails have long been assumed to result from inelastic collisions of meteor atoms with those of the atmosphere after their ablation from the meteoroid surface. This assumption is based on the premise that the surface temperature of meteoroids is inadequate to cause excitation and ionization. Unfortunately, meteor velocities are such that the quantum mechanical calculation of excitation and ionization cross sections is difficult because neither the high-energy Born approximation nor the assumption of adiabatic collisions is really valid. In addition, the complex electronic structure of the meteor constituents and the atoms of the atmosphere make the form of their interaction mathematically unwieldy. Lastly, suitable analytical wave functions are not available for most of the atoms in question.

However, it is possible to make reasonable approximations to the form of the interaction and to the wave functions. The problem of wave-function distortion in the case of near adiabatic collisions is not so easily handled, but its expected effect is discussed in our analysis of the predictions of various cross-section calculations.

## The ionization cross section

Inelastic atomic collisions are most conveniently classified by the ratio of the duration of the collision to the period of the internal motion of the electron to be excited (Massey, 1949). This ratio is conveniently given (Bates and Massey, 1954) by the expression

$$\frac{T}{\tau} \approx \frac{6\ell\Delta EM_1^{1/2}}{E^{1/2}}, \quad (1)$$

<sup>1</sup> Yale University, New Haven, Conn.; and Harvard College Observatory, Cambridge, Mass.

<sup>2</sup> Boston University, Boston, Mass.; Smithsonian Astrophysical Observatory, Cambridge, Mass.; and Harvard College Observatory, Cambridge, Mass.

where  $\ell$  is the atomic radius in units of  $a_0$ ;  $\Delta E$  is the energy of the transition in ev;  $M_1$  is the mass of the incident atom relative to the proton mass; and  $E$  the impact energy in ev. For fast collisions,  $T/\tau \ll 1$ , and the Born approximation is valid. When  $T/\tau \gg 1$ , the encounter is said to be near adiabatic. For  $\Delta E = 5$  ev,  $T/\tau$  varies between 12 and 7 for velocities between 35 and 60 km/sec. Bates and Massey (1954) have pointed out that in this instance it is necessary to treat the colliding atoms as a quasi-molecule. The perturbed stationary-state method (Massey and Smith, 1933) could then be applied, taking into account the effect of the interaction on the wave functions during the collision. Unfortunately, this treatment is not a useful one in practice as the wave functions and potential energy curves for the pseudo-molecule are generally neither known nor readily calculable. However, if the interaction does not produce a near crossing of the potential energy curves of the atoms in the initial and final states in question, then a result similar to a Born approximation calculation would be found (Mott, 1931), except for the fact that a reduction of the cross section at low energies occurs because of distortion. If, however, there is a near crossing of the potential energy curves, an adiabatic transition becomes more probable. The probability for this type of transition has been calculated by Landau (1932), Zener (1932), and Stueckelberg (1932), and applied to transitions into the continuum by Bates and Massey (1954) with the result that the cross section for ionization is given approximately by the relation,

$$\sigma = \left( \frac{3.8 \times 10^{-15} g M_1^{1/2} R_x^3}{E^{1/2} t} \right) \pi a_0^2, \quad (2)$$

when the expression in parentheses is small compared with unity. The symbol  $g$  is the

ratio of the statistical weight of the initial state to all other possible initial states;  $R_x$  is the internuclear distance at which the separation of the initial and final states of the potential energy curves is a minimum; and  $t$  is the lifetime for auto-ionization of the quasi-molecule.

The formulation used in this paper is that of the variation of parameters (Schiff, 1955, chap. 8, sec. 30), which in first order gives the same result and has the same range of validity as the first Born approximation.

The interaction, i.e., the electric potential due to the atmospheric atom at the positions  $r_i$  of the electrons of the sodium atom, is taken to be the screened coulomb potential,

$$V = \sum_i \frac{A}{|r_1 - r_i|} e^{-\alpha|r_1 - r_i|}, \quad (3)$$

where  $r_1$  is the internuclear separation,  $r_i$  the position of the  $i^{\text{th}}$  electron of the sodium atom relative to its nucleus, and  $\alpha$  and  $A$  are interaction parameters. We assume that the electron wave-functions can be separated, and that removal of the 3s electron does not appreciably change the wave function of the inner electrons. With these approximations, the matrix element for the transition to the continuum becomes

$$H' = L^{-3} \iint e^{i(\vec{k}_0 - \vec{k}) \cdot \vec{r}_1} \psi_{k'}(r_2) \frac{A}{r_{12}} e^{-\alpha r_{12}} \psi_0(r_2) d\tau_1 d\tau_2, \quad (4)$$

where  $\psi_{k'}(r_2)$  and  $\psi_0(r_2)$  are the ionized and initial state functions, respectively, and  $L^3$  is the volume in which the atoms are normalized. As usual,  $\vec{k}_0$  and  $\vec{k}$  are the initial and final propagation vectors for the interaction potential in center of mass coordinates, and  $r_{12} = |\vec{r}_1 - \vec{r}_2|$ . Any sophistication in the choice of the analytical wave functions  $\psi_{k'}(r_2)$  and  $\psi_0(r_2)$  leads to a matrix element that is totally unwieldy for calculation. The functions were therefore taken to be

$$\psi_{k'}(r_2) = (L')^{-3/2} e^{-i\vec{k}' \cdot \vec{r}_2} \quad (5)$$

for the ejected electron; with  $\vec{k}' = m\vec{v}'/\hbar$ , the electron momentum divided by Planck's constant over  $2\pi$ ,

$$\psi_0(r_2) = Br_2^2 e^{-br_2} \quad (6)$$

for the normal state, where  $(L')^{-3/2}$  and  $B$  are the usual normalizing factors, and  $b$  is a constant parameter. The lack of orthogonality of the initial and final state functions has been investigated. It can be shown that adding an orthogonalizing term to equation (5) by the Schmidt process affects the matrix element only slightly. This term vanishes as  $r_2 \rightarrow \infty$ , so that the asymptotic form of  $\psi_{k'}(r_2)$  is not affected.

By integration with the usual substitution  $\vec{K} = \vec{k}_0 - \vec{k}$ , the matrix element becomes

$$H' = L^{-3} (L')^{-3/2} \frac{(4\pi)^2 AB}{\alpha^2 + K^2} \cdot \frac{24b(b^2 - |\vec{K} - \vec{k}'|^2)}{(b^2 + |\vec{K} - \vec{k}'|^2)^4}. \quad (7)$$

If we define  $\vec{K}' \equiv \vec{K} - \vec{k}'$ , equation (7) becomes

$$|H'|^2 = L^{-6} L'^{-3} \frac{9 \times 2^{14} A^2 B^2 b^2 (b^2 - K'^2)^2}{(\alpha^2 + K^2)^2 (b^2 + K'^2)^8}. \quad (8)$$

The probability for the ejection of the valence electron with wave number  $k'$  in the direction  $\theta', \varphi'$ , accompanied by the scattering of the atmospheric atom with wave number  $k$  in the direction  $\theta, \varphi$ , is given by the expression

$$\begin{aligned} \sigma_{k'}(\theta\varphi\theta'\varphi'k') \sin\theta d\theta d\varphi \sin\theta' d\theta' d\varphi' \\ = \frac{2\pi\mu L^3}{\hbar^2 k_0} \rho(k) \rho(k') |H'|^2, \quad (9) \end{aligned}$$

where  $\sigma_{k'}(\theta\varphi\theta'\varphi'k')$  is the differential cross section for the process;  $\mu$  the reduced mass so that  $\vec{k}_0 = \mu\vec{v}_0/\hbar$  and  $\vec{k} = \mu\vec{v}/\hbar$  where  $\vec{v}_0$  and  $\vec{v}$  are the initial and final relative velocities, respectively; and  $\rho(k)$  and  $\rho(k')$  the densities of states in the vicinity of  $\vec{k}$  and  $\vec{k}'$ , respectively. The densities are

$$\left. \begin{aligned} \rho(k) &= \frac{\mu L^3}{(2\pi)^3} k \sin\theta d\theta d\varphi, \\ \rho(k') &= \frac{m L'^3}{(2\pi)^3} k' \sin\theta' d\theta' d\varphi', \end{aligned} \right\} \quad (10)$$

so that the total cross section for ionization from the ground state is given by the expression,

$$\sigma_I(k_0) = \iiint \int \sigma(\theta\varphi\theta'\varphi'k') \sin\theta d\theta d\varphi \sin\theta' d\theta' d\varphi' dk' \quad (11)$$

$$= \frac{m\mu^2 L^6 L'^3}{(2\pi)^6 \hbar^2 k_0} \iiint \int |H'|^2 k k' \sin\theta d\theta d\varphi \sin\theta' d\theta' d\varphi' dk'. \quad (12)$$

Transforming from angular to momentum variables, we obtain

$$\left. \begin{aligned} K^2 &= k_0^2 + k^2 - 2kk_0 \cos\theta, \\ k \sin\theta d\theta &= \frac{K}{k_0} dK; \end{aligned} \right\} \quad (13)$$

and

$$\left. \begin{aligned} K'^2 &= K^2 + k'^2 - 2Kk' \cos\theta', \\ Kk' \sin\theta' d\theta' &= K' dK'. \end{aligned} \right\} \quad (14)$$

Substituting equation (8) in equation (12) and carrying out the integrations over  $\varphi$  and  $\varphi'$ , we obtain

$$\sigma_I(k_0) = \frac{9 \times 2^{11} \pi m \mu^2 b^2 A^2 B^2}{\hbar^2 k_0^2} \int_0^{K^{\max}} dk' \int_{k_0-k}^{k_0+k} \frac{dK}{(\alpha^2 + K^2)^2} \int_{K-k'}^{K+k'} \frac{(b^2 - K'^2)^2}{(b^2 + K'^2)^3} K' dK'. \quad (15)$$

The first integral is easily evaluated:

$$\begin{aligned} & \int_{K-k'}^{K+k'} \frac{(b^2 - K'^2)^2}{(b^2 + K'^2)^3} K' dK' \\ &= \frac{2b^4}{7} \left\{ \frac{1}{[b^2 + (K-k')^2]^7} - \frac{1}{[b^2 + (K+k')^2]^7} \right\} \\ & \quad - \frac{b^2}{3} \left\{ \frac{1}{[b^2 + (K-k')^2]^6} - \frac{1}{[b^2 + (K+k')^2]^6} \right\} \\ & \quad + \frac{1}{10} \left\{ \frac{1}{[b^2 + (K-k')^2]^5} - \frac{1}{[b^2 + (K+k')^2]^5} \right\}. \end{aligned}$$

The lower limit  $k_0 - k$  for the second integration is determined by applying the principle of the conservation of energy:

$$(k_0 - k)(k_0 + k) = 2\mu \left[ E_I + \frac{\hbar^2}{2m} k'^2 \right], \quad (16)$$

where  $E_I$  is the ionization energy. The upper limit is taken as infinity since the greatest

contribution to the integral is for small values of  $K$ .

For small values of  $k_0$ ,

$$(k - k_0) \approx \frac{\mu}{k_0} \left( E_I + \frac{\hbar^2 k'^2}{2m} \right) \left[ 1 + \frac{\mu}{2k_0^2} \left( E_I + \frac{\hbar^2 k'^2}{2m} \right) \right] \gg 1. \quad (17)$$

It is therefore possible to expand:

$$\frac{1}{(\alpha^2 + K^2)^2} = \frac{1}{K^4} \left( 1 - \frac{\alpha^2}{K^2} + \dots \right). \quad (18)$$

If we retain the first two terms in equation (18) and the leading term in equation (17) and introduce the notation,

$$Z_{\pm} = \left( \frac{\mu E_I}{k_0} \right)^2 \pm 2k' \left( \frac{\mu E_I}{k_0} \right) + b^2 + k'^2, \quad (19)$$

the cross section becomes

$$\begin{aligned} \sigma_I(k_0) &= \frac{9 \times 2^{11} \pi m \mu^2 b^2 A^2 B^2}{\hbar^2 k_0^2} \int_0^{k'^{\max}} dk' \left\{ S \ln \left( \frac{Z_-}{Z_+} \right) \right. \\ & \quad + R \left[ \tan^{-1} \left( \frac{k_0 + k'}{b} \right) - \frac{\pi}{2} \right] + Q \left( \frac{1}{Z_+} - \frac{1}{Z_-} \right) \\ & \quad \left. + P \left( \frac{1}{Z_+^2} - \frac{1}{Z_-^2} \right) + \dots \right\}. \quad (20) \end{aligned}$$

The coefficients  $S$ ,  $R$ ,  $Q$ , and  $P$  are functions of  $\alpha$ ,  $b$ ,  $k_0$ , and  $k'$ . The interaction parameters  $A$  and  $\alpha$  were chosen to give the best possible fit to the oxygen potential determined by the numerical integration of the radial charge distribution obtained from the Hartree (1957) numerical wave-functions. The value of  $b$  was taken from the Slater (1951, app. 13, p. 476) screening constants.

The numerical integration of equation (20) was performed for several values of  $k_0$  and the resulting cross section is plotted in figure 1.

### The ionization probability

The probability of ionization of an atom with wave number  $k_i$  in one collision is

$$\beta_i = \frac{\sigma_I(k_i)}{\sigma_0(k_i) + \Sigma\sigma_E(k_i) + \sigma_I(k_i)}, \quad (21)$$

where  $\sigma_0(k_i)$  is the elastic scattering cross section; and  $\Sigma\sigma_E(k_i)$  is the sum of all possible excitation cross sections. The elastic scattering cross section for a single charged particle encountering a screened coulomb field is, in the

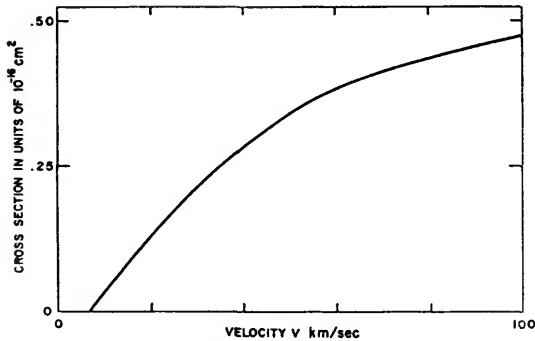


FIGURE 1.—The dependence of ionizing cross section on velocity.

first Born approximation (Schiff, 1955, chap. 7, sec. 26),

$$\sigma_0(k_i) = \frac{16\pi\mu^2 Z^2 e^4 a^4}{\hbar^4 (4k_i^2 a^2 + 1)}, \quad (22)$$

where  $a \approx \frac{\hbar^2}{m e^2 Z^{1/3}}$ ;  $e$  represents the electronic, and  $Ze$  the nuclear charge. In the energy range under consideration,  $\sigma_0(k_i)$  is much greater than  $\sigma_I(k_i)$ , and it will be assumed also to be much greater than  $\Sigma \sigma_{\pi}(k_i)$ . Therefore,

$$\beta_i \approx \frac{\sigma_I(k_i)}{\sigma_0(k_i)}. \quad (23)$$

If we let  $P_i$  be the probability that ionization will result from the  $i^{\text{th}}$  collision, it is easily seen that

$$\begin{cases} P_1 = \beta_1, \\ P_2 = \beta_2(1 - \beta_1), \\ P_i = \beta_i \left\{ 1 - \sum_{j=1}^{i-1} \beta_j + \sum_{j>k}^{i-1} \sum_{k=1}^{i-2} \beta_j \beta_k - \dots - \prod_{s=1}^{i-1} \beta_s \right\}. \end{cases} \quad (24)$$

The possibility of ionization from an excited state has been neglected because the lifetimes of excited states are much less than the average time between encounters in the upper atmosphere.

Since  $\beta_i \ll 1$ , it is possible to simplify the last of equations (24) to the expression

$$P_i \approx \beta_i, \quad (25)$$

so that the total probability for the ionization of an evaporated meteor atom becomes

$$\beta = \sum_i \beta_i. \quad (26)$$

Let  $\eta_i$  be the fraction of the velocity lost in an elastic collision with an atmospheric atom. By combining the equations for conservation of momentum and energy, we can then give  $\eta_i$  as

$$\eta_i = \frac{\mu_1}{\mu_1 + \mu_2} [\cos \theta_i \pm (\mu_2^2/\mu_1^2 - \sin^2 \theta_i)^{1/2}], \quad (27)$$

where  $\mu_1$  is the mass of a meteor atom,  $\theta_i$  the angle of scattering of the meteor atom, and  $\mu_2$  the mass of the atmospheric atom. The average of  $\eta_i$  over the normalized angular distribution in the approximation  $k_i^2 a^2 \gg 1$  is

$$\bar{\eta} \approx \frac{\mu_1}{\mu_1 + \mu_2}. \quad (28)$$

In the range of meteor velocities, the ionization cross section given in figure 1 can be approximated by the expression,

$$\sigma_I(k_i) \approx \alpha k_i - \sigma_0. \quad (29)$$

Inserting equations (22) and (29) into equation (23) and retaining only the two leading terms in  $k_i$  (the other two terms give a negligible contribution), we obtain

$$\begin{aligned} \beta &\approx \frac{\alpha}{4\pi} \left(\frac{m}{\mu}\right)^2 \sum_i \left[ k_i^3 - \frac{\sigma_0}{\alpha} k_i^2 \right] \\ &\approx \frac{\alpha}{4\pi} \left(\frac{m}{\mu}\right)^2 \left[ (1 + \bar{\eta}^3 + \bar{\eta}^6 + \dots \bar{\eta}^{3n}) k_0^3 \right. \\ &\quad \left. - \frac{\sigma_0}{\alpha} (1 + \bar{\eta}^2 + \bar{\eta}^4 + \dots \bar{\eta}^{2n}) k_0^2 \right] \\ &\approx \frac{\alpha}{4\pi} \left(\frac{m}{\mu}\right)^2 \left[ \left(\frac{1 - \bar{\eta}^{3n}}{1 - \bar{\eta}^3}\right) k_0^3 - \frac{\sigma_0}{\alpha} \left(\frac{1 - \bar{\eta}^{2n}}{1 - \bar{\eta}^2}\right) k_0^2 \right], \end{aligned} \quad (30)$$

if the  $n^{\text{th}}$  collision is the last one in which sufficient energy is available for ionization. However,

$$\bar{\eta}^n k_0 \approx k_n, \quad (31)$$

so that

$$\begin{aligned} \beta &\approx \frac{\alpha}{4\pi} \left(\frac{m}{\mu}\right)^2 \left[ \left(\frac{1 - (k_n/k_0)^3}{1 - \bar{\eta}^3}\right) k_0^3 \right. \\ &\quad \left. - \frac{\sigma_0}{\alpha} \left(\frac{1 - (k_n/k_0)^2}{1 - \bar{\eta}^2}\right) k_0^2 \right]. \end{aligned} \quad (32)$$

The elastic scattering cross section used in the calculation of  $\beta$  is subject to the same criti-

cism as the ionization cross section; i.e., it gives too large a cross section at low energies because distortion is not taken into account. Since  $\beta$  involves the ratio of the cross sections, it is likely that the effect of neglecting distortion will be reduced. The effect on the inelastic cross section is generally greater than in the elastic collision so that  $\beta$  will remain an overestimate.

From the cross section given by equation (2), which results from the near crossing of potential energy curves, we obtain for this process an ionization probability of

$$\beta \approx \left\{ \frac{3 \times 10^{-14} M_1 g R_z^2 \hbar^4}{t \mu^2 Z^2 e^4 \alpha^2} \left( \frac{1 - k_n/k_0}{1 - \bar{\eta}} \right) k_0 \right\} \pi a_0^2 \quad (33)$$

The velocity dependence of the probability resulting from curve crossing appears to be in better agreement with radio-meteor measurements than with the Born approximation result. Nevertheless, it is doubtful whether this type of collision would be prevalent in the majority of encounters between meteor and atmospheric atoms.

The Born approximation cross section appears to be more compatible with the great majority of experimental results (Massey and Burhop, 1952, ch. 7). Moreover, the manner in which the Born approximation is expected to fail in low-energy collisions (Massey and Smith, 1933; Mott and Massey, 1949, ch. 11; Mott, 1931) is well known, and has been discussed above. It has been used with considerable success to derive the range-energy relations for alpha particles and protons.

One of the assumptions made in applying these conclusions to meteor phenomena is that the upper atmosphere is monatomic. This assumption, of course, is not precisely correct although it is true for the majority of atmospheric atoms at 100 km. Those diatomic molecules present in the upper atmosphere will tend to reduce  $\beta$  because of the large cross section for rotational excitation. This competing process may lead to a term  $\Sigma \sigma_{\mathcal{R}}(k_i)$  in equation (21) which is comparable with  $\sigma_e(k_i)$ . The calculated  $\beta$  must therefore be considered an upper limit. Processes in which excitation of the

meteor atom and the atmospheric constituent occur during a single collision have been neglected because such events are much less probable than single-excitation collisions.

### Application to meteoroids

The number of ions produced in an infinitesimal volume of a meteor trail is related to the mass of ablated meteor material in that volume by the equation

$$dQ = \frac{\beta}{\mu_1} dm_0, \quad (34)$$

where  $\mu_1$  is the average mass of a meteor atom and  $\beta$  is the ionization probability. The calculation of  $\beta$  enables one to determine the mass of a meteor by the integration of equation (34). If the velocity is constant, the number of ions per unit length of trail is related to the visual magnitude  $M$  at that point by the equation

$$M = M_0 - 2.5 \log_{10} \frac{dQ}{dx}, \quad (35)$$

which is derived in the appendix (p. 227).

Making use of the relation between trail length  $x$  and height  $H$ , where  $\zeta$  is the zenith angle, we find that

$$dx = \frac{1}{\cos \zeta} dH, \quad (36)$$

and equation (35) can be written in the form

$$dQ = 10^{\left[ \frac{M_0 - M}{2.5} \right]} \frac{1}{\cos \zeta} dH. \quad (37)$$

The variation of magnitude  $M$  along the trail is given by the normalized light-curve (Whipple and Hawkins, 1958, sec. 3, p. 525) which, for 360 measured meteors, is closely approximated by the parabolic form

$$M = M_{\max} + \left( \frac{H - H_{\max}}{H_0} \right)^2, \quad (38)$$

where  $H_0$  is a two-value parameter. We take  $H_0 = H_b$  for the portion of the light curve between the beginning and the maximum, and  $H_e$  for the portion between the maximum and the end. From the experimental data,  $H_b = 3.5 \times 10^3$  meters, and  $H_e = 2.0 \times 10^3$  meters.

Thus

$$dQ = \frac{1}{\cos \zeta} \exp \left[ \frac{2.3}{2.5} (M_0 - M_{\max}) - \frac{2.3}{2.5} \left( \frac{H - H_{\max}}{H_0} \right)^2 \right] dH, \quad (39)$$

which is readily integrated to give for equation (34) the value

$$m_0 = \frac{\bar{\mu}_1}{\beta} \frac{1}{\cos \zeta} \sqrt{\frac{2.5\pi}{2.3}} \frac{H_b + H_e}{2} 10^{\left[ \frac{M_0 - M_{\max}}{2.5} \right]}. \quad (40)$$

Let us assume for the moment that the meteoroid consists entirely of sodium. For a sodium-oxygen collision  $\bar{\eta} = 0.42$ , and the following values of  $\beta$  are obtained: for a Perseid of velocity 60 km/sec,  $\beta = 1.6 \times 10^{-2}$ ; and for a Geminid of velocity 35 km/sec,  $\beta = 2.7 \times 10^{-3}$ . Hawkins (1956) has shown that  $M_0 = 40.75$  for a Perseid and 38.89 for a Geminid. The mass  $m_0$  is obtained with these radar values for meteors of maximum magnitude,  $M_{\max} = 0$ . Thus for the Perseid,  $m_0 = 0.212(1/\cos \zeta)$  gm, and for the Geminid,  $m_0 = 0.620(1/\cos \zeta)$  gm.

These results do not, of course, represent the mass of a meteoroid since the calculations were performed for sodium-oxygen collisions. The oxygen may be considered a reasonable approximation to the average atmospheric atom, but the properties of the other meteor constituents may lead to different masses than those obtained for the above "sodium meteor." The proper approach (determining an average  $\bar{\beta}$  and  $\bar{\mu}_1$ ) is to evaluate the ionization cross sections and the respective ionization probabilities for each constituent, and weight each by its abundance in meteoroids. Since the calculations of the cross sections for all meteor constituents is not feasible, and since their velocity dependence is expected to be similar to that of sodium, the following rough approximation will be used to obtain some idea of the effects of these elements on the calculation of meteor masses.

The average atomic mass is easily evaluated from the cosmic abundances of the elements (Brown, 1949). If the ionization probabilities for the various elements have the same form, they will differ only in magnitude. The magnitude of the cross section is inversely proportional to a high power of the energy required

for ionization, and directly proportional to the reduced mass of the particles.

It is not unreasonable to assume that the ionization cross section varies as  $E_I^{-6}$ , where  $E_I$  is the ionization energy (Bates and Griffing, 1953). In addition, it is necessary to multiply the cross sections by  $n$ , the number of valence electrons available for ionization. Thus the relative ionization probabilities are related by the ratios of  $n \left( \frac{\mu}{E_I^6} \right)$ . Table 1 gives these factors and the abundances.

TABLE 1.—Total ionizing probability

Element	Number of atoms per 100	Estimated $\beta$ (Na=1)	Weighted contribution per atom
Na	0.8	1.000	0.0080
Mg	14.6	.198	.0290
Al	1.4	1.518	.0213
Si	16.2	.288	.0468
Ca	1.1	.972	.0106
Fe	6.2	.384	.0238
Inert	59.6	.000	.0000
Mean $\beta$ per atom			.1323 $\beta$ (Na)

The average ionization probability  $\bar{\beta}$  is 0.1323  $\beta_{Na}$ , and the average mass of a meteor atom is  $3.72 \times 10^{-23}$  gm. The insertion of these values in equation (40) gives  $m_0 = 1.66(1/\cos \zeta)$  gm for the Perseid, and  $4.85(1/\cos \zeta)$  gm for the Geminid. There are additional uncertainties in these figures due to the assumption of the cosmic mix, and the sodium-like behavior of all atoms. Unfortunately, this uncertainty cannot be adequately assessed.

Using the radio meteor values for  $M_0$  given by Hawkins, one readily obtains an upper limit for the luminous efficiency from equation (7) of the appendix. For a meteor of visual magnitude 0,

$$\tau/\beta = 3.194 \times 10^{-3} \text{ for } v = 60 \text{ km/sec,}$$

and

$$\tau/\beta = 3.295 \times 10^{-2} \text{ for } v = 35 \text{ km/sec,}$$

so that the upper limits are

$$\tau = 8.9 \times 10^{-5} \text{ for } v = 35 \text{ km/sec}$$

and

$$\tau = 5.1 \times 10^{-5} \text{ for } v = 60 \text{ km/sec,}$$

with the computed values of  $\beta$ .

**Appendix**

The luminous efficiency  $\tau$  is defined by the relation between  $I$ , the visible energy produced per second, and the rate of ablation:

$$I = -\frac{1}{2} \frac{dm_0}{dt} v^2 \tau. \quad (1)$$

By dividing equation (34) by  $dx = -vdt$ , we obtain

$$\frac{dQ}{dx} = \frac{\beta}{\mu_1} \frac{dm_0}{dt} \frac{1}{v}, \quad (2)$$

and eliminating  $dm_0/dt$  between equations (1) and (2) gives

$$I = \frac{1}{2} \frac{\tau \bar{\mu}_1}{\beta} v^3 \frac{dQ}{dx}. \quad (3)$$

Öpik (1937) obtained the luminosity relation

$$M = 7.1 - 2.5 \log_{10} I \quad (4)$$

from the standard fluxes of established stars. Combining equations (3) and (4), we find for the visual magnitude

$$M = 7.1 - 2.5 \log_{10} \left( \frac{1}{2} \frac{\tau \bar{\mu}_1}{\beta} v^3 \right) - 2.5 \log_{10} \frac{dQ}{dx}. \quad (5)$$

Finally, for constant velocity, the second term in equation (5) is a constant and can be combined with the first term to yield

$$M = M_0 - 2.5 \log_{10} \frac{dQ}{dx}, \quad (6)$$

where

$$M_0 = 7.1 - 2.5 \log_{10} \left( \frac{1}{2} \frac{\tau \bar{\mu}_1}{\beta} v^3 \right). \quad (7)$$

**Acknowledgment**

The research in this paper was supported jointly by the U.S. Army, Navy, and Air Force, under contract with the Massachusetts Institute of Technology.

**References**

BATES, D. R., AND GRIFFING, G.  
 1953. Inelastic collisions between heavy particles. I. Excitation and ionization of hydrogen atoms in fast encounters with protons and with other hydrogen atoms. *Proc. Phys. Soc. London*, vol. 66A, pp. 961-971.

BATES, D. R., AND MASSEY, H. S. W.  
 1954. Slow inelastic collisions between atomic systems. *Phil. Mag.*, ser. 7, vol. 45, pp. 111-122.

BROWN, H.  
 1949. A table of relative abundances of nuclear species. *Rev. Mod. Phys.*, vol. 21, pp. 625-634.

HARTREE, D. R.  
 1957. The calculation of atomic structures. John Wiley & Sons, New York.

HAWKINS, G. S.  
 1956. Meteor ionization and its dependence on velocity. *Astrophys. Journ.*, vol. 124, pp. 311-313.

LANDAU, L. D.  
 1932. Theory of superconductivity. *Phys. Zeitschr. Sowjetunion*, vol. 2, p. 46.

MASSEY, H. S. W.  
 1949. Collisions between atoms and molecules at ordinary temperatures. *Phys. Soc., Rep. Progr. Phys.*, vol. 12, pp. 248-269.

MASSEY, H. S. W., AND BURHOP, E. H. S.  
 1952. Electronic and ionic impact phenomena. Clarendon Press, Oxford.

MASSEY, H. S. W., AND SMITH, R. A.  
 1933. The passage of positive ions through gases. *Proc. Roy. Soc. London*, ser. A, vol. 142, pp. 142-172.

MOTT, N. F.  
 1931. On the theory of excitation by collision with heavy particles. *Proc. Cambridge Phil. Soc.*, vol. 27, pp. 553-560.

MOTT, N. F., AND MASSEY, H. S. W.  
 1949. Theory of atomic collisions. Ed. 2. Clarendon Press, Oxford.

ÖPIK, E. J.  
 1937. Researches on the physical theory of meteor phenomena. III. Basis of the physical theory of meteor phenomena. *Publ. Obs. Astron. Univ. Tartu*, vol. 29, no. 5.

SCHIFF, L. I.  
 1955. Quantum mechanics. Ed. 2. McGraw-Hill, New York.

SLATER, J. C.  
 1951. Quantum theory of matter. Ed. 1. McGraw-Hill, New York.

STUECKELBERG, E. C. G.  
 1932. Theorie der unelastischen Stöße zwischen Atomen. *Helvetica Phys. Acta*, vol. 5, pp. 369-422.

WHIPPLE, F. L., AND HAWKINS, G. S.

1958. Meteors. *In* Handbuch der Physik, S. Flüge, ed., vol. 52, pp. 519-564. Springer-Verlag, Berlin.

ZENER, C.

1932. Non-adiabatic crossing of energy levels. Proc. Roy. Soc. London, ser. A, vol. 137, pp. 696-702.

### ***Abstract***

An upper limit for the ionizing probability  $\beta$  is obtained for sodium atoms that have evaporated from the surface of a meteoroid entering the atmosphere, and the result is generalized to apply to the other meteor constituents. Comparison of this result with radio meteor measurements leads to a meteor mass which suggests an upward revision of the meteor mass scale. An upper limit for the luminous efficiency is also obtained. The lower limit for the mass of a zero-magnitude Geminid meteor incident at  $45^\circ$  is found to be 6.86 gm, and the mass of a zero magnitude Perseid is 2.35 gm.

# Statistical Verification of the Physical Theory of Meteors

By B. J. Levin<sup>1</sup> and S. V. Majeva<sup>1</sup>

Hawkins and Southworth (1958), using the photographs of 360 meteors obtained with Baker Super-Schmidt cameras, compared their light curves (for three points—beginning, maximum light, end) with the theoretical curve for nonfragmenting meteor bodies. They showed (see fig. 5 of their paper) that almost all measured points lie within the theoretical light curve. The same is true if, instead of taking a curve for  $\mu = \frac{1}{2}$  as was done by Hawkins and Southworth, we take a curve for  $\mu = \frac{1}{3}$  which gives a shorter path length. The parameter  $\mu$  characterizes the relation between the changes of the frontal cross-sectional area  $S$  and of the mass  $M$  of the meteor body according to the formula  $S \sim M^\mu$  (Levin, 1956, formula 3.24). The rising branches of these curves are similar, but the descending branch for  $\mu = \frac{1}{2}$  is much steeper than for  $\mu = \frac{1}{3}$ , and even steeper than the curve drawn by Ananthakrishnan (1960) according to the hypothesis that the luminosity factor  $\tau \sim v\rho$  (instead of the conventional  $\tau \sim v$ ).

Jacchia (1955) noted that the observed path length of meteors is shorter than the theoretical one, and he ascribed this to fragmentation of meteor bodies. More convincing evidence in favor of the fragmentation theory can be obtained by comparing the positions of beginning and end points (relative to the point of maximum light) for the same meteor. This was done by using the data of Hawkins and Southworth. Moderate deviations of points from the theoretical curves were not taken into account, and only those beginning or end points were regarded as anomalous for which  $H_B - H_{ML}$  or  $H_{ML} - H_E$  were less than a half of correspond-

ing values for  $\mu = \frac{1}{2}$  for the same value of  $\Delta m = m_{im} - m_{ML}$ . Only 13 meteors (3.5 percent) have anomalous position of both points, i.e., a very short path; this means that only a flare was photographed. For seven meteors (2 percent) the approximately normal position of the beginning point is accompanied by the anomalous position of the end point; this means that the meteor ended in a terminal flare or shortly after a flare.

In spite of a very liberal classification of beginning and end points as "normal," only 117 meteors (33 percent) have approximately normal positions of both points. At the same time, for 221 meteors (62 percent) the position of the beginning points is anomalous, i.e., they lie too close to the points of maximum light, while the end points lie more or less normal. Such deviations from theoretical light curves indicate the fragmentation of meteor bodies. If we are to regard as normal only those beginning points which lie in the region of theoretical light curves for different values of  $\mu$ , i.e., those which lie to the upper left from the straight line corresponding to  $\mu = 0$ , then 87 percent of meteors become anomalous. For them the mean increase of light intensity is greater than the maximum theoretical value for meteors produced by nonfragmenting bodies.

Levin (1956) used the data on 140 meteors photographed at Harvard by conventional cameras to obtain a statistical verification of two basic formulas for the physical theory of meteors. Below are given the results of an analogous verification of these formulas using the data for 337 meteors photographed by Super-Schmidt cameras. Hawkins and Southworth kindly sent us their unpublished data on the masses of meteor bodies. These masses

<sup>1</sup> O. Schmidt Institute of Physics of the Earth, U.S.S.R. Academy of Sciences, Moscow.

were obtained by the photometric method (by integrating the light curve) and are expressed in the Öpik-Jacchia scale. They are averages of values found for each film of a pair. Southworth informed us that there is frequently a large difference between these individual values.

According to nonfragmentation theory, the air density at the height of maximum light  $\rho_{ML}$  can be represented by the formula (Levin, 1956, formula 3.40)

$$\rho_{ML} \sim M_0^2 v_0^2 \cos^c Z,$$

and if the drag coefficient and the heat-transfer coefficient are constant,  $a=0.33$ ,  $b=2$ , and  $c=1$ . The data for 116 "normal" meteors and for 221 meteors produced by obviously fragmenting bodies were analyzed separately with the theoretical values of  $a$ ,  $b$ ,  $c$  given above, the dispersion  $\epsilon$  of the reduced  $H_{ML}$  is 4.7 km for "normal" and 4.8 km for fragmenting meteors. The least-squares solution leads to a marked reduction of dispersion and gives the values of the parameters shown in table 1. It remains

TABLE 1.—Observed parameters in the equation  $\rho_{ML}$

	"Normal" meteors	Fragmenting meteors
$a$	$0.32 \pm 0.05$	$0.15 \pm 0.05$
$b$	$0.89 \pm 0.18$	$1.9 \pm 0.14$
$c$	$0.85 \pm 0.21$	$0.55 \pm 0.15$
$\epsilon$	$\pm 3.6$ km	$\pm 3.9$ km

unclear why the value for  $b$  for "normal" meteors is about half the theoretical value, while the values for  $a$  and  $c$  are close to theory, and why for fragmenting meteors the reverse is true.

The analogous verification was done for the maximum light formula

$$I_M \sim M_0^2 v_0^2 \cos^r Z$$

(Levin, 1956, formula 3.60). The values  $\alpha=1$ ,  $\beta=4$ , and  $\gamma=1$  correspond to the theoretical basis of the photometric method for the determination of masses of meteor bodies. However, since the masses are obtained by integration of the light curve which for real meteors deviates from the theoretical one, the least-squares solution gives somewhat different values for  $\alpha$ ,  $\beta$ ,  $\gamma$ .

The reduction of the observed maximum magnitudes  $m_{ML}$ , with theoretical values for  $\alpha$ ,  $\beta$ ,  $\gamma$ , gave for "normal" meteors a dispersion  $\epsilon=0^m29$ , and for fragmenting meteors  $\epsilon=0^m64$ .

The least-squares solution is given in table 2.

TABLE 2.—Observed parameters in the equation for  $I_{ML}$

	"Normal" meteors	Fragmenting meteors
$\alpha$	$0.86 \pm 0.08$	$0.73 \pm 0.03$
$\beta$	$3.67 \pm 0.08$	$2.67 \pm 0.10$
$\gamma$	$0.72 \pm 0.09$	$0.46 \pm 0.10$
$\epsilon$	$\pm 0^m28$	$\pm 0^m49$

For meteors produced by obviously fragmenting bodies, the values for  $\alpha$ ,  $\beta$ ,  $\gamma$  are substantially smaller than the theoretical ones. This probably shows that the fragmentation masks the dependence of  $m_{ML}$  on  $M_0$ ,  $v_0$ ,  $\cos Z$ . For "normal" meteors,  $\alpha$ ,  $\beta$ ,  $\gamma$  have intermediate values, probably also because of fragmentation in a more moderate form.<sup>2</sup>

The least-squares solution also gives values of  $(m_{ML})_{10}$ , the maximum absolute magnitude of a meteor produced by a body with  $M_0=1$  gm, flying vertically into the atmosphere at a velocity of  $v_0=10$  km/sec. We obtain

$$\text{for "normal" meteors: } (m_{ML})_{10} = +1^m2$$

and

$$\text{for fragmenting meteors: } (m_{ML})_{10} = +0^m4.$$

These values are expressed in photographic magnitudes. If we convert them to a visual scale and, in spite of some doubts, use the same correction  $+1^m8$  as for meteors photographed by conventional cameras, we obtain the values  $+3^m0$  and  $+2^m2$ , respectively. The first value (for "normal" meteors) is close to the previously obtained value  $+2^m86$  (Levin, 1956). Accordingly, meteor bodies that produce a meteor of zero visual magnitude during vertical motion with initial velocity  $v_0=40$  km/sec must have initial masses 0.062 gm and 0.030 gm, respectively (instead of  $M_0=0.055$  gm obtained in 1956). It is clear that fragmentation decreases the path length of a meteor and at the same time increases its brightness; therefore

<sup>2</sup> Note added in March 1962. Further investigation showed that after a simple allowance for fractionation, the theoretical values of  $\alpha$ ,  $\beta$ ,  $\gamma$  give a good representation of all observations together with a dispersion  $+0^m16$ ; i.e., even better than a least-squares solution for "normal" meteors. (Levin, in press.)

a smaller initial mass is needed to produce a meteor with a given maximum magnitude.

The manner in which the fragmentation influences the estimates of the masses of meteor bodies and of the amount of meteoric material accreted by the earth deserves further investigation.

#### References

- ANANTHAKRISHNAN, R.  
1960. Light curves of meteors. *Nature*, vol. 187, pp. 675-676.
- HAWKINS, G. S., AND SOUTHWORTH, R. B.  
1958. The statistics of meteors in the earth's atmosphere. *Smithsonian Contr. Astrophys.*, vol. 2, no. 11, pp. 349-364.
- JACCHIA, L. G.  
1955. The physical theory of meteors. VIII. Fragmentation as a cause of the faint-meteor anomaly. *Astrophys. Journ.*, vol. 121, pp. 521-527.
- LEVIN, B. J.  
1956. The physical theory of meteors and meteoric matter in the solar system. *Publ. House Acad. Sci. U.S.S.R.*, Moscow.



# On the Color Index of Meteors

By John Davis<sup>1</sup>

A comparison of photographic and visual meteor magnitudes reveals an interesting relationship. Jacchia (1957) has compared the meteor color index, defined as the difference between the photographic magnitude and the corresponding visual magnitude, with the maximum intrinsic brightness of a meteor as measured with a photographic system. The photographic system used was a Super-Schmidt camera (Whipple and Hawkins, 1958) with blue-sensitive film corresponding approximately to the International Photographic system (Allen, 1955), and the visual magnitudes were the direct estimates of an observer. Jacchia found that the color index showed very little variation with meteor velocity but a large variation with maximum photographic brightness, the ratio of "photographic" to "visual" light decreasing with maximum meteor brightness. The author has confirmed Jacchia's results during the combined photographic and radio-echo meteor program at Jodrell Bank (Davis, Greenhow, and Hall, 1959; Davis, 1959). The results of both Jacchia and the author are shown in figure 1, where color index has been plotted against visual magnitude in order that comparison may be made with results obtained with a photographic system of different spectral sensitivity. Jacchia has divided the observations of 294 meteors into four groups according to absolute photographic magnitude, and deduced the mean color index for each group. The two points given by Jacchia for the brightest meteors were derived from the observations of 45 meteors made with the Harvard small cameras. It is possible that color indices derived from small cameras may differ from those from Schmidt cameras due to differences in their relative

spectral transmission curves. The author has reduced his data in the same way as Jacchia, but only 53 meteor observations were available, and the larger errors associated with the mean points in figure 1 can be accounted for by the difference in the number of observations.

The variation of color index with brightness has been explained by Jacchia in terms of the Purkyně effect. He suggested that the variation is a spurious physiological effect due to the difference in the spectral sensitivity of the eye for bright and faint sources (photopic and scotopic vision).

Ceplecha (1959) has made a similar study with the difference that he used panchromatic film, sensitive to approximately 6700 Å, to obtain his "photographic" magnitudes. He thus obtained a panchromatic index which he found to increase as the maximum brightness of the meteor decreased. This is shown in figure 1 for comparison with the color index. The quite different results obtained with blue and with panchromatic systems have been suggested by Ceplecha to originate in real spectral changes of the meteor light with a previously unsuspected high emission in the red becoming relatively predominant in fainter meteors.

All the observations described have been based on subjective estimates of visual magnitudes, and these are suspect. Systematic differences up to 0.5 magnitude between experienced observers have been found, and it appears that a single visual magnitude estimate has a standard deviation of the order of  $\pm 0.8$  magnitude. Inspection of the data included in figure 1 shows that the standard deviation of a single visual estimate is  $\pm 0.8$  from the author's observations. Jacchia's results give a standard deviation of  $\pm 0.6$  magnitude, but since the majority of his results are based on

<sup>1</sup> Nuffield Radio Astronomy Laboratories, Jodrell Bank, England. Now at School of Physics, University of Sydney, Australia.

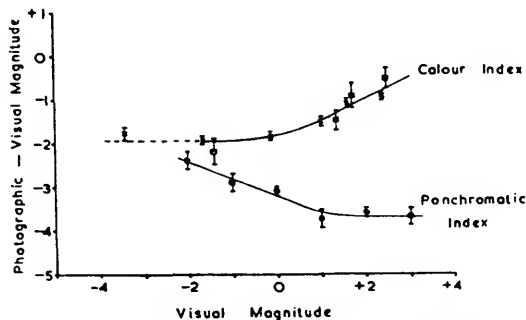


FIGURE 1.—The variation of meteor color index with meteor brightness. X, The results of Jacchia obtained with a blue photographic system;  $\square$ , results of Davis obtained with a blue photographic system;  $\circ$ , results of Ceplecha obtained with a panchromatic photographic system.

the mean of two visual-magnitude estimates, these figures are in good agreement. They suggest that the main cause of scatter in color index can be ascribed to the inaccuracy of the estimates of visual brightness. Objective measurements of visual magnitudes are therefore very desirable in this kind of work.

Two photomultipliers with Tri-alkali cathodes of 5-inch diameter have been used in a study of this problem. They have been set up with a screen above them to define a zenithal field of  $50^\circ$  diameter and with Chance glass filters to provide the required spectral responses. One tube has been fitted with an OB10 filter to give a spectral sensitivity corresponding approximately to a blue photographic system, and the other has an OGr2 filter to give a response corresponding to a mean visual observer (mean photopic and scotopic). The relative spectral responses of the photocathode-filter combinations are shown in figure 2. The relative spectral sensitivities of the photocathodes and the spectral transmission of the filters have been measured at the National Physical Laboratory, Teddington, England. The relative spectral sensitivity curve of the photographic system (Davis, in preparation) is shown in figure 2 for comparison with the blue photoelectric system. The spectral transmission curve for the Royal Society Meniscus Schmidt camera has been computed from data supplied by Chance Brothers Ltd. The transmission of the lenses, reflection at mirror and at all glass-air surfaces

have been taken into account in the calculations. The results have been combined with the spectral sensitivity curve of the Kodak photographic emulsion (V6010) to give the relative spectral sensitivity curve of the camera-emulsion combination. Spectral sensitivity curves for the normal and dark-adapted eye (Allen, 1955) are also included for comparison with the green photoelectric system. Common filter glasses have been used; nevertheless, a reasonably good match has been obtained, particularly in the case of the blue system. The varying components of the photomultiplier outputs over a bandwidth of 1/10 to 20 c.p.s. have been recorded with a Siemens high-speed pen recorder.

The amplitudes of meteor signals from the blue (OB10) and green (OGr2) channels have been converted to arbitrary magnitude scales which correspond to the photographic and visual magnitude scales respectively, except for the addition of constants which at this stage have not been determined. In figure 3, green magnitudes have been plotted against the author's direct visual estimates of meteor magnitude. The broken line represents a linear, 1:1 relationship between the two magnitude scales, whereas the full line has been derived from figure 1 for the hypothetical case of a constant color index with the observed

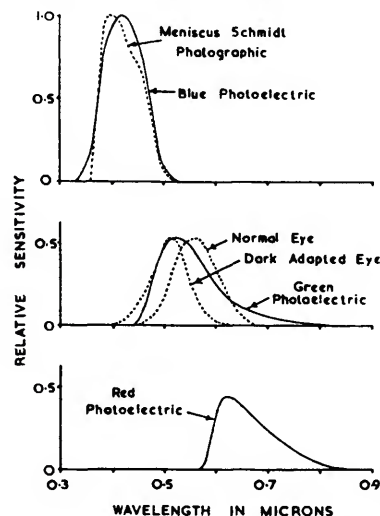


FIGURE 2.—The relative spectral sensitivity curves of the three photocathode-filter combinations.

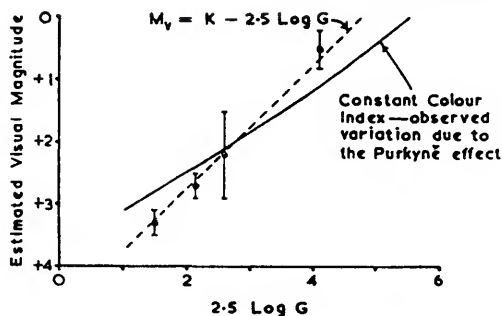


FIGURE 3.—A comparison between visual magnitudes and the green photoelectric brightness.

variation being due to the Purkyně effect. A total of 24 meteors has been used in this diagram. Since the major error lies in the estimate of visual magnitude, the data have been divided into four groups according to their value of  $2.5 \log G$ , and the mean values of visual magnitude have been derived ( $G$  is the amplitude of the "visual" photoelectric signal on an arbitrary scale and is proportional to the incident light intensity). The diagram shows clearly that it is not possible to explain the variation in terms of the Purkyně effect alone. This conclusion is further supported by figure 4 in which the photoelectrically determined color index is plotted against blue magnitude. Some 40 meteors have been used in this diagram and, since the error in  $2.5 \log B/G$  is the greater, the data have been divided into five groups according to their values of  $2.5 \log B$ , and mean values of  $2.5 \log B/G$  have

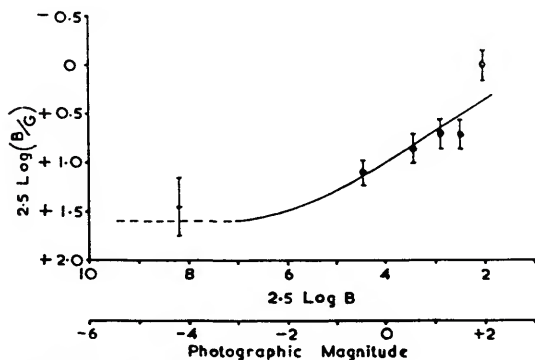


FIGURE 4.—The variation of photoelectric color index ( $2.5 \log B/G$ ) with meteor brightness.  $\odot$ , Points representing the mean of 8 meteors;  $+$ , point representing a single bright meteor.

been derived ( $B$  is the amplitude of the blue photoelectric signal on an arbitrary scale).

An absolute calibration of the blue magnitude scale has been made from fifteen meteors photographed and recorded photoelectrically. The photographic magnitude scale is indicated in figure 4 alongside the blue scale, the uncertainty in the calibration being  $\pm 0.1$  magnitude. The curve representing the variation in color index with meteor brightness determined from visual and photographic observations, which is shown in figure 1, has been transposed to figure 4. It must be noted that the color index given in figure 4 is not absolute but gives only the relative change in index with meteor brightness. Owing to the uncertainty in the calibration of the blue and the green magnitude scales against the photographic and visual scales, it is not possible to fix the position of the curve relative to the ordinate of figure 4 with sufficient accuracy for comparison with the photoelectric color indices. Therefore the position of the curve relative to the ordinate scale has been chosen arbitrarily to give the best fit to the points. It will be seen that a good fit is obtained, thus supporting the conclusion drawn from figure 3. The implication is that the variation is due to a real change in the meteor spectrum. The Purkyně effect has a much smaller influence on the results than was envisaged by Jacchia.

Another series of observations has been made in which the OGr2 filter was replaced by an OR2 filter to give a response from approximately 6000 to 7000 Å with the peak sensitivity from 6100 to 6500 Å. The relative sensitivity curve of this photocathode-filter combination is shown in figure 2. A red index, which is defined as the difference between blue (OB10) magnitude and red (OR2) magnitude, has been plotted against blue magnitude in figure 5, in which 44 meteors have been used. The data have been treated in the same manner as for figure 3, being divided into five  $2.5 \log B$  groups, and mean values of  $2.5 \log B/R$  have been derived. Again the index is only relative, but it shows clearly that faint meteors are relatively redder than bright meteors. A smooth curve has been drawn through the points in figure 5 to indicate the trend of the results.

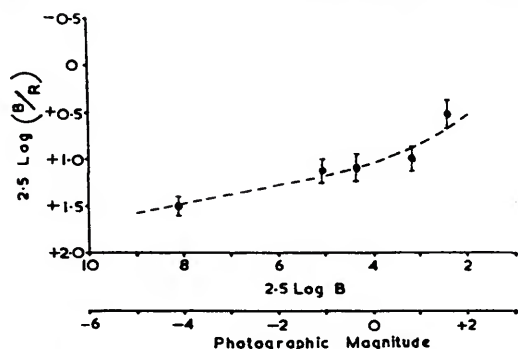


FIGURE 5.—The variation of the photoelectric red index ( $2.5 \log B/R$ ) determined photoelectrically with meteor brightness. Each point represents the mean of 8 meteors.

Approximately half of the meteors observed in the photoelectric program have been Geminids, and the remainder sporadics. No significant difference has been found between meteors of the Geminid shower and sporadic meteors.

The preliminary examination has shown that Cep-lecha's proposed explanation of the observed variation of color and panchromatic indices with meteor brightness in terms of a changing spectrum is correct. If the total light from a meteor is considered, faint meteors have relatively greater emission in the green and red regions of the spectrum than bright meteors. The transition in the emission spectrum over the range of visual magnitudes from  $-2$  to  $+3$  is apparently a gradual one.

Dr. Peter Millman (personal communication) has pointed out that the spectra of bright meteors exhibit changes along the meteor trail. The great majority of all spectra containing sufficient detail show an increasing ratio of blue

to red light as the meteor passes from the faint beginning, through maximum brightness, to the lower end of the trail. Millman suggests that faint meteors may exhibit a spectrum similar to the faint early parts of bright meteor trails. If this is so, changes in color index along the light curve of a bright meteor should be observable with the photoelectric system. No evidence to support this has been found so far, but the problem is being investigated further.

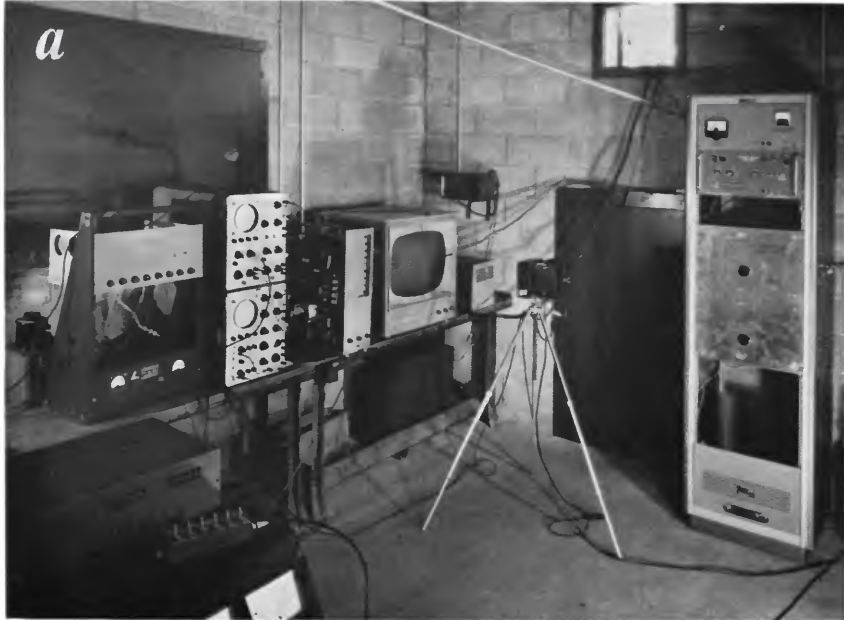
I am grateful to Sir Bernard Lovell for his encouragement in this work and for the research facilities at Jodrell Bank. I also thank Messrs. Turner and Newall for a research fellowship.

### References

- ALLEN, C. W.  
1955. *Astrophysical quantities*. Athlone Press, London.
- CEPLECHA, Z.  
1959. On the colour index of meteors. *Bull. Astron. Inst. Czechoslovakia*, vol. 10, p. 39.
- DAVIS, J.  
1959. Simultaneous photographic and radio echo observations of meteors. Thesis, University of Manchester.
- DAVIS, J.; GREENHOW, J. S.; AND HALL, J. E.  
1959. Combined photographic and radio echo observations of meteors. *Proc. Roy. Soc. London*, ser. A, vol. 253, pp. 121-129.
- JACCHIA, L. G.  
1957. On the "color index" of meteors. *Astron. Journ.*, vol. 62, pp. 358-362.
- WHIPPLE, F. L., AND HAWKINS, G. S.  
1958. Meteors. In S. Flüge, ed., *Handbuch der Physik*, vol. 52, pp. 519-564. Springer-Verlag, Berlin.

### Abstract

Objective measures of meteor color indices have been made with a two-channel photoelectric apparatus. Photocathode-filter combinations giving spectral responses corresponding to a Super-Schmidt photographic system and a mean visual observer have been used. The results show a variation of color index with meteor brightness in agreement with the subjective results of Jacchia and Davis. However, the variation can no longer be accounted for in terms of a physiological effect alone as proposed by Jacchia. It must arise from a real change in the meteor spectrum with meteor brightness as Cep-lecha has suggested. This interpretation is further supported by the observations made with blue and red sensitive photoelectric channels.



*a*, The electronic equipment. *b*, Three motion-picture sequences of Perseid meteors.





*a*, Perseid meteor photographed in August 1960. *b*, Photograph of a bright meteor.



# Image-Orthicon Photographs of Meteors

By J. Spalding,<sup>1</sup> G. Colter,<sup>2</sup> C. L. Hemenway,<sup>3</sup> J. A. Cole,<sup>3</sup>  
and J. F. Dugan<sup>3</sup>

The function of this brief communication is threefold: First, to show some image-orthicon photographs of meteors; second, to make sure that the characteristics of image-orthicon techniques are understood by the scientists interested in the study of meteors; and third, to seek advice for the best possible means of exploiting the capabilities of these techniques for meteor research.

The most important characteristic of image-orthicon techniques for the study of meteors is their very high sensitivity, which ranges from 200 to 400 times that of the fastest photographic films. This high sensitivity permits good time resolution at the expense of some loss in spatial resolution. Typical resolution for meteor studies is of the order of 10 lines per millimeter. The photo cathodes presently available are approximately 1.75 inches in diameter. The readout from such equipment is extremely rapid, and 30 pictures per second can be recorded with little difficulty. Image orthicons are available with different spectral sensitivities. There are tubes sensitive in the ultraviolet, in the infrared, and in the visual. Images can be stored on an image-orthicon target if desired. In fact, we have stored an image of stars for a half-hour without refrigeration and found that the image brightness decayed by less than a magnitude. By pulsing the cathode to target potential, one can take exposures as short as a millisecond without difficulty.

The operational characteristics of the system, as used this past summer for motion picture photography of meteors, are as follows:

Objective: 50 mm. fl, f/1.4  
Tube: GE Z5396 (visual sensitivity)

<sup>1</sup> General Electric Company, Schenectady, N.Y., and Dudley Observatory, Albany, N.Y.

<sup>2</sup> General Electric Company, Schenectady, N.Y.

<sup>3</sup> Dudley Observatory, Albany, N.Y.

Equivalent speed: ASA 1,000,000  
Operating mode: 500 lines, non-interlaced  
Limiting magnitude:  $>6^m.0$  for 1/30 sec exposure.

Plate 1a is a photograph of the electronic equipment employed. The image-orthicon camera is not shown and is outside the building directed toward the sky. This system has the advantage that the observer is in a comfortable, heated room. The recording technique that we have used is direct photography of the monitor screen. The video tape technique suggested by D. W. R. McKinley<sup>4</sup> offers a number of advantages.

Plate 2a is a picture of a 3d-magnitude Perseid meteor that we obtained in August 1960; the meteor motion is effectively "frozen," and the meteor wake is clearly separated from the meteoroid. Thus it is possible to study separately the time and spatial development of the meteor, and its wake and train phenomena.

Plate 2b shows what happens when a bright meteor comes into view. Although this -1 magnitude meteor overloaded the system, the meteor wake can still be distinguished. Note that this system has sufficient speed to photograph a weak aurora (below the meteor) in 1/30th of a second.

Plate 1b shows three motion-picture sequences of meteors taken at 1/8th of a second intervals during the last Perseid shower. The first sequence shows a faint meteor with a short-duration train. The second and third sequences show meteors that fragmented, and the spatial developments of the associated flares are seen along with longer-duration trains.

In summary, faint meteors, wakes, and trains can readily be studied by image-orthicon

<sup>4</sup> *Meteor Science and Engineering*, McGraw-Hill, New York, 1961.

techniques. We note that the magnitudes of meteors can be measured by direct comparison with the stars since short-duration exposures are used. The equipment is suitable for taking motion pictures, which permit study of time and spatial development of meteors and their spectra.

We welcome comments and suggestions for the exploitation of this equipment. We have already obtained low-resolution spectra of meteors and trains with an objective prism coupled to this equipment. A transmission grating spectrograph has been constructed and will be in use shortly.

# Meteoritic Erosion in Space

By Fred L. Whipple<sup>1</sup>

Recently developed techniques in meteoritic astronomy now enable us to determine upper limits, or rough evaluations, of the erosion rates on the surfaces of meteoroids moving in orbits about the sun.

Successive sections of this paper discuss the observational data on erosion rates, the theory of high-velocity cratering, the deduced mean density of the interplanetary dust component and evidence for a dust cloud about the earth, general physical effects on meteoroids in space, and effects that meteoroids may have on space vehicles.

## Evidence for erosion of meteoroids in space

When cosmic rays penetrate solids in space, they produce a number of transmutation or spallation products in the material of the solid. Some of the atomic species so produced are stable against radioactive decay, while others have a half-life that may be short or long. A measurement of a stable isotope so produced establishes the integrated effect of cosmic rays over the period of exposure, while a measurement of a short-lived isotope provides the cosmic-ray spallation rate over a recent, short interval of time. After correction for spallation cross sections, the ratio of the observed abundances of two such isotopes in a recovered meteorite provides a determination of the *exposure age*.

The penetrating powers of cosmic rays are definitely limited. One may assume that the cosmic-ray rate has been statistically constant in the past and conclude that the exposure age represents the interval of time since the individually recovered meteorite was separated from a larger body. Whipple and Fireman (1959) showed that an alternative interpreta-

tion of exposure age leads to a determination of an upper limit to the rate of erosion acting on the meteorite while it was in space. The actual erosion rate experienced by the meteorite may well have been smaller, depending upon the unknown time at which the meteorite was separated from a larger parent body.

Suppose, as an example, that in a recently fallen meteorite the quantity of the stable argon isotope  $A^{38}$  is measured, as well as that of the isotope  $A^{39}$ , which has a half-life of some 325 years. Since the relative cross sections for average cosmic-ray spallation are known for these two isotopes, the  $A^{39}$  measurement provides a determination of the average rate of production of  $A^{38}$  over some 100 revolutions of the meteoroid in orbit about the sun and over a large number of sunspot cycles (the latter in case the cosmic-ray activity is dependent upon solar activity).

Let us assume that the measurements are made somewhere near what was the center of the meteoroid before it was ablated and broken by atmospheric passage, and that the meteoroid was roughly spherical, of radius  $R$ . Let  $L$  be the distance through which the cosmic-ray spallation effect is reduced by a factor of  $e$ . Then the measured  $A^{39}$  content leads to the rate of production of  $A^{38}$  given by the equation

$$\frac{dA^{38}}{dt} = C \exp(-R/L), \quad (1)$$

where  $C$  is the constant determined by the measurement.

If we postulate a statistically linear erosion rate of the external surfaces by all causes while the meteoroid was in space, the accumulated  $A^{38}$  will amount to

$$A^{38} = C \int_0^{T'} \exp[-(R + \epsilon t)/L] dt, \quad (2)$$

<sup>1</sup> Smithsonian Astrophysical Observatory, and Harvard College Observatory, Cambridge, Mass.

where  $T'$  is the interval of time since the meteoroid was exposed to cosmic rays, presumably by separation from a parent body.

The usually defined *exposure age*  $T$  follows from a constant rate of production by cosmic rays producing the  $A^{38}$ ; from equation (1) the accumulated  $A^{38}$  is given by

$$A^{38} = CT \exp(-R/L). \quad (3)$$

On integrating equation (2) and equating the values of  $A^{38}$  to that given by equation (3), we find

$$\epsilon = \frac{L}{T} \{1 - \exp(-\epsilon T'/L)\}. \quad (4)$$

If we assume that  $T'$  is very great compared to  $T$ , we obtain an upper limit to the erosion rate by the simple expression,

$$\epsilon = L/T. \quad (5)$$

Eventually our knowledge of the breakup of asteroids in the formation of meteorites may be adequate to enable us to put in a significant value of  $T'$  in equation (4). At present, the upper limit to the erosion rate given by equation (5) represents an adequate statement of our knowledge.

For the Sikhote-Alin nickel-iron meteorite Fireman (1958) found  $T = 5 \times 10^8$  years by a measurement of the decay rate of  $A^{39}$  and an evaluation of the  $A^{38}$  content from the  $He^3$  measured in that meteorite. Whipple and Fireman (1959) adopted a shielding constant  $L = 72$  cm on the basis of spallation measures in a high-energy accelerator, and thus derived an upper limit to the erosion rate of a nickel-iron meteorite as  $\epsilon = 1.5 \times 10^{-7}$  cm yr $^{-1}$ . Fisher (1961) has criticized this determination; he prefers a value based upon  $Ne^{21}$  measurements in the Grant meteorite leading to a value  $\epsilon = 1.1 \times 10^{-8}$  cm yr $^{-1}$ . A detailed critical discussion of the pros and cons concerning meteorite exposure ages by various isotopic measurements would become too involved for the present paper and probably would not result in any definitive conclusions in the present state of the art. Measurements of 17 iron meteorites giving exposure ages by  $A^{39}$  or  $Cl^{36}$  rates are listed by Anders (private communication) and average about  $3.4 \times 10^8$  years. The

five oldest average about  $6 \times 10^8$  years. I shall, therefore, adopt as a significant estimate, probably correct to within a factor of 2, an upper limit to the erosion rate of nickel-iron meteorites in space,  $\epsilon = 1.2 \times 10^{-7}$  cm yr $^{-1}$ , to be used in the present discussion.

The fact that the exposure ages by the argon method and by similar methods have consistently come out much smaller for stony meteorites than for iron meteorites has been a subject of considerable interest for several years. Fireman and DeFelice (1960) suggested that the difference results from the physical weakness of stones as compared to irons, resulting in a more rapid etching of the stones, a major assumption of this paper. In a summary of argon measurements for various stony meteorites, Fireman and DeFelice (1961) find that for nine chondrites the  $A^{39}$  decay rate ranges only from 5 to 12 kg $^{-1}$  min $^{-1}$ . The exposure ages and the  $A^{38}$  contents are similarly confined in range (e.g.,  $A^{38}$  only from 1 to  $2 \times 10^{-8}$  sec gm $^{-1}$ ). Typical exposure ages by the argon method and also by similar methods for chondrites generally are less than  $10^8$  years. Until more definitive results are available, I shall adopt the typical exposure age of  $4 \times 10^7$  years determined for the Bruderheim meteorite by Fireman and DeFelice, and a shielding constant  $L = 70$  cm, suggested by these authors. The upper limit to the erosion rate for typical stony meteorites then becomes  $\epsilon = 1.7 \times 10^{-6}$  cm yr $^{-1}$ . Again the uncertainty may be comparable to a factor of 2.

For photographic meteoroids, Jacchia and Whipple (1961) find semi-definitive evidence that the lifetime of photographic meteoroids in space is relatively short, of the order of 10,000 years or perhaps less. Some 60 percent of the precisely reduced photographic meteors can be assigned to streams or associations; also there is no tendency for meteors having aphelion distances within the perihelion distance of Jupiter to have their lines of apsides aligned with those of Jupiter, as is so conspicuous for the asteroids.

Since so many of the meteor orbits cross that of Jupiter and are subject to relatively great perturbations by that planet, the tendency to streaming among photographic meteors indicates a relatively short lifetime. Over

periods of time adequate for the Poynting-Robertson effect to reduce the aphelia appreciably, Jupiter perturbations should cause most of the stream identities to become unrecognizable. The lack of systematic alignment of the apsides among the meteors of smaller aphelion distance again indicates that Jupiter perturbations have not had time to play an appreciable role for these meteoroids. More precise evaluation of the time scale involved is under study by S. Hamid at the Smithsonian Astrophysical Observatory, but for the moment, an estimate of  $10^4$  years appears to be reasonable, although perhaps too long.

Destructive forces are thus clearly at work among the cometary meteoroids. Barring totally destructive collisions, an erosion rate should fairly describe the destructive processes. Thus, to determine the erosion rate for the photographic meteoroids, we need a determination of the meteoroid dimensions. Again, to provide an upper limit, let us assume that the  $10^4$ -year period of destruction applies to a zero-magnitude meteor with an entry velocity of  $30 \text{ km sec}^{-1}$ . Until the luminous efficiency factor or the ionizing efficiency factor has been theoretically or experimentally determined for photographic meteoroids, we have available for dimensional determination primarily the drag measurements in the Harvard photographic meteor program. These measurements provide the following relation between meteoroid radius  $R$  and density  $\rho$ , for a  $0^{\text{th}}$  magnitude meteor at velocity  $30 \text{ km sec}^{-1}$ :

$$R\rho = 0.23 \text{ (cgs)}. \quad (6)$$

I am indebted to Allan F. Cook and Luigi G. Jacchia for this evaluation, which is probably significant to 20 or 30 percent. The largest uncertainty rests in the assumed shape factor of the meteoroid, which was taken to be 1.66, and the drag coefficient, taken as  $C_d = 2.0$ ; both enter linearly on the right side of the equation.

Accepting a time of  $10^4$  years for total erosion, we estimate for the erosion rate in equation (6),

$$\epsilon \text{ (phot. met.)} = 2.3 \times 10^{-5} / \rho \text{ (cm yr}^{-1}\text{)}. \quad (7)$$

This value may be taken as a rather high estimate since we might well have chosen a

third-magnitude meteor as representative of the fainter limit of the photographic determinations. This assumption would reduce the value in equation (7) to a rate of approximately  $10^{-5} / \rho \text{ cm yr}^{-1}$ . However, the determinations for iron and stony meteorites are both upper limits, and tentative indications suggest that the photographic meteoroids may, indeed, be destroyed in a shorter mean time than  $10^4$  years in the inner region of the solar system typical of the orbital paths expected for recovered meteorites. No clearcut information is yet available concerning the density  $\rho$  to be applied in equation (7). The lowest mean value is  $\rho = 0.05 \text{ gm cm}^{-3}$  suggested by Cook and Whipple (Whipple, 1955), but based upon a rather unreliable method of mass determination that depends upon the forward motion in the incoming train of a bright photographic meteor. There is little question but that some stream meteoroids may average densities even smaller than this, for example, the Giacobinid stream of 1946, but average values for more typical photographic meteoroids may more probably lie near  $0.3 \text{ gm cm}^{-3}$ . This problem of meteoroid density is under continuous investigation; better values will be obtainable when more definitive examples of stony meteors have been investigated by photographic meteor techniques. We have clearcut evidence, particularly that by McCrosky (1955), that photographic meteoroids are weak structures and that many of them crush under dynamic pressure of the order of one-third atmospheric pressure, approximately  $10^{-4} \text{ dyn cm}^{-2}$ . Öpik (1955) previously deduced such a crushing strength from less definitive observational data.

The basic assumption of this paper, that the erosion rates calculated above for iron, stony, and cometary meteoroids are actually measures of space erosion, is an *ad hoc* assumption for which no great affirmative evidence can be amassed. Its chief *raison d'être* rests on the fact that the values increase sequentially as we go from materials of stronger to weaker structural strength, or better, from greater to lesser crushing strengths. Also there seems little reason to believe that etching processes such as ionic sputtering would be highly sensitive to strength of materials. The binding in crystalline structures is not so vastly variable

from one material to another (see, for example, Reiffel, 1960). Crater formation, however, where there is no gravitational or other mechanism for retaining crushed material, should increase markedly as the target material becomes weaker structurally.

Anders (private communication) carefully discusses the pros and cons of the erosion concept for irons and stones, and questions the conclusion severely on the following grounds: (a) Some of the harder stones have short exposure ages, while the "friable" Norton County has an age of 2 to  $5 \times 10^8$  years. (b) Macroscopic strength cannot be the major factor in cratering by dust, only the microstructure; the mechanical strength of iron and stone crystals do not differ much; also from Buddhue's (1942) measures of crushing strength even the macroscopic strengths of some stones are comparable to that of the Descubridora, Mexico, iron (Om),  $3.7 \times 10^9$  dyn  $\text{cm}^{-2}$ . (c) Strong clustering of ages occurs for the chondrites near  $22 \times 10^6$  years versus much shorter ages; clustering also occurs for the irons near  $3 \times 10^8$  years and  $6 \times 10^8$  years; the hexahedrites seem to show shorter lifetimes than the medium octahedrites. Some of these objections are also voiced by Eberhardt and Hess (1960).

The shorter derived exposure ages, whether for irons or stones, whether for hard or soft material, whether or not clustered in time, really do not bear on the erosion problem. There is every reason to believe that collisions and breakage among meteoroids must occur. Thus the shorter exposure ages (when not due to leakage of gas) are reasonably interpreted in the now classical fashion as measuring some mean time since a breakup or breakups.

The great age for the Norton County achondrite presents a problem. Edward L. Fireman has permitted me to express his opinion as follows: "The exposure age of Norton County is more uncertain than that of other meteorites because its Fe content ( $\sim 1$  percent) is the lowest of any meteorite. Thus argon is produced mainly from Ca and K; the He may be produced by a high Li<sup>6</sup> content. Some Li and target measurements in Norton County are necessary to put its exposure age on a firmer basis." Until these experiments have been done, and until complete measures on single

samples are made, the problem does not appear damning to the erosion concept.

It is quite clear, as Anders points out, that pure compressive strength is not the vital quantity that should measure the cratering efficiency of high-velocity impact. Some numerical measures of malleability or of brittleness should enter the cratering formula. Everyone knows that violent shock on a meteorite will break more stone than iron. The volume of displaced material is mostly determined by whether the material breaks when compressed violently as the exposure shock wave spreads and attenuates. The iron in most chondrites is usually not adequate by volume (5 to 10 percent), and is too poorly distributed to offer major protection to the stony material against crushing and shattering. Undoubtedly it does offer appreciable protection in some chondrites, but the stronger crystals in the stone will fall apart when the softer matrix is worn away by cratering impact.

The questions raised by Anders cannot be ignored and suggest a number of experiments and measurements that must be made to finally clarify the situation. I prefer for the moment, however, to adopt the erosion concept as a working hypothesis applying to the older exposure ages, and to pursue the consequences of this hypothesis.

#### Cratering by high-velocity impact

No definitive theory or experiment yet defines the laws of crater formation by high-velocity impact. Indeed, the broad dependence of the phenomena upon velocity or nature of the materials is not yet established. Rapid progress, however, is now being made in this area of research, both in theory and in experiment.

The only theory that appears broad enough to cover the types of target materials of interest in meteoroids is by Öpik (1958). He calculates that a projectile (or meteoroid) of mass  $\mu$ , striking a large solid surface of density  $\rho$ , and compressive strength  $S$ , at a meteoric velocity  $v$ , will crush and displace a mass  $M$ , according to the equation

$$\frac{M}{\mu} = kv(\rho/S)^{1/2}, \quad (8)$$

where  $k$  is a dimensionless constant that depends

upon the shape and nature of the impinging body. He derives values of  $k=4.7$  for iron impinging on stone, and  $k=4.3$  for stone on iron. Fireman and DeFelice (1960) apply his theory to the problem of erosion rates and meteoritic collision in space.

From effects of surface nuclear bursts, S. Glasstone (1957, par. 5.8) adopts a scaling law in which the linear dimensions of the displaced earth vary as the cube root of the energy  $E$ . Thus, the volume or mass of the earth displaced and brecciated varies as the energy of the explosion (with dependence upon the scaled depth of the explosion). His constants lead to an energy per unit mass of dry earth displaced equal to about  $1 \times 10^9$  erg gm $^{-1}$ .

Shoemaker (1960), in his calculations of the mass that produced the Arizona Meteorite Crater (Barringer Crater), adopts Glasstone's scaling law and uses constants equivalent to  $2.3 \times 10^8$  erg gm $^{-1}$  for displaced earth at an impact velocity of 15 km sec $^{-1}$ . He also uses the scaling law  $(E)^{1/3.4}$ , which would further reduce the required ergs per gram for microscopic particles. I used the energy-scaling law and a constant of  $1.2 \times 10^{10}$  erg gm $^{-1}$  for aluminum (Whipple, 1957).

Öpik's relation (eq. 8) produces a volume of displaced material proportional to the momentum rather than to the energy of impact. Thus, at  $v=15$  km sec $^{-1}$ , he calculates the impacting mass of the Arizona iron meteoroid to be some 20 times greater than does Shoemaker ( $1.5 \times 10^{12}$  gm vs.  $6.3 \times 10^{10}$  gm). Öpik adopts, however, a crushed mass of  $10^{15}$  gm, about three times the value adopted by Shoemaker, reducing the theoretical discrepancy to a factor of eight times. From equation (8), if  $v=15$  km sec $^{-1}$ , and  $S=9 \times 10^8$  dyn cm $^{-2}$  and  $\rho=2.6$  gm cm $^{-3}$  for dry earth, Öpik's value of energy per gram of displaced rock becomes  $3.0 \times 10^9$  erg gm $^{-1}$  compared to  $1 \times 10^9$  erg gm $^{-1}$  by Glasstone and  $2.3 \times 10^8$  erg gm $^{-1}$  by Shoemaker.

In his calculations of impact craters and meteoritic penetration at impact velocities of 5.5, 20, and 72 km sec $^{-1}$ , Bjork (1961a) finds the momentum scaling law. His calculations have been confirmed experimentally at  $v \sim 6.5$  km sec $^{-1}$ . In his preliminary report on the formation of the Arizona Meteor Crater, he (1961b) also adopts the momentum scaling law.

For hemispherical craters in aluminum or stone, his formula (1961a) is

$$\text{Penetration} = 2.35 \times 10^{-2} (\mu v)^{1/3} \text{ (cgs units)}. \quad (9)$$

Thus, Bjork's equation for crater formation agrees with Öpik's insofar as velocity is concerned, but carries no explicit term for the strength or ductility of the material. For stone ( $\rho=2.64$  gm cm $^{-3}$ ) his equation for ratio of crater mass to projectile mass is closely

$$\frac{M}{\mu} = 7.0 \times 10^{-5} v \text{ (cgs units)}. \quad (10)$$

The corresponding energy per gram displaced at  $v=15$  km sec $^{-1}$  becomes  $1.0 \times 10^{10}$  ergs gm $^{-1}$ , a relatively high value.

I can find little experimental evidence concerning the dependence of cratering upon the density, strength, or nature of materials. Birkhoff et al. (1948) find that the depth of penetration of a high-velocity jet varies as  $\rho^{-1/2}$ . Thus, the volume of material displaced in a jet-produced crater should vary more rapidly than  $\rho^{-1}$ , perhaps as much as  $\rho^{-3/2}$ , and the mass as  $\rho^0$  to  $\rho^{-1/2}$ , in contrast to Öpik's conclusion,  $\rho^{+1/2}$ .

Summers and Charters (1959), from relatively low-velocity impact (to 3 km sec $^{-1}$ ) of copper and lead projectiles on both copper and lead targets, find a relation which becomes closely

$$\frac{M}{\mu} = 5.93 \frac{\rho_m}{\rho} \left(\frac{v}{c}\right)^2 \text{ (cgs units)}, \quad (11)$$

where  $\rho_m$  is the density of the projectile, and  $c$  is the velocity of sound in the target material. Equation (11) follows the energy scaling law; the calculated energy per unit mass displaced for ordinary materials is high, on the order of  $10^{10}$  ergs gm $^{-1}$ . The displaced mass varies inversely as the target material.

Applicable to the present discussion are photographs by Charters (1960) of the crater formed in granite by a ¼-inch-diameter nylon sphere at  $v=5.34$  km sec $^{-1}$ . By measuring the photographs and assuming that  $\rho$  (nylon) = 1.14 gm cm $^{-3}$  and  $\rho$  (granite) = 2.64 gm cm $^{-3}$ , I calculate that the ratio of the displaced mass to projectile mass is  $M/\mu=220$ , and that the energy of displaced material per unit mass is  $6.6 \times 10^8$  ergs gm $^{-1}$ , a relatively low value.

I have compared the various theories and formulas for crater formation with the Charters photographs of the crater formed in granite by a nylon ball (see table 1). The theories or formulas by Öpik, Glasstone, and Shoemaker fit the results from the photographs fairly well, while the predictions by Summers and Charters, Whipple, and Bjork are less satisfactory, predicting too small a crater volume by one to two orders of magnitude.

TABLE 1.—Crater by nylon ball on granite at  
 $v=5.34$  km sec<sup>-1</sup>

Source	Energy of displaced mass erg gm <sup>-1</sup>	Mass displaced Mass projectile M/μ
Öpik (eq. 8) <sup>a</sup>	-----	90
Whipple	1.1 × 10 <sup>10</sup>	-----
Glasstone	1 × 10 <sup>9</sup>	-----
Shoemaker	2.3 × 10 <sup>8</sup>	-----
Bjork	-----	38
Summers and Charters (eq. 11) <sup>b</sup>	7.0 × 10 <sup>10</sup>	2.0
Photographs by Charters	6.6 × 10 <sup>8</sup>	220

<sup>a</sup> Assumed crushing strength of granite,  $S=1.5 \times 10^9$  dyn cm<sup>-2</sup>.

<sup>b</sup> Assumed velocity of sound in granite,  $c=6.0 \times 10^4$  cm sec<sup>-1</sup>.

I shall adopt Öpik's solution and constants in this paper, since they appear to apply fairly well in an experimental example that simulates the actual situation in space. There can be no doubt that some other quantity than compressive strength, perhaps some function of ductility or brittleness, must more appropriately measure the material displaced in crater formation by high-velocity impact. Also density seemingly should enter the equation in a different manner. More theoretical and experimental results are sorely needed. Fortunately, the velocities of interest are near enough to the observed velocity so that the still unresolved question of momentum or energy scaling does not greatly affect the calculated results. In both cases the scaling is proportional to mass, and no theory suggests much deviation from mass scaling so long as the projectile contains a very large number of atoms.

Let us then adopt  $k=4.0$  in equation (8), since the meteoroid will probably be less dense than stone ( $k=4.3$  for stone striking iron). At a relative velocity  $v$ , interplanetary material of mean space density  $\rho_s$  will, upon encountering a randomly oriented surface, contribute a mass  $v\rho_s/4$  per unit area per unit time. The linear erosion rate  $dR/dt$  will vary as  $\rho_s^{-1}$  times the mass erosion rate; hence by equation (8), the linear erosion rate becomes

$$\frac{dR}{dt} = \epsilon = 1.0 \times \frac{\rho_s v^2}{(\rho S)^{1/2}}. \quad (12)$$

### Mean space density of dust and comparisons

We can now apply the observed etching rates to determine a mean space density of particles by means of equation (12); hence

$$\rho_s = \frac{\epsilon(\rho S)^{1/2}}{v^2}. \quad (13)$$

The space density and the velocity of encounter both vary in some inverse fashion with solar distance ( $\sim r^{-1/2}$ ?), while the time of passage varies in a direct fashion ( $\sim r^{3/2}$ ?). Hence the mean value of  $\rho_s$  will be somewhat weighted towards the outer parts of the meteoroid orbits. A more refined treatment is scarcely justified at this stage of the study.

The last column of table 2 gives calculated values of the mean space density based on equation (13) and the adopted values of the erosion rates for irons, stones, and photographic meteoroids. For irons the value of crushing strength is probably too great, but is intended to include some effect of ductility or malleability, as compared to the value for stones, checked generally by the experiment of the nylon ball on granite. For photographic meteoroids the value of  $S$  is probably too small, representing the most fragile 20 percent observed. The mean velocity is taken at 10 km sec<sup>-1</sup>, as representing a value corresponding more to the

TABLE 2.—Calculations of space density from erosion rates

	Erosion rate $\epsilon$ (cm sec <sup>-1</sup> )	Density $\rho$ (gm cm <sup>-3</sup> )	Compressive strength $S$ (dyn cm <sup>-2</sup> )	Meteoroid velocity $v$ (km sec <sup>-1</sup> )	Mean space density $\rho_s$ (gm cm <sup>-3</sup> )
Irons	$3.8 \times 10^{-15}$	7.8	$2 \times 10^{10}$	10	$1.5 \times 10^{-21}$
Stones	$5.4 \times 10^{-14}$	2.6	$2 \times 10^9$	10	$3.9 \times 10^{-21}$
Phot. met.	$7.3 \times 10^{-13} \rho^{-1}$	$\rho$	$2 \times 10^4$	10	$0.10 \times 10^{-21} \rho^{-1/2}$

distance of the earth or Mars from the sun than to the value in the asteroid belt ( $\sim 5$  km sec $^{-1}$ ). The value  $v=10$  km sec $^{-1}$  is small for meteors, even after neglecting earth gravity.

The mean space density calculated from data on photographic meteoroids is more than an order of magnitude smaller than those based on erosion of irons and stones, if we adopt  $\rho \sim 1$  gm cm $^{-3}$ . A smaller value of  $\rho$  is possible and the crushing strength is probably underestimated; hence the fit is satisfactory in view of the uncertainties in all the critical data. A somewhat higher value of  $v$  than 10 km sec $^{-1}$  might be more applicable to cometary meteoroids than to asteroidal material, because of the greater orbital inclinations and eccentricities. This would increase the discrepancy. On the other hand, the greater mean applicable solar distance and inclination would be expected to reduce the average space density of material encountered by cometary meteoroids. Hence the discrepancy is in the expected direction and may represent reality.

Comparison with other data is difficult. For the Zodiacal Cloud in the neighborhood of the earth's path, van de Hulst (1947) derives  $1.0 \times 10^{-21}$   $\rho$  gm cm $^{-3}$  as the density near the earth's orbit. If we accept a fraction  $f$  of this density as applying to the mean region of cometary asteroids, and assume that the density of interplanetary particles equals that of the cometary meteoroids, we can solve for  $\rho$  and  $\rho_s$  by this relation and by table 2, leading to

$$\rho_s^{3/2} = 0.1/f \text{ (cgs units)}. \quad (14)$$

If we arbitrarily adopt some reasonable value for  $f$ , say 1/4, allowing for a decrease in  $\rho_s$  with solar distance and away from the ecliptic plane, we solve equation (14) to derive  $\rho \sim 0.5$  gm cm $^{-3}$  and  $\rho_s = 1.2 \times 10^{-22}$  gm cm $^{-3}$ . The corresponding value of the mean density near the earth's orbit is then  $5 \times 10^{-22}$  gm cm $^{-3}$ .

Other analyses of the Zodiacal Cloud obtain lower values of  $\rho_s$  than van de Hulst by factors of 10 or more times (see, for example, the list by Nazarova, 1961). The derived density is very sensitive to the upper limit of the cutoff in the distribution law applicable to the smallest particles. Typical is van de Hulst's derived law

$$N(R) = \frac{3.5 \times 10^{-20}}{R^{2.6}}, \quad (15)$$

where  $N(R)dR$  represents the number of particles per cm $^3$  in the particle-radius range  $dR$ . In his integration he cuts off the upper limit at  $R=0.035$  cm; the lower limit does not much affect the sum.

The mean space density derived by McCracken, Alexander, and Dubin (1961) from measures on space vehicles near the earth is considerably greater than van de Hulst's value. Comparison, however, is specious since their particle-size distribution law is

$$N(R) = \frac{6.0 \times 10^{-28}}{\rho^{1.7} R^{6.1}} \text{ (cgs units)}. \quad (16)$$

The mass integral depends almost solely upon the *lower* limit in  $R$ , which at mass  $\sim 10^{-10}$  gm leads to a mean space density near the earth of  $3.2 \times 10^{-20}$  gm cm $^{-3}$ . The space density is doubled if the mean velocity of impact is taken as 15 instead of 30 km sec $^{-1}$ , and increases rapidly as the limiting particle radius is reduced.

But the real difficulty in comparison lies in the area provided for diffraction of light by small particles, diffraction being proportional to the total area. From McCracken et al. (1961) the particle area per unit volume is  $5.7 \times 10^{-17}$   $\rho^{-2/3}$  cm $^2$  per cm $^3$ , while van de Hulst requires only  $6 \times 10^{-20}$  cm $^2$  per cm $^3$  near the earth, or about one thousandth as much. The newer measures by Blackwell, as indicated by the calculations of Ingham (1961), require even a lower scattering area, roughly  $10^{-21}$  cm $^2$  per cm $^3$  at the earth's distance from the sun. The great diffracting area observed by McCracken et al. is provided by particles largely in the dimension range from  $10^{-4}$  to  $10^{-3}$  cm that are most responsible for scattering at angles of from  $1^\circ$  to  $10^\circ$  from the sun. Hence their deduced particle density would increase the intensity of the Fraunhofer Corona a thousand times its observed intensity, unless the particles are confined to a small volume near the earth, essentially within the moon's distance. This evidence seems to confirm the existence of a dust cloud about the earth (Whipple, 1961a, 1961b; Hibbs, 1961a, 1961b; questioned by Dubin, 1961).

### Consequences of erosion to the Poynting-Robertson effect

Let us again accept the postulate made above that cometary meteoroids capable of producing photographic meteors are eliminated by space erosion of some kind in the order of  $10^4$  years. The average lifetime  $t$  of any such meteoroid will then be  $R/\epsilon$ , or by equation (7),

$$t = R\rho \times 4.3 \times 10^4 \text{ years,} \quad (17)$$

where  $R$  and  $\rho$ , the radius and density, respectively, of the meteoroid, are measured in cgs units.

Now the Poynting-Robertson effect (Wyatt and Whipple, 1950) will cause a particle to spiral from an initial orbit into the sun in a time

$$t = R\rho K \times 10^7 \text{ years,} \quad (18)$$

where  $K$  depends upon the initial eccentricity and perihelion distance of the orbit, and is of the order of unity for short-period comet orbits.

Typical values of  $K$  are: 0.14 for the Geminid meteor shower; 0.6 for the Taurids and Encke's comet; 2.8 for the Bielids; 7.2 for the Leonids; and 18.6 for the Lyrids. We see that the Poynting-Robertson effect acts at a rate  $10^{-2}$  to  $10^{-4}$  times as fast as the estimated erosion for typical meteor showers. Thus, if we take the erosion rate as fixed for particles of all sizes, the Poynting-Robertson effect can be neglected for all cometary meteoroids, but could possibly be effective for some of the asteroidal particles (see table 2), such as irons in highly inclined orbits. Even for stones, however, the effect could probably be neglected.

At least two other factors must be considered as we apply the above reasoning to smaller particles: (a) erosion changes to destructive collision when the eroding mass is the order of  $10^{-2}$  times the mass of the particle eroded or greater; and (b) the physical properties of cometary meteoroids may depend upon their size.

Thus, as we consider erosion of smaller particles, the upper limit of mass for the eroding particles must be reduced proportionally to the mass of the particle eroded. The cross section for destructive collision by larger

particles can be neglected. The Poynting-Robertson effect becomes operative when only  $10^{-2}$  to  $10^{-4}$  of the total space density remains in particles the order of  $10^{-2}$  times the mass of the particle eroded. If, for example, van de Hulst's law (eq. 15) is valid to  $R=10^{-4}$  cm, 1 percent of the mass would then be contained in the range 1 to  $13 \times 10^{-4}$  cm. Hence, cometary particles less than approximately  $60\mu$  in radius and initially in very short-period orbits, or in longer orbits of high inclination to the ecliptic, might survive long enough to spiral into the sun. Note that high-inclination orbits are always favored because of the *observed* concentration of dust to the ecliptic (really Jupiter's orbit plane). Note also, however, that these smaller particles are already counted in the diffraction theory for the origin of the Fraunhofer Corona.

As the exponent  $\alpha$  of  $R$  in the relation  $N(R) \sim R^{-\alpha}$  becomes greater than 4, where the increase in mass per logarithmic step in  $R$  or  $\mu$  is constant, only the smallest particles allowed by light pressure survive long enough to spiral into the sun. The total fraction of the mass in these small particles, however, becomes larger as  $\alpha$  increases. If high-energy ions contribute appreciably to space erosion, however, small particles may fare no better than large ones with regard to the Poynting-Robertson effect (see, for example, Whipple, 1959; and Reiffel, 1960).

On the other hand, if the small cometary meteoroids are stronger and tougher than are the larger ones, erosion may be less serious for them. An increase by a factor of 100 in compressive strength would increase the limiting particle size by a factor of 10 and the limiting mass by a factor of 1,000.

We may conclude, therefore, that the data and assumptions of the present paper would preclude most of the small particles from attaining low inclination, nearly circular orbits, unless they are much stronger physically than the average photographic meteoroids. Higher inclination orbits would somewhat favor Poynting-Robertson reduction in orbit dimensions for all particles. Unfortunately, we have no satisfactory information about the physical or chemical nature of the small particles (below  $\mu \sim 10^{-2}$  gm).

### Dust as a hazard to space vehicles

Penetration rates for exposed surfaces in space near the ecliptic between Venus and Mars well away from the earth should probably be considerably smaller than the values given by the author in 1957. The mean space density near the earth was taken as  $4 \times 10^{-20}$  gm cm<sup>-3</sup> as compared to the values derived here, in the range from  $4 \times 10^{-22}$  to  $\sim 1 \times 10^{-20}$  gm cm<sup>-3</sup> near the earth's orbit. Bjork (1961a) finds slightly smaller penetrations for given masses and velocities, while possible low densities of the particles themselves may reduce their penetration powers. Lower average velocities also will apply, especially towards Mars, again reducing the penetrating power.

In the immediate neighborhood of the earth we still have no reliable information on the distribution of particles in the mass range from  $10^{-5}$  to  $10^{-3}$  gm. Extrapolations from McCracken et al. suggest that my 1957 estimates may be too large. On the other hand, the rough agreement of values of mean space density derived from etching rates and from the Zodiacal Cloud calculations suggests that most of the mass (or mean density) in space is carried by particles intermediate in size between the finest dust and optical meteoroids; i.e., in the range  $10^{-7}$  to  $10^{-3}$  gm. Hence my 1957 estimates may, in fact, be realistic values rather than safe upper limits near the earth.

The etching rates for exposed surfaces can be determined with some confidence from table 2 as safe limits near the ecliptic between Venus and Mars, but not in the immediate vicinity of the earth. McCracken et al. have produced almost incontestable evidence that a high concentration of fine dust exists near the earth. Thus etching rates within the moon's distance may be a few times greater, perhaps even orders of magnitude greater, than at much larger distances from the earth, but still negligible for metals as tough as aluminum.

Exposed surfaces of weak and brittle materials should be avoided in space vehicles where an etching rate of 1 micron a year would be undesirable. On the moon, the etching (and possibly even penetration) may be aggravated by material ejected from meteoritic impacts. When not in use, transparent or delicate surfaces

should be protected on the moon, and "tough" material should be chosen insofar as is practicable for exposed surfaces whose function could be impaired by etching.

Note that the continued operation of Vanguard I for nearly three years does not guarantee that the protecting windows for the solar cells are not severely etched. Even severe etching of a glass surface does not necessarily reduce much of its transparency to light.

### Acknowledgment

I am indebted to Dr. Edward Anders for pre-publication material, and especially to Dr. Edward L. Fireman for helpful advice and discussion.

### References

- BIRKHOFF, G.; MACDOUGALL, D. P.; PUGH, E. M.:  
AND TAYLOR, G.  
1948. Explosives with lined cavities. *Journ. Appl. Phys.*, vol. 19, pp. 563-582.
- BJORK, R. L.  
1961a. Meteoroids vs. space vehicles. *Journ. Amer. Rocket Soc.*, vol. 31, pp. 803-807.  
1961b. Analysis of the formation of Meteor Crater, Arizona: A preliminary report. *Journ. Geophys. Res.*, vol. 66, pp. 3379-3387.
- BUDDHUE, J. D.  
1942. The compressive strength of meteorites. *Pop. Astron.*, vol. 50, pp. 390-391.
- CHARTERS, A. C.  
1960. High-speed impact. *Sci. American*, vol. 203, no. 4, pp. 128-140.
- DUBIN, M.  
1961. Remarks on the article by A. R. Hibbs, "The distribution of micrometeorites near the earth." *Journ. Geophys. Res.*, vol. 66, pp. 2592-2594.
- EBERHARDT, P., AND HESS, D. C.  
1960. Helium in stone meteorites. *Astrophys. Journ.*, vol. 131, pp. 38-46.
- FIREMAN, E. L.  
1958. Argon-39 in the Sikhote-Alin meteorite fall. *Nature*, vol. 181, pp. 1613-1614.
- FIREMAN, E. L., AND DEFELICE, J.  
1960. Argon-39 and tritium in meteorites. *Geochim. et Cosmochim. Acta*, vol. 18, pp. 183-192.  
1961. Tritium, argon 37, and argon 39 in the Bruderheim meteorite. *Journ. Geophys. Res.*, vol. 66, pp. 3547-3551.
- FISHER, D. E.  
1961. Space erosion of the Grant meteorite. *Journ. Geophys. Res.*, vol. 66, pp. 1509-1511.

- GLASSTONE, S., ED.  
1957. The effects of nuclear weapons. U.S. Atomic Energy Commission, Washington, D.C.
- HIBBS, A. R.  
1961a. The distribution of micrometeorites near the earth. *Journ. Geophys. Res.*, vol. 66, pp. 371-377.  
1961b. Author's reply to the preceding discussion on the article, "The distribution of micrometeorites near the earth." *Journ. Geophys. Res.*, vol. 66, pp. 2595-2596.
- VAN DE HULST, H. C.  
1947. Zodiacal light in the solar corona. *Astro-phys. Journ.*, vol. 105, pp. 471-488.
- INGHAM, M. F.  
1961. Observations of the zodiacal light from a very high altitude station. IV. The nature and distribution of the interplanetary dust. *Monthly Notices Roy. Astron. Soc.*, vol. 122, pp. 157-176.
- JACCHIA, L. G., AND WHIPPLE, F. L.  
1961. Precision orbits of 413 photographic meteors. *Smithsonian Contr. Astrophys.*, vol. 4, no. 4, pp. 97-129.
- MCCRACKEN, C. W.; ALEXANDER, W. M.; AND DUBIN, M.  
1961. Direct measurement of interplanetary dust particles in the vicinity of Earth. *Nature*, vol. 192, pp. 441-442.
- MCCROSKY, R. E.  
1955. Fragmentation of faint meteors. *Astron. Journ.*, vol. 60, p. 170.
- NAZAROVA, T. N.  
1961. Investigation of meteoric particles on the third Soviet artificial earth satellite. *Planetary Space Sci.*, vol. 8, pp. 82-85.
- ÖPIK, E. J.  
1955. The masses and structure of meteors. *In* *Meteors*, T. R. Kaiser, ed., pp. 33-35. Pergamon Press, New York.
1958. Meteor impact on solid surface. *Irish Astron. Journ.*, vol. 5, pp. 14-33.
- REIFFEL, L.  
1960. Erosion of meteorites in space and the density of interplanetary gas. *Nature*, vol. 185, pp. 821-823.
- SHOEMAKER, E. M.  
1960. Penetration mechanics of high velocity meteorites, illustrated by Meteor Crater, Arizona. *In* *Report Int. Geol. Congr.*, 21st Session, Norden, 1960, Part 18, pp. 418-434.
- SUMMERS, J. L., AND CHARTERS, A. C.  
1959. High-speed impact of metal projectiles in targets of various materials. *In* *Proc. Third Symposium on Hypervelocity Impact*, F. Genevese, ed., pp. 101-110. Armour Research Foundation, Chicago.
- WHIPPLE, F. L.  
1955. On the mass-luminosity relation for meteors. *Astron. Journ.*, vol. 60, pp. 182-183.  
1957. The meteoritic risk to space vehicles. *In* *Proc. 8th Int. Astronautical Congr.*, Barcelona, 1957, pp. 418-428. Springer-Verlag, Vienna, 1958.  
1959. Solid particles in the solar system. *Journ. Geophys. Res.*, vol. 64, pp. 1653-1664.  
1961a. The dust cloud about the earth. *Nature*, vol. 189, pp. 127-128.  
1961b. Particulate contents of space. *In* *Medical and biological aspects of the energies of space*, P. Campbell, ed., pp. 49-70. Columbia University Press, New York.
- WHIPPLE, F. L., AND FIREMAN, E. L.  
1959. Calculation of erosion in space from the cosmic-ray exposure ages of meteorites. *Nature*, vol. 183, p. 1315.
- WYATT, S. P., JR., AND WHIPPLE, F. L.  
1950. The Poynting-Robertson effect on meteor orbits. *Astrophys. Journ.*, vol. 111, pp. 134-141.

### Abstract

Photographic meteor studies and spallation products of cosmic rays in meteorites provide upper limits or evaluations of erosion rates for meteoroids in orbit. The rate increases by several orders of magnitude in the sequence: irons, stones, and photographic meteoroids. The sequence suggests that the erosion rate depends in some inverse fashion upon the strength or brittleness of the materials, a natural expectation if erosion is produced by crater-forming impacts with interplanetary dust. On this assumption and by applying Öpik's high-velocity impact theory, the author derives a mean space density for the dust at roughly  $10^{-21}$  gm cm<sup>-3</sup>.

Only the very smallest cometary meteoroids can spiral into the sun by the Poynting-Robertson effect if the assumptions of this paper are true. Strong evidence for a high concentration of dust in the earth's immediate vicinity suggests that erosion rates may be greater near the earth than in deep space from Venus to Mars and even beyond. The surface of space vehicles should be carefully chosen or protected to minimize etching by interplanetary dust, if long exposure times are anticipated. The hazard may be greatest at the moon's surface.

# The Absence of Magnetic Micropulsations of Meteor Origin

By C. Ellyett<sup>1</sup> and G. B. Gillion<sup>1</sup>

Kalashnikov (1949) claimed to have found an increase in the occurrence of micropulsations of the earth's magnetic field during the dates of certain northern hemisphere meteor showers. Pulsations of  $4m\gamma$  amplitude could be recorded. The measured band of micropulsation frequencies unfortunately extended upwards beyond 2 c/s, and hence into the region of sferics of thunderstorm origin. Campbell (1960) has reviewed this work, and concludes that the validity of the results is increased by the fact that the observations were made in November, December, and January—a period of minimum activity in the annual cycle of thunderstorm activity.

Hawkins (1958) repeated Kalashnikov's investigations using apparatus of about the same sensitivity, and found no significant increase. His equipment, however, covered the band 0.5 to 10.0 c/s, and hence could also have recorded sferics.

Further work was done by Campbell (1960), who carried out a 7-month series of micropulsation measurements in California in 1958, with a limiting sensitivity of  $20m\gamma$ . The periods recorded lay between 0.04 and 0.4 c/s. An average amplitude was obtained for each hour. Normalizing factors ranging from 1.02 to 33.3 for various hours of the day, compared with the rate at 10 a.m. L.T. as reference, were applied to determine an average daily value. Departures in micropulsation amplitude from this daily average were then compared with the occurrence of the meteor showers. This procedure would appear to be doubtful in two respects. First, undue weight in scaling within the day appears to be given to the 10 a.m. micropulsation amplitudes. Meteor shower occurrence normally peaks well before 6 a.m. L.T., and it is

only in very limited parts of the year that a second peak of shower activity occurs around 8 to 10 a.m. Second, the association of the two phenomena, which was claimed to exist, was based on low-rate meteor observations (Whipple and Hawkins, 1958). If the percentage occurrence of micropulsation activity is to increase appreciably, an accompanying large increase of subvisual meteors is implied. Observations at high radar-meteor rates, however, have now shown that major showers comprise a relatively small proportion of the total count (Whipple and Hawkins, 1958; Ellyett and Keay, 1956).

Finally, Jenkins, Phillips, and Maple (1960) observed micropulsations at 1.5 c/s, with an improved sensitivity of  $0.3m\gamma$ . They claim an occasional big increase in the occurrence of these micropulsations on some nights, correlating with meteor showers. The graphical correlation does not look convincing, and in any case the meteor data used are the Harvard visual meteor observations taken during the first half of the century. These are again low-rate observations.

On general grounds, there is little in the diurnal distribution of micropulsations that fits the picture of meteor occurrence. Continuous micropulsations ( $Pc$ ), trains ( $Pt$ ), giant pulsations ( $Pg$ ), and long-period fluctuations ( $LPc$ ) all increase in amplitude toward the auroral regions. Observations of  $Pc$  show a 27-day solar period, and both  $Pt$  and  $Pg$  are essentially nighttime phenomena. The possible exception is "pearls" at about 1 c/s, but these on occasion last fairly regularly for many hours.

If a single meteor produces a magnetic pulse or train of pulses—as it must if the suggestion of meteor origin is correct—then it is obviously desirable that both sets of phenomena be observed at the same site. This has not previously been done.

<sup>1</sup> Physics Department, University of Canterbury, Christchurch, New Zealand.

### Meteor equipment

A radar transmitter maintained a signal of 81 kw peak power and  $26\ \mu$  pulse width at 69.5 Mc/s, with a pulse recurrence frequency of 150 c/s. Single crossed folded dipoles above wire-mesh artificial earth screens were used for transmitting and receiving, and resulted in all-sky viewing. The receiver, followed by normal oscillograph and camera recording, contained design features that eliminated false meteor rate variations due to both slow variations of the background noise (MacLauchlan, 1960) and pulse-type interference. Meteors were recorded down to a magnitude of +9.1.

### Micropulsation equipment

Magnetic flux variations were detected by a two-turn buried loop, with an effective area of  $1.6 \times 10^4$  square meters, leading to a galvanometer. Light from the undisturbed galvanometer mirror fell centrally on two photocells placed side by side. Deflection of the mirror by an incoming signal altered the photocell current, which was then amplified by a triode that formed one arm of a bridge. A twin-T rejection filter, tuned to 1.5 c/s, supplied negative feedback. The overall gain of the detection circuit, including an amplifier in the pen-recording unit, was  $4 \times 10^8$ , giving a

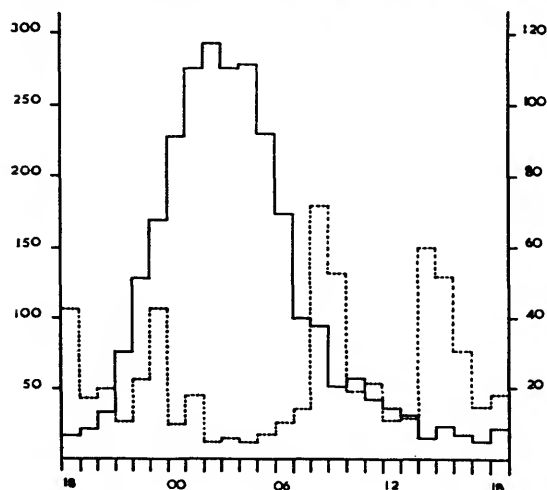


FIGURE 1.—Number of meteors/hr compared with the number of  $\frac{1}{2}$ -mins/hr containing 1.5 c/s micropulsations. Observations commenced at 6 p.m., local time, on 29 July 1961. Heavy line, meteors; dotted line, micropulsations.

minimum readable input level of  $0.04\ \mu\text{V}$ , corresponding to a magnetic field change of  $0.3\text{m}\gamma$  ( $=0.3 \times 10^{-8}$  gauss). The sensitivity, and the frequency filtering at 1.5 c/s, was thus purposely made the same as that of Jenkins, Phillips, and Maple (1960). (There is no reason why the particular micropulsation frequency of 1.5 c/s should be associated with meteors. Two advantages of this frequency are that it is below sferics interference, and is in a region of high loop sensitivity.) The recording paper passed through the pen recorder at a rate of 3 inches per minute, which just allowed 1.5 c/s to be resolved.

### Results

A period of 24 hours of continuous observing commenced at 6 p.m. L.T. on 29 July 1961. Both equipments were looking at approximately the same sky area.

During this period the  $\delta$ -Aquadrid shower ( $\alpha=340^\circ$ ,  $\delta=-19^\circ$ ), which is the strongest known meteor shower to occur in either hemisphere (Ellyett, Keay, Roth, and Bennett, 1961; Keay and Ellyett, 1961), exerted its peak effect at about 3 a.m. L.T. and was above the horizon for several hours centered on this time.

The time of occurrence of each individual meteor was read to an accuracy of  $\pm 2$  seconds. The micropulsation and the meteor time scales were locked together, and a correlation was considered positive if the two phenomena commenced within 4 seconds of each other. A total of 2,750 meteors was recorded during the 24 hours.

First, large-amplitude low-range meteors, with durations in many cases of up to 30 seconds, were individually compared with the micropulsation trace. There was an obvious absence of any correlation.

The number of half-minutes in each hour when micropulsations at 1.5 c/s were present was then plotted against the total hourly meteor count. The micropulsation distribution was as expected, with a noon dip. As shown in figure 1, there is no correlation between the two rates of occurrence.

It would thus appear fairly conclusive that no correlation exists within the present limits of sensitivity. Further work is proceeding.

**Acknowledgments**

This work has received contract assistance from the Electronics Research Directorate of the Air Research and Development Command, U.S. Air Force, under contract AF64(500)-6 (Meteors); and from the Office of Naval Research, U.S. Navy, under contract Nonr(G)-00027-62 (Micropulsations).

**References**

- CAMPBELL, W. H.  
1960. Magnetic micropulsations accompanying meteor activity. *Journ. Geophys. Res.*, vol. 65, pp. 2241-2245.
- ELLYETT, C. D., AND KEAY, C. S. L.  
1956. Radio echo observations of meteor activity in the southern hemisphere. *Australian Journ. Phys.*, vol. 9, pp. 471-480.
- ELLYETT, C. D.; KEAY, C. S. L.; ROTH, K. W.; AND BENNETT, R. G. T.  
1961. The identification of meteor showers with application to southern hemisphere results. *Monthly Notices Roy. Astron. Soc.*, vol. 123, pp. 37-50.
- HAWKINS, G. S.  
1958. A search for magnetic effects from meteors. *Journ. Geophys. Res.*, vol. 63, pp. 467-475.
- JENKINS, A. W.; PHILLIPS, C. A.; AND MAPLE, E.  
1960. Observed magnetic effects from meteors. *Journ. Geophys. Res.*, vol. 65, pp. 1617-1619.
- KALASHNIKOV, A. G.  
1949. On observations of the magnetic effect of meteors by the inductive method. *Dokl. Acad. Sci. U.S.S.R.*, vol. 66, pp. 373-376. (Translated by E. R. Hope, Canadian Def. Res. Board, T-130-R, 1954.)
- KEAY, C. S. L., AND ELLYETT, C. D.  
1961. The latitude dependence of radar meteor shower observations. *Journ. Geophys. Res.*, vol. 66, pp. 2337-2343.
- MACLAUCHLAN, E. C.  
1960. Noise suppression in pulse receivers. *Australian Journ. Phys.*, vol. 13, pp. 750-752.
- WHIPPLE, F. L., AND HAWKINS, G. S.  
1958. Meteors. *In Handbuch der Physik*, S. Flügge, ed., vol. 52, pp. 519-564. Springer-Verlag, Berlin.

**Abstract**

Simultaneous observations of micropulsations greater than  $0.3m\gamma$  at 1.5 c/s, and of meteors greater than magnitude +9.1, at the same site during the peak of occurrence of the  $\delta$ -Aquadrid meteor shower, failed to show any correlation, either with individual meteors, or on an hourly rate basis.



# The Density Distribution of Telescopic Meteors Around the Earth's Orbit

By L. Kresák and M. Kresáková<sup>1</sup>

Recent studies have provided substantial evidence that the rate of meteoric particles encountered by the earth varies considerably, owing both to the occurrence of recognized meteor showers and to the nonuniform density distribution of the sporadic background. These irregularities, appearing periodically in the form of annual variation of meteor rates, are of particular interest in connection with the constitution of minor meteor streams at advanced stages of dispersion, and with the meteoric risk to space vehicles, especially those moving in satellite orbits around the earth or launched to the moon. The evaluation of the annual variation is made difficult by the variability of the geometrical conditions depending on geographic latitude and by the additional effect of diurnal variation produced by the rotation of the earth. Another difficulty in the interpretation of observed rates lies in the variability of the velocity distribution; the different sensitivities of individual observing techniques to meteors of different velocities complicate this problem.

The main purpose of this paper is to analyze the distribution of meteor orbits around that of the earth, on the basis of telescopic observations made at the Skalnaté Pleso Observatory for the period 1946–1959. These include faint telescopic meteors down to the 10th apparent magnitude; more than half of the data are concerned with meteors of 8th and 9th magnitude. These faint meteors are of particular significance for two reasons: (1) In the constitution of meteor streams they may reveal evolutionary changes caused by the effects of solar radiation, which are substantially greater on smaller particles; (2) the likelihood of a collision with a space

vehicle is greater for smaller meteors, approximately by a factor of ten for each two magnitudes. For the telescopic meteors recorded during the Skalnaté Pleso program, the average probability of collision is estimated at about  $10^{-6} \text{ m}^{-2} \text{ day}^{-1}$ ; this is not a negligible figure even for the space vehicles and durations of flight expected in the near future.

Supplementing the results of earlier studies (Kresáková and Kresák, 1955), we report here on a total of 4,573 meteors recorded during 1,364 hours of observation more or less uniformly distributed over the various dates and hours of the night. All observations were made with the same type of instrument, 4-inch binoculars with a magnification of 25.

The net annual variation produced by the changes of meteor density around the orbit of the earth may be established only after eliminating the effect of nonuniform radiant distribution on the visible and invisible hemisphere. This may be done by separating the annual and diurnal variation with the use of a reference model of apparent radiant distribution. In the present work we used three such models: Model A, the uniform apparent radiant distribution, giving constant hourly rates; Model B, an isotropic distribution with respect to the apex, with a continuous decline of radiant density towards the antapex (Hoffmeister, 1931) (the “equivalent velocity” constant ( $c=3.9$ ) was computed directly from our observations); and Model C, the standard distribution derived by Hawkins (1956) from the radio-echo data. This distribution is characterized by a pronounced ecliptical concentration, two main maxima near the sun and antihelion point, and a secondary maximum at the apex.

<sup>1</sup> Astronomical Institute of the Slovak Academy of Sciences, Bratislava, Czechoslovakia.

For each of the models the expected hourly rates for any instant may be predicted and compared with the observation. An overall comparison is shown in figure 1, where the abscissae indicate the solar longitudes and the ordinates the time in M.E.T. In this network of coordinates we plotted curves of constant reduced hourly rates obtained by combining the observations into normal places, interpolating, and smoothing the results. For a perfect representation of the diurnal variation, the curves should change into vertical straight lines; for a perfect representation of the annual variation, they should change into horizontal straight lines; and for an entire agreement between theory and observation they should vanish. Obviously, systematic departures may be anticipated in the annual rather than in the diurnal variation, and the vanishing of the diurnal variation alone would offer convincing proof of a nonuniform distribution of meteors around the orbit of the earth.

Figure 1 indicates that model A is distinctly inferior to models B and C. A systematic increase of meteor rates from the evening to the morning hours and a sharp maximum in the autumn reveal the main features of diurnal and annual variations, established long ago in the naked-eye range. In model B the total amplitude is essentially reduced, and the curves, as expected, run mainly in the vertical direction. Model C, which represents satisfactorily the radio observations (Hawkins, 1956) and the naked-eye observations (Hawkins and Pren-

tice, 1957), is, surprisingly, less consistent with the telescopic observations than is model B. It appears as if there were an overcorrection of the observed variation (a mirror-like image of model A); the radiant distribution suggested by Hawkins would fit better with a diminished density gradient. This may be attributed either to the selective effect of angular velocities applying to telescopic observations, or to an increasing preponderance of direct orbits with decreasing size of particles. It may be noted that for model B this effect was already indirectly taken into account by determining the basic constant ("equivalent velocity") from the telescopic data; a lower degree of apical concentration than indicated by the naked-eye observations was also found.

It is clear that none of the models of radiant distribution can account for the annual variation in terms of the earth's rotation combined with the obliquity of the ecliptic. Evidently, such features as a rapid increase of meteor rates in June and July, or a decrease in December and January cannot be explained by any other acceptable model of radiant distribution. Although the trend of diurnal variation in model A is entirely reversed in model C, nevertheless the annual variation preserves its main features unchanged. Hence the actual variations of meteor density around the earth's orbit are established beyond doubt.

The course of the net annual variation, freed from the effects of the earth's orientation according to the three models, is shown in figure

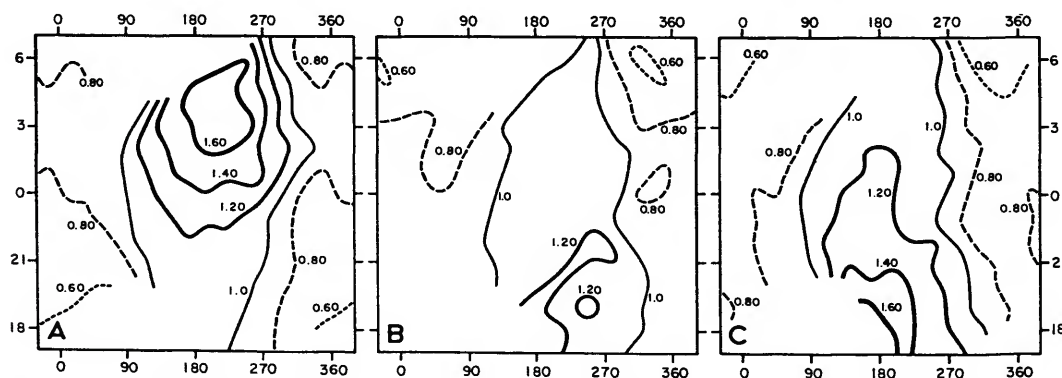


FIGURE 1.—The combined pattern of annual and diurnal variation referred to models A, B, C. The first solid line corresponds to the median hourly rate, the next solid lines to 1.20, 1.40, etc., and the broken lines to 0.80, 0.60 of the median value. Abscissae, solar longitudes; ordinates, time M.E.T.

2. Here the amplitudes of the annual variation for models B and C are 1:1.8 and 1:2.2, respectively. Despite considerable differences between these two models, the curves are similar enough, indicating in each case a lower level of activity in the first half of the year ( $\odot=280^\circ$  to  $100^\circ$ ) and a higher level in the second half ( $\odot=100^\circ$  to  $280^\circ$ ). Even the three maxima near  $\odot=130^\circ$ ,  $190^\circ$ , and  $250^\circ$  are consistently reproduced in both types of representation.

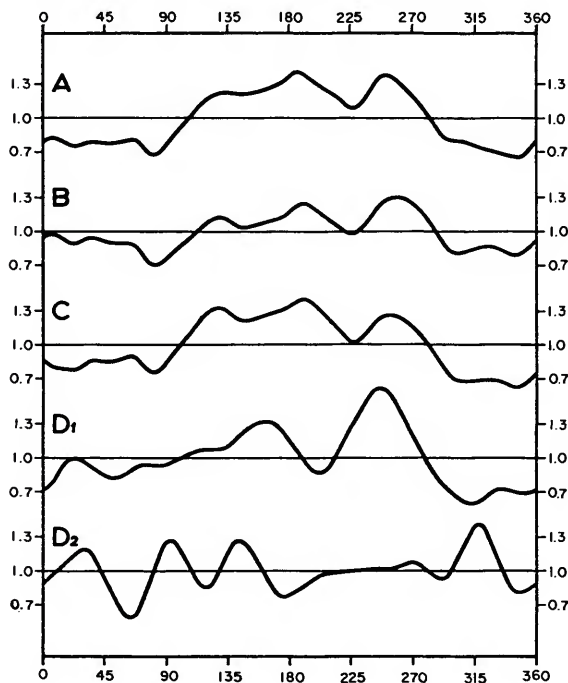


FIGURE 2.—The net annual variation referred to models A, B, C, compared with the distribution of comet approaches D1 ( $P < 500$  years) and D2 ( $P > 500$  years). Abscissae—solar longitudes.

We have attempted to test the source of the irregularities of the annual variation by means of cometary statistics. For the reasons pointed out by Levin (1961), Hoffmeister's (1948, p. 100) cometary indices are not suitable for this purpose, i.e., for taking the periodic comets together with the non-periodic comets that appeared in a relatively short time-interval. Instead, we used as a reference catalogue Kramer's (1953) extensive list of cometary orbits approaching the earth within 0.3 A.U. The comets of this list were divided into two

groups according as their periods were less than or greater than 500 years. With regard to the periods of recognized meteor showers, a correlation appears possible for the former group but highly improbable for the latter. The stream associated with each of the comets was considered as possibly active within  $30^\circ$  of solar longitude before and after the closest approach for the former group of comets (regularly of low inclination), and within  $15^\circ$  for the latter group. The results are shown in the lower part of figure 2, where we see that the density distribution D1 of short-periodic cometary orbits agrees well with the density distribution of telescopic meteors. As expected, the comets moving in very prolonged orbits (D2) exhibit no correlation at all, and this excludes any alternative explanation of the agreement in terms of seasonal selective effects of the discoveries of comets on the distribution of their nodes. Consequently, there is strong evidence that at least some of the irregularities of the annual variation are due to minor meteor streams of cometary origin, with the parent comets known, but too dispersed to be distinguished separately.

Analyses of the annual variation determined by radio techniques have been published by Hawkins (1956) for Jodrell Bank, and by Weiss (1957) for Adelaide. The net variation determined by Hawkins is based on model C, and is directly comparable with our results. The model chosen by Weiss is different. It assumes a line source round the ecliptic with an apparent strength up to the distance of  $90^\circ$  from the apex four times higher than in the remaining part of the ecliptic. Experience with different models, however, including those used by Weiss, indicates that the result will not differ greatly from those based on model C.

A comparison of the annual variation determined at Adelaide, Jodrell Bank, and Skalnaté Pleso is shown in figure 3. A previous study (Kresáková and Kresák, 1955) demonstrated that the annual variation of the telescopic meteors obtained at Skalnaté Pleso agrees well with the results of Hoffmeister (1937), derived from the naked-eye observations of Schmidt, Heybrock, and himself. Hence it may be concluded that the difference in the magnitude range covered by the different methods of

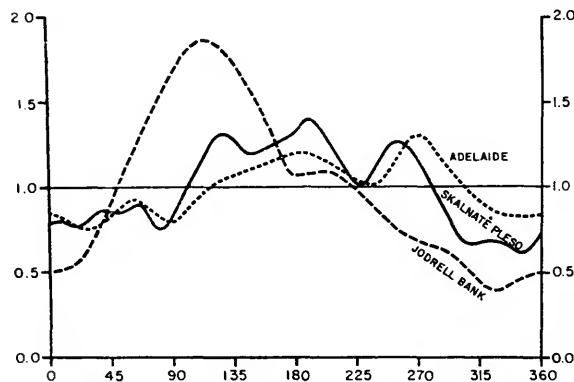


FIGURE 3.—The comparison of the net annual variation obtained at Adelaide (dotted line), Jodrell Bank (broken line) and Skalnate Pleso (solid line). Abscissae—solar longitudes.

observation cannot represent the essential source of the discrepancies. These discrepancies may result either from the difference in geographic latitudes or from the difference in the type of technique used for the determination of meteor rates.

It is surprising that our telescopic observations agree much more closely with the observations at Adelaide, in the southern hemisphere, than with those at Jodrell Bank, located in approximately the same geographic latitude as Skalnate Pleso. From this fact it follows that the main discrepancies are not due to the actual distribution of the radiants in declination. The difference between the annual variation of radio-echo and that of photographic rates was pointed out by Hawkins and Prentice (1957), who attribute it to the fact that the sensitivities of the two methods of observation vary with the geocentric velocities of the meteors. This interpretation requires a concentration of high-velocity meteors in the sector of the earth's orbit traversed in the summer months. However, direct measurements of meteor velocities, e.g., those by McKinley (1951), show, on the contrary, that there is only an average number of high-velocity meteors in June and July, and a maximum in September and October, consistent with the extreme declination of the apex.

Figure 4 shows the annual variation of the ratios of the hourly rates at Jodrell Bank and at Adelaide to those at Skalnate Pleso. A

striking feature of the first of these curves is its symmetry with respect to the summer solstice. This feature suggests some seasonal effect producing a correlation between the duration of the daily illumination by the sun and the ratio of ionizing to luminous efficiency of meteors. Such an explanation would require an inverse trend of the annual variation in the southern hemisphere, where the seasonal shift is in six-month periods. Some indications of such inversion actually appear in the figure, but they are not sufficiently conclusive. If, however, we take into account the annual variation of naked-eye meteors, determined for the southern latitudes by McIntosh (1934) and by Hoffmeister (1937, p. 60), with a deep minimum in January and February, the inversion of the curve becomes more distinct. There is a considerable difference between the amplitudes of the two curves in figure 4. In fact, the explanation suggested requires a difference of this kind, since the conditions of illumination are much more variable during the year at Jodrell Bank ( $\phi = +53^{\circ}.4$ ) than at Adelaide ( $\phi = -34^{\circ}.9$ ). At Jodrell Bank the atmospheric levels in which meteors appear are almost continuously illuminated at the time of the summer solstice. If this explanation is valid, it would partially account for the abundance of the summer daytime meteor showers detected only by radio techniques. Since all these streams encounter the earth at about the time of the summer solstice, they should be relatively



FIGURE 4.—The annual variation of the ratio of reduced hourly rates Adelaide:Skalnate Pleso (broken line), and Jodrell Bank:Skalnate Pleso (solid line). Abscissae—solar longitudes.

much weaker if they could be observed optically. It is important to emphasize that the basic data of Hawkins and Weiss were obtained at substantially different wavelengths (4.2 and 11.2 m, respectively), but the effect of this difference is difficult to determine.

From the similarity of the curves of annual variation at Adelaide and Skalnaté Pleso, despite their difference of  $84^\circ$  in geographic latitude, we deduce that the main contribution of the annual variation is due to meteor radiants of low declination. This conclusion offers an additional proof of the ecliptical concentration of radiants produced by a significant prevalence of direct meteor orbits of low inclination and short period. An earlier discussion of the telescopic meteor directions (Kresák, 1955) led to the same conclusion. The correlation between the annual variation and the distribution of the points of approach of short-periodic cometary orbits (fig.2) requires an ecliptical concentration as well. Thus three entirely independent types of evidence suggest that in the range of faint telescopic meteors the orbits are distinctly concentrated toward the plane of the ecliptic.

We shall now comment on the occurrence of shower meteors in the telescopic observations. The permanent showers, which at their maxima contribute a majority of the meteors observed, are hardly detectable in the range of telescopic meteors of 7th to 9th magnitudes. In the total for the whole year they were at least seven times less frequent with respect to the sporadic background than in the naked-eye observations. This lack of faint shower-meteors is consistent with the recent results obtained by Kresáková (unpublished), who, from naked-eye observations at Skalnaté Pleso, found a systematic difference between the magnitude functions of shower meteors and of sporadic meteors, with the constant  $\kappa=2.6$  and 3.5, respectively. An extrapolation would require the ratio of shower to sporadic meteors to be four times lower in the present telescopic observations than in those made by the naked eye. The actual relative decrease in the number of shower meteors appears even sharper, presumably because of the effect of corpuscular

radiation on the evolution of meteor streams (Kresák, 1960).

In addition to the showers known from other techniques of observation, eight showers of telescopic meteors have been established with a sufficient degree of probability. They appeared at solar longitudes  $25^\circ$ ,  $131^\circ$ ,  $158^\circ$ ,  $184^\circ$ ,  $194^\circ$ ,  $248^\circ$ , and  $316^\circ$ , most of them with out any indication of periodicity. Only rarely did their hourly rates exceed those of the sporadic background by a factor of two; striking phenomena, comparable to the Perseids or Geminids in the naked-eye range, are absent at 7th to 9th magnitudes. In general, it may be concluded that the phenomenon of meteor streaming becomes gradually less prominent as we pass from photographic through naked-eye to telescopic meteors. This phenomenon probably reappears again, to a much greater extent, in the range of much smaller particles for which rapid variations in frequency have been established by the impact measurements on high-altitude rockets and artificial satellites. Among faint telescopic meteors there is rather a system of minor, considerably dispersed streams that do not produce abrupt changes in meteor rates over a period of a few days, but that do influence the total annual variation.

As for the meteoric risk to space vehicles moving in the vicinity of the earth's orbit, we conclude primarily that:

(1) At the level of the probability of encounter  $10^{-6} \text{ m}^{-2} \text{ day}^{-1}$ , the risk from the sporadic background varies with a maximum seasonal amplitude of about 1:2, the safest period of permanently low activity lasting from January till May. The periods of highest activity occur in August, September, the first half of October, and in December.

(2) The particles producing this activity are very likely of cometary origin and constitution, as indicated by the relation of meteor rates to the distribution of nodes of short periodic cometary orbits.

(3) The permanent meteor showers represent a risk that is negligible in most cases, and is generally much lower than might be anticipated from photographic and naked-eye observations of larger bodies, or from impact measurements of smaller bodies.

(4) Showers rich in telescopic meteors are scarce and without distinct periodicity. Only quite exceptionally do they increase the risk by a factor of two or three. It must be remembered, however, that this result is derived from night-time observations, in which meteor showers with apparent radiants near the sun could not be detected.

#### Acknowledgments

The authors are greatly indebted to all members of the staff of the Skalnaté Pleso Observatory who took part in the observations analyzed here, especially to the most active observers: Dr. L. Padjušáková, Mr. A. Mrkos, Dr. A. Bečvář, Mr. M. Dzubák, and Mrs. A. Antalová. Our thanks are due to Mrs. L. Ďurkovičová and Mr. A. Aldor for their aid in numerical computations.

#### References

- HAWKINS, G. S.  
1956. Variations in the occurrence rate of meteors. *Astron. Journ.*, vol. 61, pp. 386-391.
- HAWKINS, G. S., and PRENTICE, J. P. M.  
1957. Visual determination of the radiant distribution of sporadic meteors. *Astron. Journ.*, vol. 62, pp. 234-240.
- HOFFMEISTER, C.  
1931. Zur Theorie der Variation der Sternschnuppenhäufigkeit. *Veröff. Univ. Berlin-Babelsberg*, vol. 9, no. 1, p. 17.  
1937. Die Meteore. *Akademische Verlagsgesellschaft*, Leipzig.  
1948. Meteorströme. *J. Barth Verlag*, Leipzig.
- KRAMER, E. N.  
1953. Cometary radiants and the association of meteor streams with comets. *Izv. Astron. Obs. Odessa*, pp. 163-247.
- KRESÁK, L.  
1955. The direction distribution of telescopic meteors. *Contr. Astron. Obs. Skalnaté Pleso*, vol. 1, pp. 9-35.  
1960. The effect of solar corpuscular emission on the magnitude distribution of meteors. *Bull. Astron. Inst. Czechoslovakia*, vol. 11, pp. 1-9.
- KRESÁKOVÁ, M., and KRESÁK, L.  
1955. On the activity of telescopic meteors and some related problems. *Contr. Astron. Obs. Skalnaté Pleso*, vol. 1, pp. 40-77.
- LEVIN, B. J.  
1961. The distribution of true radiants of meteor bodies down to a definite limit of mass. Symposia at the 5th meeting of CSAGI, Moscow, 1958. *In Annals of the International Geophysical Year*, vol. 11, pp. 187-193. Published by Pergamon Press.
- MCINTOSH, R. A.  
1934. Report of the section for the observation of meteors, 1929-1931. *New Zealand Astron. Soc. Bull.*, no. 21.
- McKINLEY, D. W. R.  
1951. Meteor velocities determined by radio observations. *Astrophys. Journ.*, vol. 113, pp. 225-267.
- WEISS, A. A.  
1957. The distribution of the orbits of sporadic meteors. *Australian Journ. Phys.*, vol. 10, pp. 77-102.

# Atmospheric Trajectories of Telescopic Meteors

Luboš Kohoutek<sup>1</sup> and Jiří Grygar<sup>1</sup>

Double-station observations of telescopic meteors were organized at the amateur meteor expedition to Mount Bezovec ( $\lambda=17^{\circ}58'$  E. Gr.,  $\varphi=+48^{\circ}40'$ , height=500 meters above sea level). Two teams of four members each gathered data on 123 pairs during the period of 8 nights (July 10 to 25, 1958). That represented 62 percent of all meteors recorded. The telescopes Somet 25×100 ( $d=3:3$ ) and binoculars 10×80 ( $d=7:3$ ) were used, with the base 2.5 km. We treated the observations by means of graphic-numerical analysis. All the distortions that might influence the determination of the mean heights were taken into account. The mean errors of some principal characteristics of meteors were also computed. The mean error of the estimates of the magnitude of one meteor was  $\pm 0^m24$ ; the error of angular length did not exceed 2/10 of the diameter of the field of view, and the error of plotted direction of meteor flight was about  $\pm 5^{\circ}$ . The errors in the determinations of the mean heights of the beginning, the center, and the end of meteor trajectories were smaller than 4 percent. The apparent frequency distribution of heights could not be represented by the Gaussian distribution, and therefore we considered the modal heights as more probable mean values. The following values were obtained for the height of the beginning, the center, and the end of meteor paths, respectively:  $H_b=98\pm 4$  km,  $H_c=93\pm 4$  km,  $H_e=88\pm 3$  km (the average corrected absolute magnitude  $m=6.0$ ). It was established that the observed beginnings of meteor trajectories agree well with the theoretical points of the beginning of rapid evaporation, and that the observed centers of paths approximately correspond to the point of maximum light of me-

<sup>1</sup> Astronomical Institute of the Czechoslovak Academy of Sciences, Praha and Ondřejov, Czechoslovakia.

teors. Next it was found that increase of the mean height with magnitude, if it exists at all, is very slight in the magnitude interval from 0<sup>m</sup>0 to 7<sup>m</sup>0. This conclusion was confirmed by recent radar observations.

No meteor with the real height below 60 km was recorded, thus the existence of isolated groups of the "low" telescopic meteors, as was suggested by Astapovich,<sup>2</sup> is hardly possible. The mean geocentric velocity,  $v_g=36\pm 5$  km/sec, was estimated and the average original radius of meteoroids was  $r_o=0.4$  to 0.5 mm, using some assumptions of the physical theory of meteors.

According to Levin's<sup>3</sup> formula, the energy necessary for the evaporation of 1 gm of meteor material was estimated to be from 1.6 to 3.5  $\times 10^{10}$  erg/gm. It follows from this that the free molecule flow occurs during the flight of telescopic meteoroids through the atmosphere. The course of diurnal variation of heights and geocentric velocities is in agreement with the assumption of nearly circular orbits of telescopic meteors, which is also confirmed by the distribution of apparent radiants. During the expedition the activity of the unusual meteor shower  $\alpha$  Lyrids, announced first by V. V. Martynenko (Simferopol, U.S.S.R.), was detected.<sup>4</sup> Unfortunately, the great angular elongation between our field of vision (North Pole) and the point of radiant made it impossible to determine accurately the radiant of telescopic meteors belonging to this shower. (For details, see also Bull. Astron. Inst. Czechoslovakia, vol. 13, pp. 9-26, 1962.)

<sup>2</sup> I. S. Astapovich, *Meteor phenomena in the earth's atmosphere*, chap. 33. Moscow, 1958. (In Russian.)

<sup>3</sup> B. J. Levin, *Physical theory of meteors and meteor matter in the solar system*, pp. 29, 97. Moscow, 1956. (In Russian.)

<sup>4</sup> J. Grygar, L. Kohoutek, Z. Kvíz, and J. Mikušek: "Observation of the  $\alpha$ -Lyrid meteor stream. Results of the Mount Bezovec meteor expedition." Bull. Astron. Inst. Czechoslovakia, vol. 11, pp. 84-86, 1960.



# Statistics of Meteor Streams

By R. B. Southworth<sup>1</sup> and G. S. Hawkins<sup>2</sup>

In the period 1954 to 1957 a random sample comprising 360 of the meteors photographed from two stations by the Baker Super-Schmidt meteor cameras were reduced under the "Short Trail" program (Hawkins and Southworth, 1958). The radiant and velocities of 359 meteors were sufficiently accurate to permit computation of dependable orbits (Hawkins and Southworth, 1961). Since this is the only random sample of photographic meteors with individually reliable orbits, it provides valuable material for a study of meteor distribution in space. The degree to which the meteors are grouped into streams is a basic feature of this distribution.

The major meteor streams are conspicuous in any random sample of photographic meteors and virtually all of their members are readily identifiable. Since in the sample there are many meteors that belong to each such stream, the characteristics of the stream are well defined, as is the range of each characteristic within the stream. Furthermore, these streams are well-known from other studies.

Members of a stream not previously known, or not well represented in the sample under study, are not as easy to identify. Early in the Short Trail program it became apparent that some of the meteors were associated into other groups or streams, apart from the previously known major streams. Numerous other meteors were doubtfully associated with streams. Several attempts, based upon a variety of principles, were made to classify the meteors into streams and a "sporadic" remainder. None of the classifications based on geocentric quantities—radiants, velocities,

and dates of occurrence—was satisfactory. It became clear that a comprehensive quantitative criterion was required that would embrace all the elements of the orbit.

## A criterion for stream membership

We may regard a meteor stream as composed of those meteors originating from a single comet during a single ejection or over an interval of time. As yet, we cannot reliably identify stream membership by physical or chemical characteristics, although some physical differences have been observed between different streams (Jacchia, 1960). Meteors arising from a comet will move in orbits similar to the comet's orbit, at least for a while. If planetary perturbations or other forces disperse the meteors so that the similarity of their orbits can no longer be seen, the stream is effectively destroyed. Thus, in practice, a meteor stream is recognized and defined as a group of meteors in similar orbits.

Occasionally meteors from two or more comets may have similar orbits. If the different origins cannot be recognized from the orbits, then the meteors form a single stream in practice, although arising from more than one comet.

A quantitative criterion for stream membership therefore requires a quantitative measure of orbit similarity (or difference). We shall consider the difference between orbits to be the difference between meteors. Let  $D(A, B)$  be such a quantitative measure of the difference between meteors  $A$  and  $B$ . Similarly, let  $D(M, N)$  be of the same mathematical form, but let it measure the difference between a mean orbit  $M$  of a stream and an individual meteor  $N$ . The two measures  $D(A, B)$  and  $D(M, N)$  correspond to two possible ways of defining a stream.

(1) A stream may be defined, for example, as

<sup>1</sup> Smithsonian Astrophysical Observatory, and Harvard College Observatory, Cambridge, Mass.

<sup>2</sup> Harvard College Observatory, Cambridge, Mass., and Boston University, Boston, Mass.

all meteors  $N$  such that  $D(M, N)$  does not exceed a given value  $D_M$ .

(2) We may define a stream by serial association between members. We may state that two meteors  $A$  and  $B$  are associated if  $D(A, B)$  does not exceed a standard value  $D_s$ . A stream may then be defined as a group of meteors in which every member is associated with one or more other members, and all members are associated together directly or indirectly.

As a third possibility we may define a phase space in which each meteor is represented by a point and the distance between points is the difference between meteors. Then a stream can be defined as the meteors in a region of high density in the phase space. This form has theoretical advantages but requires far more data than we possess. We shall therefore use the first two alternatives.

No particular measure of orbit difference is specified a priori. Indeed, we have found no way of determining a "best" or "optimum" measure. The magnitude of the cause of orbit difference, when known, is often the best measure of the difference. We do not know the causes of the dispersion within meteor streams in any quantitative manner, however, and it would be quite wrong to assume the causes. Consequently, we have looked for a measure that is as simple as possible and is expressed in terms of orbital elements as far as possible, since these are the most familiar indices of orbit differences. Because differences within streams are small, our measure need not be accurate for large differences in order to be useful.

One orbit may differ from another in any of six independent ways. One of these, the position of the meteor in the orbit at a given time, is not significant for our purpose because the meteors of a stream rapidly spread out all along the orbit. Apart from the instantaneous position of the meteor, the orbit may be specified by five elements. These may be the usual elements:  $a, e, \omega, \delta, i$ ; or they may be any set, out of an infinite number of possible sets, of five independent functions of the usual elements:  $C_j$ , where  $j=1, 2, 3, 4, 5$ . Each of the five differences between two orbits  $A, B$  may be expressed as the difference between the values of an element:  $C_j(A) - C_j(B)$ .

The fact that all the observed meteors pass close to the orbit of the earth imposes one constraint on the observed five elements, and thus reduces the number of independent elements to four. The earth is not important in the evolution of meteor streams, however, so that this constraint is not relevant to the differences within streams. Accordingly, we disregard it in formulating  $D$ .

In order to construct a single measure comprising five independent differences, we draw an analogy with a five-dimensional orthogonal coordinate system and consider each element as a coordinate. Any orbit then corresponds to a point in this conceptual space, and the distance between two points is a natural measure of the difference between the two corresponding orbits. Although orthogonal, the coordinates need not be rectangular; usually these will be curvilinear coordinates. We may approximate them by rectangular coordinates in any sufficiently small region, however, and this approximation will prove to be adequate for our purpose. The difference between meteors  $A, B$  is then of the form

$$D(A, B) = \left\{ \sum_{j=1}^5 c_j^2 [C_j(A) - C_j(B)]^2 \right\}^{1/2}, \quad (1)$$

where  $c_j$  are functions of the elements which are at our disposal and which determine the geometry of the space.

The value of  $D$  as a measure of difference depends on how well the  $c_j$  are chosen or can be chosen. The  $c_j$ , for our purpose, are scale factors determining the relative importance of the different  $C_j$  in  $D$ . Each  $c_j$  should be inversely proportional to the expected standard deviation of the corresponding element  $C_j$  in a stream.

An attempt to base the scale factors only on the streams would be an attempt to lift ourselves by our own bootstraps, because we are still trying to determine which meteors are stream members and which are not. We have checked the reasonability of the scale factors that were ultimately chosen by computing the mean standard deviation of each element on the assumption of an idealized dispersing mechanism. This is discussed below.

In accordance with all the foregoing, we have selected the elements and scale factors

described below. Angles, and thus the differences of angular elements, are measured by their chords, i.e., by twice the sine of half the angle. This is convenient; for small angles it is a close approximation to radian measure, and for all angles from 0 to  $2\pi$  it is a smooth continuous measure of the absolute value, without difficulties of sign or definition. We measure a difference in orbital plane by the angle  $I_{AB}$  between the orbital planes.  $I_{AB}$  comprises two elements and their scale factors; this appears explicitly in the identity

$$\left(2 \sin \frac{I_{AB}}{2}\right)^2 = \left(2 \sin \frac{i_B - i_A}{2}\right)^2 + \sin i_A \sin i_B \left(2 \sin \frac{\delta\omega_B - \delta\omega_A}{2}\right)^2. \quad (2)$$

Three elements describe an orbit within the orbital plane. We measure a difference of shape by the difference in eccentricity  $e$ , and of size by the difference in perihelion distance  $q$ . In contrast to the major semi-axis  $a$ ,  $q$  is well determined by observation and has a small range of values. A difference in orientation of the orbit within the plane is measured by the angle  $\Pi_{AB}$  between the major axes, weighted by the scale factor  $e$ . Thus  $\Pi_{AB}$  is the difference between the longitudes of perihelion. When the orbits are in different planes,  $\Pi_{AB}$  is the difference between the longitudes of perihelion measured from the intersection of the orbits. In terms of familiar elements,

$$\Pi_{AB} = \omega_B - \omega_A + 2 \arcsin \left[ \cos \frac{i_A + i_B}{2} \sin \frac{\delta\omega_B - \delta\omega_A}{2} \sec \frac{I_{AB}}{2} \right], \quad (3a)$$

or, to a sufficient approximation when  $i_A$  and  $i_B$  are small,

$$\Pi_{AB} = (\delta\omega_B + \omega_B) - (\delta\omega_A + \omega_A). \quad (3b)$$

By combining equations (1), (2), and (3a), we find

$$\begin{aligned} [D(A, B)]^2 = & [e_B - e_A]^2 \\ & + [q_B - q_A]^2 + \left[ 2 \sin \frac{i_B - i_A}{2} \right]^2 \\ & + \sin i_A \sin i_B \left[ 2 \sin \frac{\delta\omega_B - \delta\omega_A}{2} \right]^2 \\ & + \left[ \left( \frac{e_A + e_B}{2} \right) 2 \sin \frac{(\delta\omega_B + \omega_B) - (\delta\omega_A + \omega_A)}{2} \right]^2 \end{aligned} \quad (4)$$

at low inclination, or, after substituting equation (3a) for (3b) in the last term, at any inclination. This expression is readily computed with a desk calculator and a special table of chords.

#### A model of stream dispersion

The scale factors  $c_i$  of the various elements in  $D$ , as shown in equation (4), were selected on a variety of grounds of simplicity, reasonability, and previous experience. By qualitative arguments we expected that, after scaling, the elements would make roughly equal contributions to  $D$ . The utility of  $D$  is empirically established below on known streams; nevertheless, a theoretical basis for  $D$  is clearly desirable if it can be found. Although we made this theoretical study after  $D$  had already been applied to the meteors, the validity of  $D$  is confirmed in the main.

An excellent measure of the difference between orbits, if it can be found, is the amount of perturbation that will transform one of the orbits into the other. A perturbation of an orbit arises from an accelerating force applied for a period of time; hence the velocity change so arising is the natural measure of the perturbation. In general, no single perturbation can suffice because the two orbits will not intersect; we may expect that an appreciable difference between a pair of orbits that were once the same will normally be the result of many perturbations. Since  $D$  comprehends all orbital elements, it appears possible that  $D$  is indeed a measure of total perturbation; we

must determine, however, whether the different elements may be so combined.

We consider an idealized model for orbit change, postulating random vectorial increments  $\delta\mathbf{V}$  to the vectorial orbital velocity  $\mathbf{V}_H$  of a meteor. The natural unit of orbital speed at any particular distance  $r$  from the sun is the speed  $U$  of a body in a circular orbit of that radius;  $U$  varies as  $r^{-1/2}$ . We take  $\delta V$  to be proportional to  $U$  because, broadly speaking, we would expect most kinds of perturbation to be more intense nearer the sun. The test applied to  $D$  consisted in finding the sensitivities of the different elements to perturbations  $\delta\mathbf{V}$ ; these sensitivities should be comparable. To measure the sensitivities, we computed the time averages, denoted "Grad," of the magnitudes of the gradients of the various elements in  $D$  with respect to perturbations  $\delta\mathbf{V}$ . They are shown in figure 1, plotted as functions of eccentricity. The computation of these gradients is described in the appendix; they are approximate, except for Grad  $I_{AB}$  which is exact. The value of Grad  $\Pi_{AB}$  on the graph has already been multiplied by the scale factor  $e$ . To obtain Grad  $q$ , the value in the figure must be multiplied by  $a$ . Broken lines in the figure indicate the extreme values of Grad  $q$  possible for a meteor observed on earth.

Grad  $e$ ,  $e$  Grad  $\Pi_{AB}$ , and Grad  $I_{AB}$  are quite satisfactorily similar for values of  $e \leq 0.85$ . Grad  $q$  is a function of both  $a$  and  $e$ , but is comparable to the others for most observed values of  $a$  when  $e \leq 0.85$ . For eccentricities near unity the model implies that the different elements in  $D$  have very different sensitivities to perturbations of the kind postulated. At these high eccentricities, the time averages primarily reflect the conditions near aphelion; the effect of this is not clear. Possibly the apparent practical success of  $D$  for high eccentricity depends upon averaging overweighted elements with underweighted elements.

If this computation had been available earlier in the analysis, we could no doubt have modified the form of  $D$  at the cost of simplicity. Except when the eccentricity is nearly one, however, we may conclude that  $D$  in its present form is approximately proportional to the average velocity increment, in units of the circular speed, which will perturb one of the

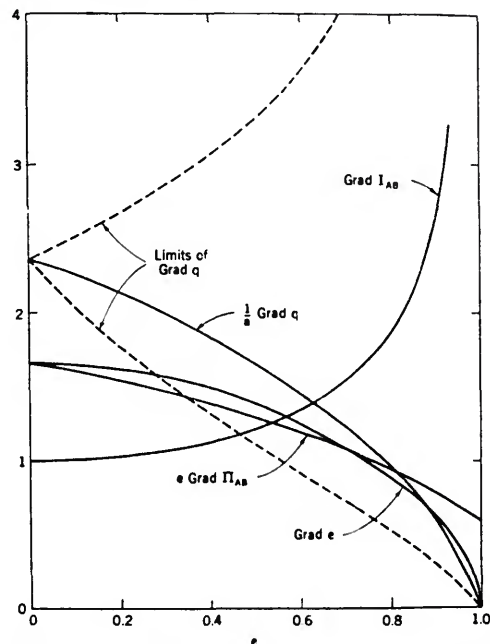


FIGURE 1.—Time average gradients of elements with respect to velocity perturbations which are proportional to the circular speed.

orbits into the other. Estimating the factor of proportionality from figure 1, we find that  $D$  is about  $3/2$  of the mean velocity increment.

#### Application to known streams

We applied  $D$  first to the known streams that were sufficiently represented in the sample, using both forms of the stream criterion discussed above. A list of the members of each stream had already been prepared by use of conventional criteria. The difference  $D(M, N)$  between the mean orbit  $M$  of the stream and the orbit of each member  $N$  was found, as were the differences  $D(A, B)$  between pairs of meteors in each stream. The values of  $D(A, B)$  were examined to find the minimum value  $D_{S \text{ min}}$  of  $D_S$  such that all the members were associated. Table 1 summarizes the values of  $D(M, N)$  and also includes  $D_{S \text{ min}}$ . There is obviously a close correlation between  $D_{S \text{ min}}$  and the mean value of  $D(M, N)$ .

Both  $D_{S \text{ min}}$  and the mean value of  $D(M, N)$  are also correlated with the average spread of a stream radiant, as found by Wright, Jacchia, and Whipple (see Whipple, 1947; Wright and

TABLE 1.—Distribution of values of  $D(M,N)$  for previously identified members of known streams, and values of  $D_{S \text{ min}}$  and  $O-C$

Streams	Range of $D(M,N)$								Total	Mean	$D_{S \text{ min}}$	$O-C$
	.00 to .04	.05 to .08	.09 to .12	.13 to .16	.17 to .20	.21 to .24	.25 to .28	.29 to .32				
Quadrantids	3	2							5	0.04	0.05	
Orionids	4	3	3	1	1				12	.08	.15	0.38
Perseids*	1	3	1	3	1				9	*.11	*.12	.68
Geminids	14	2							16	.02	.04	.22
S. $\iota$ Aquarids†			2						2	.10	.20	1.8
S. $\delta$ Aquarids	2	1							3	.03	.07	.80
N. $\delta$ Aquarids		1	1	1					3	.10	.15	1.2
$\alpha$ Capricornid		2							2	.08	.16	2.1
S. Taurid-Arietid		1	2	2	1	1	2	1	10	.18	.19	.83
N. Taurids		1	2	3		1			7	.13	.19	1.02
Andromedids		2							2	.08	.16	
Total	24	18	11	10	3	2	2	1	71	.09		

\*Incomplete observations; shower peak missed.

†One meteor, characterized as a "very doubtful member" by Wright, Jacchia, and Whipple (1957), has been omitted.

Whipple, 1948, 1950, 1953; Wright, Jacchia, and Whipple, 1954, 1956, 1957). Their value of the average deviation  $|O-C|$  of an extended trail from the least-squares moving radiant appears in table 1 for nine streams. They have not determined a value of  $|O-C|$  for Quadrantids or Andromedids. Figure 2 shows the correlations with  $D_{S \text{ min}}$  and the average  $D(M,N)$ . There is a well-known correlation

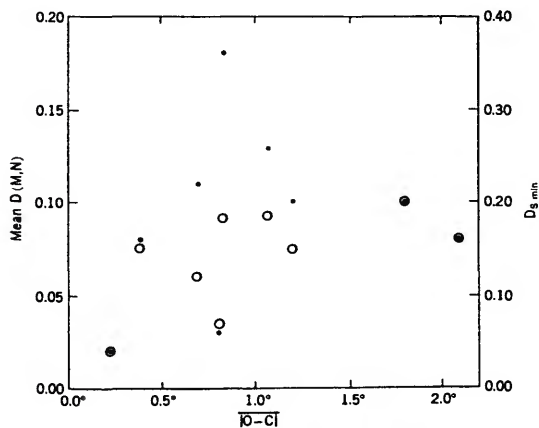


FIGURE 2.—Correlations of mean  $D(M,N)$  (solid dots) and of  $D_{S \text{ min}}$  (open circles) with Wright, Jacchia, and Whipple's average radiant deviations  $|O-C|$ , for nine streams.

between radiant spread and shower duration (Wright, Jacchia, and Whipple, 1957), and a correlation of either  $D_{S \text{ min}}$  or mean  $D(M,N)$  with shower duration is easily shown. Thus all these measures of meteor orbit difference within a stream are intercorrelated.

It will be seen in table 1 that  $D(M,N)$  exceeds 0.20 for only four meteors, one Northern Taurid and three Southern Taurid-Arietids. Thus we may use the condition  $D(M,N) \leq D_M$ , where  $D_M=0.20$ , as an empirical test for membership in these known streams. Similarly, no value of  $D_{S \text{ min}}$  exceeds 0.20, and we may use  $D_S=0.20$  as an empirical test. For all but four streams in table 1, either test gives the same results as conventional criteria, including all meteors previously selected as members and excluding all others. The Southern  $\iota$ -Aquadrid stream has presented difficulties to conventional classification (Wright, Jacchia, and Whipple, 1957); the  $D_S$  test includes two additional meteors, one of which had been considered a member but was subsequently rejected.

The Andromedid stream has recently been shown to be much more extensive than was believed when the members were identified for table 1 (Hawkins, Southworth, and Stienon, 1959) and both tests add several additional

members. The  $D_s$  test adds one new Northern Taurid and one new Southern Taurid-Arietid, and excludes no previous members. The  $D_M$  test includes these two additional meteors and excludes one Northern Taurid and three Southern Taurid-Arietids. Almost all of the additional and rejected meteors are close to the dividing lines of the tests.

We conclude that  $D$  provides valid tests for membership in a stream known to exist. The essential value of these tests is that they have the same formulation for every stream and do not depend on prior study of it. Thus they may be used to look for new streams.

The numerical values  $D_M = D_s = 0.20$ , which were empirically determined from this sample of meteors, will require re-evaluation if applied to a different sample, particularly to a much larger sample. Certainly  $D_s$  should be decreased in a larger sample. If, as above, we use a four-dimensional point distribution as a model of the distribution of meteor orbits,  $D_s$  should vary inversely as the fourth root of the sample size in random samples.

#### Search for new streams

We next applied the  $D_s$  test to our entire sample by computing every value of  $D(A, B) \leq 0.20$  for any pair of meteors in the sample, as follows. There already existed a card for each meteor, on which its orbital elements had been written. These cards were sorted and then compared in pairs.  $D(A, B)$  was computed for every pair unless it could be seen by inspection that  $D$  exceeded 0.20. Because members of some known streams had already been treated they were not included in this process, but special pains were taken to see that any association existing between these stream members and other meteors was not overlooked.

The  $D_s$  test found 25 groups of meteors, which we may therefore consider as possible streams.

As will be discussed below, we define the "major" streams as those whose mean photographic rates exceed three per hour. Table 2 includes all others, termed "minor" streams, including the 25 newly-found possible streams. For the minor streams previously known it includes all members as defined by the  $D_s$  test. Three known streams, each having one member

in our sample, are included for completeness; they are not considered further in this study.

One of the 25 possible streams has been called the "Cyclids" because of its nearly circular orbit. (This stream includes two meteors that were assigned the earth's orbit because their observed velocity falls short of the velocity of escape.) Each of the other streams is identified for convenience by a name formed in the traditional manner from a star near the radiant. Mean values of the orbital elements, the corrected radiant (equinox 1950.0), and the extra-atmospheric velocity are tabulated for each stream. Several of the streams near the ecliptic have members whose node differs by  $180^\circ$  from the rest. To form mean elements of streams, we have added  $180^\circ$  to the node of such meteors, and interpreted them as having negative inclinations. Individual values of the same quantities as for the streams, of the date of occurrence, and of  $D(M, N)$  are tabulated for each member. One readily sees that the  $D_M$  test (i.e.,  $D \leq 0.20$ ) is also fulfilled for the great majority of the meteors in table 2.

Several of the possible streams in table 2 are discussed below, after a general discussion of the statistical significance of these streams.

#### Probability of chance association

To evaluate the importance of the "possible" streams listed in table 2, we clearly must know the probability that such groups would occur by chance. It is not proper to compare the observed groups with the groups that would be found in a random sample of orbits because, quite apart from any grouping, the observed distribution is far from random. Furthermore, we know the distribution of meteor orbits very imperfectly, with or without selection effects. In order to estimate the degree of chance grouping, therefore, we have taken the observed distribution and smoothed out its grouping as far as possible, and then looked for chance groups.

Each meteor is described by the elements  $q$ ,  $e$ ,  $\omega$ ,  $i$ , and  $\Omega$ . The smoothing process consisted in removing the values of  $\Omega$  from all the meteors not originally classified in known streams, mixing them up, and reassigning them at random; and in doing the same with

the values of  $i$ . This substantially effaces the grouping. To offset any residual grouping, this process also eliminated the weak correlations between  $\Omega$  or  $i$  and other elements. Any further randomizing is hardly feasible since there is an almost exact relation among  $q$ ,  $e$ , and  $\omega$ . The resulting artificial orbits in the range  $0^\circ \leq \Omega \leq 100^\circ$  were then treated in the same way as the observed orbits. In this way, although the sample size was reduced, we would expect the same percentage of "stream" meteors if table 2 were a result of chance. Table 3 shows the groups found.

The artificial sample may be compared with the observed meteors not originally classified in known streams, as follows:

	Observed sample	Artificial sample
Meteors	290	103
New groups found	24	8
Known streams enlarged	4	
Meteors classified into groups:		
Number	119	22
Percent of sample	41	21

Since the random sample has produced 21 percent of "stream meteors," we conclude that approximately one half of the groups found by the  $D_s$  test are chance associations. Approximately 14 groups or 62 meteors in table 2 then are included by chance; the remaining streams and meteors are genuinely associated.

We do not know which groups in table 2 are spurious, but it is possible to develop criteria for the probability that a group is a genuine meteor stream.

It is clear that the chance associations in table 2 are principally the result of the non-random overall distribution of orbits. The chance associations occur almost entirely in the regions of the phase space most densely populated with orbits. We have stated earlier that the value of  $D_s$  should be adjusted to the total number in a sample. A more refined test should take account of crowding in part of a sample, but the present data are insufficient to warrant refinements. One result of the non-random distribution is obvious; the "Cyclid" stream, in all probability, does not exist as a physical entity but only represents the peak of the distribution of probability of meeting the earth. Another result of crowding will be

the association into larger groups of streams which are genuinely distinct. The " $\sigma$  Leonids" are certainly composite; possibly an improved test can separate this group into independent parts.

#### Hourly rates of streams; major and minor streams

For each stream, we have computed the average number of photographic meteors per hour that are members of that stream, as follows. The number of meteors photographed is taken as ten times the number in the sample, because the sample originally consisted of every tenth meteor photographed (Hawkins and Southworth, 1958). If there were two meteors from one stream on a single plate because additional meteors on the same plates as "tenth" meteors had been reduced, the additional meteor was not counted for this purpose. We define the period of visibility of each stream by the earliest and latest observed dates in the sample, and by the rising and setting of the mean radiant. The total number of hours of double-station observing time within these limits, and within the overall limits of the sample (26 February, 1952, to 3 July, 1954) was found from the records. The hourly rate is then the number of meteors photographed divided by the number of hours observed. Table 4 lists these hourly rates, and also the average  $D(M, N)$  within each stream. A meaningful hourly rate for the "Cyclid" stream cannot be computed. The other columns of table 4 are discussed further on. Figure 3 is a plot of mean hourly rate versus mean  $D(M, N)$ .

Three streams—the Geminids, Orionids, and Quadrantids—are well separated from all others in figure 3 by their high hourly rate. Their internal dispersions are smaller than those of almost all the other streams. We shall call these the major streams, and treat them as a class apart.

The position of the Perseids in figure 3 is anomalous in view of the known importance of this shower. On closer examination, we find that the shower maximum in fact is hardly represented in our sample, observations having been prevented in 1952 by moonlight and almost entirely prevented in 1953 by clouds.

TABLE 2.—*Minor streams*

(Asterisk represents newly found members of known streams)

Stream	Greenwich date	$\alpha$ (a.u.)	$e$	$i$ (deg)	$\delta$ (deg)	$\pi$ (deg)	Corr. R.A. (deg)	Rad. dec. (deg)	$V_{\infty}$ (km/ sec)	$D(M,N)$
KNOWN STREAMS										
South ♄ Aquarids	52 June 29.43208	1.50	0.852	7.4	97.6	51.8	299.3	-16.1	32.1	0.38
	53 July 21.35918	1.37	0.921	2.9	298.2	87.9	328.7	-13.9	35.9	0.24
	*53 Aug 6.17192	1.71	0.827	1.9	313.4	77.8	331.9	-13.1	30.9	0.11
	53 Aug 8.19278	3.32	0.927	7.5	315.3	80.8	335.1	-15.1	36.1	0.16
	<i>Mean values</i>	<i>1.98</i>	<i>0.882</i>	<i>1.2</i>	<i>301.1</i>	<i>74.6</i>	<i>323.8</i>	<i>-14.6</i>	<i>33.8</i>	<i>0.22</i>
South ♁ Aquarids	52 July 25.44425	2.85	0.978	27.3	302.4	96.2	335.9	-17.1	43.0	0.05
	52 July 28.31172	2.36	0.973	30.0	305.1	99.3	339.6	-16.5	43.7	0.03
	52 July 29.40913	2.40	0.970	29.4	306.2	98.8	340.2	-16.6	42.2	0.02
	<i>Mean values</i>	<i>2.54</i>	<i>0.974</i>	<i>28.9</i>	<i>304.6</i>	<i>98.1</i>	<i>338.6</i>	<i>-16.7</i>	<i>42.6</i>	<i>0.03</i>
North ♁ Aquarids	52 Aug 25.35970	2.38	0.947	17.0	152.0	114.9	354.3	+4.7	39.0	0.15
	53 Aug 10.43442	2.41	0.960	22.5	137.4	105.2	342.8	+0.5	40.5	0.06
	53 Aug 13.19186	2.50	0.949	24.1	140.1	102.8	343.0	+2.5	40.0	0.09
	<i>Mean values</i>	<i>2.43</i>	<i>0.952</i>	<i>21.2</i>	<i>143.2</i>	<i>107.6</i>	<i>346.7</i>	<i>+2.6</i>	<i>39.8</i>	<i>0.10</i>
♈ Capri- cornids	52 Aug 22.20417	3.19	0.793	8.3	149.0	46.6	321.2	-2.2	24.3	0.08
	53 Aug 8.36042	2.65	0.753	7.7	135.4	35.5	309.8	-6.3	23.5	0.08
	<i>Mean values</i>	<i>2.92</i>	<i>0.773</i>	<i>8.0</i>	<i>142.2</i>	<i>41.0</i>	<i>315.6</i>	<i>-4.2</i>	<i>23.9</i>	<i>0.08</i>
S. Taurid- Arietids	52 Sept 17.31692	2.47	0.894	4.5	354.3	118.7	10.6	+1.4	33.8	0.28
	52 Sept 19.37056	1.17	0.736	6.1	356.3	125.7	16.8	+1.2	26.5	0.17
	52 Sept 20.28367	1.37	0.741	3.0	357.2	118.4	12.5	+2.2	29.9	0.26
	52 Sept 25.36076	1.52	0.846	7.9	2.2	134.5	22.8	+4.0	31.8	0.10
	52 Oct 13.28086	1.85	0.840	5.9	19.8	142.6	34.8	+9.2	31.4	0.10
	52 Oct 14.35000	1.47	0.844	6.2	20.9	154.1	40.6	+11.5	31.8	0.27
	52 Oct 19.26487	1.95	0.806	4.3	25.8	138.6	36.0	+10.1	29.2	0.08
	52 Oct 22.47095	2.76	0.829	5.3	29.0	128.1	33.6	+7.4	27.9	0.12
	52 Oct 27.35625	1.79	0.869	9.9	33.8	163.8	52.5	+12.5	33.3	0.42
	*53 Oct 9.24410	1.73	0.791	5.4	195.6	131.9	24.7	+15.6	28.8	0.20
	53 Oct 9.24725	1.45	0.813	7.5	15.6	144.1	34.1	+7.7	30.4	0.12
	<i>Mean values</i>	<i>1.78</i>	<i>0.819</i>	<i>5.0</i>	<i>13.7</i>	<i>136.4</i>	<i>29.0</i>	<i>+7.5</i>	<i>30.4</i>	<i>0.19</i>
	North ♉ Taurids	52 Oct 16.33975	2.26	0.912	3.4	202.9	155.6	39.7	+17.4	35.7
52 Oct 19.38343		1.44	0.782	5.0	205.9	149.9	38.8	+19.6	28.6	0.12
52 Oct 27.35799		2.40	0.856	3.0	213.8	148.4	42.6	+18.9	31.1	0.13
52 Nov 12.19596		2.25	0.839	3.1	229.7	162.8	58.4	+23.0	30.7	0.10
52 Nov 12.37045		2.35	0.836	2.3	229.9	159.7	57.1	+22.1	29.8	0.10
52 Nov 12.37333		1.98	0.855	5.3	229.9	172.5	53.0	+25.1	32.0	0.23
*53 Oct 10.21343		2.18	0.929	4.7	196.6	155.5	36.0	+16.6	37.4	0.17
53 Nov 3.29681		1.97	0.800	3.6	220.5	151.4	47.6	+21.3	28.8	0.13
<i>Mean values</i>		<i>2.10</i>	<i>0.851</i>	<i>3.8</i>	<i>216.1</i>	<i>157.0</i>	<i>47.9</i>	<i>+20.5</i>	<i>31.9</i>	<i>0.14</i>

TABLE 2.—*Minor streams*—Continued

Stream	Greenwich date	<i>a</i> (a.u.)	<i>e</i>	<i>i</i> (deg)	$\Omega$ (deg)	$\pi$ (deg)	Corr. R.A. (deg)	Rad. dec. (deg)	$V_{\infty}$ (km/ sec)	$D(M,N)$
KNOWN STREAMS—Continued										
Androme- dids (Bieliids)	*52 Sept 20.28438	2.80	0.764	0.8	357.2	75.0	351.8	-4.9	23.0	0.33
	*52 Sept 25.36001	2.80	0.775	4.7	182.2	83.6	355.2	+5.5	23.8	0.25
	*52 Oct 9.19792	2.50	0.773	2.1	195.8	105.2	13.3	+8.7	25.2	0.16
	*52 Oct 13.27778	2.38	0.787	8.1	199.8	116.6	18.5	+18.1	26.8	0.32
	*52 Oct 21.32940	1.75	0.558	8.0	27.8	95.4	22.6	-10.4	18.1	0.22
	*52 Oct 24.35000	2.48	0.707	4.1	30.8	100.4	21.4	+0.6	20.7	0.07
	52 Nov 7.10870	2.59	0.708	8.4	224.6	108.9	22.9	+27.6	20.9	0.20
	*52 Dec 9.26872	2.68	0.666	3.5	77.1	116.8	44.8	+6.0	16.5	0.29
	*53 Oct 2.31090	2.54	0.773	3.7	188.8	97.0	5.4	+7.7	24.8	0.16
	*53 Oct 6.28447	1.81	0.703	3.6	12.7	109.6	16.9	+2.0	24.1	0.20
	*53 Oct 7.39307	1.92	0.649	1.9	13.8	93.9	9.3	+0.3	20.6	0.07
	*53 Oct 10.31215	2.39	0.700	7.5	16.6	88.3	12.3	-9.6	21.2	0.16
	53 Nov 7.46139	2.29	0.679	0.0	224.7	113.5	31.1	+12.7	19.8	0.17
	*53 Nov 13.24583	2.02	0.577	3.8	50.5	102.0	29.5	+0.6	16.6	0.25
<i>Mean values</i>	<i>2.85</i>	<i>0.701</i>	<i>0.4</i>	<i>25.9</i>	<i>100.4</i>	<i>18.6</i>	<i>+4.6</i>	<i>21.6</i>	<i>0.20</i>	
KNOWN STREAMS HAVING ONE MEMBER IN OUR SAMPLE										
North Aquarids	52 July 27.22705	3.48	0.947	15.0	124.1	76.9	323.8	-6.8	38.5	—
Draconids (Giacobi- nids)	53 Oct 9.19222	3.37	0.704	24.6	195.5	12.5	270.9	+47.2	20.2	—
Monoce- rotids	53 Dec 10.51604	20.16	0.992	39.8	78.1	209.4	101.6	+7.7	43.9	—
NEWLY FOUND POSSIBLE STREAMS										
$\chi$ Geminids	53 Jan 13.29493	2.01	0.739	1.0	292.8	208.3	118.4	+22.1	25.6	0.11
	53 Jan 13.45089	2.58	0.779	17.2	292.9	200.6	123.0	+41.8	27.0	0.19
	53 Jan 13.45411	2.52	0.798	11.3	292.9	208.1	122.4	+33.2	27.6	0.13
	53 Jan 23.38956	2.41	0.725	4.2	123.1	200.0	117.9	+14.0	22.7	0.20
	<i>Mean values</i>	<i>2.88</i>	<i>0.760</i>	<i>6.3</i>	<i>295.4</i>	<i>204.2</i>	<i>120.4</i>	<i>+27.8</i>	<i>25.7</i>	<i>0.16</i>
$\rho$ Geminids	53 Jan 15.40959	2.41	0.716	7.4	294.9	189.0	111.6	+34.6	22.3	0.11
	53 Jan 19.19278	2.55	0.694	4.4	298.8	179.5	105.5	+31.9	20.1	0.06
	53 Jan 21.37852	2.81	0.723	1.1	301.0	180.6	105.9	+24.9	20.0	0.08
	54 Jan 28.17159	3.34	0.762	7.9	307.6	184.1	114.6	+37.8	21.0	0.07
	<i>Mean values</i>	<i>2.78</i>	<i>0.724</i>	<i>5.2</i>	<i>300.6</i>	<i>183.3</i>	<i>109.4</i>	<i>+32.3</i>	<i>20.8</i>	<i>0.08</i>

TABLE 2.—Minor streams—Continued

Stream	Greenwich date	$a$ (a. u.)	$e$	$i$ (deg)	$\Omega$ (deg)	$\pi$ (deg)	Corr. R. A. (deg)	Rad. dec. (deg)	$V_{\infty}$ (km/ sec)	$D(M,N)$
NEWLY FOUND POSSIBLE STREAMS—Continued										
$\sigma$ Leonids	52 Feb 26.40208	1.65	0.621	8.9	336.7	244.6	164.6	+21.8	22.1	0.17
	52 Apr 26.28750	1.98	0.592	4.6	216.0	278.2	195.3	-17.6	18.5	0.35
	52 May 22.28093	2.04	0.581	2.2	61.1	295.9	219.6	-9.7	17.3	0.51
	53 Feb 5.14883	2.71	0.858	0.8	136.0	244.8	147.2	+12.4	31.7	0.39
	53 Feb 17.20441	2.49	0.758	2.4	148.2	232.5	147.0	+9.7	25.0	0.28
	53 Feb 17.20626	1.89	0.720	14.5	328.2	244.6	162.9	+26.2	26.6	0.30
	53 Feb 18.35000	1.95	0.701	4.8	329.4	239.3	154.6	+17.7	24.1	0.20
	53 Mar 12.17613	1.53	0.456	9.6	171.3	232.3	150.4	-15.2	17.1	0.37
	53 Mar 12.27841	2.53	0.671	0.5	351.4	225.2	153.2	+12.2	18.7	0.32
	53 Mar 13.29792	1.55	0.414	5.6	172.4	217.9	143.0	-6.6	14.6	0.47
	53 Mar 14.34103	1.68	0.596	4.4	173.4	255.1	167.6	-3.1	20.6	0.15
	53 Mar 18.33892	1.35	0.492	2.3	177.4	264.3	174.7	-2.8	18.6	0.24
	53 Mar 19.31853	2.91	0.731	11.5	358.4	238.8	174.8	+26.3	21.6	0.24
	53 Mar 19.39518	8.49	0.913	9.5	358.4	241.5	172.2	+20.0	24.7	0.30
	53 Mar 20.42303	2.14	0.625	7.5	179.5	239.8	159.8	-9.0	19.0	0.23
	53 Mar 21.40331	2.71	0.710	4.3	0.4	240.8	169.6	+14.2	20.2	0.15
	53 Apr 9.29081	2.77	0.688	8.9	19.1	247.6	184.8	+20.9	19.0	0.20
	53 Apr 11.22535	2.58	0.682	4.9	21.0	257.4	186.3	+9.0	19.6	0.14
	53 Apr 11.34984	2.30	0.694	4.2	21.1	275.4	194.9	+1.4	21.9	0.29
	53 Apr 14.28612	2.01	0.605	2.6	24.0	267.3	191.0	+1.4	18.8	0.21
	53 Apr 15.24583	2.92	0.708	2.4	204.9	255.3	178.9	-5.7	18.8	0.17
	53 May 6.28495	2.15	0.671	0.5	225.4	300.6	214.7	-14.8	21.4	0.56
	53 May 7.22324	2.37	0.674	1.0	46.3	291.7	211.0	-10.6	20.4	0.47
	54 Feb 6.38914	2.63	0.810	16.6	317.0	233.0	152.0	+30.5	29.0	0.43
	54 Feb 6.42292	2.45	0.807	2.6	317.0	236.4	145.4	+16.8	28.1	0.34
	54 Feb 26.30579	1.91	0.660	4.6	157.1	239.5	153.2	+3.2	22.3	0.19
54 Mar 1.36968	2.01	0.639	7.3	340.2	231.9	159.3	+23.5	20.7	0.24	
<i>Mean values</i>	<i>2.43</i>	<i>0.670</i>	<i>2.2</i>	<i>359.0</i>	<i>250.8</i>	<i>171.4</i>	<i>6.4</i>	<i>21.5</i>	<i>0.29</i>	
$\xi$ Orionids	53 Mar 14.16204	1.94	0.488	4.2	173.2	169.1	80.6	+0.2	12.9	0.09
	54 Feb 11.42659	1.80	0.479	3.4	322.1	173.9	106.4	+36.5	13.9	0.09
	54 Mar 5.29565	1.84	0.472	1.0	164.1	185.6	113.6	+12.6	13.2	0.08
	<i>Mean values</i>	<i>1.86</i>	<i>0.480</i>	<i>0.9</i>	<i>159.8</i>	<i>176.2</i>	<i>100.2</i>	<i>+16.4</i>	<i>13.3</i>	<i>0.09</i>
$\psi$ Ursa Majorids	53 Mar 18.33889	1.80	0.497	6.9	357.4	220.9	161.8	+31.8	15.6	0.08
	53 Apr 10.24583	1.63	0.398	12.0	20.0	222.5	185.4	+53.7	14.6	0.09
	<i>Mean values</i>	<i>1.72</i>	<i>0.448</i>	<i>9.4</i>	<i>8.7</i>	<i>221.7</i>	<i>173.6</i>	<i>+42.8</i>	<i>15.1</i>	<i>0.08</i>
$\alpha$ Bootids	53 Apr 9.35927	1.90	0.599	21.0	19.2	268.3	209.8	+27.6	22.4	0.10
	53 Apr 16.28881	2.13	0.674	16.0	26.0	282.3	210.4	+14.8	23.4	0.10
	<i>Mean values</i>	<i>2.02</i>	<i>0.636</i>	<i>18.5</i>	<i>22.6</i>	<i>275.3</i>	<i>210.1</i>	<i>+21.2</i>	<i>22.9</i>	<i>0.10</i>
$\gamma$ Bootids	53 Apr 13.25625	3.76	0.786	26.6	23.0	259.5	213.0	+33.4	25.9	0.08
	53 Apr 21.36280	3.34	0.733	29.1	30.9	253.3	222.3	+42.7	24.5	0.08
	<i>Mean values</i>	<i>3.55</i>	<i>0.760</i>	<i>27.8</i>	<i>27.0</i>	<i>256.4</i>	<i>217.6</i>	<i>+38.0</i>	<i>25.2</i>	<i>0.08</i>
$\xi$ Librids	53 Apr 13.25916	1.71	0.914	2.8	23.0	344.9	224.4	-15.6	37.0	0.09
	53 May 5.28417	2.95	0.925	3.2	224.4	353.3	239.1	-22.2	36.8	0.09
	<i>Mean values</i>	<i>2.33</i>	<i>0.920</i>	<i>0.2</i>	<i>213.7</i>	<i>349.0</i>	<i>231.8</i>	<i>-18.9</i>	<i>36.9</i>	<i>0.09</i>

TABLE 2.—Minor streams—Continued

Stream	Greenwich date	$a$ (a.u.)	$e$	$i$ (deg)	$\Omega$ (deg)	$\pi$ (deg)	Corr. R.A. (deg)	Rad. dec. (deg)	$V_{\infty}$ (km/ sec)	$D(M,N)$
NEWLY FOUND POSSIBLE STREAMS—Continued										
$\mu$ Draconids	53 Apr 16.42532	4.32	0.770	43.6	26.1	218.3	256.6	+59.8	29.6	0.09
	53 Apr 21.36042	15.72	0.936	47.1	30.9	217.9	263.4	+61.0	32.4	0.09
	<i>Mean values</i>	<i>10.02</i>	<i>0.853</i>	<i>45.4</i>	<i>28.5</i>	<i>218.1</i>	<i>260.0</i>	<i>+60.4</i>	<i>31.0</i>	<i>0.09</i>
$\phi$ Bootids	53 May 7.33958	1.50	0.379	19.9	46.4	270.3	231.6	+40.4	17.6	0.06
	53 May 8.38998	1.39	0.321	17.9	47.4	270.1	231.8	+41.5	16.2	0.08
	54 June 4.24583	1.70	0.417	22.7	73.0	275.0	245.0	+50.5	18.2	0.13
	<i>Mean values</i>	<i>1.53</i>	<i>0.372</i>	<i>20.2</i>	<i>55.6</i>	<i>271.8</i>	<i>236.1</i>	<i>+44.1</i>	<i>17.3</i>	<i>0.09</i>
$\xi$ Cepheids	53 May 9.42072	1.00	0.157	16.4	48.4	127.4	341.8	+63.9	14.7	0.10
	54 Apr 28.30873	1.15	0.172	22.1	37.4	164.7	313.8	+68.3	16.6	0.10
	<i>Mean values</i>	<i>1.08</i>	<i>0.164</i>	<i>19.2</i>	<i>42.9</i>	<i>146.0</i>	<i>327.8</i>	<i>+66.1</i>	<i>15.6</i>	<i>0.10</i>
$\omega$ Ursa Majorids	53 May 13.16348	2.04	0.512	2.8	52.0	248.3	178.0	+15.1	13.6	0.16
	53 June 5.17987	2.48	0.596	9.4	74.2	240.5	161.0	+49.0	14.8	0.03
	53 June 6.19792	3.55	0.725	13.3	75.1	230.6	143.5	+57.9	17.2	0.18
	<i>Mean values</i>	<i>2.69</i>	<i>0.611</i>	<i>8.5</i>	<i>67.1</i>	<i>239.8</i>	<i>160.8</i>	<i>+40.7</i>	<i>15.1</i>	<i>0.12</i>
Cylids	52 May 19.21518	1.03	0.131	0.8	58.1	148.7	57.5	+27.2	11.5	0.06
	52 Oct 19.44228	0.95	0.120	2.7	26.0	144.7	50.2	-7.4	11.4	0.10
	53 Apr 11.14238	1.00	0.017	0.0	—	101.2	—	—	10.6	0.10
	53 Apr 15.24742	1.00	0.017	0.0	—	101.2	—	—	11.0	0.10
	54 June 3.25929	1.08	0.148	6.2	72.1	179.9	76.9	+62.8	12.2	0.14
<i>Mean values</i>	<i>1.01</i>	<i>0.087</i>	<i>1.9</i>	<i>52.1</i>	<i>135.1</i>	<i>60.5</i>	<i>+27.5</i>	<i>11.3</i>	<i>0.10</i>	
$\theta$ Ophiucids	52 May 21.36274	2.62	0.915	4.5	240.2	9.4	256.3	-25.4	36.0	0.19
	53 June 4.20432	2.34	0.838	3.0	253.2	5.2	262.4	-25.9	30.8	0.03
	53 June 8.37832	3.42	0.893	3.1	257.2	8.2	266.3	-25.8	32.4	0.06
	53 June 16.30529	3.11	0.827	4.5	264.8	357.0	265.0	-28.6	27.4	0.19
	53 June 16.31098	2.86	0.837	4.9	264.8	5.7	269.7	-28.4	29.0	0.08
	<i>Mean values</i>	<i>2.87</i>	<i>0.862</i>	<i>4.0</i>	<i>256.0</i>	<i>5.1</i>	<i>264.0</i>	<i>-26.8</i>	<i>31.1</i>	<i>0.11</i>
$\mu$ Draconids	52 June 17.36898	2.83	0.641	26.7	86.1	269.4	238.4	+60.3	20.6	0.18
	53 June 8.28750	3.28	0.720	31.8	77.1	296.2	255.5	+37.9	25.0	0.24
	53 June 13.26806	3.70	0.736	31.3	81.9	286.4	253.1	+46.8	24.1	0.12
	54 June 9.37083	2.81	0.644	39.6	77.9	273.5	267.7	+56.6	26.7	0.13
	54 June 11.38442	3.27	0.697	33.6	79.8	280.1	255.9	+51.7	24.4	0.04
	54 June 23.21042	2.74	0.629	38.2	91.1	270.1	267.8	+66.9	25.9	0.18
<i>Mean values</i>	<i>3.10</i>	<i>0.678</i>	<i>33.5</i>	<i>82.3</i>	<i>279.3</i>	<i>256.4</i>	<i>+53.4</i>	<i>24.4</i>	<i>0.15</i>	
$\tau$ Herculids	53 June 20.35000	2.07	0.521	28.9	88.7	291.0	258.6	+50.4	21.2	0.10
	54 June 25.24461	2.81	0.642	21.3	93.1	286.2	237.8	+46.4	18.8	0.10
	<i>Mean Values</i>	<i>2.44</i>	<i>0.582</i>	<i>25.1</i>	<i>90.9</i>	<i>288.6</i>	<i>248.2</i>	<i>+48.4</i>	<i>20.0</i>	<i>0.10</i>
$\mu$ Ophiucids	53 Aug 6.16985	2.53	0.624	1.2	313.4	347.0	272.3	-27.4	15.5	0.12
	53 Aug 7.39845	2.06	0.515	7.7	134.5	330.7	254.0	+11.6	13.7	0.13
	53 Aug 10.22697	2.36	0.587	4.3	137.2	343.1	266.9	-6.6	14.5	0.10
	<i>Mean values</i>	<i>2.32</i>	<i>0.575</i>	<i>3.6</i>	<i>135.0</i>	<i>340.3</i>	<i>264.4</i>	<i>-7.5</i>	<i>14.6</i>	<i>0.10</i>

TABLE 2.—Minor streams—Continued

Stream	Greenwich date	$a$ (a.u.)	$e$	$i$ (deg)	$\Omega$ (deg)	$\pi$ (deg)	Corr. R.A. (deg)	Rad dec. (deg)	$V_{\infty}$ (km/ sec)	$D(M,N)$
NEWLY FOUND POSSIBLE STREAMS—Continued										
♁ Herculids	53 Aug 9. 23255	2. 59	0. 611	18. 6	136. 3	327. 5	257. 1	+38. 8	17. 4	0. 04
	53 Aug 13. 42525	2. 50	0. 617	17. 3	140. 3	352. 1	280. 1	+26. 6	17. 7	0. 13
	53 Aug 15. 42275	2. 06	0. 518	18. 7	142. 2	341. 2	270. 2	+38. 8	16. 9	0. 06
	<i>Mean values</i>	<i>2. 38</i>	<i>0. 582</i>	<i>18. 2</i>	<i>139. 6</i>	<i>340. 3</i>	<i>269. 1</i>	<i>+34. 7</i>	<i>17. 2</i>	<i>0. 08</i>
♋ Cetids	52 Sept 14. 37389	1. 93	0. 720	12. 0	351. 4	87. 4	2. 5	-15. 7	25. 0	0. 09
	52 Sept 20. 29047	1. 40	0. 592	15. 5	357. 2	96. 7	14. 0	-18. 8	22. 5	0. 09
	<i>Mean values</i>	<i>1. 66</i>	<i>0. 656</i>	<i>13. 8</i>	<i>354. 3</i>	<i>92. 0</i>	<i>8. 2</i>	<i>-17. 2</i>	<i>23. 3</i>	<i>0. 09</i>
♌ Capri- cornids	52 Sept 16. 33958	1. 57	0. 422	1. 0	173. 4	41. 6	327. 2	-9. 0	13. 9	0. 13
	52 Oct 9. 19742	1. 46	0. 314	8. 9	195. 8	17. 6	278. 6	+30. 2	12. 7	0. 10
	53 Aug 13. 35836	1. 37	0. 348	0. 9	320. 2	17. 1	302. 4	-23. 7	13. 6	0. 14
	<i>Mean values</i>	<i>1. 47</i>	<i>0. 361</i>	<i>3. 0</i>	<i>169. 8</i>	<i>25. 4</i>	<i>302. 7</i>	<i>-0. 8</i>	<i>13. 5</i>	<i>0. 12</i>
♍ Pegasids	52 Sept 19. 23462	2. 70	0. 713	0. 7	176. 2	59. 4	341. 4	-6. 3	20. 0	0. 20
	52 Sept 27. 30972	1. 79	0. 599	10. 9	184. 1	79. 8	349. 8	+18. 5	20. 0	0. 22
	52 Oct 16. 21458	2. 61	0. 670	2. 6	22. 8	71. 3	359. 5	-7. 7	17. 5	0. 13
	52 Nov 12. 19033	3. 41	0. 717	7. 6	229. 7	70. 1	342. 2	+22. 1	15. 6	0. 14
	52 Nov 12. 19349	2. 46	0. 605	6. 9	229. 7	68. 7	339. 8	+22. 4	14. 4	0. 12
	52 Nov 12. 26391	3. 42	0. 719	7. 4	229. 8	70. 6	343. 0	+21. 9	15. 5	0. 14
	53 Oct 3. 25367	1. 46	0. 432	11. 5	189. 7	74. 5	345. 0	+28. 5	16. 5	0. 24
	53 Oct 3. 29383	1. 73	0. 501	5. 4	189. 7	64. 0	343. 1	+10. 4	15. 7	0. 15
	53 Nov 6. 33041	3. 06	0. 704	7. 0	43. 6	81. 2	15. 8	-15. 5	16. 8	0. 25
<i>Mean values</i>	<i>2. 52</i>	<i>0. 629</i>	<i>4. 5</i>	<i>206. 1</i>	<i>71. 1</i>	<i>343. 8</i>	<i>+10. 5</i>	<i>16. 9</i>	<i>0. 18</i>	
♎ Draconids	52 Oct 12. 33141	5. 49	0. 818	72. 1	198. 9	18. 4	181. 9	+81. 4	43. 5	0. 10
	52 Oct 19. 44602	3. 14	0. 683	77. 4	206. 0	24. 3	167. 3	+76. 0	45. 0	0. 10
	<i>Mean values</i>	<i>4. 32</i>	<i>0. 750</i>	<i>74. 8</i>	<i>202. 4</i>	<i>21. 4</i>	<i>174. 6</i>	<i>+73. 7</i>	<i>44. 2</i>	<i>0. 10</i>
♏ Geminids	52 Oct 17. 40034	10. 37	0. 919	173. 8	203. 9	71. 4	102. 4	+26. 3	70. 6	0. 11
	52 Oct 22. 26372	26. 77	0. 971	173. 0	208. 8	85. 6	104. 2	+26. 5	70. 6	0. 14
	53 Oct 16. 42579	22. 87	0. 965	173. 3	202. 7	76. 3	98. 6	+26. 8	70. 5	0. 03
	<i>Mean values</i>	<i>20. 00</i>	<i>0. 952</i>	<i>173. 4</i>	<i>205. 1</i>	<i>77. 8</i>	<i>101. 7</i>	<i>+26. 5</i>	<i>70. 6</i>	<i>0. 09</i>
♐ Taurids	52 Dec 9. 26560	2. 60	0. 682	2. 1	257. 1	130. 3	51. 0	+24. 0	18. 3	0. 10
	53 Jan 15. 21244	3. 98	0. 763	0. 7	114. 7	140. 7	65. 3	+19. 3	16. 0	0. 10
	<i>Mean values</i>	<i>3. 29</i>	<i>0. 722</i>	<i>0. 7</i>	<i>275. 9</i>	<i>135. 5</i>	<i>58. 2</i>	<i>+21. 6</i>	<i>17. 2</i>	<i>0. 10</i>

TABLE 3.—*Spurious streams found in the artificial sample*

Stream	Greenwich Date	$a$ (a.u.)	$e$	$i$ (deg)	$\Omega$ (deg)	$\tau$ (deg)	Original Classification	$D(M,N)$
(A)	52 Mar 21. 36111	3. 23	0. 713	4. 3	43. 6	257. 2	Sporadic	0. 13
	52 Sept 25. 17361	1. 79	0. 510	11. 5	25. 1	256. 4	Sporadic	0. 14
	53 Aug 13. 42525	2. 50	0. 617	4. 8	46. 4	258. 2	$\vartheta$ Herculid	0. 06
	53 Aug 15. 42275	2. 06	0. 518	4. 6	47. 4	246. 4	Sporadic	0. 12
	<i>Mean values</i>	<i>2. 40</i>	<i>0. 590</i>	<i>6. 3</i>	<i>40. 6</i>	<i>254. 6</i>		
(B)	52 Apr 2. 38125	2. 80	0. 644	1. 9	21. 1	210. 4	Sporadic	0. 07
	53 May 13. 16348	2. 04	0. 512	4. 9	0. 6	196. 8	$\omega$ Ursa Majorid	0. 13
	54 June 25. 24461	2. 81	0. 642	1. 2	16. 6	209. 7	$\tau$ Herculid	0. 07
	<i>Mean values</i>	<i>2. 55</i>	<i>0. 599</i>	<i>2. 7</i>	<i>12. 8</i>	<i>205. 6</i>		
(C)	52 June 24. 20301	2. 79	0. 720	8. 6	39. 6	283. 2	Sporadic	0. 15
	52 Sept 16. 33958	1. 57	0. 422	4. 4	48. 4	276. 7	$\xi$ Capricornid	0. 20
	52 Sept 19. 23462	2. 70	0. 713	7. 6	30. 0	273. 2	$\alpha$ Pegasid	0. 14
	53 Oct 3. 29383	1. 73	0. 501	4. 2	46. 3	280. 5	$\alpha$ Pegasid	0. 12
	54 Mar 1. 36968	2. 01	0. 639	4. 8	25. 1	276. 8	$\sigma$ Leonid	0. 10
<i>Mean values</i>	<i>2. 16</i>	<i>0. 599</i>	<i>5. 9</i>	<i>37. 9</i>	<i>278. 1</i>			
(D)	52 Sept 16. 33723	3. 22	0. 937	8. 9	63. 1	13. 6	Sporadic	0. 07
	53 Apr 13. 25916	1. 71	0. 914	3. 9	46. 5	8. 4	$\zeta$ Librid	0. 07
	<i>Mean values</i>	<i>2. 96</i>	<i>0. 926</i>	<i>6. 4</i>	<i>54. 8</i>	<i>11. 0</i>		
(E)	52 Sept 25. 17579	15. 94	0. 947	7. 0	48. 4	275. 9	Sporadic	0. 08
	53 Nov 2. 35675	6. 87	0. 872	13. 3	51. 2	271. 7	Sporadic	0. 07
	<i>Mean values</i>	<i>11. 41</i>	<i>0. 910</i>	<i>10. 2</i>	<i>49. 8</i>	<i>273. 8</i>		
(F)	52 Aug 18. 25543	20. 92	0. 952	0. 2	24. 0	207. 4	Sporadic	0. 08
	53 Oct 9. 31647	19. 45	0. 949	9. 7	30. 9	207. 9	Sporadic	0. 08
	<i>Mean values</i>	<i>20. 18</i>	<i>0. 950</i>	<i>5. 0</i>	<i>27. 4</i>	<i>207. 6</i>		
(G)	53 Jan 13. 45411	2. 52	0. 798	1. 9	23. 2	298. 4	$\chi$ Geminid	0. 06
	54 Feb 6. 38914	2. 63	0. 810	2. 4	32. 1	308. 1	$\sigma$ Leonid	0. 07
	<i>Mean values</i>	<i>2. 58</i>	<i>0. 804</i>	<i>2. 2</i>	<i>27. 6</i>	<i>303. 2</i>		
(H)	53 Apr 7. 28372	1. 98	0. 809	4. 2	53. 0	346. 0	Sporadic	0. 09
	54 Feb 10. 40343	3. 69	0. 871	0. 9	77. 9	354. 2	Sporadic	0. 09
	<i>Mean values</i>	<i>2. 84</i>	<i>0. 840</i>	<i>2. 6</i>	<i>65. 4</i>	<i>350. 1</i>		

TABLE 4.—Further data on streams

Stream	Hourly rate	Number of members	Inclination	Mean $D(M,N)$	Radiant $\lambda - \lambda_{\odot}$ $\beta$	
MAJOR STREAMS						
Quadrantids	4.30	5	71°6	0.04	278°	64°
Orionids	3.69	12	164.9	.08	247	-7
Perseids*	*1.67	9	113.8	*.11	283	37
Geminids	5.92	16	23.3	.02	208	10
KNOWN MINOR STREAMS						
S. $\iota$ Aquarids	0.46	4	1°2	0.22	201°	-1°
S. $\delta$ Aquarids	1.80	3	28.9	.03	210	-7
N. $\delta$ Aquarids	0.37	3	21.2	.10	207	7
$\alpha$ Capricornids	0.29	2	8.0	.08	175	12
S. Taurid-Arietids	0.71	11	5.0	.19	197	-5
N. Taurids	0.54	8	3.8	.14	195	2
Andromedids	0.67	14	0.4	.20	172	-1
KNOWN MINOR STREAMS HAVING ONE MEMBER IN OUR SAMPLE						
N. Aquarids	—	1	15°0	—	202°	7°
Draconids	—	1	24.6	—	78	70
Monocerotids	—	1	39.8	—	205	-14
NEWLY FOUND POSSIBLE MINOR STREAMS						
$\chi$ Geminids	0.63	4	6°3	0.16	182°	8°
$\rho$ Geminids	0.89	4	5.2	.08	166	10
$\sigma$ Leonids	0.74	27	2.2	.29	171	2
$\xi$ Orionids	0.43	3	0.9	.09	119	-2
$\psi$ Ursae Majorids	0.20	2	9.4	.08	144	36
$\alpha$ Bootids	0.44	2	18°5	.10	176°	31°
$\gamma$ Bootids	0.67	2	27.8	.08	171	49
$\delta$ Librids	0.24	2	0.2	.09	201	0
$\nu$ Draconids	1.24	2	45.4	.09	204	82
$\varphi$ Bootids**	0.29	3	20.2	.09	159	60
$\xi$ Cepheids	0.32	2	19°2	.10	344°	68°
$\omega$ Ursae Majorids	0.38	3	8.5	.12	79	31
Cyclids	—	5	1.9	.10	—	—
$\theta$ Ophiucids	0.37	5	4.0	.11	189	-4
$\mu$ Draconids**	1.31	6	33.5	.15	148	74
$\tau$ Herculids	0.84	2	25°1	.10	140°	68°
$\mu$ Ophiucids	1.76	3	3.6	.12	128	15
$\varphi$ Herculids**	0.92	3	18.2	.08	129	58
$\beta$ Cetids	0.71	2	13.8	.09	186	-20
$\xi$ Capricornids	0.24	3	3.0	.12	134	18
$\alpha$ Pegasids	0.56	9	4°5	.18	148°	15°
$\lambda$ Draconids	0.57	2	74.8	.10	273	68
$\epsilon$ Geminids**	1.09	3	173.4	.09	256	3
$\eta$ Taurids	0.15	2	0.7	.10	145	2

TABLE 4.—Further data on streams—Continued

Stream	Hourly rate	Number of members	Inclination	Mean $D(M,N)$	Radiant $\lambda-\lambda_{\odot}$	$\beta$
SPURIOUS STREAMS						
(A)	—	4	6°3	0.11	136°	22°
(B)	—	3	2.7	.09	98	13
(C)	—	5	5.9	.14	161	14
(D)	—	2	6.4	.07	202	6
(E)	—	2	10.2	.08	152	22
(F)	—	2	5.0	.08	90	16
(G)	—	2	2.2	.06	183	2
(H)	—	2	2.6	.09	192	2

\*Incomplete observations; shower peak missed.  
 \*\*The most probable streams.

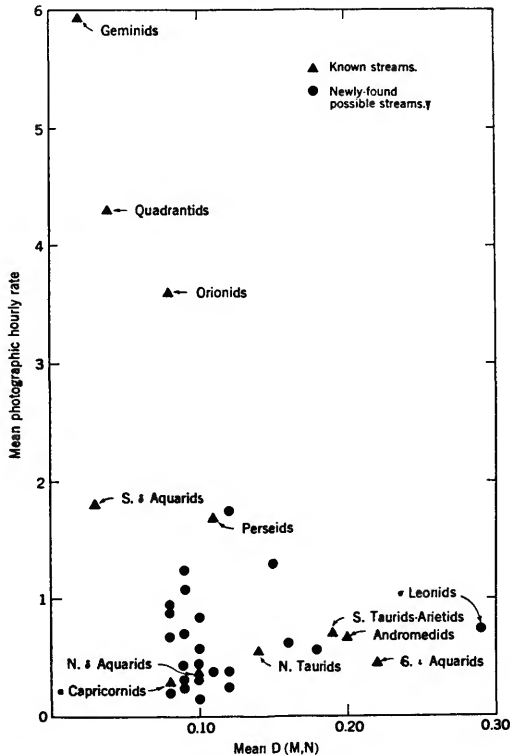


FIGURE 3.—Relation between hourly rate and internal dispersion of streams.

Thus neither our value of the rate nor of the mean dispersion within the stream is representative of the stream. Accordingly, no further use is made of values of  $D$  from the Perseid stream.

Streams with a photographic rate less than three per hour we shall call the minor streams. The Southern  $\delta$  Aquarids are the only minor stream in our sample with a mean  $D(M,N)$  less than 0.08. Because the duration of a shower is correlated with its mean  $D(M,N)$ , the total number of meteors in the sample is correlated with the product of ordinate and abscissa in figure 3; thus a stream in the lower left corner is comparatively unlikely to be detected. Nevertheless, the sharp boundary of the points at  $D=0.08$  seems meaningful as an approximate lower bound to the mean dispersion within the majority of minor streams.

On the right edge of figure 3, the " $\sigma$  Leonids" are doubtless a composite of two or more streams. The Southern Taurid-Arietid stream is known to be composite, as its name indicates. Either of these composite streams, if it could be divided into its originally independent parts, would be represented by two or more points nearer to the majority of streams in the diagram.

**Nature of the newly found minor streams**

Figure 4 shows histograms of the normalized distribution of values of  $D(M,N)$  in each of four classes of streams. The data for major streams and previously known minor streams are drawn from table 1, Perseids being omitted; for newly found minor streams from table 2; and for spurious streams from table 3. For each class of stream the ordinate is the percent

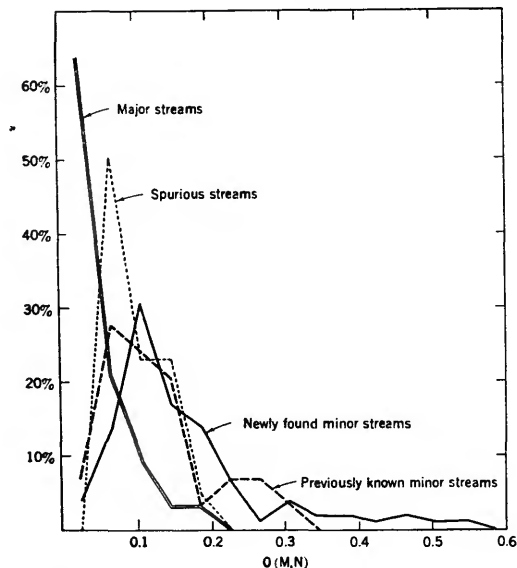


FIGURE 4.—Normalized distribution of  $D(M,N)$  in different classes of streams.

of values of  $D$  within an interval 0.04 unit wide.

All these curves indicate high central condensation in the streams.  $D$  may be interpreted as distance in a four-dimensional phase

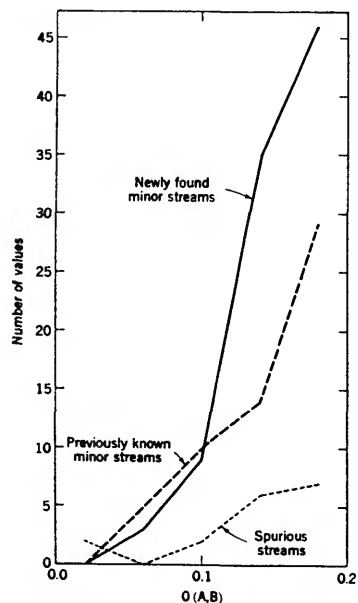


FIGURE 5.—Distribution of  $D(A,B)$  in different classes of streams.

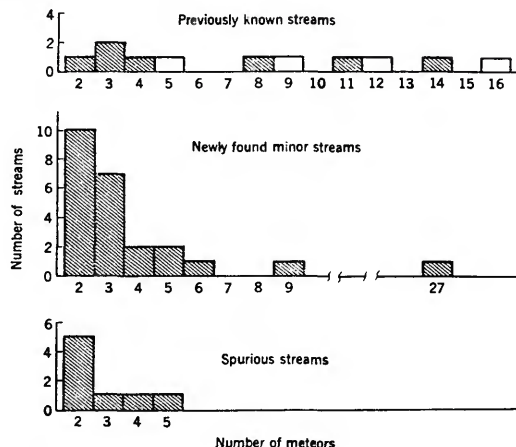


FIGURE 6.—Distribution of number of meteors in a stream. Major streams are unshaded.

space from the mean elements of the stream. A stream with members uniformly distributed through a volume in this phase space would have a histogram in which the ordinate varied as the cube of the abscissa. Thus, the histogram for newly found minor streams indicates, so far as the numbers are significant, that the density of points at  $D(M,N)=0.1$  has actually decreased from the density at lower values of  $D$ .

Figure 5 shows the distribution of values of  $D(A,B)$  within streams. It is clear in both figures 4 and 5 that the newly found streams are less compact than the previously known minor streams. Figure 6 shows the distribution of the number of meteors in a stream. The comparatively low values of  $D(M,N)$  for spurious streams occur because such a large proportion of the spurious streams have two members only. We may also conclude from figure 6 that it is the newly found minor streams with two or few members that are more likely to be chance groupings.

Figure 7 shows the distribution of the inclinations of the mean orbits of streams. From the concentration of all the spurious stream inclinations to low values we conclude that the newly found minor streams with low inclinations, like those with few members, are less likely to be genuine streams.

The distribution of radiant of meteors and streams in our sample is shown in figures 8 and 9, referred to a system of coordinates defined by the ecliptic plane and the direction to the sun.

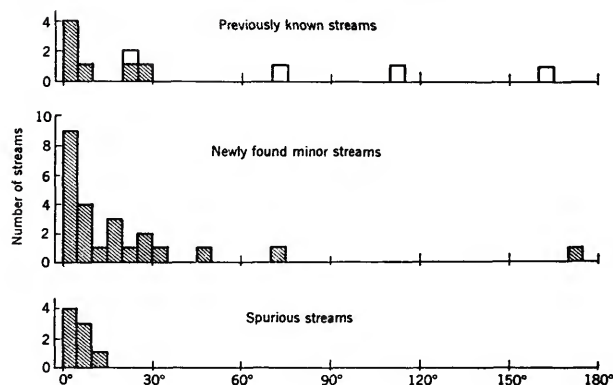


FIGURE 7.—Distribution of inclinations. Major streams are unshaded.

These radiant have been corrected for zenith attraction and diurnal aberration. We found the ecliptic latitude  $\beta$  of each radiant and also the ecliptic longitude  $\lambda - \lambda_{\odot}$  measured from the sun's direction as origin. The radiants of major streams and of all other meteors in the sample are so plotted in figure 8. The apex of the earth's motion is in the center of the diagram, the antapex at the right and left ends. The large cluster of points at the right is nearly centered on the anti-sun at  $\lambda - \lambda_{\odot} = 180^{\circ}$ ,  $\beta = 0^{\circ}$ ; while the direction to the sun at left center is  $\lambda - \lambda_{\odot} = \beta = 0^{\circ}$ .

The last two columns of table 4 list the mean values of  $\lambda - \lambda_{\odot}$  and  $\beta$  for each stream radiant. Figure 9 repeats figure 8, substituting mean radiants of minor streams for the individual radiants of their members. The "Cyclid" radiant spread is too large to permit plotting.

In figure 9, the minor streams are seen to cluster principally around the ecliptic in longitude  $120^{\circ}$  to  $210^{\circ}$  with respect to the sun. Table 4 also lists the mean radiants of the spurious streams, computed from their orbital elements neglecting the eccentricity of the earth's orbit. These spurious stream radiants are all in or close to this cluster of stream radiants. All the streams with low inclination are in this cluster, and no stream with high inclination; thus we again conclude that the newly found streams with high inclination are much more probably genuine.

All the information that we have found useful in estimating the probability of a stream has been assembled in table 4, although some of it appears also in the other tables. By means of the criteria described above, we have

selected four of the provisional streams as the most probable, the  $\varphi$  Bootids,  $\mu$  Draconids,  $\theta$  Herculis, and  $\epsilon$  Geminids. We have indicated above that the Cyclids are quite probably not a stream, and that the  $\sigma$  Leonids are certainly not a single stream. More definite conclusions can hardly be drawn from our sample.

#### Comparison with other results

McCrosky and Posen (1959) have examined 2538 meteors photographed by the Super-Schmidt cameras, and by comparing radiants, velocities, and dates, have found seven new streams. Substantially all of our meteor sample is included in theirs. Four of the streams in each list are associated. The  $\epsilon$  Geminid stream bears the same name in both lists. Their  $\delta$  Arietids are the same as our  $\eta$  Taurids, and their  $\mu$  Pegasids are included in our  $\gamma$  Piscids. Finally, their  $\alpha$  Virginids are included within our overgrown  $\sigma$ -Leonid association. This result emphasizes the difficulty of deciding the validity of a possible stream in our sample for, while the  $\epsilon$  Geminids had already been selected as one of the most probable, there was hardly a less promising stream than the  $\eta$  Taurids.

#### Associations with comets

We have compared the mean orbits of the possible streams with the orbits of comets observed since 1700, seeking similarities. The nearest associations found appear in table 5. The comets listed have been seen on only one revolution, except Comet De Vico-Swift, for which we list all three observed perihelion passages. The difference  $D$  between each stream and its provisionally associated comet is tabulated.

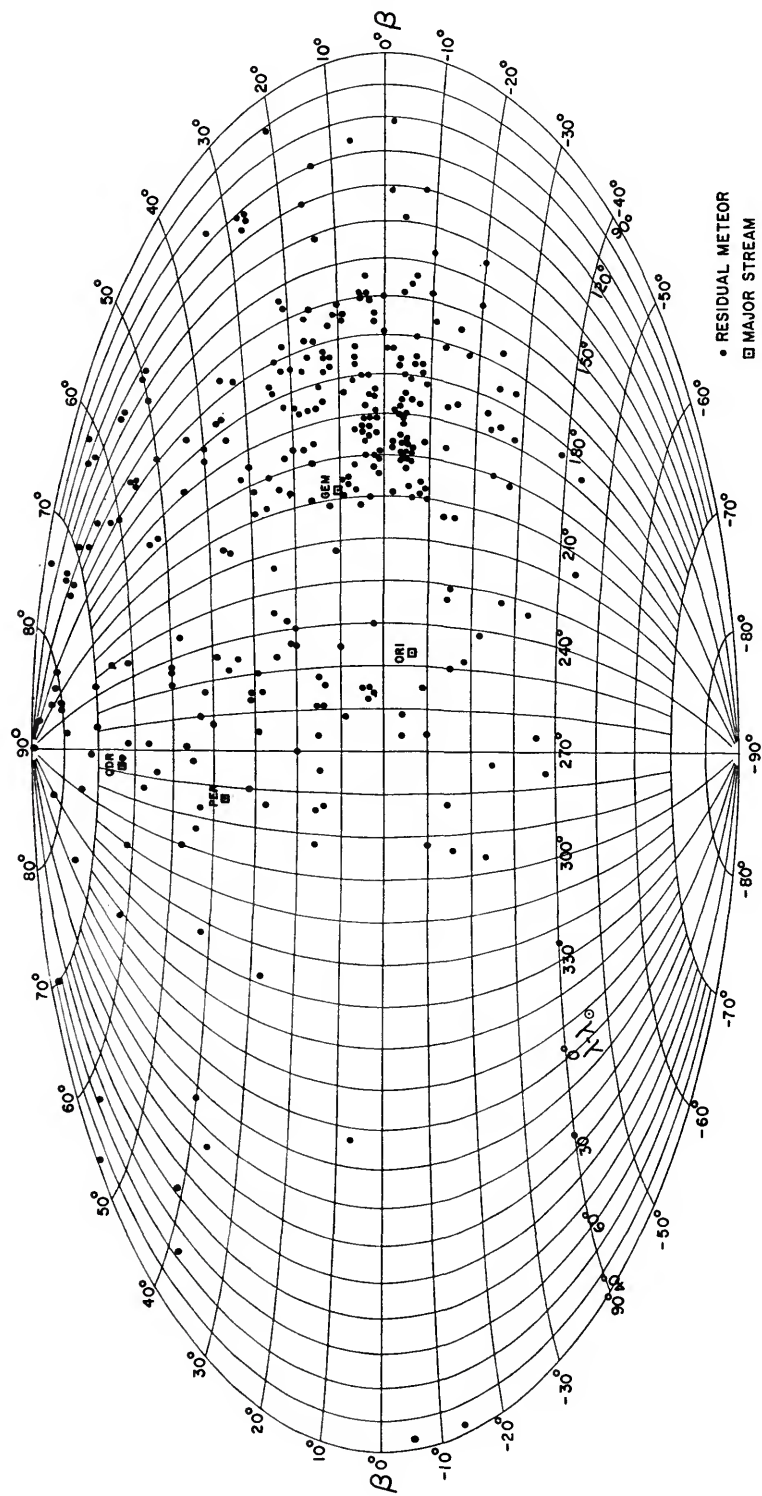


Figure 8.—Distribution of radiants of major streams and residual meteors.

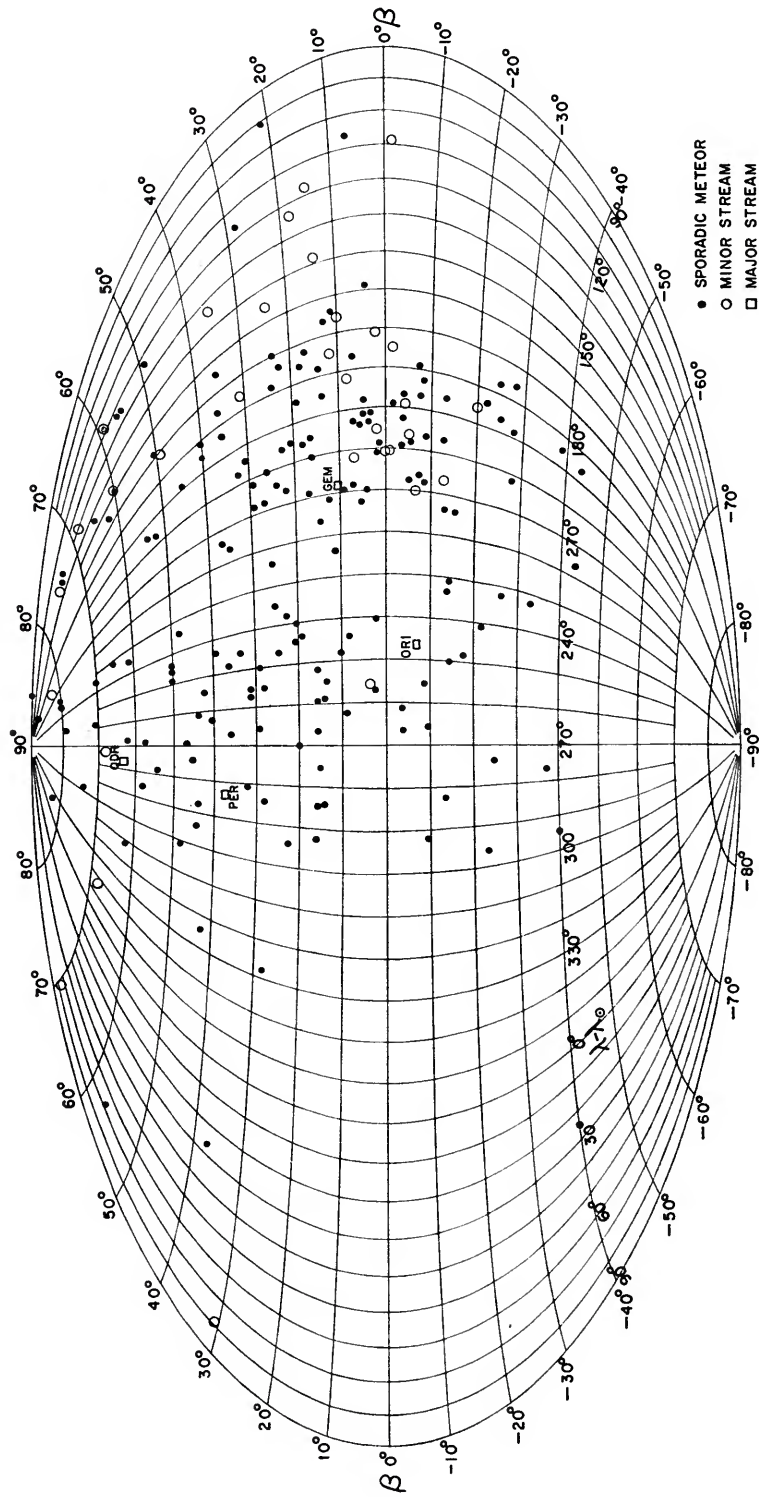


FIGURE 9.—Distribution of radiants of major streams, minor streams, and sporadic meteors.

TABLE 5.—The closest correspondences between newly found possible streams and known comets

Stream	<i>a</i>	<i>e</i>	<i>q</i>	<i>i</i>	$\Omega$	$\omega$	$\pi$	Equinox	<i>D</i>
$\xi$ Orionids	1. 86	. 480	. 947	0°9	159°8	16°4	176°2	1950	
Comet 1928 III	3. 43	. 71	. 995	1. 4	196. 8	345. 2	182. 0	1928	. 24
$\tau$ Herculids	2. 44	. 582	. 998	25°1	90°9	197°7	288°6	1950	
Comet 1930 VI	3. 09	. 672	1. 011	17. 4	76. 8	192. 3	269. 1	1930	. 28
$\mu$ Ophiucids	2. 32	. 575	. 975	3°6	135°0	205°3	340°3	1950	
Comet } 1678	3. 07	. 627	1. 145	2. 9	163. 3	159. 5	322. 8	1678	. 26
De Vico- } 1844 I	3. 10	. 617	1. 186	2. 9	63. 8	278. 7	342. 5	1844	. 23
Swift } 1894 IV	3. 25	. 572	1. 392	3. 0	48. 8	296. 6	345. 4	1900	. 43
$\alpha$ Pegasids	2. 52	. 629	. 872	4°5	206°1	225°0	71°1	1950	
Comet 1819 IV	2. 96	. 699	. 892	9. 1	77. 4	350. 1	67. 5	1820	. 23
$\eta$ Taurids	3. 29	. 722	. 885	0°7	275°9	219°6	135°5	1950	
Comet 1894 I	3. 80	. 698	1. 147	5. 5	84. 4	46. 2	130. 6	1894	. 29

Only the connection between the  $\alpha$  Pegasids and Comet 1819 IV, which was previously found by McCrosky and Posen (1959), is fully convincing. We should expect a parent comet to differ from the mean of an observed stream by more than the average observed meteor because the observed meteors, all of which strike the earth, are a restricted sample of the stream. Since all these comets except 1819 IV differ from the streams by more than 0.2, however, and since some of the streams themselves may not exist, anything more than the possibility of association between these remaining streams and comets remains to be shown.

**Space density of minor streams**

In this discussion we shall use the symbols defined as follows:

- $V_H$ : Heliocentric velocity of meteors.
- $V_G$ : Geocentric velocity of the meteors, neglecting the earth's attraction.
- $V_a$ : Accelerated geocentric velocity of the meteors, at the top of the atmosphere.
- $V_\infty$ : Velocity of the meteors with respect to the earth's surface, at the top of the atmosphere.
- $L$ : Angular elongation of the corrected radiant from the apex of the earth's way.
- $\gamma$ : Angle between  $V_G$  and  $V_H$ .
- $w$ : Width of meteor stream in the plane of the figure.
- $\rho$ : Density of meteors in the stream.
- $X$ : Earth's collisional cross-section for meteors.
- $R$ : Earth's radius including the atmosphere.
- $V_E$ : Earth's orbital velocity.

The number of meteors swept up by the earth in one pass through the stream is  $N_1 = X\rho w \operatorname{cosec} \gamma$ . The number of meteors in the

stream passing within any given small distance  $h$  from the earth's orbit per unit time is  $N_2 = 2hw\rho V_E$ . It is well known (see, for example, Schiaparelli, 1871, p. 116) that  $X = \pi R^2 V_c^2 / V_G^2$ . From figure 10 we see that  $V_E \operatorname{cosec} \gamma = V_H \operatorname{cosec} L$ . Thus the ratio of the number of meteors striking the earth to those crossing its orbit,

$$\frac{N_1}{N_2} = \frac{\pi R^2}{2hV_E} \frac{V_c^2}{V_G^2 \sin L}$$

is independent of  $w$  and  $\rho$ . Following Whipple (1954), we approximate by  $V_\infty^2$  the velocity dependence of the ratio of the number of meteors brighter than a given magnitude on photographs to the number above a given mass, but omit his special factor for velocities

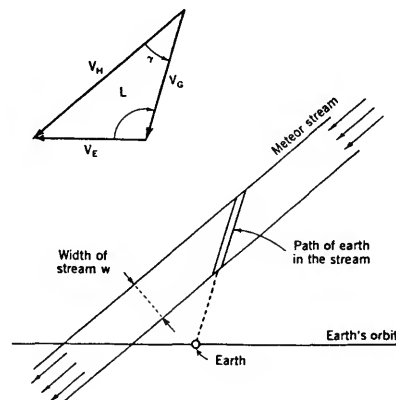


FIGURE 10.—Geometry of the intersection of the earth with a meteor stream.

below 19 km/sec. The qualitative result is not sensitive to a fractional change in the power of  $V_\infty$ . We approximate  $V_\infty$  by the closely similar  $V_c$ . Thus (neglecting constants) we find that the ratio of the number of meteors passing near the earth's orbit to those photographed is given by

$$W = \frac{V_c^2 \sin L}{V_c^4}, \quad (5)$$

which may be interpreted as a weight of a photographic meteor in determining the present strength of its stream at the earth's orbit. Figure 11 shows  $W$  as a function of  $L$  for various values of the stream major semi-axis  $a$ . For all except nearly circular orbits,  $W$  has a strong maximum between  $L=90^\circ$  and  $L=130^\circ$ .

Figure 9 contains, in addition to the cluster of stream radiants already discussed, a smaller group in high latitudes which includes three of the most probable streams. All of this group, and most of the larger group fall within the range of high  $W$ ,  $90^\circ \leq L \leq 130^\circ$ . The minor streams, therefore, are perhaps twice as important numerically in the earth's neighborhood with respect to sporadic meteors, as the observed numbers indicate.

**Origin of the newly found minor streams**

As shown above, the newly found streams are broader and more diffuse than the major streams, or than most of the previously known minor streams. By this characteristic, we readily recognize that in the dynamical sense they are old streams, which have been more disturbed and perturbed than previously known

streams. The absence of closely associated comets corroborates their relatively great age.

There are some interesting relationships among certain of these streams. The  $\mu$  Ophiucids and  $\vartheta$  Herculids form a pair of very similar streams differing only in inclination. In contrast to known pairs of streams on either side of the ecliptic, the  $\mu$  Ophiucids are nearly in the ecliptic while the  $\vartheta$  Herculids have an inclination of  $18^\circ$ . The  $\epsilon$  Geminids bear a somewhat similar relation to the Orionids, but in this case the longitudes of perihelion also differ.

In figure 12 the orbits of all the newly found minor streams with inclinations less than  $15^\circ$  are projected onto the plane of the ecliptic. Although the majority of the streams plotted here doubtless are chance associations, some conclusions can be drawn. The tendency of these orbits to be approximately tangent to the earth's orbit is clearly a selection effect. The tendency to have aphelia at or near Jupiter's orbit appears to be significant. Jupiter will strongly affect these streams, and they will age rapidly.

**Conclusions**

The differences  $D$  between meteors may be used as a means of determining membership in known streams, or of finding new streams. As we have applied  $D$  to the search for streams, the result is certainly complete in the sense that all streams with two or more members in the sample doubtless were found. Unfortunately, the method as applied was not very discriminating, since many streams were "found"

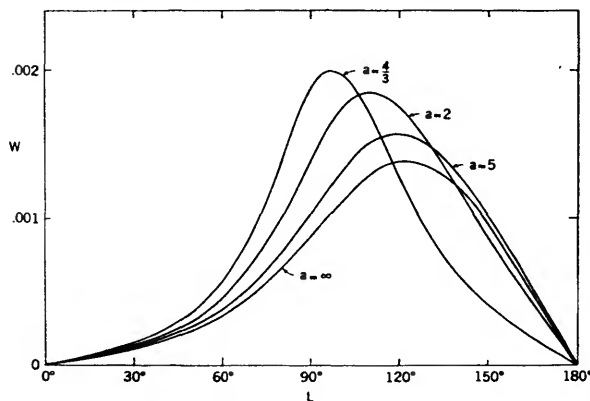


FIGURE 11.—Weight  $W$  of a photographic meteor in determining the present strength of its stream at the earth's orbit, as a function of the angular elongation  $L$  of the radiant from the apex, and the major semi-axis  $a$ .

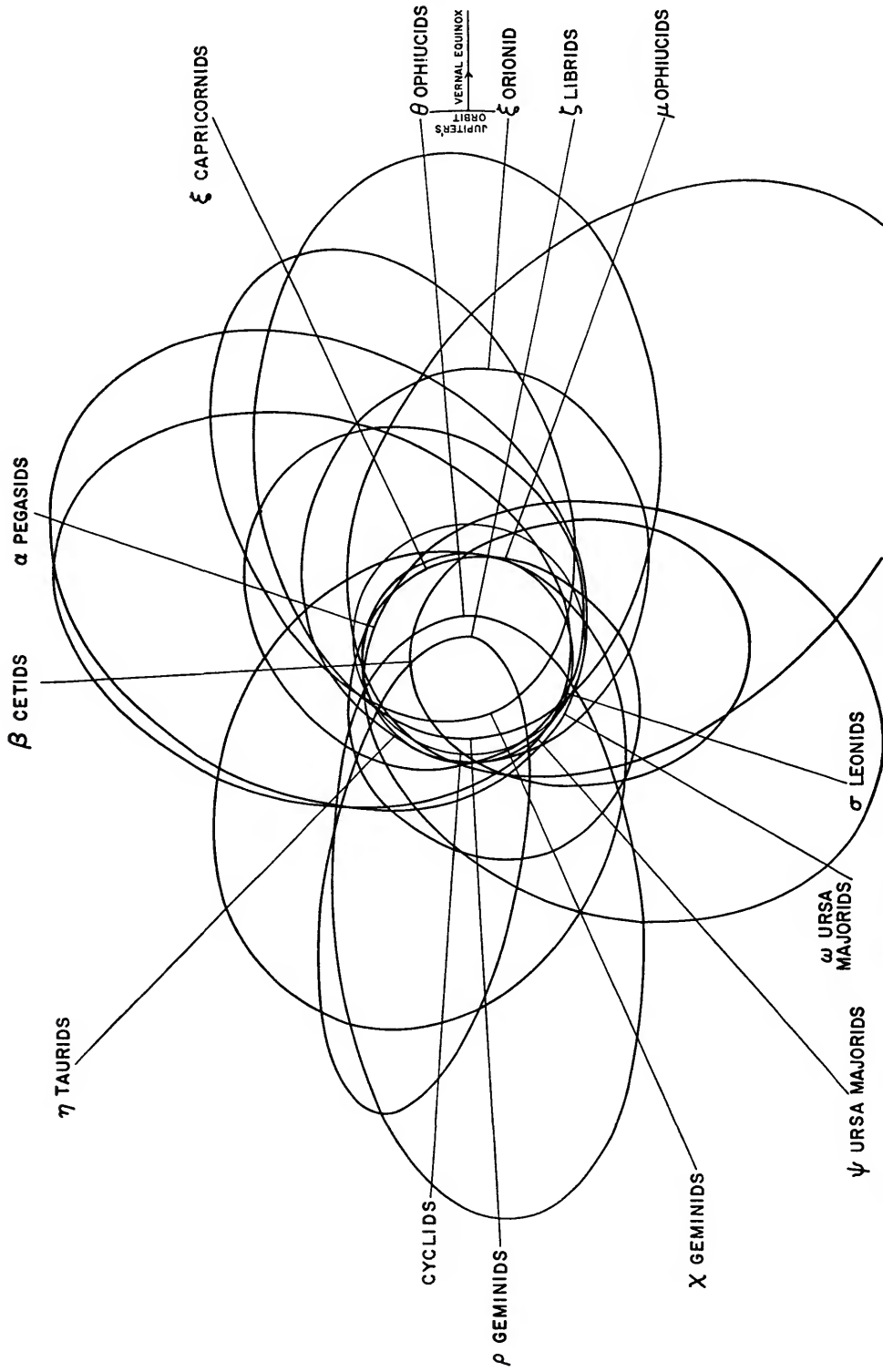


FIGURE 12.—Orbits of all the newly found minor streams with inclinations less than 15° are projected onto the plane of the ecliptic.

which no doubt do not exist, but the number of spurious streams may be estimated. Streams too small to have at least two meteors in our sample, streams with brief showers during a gap in the observing, variable and temporary streams: all may or will be missed.

Of the 359 meteors in the sample, 42 or 12 percent belong to major streams, i.e., those with mean photographic hourly rates exceeding three; 48 or 13 percent belong to previously known minor streams, and approximately 39 or 11 percent to newly found streams. About 64 percent of the sample is sporadic. In the immediate neighborhood of the earth's orbit, the minor streams, compared to other meteors, are roughly twice as numerous as in the photographic sample.

The newly found streams are in fact old streams; they have been much perturbed, and some show obvious relationships with Jupiter. In overall orbital distribution, the minor streams do not differ, in any way that has been conspicuous to us without special scrutiny, from the sporadic meteors with which they are intermingled.

**Appendix**

To compute the average gradients of orbital elements with respect to perturbations, let the units be the astronomical unit, the solar mass, and  $\frac{1}{2\pi}$  year. Consider perturbations at a point  $P$  in a meteor orbit, at a distance  $r$  from the sun. Resolve the meteor's heliocentric velocity  $\mathbf{V}_H$  into components as in figure 13:  $V_R$  directed away from the sun, and  $V_S$  directed forward in the orbit plane normal to  $V_R$ . Resolve the perturbations in velocity into components:  $\delta V_R$  and  $\delta V_S$  along  $V_R$  and  $V_S$ , respectively, and  $\delta V_T$  normal to the orbit plane forming a right-handed set with  $\delta V_R$  and  $\delta V_S$ .

Let  $G$  denote any orbital element, and  $|\nabla G|$  the magnitude of the gradient of  $G$  with respect to perturbations in velocity. Then

$$|\nabla G| = \left[ \left( \frac{\partial G}{\partial \delta V_R} \right)^2 + \left( \frac{\partial G}{\partial \delta V_S} \right)^2 + \left( \frac{\partial G}{\partial \delta V_T} \right)^2 \right]^{1/2} \tag{A1}$$

It is evident that differentiation with respect to  $\delta V_R$  and  $\delta V_S$  may be replaced by differentiation with respect to  $V_R$  and  $V_S$ , respectively.

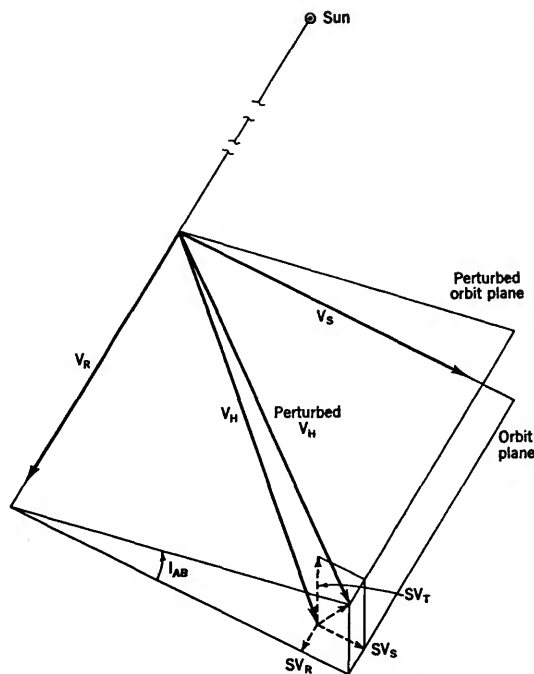


FIGURE 13.—Components of velocity and of perturbations in velocity.

Let the perturbations be expressed in units of the circular speed  $U=r^{-1/2}$ ; the magnitude of the gradient of  $G$  with respect to such perturbations is

$$|\nabla G|_c = r^{1/2} |\nabla G|. \tag{A2}$$

Let  $\text{Grad } G$  denote the average of  $|\nabla G|_c$  over the orbit with respect to time. Let  $t$  be the time of the meteor's arrival at  $P$ , counted from perihelion passage. Then, since the period of revolution is  $2\pi a^{3/2}$ ,

$$\text{Grad } G = \frac{1}{2\pi a^{3/2}} \int_0^{2\pi a^{3/2}} r^{1/2} |\nabla G| dt \tag{A3}$$

$$= \frac{1}{2\pi a^{3/2}} \int_0^{2\pi a^{3/2}} r^{1/2} \left[ \left( \frac{\partial G}{\partial V_R} \right)^2 + \left( \frac{\partial G}{\partial V_S} \right)^2 + \left( \frac{\partial G}{\partial \delta V_T} \right)^2 \right]^{1/2} dt. \tag{A4}$$

This is the desired measure of the importance of  $G$  in  $D$ .

Of the components of  $D$ , differences within the orbital plane are measured by  $\delta e$ ,  $\delta q$ ,  $\Pi_{AB}$ . Obviously,  $\text{Grad } \delta e = \text{Grad } e$ , and  $\text{Grad } \delta q =$

Grad  $q$ . Let  $v$  be the true anomaly at  $P$ . Any perturbation  $\delta v$  in true anomaly implies a perturbation  $-\delta v$  in the direction of perihelion; thus

$$\text{Grad } \Pi_{AB} = \text{Grad } v. \tag{A5}$$

By standard formulae, if  $p = a(1 - e^2)$  is the parameter of the orbit, then

$$\left. \begin{aligned} r &= p/(1 + e \cos v), \\ V_R &= (e \sin v)/p^{1/2}, \\ V_S &= (1 + e \cos v)/p^{1/2}, \\ dv/dt &= V_S/r. \end{aligned} \right\} \tag{A6}$$

If  $r, V_R, V_S$  are given at any point, then by equally standard formulae:

$$\left. \begin{aligned} e \sin v &= r V_R V_S, \\ e \cos v &= r V_S^2 - 1, \\ q &= r^2 V_S^2 / (1 + e). \end{aligned} \right\} \tag{A7}$$

Straightforward analysis yields:

$$\left. \begin{aligned} \partial e / \partial V_R &= r^2 V_R V_S^2 / e, \\ \partial e / \partial V_S &= r^2 V_S (V_S^2 - 1/a) / e, \\ \partial v / \partial V_R &= r V_S (r V_S^2 - 1) / e^2, \\ \partial v / \partial V_S &= -r V_R (r V_S^2 + 1) / e^2, \\ \partial q / \partial V_R &= -V_R q^2 / e, \\ \partial q / \partial V_S &= V_S (r - q)^2 / e. \end{aligned} \right\} \tag{A8}$$

Since  $e, v, q$  are functions of  $r, V_R, V_S$  only,

$$\partial e / \partial \delta V_T = \partial v / \partial \delta V_T = \partial q / \partial \delta V_T = 0. \tag{A9}$$

Expressions for Grad  $e$ , Grad  $v$ , Grad  $q$  may now be found by substitution of equations (A6), (A8), (A9) into equation (A4). We have not found it possible to evaluate those expressions in closed form. Since an approximate result is sufficient for the purpose, we take advantage of the following lemma.

Lemma: If  $y$  and  $z$  are functions of  $x$  which are finite throughout  $a \leq x \leq b$ , and if

$$y \geq 0, \tag{A10}$$

$$z \geq 0, \tag{A11}$$

$$Y = \int_a^b y dx, \tag{A12}$$

$$Z = \int_a^b z dx, \tag{A13}$$

$$R = \int_a^b (y^2 + z^2)^{1/2} dx, \tag{A14}$$

then

$$(Y^2 + Z^2)^{1/2} \leq R \leq Y + Z. \tag{A15}$$

If  $y$  bears a constant proportion to  $z$  for all  $x$  in  $a \leq x \leq b$ , then  $R = (Y^2 + Z^2)^{1/2}$ . Any deviation from constant proportionality between  $y$  and  $z$  increases  $R$ ; for example, if  $y(x_1)$  is increased by  $\Delta y$  over a range  $dx$  about  $x_1$ , and then  $y(x_2)$  is decreased by  $\Delta y$  over a range  $dx$  about  $x_2$  in order to satisfy equation (A12), some algebra will show that  $R$  increases. If  $y = 0$  for all  $x$  such that  $z > 0$  and vice versa, then  $R = Y + Z$ ; if there is any range in  $x$  in which both  $y > 0$  and  $z > 0$ , then  $R < Y + Z$  because  $(y^2 + z^2)^{1/2} < y + z$ .

By substituting equation (A9) into (A4), and taking the mean of the limits in equation (A15), we find that an approximation to equation (A4) when  $G$  is  $\delta e, \Pi_{AB}$ , or  $\delta q$  is

$$\text{Grad } G = \frac{1}{2} \left\{ \left[ \left\langle \frac{\partial G}{\partial V_R} \right\rangle^2 + \left\langle \frac{\partial G}{\partial V_S} \right\rangle^2 \right]^{1/2} + \left\langle \frac{\partial G}{\partial V_R} \right\rangle + \left\langle \frac{\partial G}{\partial V_S} \right\rangle \right\}, \tag{A16}$$

where

$$\left\langle \frac{\partial G}{\partial V_R} \right\rangle = \frac{1}{2\pi a^{3/2}} \int_0^{2\pi a^{3/2}} r^{1/2} \frac{\partial G}{\partial V_R} dt, \tag{A17}$$

and  $\left\langle \frac{\partial G}{\partial V_S} \right\rangle$  is similarly defined.

With the aid of a particular set of elliptic integrals,

$$F'(\phi) = \int_0^\phi [1 - 2e(1+e)^{-1} \sin^2 u]^{-1/2} du, \tag{A18}$$

$$E'(\phi) = \int_0^\phi [1 - 2e(1+e)^{-1} \sin^2 u]^{1/2} du, \tag{A19}$$

we may now evaluate Grad  $G$ . By substituting equations (A6) and (A8) into (A17), and performing the necessary algebra, we find:

$$\langle \partial e / \partial V_R \rangle = 2(1 - e^2) [(1 + e)^{1/2} - (1 - e)^{1/2}] / \pi e, \tag{A20}$$

$$\begin{aligned} \langle \partial e / \partial V_S \rangle &= 8(1 - e^2) \{ (1 - e)^{1/2} [2F'(\pi/2) - F'(\pi/2)] \\ &\quad - (1 - e)^{-1/2} [2E'(\pi/2) - E'(\pi/2)] + [2 \\ &\quad - 2(1 - e^2)^{1/2}]^{1/2} [2(1 - e^2)^{-1/2} + 1/2] \} / 3\pi e, \end{aligned} \tag{A21}$$

where

$$A = \frac{1}{2} \arccos \{ [-1 + (1 - e^2)^{1/2}] / e \}. \quad (\text{A22})$$

Also,

$$\begin{aligned} \langle \partial v / \partial V_R \rangle &= 2(1 - e^2)(1 - e)^{1/2} \{ 2F'(\pi/4) - F'(\pi/2) \\ &\quad - (1 - e)^{-1} [2E'(\pi/4) - E'(\pi/2)] \\ &\quad + 2e(1 - e)^{-1}(1 + e)^{-1/2} \} / \pi e^2, \quad (\text{A23}) \end{aligned}$$

$$\begin{aligned} \langle \partial v / \partial V_S \rangle &= 2 \{ (1 + e)^{3/2} - (1 - e)^{3/2} \\ &\quad + 3(1 - e^2)[(1 + e)^{1/2} - (1 - e)^{1/2}] \} / 3\pi e^2, \quad (\text{A24}) \end{aligned}$$

$$\begin{aligned} \langle \partial q / \partial V_R \rangle &= 2a(1 - e^2)[(1 + e)^{1/2} - (1 - e)^{1/2}] / \pi e, \\ & \quad (\text{A25}) \end{aligned}$$

$$\begin{aligned} \langle \partial q / \partial V_S \rangle &= 4a(1 - e)^{1/2} [2(1 + e)E'(\pi/2) \\ &\quad - (2 - e)(1 - e)F'(\pi/2)] / 3\pi e. \quad (\text{A26}) \end{aligned}$$

The values of Grad  $e$ ,  $e$  Grad  $\Pi_{AB}$ , and of  $1/a$  Grad  $q$  in figure 1 were computed from equations (A5) and (A16) through (A26). The largest possible error, computed by equation (A15), is 15 percent.

Grad  $I_{AB}$  remains to be discussed. Since  $I_{AB}$  measures the change of orbital plane, it is independent of velocity changes within the plane; hence

$$\partial I_{AB} / \partial \delta V_R = \partial I_{AB} / \partial \delta V_S = 0. \quad (\text{A27})$$

From figure 13 we see that

$$\partial I_{AB} / \partial \delta V_T = 1 / V_S. \quad (\text{A28})$$

Thus Grad  $I_{AB}$  may be found exactly from equations (A4), (A6), (A18), (A19), (A27), (A28), as

$$\begin{aligned} \text{Grad } I_{AB} &= 2(1 - e)^{-1/2} [4E'(\pi/2) \\ &\quad - (1 - e)F'(\pi/2)] / 3\pi, \quad (\text{A29}) \end{aligned}$$

and the values in figure 1 were so computed.

## References

- HAWKINS, G. S., AND SOUTHWORTH, R. B.  
 1958. The statistics of meteors in the earth's atmosphere. *Smithsonian Contr. Astrophys.*, vol. 2, no. 11, pp. 349-364.  
 1961. Orbital elements of meteors. *Smithsonian Contr. Astrophys.*, vol. 4, no. 3, pp. 85-95.
- HAWKINS, G. S.; SOUTHWORTH, R. B.; AND STIENON, F.  
 1959. Recovery of the Andromedids. *Astron. Journ.*, vol. 64, pp. 183-188.
- JACCHIA, L. G.  
 1960. Individual characteristics of meteor families (abstract). *Astron. Journ.*, vol. 60, pp. 53-54.
- MCCROSKY, R. E., AND POSEN, A.  
 1959. New photographic meteor showers. *Astron. Journ.*, vol. 64, pp. 25-27.
- SCHIAPARELLI, G. V.  
 1871. Entwurf einer Astronomischen Theorie der Sternschnuppen. G. von Boguslawski, transl. Stettin.
- WHIPPLE, F. L.  
 1947. Photographic meteor studies. IV. The Geminid shower. *Proc. Amer. Phil. Soc.*, vol. 91, pp. 189-200.  
 1954. Photographic meteor orbits and their distribution in space. *Astron. Journ.*, vol. 59, pp. 201-217.
- WRIGHT, F. W.; JACCHIA, L. G.; AND WHIPPLE, F. L.  
 1954. Photographic  $\delta$ -Aquadrid meteors. *Astron. Journ.*, vol. 59, pp. 400-406.  
 1956. Photographic  $\alpha$ -Capricornid meteors. *Astron. Journ.*, vol. 61, pp. 61-69.  
 1957. Photographic  $\delta$ -Aquadrid meteors and evidence for the northern  $\delta$ -Aquadrids. *Astron. Journ.*, vol. 62, pp. 225-233.
- WRIGHT, F. W., AND WHIPPLE, F. L.  
 1948. Photographic meteor results for the month of October (abstract). *Astron. Journ.*, vol. 54, p. 54.  
 1950. The photographic Taurid meteors. *Harvard Coll. Obs. Reprints*, ser. 2, no. 35.  
 1953. The photographic Perseid meteors. *Harvard Coll. Obs. Reprints*, ser. 2, no. 47.



# Orbital Elements of Photographic Meteors

By P. Babadjanov<sup>1</sup>

During the period June 1957 to December 1959, 592 meteors were photographed at two stations of the Institute of Astrophysics of the Academy of Sciences of Tadzhikistan, 359 of them from both stations; 185 doubly photographed meteors were selected for accurate reduction on the basis of trial length and quality of image. The photographs were taken with cameras NAFA 3C/25 (D=100 mm, F=250 mm); a panchromatic emulsion with sensitivity 1,100–1,300 units of GOST 0.85 (approx.=350–400 ASA) was used.

The details of the cameras and the methods of reduction have been described elsewhere (Babadjanov and Sosnova, 1960). The velocity of the meteor outside the atmosphere was computed on the basis of the formula:

$$v=v_{\infty}+kce^{kt}.$$

The parameter  $k$  was determined by a grapho-analytical method, and  $v_{\infty}$  and  $c$  were evaluated by the method of least squares. The instants of the meteors were determined by using a shutter with a gradually changing width. The error of a time observation did not exceed 1 minute.

Table 1 presents orbital data for 132 meteors that have been reduced up to the present. Following are definitions of the column heads of the table:

No: Meteor number, of the year of observation minus 1900 (the first two digits); number of the exposure in the current year (the next three digits); number of the camera (the last digit). If two or more

meteors were photographed simultaneously on one camera, they are distinguished by an added Roman letter.

Date: Day and month.

U.T.: Hour and minute in Universal Time.

Shower: Name of the shower.

Corr. rad.: Radiant (right ascension  $\alpha$  and declination  $\delta$ ) after correction for the earth's attraction and diurnal aberration, in degrees. Equinox 1950.0.

Sin  $Q$ :  $Q$  is the angle between the great circles traced by the meteor, as seen from two stations.

$\epsilon$ : Elongation of the corrected radiant from the apex of the earth's motion, in degrees.

$v_{\infty}$ : Pre-atmospheric velocity, km/sec.

$v_G$ : Geocentric velocity, km/sec.

$v_H$ : Heliocentric velocity, km/sec.

$a$ : Semimajor axis, in a.u.

$e$ : Eccentricity.

$q$ : Perihelion distance, in a.u.

$q'$ : Aphelion distance, in a.u.

$\Omega$ : Longitude of the ascending node, in degrees. Equinox 1950.0.

$\omega$ : Argument of perihelion, in degrees. Equinox 1950.0.

$i$ : Inclination of the orbit plane to the ecliptic, in degrees. Equinox 1950.0.

$\pi$ : Longitude of perihelion, in degrees.

$k$ : Whipple's comet-asteroid criterion.

$\alpha$ CAP:  $\alpha$  Capricornids.

$\iota$ AQU:  $\iota$  Aquarids.

$\delta$ AQU:  $\delta$  Aquarids.

PER: Perseids.

S.T.: Southern Taurids.

LMIN: Leo Minorids.

N.T.: Northern Taurids.

GEM: Geminids.

<sup>1</sup> Astrophysical Institute of the Academy of Sciences of Tadzhikistan, U.S.S.R.

Table 1 contains many meteors belonging to well-known showers: 30 Perseids, 4 Geminids, 3  $\delta$  Aquarids, 3 Northern and Southern Taurids, and 6  $\alpha$  Capricornids. The sporadic meteors also form some groups with analogous radiant, velocities, and orbital elements. One group, designated as "I," is formed by the meteors Nos. 570673, 570706, 570774, and 582565b, and possesses the following mean characteristics:

$\alpha=278^{\circ}5$	$a^{-1}=0.16$	$\Omega=127^{\circ}6$
$\delta=48^{\circ}8$	$e=0.86$	$\omega=202^{\circ}2$
$v_{\infty}=27.0$	$q=0.98$	$i=36^{\circ}2$

The mean coordinates of the radiant are close to that of Maltsev's (1930) radiant No. 76 near  $\epsilon$  Draconis ( $\alpha=279^{\circ}$ ,  $\delta=55^{\circ}$ ); moreover, the Harvard meteor No. 8089 has almost the same characteristics.

The second group, designated as "II," consists of three meteors, Nos. 572181, 572182, and 572384, and has the following mean characteristics:

$\alpha=0^{\circ}9$	$a^{-1}=0.33$	$\Omega=2^{\circ}7$
$\delta=-8^{\circ}9$	$e=0.77$	$\omega=79^{\circ}3$
$v_{\infty}=23.7$	$q=0.65$	$i=5^{\circ}6$

No known visual radiant corresponds to the mean coordinates of the radiant of this group.

Some meteors can be related to the meteor associations discovered recently by Jacchia and Whipple (1961). Such meteors are Nos. 591444 and 570214, related to the association

63; No. 570233 (association 61 or 62); Nos. 591774, 570556, and 570582 (association 72 or 73); No. 570354 (association 69); and No. 573162 (association 88).

Thus, we see that an increase in the observational material results in a decrease in the number of the so-called sporadic meteors. Evidently the majority of sporadic meteors belong to various not-yet-known showers. Application of Whipple's K criterion to the elliptic orbits of sporadic meteors shows that 73 percent are connected with comets ( $K>0$ ), the rest being of asteroidal origin ( $K<0$ ).

Table 1 contains 26 hyperbolic orbits, but almost all of them are perhaps due to observational errors. Only one hyperbolic orbit, that of meteor No. 570707, is probably real. This indicates that the actually hyperbolic orbits constitute less than 1 percent of the whole material.

#### References

- BABADJANOV, P. B., AND SOSNOVA, A. K.  
1960. Photographic observations of meteors in 1957. *Bull. Astrophys. Inst. Acad. Sci. Tadjikistan, U.S.S.R.*, no. 29, pp. 3-15.
- JACCHIA, L. G., AND WHIPPLE, F. L.  
1961. Precision orbits of 413 photographic meteors. *Smithsonian Contr. Astrophys.*, vol. 4, no. 4, pp. 97-129.
- MALTSEV, V. A.  
1930. Radiants of the most important meteor streams. *Russian Astron. Calendar*, ed. 4-e (permanent section), pp. 448-453.

TABLE 1.—Orbital elements of meteors

No.	Day	Mo.	U. T.	Showers	Corr. radiant	$\alpha$	$\delta$	$\varpi$	$\varpi_0$	$\varpi_1$	$\varpi_2$	$\epsilon$	$\phi$	$\theta$	$\phi$	$\psi$	$\Omega$	$i$	$\nu$	$\lambda$	
590065	16	1	14 05		52 38	04 41	0.268	121.0	18.8	15.2	40.4	5.11	0.514	0.945	9.27	205.5	156.0	15.4	92.4	0.70	
590212	10	2	17 16		173 47	8 50	.087	60.1	41.1	36.8	33.0	1.68	.960	.067	3.29	321.3	25.4	20.6	344.8	.91	
590322	11	2	19 21		326 30	52 43	.123	108.6	18.9	15.4	33.0	2.50	.610	.951	4.05	322.5	154.6	20.7	117.0	.02	
590624	11	2	19 13		146 24	17 34	.132	89.3	28.5	26.2	39.7	4.03	.867	.531	7.52	322.4	269.1	3.3	231.6	.45	
590641	6	3	17 52		158 35	78 18	.206	113.0	18.7	16.1	38.5	2.89	.661	.960	4.80	345.3	194.4	20.0	179.7	.16	
590682	24	6	20 33		260 45	28 15	.180	89.6	38.3	36.7	46.8	-2.02	1.40	.795	-4.83	63.0	230.7	43.6	263.7		
570037	4	6	21 07		212 09	26 51	.132	130.6	16.0	10.6	37.1	2.26	.579	.993	3.73	73.8	119.3	9.9	193.2		
591444	6	6	17 05		223 48	-20 56	.095	116.2	16.5	12.2	36.4	2.08	.571	.865	3.27	254.1	47.7	1.4	301.8	-0.05	
591683	12	6	21 04		326 28	19 20	.066	33.6	67.0	65.9	44.5	-3.80	1.24	.921	-3.51	81.0	213.6	177.0	294.7	-0.12	
591125	13	6	19 31		335 27	3 16	.064	31.8	67.5	66.4	44.2	-4.31	1.12	.520	-9.14	82.2	94.4	152.1	176.6		
570214	24	6	16 57		224 57	38 43	.339	124.8	16.7	12.5	37.8	2.80	.639	1.01	4.59	92.8	160.9	15.3	283.7	.10	
570233	24	6	16 54		228 38	-23 10	.107	130.0	18.1	10.3	36.8	2.24	.574	.954	3.53	272.8	33.6	1.5	306.3	-0.08	
581663	25	6	22 21		9 18	18 11	.264	17.8	62.2	61.0	34.2	1.54	.484	.797	2.28	92.7	109.7	154.5	302.4	1.30	
591774	27	6	17 13		257 55	30 43	.123	103.2	19.2	16.5	36.2	2.02	.537	.996	3.10	95.2	219.4	20.8	314.5	-0.85	
592141	1	7	20 52		277 50	-16 30	.039	91.9	25.0	22.6	37.6	2.65	.774	.597	4.70	90.6	206.8	4.9	6.5	-0.32	
570443	3	7	19 17		322 32	54 44	.156	63.3	53.2	51.9	46.7	-2.03	1.50	1.01	-5.08	101.4	180.4	82.6	290.8		
581973	13	7	17 43	$\alpha$ OAP	336 55	48 52	.070	54.0	62.5	61.0	41.3	21.5	.955	.974	42.0	110.7	302.8	91.0	313.6	1.97	
582027	13	7	20 44	$\lambda$ AQU	315 41	33 10	.134	63.6	46.2	44.8	41.2	18.2	.962	.694	35.7	110.8	248.3	74.2	359.1	1.97	
592141	21	7	20 20		28 10	32 02	.070	21.1	62.4	61.1	35.4	1.79	.492	.909	2.57	118.4	133.0	144.1	251.4	-0.40	
582163	21	7	21 43		354 18	1 40	.032	33.5	66.1	65.0	43.7	-3.43	1.07	.366	-11.4	118.5	103.9	169.9	222.4		
570542	22	7	16 03	$\alpha$ OAP	300 58	-10 47	.142	88.9	23.4	22.6	36.7	2.20	.745	.561	3.84	119.4	272.8	7.3	32.2	.18	
582194A	22	7	19 40		315 15	-17 43	.082	77.1	31.9	29.9	36.9	2.29	.565	.994	3.58	290.5	340.2	.6	279.7	-0.08	
582194B	22	7	19 36		300 18	-13 47	.068	90.1	25.5	23.9	37.2	2.47	.766	.576	4.26	119.5	90.2	5.1	209.6	-0.27	
570556	23	7	16 25		293 51	44 24	.087	104.9	19.8	16.3	37.0	2.35	.578	.992	3.71	120.4	200.3	24.2	320.7	-0.06	
570682	25	7	16 16		238 23	53 27	.266	116.3	17.0	12.6	36.6	2.16	.541	.992	3.33	123.3	203.3	41.7	326.0	-0.14	
570706	26	7	18 57	I	279 50	49 25	.279	93.7	31.3	29.2	42.7	120.	1.08	.900	-280.	12.3	123.4	201.7	38.4	325.1	.92
570707	26	7	18 48	I	294 49	-7 05	.109	98.0	45.7	44.3	56.5	-0.016	1.89	.547	-1.78	123.4	252.8	17.1	16.2		
570774	27	7	18 12	I	277 36	48 06	.060	96.0	26.8	24.4	40.1	6.30	.845	.975	11.6	124.3	204.2	36.0	328.5	.87	
570804	27	7	18 19		273 10	-20 48	.068	121.7	17.9	14.2	38.7	3.59	.750	.896	6.28	124.4	223.6	1.0	347.9	.40	
570804	27	7	20 06	$\alpha$ CAP	304 13	-7 27	.061	90.0	24.6	22.0	36.7	2.20	.734	.585	3.81	124.4	270.1	8.9	34.4	.16	
570827A	28	7	16 11	$\alpha$ OAP	298 23	-9 10	.085	96.8	27.5	24.9	40.7	9.00	.934	.635	18.6	125.2	257.0	8.7	22.2	1.45	
570827B	28	7	16 15		276 18	39 17	.029	101.2	29.0	26.7	43.4	-0.80	1.14	.949	-14.6	125.2	208.6	84.6	333.8		
570872	28	7	19 40	$\alpha$ CAP	310 58	-4 46	.016	83.8	32.7	30.8	40.2	6.49	.934	.428	4.10	305.3	251.2	22.9	97.6	1.28	
570876	28	7	19 42	$\lambda$ AQU	338 24	-15 56	.118	61.8	41.2	36.5	36.4	2.09	.964	.076	4.10	305.3	152.2	22.9	97.6	1.06	
570883	28	7	20 45	$\lambda$ AQU	338 11	-17 50	.102	62.2	38.1	36.2	34.4	1.66	.932	.106	3.01	304.7	148.9	22.8	93.6	.65	
570887	28	7	20 57	$\alpha$ OAP	303 26	-11 43	.136	92.7	21.8	18.9	35.7	1.80	.666	.641	3.08	125.4	266.0	5.0	31.4	-0.06	
570916	29	7	18 06		14 19	1 25	.074	23.3	65.6	64.3	36.1	4.00	.868	.570	7.43	306.2	86.6	170.7	32.8		
570951	29	7	20 35		281 46	3 19	.191	26.1	72.4	71.3	46.8	-2.03	1.30	.618	-4.67	306.3	72.4	178.0	18.7	-2.1	
570985	31	7	18 10		291 48	-4 22	.149	114.7	19.2	15.7	38.6	3.43	.747	.807	5.99	128.1	228.7	7.9	356.8	.37	
571086A	4	8	20 25	PER	35 24	55 27	.024	40.0	58.9	57.7	39.9	5.66	.829	.967	10.4	132.0	151.7	112.2	283.8	.78	
571086B	4	8	20 26	PER	32 69	60 34	.029	46.2	53.9	52.6	38.1	2.96	.676	.937	4.96	132.0	148.5	101.8	280.6	.18	
571117	4	8	22 16	PER	39 31	50 59	.046	41.4	58.4	57.2	40.1	6.38	.930	.854	11.8	132.0	144.3	110.4	276.4	.91	
571141	5	8	21 23		304 29	36 10	.208	86.6	26.8	24.6	37.2	2.41	.662	.816	4.00	133.0	239.3	35.6	12.4	-0.11	
592895	7	8	22 07	PER	40 34	57 02	.085	40.7	54.4	53.1	36.3	2.05	.551	.919	3.18	134.5	137.4	107.9	272.0	-0.15	
592904	7	8	23 05	PER	37 42	58 46	.118	42.6	61.8	60.7	43.8	-0.30	1.18	.969	-11.6	134.6	156.7	110.9	291.3		
562964A	8	8	19 43	PER	42 29	59 38	.100	42.8	64.1	62.8	37.0	2.53	.602	.928	3.73	136.5	140.8	105.0	277.2	-0.03	
563013B	8	8	22 32	PER	42 46	57 23	.269	40.8	60.7	59.6	42.0	-87.3	1.01	.944	-173.0	135.5	149.9	112.7	285.4		
593035	9	8	17 39	$\alpha$ CAP	327 54	-7 00	.104	79.4	32.0	29.6	37.6	2.60	.867	.352	4.97	136.4	283.9	7.0	70.4	.57	

TABLE 1.—Orbital elements of meteors—Continued

No.	Day	Mo.	U.T.	Shower	Corr. radiant α	sin Q	δ	ρ	σ	τ	φ	ψ	ω	i	r	k	
552301	9	8	19 23	PER	42 21	59 13	.052	42.3	59.8	48.6	173.	.994	136.6	151.8	109.9	288.4	
552424	11	8	17 35	PER	45 54	57 02	.022	39.6	61.8	41.8	-94.2	1.04	138.4	152.1	114.8	290.5	
552444	11	8	19 02	PER	49 42	59 59	.078	42.6	57.7	56.5	6.16	.851	138.5	142.0	108.4	279.4	
562523	11	8	21 20	PER	44 59	57 41	.107	50.2	61.3	60.1	-80.6	1.03	138.5	138.0	113.6	291.5	
552463	12	8	16 14	PER	45 52	57 38	.124	39.0	59.4	58.2	7.12	.865	133.3	151.3	112.7	290.6	
552473	12	8	17 02	PER	302 45	20 25	.036	94.9	25.6	23.0	4.48	.825	139.4	240.2	24.4	191.6	
552474	12	8	16 51	PER	19 46	51 16	.063	40.1	53.4	52.0	1.70	.489	139.4	215.2	107.7	354.6	
552502	12	8	19 06	AQU	350 19	-13 47	.418	64.7	44.9	43.3	8.70	.990	17.3	319.4	144.4	32.4	105.8
552504A	12	8	19 01	PER	46 10	57 17	.038	39.5	65.6	64.5	-2.57	1.38	139.4	157.5	117.0	291.1	
552504B	12	8	19 05	PER	45 54	58 33	.270	40.8	59.5	58.4	11.2	.915	139.4	151.7	111.6	291.0	
552511	12	8	19 50	PER	46 28	58 21	.056	40.6	65.0	63.8	-2.62	1.37	139.5	156.6	115.2	295.0	
552514	12	8	19 27	PER	46 45	56 34	.219	38.8	63.6	62.5	-6.83	1.16	139.4	154.8	116.8	294.3	
552544A	12	8	21 01	PER	45 03	56 53	.087	39.2	57.8	56.6	3.38	.717	139.6	149.1	118.6	288.7	
552546B	12	8	23 01	PER	47 34	57 13	.110	39.4	59.4	58.4	6.81	.861	140.4	147.2	113.2	287.6	
552546B	12	8	22 52	I	278 10	46 31	.134	101.3	22.0	19.8	3.02	.675	140.4	151.8	112.5	292.2	
552604	13	8	18 35	PER	344 28	18 23	.068	60.5	51.5	50.1	-6.16	1.04	140.4	142.1	113.7	286.2	
552622A	13	8	19 16	PER	00 10	21 04	.188	45.5	57.2	55.9	13.3	.981	140.4	140.4	118.6	288.7	
552622A	13	8	20 11	PER	46 03	57 42	.066	39.7	61.8	60.6	-22.2	1.04	140.4	147.2	113.2	287.6	
552623A	13	8	20 09	PER	50 19	57 55	.100	39.9	59.8	58.6	9.19	.898	140.4	147.2	113.2	287.6	
552623B	13	8	20 52	PER	48 09	58 44	.139	40.7	60.6	59.4	98.9	.900	140.4	151.8	112.5	292.2	
552624	13	8	19 54	PER	320 56	25 23	.060	36.2	34.5	41.4	24.3	.976	140.4	140.4	116.6	292.6	
552625	13	8	20 02	PER	46 17	54 57	.065	37.0	59.6	58.4	3.99	.759	140.4	152.2	112.9	292.6	
552632	13	8	20 34	PER	48 10	55 37	.052	40.6	60.9	59.8	-87.8	1.01	140.4	145.8	113.7	286.2	
552634	13	8	20 24	PER	50 51	57 24	.099	39.4	59.5	58.4	6.69	.860	140.4	145.8	113.7	286.2	
552655	13	8	22 51	PER	50 31	58 13	.088	40.2	60.4	59.2	19.9	.953	140.5	147.8	113.2	288.4	
552664	13	8	22 01	PER	49 22	58 10	.495	40.1	59.0	57.8	6.10	.846	140.5	147.8	113.2	288.4	
552665	13	8	22 42	PER	49 01	56 50	.109	38.8	59.2	58.0	4.90	.807	140.5	147.6	114.2	288.1	
552667A	13	8	22 43	PER	53 22	59 59	.035	42.1	59.5	58.3	25.9	.965	140.5	148.7	110.4	284.2	
552667B	13	8	22 44	PER	49 02	58 32	.043	40.4	61.5	60.4	-16.6	1.06	140.5	162.1	113.5	292.8	
552765	16	8	19 23	PER	54 07	55 14	.044	36.5	63.3	62.2	-24.6	1.04	140.6	143.3	150.6	119.9	293.9
552804	16	8	22 03	PER	53 20	57 27	.161	37.8	59.9	58.7	5.04	.806	143.4	143.4	157.5	115.6	300.9
571835	23	8	18 51	PER	256 57	66 33	.225	92.0	19.7	13.0	1.28	.214	1.65	150.2	172.9	23.4	323.2
571853	24	8	18 06	PER	289 16	63 09	.126	87.8	16.6	10.7	1.11	.112	1.23	151.2	217.9	20.1	9.1
571871	30	8	20 23	PER	353 11	-4 43	.081	76.0	32.9	31.0	2.38	.813	4.31	237.0	104.1	1.9	341.2
552995	7	9	18 16	PER	296 36	-44 48	.075	145.4	13.2	7.3	35.9	1.87	2.75	344.5	18.4	4.4	2.9
594472	10	9	20 24	PER	27 51	59 30	.106	50.2	60.0	58.9	-2.58	1.33	-6.01	167.2	137.0	100.8	304.2
583135	12	9	19 01	PER	283 24	56 10	.116	70.3	49.5	48.2	6.38	.813	9.76	168.4	170.3	63.5	345.7
583194	13	9	21 42	PER	1 24	71 54	.147	64.6	49.5	48.2	-4.16	1.22	-9.24	170.3	208.6	78.2	18.9
583371	14	9	21 42	PER	92 41	26 35	.078	6.0	60.4	59.1	1.01	.189	1.20	171.4	81.2	173.0	252.6
583414	17	9	18 14	PER	20 40	9 56	.070	62.4	49.8	39.0	2.04	.968	3.99	174.2	29.6	3.8	203.8
583464	17	9	21 39	PER	9 14	7 41	.060	73.8	33.0	31.2	2.07	.877	3.88	174.4	306.6	6.2	121.0
571817	18	9	17 05	PER	16 07	9 14	.018	68.9	33.0	30.8	1.48	.865	2.78	175.4	316.5	4.4	131.9
571925	21	9	19 05	PER	16 16	16 05	.016	72.4	36.7	34.5	3.00	.932	6.90	333.4	130.6	2.9	129.1
571942	22	9	16 09	PER	11 11	2 02	.078	79.1	36.0	34.0	7.66	.931	15.0	359.3	115.5	3.8	114.7
571943	22	9	16 14	PER	325 33	71 57	.314	77.5	32.8	30.8	2.68	.648	4.42	179.3	212.3	51.8	31.6
571953	22	9	18 47	PER	18 07	14 29	.029	68.2	43.3	41.7	13.4	.991	21.7	179.4	320.7	18.6	140.1
583606	22	9	23 25	PER	68 48	-17 30	.114	51.3	53.7	52.6	11.1	.947	26.7	359.4	81.5	83.5	81.0
572072	23	9	19 25	PER	299 45	-24 37	.049	154.2	13.0	6.8	1.76	.435	2.51	178.4	17.8	18.1	7.0
572106	24	9	17 33	PER	276 59	67 34	.190	89.0	26.4	24.0	2.64	.621	4.28	180.6	186.4	39.4	7.0
594674	25	9	16 31	PER	324 58	4 54	.086	121.9	18.2	14.8	4.36	.796	3.47	181.7	221.3	6.9	43.0
572181	25	9	17 31	II	00 21	-8 34	.263	96.2	25.6	22.7	3.97	.841	7.31	2.3	79.4	5.7	81.6
572182	25	9	17 32	II	00 31	-8 58	.262	96.2	24.4	21.4	3.04	.788	5.44	2.2	79.4	5.7	81.6
572384	27	9	20 00	II	1 50	-9 06	.051	96.4	21.2	15.4	2.08	.675	3.45	3.6	79.1	5.3	82.6

TABLE 1.—Orbital elements of meteors—Continued

No.	Day Mo.	U.T.	Shower	Corr. radiant α	δ	ρ <sub>∞</sub>	v <sub>H</sub>	g	ε	q	q'	Ω	ω	ι	r	k			
572452	28	9	20 56	114 16	22 26	.026	16.0	60.3	65.1	37.4	2.37	.704	.700	4.04	185.3	108.7	178.3	291.0	.13
572513	29	9	20 51	81 11	46 34	.129	26.9	66.1	65.2	40.9	9.06	.903	.880	17.2	186.3	221.9	138.0	47.2	1.25
572514	29	9	20 42	47 16	11 11	.065	49.6	53.0	51.7	39.5	4.23	.767	.987	7.47	6.3	14.7	171.8	21.0	.51
572544	29	9	22 40	74 44	32 54	.061	22.6	68.9	67.9	42.0	144.	.965	.708	287	186.4	245.4	160.2	71.8	3.57
572581	30	9	20 05	359 10	11 16	.089	92.5	24.3	21.8	37.9	2.48	.744	.635	4.32	187.3	261.8	7.4	89.0	.23
572593	30	9	20 45	19 33	1 54	.018	78.6	27.4	25.1	35.3	1.68	.762	.400	2.96	7.3	118.1	5.9	128.4	.09
565755	7	10	19 05	29 47	36 57	.154	65.8	18.9	15.2	27.4	.863	.491	.439	1.28	163.6	314.5	14.3	148.1	-.60
565985	11	10	23 45	174 56	76 51	.071	62.5	57.8	56.7	50.4	-1.17	1.84	.988	-3.32	197.8	170.1	85.7	7.9	
583777	13	10	18 49	331 04	16 51	.345	125.9	15.9	11.6	37.9	2.56	.636	.834	4.19	199.8	213.4	8.2	53.2	.06
563815	13	10	21 28	34 04	9 17	.086	76.0	30.8	28.9	36.2	1.88	.836	.309	3.45	19.9	121.1	5.3	141.0	.32
563972	15	9	17 31	37 14	10 36	.036	74.4	34.5	32.4	37.7	2.46	.897	.265	4.67	21.8	125.1	6.1	146.9	.66
572813	23	10	21 41	160 21	37 23	.028	39.6	62.2	60.9	41.0	8.27	.922	.642	15.9	210.1	104.6	124.0	314.7	1.31
573027	28	10	21 59	102 23	38 20	.021	29.0	71.4	70.4	46.5	-3.39	1.28	.697	-5.45	214.1	245.6	149.8	99.6	
573065	2	11	23 37	124 55	29 20	.112	14.4	74.0	73.9	44.6	-4.56	1.20	.916	-10.0	220.0	210.8	163.6	70.8	
564193	4	11	14 21	52 01	13 15	.114	78.4	25.6	22.6	34.2	1.42	.697	.429	2.40	61.5	112.2	4.8	173.7	-10
564214	4	11	19 30	24 44	12 41	.101	104.9	20.6	17.1	38.2	2.66	.716	.764	4.55	221.6	244.8	1.1	106.4	.20
564412	17	11	19 18	62 46	23 15	.138	80.4	29.2	26.9	36.9	2.05	.809	.391	3.71	234.8	290.6	2.2	165.3	.29
564501A	19	11	22 03	86 22	55 08	.421	64.9	45.9	45.6	42.7	-35.8	1.01	.374	-72.0	237.0	283.7	66.6	160.7	
564591B	19	11	21 51	91 49	47 27	.636	62.2	47.7	46.4	41.9	21.4	.989	.241	21.2	237.0	283.6	64.8	295.6	2.28
564687	6	12	16 36	70 29	25 09	.017	92.0	18.5	14.6	34.0	1.33	.505	.682	2.08	253.9	245.3	1.4	139.2	-38
573136	12	12	15 28	32 40	-11 49	.174	138.3	16.6	12.2	40.2	4.79	.801	.953	8.63	80.2	21.8	7.0	102.0	.64
573162	13	12	15 05	308 08	52 24	.119	113.0	18.8	15.4	39.0	3.12	.685	.983	5.26	261.2	177.0	21.3	78.2	.22
573185	13	12	16 07	112 55	31 32	.025	62.9	36.8	34.5	34.2	1.41	.905	.134	2.69	261.3	326.0	22.4	226.3	.45
573191	13	12	17 07	112 43	32 21	.039	62.8	35.5	33.4	33.3	1.28	.984	.148	2.41	261.3	324.2	22.2	225.6	.32
564622	14	12	16 19	114 42	33 12	.028	62.1	45.8	44.2	40.2	4.73	.981	.091	9.37	262.1	6.3	43.3	268.4	1.69
564652	14	12	18 18	113 30	32 13	.249	62.9	35.0	32.9	33.0	1.25	.877	.153	2.35	262.1	323.8	21.5	225.9	.28
564692	14	12	19 14	113 43	31 52	.124	56.8	35.4	33.4	31.9	1.28	.885	.147	2.41	262.2	324.3	21.6	226.5	.32
564695	14	12	19 12	113 22	15 11	.112	60.0	43.2	41.6	37.2	2.13	.971	.060	4.20	262.2	154.7	26.4	56.8	1.16
573287	19	12	19 23	164 53	30 39	.010	32.2	58.8	57.4	35.6	1.56	.684	.524	2.80	267.5	273.6	130.2	186.1	.05



# On the Structure of the $\delta$ -Aquarid Meteor Stream

By A. K. Terentjeva<sup>1</sup>

The  $\delta$ -Aquarid meteor stream has some exclusive and peculiar properties:

(1) The perihelion distance  $q=0.06$  a.u. is shorter than that of all other streams (having  $q \geq 0.1$  a.u.). The theoretical temperature  $T$  of the meteor bodies near the perihelion should be  $T \sim 1100^\circ$  K (melting point of silicates). It is possible that this high temperature accounts for the peculiar general appearance of the shower meteors which are sharp, show no wakes, and give off no sparks. The  $\delta$ Aquarids are also observed at the ascending nodes of their orbits as a daytime meteor shower, the Arietids.

(2) The radiants of this shower cover a large area, and many other radiants of some minor ecliptical streams occur in the same region.

(3) The  $\delta$ Aquarids are the richest shower of the southern hemisphere, but the number of good photographic and visual observations is insufficient. There have been some attempts (Wright, Jacchia, and Whipple, 1956; 1957) to obtain the structure of  $\delta$ Aquarids and neighboring streams ( $\iota$ Aquarids,  $\alpha$ Capricornids), based upon an insufficient number of double-station photographs; only some of the single-station meteors are genuine  $\delta$ Aquarids.

Much reliable data concerning a great number of the  $\delta$ -Aquarids' visual radiants have been compiled in the U.S.S.R., some with a determination of geocentric velocities. These data were published in Russian, and have remained insufficiently known abroad. A new paper (Terentjeva, to appear) tabulates all double-station photographs, visual radiants, and radar observations of the  $\delta$ Aquarids since their discovery in 1871. The total number of radiants is about 600, and they include radiants of the neighboring showers ( $\iota$ Aquarids,  $\alpha$ Capricornids, etc).

The general study of the radiants shows the complexity of the  $\delta$ Aquarids and their large area with some "centers" (Pokrovsky, 1922; Astapovich, 1950). A study of the improved geocentric radiants and all the orbital data gives the following results:

(1) The  $\delta$ Aquarids show two groups of radiants: one north and one south (main group) of the ecliptic; the symmetry line is parallel to the ecliptic and lies  $1^\circ 3'$  to the south. The north and south branches are symmetrical relative to the plane of Jupiter's orbit. This may be the effect of perturbations. The visually determined third "ecliptic branch" of the  $\delta$ Aquarids is, apparently, a group of different radiants of many minor streams and of sporadic meteors. Simultaneous visual and photographic observations of this group are needed. The new ephemeris (daily motion) of the improved geocentric radiants is given in table 1. McIntosh's (1935) ephemeris is in good agreement with these data for the southern  $\delta$ Aquarids. Derbeneva (Stalinabad) in 1960 obtained the following ephemeris for the radiant from telescopic meteors (Equinox 1950.0):

$$\alpha_R = 338^\circ 8' + 0^\circ 89 \text{ (Long. of } \odot - 122^\circ 4'),$$

$$\delta_R = -15^\circ 4' + 0^\circ 39 \text{ (Long. of } \odot - 122^\circ 4').$$

(2) The period of visibility is apparently from long. of  $\odot = 120^\circ$  (July 23) to long. of  $\odot = 148^\circ$  (August 22), with maximum at long. of  $\odot = 125^\circ - 126^\circ$  (maximum of southern  $\delta$ Aquarids only, about July 29), Equinox 1950.0. The 600 fireballs observed in China (10th to 12th centuries) give for the  $\delta$ Aquarids a shift of 4 to 5 days in the maximum date over 1000 years; the radiant area then was also very large. Undoubtedly, Jupiter disturbed this stream. During a period of 28 days the earth passes through the stream, which passes very close to

<sup>1</sup>Kiev Astronomical Observatory, U.S.S.R.

the sun; therefore a very small variation in radiant position gives a great difference in inclination, perihelion distance, and other elements. The perturbations alone are insufficient to explain all the peculiarities of the observed orbit which may be affected by physical agents as well.

The velocities of the photographic  $\delta$ -Aquadrid meteors show a systematic difference  $\Delta V_s$  of about +4 km/sec relative to the velocities obtained by radar (Almond, Bullough, and Hawkins, 1952; Almond, 1952). The semimajor axes of photographic orbits are thus enlarged by a factor of 2. The mass distribution and the space density in the stream were studied in detail (Terentjeva, 1961); the mass distribution  $f(M) \sim M^{-2.0}$ , the mean space density  $D(M) = 12 \times 10^{-9} \text{ km}^{-3}$ , in accord with the later determination by Moscow Section of VAGO, Crimea Expedition of 1960.

A fine shower of  $\iota$  Aquarids and more than three other showers are acting simultaneously in the same region; to separate them we need double-station photographic and exact visual observations. The data obtained by Wright, Jacchia, and Whipple (1957) concerning  $\iota$  Aquarids are doubtful: of nine double-station meteors, some are not  $\iota$  Aquarids. The radiants of the  $\iota$  Aquarids are also near the ecliptic, in a very confusing region. There are many radiants of meteor streams near the ecliptic, acting successively; they correspond to the orbits of short period (Astapovich, 1950). The study of these streams ( $\iota$  Aquarids,  $\alpha$  Capricornids,  $\delta$  Aquarids) therefore demands great care.

The neighboring shower of the  $\alpha$  Capricornids has two groups of radiants: the proper  $\alpha$  Capricornids (an old meteor stream observed in the 19th century), and a possibly new group of ecliptical  $\alpha$  Capricornids. Their correlation

cannot be explored because of the absence of exact observations of the later shower. It is possible that the structure of the Capricornids is identical with that of the  $\delta$  Aquarids: McIntosh's (1935) radiant No. 250 being the southern branch, the  $\alpha$  Capricornids the northern one. McIntosh's radiants Nos 240 and 264 apparently fit the ecliptical branch of the Capricornids, but not that of the "southern  $\iota$  Aquarids," as suggested by Wright, Jacchia, and Whipple (1957). The ecliptical group of "August  $\alpha$  Capricornids" (Wright, Jacchia, and Whipple, 1956) is doubtful. If the "August  $\alpha$  Capricornids" were real, the photographic error of the radiant would be  $6^\circ$  to  $8^\circ$ . The preliminary ephemeris of the  $\alpha$  Capricornids (Equinox 1950.0) is:

$$\alpha_R = 303^\circ.1 + 0.63 \text{ (Long. of } \odot - 124^\circ.0)$$

$$\delta_R = -10^\circ.4 + 0.17 \text{ (Long. of } \odot - 124^\circ.0)$$

(photographic obs.)

The association between the  $\alpha$  Capricornids and Comet Lexell 1770 I is more probable than that with Comet 1948n (=1948 XII) as suggested by Wright, Jacchia, and Whipple (1956).

Comet 1770 I is also connected with some ecliptical streams and may be related to Comet 1948 XII (Tisserand's criterion). The application of Tisserand's criterion to the study of the connection between comets and streams gives a considerable dispersion of the C-constant (for a single meteor orbit). Apparently the meteor bodies not only suffer gravitational perturbations, but are possibly influenced by other physical agents. In these cases Tisserand's criterion cannot be applied.

A lengthy paper on this subject with a bibliography of sources (over 100 references) will be published in Russian.

TABLE 1.—New ephemeris of geocentric  $\delta$ -Aquadrid radiants (Equinox 1950.0)

Stream	Radiants	Daily motion	Long. of $\odot$	Type of observation
Northern $\delta$ Aquarids	$\alpha_R = 334^\circ.5$ $\delta_R = -5^\circ.4$	+0 $^\circ$ .85 +0 $^\circ$ .35	125 $^\circ$ .0 125 $^\circ$ .0	All photographic and visual
Southern $\delta$ Aquarids	$\alpha_R = 338^\circ.5$ $\delta_R = -16^\circ.9$	+0 $^\circ$ .88 +0 $^\circ$ .36	125 $^\circ$ .0 125 $^\circ$ .0	All photographic

## References

- ALMOND, M.  
1952. The orbit of the  $\delta$  Aquarid meteor stream. *Jodrell Bank Ann.*, vol. 1, pp. 22-28.
- ALMOND, M.; BULLOUGH, K.; AND HAWKINS, G. S.  
1952. Radio echo observations of the daytime meteor streams in 1952. *Jodrell Bank Ann.*, vol. 1, pp. 13-21.
- ASTAPOVICH, I. S.  
1950. The ecliptic orbits of meteor bodies in the solar system. *Izv. Turkmen Sec. Acad. Sci. U.S.S.R.*, no. 4, pp. 95-96.
- McINTOSH, R. A.  
1935. An index to southern meteor showers. *Monthly Notices Roy. Astron. Soc.*, vol. 95, pp. 709-718.
- POKROVSKY, K. D.  
1922. Meteor showers of the southern hemisphere. *In* *Trans. 1st Meeting of the Russian Society of Amateur Astronomers (Mir-ovédénié)*, pp. 172-173. Petrograd.
- TERENTJEVA, A. K.  
1961. Results of the  $\delta$ -Auarid and Perseid meteor showers observations in 1959. *Bull. Comiss. Comets and Meteors, Acad. Sci. U.S.S.R.*, no. 5, pp. 29-35.
- WRIGHT, F. W.; JACCHIA, L. G.; AND WHIPPLE, F. L.  
1956. Photographic  $\alpha$ -Capricornid meteors. *Astron. Journ.*, vol. 61, pp. 61-69.  
1957. Photographic  $\iota$ -Auarid meteors and evidence for the northern  $\delta$  Aquarids. *Astron. Journ.*, vol. 62, pp. 225-233.



# Masses of Comet Giacobini-Zinner and the Draconid Meteor Stream

By Y. V. Yevdokimov<sup>1</sup>

Comet Giacobini-Zinner is of great interest because of the many valuable observations made of the related Draconid meteor showers. A precise study of the comet's motions leads to some striking conclusions about the manner in which meteor particles are ejected from the comet's nucleus.

An earlier paper (Yevdokimov, 1955) on the relation between the comet and the Draconid meteor stream gave the exact value of the longitude of the ascending node of the meteor stream in 1946 at its maximum as

$$\Omega_{\max} = 196^{\circ}14'31''.6 \pm 3''.2 \quad (1946.0).$$

This paper also established the displacement of the plane of the central part of the stream's orbit. The longitude of the ascending node of the stream was greater than that of the comet. In 1898 the comet approached Jupiter and markedly changed its orbit. Table 1 shows the changes in the perihelion distances since 1897.

In view of these data we may conclude that the earth could encounter only the meteoritic bodies of the stream ejected since 1900. Hence, the tangential component of velocity could not be less than 14.5 meters/second.

The minor distance along the orbit between the comet and the meteors that encountered the earth in 1946 (15.4 days) indicates that the tangential component of velocity must not be greater than 13.7 meters/second.

If we suppose that the meteors were ejected earlier (in 1913, 1926, or 1933), the ejection velocities would be lower than those of the meteors observed in 1933. Thus we conclude that the main mass of meteors observed in 1946 at maximum was ejected by the comet

in 1940, with a tangential component of velocity not greater than 13.7 meters/second.

We have recently worked at combining observations of the comet in 1933, 1939, and 1946. The perturbations from five planets, in the period from 1933 to 1946, have been computed, and we have obtained two systems of elements:

(1) For observations in 1933 and 1939, osculation 1939, Oct. 14.0:

$$\left. \begin{aligned} M_0 &= 341^{\circ}06'57''.45 \pm 0''.22 \\ a &= 3.5138522 \pm 16 \\ e &= 0.7166606 \pm 7 \\ \omega &= 171^{\circ}47'27''.62 \pm 0''.93 \\ i &= 30^{\circ}44'28''.67 \pm 0''.62 \\ \Omega &= 196^{\circ}14'59''.75 \pm 1''.64 \end{aligned} \right\} (1950.0)$$

(2) For observations in 1939 and 1946, osculation 1939, Oct. 14.0:

$$\left. \begin{aligned} M_0 &= 341^{\circ}06'55''.46 \pm 3''.71 \\ a &= 3.5139365 \pm 63 \\ e &= 0.7166601 \pm 9 \\ \omega &= 171^{\circ}47'31''.49 \pm 0''.93 \\ i &= 30^{\circ}44'28''.52 \pm 1''.14 \\ \Omega &= 196^{\circ}14'56''.71 \pm 1''.73 \end{aligned} \right\} (1950.0)$$

A comparison of these elements shows the changes from one revolution (1933-1939) to another (1939-1946), as follows:

$$\begin{aligned} \Delta M_0 &= -1''.99 \\ \Delta a &= +0.0000843 \\ \Delta e &= -0.0000005 \\ \Delta \omega &= +3''.87 \\ \Delta i &= -0''.15 \\ \Delta \Omega &= -3''.04 \end{aligned}$$

<sup>1</sup> Kazan University, U.S.S.R.

TABLE 1.—Changes in perihelion distance

Year	Perihelion distance (a.u.)
1897	1.20
1900	.93
1913	.98
1926	.99
1933	1.00
1940	1.00
1946	1.00
1959	.94

In contrast to the change in the longitude of the ascending node of the meteor stream (+16°8), that of the comet diminished (−3°04) and became equal to

$$196^{\circ}14'11''.82 \pm 1''.73 \quad (1946.0).$$

It is well known that a change in the longitude of the ascending node depends only on the force perpendicular to the plane of an orbit. Hence we may conclude that the changes in the longitude of the ascending node of both comet and meteor stream resulted from the same force at the time of ejection in 1940, and that some component of that force was perpendicular to the plane of the orbit. This may be expressed as follows:

$$\Delta\Omega_{\text{com.}} = r \sin(v+\omega) \operatorname{cosec} i \frac{F_z}{M_{\text{com.}}}$$

$$\Delta\Omega_{\text{met.}} = r \sin(v+\omega) \operatorname{cosec} i \frac{-F_z}{M_{\text{met.}}}$$

$$\Delta\Omega_{\text{com.}} \cdot M_{\text{com.}} = -\Delta\Omega_{\text{met.}} \cdot M_{\text{met.}}$$

$$\frac{M_{\text{met.}}}{M_{\text{com.}}} = -\frac{\Delta\Omega_{\text{com.}}}{\Delta\Omega_{\text{met.}}} = \frac{3.04}{16.8}$$

Hence we conclude that during the period of one revolution, from 1939 to 1946, Comet Giacobini-Zinner ejected 17.5 percent of its mass.

This result is consistent with that obtained by DUBYAGO (1948), who concluded that the velocity of the ejected meteor particles multiplied by the ratio of their mass to the mass of the comet ( $v \frac{M_{\text{met.}}}{M_{\text{com.}}}$  in cm/sec) has the following values: for Comet Encke, 19; for Comet Biela, 14; for Comet Brooks, 17.

If we assume the velocity of ejected particles to be 10 meters/second, we obtain for Comet Encke 2 percent, and for Comets Biela and Brooks 1.5 percent of mass lost. Thus, our conclusions that a considerable loss of mass occurs during each cometary revolution are proved in various ways.

### References

DUBYAGO, A. D.

1948. On secular acceleration in the motion of periodic comets. *Astron. Journ.*, U.S.S.R., vol. 25, pp. 361-368.

YEVDOKIMOV, Y. V.

1955. Concerning the association of the Giacobini-Zinner comet with the Draconid stream. *Astron. Circular, Acad. Sci.*, U.S.S.R., no. 159, pp. 21-24.

# Dynamical Evolution of the Perseids and Orionids

By Richard B. Southworth<sup>1</sup>

This report sketches the methods and the conclusions to date in a study of the effects of planetary perturbations on meteor streams. The research is continuing, and the material will be published in greater detail in another volume of these Contributions.

## Method

Chiefly to be considered here are the differences among the orbits of different meteors in a stream, or equivalently the distribution of meteors in a stream. Since these differences can be directly observed in photographs, the principal task here is to predict them. Neither the observation nor the prediction would have been possible a few years ago; now, however, the Harvard Meteor Program has made sufficiently accurate observations, and the IBM 704 and 7090 computing machines at the Smithsonian Observatory have been able to perform the computing.

The only streams treated thus far in the study are the Perseids and Orionids. Sufficiently accurate observations have been published for 30 Perseids and 19 Orionids (Wright and Whipple, 1953; Whipple, 1954; Jacchia and Whipple, 1961; Hawkins and Southworth, 1961). Every meteor within about 10 km/sec in speed, 10 degrees in radiant, and 10 days in date from the shower mean has been included. The observational errors are all probably less than 0.2 km/sec or 0°.2.

For each stream a reference orbit was computed for a hypothetical meteor coming from the observed mean radiant at the observed mean speed on the observed mean date. The analysis deals primarily with differences from this reference orbit, but neglects squares and

products of the differences; in that sense, it is a first-order computation.

The secular perturbations of an orbit by a planet are the average of the total perturbations by that planet, where the average is taken over all positions of the planet in its own orbit. The effect of secular perturbations on a meteor stream is a gradual shift of the whole stream; differential secular perturbations between different parts of the stream may gradually further distort the stream. The secular perturbations of the Perseids and Orionids were computed by Smart's (1953, pp. 218-231) formulation of Gauss's method. The results, especially the differential secular perturbations, were found to be negligible compared to the other perturbations to be discussed next.

The average perturbation of a planet over a few revolutions does not differ much from the secular perturbation. This is not true, however, for meteor streams. In particular, when as in the case of the Perseids and Orionids the stream passes close to the orbit of Jupiter or Saturn and has a long period, the meteors undergo large perturbations at irregular intervals. The effects of these perturbations on the stream are treated here by a numerical method, partly due to Hamid (1950). This method, which involves a good deal of computing, is described as follows.

First, tables are prepared of the perturbation of a single meteor during one complete revolution from aphelion to aphelion. The values are found by numerical integration along the orbit. A table is prepared for every perturbing planet that may be considered, and a set of initial positions of the planet is chosen, uniformly spaced around its orbit. The different values in each table are the perturbations that would occur if the planet were at these

---

<sup>1</sup>Harvard College Observatory, and Smithsonian Astrophysical Observatory, Cambridge, Mass.

different initial positions when the meteor was at aphelion. The chief approximation in this entire study is that these perturbations are computed only for meteors moving in the reference orbit. From another point of view, this is the limitation of the first-order formulation. This approximation should be adequate for the Perseids and Orionids, but will be discontinued in future studies of other streams.

The second part of the perturbation computation is a Monte Carlo computation. This consists in tracing out the individual perturbations of a set of meteors chosen at random from an initial Gaussian distribution. Each chosen meteor is treated one revolution at a time. The initial elements and the initial positions of the perturbing planets are given. The meteor's perturbations in its first revolution are found by interpolation in the tables previously computed from the initial planet positions. Thus the elements at the end of the first revolution are found, and then, from the new value of the period, the positions of the planets at the end of the revolution. It is then possible to compute the perturbations in the second revolution, and so on. This process is performed about a hundred times on about a hundred meteors.

One can theoretically predict the general behavior of the perturbed meteors, but it will be sufficient here to examine the computed results, which agree with the theory. The first feature is the well-known rapid speed of the meteors along the orbit of the stream. Of course, the time required to spread out depends on initial circumstances, but, for example, a set of Perseids leaving their comet in the vicinity of the earth with root-mean-square relative velocities of 30 meteors per second were spread all along the orbit four revolutions later. Consequently, it has not been necessary to take account of the distribution in the stream along its orbit.

Once the meteors are well separated, they undergo independent perturbations which are (effectively) a random walk in the elements. It is not a true random walk because, if only one perturbing planet is considered, the perturbations have a complicated periodic char-

acter. Saturn's perturbations upset the periodicity of Jupiter's, however, at least for the Perseids and Orionids. It is convenient to express the average difference between meteors in the stream by the variances and covariances of the elements. The computed variances increase approximately linearly with the time, as they would in the case of a true random walk.

The last part of the perturbation computation is the calculation of the effects of the perturbations on the observable part of the stream. The observable meteors—those whose orbits intersect the earth's orbit—form only a four-dimensional cross section of the five-dimensional distribution of meteors in the stream. It is convenient to define a set of descriptive parameters called "local quantities"; these comprise the (unobservable) minimum distance between a meteor's orbit and the earth's orbit, and four observable quantities: the right ascension and declination of the true radiant, the geocentric speed, and the date of observation. To the first order, there is a linear matrix transformation between orbital elements and local quantities, and the two modes of description are equivalent. This transformation is applied, in fact, to the tables of perturbations per revolution, and the Monte Carlo computations are actually performed in terms of local quantities. Thus the time rates of increase of the variances of the local quantities are computed directly, and the rates of increase of the variances in the observable sample can be found by subtracting the parts of the overall variances that depend on correlation with the distance from the earth's orbit. For the Perseids and Orionids, it is found that the observable quantities are highly correlated with the distance from the earth's orbit; thus the variance in the observable sample is much smaller than in the stream. From another point of view, this means that perturbations tend to disperse meteors of both streams mostly within the orbit planes.

### Perseids

The Perseid reference orbit is very similar to the orbit of the parent Comet 1862 III, except

TABLE 1.—Differences within the Perseid stream

	$\alpha_R$	$\delta_R$	$V_G$	Date
Observed standard deviation	4.7	1.7	1.0 km/sec	3.4 days
Observed variances	$\alpha_R$ 21.9	$\delta_R$ 1.2 2.8	$V_G$ 0.5 -1.3 1.0	Date 15.0 1.1 0.5 11.6
Computed increase in variances per revolution (per 100 years)	$\alpha_R$ .08	$\delta_R$ .08 .11	$V_G$ -.04 -.04 .02	Date .08 .09 -.04 .09
Deduced age (years)	27,000	2,600	5,300	13,200

for a shorter period. The reference orbit passes 1.3 a.u. from Jupiter's orbit, and only 0.3 a.u. from Saturn's.

ORBITAL ELEMENTS (1950.0)

	Reference	1862 III
$a$	21.56	24.28
$e$	.956	.960
$q$	.946	.963
$P$	100.1	119.6
$i$	113°2	113°6
$\omega$	149°8	152°8
$\Omega$	137°9	138°7

The first line of table 1 shows the standard deviation of Perseids from the mean.  $\alpha_R$  and  $\delta_R$  are the right ascension and declination of the radiant, and  $V_G$  is the geocentric speed. The radiant deviations are from a fixed mean; standard deviations from a moving mean radiant are 1.6 in both coordinates. The next four lines show observed values of the four variances and six covariances in the same units as the standard deviations.

The computed increase of the variances per revolution (i.e., per century) is shown in lines 6 through 9 of table 1. On the simplest model for the stream history—all the meteors leaving the comet at one time—the age of the stream would be found by dividing the present variances by their rates of increase. Line 10 shows these ages; they are quite discordant. If one considers models in which the meteors leave the comet at different times, the average age

of the meteors would be somewhat less than these ages, but the results agree no better.

It follows from table 1 that planetary perturbations alone cannot explain the present Perseid distribution. Since other processes can scatter the meteors, but can hardly bring them back together, the ages in line 10 are upper limits. If we take the smallest of those, and allow an additional 400 years for the initial spread along the orbit, the conclusion is that the average age of the Perseids does not exceed 3,000 years, and that the overall age is not likely to exceed 6,000 years.

To explain the remaining variances, there must be another force that must be nongravitational and must have large components perpendicular to the orbit plane. It is impossible to determine the nature of this force definitely because only a sample of the stream is observed; nonetheless it is possible to guess. Guigay (1947, 1948) pointed out that the observed Perseid orbits tend to diverge from a point on the comet orbit before perihelion. Accordingly, the hypothesis was made that an explosion took place there in the past, and several Monte Carlo computations were performed to study the subsequent perturbations. By adjusting the date and place of the explosion, and the relative speed, the best fit to the observed variances was found to be with an explosion 1.5 a.u. from the sun, 1.3 a.u. north of the ecliptic plane, roughly a thousand years ago.

Table 2 shows the computed variances, which are a passable fit. The root-mean-square relative velocity found is 2.6 km/sec, which is very high, but is actually observed in dust outbursts from comets (Whitney, 1955). These outbursts are not well understood, but it is clear that a large quantity of material is ejected at high velocity; hence some connection with meteors seems likely.

### Orionids

There has long been a doubtful association between the Orionids and Comet Halley. Although the reference orbit is quite similar in size and shape to the comet orbit, the mutual inclination is eight degrees. All the observed Orionid orbits lie in nearly the same plane and are scattered in that plane. The comet orbit is well outside the apparent distribution of meteor orbits.

ORBITAL ELEMENTS (1950.0)

	<i>Reference</i>	<i>Halley</i>
<i>a</i>	17.80	17.95
<i>e</i>	.968	.967
<i>q</i>	.569	.587
<i>P</i>	75.1	76.0
<i>i</i>	164°7	162°2
$\omega$	82°6	111°7
$\Omega$	29°1	56°7

Table 3 shows the observed and computed differences within the Orionid stream. As in

TABLE 2.—*Computed Perseid variances on the explosion hypothesis*

	$\alpha_R$	$\delta_R$	$V_G$	Date
$\alpha_R$	23.1	4.1	2.5	11.6
$\delta_R$		2.0	-0.1	2.4
$V_G$			1.1	0.4
Date				10.5

the case of the Perseids, line 10 contains upper limits to the average time since the meteors were spread along the orbit. The observed dispersions in the declination of the radiant and in the speed are both so small that they are certainly affected by observational errors, and should in fact be even smaller. Furthermore, it is not difficult to produce small dispersions—for example, by collision with dust particles (see Whipple, this symposium, p. 239). Thus one can accept the results from the right ascensions and dates without being troubled by the declinations and speeds. The conclusion is that the Orionids have been spread along the orbit for only 400 or 500 years, and are perhaps 700 years old in all.

### Conclusions

The perturbations of individual meteors in a stream can be much more important than the secular perturbations of the stream as a whole. The dust outbursts from comets deserve more attention as a possible source of meteor streams.

TABLE 3.—*Differences within the Orionid stream*

	$\alpha_R$	$\delta_R$	$V_G$	Date
Observed standard deviation	1°03	0°48	.87 km/sec	1.23 days
Observed variances	$\alpha_R$ $\delta_R$ $V_G$ Date	1.06	-.03 .23 .57 .02 .75	.72 .25 .51 1.52
Computed increase in variances per revolution (per 75 years)	$\alpha_R$ $\delta_R$ $V_G$ Date	.170	.006 .0004 -.019 -.001 .002	.228 .008 -.025 .304
Deduced age (years)	470	44,000	26,000	380

**References**

GUIGAY, M. G.

1947. Recherches sur la constitution du courant d'étoiles filantes des Perseides. *Journ. Observateurs*, vol. 30, pp. 33-48, 69-87.
1948. Recherches sur la constitution du courant d'étoiles filantes des Perseides (suite). *Journ. Observateurs*, vol. 31, pp. 1-32, 49-64, 77-94.

HAMID, S. E.

1950. The formation and evolution of the Perseid meteor stream. Doctoral thesis, Harvard University.

HAWKINS, G. S., and SOUTHWORTH, R. B.

1961. Orbital elements of meteors. *Smithsonian Contr. Astrophys.*, vol. 4, no. 3, pp. 85-95.

JACCHIA, L. G., AND WHIPPLE, F. L.

1961. Precision orbits of 413 photographic meteors. *Smithsonian Contr. Astrophys.*, vol. 4, no. 4, pp. 97-129.

SMART, W. M.

1953. *Celestial mechanics*. Longmans, Green and Co., New York.

WHIPPLE, F. L.

1954. Photographic meteor orbits and their distribution in space. *Astron. Journ.*, vol. 59, pp. 201-217.

WHITNEY, C. A.

1955. Comet outbursts. *Astrophys. Journ.*, vol. 122, 190-195.

WRIGHT, F. W., AND WHIPPLE, F. L.

1953. The photographic Perseid meteors. *Harvard Coll. Obs. Reprints*, ser. 2, no. 47.



# A Note on the Cometary Nature of the Tungus Meteorites

By V. Fessenkov<sup>1</sup>

The Tungus meteorite appeared in the early morning of June 30, 1908, at 0<sup>h</sup>17<sup>m</sup> UT near Vanovara, Central Siberia ( $\lambda=6^{\text{h}}47^{\text{m}}2^{\text{s}}$ ,  $\varphi=60^{\circ}9'$ ). Its trajectory was oriented nearly along the meridian from south to north, inclined toward the horizon at  $10^{\circ}$  to  $15^{\circ}$ . The meteorite moved toward the earth with an apparent relative velocity of about 40 to 50 km/sec. According to all evidence, this body possessed a retrograde motion in the solar system and consequently could not be any fragment of an asteroid; i.e., an ordinary meteorite.

It is known that all meteorites so far studied in our laboratories are the ancient constituent parts of asteroids separated apparently by their mutual collisions with a small kinetic energy, leaving their internal structure unaltered. In the solar system only comets may possess retrograde motion. For this reason the Tungus meteorite must be considered as a small comet encountering the earth. Several other data strongly support this conclusion.

This meteorite produced an exceptionally strong aerial explosion wave that spread over the world and was registered at many stations. Especially significant was the barogram obtained at Potsdam, Germany; it contained the direct as well as the inverse wave propagation and, consequently, the corresponding height above sea level, which was found to be only 5 to 6 km.

The meteoritic matter dispersed by the explosion was spread as far as California during the following two weeks and produced a marked increase in the atmospheric extinction not strongly dependent on wavelength.

If we suppose that the absorbing matter was uniformly distributed over the whole of the

Northern Hemisphere, its total amount could be roughly estimated to be  $10^6$  tons. Nevertheless, no meteoritic fragments were discovered either at the place where the explosion occurred or in the neighborhood, although very careful search was made by numerous parties during 1958, 1959, and 1960. Boring in the marshes and in the lakes situated in the central area of the fall likewise produced no results.

There were no traces of direct blow or explosion at the surface, no craters or even cavities. The only remnants of the material substance of the meteorite were the microscopic spherules, about 0.01 to 0.1 mm in diameter, which were very irregularly distributed over the central area where the forest was greatly damaged. These spherules could perhaps have originated by the condensation of melting products of the explosion of the meteorite. On the other hand, the explosion energy was enormous, as was evident from the crushing of the trees in an area of several hundred square kilometers. At a certain distance, the fallen trees clearly assumed a radial character. The corresponding energy manifested by this effect in the central area was evaluated to be  $10^{23}$  ergs. This is only about 1 percent of the initial kinetic energy of the Tungus meteorite if its mass is taken to be  $10^6$  tons and the relative velocity as 50 km.

The first night following the fall of the meteorite appeared unusually bright in the areas westward from the spot of the fall. This unusual illumination was due not to the intensifying of emission lines in the spectrum of the night sky but uniquely to the continuous part of the spectrum and, therefore, was produced by the scattering of the solar light by dust particles.

<sup>1</sup> Director, Astrophysical Institute, Alma Ata, U.S.S.R.

The numerous reports obtained by the Committee of Meteorites of the U.S.S.R. from all over the world established the region at the earth's surface where bright nights occurred. The western boundary was apparently limited by Ireland. At least there is no knowledge of a similar anomaly in the Atlantic, and it is certain that nothing unusual occurred in the United States. The southern boundary was placed at  $\varphi=45^\circ$  to  $46^\circ$  in Western Europe and apparently descended to  $42^\circ$  in Central Asia. In Tashkent the nocturnal sky was of such a brightness that photographic exposures with a normal astrograph were not possible at all. The next night the brightness of the night sky became much fainter and then completely disappeared.

All these striking phenomena can be easily understood if we imagine that simultaneously with the meteorite a dust cometary tail penetrated into the atmosphere and was detained in its upper strata. It is evident that the dust particles composing the tail must have invaded the atmosphere in the Northern Hemisphere and were restricted only to an area determined by longitude  $180^\circ$  relative to the sun. The western borders of Ireland are just within this area. On the other hand, the southern boundary of the nocturnal illumination was determined evidently by the height of the atmospheric layers still illuminated by the direct solar rays at midnight near solstice. For Europe this corresponds to nearly 350 km, but for Central Asia to 700 km. In order to be detained at these altitudes, dust particles must be exceedingly small. In fact, their dimensions must be of the order of some tenths of a micron. The abundance of such matter in the atmosphere corresponds to an optical thickness of the order of  $10^{-6}$ . Evidently this insignificant amount cannot be found in some optical anomaly in daylight conditions. It is in striking contrast to the matter provided from the explosion of the head of the meteorite; it had gradually dispersed over the whole of the atmosphere and resulted, as mentioned above, in an increase in atmospheric extinction but not in any discernible change in nocturnal brightness.

It is highly probable that all these data show that the Tungus meteorite was in fact a small comet with a dust tail oriented in the direc-

tion opposite to the sun. The central area of the meteorite explosion was characterized by the fall of trees generally oriented radially. The direction of the fallen trunks marked the initial propagation of the explosion waves. This orientation can still be seen at the spot where the explosion occurred and also on the photographs made by an aerial survey of this area in 1939 (scale 1:5000), which clearly show the separate trunks of the fallen trees. The whole picture is nevertheless a very complex one. In the very center of the area of devastation there are many trees standing with torn branches and looking like telegraph poles.

The orientation of the fallen trees cannot be accounted for by one single center of explosion. Clearly, aerial waves issued from the flying body with at least three major outbursts lying apparently not exactly on the same straight trajectory. It is possible to localize approximately the places of projection on the ground of these outbursts occurring at a height of several kilometers.

The first outburst corresponds to the so-called South Marsh and was found to be at a distance of 1.4 km in a southerly direction from the Kulik camp; the second outburst, apparently much stronger, occurred at a distance of about 0.8 km in a northeasterly direction from this camp; and the third one at a distance of 2.2 km to the north-northwest. The consecutive and nearly simultaneous explosion waves interfered with each other and produced a complex picture that cannot easily be interpreted with any exactitude. Only at a certain distance from the central area does the direction of the fallen trees become more homogenous and nearly uniformly radial. The mountains, some hundred meters in height, and other elevations in the close neighborhood of the area appear to have had no influence on wave propagation.

Finally, one may ask how it is possible that a comet, representing even in its nucleus a dispersed state of matter similar to a very dense cluster of particles, can penetrate into the lower layers of the atmosphere.

A single body of a mass of  $10^9$  tons must fall on the ground with a considerable remnant of its initial mass and cosmic velocity. As a result, a crater or even a field of craters can be

expected, and actually has occurred in many similar cases. Nevertheless, the dimensions of the nucleus of the Tungus comet could not have been very large, perhaps only about 0.5 km in diameter with a mean density of several hundredths gm/cm<sup>3</sup>. The mutual separation in the nucleus between the particles appears to be several times greater than their linear dimensions.

These are the preliminary results of the examination of different data concerning this exceptional phenomenon. A further study being undertaken by the Academy of Sciences of the U.S.S.R. (Committee of Meteorites) and other institutions will help to elucidate many questions about the Tungus fall and its cometary nature, and may well have some bearing on other comets.



# A Short Note on the Origin and Age of the Quadrantids

By S. E. Hamid <sup>1</sup> and Mary N. Youssef <sup>1</sup>

The Quadrantid shower is distinguished among the periodic meteor streams by its very short duration ( $<1^\circ$  in longitude of node), very high inclination ( $\simeq 70^\circ$ ), short period ( $\simeq 5$  years), and high eccentricity ( $\simeq 0.70$ ).

The stream, meeting the earth at descending node, approaches the orbit of Jupiter (its radius vector at ascending node is  $\simeq 4.8$  a.u.). The stream's orbit, except for its high inclination, is similar to that of Jupiter's short period cometary group.

The present study is based on six doubly photographed meteors whose orbital elements are given in table 1.

By integrating numerically the secular perturbation of Jupiter on these orbital elements and carrying the integration back 5000 years, we find that:

(1) The inclination of the stream decreases from its present high value to a minimum value ( $\simeq 13^\circ$ ) around 1500 years ago, and then increases again to a maximum value ( $\simeq 76^\circ$ ) around 4000 years ago.

(2) The perihelion distance of the stream decreases from its present value ( $\simeq 1$  a.u.) to

a minimum value ( $<0.1$  a.u.) around 1500 years ago (time of minimum inclination), and then increases again to maximum ( $\simeq 1.0$  a.u.) around 4000 years ago (time of maximum inclination).

(3) As we go back in time, the stream recedes from Jupiter's orbit, arrives at its maximum distance about 1500 years ago, and then approaches Jupiter's orbit again to within 0.2 a.u. about 4000 years ago.

(4) The longitude of the perihelion of the stream undergoes periodic variation, with its minimum value  $\sim 86^\circ$  around 500 years and its maximum value  $\simeq 111^\circ$  around 2800 years.

Figures 1 to 5 show typical changes of the orbital elements of a Quadrantid meteor (No. 9983). Comparing the orbital elements of the six meteors in the past, it is found that they agree around 3000 years ago (see table 2).

We are suggesting that sometime around 4000 years ago (see fig. 1) a comet was captured by Jupiter. After the capture the comet developed meteors along its path. Because an appreciable number of these meteors, which now form the Quadrantids, did not suffer another close approach to Jupiter, the shower is observed to be compact.

<sup>1</sup> National Planning Institute, Cairo, Egypt.

TABLE 1.—Orbital elements of Quadrantid meteors

Trail no.	$a$ (a.u.)	$e$	$i$ (degrees)	$\omega$ (degrees)	$\Omega$ (degrees)	$\pi$ (degrees)	Reference
9945	3.046	0.682	68.6	165.2	282.5	87.7	(1)
9985	3.074	0.683	70.8	168.3	282.5	90.8	(1)
9953	2.906	0.664	72.7	170.3	282.5	92.8	(1)
9983	3.002	0.675	72.4	169.6	282.5	92.1	(1)
9974	2.999	0.674	72.5	170.4	282.5	92.9	(1)
9907	2.880	0.659	72.1	177.2	281.4	98.6	(2)

(1) L. G. Jacchia, and F. L. Whipple, "Precision Orbits of 413 Photographic Meteors," Smithsonian Contribution to Astrophysics, vol. 4, no. 4, pp. 97-129, 1961.

(2) G. S. Hawkins, and R. B. Southworth, "Orbital Elements of Meteors," Smithsonian Contribution to Astrophysics, vol. 4, no. 3, pp. 85-95, 1961.

TABLE 2.—Angular orbital elements (in degrees) of the Quadrantids in the past

Time (years)	Trail no.																	
	9945			9985			9953			9983			9974			9907		
	<i>i</i>	$\omega$	$\Omega$	<i>i</i>	$\omega$	$\Omega$	<i>i</i>	$\omega$	$\Omega$	<i>i</i>	$\omega$	$\Omega$	<i>i</i>	$\omega$	$\Omega$	<i>i</i>	$\omega$	$\Omega$
0	69	165	282	71	168	282	73	170	282	72	170	282	73	170	282	72	177	281
-400	65	162	284	68	164	284	71	165	284	70	164	284	70	165	284	71	169	283
-800	58	160	288	60	163	287	67	162	286	64	163	286	65	163	286	68	164	284
-1200	42	157	295	40	159	295	58	161	289	50	161	292	51	161	291	62	162	287
-1600	15	107	351	14	66	394	36	153	302	17	128	331	17	128	331	46	158	294
-2000	37	24	440	47	18	449	22	42	420	41	21	445	41	20	445	14	94	365
-2400	57	18	450	63	16	455	53	19	449	62	16	454	62	16	454	46	20	446
-2800	66	17	454	71	14	457	67	17	454	71	15	456	71	15	457	64	16	452
-3200	71	14	456	74	9	458	73	15	456	74	12	458	75	11	458	71	14	456
-3600	73	8	457	75	-1	459	75	11	458	76	4	459	76	3	459	74	9	457
-4000	73	-2	459	74	-10	461	76	3	459	76	-6	460	76	-7	460	75	1	458
-4400	72	-11	460	71	-16	463	76	-6	460	75	-13	461	74	-14	462	75	-8	459
-4800	70	-17	462	65	-17	465	75	-13	461	71	-17	463	70	-17	463	73	-14	461

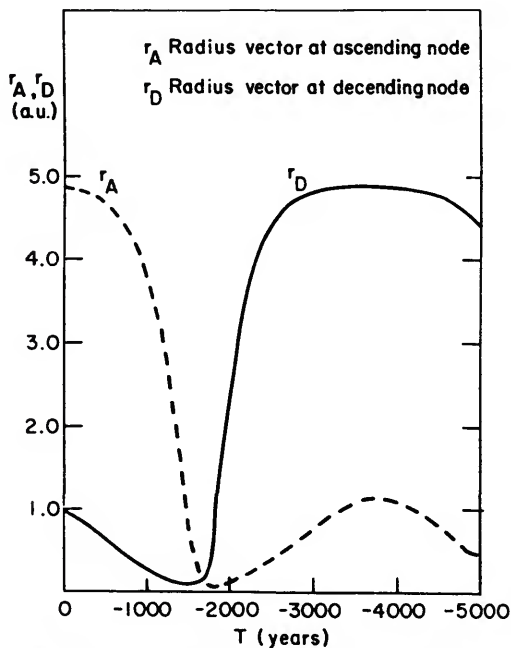


FIGURE 1.—Quadrantid meteor no. 9983. Radius vectors at the nodes plotted against time in the past.

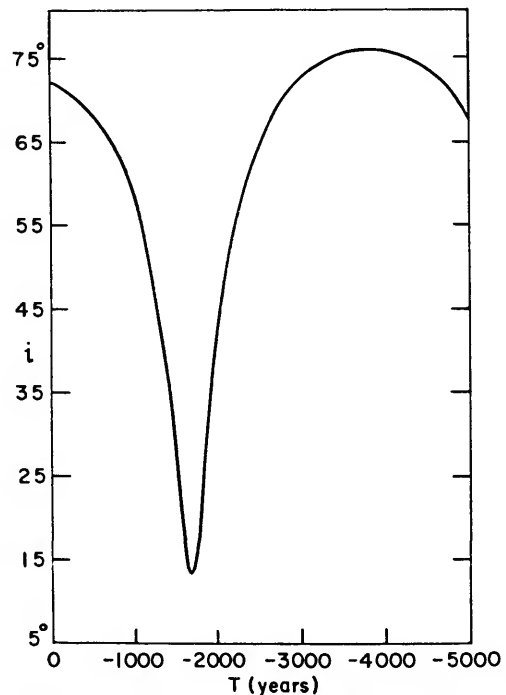


FIGURE 2.—Quadrantid meteor no. 9983. Orbital inclination *i* plotted against time in the past.

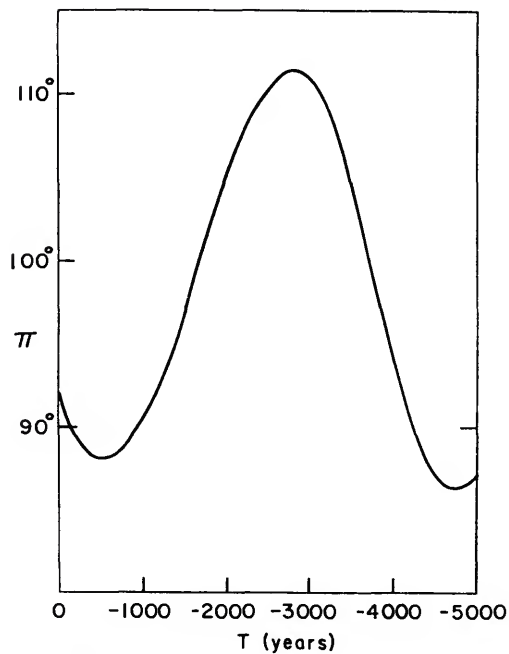


FIGURE 3.—Quadrantid meteor no. 9983. Longitude of perihelion  $\pi$  plotted against time in the past.

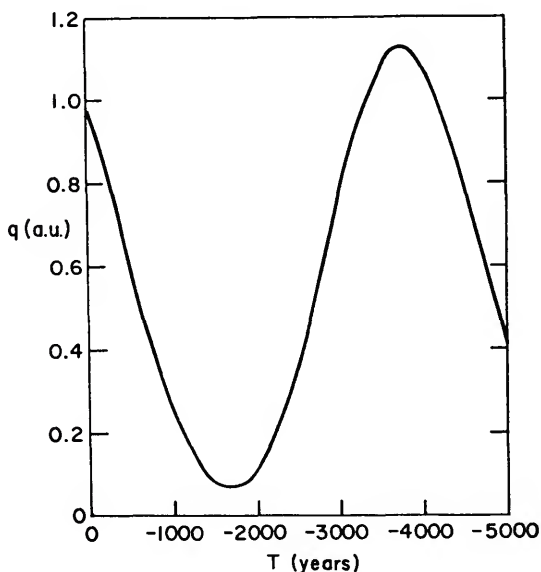


FIGURE 4.—Quadrantid meteor no. 9983. Perihelion distance  $q$  plotted against time in the past.

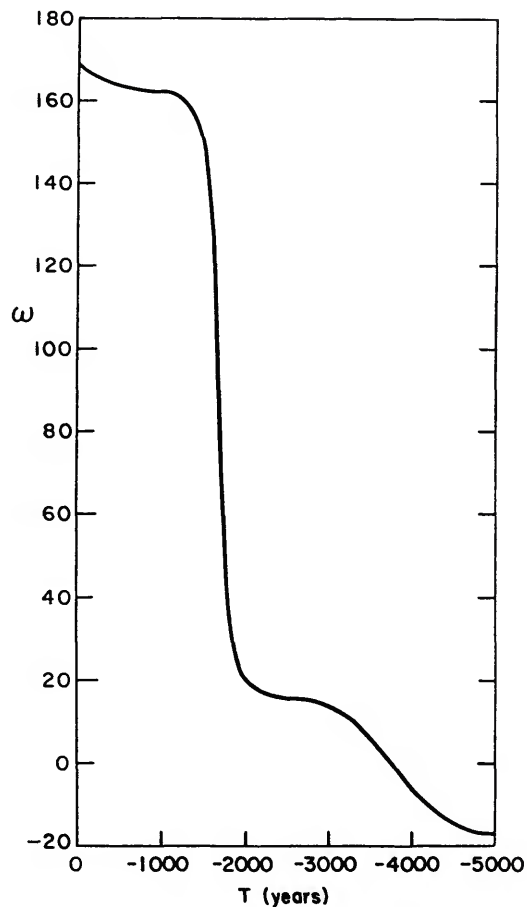


FIGURE 5.—Argument of perihelion  $\omega$  plotted against time in the past.



## Abstracts of Other Papers

*Southern Hemisphere Vela-Puppis Meteor Activity:* C. Ellyett and K. W. Roth<sup>1</sup>.—It has gradually become established from radar surveys at Christchurch, New Zealand, in 1953, 1956, and 1960, that intense meteor shower activity occurs annually in early December, with radiant in both the Vela and the Puppis constellations. The Vela group has a mean right ascension of about 133°, and the Puppis group is somewhat widely spread around 110°. The declination of both showers is about -45°.

*The Absence of Detectable Infrared Radiation from Meteor Trails:* B. A. Tinsley, J. J. Tait, and C. Ellyett<sup>1</sup>.—A lead sulphide cell immersed in dry ice was used in conjunction with an arsenic trisulphide lens to look from ground level for transient infrared bursts radiated from the trails produced by large incoming meteors in the upper atmosphere. No bursts were detected. A theoretical analysis was then made of the probability of detection. The mechanism of infrared radiation from meteor trails is largely unknown, so assumptions must be made in order to give a figure for radiated power. It is then possible to calculate the infrared flux at the ground. The conclusion reached was that, with the equipment available, an average of 200 hours of clear night-time observing would be required to detect a single meteor.

*The Latitude Dependence of Radar Meteor Shower Observations:*<sup>2</sup> C. S. L. Keay and C. Ellyett.<sup>1</sup>—A simplified method of assessing the relative significance of meteor showers is discussed. Most of the tables of meteor showers quoted in the literature give a false impression of the actual influx of meteoric shower particles into the earth's atmosphere, particularly when rate measurements are quoted. The bias inherent in single-station rate measurements is largely eliminated by the present method, and

the importance of short-range echoes is emphasized. Comparison of results obtained from both hemispheres reveals a considerable measure of agreement between various surveys.

*The Seasonal Variation of the Twilight Sodium Airglow in the Southern Hemisphere:*<sup>3</sup> B. A. Tinsley<sup>4</sup> and A. Vallance Jones.<sup>5</sup>—The plateau brightness of the sodium twilight airglow has been measured near Christchurch, New Zealand, by photographic spectroscopy between July 1960 and September 1961. A seasonal variation with a maximum in mid-winter and a minimum in mid-summer was observed. This is similar to the seasonal variation in the northern hemisphere, indicating a six-month phase difference between the two hemispheres.

The annual distribution of meteors at high rates has just been determined at Christchurch, New Zealand, for a complete year. The southern hemisphere meteor distribution is out of phase with the northern hemisphere, and both are out of phase with their own sodium distributions. Thus, unless the concept of long-term storage of sodium in the upper atmosphere is introduced, it is unlikely that upper atmospheric sodium is of meteor origin, at least from meteors of a size detectable by radar methods.

*All-Sky Meteor Rates in the Southern Hemisphere:*<sup>6</sup> C. Ellyett and C. S. L. Keay.<sup>1</sup>—An extensive experiment has been carried out at Christchurch, New Zealand (43°37'S, 172°24'E), to determine meteor rates over the visible sky, using radar equipment with all parameters maintained constant throughout a complete year. The effect of varying background noise was eliminated.

From a total of 724,681 meteors, a seasonal variation has been established, with a peak rate in local summer. The meteor rate at 69.5 Mc/s was found to be unaffected by iono-

<sup>1</sup> The authors are associated with the University of Canterbury, Christchurch, New Zealand.

<sup>2</sup> Published in *Journ. Geophys. Res.*, vol. 66, pp. 2337-2343, 1961.

<sup>3</sup> Published in *Journ. Atmosph. Terr. Phys.* vol. 24, pp. 345-351, 1962.

<sup>4</sup> University of Canterbury, Christchurch, New Zealand.

<sup>5</sup> University of Saskatchewan, Canada.

<sup>6</sup> Published in *Journ. Geophys. Res.*, vol. 66, pp. 2590-2591, 1961.

spheric behavior, such as increased absorption, magnetic storms, or aurorae.

*The Identification of Meteor Showers with Application to Southern Hemisphere Results:*<sup>7</sup> C. Ellyett, C. S. L. Keay, K. W. Roth, and R. G. T. Bennett.<sup>8</sup>—Further meteor shower results observed by radar at Christchurch, New Zealand, are now given, including results at high rates, and all Christchurch data are compared with visual observations, and radar results from Adelaide, for the declination range from  $+26^{\circ}.5$  to about  $-50^{\circ}$ . Seven meteor showers appear in all three surveys, and can be regarded as certain, and another 6 to 9, which are each reported twice, are probable.

---

<sup>7</sup> Published in *Monthly Notices, Roy. Astron. Soc.*, vol. 123, pp. 37-50, 1961.

<sup>8</sup> The authors are associated with the University of Canterbury, Christchurch, New Zealand.

An additional 9 to 10 radiant, however, are found by each survey alone.

The errors inherent in the identification of meteor showers from radar data are considered. Different techniques have been used at Christchurch and at Adelaide. It is concluded that no single method of analysis is fundamentally better than any other.

The technique of shower identification depends partly on the nature of the background rate, which may be due either to sporadic meteors, or to the resultant of many minor radiants. The resolution of this uncertainty is necessary before the occurrence of less active showers can be confirmed.

The rate-count method has been extended to multiple range bands, resulting in a useful additional means of sorting out the significance of peaks in the rate curves.







